Morten Hjorth-Jensen, Maria Paola Lombardo, and Ubirajara van Kolck, Editors

An advanced course in computational nuclear physics

Bridging the scales from quarks to neutron stars

June 21, 2016

Springer

No Title Given

No Author Given

Preface

This graduate-level text collects and synthesizes nine series of lectures on the nuclear quantum many-body problem - starting from our present understanding of the underlying forces with a presentation of recent advances within the field of lattice quantum chromodynamics, via effective field theories to central many-body methods like Monte Carlo methods, coupled cluster theories, similarity renormalization group and large-scale diagonalization approaches.

In particular algorithmic and computational advances show promise for breakthroughs in predictive power including proper error estimates, a better understanding of the underlying effective degrees of freedom and of the respective forces at play.

Enabled by recent advances in theoretical, experimental and numerical techniques, the modern and state-of-the art applications considered in this volume span the entire range from our smallest components, quarks and gluons as the mediators of the strong force to the computation of the equation of state for neutron star matter.

The present lectures provide a proper exposition of the underlying theoretical and algorithmic approaches as well as strong ties to the numerical implementation of the exposed methods. Each series of lectures provides a proper link to actual numerical software. The latter will enable the reader to build upon these and develop his/her own insights about these methods, as well as using the corresponding codes for developing own programs for tackling challenging nuclear many-body problems.

Contents

Chapter 1
Motivation and overarching aims

Morten Hjorth-Jensen, Maria Paola Lombardo, and Ubirajara van Kolck

Abstract Our presentation

Nuclear physics has recently experienced several discoveries and technological advances that address the fundamental questions of the field, in particular how nuclei emerge from the strong dynamics of quantum chromodynamics (QCD). Many of these advances have been made possible by significant investments in frontier research facilities worldwide over the last two decades. Some of these discoveries are the detection of perhaps the most exotic state of matter, the quark-gluon plasma, which is believed to have existed in the very first moments of the Universe (refs). Recent experiments have validated the standard solar model and established that neutrinos have mass (refs). High-precision measurements of the quark structure of the nucleon are challenging existing theoretical understanding. Nuclear physicists have started to explore a completely unknown landscape of nuclei with extreme neutron-to-proton ratios using radioactive and short-lived ions, including rare and very neutron-rich isotopes. These experiments push us towards the extremes of nuclear stability. Moreover, these rare nuclei lie at the heart of nucleosynthesis processes in the universe and are therefore an important component in the puzzle of matter generation in the universe.

A firm experimental and theoretical understanding of nuclear stability in terms of the basic constituents is a huge intellectual endeavor. Experiments indicate that developing a comprehensive description of all nuclei and their reactions requires theoretical and experimental investigations of rare isotopes with unusual neutron-to-proton ratios that are very different from their stable counterparts. These rare nuclei are difficult to produce and study experimentally since they can have extremely short lifetimes. Theoretical approaches to these nuclei involve solving the nuclear many-body problem.

Accompanying these developments, a qualitative change has swept the nuclear theory landscape thanks to a combination of techniques that is allowing, for the first time, th direct connection between QCD and nuclear structure. This transformation has been brought by a dramatic improvement in the capability of numerical calculations both in QCD, via lattice simulations, and in the nuclear many-body problem, via "ab initio" methods for the diagonilization of non-relativistic Hamiltonians. Simultaneously, the framework of effective field

Morten Hjorth-Jensen

Department of Physics and Astronomy and National Superconducting Cyclotron Laboratory, Michigan State University, East Lansing, Michigan, USA and Department of Physics, University of Oslo, Oslo, Norway, e-mail: hjensen@msu.edu,

Maria Paola Lombardo

INFN, Laboratori Nazionali di Frascati, Frascati, Italy, e-mail: mariapaola.lombardo@lnf.infn.it,

Ubirajara van Kolck

Department of Physics, University of Arizona, Tucson, Arizona, USA and Institut de Physique NuclÃl'aire, Orsay, France, e-mail: vankolck@ipno.in2p3.fr

theories builts a bridge between the two numerical approaches, allowing to convert the results of lattice QCD into input to ab initio methods.

Now, algorithmic and computational advances hold promise for breakthroughs in predictive power including proper error estimates, enhancing the already strong links between theory and experiment. These advances include better ab initio many-body methods as well as a better understanding of the underlying effective degrees of freedom and the respective forces at play. And obviously better numerical algorithms as well as developments in high-performance computing. This will provide us with important new insights about the stability of nuclear matter and allow us to relate these novel understandings to the underlying laws of motion, the corresponding forces and the pertinent fundamental building blocks.

Important issues such as whether we can explain from first-principle methods the existence of magic numbers and their vanishing as we add more and more nucleons, how the binding energy of neutron-rich nuclei behaves, or the radii, neutron skins, and many many other probes that extract information about many-body correlations as nuclei evolve towards their limits of stability — these are all fundamental questions which, combined with recent experimental and theoretical advances, will allow us to advance our basic knowledge about the limits of stability of matter, and, hopefully, help us in gaining a better understanding of visible matter.

It is within this framework the present texts finds its rationale. This text collects and synthesizes seven series of lectures on the nuclear many-body problem, starting from our present understanding of the underlying forces with a presentation of recent advances within the field of lattice QCD, via effective field theories to central many-body methods like Monte Carlo, coupled-cluster, and large-scale diagonalization methods. The applications span from our smallest components, quarks and gluons as the mediators of the strong force to the computation of the equation of state for infinite nuclear matter and neutron star matter. The lectures provide a proper exposition of the underlying theoretical and algorithmic approaches as well as strong ties to the numerical implementation of the exposed methods. The lectures propose exercises, often providing a proper link to actual numerical software The latter will enable the reader to build upon these and develop his/her own insights about these methods, as well as using these codes for developing his/her own programs for tackling complicated many-body problems.

A proper understanding of the role of correlations beyond a mean-field description is of great importance for quantum many-particle theories. For many quantum-mechanical systems, either finite ones or infinite systems like the homogeneous electron gas in two or three dimensions [1–3] or nuclear or neutron star matter [4–8], the concept of an independent particle motion plays a fundamental role in studies of many-particle systems. Deviations from such an independent particle, or mean-field, picture have normally been interpreted as a possible measure of correlations. The latter are expected to reveal important features about the structure and the dynamics of a many-particle system beyond a mean-field approximation. However, even for a system like the homogeneous electron gas, defined by a rather simple model Hamiltonian that results in mean-field solutions in closed form, to obtain a reliable estimate of correlations beyond the mean field with different many-body methods, is rather difficult. The nuclear many-body problem for infinite nuclear matter, which is an idealized system of infinitely many interacting baryons, is no exception. There as well, the simplicity of the infinite system at the one-body level offers a good starting point for various many-body approximations. However, to understand properly correlations beyond the mean field level for nuclear matter has proven to be a very hard problem to solve. Being able to compute reliably properties of infinite nuclear matter is thus one of the fundamental goals of nuclear physics and many-particle theories, with far reaching consequences for our basic understanding of hadronic matter, as seen in the physics of compact objects like neutron stars or in explosive phenomena in astrophysics.

References

1. D.M. Ceperley, B.J. Alder, Phys. Rev. Lett. **45**, 566 (1980)
2. B. Tanatar, D.M. Ceperley, Phys. Rev. B **39**, 5005 (1989)
3. J.J. Shepherd, G.H. Booth, A. Grüneis, A. Alavi, Phys. Rev. B **85**, 081103 (2012)
4. B.D. Day, Rev. Mod. Phys. **39**, 719 (1967). DOI 10.1103/RevModPhys.39.719. URL `http://link.aps.org/doi/10.1103/RevModPhys.39.719`
5. S.L. Shapiro, S.A. Teukolsky, *Black holes, white dwarfs, and neutron stars: the physics of compact objects* (Wiley, 1983)
6. J.D. Walecka, *Theoretical Nuclear and Subnuclear Physics* (World Scientific, 2004)
7. F. Weber, *Pulsars as Astrophysical Laboratories for Nuclear and Particle Physics* (Institute of Physics Publishing, London, 1999)
8. H. Heiselberg, M. Hjorth-Jensen, Phys. Rep. **328**, 237 (2000)

Chapter 2
Quantum Chromodynamics

Thomas Schäfer

Abstract We present a brief introduction to QCD, the QCD phase diagram, and non-equilibrium phenomena in QCD. We emphasize aspects of the theory that can be addressed using computational methods, in particular euclidean path integral Monte Carlo, fluid dynamics, kinetic theory, classical field theory and holographic duality.

2.1 Introduction

The goal of this chapter is to provide a brief summary of Quantum Chromodynamics (QCD) and the QCD phase diagram, and to give an introduction to computational methods that are being used to study different aspects of QCD. Quantum Chromodynamics is a remarkable theory in many respects. QCD is an almost parameter free theory. Indeed, in the context of nuclear physics QCD is completely characterized by the masses of the up, down, and strange quark, and a reasonable caricature of nuclear physics emerges in the even simpler case in which the up and down quark are taken to be massless, and the strange quark is infinitely heavy. QCD nevertheless accounts for the incredible richness of the phase diagram of strongly interacting matter. QCD describes finite nuclei, normal and superfluid states of nuclear matter, color superconductors, hadronic gases, quark gluon plasma, and many other states. This rich variety of states is reflected in the large number of computational methods that have been brought to bear on problems in QCD. This includes a large number of methods for the structure and excitations of finite Fermi systems, quantum Monte Carlo methods, and a variety of tools for equilibrium and non-equilibrium statistical mechanics.

The bulk of this book is devoted to the study of few and many nucleon systems. Summarizing everything else in one brief chapter is obviously out of the question, both because of limitations of space and because of my limited expertise. I will therefore be very selective, and focus on a number of very simple yet powerful ideas. This reflects, in part, my background, which is not primarily in computational physics. It also reflects my conviction that progress in computational physics is unfortunately often reflected in increasingly complicated codes that obscure the simplicity of the underlying methods.

Thomas Schäfer

Department of Physics, North Carolina State University, Raleigh, NC 27695, USA, e-mail: `tmschaef@ncsu.edu`

2.2 Path integrals and the Metropolis algorithm

Consider a simple quantum mechanical problem, the motion of a particle in a one-dimensional potential. In order to be specific I will focus on the double well potential $V(x) = \lambda(x^2 - \eta^2)^2$, where η and λ are parameters. The Hamiltonian is

$$H = \frac{p^2}{2m} + \lambda(x^2 - \eta^2)^2. \tag{2.1}$$

Using a change of variables I can set $2m = \lambda = 1$. This implies that there is only one physical parameter in this problem, the barrier separation η. The regime $\eta \gg 1$ corresponds to the limit in which the system has two almost degenerate minima that are split by semi-classical tunneling events. The energy eigenstates and wave functions are solutions of the eigenvalue problem $H|n\rangle = |n\rangle E_n$. Once the eigenstates are known I can compute all possible correlation functions

$$\Pi_n(t_1, t_2, \ldots, t_n) = \langle 0|x(t_1)x(t_2)\ldots x(t_n)|0\rangle, \tag{2.2}$$

by inserting complete sets of states. An alternative to the Hamiltonian formulation of the problem is the Feynman path integral [1]. The path integral for the anharmonic oscillator is given by

$$\langle x_1|e^{-iHt_f}|x_0\rangle = \int_{x(0)=x_0}^{x(t_f)=x_1} \mathscr{D}x\, e^{iS}, \qquad S = \int_0^{t_f} dt\left(\frac{1}{4}\dot{x}^4 - (x^2 - \eta^2)^2\right). \tag{2.3}$$

This expression contains a rapidly oscillating phase factor e^{iS}, which prohibits any direct numerical attempt at computing the path integral. The standard approach is based on analytic continuation to imaginary time $\tau = it$. This is also referred to as Euclidean time, because the Minkowski interval $dx^2 - dt^2$ turns into the Euclidean expression $dx^2 + d\tau^2$. In the following I will consider the euclidean partition function

$$Z(T) = \int \mathscr{D}x\, e^{-S_E}, \qquad S_E = \int_0^\beta d\tau\left(\frac{1}{4}\dot{x}^4 + (x^2 - \eta^2)^2\right), \tag{2.4}$$

where $\beta = 1/T$ is the inverse temperature. To see that equ. (2.4) we can use equ. (2.3) to show that $Z(T)$ can be expressed in terms of the eigenvalues of the Hamiltonian, $Z(T) = \sum_n \exp(-E_n/T)$. In the following I will describe numerical simulations using a discretized version of the euclidean action. For this purpose I discretize the euclidean time coordinate $\tau_j = ja, i = 1, \ldots n$ where $a = \beta/n$ is the length of time interval. The discretized action is given by

$$S = \sum_{i=1}^n \left\{\frac{1}{4a}(x_i - x_{i-1})^2 + a(x_i^2 - \eta^2)^2\right\}, \tag{2.5}$$

where $x_i = x(\tau_i)$. I consider periodic boundary conditions $x_0 = x_n$. The discretized euclidean path integral is formally equivalent to the partition function of a statistical system of (continuous) "spins" x_i arranged on a one-dimensional lattice. This statistical system can be studied using standard Monte-Carlo sampling methods. In the following I will use the Metropolis algorithm [2]. Detailed numerical studies of the euclidean path integral can be found in [3–6].

The Metropolis method generates an ensemble of configurations $\{x_i\}^{(k)}$ where $i = 1, \ldots, n$ labels the lattice points and $k = 1, \ldots, N_{conf}$ labels the configurations. Quantum mechanical averages are computed by averaging observables over many configurations,

$$\langle \mathscr{O}\rangle = \lim_{N_{conf}\to\infty} \frac{1}{N_{conf}} \sum_{k=1}^{N_{conf}} \mathscr{O}^{(k)} \tag{2.6}$$

where $\mathcal{O}^{(k)}$ is the value of the classical observable $\mathcal{O}$ in the configuration $\{x_i\}^{(k)}$. The configurations are generated using Metropolis updates $\{x_i\}^{(k)} \rightarrow \{x_i\}^{(k+1)}$. The update consists of a sweep through the lattice during which a trial update $x_i^{(k+1)} = x_i^{(k)} + \delta x$ is performed for every lattice site. Here, δx is a random number. The trial update is accepted with probability

$$P\left(x_i^{(k)} \rightarrow x_i^{(k+1)}\right) = \min\left\{\exp(-\Delta S), 1\right\}, \tag{2.7}$$

where ΔS is the change in the action equ. (2.5). This ensures that the configurations $\{x_i\}^{(k)}$ are distributed according the "Boltzmann" distribution $\exp(-S)$. The distribution of δx is arbitrary as long as the trial update is micro-reversible, i. e. is equally likely to change $x_i^{(k)}$ to $x_i^{(k+1)}$ and back. The initial configuration is arbitrary. In order to study equilibration it is useful to compare an ordered (cold) start with $\{x_i\}^{(0)} = \{\eta\}$ to a disordered (hot) start $\{x_i\}^{(0)} = \{r_i\}$, where r_i is a random variable.

The advantage of the Metropolis algorithm is its simplicity and robustness. The only parameter to adjust is the distribution of δx. A simple choice is to take δx to be a Gaussian random number, and choose the width of the distribution so that the average acceptance rate for the trial updates is around 50%. Fluctuations of $\mathcal{O}$ provide an estimate in the error of $\langle \mathcal{O} \rangle$. The uncertainty is given by

$$\Delta\langle\mathcal{O}\rangle = \sqrt{\frac{\langle\mathcal{O}^2\rangle - \langle\mathcal{O}\rangle^2}{N_{conf}}}. \tag{2.8}$$

This requires some care, because the error estimate is based on the assumption that the configurations are statistically independent. In practice this can be monitored by computing the auto-correlation "time" in successive measurements $\mathcal{O}(\{x_i\}^{(k)})$.

I have written a simple fortran code that implements the Metropolis algorithm for euclidean path integrals [6]. The most important part of that code is a sweep through the lattice with a Metropolis update on every site τ_j:

```fortran
do j=1,n-1

    nhit = nhit+1

    xpm = (x(j)-x(j-1))/a
    xpp = (x(j+1)-x(j))/a
    t = 1.0/4.0*(xpm**2+xpp**2)
    v = (x(j)**2-f**2)**2
    sold = a*(t+v)

    xnew = x(j) + delx*(2.0*ran2(iseed)-1.0)

    xpm = (xnew-x(j-1))/a
    xpp = (x(j+1)-xnew)/a
    t = 1.0/4.0*(xpm**2+xpp**2)
    v = (xnew**2-f**2)**2
    snew = a*(t+v)
    dels = snew-sold

    p = ran2(iseed)
    if (exp(-dels) .gt. p) then
      x(j) = xnew
      nacc = nacc + 1
    endif

enddo
```
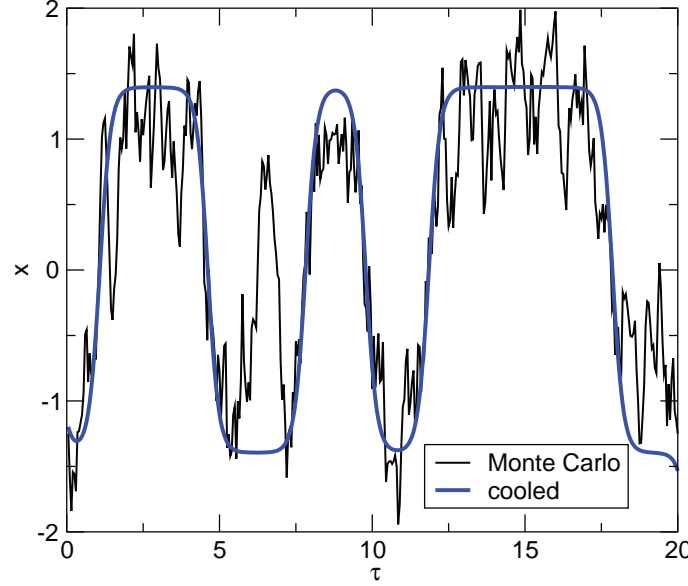
Fig. 2.1 Typical euclidean path obtained in a Monte Carlo simulation of the discretized euclidean action of the double well potential for $\eta = 1.4$. The lattice spacing in the euclidean time direction is $a = 0.05$ and the total number of lattice points is $N_\tau = 800$. The green curve shows the corresponding smooth path obtained by running 100 cooling sweeps on the original path.

Here, `sold` is the local action corresponding to the initial value of `x(j)`, and `snew` is the action after the trial update. The trial update is accepted if `exp(-dels)` is greater that the random variable p. The function `ran2()` generates a random number between 0 and 1, and `nacc/nhit` measures the acceptance rate. A typical path is shown in Fig. 2.1. An important feature of the paths in the double well potential is the presence of tunneling events. Indeed, in the semi-classical regime $\eta \gg 1$, a typical path can be understood as Gaussian fluctuations superimposed on a series of tunneling events (instantons).

The path integral method does not provide direct access to the eigenvalues of the Hamiltonian, but it can be used to compute imaginary time correlation functions

$$\Pi_n^E(\tau) = \langle x(\tau_1)\ldots x(\tau_n)\rangle. \tag{2.9}$$

Note that the average is carried out with respect to the partition function in equ. (2.4). In the limit $\beta \to \infty$ this corresponds to the ground state expectation value. A very important observable is the two-point function $\Pi^E(\tau) \equiv \Pi_2^E(0,\tau)$. The euclidean correlation functions is related to the eigenstates of the Hamiltonian via a spectral representations. This representation is obtained by inserting a complete set of states into equ. (2.9). The result is

$$\Pi^E(\tau) = \sum_n |\langle 0|x|n\rangle|^2 \exp(-(E_n - E_0)\tau), \tag{2.10}$$

where E_n is the energy of the state $|n\rangle$. This can be written as

$$\Pi^E(\tau) = \int dE\, \rho(E) \exp(-(E - E_0)\tau), \tag{2.11}$$

where $\rho(E)$ is the spectral function. In the case of the double well potential there are only bound states and the spectral function is a sum of delta-functions. Equ. (2.10) shows that the

euclidean correlation function is easy to construct once the energy eigenvalues and eigenfunctions are known. The inverse problem is well defined in principle, but numerically much more difficult. The excitation energy of the first excited state $\Delta E_1 = E_1 - E_0$ is easy to extract from the exponential decay of the two-point functions, but higher states are more difficult to compute. A technique that can be used on order determine the spectral function from euclidean correlation functions is the maximum entropy image reconstruction method, see [7,8].

The calculation of correlation functions in a Monte Carlo simulation is very straightforward. All I need to do is multiply the values of $x(\tau_i)$ for a given path, and then average over all paths:

```
do ic=1,nc

    ncor = ncor + 1
    ip0 = int( (n-np)*ran2(iseed) )
    x0 = x(ip0)

    do ip=1,np
      x1 = x(ip0+ip)
      xcor = x0*x1
      x2cor= xcor**2
      xcor_sum(ip) = xcor_sum(ip) + xcor
      xcor2_sum(ip) = xcor2_sum(ip) + xcor**2
  enddo
enddo
```

The advantages of this method are that it is extremely robust, that it requires no knowledge (or preconceived notion) of what the wave function looks like, and that it can explore a very complicated configuration space. On the other hand, in the case of one-dimensional quantum mechanics, the Metropolis method is very inefficient. Using direct diagonalization in a finite basis it is not difficult to compute the energies of the first several states in the potential in equ. 2.1 with a very high accuracy, $\Delta E/E_0 \sim O(10^{-6})$ or better. On the other hand, using the Monte Carlo method, it is quite difficult to achieve an accuracy of $O(10^{-2})$ for observable other than $(E_1 - E_0)/E_0$. The advantage of the Monte Carlo method is that it scales much better towards high dimensional systems, such as quantum mechanics of many particles, or quantum field theory.

The Monte Carlo method also does not directly provide the ground state energy, or the partition function and free energy at finite temperature. In quantum mechanics we can compute the ground state energy from the expectation value of the Hamiltonian $\langle H \rangle = \langle T + V \rangle$ in the limit $\beta \to \infty$. The expectation value of the kinetic energy is singular as $a \to 0$, but this problem can be overcome by using the Virial theorem

$$\langle H \rangle = \left\langle \frac{x}{2} V' + V \right\rangle. \tag{2.12}$$

There is no simple analog of this method in quantum field theory. A method for computing the free energy which does generalize to quantum field theory is the adiabatic switching technique. The idea is to start from a reference system for which the free energy is known and calculate the free energy difference to the real system using Monte Carlo methods. For this purpose I write the action as

$$S_\alpha = S_0 + \alpha \Delta S, \tag{2.13}$$

where S is the full action, S_0 is the action of the reference system, ΔS is defined by $\Delta S = S - S_0$, and α is a coupling constant. The action S_α interpolates between the physical system and the reference system. Integrating the relation $\partial \log Z(\alpha)/(\partial \alpha) = -\langle \Delta S \rangle_\alpha$ I find

$$\log(Z(\alpha = 1)) = \log(Z(\alpha = 0)) - \int_0^1 d\alpha' \langle \Delta S \rangle_{\alpha'} \; , \tag{2.14}$$

where $\langle . \rangle_\alpha$ is computed using the action S_α. In the case of the anharmonic oscillator it is natural to use the harmonic oscillator as a reference system. In that case

$$Z(\alpha = 0) = \sum_n \exp(-\beta E_n^0) = \frac{\exp(-\beta \omega_0/2)}{1 - \exp(-\beta \omega_0)}, \tag{2.15}$$

where ω_0 is the oscillator constant. Note that the free energy of the anharmonic oscillator should be independent of the reference frequency ω_0. The integral over the coupling constant α can be calculated in a Monte Carlo simulation by slowly changing α from 0 to 1 during the simulation. Free energy calculations of this type play an important role in quantum chemistry, and more efficient methods for determining ΔF have been developed [9].

2.3 Quantumchromodynamics

2.3.1 QCD at zero temperature and density

The rich phenomenology of strong interacting matter is encoded in a deceptively simple Lagrangian. The fundamental fields in the Lagrangian are quark fields $q_{\alpha f}^c$ and gluon fields A_μ^a. Here, $\alpha = 1, \ldots, 4$ is a Dirac spinor index, $c = 1, \ldots, N_c$ with $N_c = 3$ is a color index, and $f = up, down, strange, charm, bottom, top$ is a flavor index. Interactions in QCD are governed by the color degrees of freedom. The gluon field A_μ^a is a vector field labeled by an index $a = 1, \ldots, N_c^2 - 1$ in the adjoint representation. The N_c^2- multiplet of gluon fields can be used to construct a matrix valued field $A_\mu = A_\mu^a \frac{\lambda^a}{2}$, where λ^a is a set of traceless, Hermitian, $N_c \times N_c$ matrices. The QCD Lagrangian is

$$\mathcal{L} = -\frac{1}{4} G_{\mu\nu}^a G_{\mu\nu}^a + \sum_f^{N_f} \bar{q}_f (i\gamma^\mu D_\mu - m_f) q_f \,, \tag{2.16}$$

where $G_{\mu\nu}^a$ is the QCD field strength tensor defined by

$$G_{\mu\nu}^a = \partial_\mu A_\nu^a - \partial_\nu A_\mu^a + g f^{abc} A_\mu^b A_\nu^c \,, \tag{2.17}$$

and $f^{abc} = 4i \text{Tr}([\lambda^a, \lambda^b] \lambda^c)$ are the $SU(N_c)$ structure constants. The action of the covariant derivative on the quark fields is

$$iD_\mu q = \left(i\partial_\mu + g A_\mu^a \frac{\lambda^a}{2} \right) q \,, \tag{2.18}$$

where m_f is the mass of the quarks. The terms in equ. (2.16) describe the interaction between quarks and gluons, as well as nonlinear three and four-gluon interactions. Note that, except for the number of flavors and their masses, the structure of the QCD Lagrangian is completely fixed by the local $SU(N_c)$ color symmetry.

A natural starting point for studying the phase diagram of hadronic matter is to consider the light flavors (up, down, and strange) as approximately massless, and the heavy flavors (charm, bottom, top) as infinitely massive. In this limit the QCD Lagrangian is completely characterized by two integer valued parameters, the number of colors $N_c = 3$ and flavors $N_f = 3$, and a single dimensionless coupling constant g. Quantum fluctuations cause the coupling constant to become scale dependent [10,11]. At one-loop order the running coupling constant

is

$$g^2(q^2) = \frac{16\pi^2}{b_0 \log(q^2/\Lambda_{QCD}^2)}, \qquad b_0 = \frac{11}{3}N_c - \frac{2}{3}N_f,$$ (2.19)

where q is a characteristic momentum and N_f is the number of active flavors. The scale dependence of the coupling implies that, as a quantum theory, QCD is not governed by a dimensionless coupling but by a dimensionful scale, the QCD scale parameter Λ_{QCD}. This phenomenon is known as dimensional transmutation [12].

A crucial aspect of the scale dependence of the coupling in QCD is that the effective interaction decreases as the energy or momentum scale is increased. This feature of QCD is called asymptotic freedom [10, 11]. It implies that high energy interactions can be analyzed using perturbative QCD. The flip side of asymptotic freedom is anti-screening, or confinement: The effective interaction between quarks increases with distance, and quarks are permanently confined into hadrons. The absence of colored states in the spectrum implies that the use of perturbation theory is subtle, even at high energy. Quantities that can be computed perturbatively either involve a sum over many hadronic states, or allow for a factorization of perturbative interactions and non-perturbative matrix elements.

If quarks are massless then QCD observables are dimensionless ratios like m_p/Λ_{QCD}, where m_p is the mass of the proton. This implies that the QCD scale is not a parameter of the theory, but reflects a choice of units. In the real world QCD is part of the standard model, quarks acquire masses by electroweak symmetry breaking, and the QCD scale is fixed by value of the coupling constant at the weak scale. Experiments determine the value of the QCD fine structure constant $\alpha_s = g^2/(4\pi)$ at the position of the Z boson pole, $\alpha_s(m_z) = 0.1184 \pm 0.0007$ [13]. The numerical value of Λ_{QCD} depends on the renormalization scheme used in computing quantum corrections to the coupling constant. Physical observables, as well as the value of b_0, are independent of this choice. In the modified minimal subtraction ($\overline{MS}$) scheme the scale parameter is $\Lambda_{QCD} \simeq 200$ MeV [13].

A schematic phase diagram of QCD is shown in Fig. 2.2. In this figure I show the phases of strongly interacting matter as a function of the temperature T and the baryon chemical potential μ. The chemical potential μ controls the baryon density ρ, defined as 1/3 times the number density of quarks minus the number density of anti-quarks. In the following I will explain that the basic structure of the phase diagram is determined by asymptotic freedom and the symmetries of QCD. For more detailed reviews see [14–16].

At small temperature and chemical potential the interaction between quarks is dominated by large distances and the effective coupling is strong. This implies that quarks and gluons are permanently confined in color singlet hadrons, with masses of order Λ_{QCD}. The proton, for example, has a mass of $m_p = 935$ MeV. A simplistic view of the structure of the proton is that it is a bound state of three constituent quarks with effective masses $m_Q \simeq m_p/3 \simeq \Lambda_{QCD}$. These masses should be compared to the bare up and down quark masses which are of the order 10 MeV.

As a consequence of strong interactions between virtual quarks and anti-quarks in the QCD ground state a vacuum condensate of $\bar{q}q$ pairs is generated, $\langle\bar{q}q\rangle \simeq -\Lambda_{QCD}^3$ [17–19]. This vacuum expectation value spontaneously breaks the approximate chiral $SU(3)_L \times SU(3)_R$ flavor symmetry of the QCD Lagrangian down to its diagonal subgroup, the flavor symmetry $SU(3)_V$. Spontaneous chiral symmetry breaking implies the existence of Goldstone bosons, massless modes with the quantum numbers of the generators of the broken axial symmetry $SU(3)_A$. The corresponding excitations in the spectrum of QCD are the π, K and η mesons. The $SU(3)_L \times SU(3)_R$ symmetry is explicitly broken by quark masses, and the mass of the charged pion is $m_\pi = 139$ MeV. This scale can be compared to the mass of the lightest non-Goldstone particle, the rho meson, which has a mass $m_\rho = 770$ MeV.

At low energy Goldstone bosons can be described in terms of an effective field theory in which composite π, K and η particles are treated as fundamental fields. The Goldstone boson
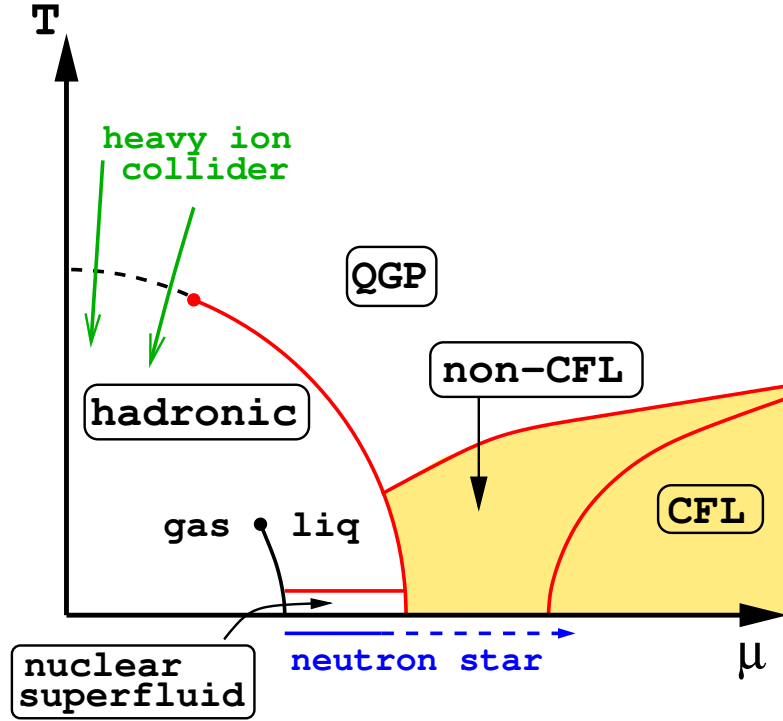
Fig. 2.2 Schematic phase diagram of QCD as a function of temperature T and baryon chemical potential μ. The quark gluon plasma phase is labeled QGP, and CFL refers to the color superconducting phase that is predicted to occur at asymptotically large chemical potential. The critical endpoints of the chiral and nuclear liquid-gas phase transitions, are denoted by red and black points, respectively. The chiral pseudo-critical line associated with the crossover transition at low temperature is shown as a dashed line. The green arrows indicate the regions of the phase diagram that can be studied by the experimental heavy ion programs at RHIC and the LHC.

field can be parametrized by unitary matrices

$$\Sigma = \exp(i\lambda^a \phi^a / f_\pi), \tag{2.20}$$

where λ^a are the Gell-Mann matrices for $SU(3)$ flavor and $f_\pi = 93$ MeV is the pion decay constant. For example, $\pi^0 = \phi^3$ and $\pi^\pm = (\phi_1 \pm i\phi_2)/2$ describe the neutral and charged pion. Other components of ϕ^a describe the neutral and charged kaons, as well as the eta. The eta prime, which is the $SU(3)_F$ singlet meson, acquires a large mass because of the axial anomaly, and is not a Goldstone boson. The axial anomaly refers to the fact that the flavor singlet axial current, which is conserved in massless QCD at the classical level, is not conserved if quantum effects are taken into account. The divergence of the axial current $A_\mu = \bar{q}\gamma_\mu\gamma_5 q$ is

$$\partial_\mu A^\mu = \frac{g^2 N_f}{32\pi^2} \varepsilon^{\mu\nu\alpha\beta} G^a_{\mu\nu} G^a_{\alpha\beta}. \tag{2.21}$$

The right hand side is the topological charge density, which I will discuss in more detail in Sect. 2.4.3.

At low energy the effective Lagrangian for the chiral field can be organized as a derivative expansion in gradients of Σ. Higher derivative terms describe interactions that scale as either the momentum or the energy of the Goldstone boson. Since Goldstone bosons are approximately massless, the energy is of the same order of magnitude as the momentum. We will see that the expansion parameter is $p/(4\pi f_\pi)$. At leading order in (∂/f_π) there is only one

possible term which is consistent with chiral symmetry, Lorentz invariance and the discrete symmetries C, P, T. This is the Lagrangian of the non-linear sigma model

$$\mathscr{L} = \frac{f_\pi^2}{4} \mathrm{Tr} \left[\partial_\mu \Sigma \partial^\mu \Sigma^\dagger \right] + \left[B \mathrm{Tr}(M \Sigma^\dagger) + h.c. \right] + \ldots, \tag{2.22}$$

where the term proportional to B takes into account explicit symmetry breaking. Here, $M = \mathrm{diag}(m_u, m_d, m_s)$ is the quark mass matrix and B is a low energy constant that I will fix below.

First, I will show that the parameter f_π controls the pion decay amplitude. For this purpose I have to gauge the non-linear sigma model. As usual, this is achieved by promoting the derivative to a gauge covariant operator $\nabla_\mu \Sigma = \partial_\mu \Sigma + i g_w W_\mu \Sigma$ where W_μ is the charged weak gauge boson and g_w is the weak coupling constant. The gauged non-linear sigma model gives a pion-W boson interaction

$$\mathscr{L} = g_w f_\pi W_\mu^\pm \partial^\mu \pi^\mp. \tag{2.23}$$

This term contributes to the amplitude for the decay $\pi^\pm \to W^\pm \to e^\pm \nu_e$. We get $\mathscr{A} = g_w f_\pi q_\mu$, where q_μ is the momentum of the pion. This result agrees with the definition of f_π in terms of the weak axial current matrix element of the pion, $\langle 0 | A_\mu^a | \pi^b \rangle = f_\pi q_\mu \delta^{ab}$.

In the ground state $\Sigma = 1$ and the ground state energy is $E_{vac} = -2B \mathrm{Tr}[M]$. Using the relation $\langle \bar{q}q \rangle = \partial E_{vac} / (\partial m)$ we find $\langle \bar{q}q \rangle = -2B$. Fluctuations around $\Sigma = 1$ determine the masses of the Goldstone bosons. The pion mass satisfies the Gell-Mann-Oaks-Renner relation (GMOR) [17]

$$m_\pi^2 f_\pi^2 = -(m_u + m_d) \langle \bar{q}q \rangle \tag{2.24}$$

and analogous relations exist for the kaon and eta masses. This result shows the characteristic non-analytic dependence of the pion mass on the quark masses, $m_\pi \sim \sqrt{m_q}$.

2.3.2 QCD at finite temperature

The structured of QCD at high temperature can be analyzed using the assumption that quarks and gluons are approximately free. We will see that this assumption is internally consistent, and that it is confirmed by lattice calculations. If the temperature is large then quarks and gluons have thermal momenta $p \sim T \gg \Lambda_{QCD}$. Asymptotic freedom implies that these particles are weakly interacting, and that they form a plasma of mobile color charges, the quark gluon plasma (QGP) [20, 21]. The pressure of a gas of quarks and gluons is

$$P = \frac{\pi^2 T^4}{90} \left(2 \left(N_c^2 - 1 \right) + 4 N_c N_f \frac{7}{8} \right). \tag{2.25}$$

This is the Stefan-Boltzmann law, where $2(N_c^2 - 1)$ is the number of bosonic degrees of freedom, and $4 N_c N_F$ is the number of fermions. The factor 7/8 takes into account the difference between Bose and Fermi statistics. The pressure of a QGP is parametrically much bigger than the pressure of a pion gas, indicating that the QGP at high temperature is thermodynamically stable.

The argument that the QGP at asymptotically high temperature is weakly coupled is somewhat more subtle than it might appear at first glance. If two quarks or gluons in the plasma interact via large angle scattering then the momentum transfer is large, and asymptotic freedom implies that the effective coupling is weak. However, the color Coulomb interaction is dominated by small angle scattering, and it is not immediately clear why the effective interaction that governs small angle scattering is weak. The basic observation is that in a high temperature plasma there is a large thermal population ($n \sim T^3$) of mobile color charges that

screen the interaction at distances beyond the Debye length $r_D \sim 1/(gT)$. We also note that even in the limit $T \gg \Lambda_{QCD}$ the QGP contains a non-perturbative sector of static magnetic color fields [22]. This sector of the theory, corresponding to energies below the magnetic screening scale $m_M \lesssim g^2 T$, is strongly coupled, but it does not contribute to thermodynamic or transport properties of the plasma in the limit $T \to \infty$.

The quark gluon plasma exhibits neither color confinement nor chiral symmetry breaking. This implies that the high temperature phase must be separated from the low temperature hadronic phase by a phase transition. The order of this transition is very sensitive to the values of the quark masses. In QCD with massless u, d and infinitely massive s, c, b, t quarks the transition is second order [23]. In the case of massless (or sufficiently light) u, d, s quarks the transition is first order. Lattice simulations show that for realistic quark masses, $m_u \simeq m_d \simeq 10$ MeV and $m_s \simeq 120$ MeV, the phase transition is a rapid crossover [24, 25]. The transition temperature, defined in terms of the chiral susceptibility, is $T_c \simeq 151 \pm 3 \pm 3$ MeV [26, 27], which is consistent with the result 154 ± 9 MeV reported in [25, 28].

The phase transition is expected to strengthen as a function of chemical potential, so that there is a critical baryon chemical potential μ at which the crossover turns into a first order phase transition [29]. This critical point is the endpoint of the chiral phase transition. Because of the fermion sign problem, which I will discuss in Sect. 2.4.4, it is very difficult to locate the critical endpoint using simulations on the lattice. Model calculations typically predict the existence of a critical point, but do not constrain its location. A number of exploratory lattice calculations have been performed [30–35], but at the time I am writing these notes it has not been demonstrated conclusively that the transition strengthens with increasing baryon chemical potential [36]. The critical endpoint is important because, with the exception of the endpoint of the nuclear liquid-gas transition, it is the only thermodynamically stable point in the QCD phase diagram at which the correlation length diverges. This means that the critical endpoint may manifest itself in heavy ion collisions in terms of enhanced fluctuation observables [37].

2.3.3 High baryon density QCD

The origin of the phase diagram, $T = \mu = 0$, corresponds to the vacuum state of QCD. If we stay on the $T = 0$ line and increase the chemical potential μ then there is no change initially. At zero temperature the chemical potential μ is the energy required to add a baryon to the system, and QCD has a large mass gap for baryonic states. The first non-vacuum state we encounter along the $T = 0$ axis of the phase diagram is nuclear matter, a strongly correlated superfluid composed of approximately non-relativistic neutrons and protons. Nuclear matter is self-bound, and the baryon density changes discontinuously at the onset transition, from $\rho = 0$ to nuclear matter saturation density $\rho = \rho_0 \simeq 0.15 \, \text{fm}^{-3}$. The discontinuity decreases as nuclear matter is heated, and the nuclear-liquid gas phase transition ends in a critical point at $T \simeq 18$ MeV and $\rho \simeq \rho_0/3$ [38–40]. Hot hadronic matter can be described quite accurately as a weakly interacting gas of hadronic resonances. Empirically, the density of states for both mesons and baryons grows exponentially. A system of this type is called a Hagedorn gas, and it is known that a Hagedorn gas has a limiting temperature. It is also known that an exponential density of states can be realized using the string model of hadronic resonances.

In the regime $\mu \gg \Lambda_{QCD}$ we can use arguments similar to those in the limit $T \gg \Lambda_{QCD}$ to establish that quarks and gluons are weakly coupled. At low temperature non-interacting quarks form a Fermi surface, where all states below the Fermi energy $E_F \simeq \mu/3$ are filled, and all states above the Fermi energy are empty. Interactions take place near the Fermi surface, and the corresponding interaction is weak. The main difference between cold quark matter

and the hot QGP is that the large density of states near the quark Fermi surface implies that even weak interactions can cause qualitative changes in the ground state of dense matter. In particular, attractive interactions between pairs of quarks $(\mathbf{p}_F, -\mathbf{p}_F)$ on opposite sides of the Fermi surface leads to color superconductivity and the formation of a $\langle qq \rangle$ diquark condensate.

Since quarks carry many different quantum numbers, color, flavor, and spin, a variety of superconducting phases are possible. The most symmetric of these, known as the color-flavor locked (CFL) phase, is predicted to exist at asymptotically high density [41, 42]. In the CFL phase the diquark order parameter is

$$\langle q_{\alpha f}^A q_{\beta g}^B \rangle = (C\gamma_5)_{\alpha\beta} \varepsilon^{ABC} \varepsilon_{fgh} \delta_C^h \Phi, \tag{2.26}$$

where $C\gamma_5$ is an anti-symmetric (spin zero) Dirac matrix, and Φ determines the magnitude of the gap near the Fermi surface. This order parameter has a number of interesting properties. It breaks the $U(1)$ symmetry associated with baryon number, leading to superfluidity, and it breaks the chiral $SU(3)_L \times SU(3)_R$ symmetry. Except for Goldstone modes the spectrum is fully gapped. Fermions acquire a BCS-pairing gap, and gauge fields are screened by the color Meissner effect. This implies that the CFL phase, even though it is predicted to occur in a very dense liquid of quarks, exhibits many properties of superfluid nuclear matter.

The CFL order parameter describes equal pair-condensates $\langle ud \rangle = \langle us \rangle = \langle ds \rangle$ of all three light quark flavors. As the density is lowered effects of the non-zero strange quark mass become important, and less symmetric phases are predicted to appear [14]. Phases that have been theoretically explored include Bose condensates of pions and kaons, hyperon matter, states with inhomogeneous quark-anti-quark or diquark condensates, and less symmetric color superconducting phases. The regimes of moderate baryon chemical potential in the phase diagram shown in Fig. 2.2 is largely conjecture. Empirical evidence shows that at low μ there is a nuclear matter phase with broken chiral symmetry and zero strangeness, and weak coupling calculations indicate that at high μ we find the CFL phase with broken chiral symmetry but non-zero strangeness. In principle the two phases could be separated by a single onset transition for strangeness [43, 44], but model calculation support a richer picture in which one or more first order transitions intervene, as indicated in Fig. 2.2.

2.4 Lattice QCD

2.4.1 The Wilson action

Symmetry arguments and perturbative calculations can be used to establish general features of the QCD phase diagram, but quantitative results can only be obtained using numerical calculations based on lattice QCD. The same is true for the masses of hadrons, their properties, and interactions. Lattice QCD is based on the euclidean path integral representation of the partition function, see [45–49] for introductions. More detailed reviews of the lattice field theory approach to hot and dense QCD can be found in [50, 51].

The euclidean partition function for QCD is

$$Z(T, \mu, V) = \int \mathscr{D}A_\mu \, \mathscr{D}q_f \, \mathscr{D}\bar{q}_f \, \exp(-S_E), \tag{2.27}$$

where S_E is the euclidean action

$$S_E = -\int_0^\beta d\tau \int_V d^3x \, \mathscr{L}^E, \tag{2.28}$$

$\beta = T^{-1}$ is the inverse temperature and $\mathscr{L}^E$ is the euclidean Lagrangian, which is obtained by analytically continuing equ. (2.16) to imaginary time $\tau = it$. As in the quantum mechanical example in equ. (2.4) the temperature enters via the boundary condition on the fields in the imaginary time direction. Gauge fields and fermions obey periodic and anti-periodic boundary conditions, respectively. The chemical potential enters through its coupling to the conserved baryon density

$$\mathscr{L}^E(\mu) = \mathscr{L}^E(0) + \mu \bar{q}_f \gamma_0 q_f. \tag{2.29}$$

In his pioneering work Wilson proposed to discretize the action on a $N_\tau \times N_\sigma^3$ space-time lattice with lattice spacings a_τ and a_σ [52]. In many cases $a_\sigma = a_\tau = a$, but we will encounter an exception in Sect. 2.5.4. when we discuss the Hamiltonian formulation of the theory.

At finite temperature we have to ensure that the spatial volume is larger than the inverse temperature, $L > \beta$. Here, $\beta = N_\tau a_\tau$, $L = N_\sigma a_\sigma$, and $V = L^3$ is the volume. Thermodynamic quantities are determined by taking derivatives of the partition function. The energy and baryon density are given by

$$\mathscr{E} = -\frac{1}{V} \left. \frac{\partial \log Z}{\partial \beta} \right|_{\beta\mu}, \tag{2.30}$$

$$\rho = \frac{1}{\beta V} \left. \frac{\partial \log Z}{\partial \mu} \right|_{\beta}. \tag{2.31}$$

The discretized action for the gauge fields originally suggested by Wilson is given by

$$S_W = -\frac{2}{g^2} \sum_n \sum_{\mu < \nu} \operatorname{Re} \operatorname{Tr} \left[W_{\mu\nu}(n) - 1 \right] \tag{2.32}$$

where $W_{\mu\nu}(n)$ is the plaquette, the product of gauge links around an elementary loop on the lattice,

$$W_{\mu\nu}(n) = U_\mu(n) U_\nu(n + \hat{\mu}) U_{-\mu}(n + \hat{\mu} + \hat{\nu}) U_{-\nu}(n + \hat{\nu}). \tag{2.33}$$

Here, $n = (n_\tau, n_i)$ labels lattice sites and $\hat{\mu}$ is a unit vector in the μ-direction. The gauge links $U_\mu(n)$ are $SU(N_c)$ matrices. We can think of the gauge links as line integrals

$$U_\mu(n) = \exp(ia A_\mu(n)), \tag{2.34}$$

and of the plaquettes as fluxes

$$W_{\mu\nu}(n)) = \exp(ia^2 G_{\mu\nu}(n)), \tag{2.35}$$

but the fundamental variables in the path integral are the (compact) group variables U_μ, not the (non-compact) gauge potentials A_μ. In particular, the path integral in pure gauge QCD takes the form

$$Z = \int \prod_{n,\mu} dU_\mu(n) \exp(-S_W), \tag{2.36}$$

where dU is the Haar measure on $SU(N_c)$. Using equ. (2.34) we can check that the Wilson action reduces to continuum pure gauge theory in the limit $a \to 0$. We note that the gauge invariance of QCD is maintained exactly, even on a finite lattice, but that Lorentz invariance is only restored in the continuum limit. We also observe that classical scale invariance implies that the massless QCD action is independent of a. The continuum limit is taken by adjusting the bare coupling at the scale of the lattice spacing according to asymptotic freedom, see equ. (2.19). In practice the lattice spacing is not small enough to ensure the accuracy of this method, and more sophisticated scale setting procedures are used [50, 51].

Monte Carlo simulations of the path integral equ. (2.36) can be performed using the Metropolis algorithm explained in Sect. 2.2:

- Initialize the link variables with random $SU(N_c)$ matrices. A simple algorithm is based on writing U in terms of N_c complex row vectors $\mathbf{u}_i$. Take each vector to be random unit vector and then use the Gram-Schmidt method to orthogonalize the different vectors, $\mathbf{u}_i \cdot \mathbf{u}_j^* = \delta_{ij}$. This ensures that U is unitary and distributed according to the $SU(N_c)$ Haar measure [53].
- Sweep through the lattice and update individual link variables. For this purpose multiply the link variable by a random $SU(N_c)$ matrix, $U_\mu \to R U_\mu$. Compute the change in the Wilson action and accept the update with probability $\exp(-\Delta S_W)$.
- Compute physical observables. The simplest observable is the average plaquette $\langle W_{\mu\nu} \rangle$, which can be related to the equation of state, see equ. (2.30). More complicated observables include the correlation function between plaquettes, and the Wilson loop

$$W(\mathscr{C}) = Tr\left[L(\mathscr{C})\right], \quad L(\mathscr{C}) = \prod_{(n,\mu)\in\mathscr{C}} U_\mu(n), \tag{2.37}$$

  where $L(\mathscr{C})$ is the product of link variables around a closed loop. The average Wilson loop is related to the potential between two static charges in the fundamental representation

$$V(R) = -\lim_{T\to\infty} \frac{1}{T} \log\left[\langle W(\mathscr{C}) \rangle\right], \tag{2.38}$$

  where $R \times T$ is the area of a rectangular loop $\mathscr{C}$.
- Tune to the continuum limit $a \to 0$ by adjusting the coupling constant according to the asymptotic freedom formula equ. (2.19). Note that the Lambda parameter for the lattice regulator is quite small, $\Lambda_{lat} = 28.8 \Lambda_{\overline{MS}}$ [54]. Note that we have to increase N_σ, N_τ to keep the physical volume constant. Indeed, we have to study the infinite volume limit $V \to \infty$. This is more difficult than it appears, because $a \to 0$ ($g \to 0$) is a critical point, and simulations exhibit critical slowing down.

Metropolis simulations with the pure gauge Wilson action are very simple and robust. As an illustration we provide a simple Z_2 lattice gauge theory code written by M. Creutz in the appendix. Reasonable results for the heavy quark potential can be obtained on fairly coarse lattices, for example an 8^4 lattice with a spacing $a \simeq 0.25$ fm [55]. However, accurate results with controlled error bars require significant computational resources. In practice the perturbative relation between a and g^2 is only valid on very fine lattices, and the scale setting has to be done non-perturbatively. Also, determining the spectrum of pure gauge theory is difficult. Purely gluonic states, glueballs, are quite heavy, with masses in the range $m \simeq 1.6$ GeV and higher. This implies that gluonic correlation functions are short range, requiring a resolution $a \simeq 0.1$ fm or better. Finally, simulations on fine lattices are affected by critical slowing down. Indeed, finding an efficient method for updating gauge fields on very fine lattices, analogous to the cluster algorithms for spin models [56], is an important unsolved problem.

2.4.2 Fermions on the lattice

The main difficulty in lattice QCD is related to the presence of light fermions. The fermion action is of the form

$$S_F = a^4 \sum_{m,n} \bar{q}(m) D_{mn} q(n). \tag{2.39}$$

Formally, the integration over the fermion fields can be performed exactly, resulting in the determinant of the Dirac operator $\det(D(A_\mu, \mu))$. Several methods exist for discretizing the Dirac operator D, and for sampling the determinant. Different discretization schemes differ in the degree to which chiral symmetry is maintained on a finite lattice. The original formulation due to Wilson [52] preserves no chiral symmetry, the staggered Fermion scheme [57] maintains a subset of the full chiral symmetry, while the domain wall [58] and overlap methods [59] aim to preserve the full chiral symmetry on a discrete lattice.

The central difficulty in implementing these methods is that the fermion determinant is a very non-local object. While updating a single gauge link only requires recalculating a small number of plaquettes (6 in $d = 4$ dimensions) in the Wilson action, recalculating the fermion action requires computing the determinant of a (very sparse) matrix of size $(N_\tau N_\sigma^3) \times (N_\tau N_\sigma^3)$ or larger. This is clearly impractical. Fermion algorithms rely on a number of tricks. The first is the observation that the Dirac operator has a property called γ_5-hermiticity, $\gamma_5 D \gamma_5 = D^\dagger$, which implies that $\det(D)$ is real. The determinant of a two-flavor theory is then real and positive. This allows us to rewrite the fermion determinant as a path integral over a bosonic field with a non-local action but positive action

$$\det(D_u)\det(D_d) = \det(DD^\dagger) = \int \mathscr{D}\phi \mathscr{D}\phi^\dagger \exp\left(-\phi^\dagger (DD^\dagger)^{-1}\phi\right). \tag{2.40}$$

The path integral over the pseudofermion field ϕ can be sampled using a combination of deterministic methods like molecular dynamics and stochastic methods such as the Metropolis algorithm. These combined algorithms are known as Hybrid Monte Carlo (HMC) methods. Codes that implement the HMC algorithm for pseudofermions are significantly more complicated than the Metropolis algorithm for the pure gauge Wilson action discussed above, and I refer the interested reader to the more specialized literature [60]. I also note that since these algorithms involve the calculation of D^{-1} the computational cost increases as the quark masses are lowered.

The calculation of correlation functions also differs from the bosonic case. Consider, for example, an operator with the quantum numbers of a charged pion, $J_\pi(x) = \bar{u}^a(x)\gamma_5 d^a(x)$. Since the fermion action is quadratic the correlation function in a given gauge configuration can be computed exactly in terms of the fermion propagator. The full correlation function is

$$\Pi_\pi(x) = \langle J_\pi(x) J_\pi(0) \rangle = \langle \text{Tr}\left[S(x,0)\gamma_5 S(0,x)\gamma_5\right]\rangle, \tag{2.41}$$

where $S(x,y) = \langle x|D^{-1}|y\rangle$ is the fermion propagator, and we have assumed exact isospin symmetry so that the propagator of the up quark is equal to the propagator of the down quark. Note that the interaction between quarks is encoded in the average over all gauge fields. The one-gluon exchange interaction, for example, corresponds to a perturbative fluctuation in the gauge field that modifies the two quark propagators. An operator with the quantum number of the proton is $\eta_\alpha(x) = \varepsilon_{abc}(u^a(x)C\gamma_\mu u^b(x))(\gamma^\mu \gamma_5 d^c(x))_\alpha$. The correlation function is

$$\Pi_{\alpha\beta}(x) = 2\varepsilon_{abc}\varepsilon_{a'b'c'}\left\langle \left(\gamma_\mu \gamma_5 S^{cc'}(0,x)\gamma_\nu \gamma_5\right)_{\alpha\beta} \text{Tr}\left[\gamma_\mu S^{aa'}(0,x)\gamma_\nu C(S^{bb'}(0,x))^T C\right]\right\rangle. \tag{2.42}$$

Note that meson correlation function involves one forward and one backward going propagator, whereas the propagators in the baryon correlation function are all forward going. A difficulty arises when we consider flavor singlet $\bar{q}q$ currents such as $J_{\eta'} = (\bar{u}^a(x)\gamma_5 u^a(x) + \bar{d}^a(x)\gamma_5 d^a(x))/\sqrt{2}$, which has the quantum numbers of the η' meson. We find

$$\Pi_{\eta'}(x) = \langle J_{\eta'}(x) J_{\eta'}(0)\rangle = \langle \text{Tr}\left[S(x,0)\gamma_5 S(0,x)\gamma_5\right] - 2\text{Tr}\left[S(x,x)\gamma_5\right]\text{Tr}\left[S(0,0)\gamma_5\right]\rangle, \tag{2.43}$$
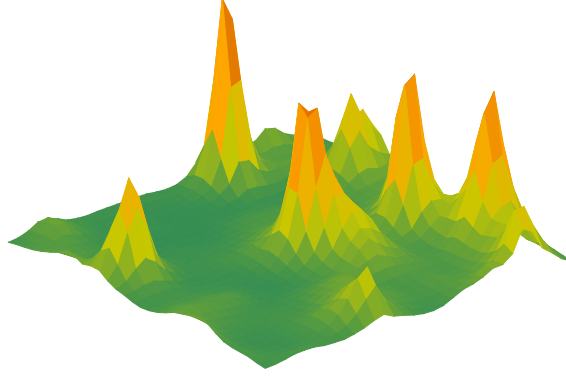
Fig. 2.3 Topological objects in lattice QCD (figure courtesy of S. Sharma, see [62]). This picture shows a slice through a low lying eigenstate of the Dirac operator in lattice QCD.

which involve propagators $S(x,x)$ that loop back to the same point. These contributions are known as quark-line disconnected diagrams, and difficult to treat numerically, see [61] for a recent discussion.

2.4.3 The QCD vacuum

It is natural to hope that lattice QCD can provide us with an intuitive picture of what the QCD vacuum looks like, similar to the picture of the quantum mechanical ground state shown in Fig. 2.1. This turns out to be more complicated, for a number of reasons. The first is that the field in QCD is a $SU(3)$ matrix, which is hard to visualize. The second, more important, problem is related to quantum fluctuations. In QCD there is no obvious separation of scales that would allow us to clearly separate perturbative fluctuations from large semi-classical fluctuations.

This has led to the idea to eliminate short range fluctuations by some kind of filtering or smoothing algorithm. The simplest of these is known as cooling [63]. In the cooling method we modify the Metropolis algorithm so that only updates that reduce the action are accepted. Since the update algorithm is local, this will tend to eliminate small structures but preserve larger objects. A modern version of cooling is gradient flow [64]. In the gradient flow method we continue the gauge fields to a 5th "time" dimension. In this direction the fields satisfy a differential equation

$$\partial_\tau A_\mu = D^\nu G_{\mu\nu}, \tag{2.44}$$

where $A_\mu(\tau = 0)$ is the four-dimensional gauge field and the rhs is computed from the gauge potentials evaluated at the flow time τ. The Lorentz indices remain four-dimensional. The rhs of the flow equations is the classical equation of motion, so that the gradient flow tends to drive gauge fields towards the closest classical solution. The only finite action solutions of the euclidean field equations on R^4 are instantons [65,66]. Instantons and anti-instantons are characterized by integer values $Q_{top} = \pm 1$ of the topological charge

$$Q_{top} = \int d^4x \, q(x) \,, \qquad q(x) = \frac{g^2}{64\pi^2} \varepsilon^{\mu\nu\alpha\beta} G^a_{\mu\nu} G^a_{\alpha\beta} \,. \tag{2.45}$$

Exact higher charge solutions exist, but the QCD vacuum is dominated by configurations with both instantons and anti-instantons. These gauge field configurations are only approximate solutions of the equations of motion [66]. Under cooling or gradient flow instantons and anti-instantons will eventually annihilate and evolve to an exact multi-instantons solution with $Q_{top} = N_I - N_A$, where $N_{I,A}$ are the numbers of (anti)instantons. However, the $N_I + N_A$ topological objects are preserved for flow times that are much longer than the decay time of ordinary quantum fluctuations, and the total number of well separated instantons and anti-instantons can be determined.

The average topological charge is zero, but the pure gauge vacuum is characterized by a non-zero topological susceptibility

$$\chi_{top} = \frac{1}{V} \langle Q^2_{top} \rangle \,, \tag{2.46}$$

where V is the euclidean four-volume. The topological charge can be determined using the naive lattice discretization of equ. (2.45), but this operator is very noisy, and in general not an integer. This problem can be addressed using the cooling or gradient flow algorithms discussed above. Recent lattice calculations based on these methods give $\chi_{top} = (190 \pm 5 \, \text{MeV})^4$ [67, 68]. A simple picture of the QCD vacuum which is consistent with this value is the dilute instanton liquid model, which assumes that the topological susceptibility is determined by Poisson fluctuations in an ensemble of instantons and anti-instantons with an average density $(N_I + N_A)/V \simeq 1 \, \text{fm}^{-4}$ [66]. This is an approximate picture, and more complicated configurations involving monopoles and fractional charges are needed to understand the large N_c limit and the role of confinement [69].

Another important development is the use of fermionic methods to analyze the vacuum structure of QCD. In a given gauge configuration the quark propagator can written as

$$S(x,y) = \sum_\lambda \frac{\psi_\lambda(x)\psi_\lambda^\dagger(y)}{\lambda + im} \,, \tag{2.47}$$

where ψ_λ is an eigenvector of the Dirac operator with eigenvalue λ: $D\psi_\lambda = (\lambda + im)\psi_\lambda$. Note that this is not how propagators are typically determined in lattice QCD, because the calculation of the complete spectrum is numerically very expensive. Gamma five hermiticity implies that eigenvalues come in pairs $\pm\lambda$. The quark condensate is given by

$$\langle \bar{q}q \rangle = -i \int d^4x \, \langle \text{Tr}\,[S(x,x)] \rangle = - \left\langle \sum_{\lambda>0} \frac{2m}{\lambda^2 + m^2} \right\rangle \,. \tag{2.48}$$

Here, I have ignored the contribution from exact zero modes because the density of zero modes is suppressed by m^{N_f}. This factor comes from the determinant in the measure. If we were to ignore the determinant (this is called the quenched approximation), then the quark condensate would diverge as $1/m$. We observe that a finite value of the quark condensate in the chiral limit $m \to 0$ requires an accumulation of eigenvalues near zero. This can be made more explicit by introducing the density of states

$$\rho(v) = \left\langle \sum_{\lambda\geq0} \delta(\lambda - v) \right\rangle \,. \tag{2.49}$$

The chiral condensate in the thermodynamic and chiral limits is given by

$$\langle \bar{q}q \rangle = -\pi\rho(0) \,. \tag{2.50}$$

This is known as the Banks-Casher relation [70]. Note that is is essential to take the thermo-dynamic $V \to \infty$ limit before the chiral limit $m \to 0$.

Exact zero modes of the Dirac operator are related to topology. The Dirac operator has one left handed zero mode in the field of an instanton, and a right handed zero mode in the field of an anti-instanton. This is consistent with the Atiyah-Singer index theorem, which states that the topological charge is equal to the index of the Dirac operator, the difference between the number of left and right handed zero modes, $Q_{top} = N_f(n_L - n_R)$. These results suggest that it is possible to give a purely fermionic definition of the topological charge density.

On the lattice, this can be achieved for a class of Dirac operators that satisfy the Ginsparg-Wilson relation [71]

$$D\gamma_5 + \gamma_5 D = a D \gamma_5 D, \tag{2.51}$$

where a is the lattice spacing. In the continuum limit we recover the expected relation $D\gamma_5 + \gamma_5 D = 0$ for the massless Dirac operator. The important observation is that even on a discrete lattice

$$q_f(n) = \frac{1}{2a^3} \text{tr}_{CD} \left[\gamma_5 D(n,n) \right], \tag{2.52}$$

where tr_{CD} is a color-Dirac trace, satisfies the index theorem

$$Q_{top} = a^4 \sum_n q_f(n). \tag{2.53}$$

Fig. 2.3 shows the absolute square of $q_f(x)$ constructed from lying eigenmodes of the Dirac operator. We observe that fermionic operators can indeed be used to probe the topological content of the QCD vacuum directly, without the need for filtering or smoothing.

The existence of zero mode implies that the topological susceptibility is zero if at least one quark flavor is massless. This is because the path integral measure contains the fermion determinant, which is vanishes if $m = 0$ and $Q_{top} \neq 0$. We can be more precise using the chiral lagrangian equ. (2.22). In order to keep track of topology we add to the QCD action a topological term $S_\theta = i\theta Q_{top}$. Then the topological susceptibility is given by the second derivative of the free energy with respect to θ. Since every zero mode in the Dirac operator contributes a factor $\det(M)$ to the partition function we know that θ enters the effective lagrangian in the combination $\theta + \arg(\det(M))$. The vacuum energy is determined by

$$V = -B\text{Tr} \left[M e^{i\theta/N_f} \Sigma^\dagger \right] + h.c., \tag{2.54}$$

and we observe that the topological susceptibility in QCD with degenerate quark masses is proportional to $m\langle \bar{q}q \rangle$. Note that equ. (2.54) is consistent with the vanishing of χ_{top} for $m_u = 0$. If $m_u = 0$ and $m_d \neq 0$ then equ. (2.54) is minimized by $\Sigma = \exp(i\phi \tau_3)$ with $\phi = \theta/2$, and the vacuum energy is independent of θ.

It is tempting to think that exact zero modes, governed by topology, and approximate zero modes, connected to chiral symmetry breaking, are related. This is the basis of the instanton liquid model [66]. In the instanton liquid model we consider an ensemble of instantons and anti-instantons with no (or small) net topology. The exact zero modes of individual instantons are lifted, and form a zero mode zone. The density of eigenvalues in the zero mode zone determines the chiral condensate via the Banks-Casher relation. This model predicts the correct order of magnitude of $\langle \bar{q}q \rangle$, but the calculation cannot be systematically improved because chiral symmetry breaking requires strong coupling. Recently, we showed that the connection of chiral symmetry breaking, instantons and monopoles can be made precise in a certain limit of QCD. The idea is to compactify QCD on $R^3 \times S_1$, where the size of the circle is much smaller than Λ_{QCD}^{-1}, and the fermions satisfy non-thermal (twisted) boundary conditions [72].

2.4.4 Lattice QCD at finite baryon density

In section 2.4.2 I discussed some of the difficulties that appear when we discretize the Dirac operator. A separate, more serious, issue with fermions is that for $\mu \neq 0$ the Dirac operator does not satisfy γ_5-hermiticity, the fermion determinant is no longer real, and that standard importance sampling methods fail. This is the "sign" problem already mentioned in Sect. 2.3.2. To understand the severity of the problem consider a generic expectation value

$$\langle \mathscr{O} \rangle = \frac{\int dU \, \det(D) \, \mathscr{O} \, e^{-S}}{\int dU \, \det(D) \, e^{-S}} \, . \tag{2.55}$$

If the determinant is complex I can write this as

$$\langle \mathscr{O} \rangle = \frac{\int dU \, |\det(D)| \, \mathscr{O} e^{i\varphi} \, e^{-S}}{\int dU \, |\det(D)| e^{i\varphi} e^{-S}} \equiv \frac{\langle \mathscr{O} e^{i\varphi} \rangle_{pq}}{\langle e^{i\varphi} \rangle_{pq}} \, , \tag{2.56}$$

where $\langle . \rangle_{pq}$ refers to a phase quenched average. This average can be computed using the Metropolis (or HMC) algorithm. The problem is that the average phase $\langle e^{i\varphi} \rangle_{pq}$ is very small. This follows from the fact that the average phase can be expressed as the ratio of two partition functions

$$\langle e^{i\varphi} \rangle_{pq} = \frac{\int dU \, \det(D) \, e^{-S}}{\int dU \, |\det(D)| e^{-S}} = \frac{Z}{Z_{pq}} = e^{-V\Delta F} \, , \tag{2.57}$$

where ΔF is the free energy density difference, and V is the volume of the system. This shows that the phase is exponentially small, and that the ratio equ. (2.56) is very difficult to compute.

As a specific example consider QCD with two degenerate flavors, up and down, and a baryon chemical potential $\mu_u = \mu_d = \mu_B/3$. Then $\det(D) = \det(D_u)\det(D_d)$ and $|\det(D)| = \det(D_u)\det(D_d)^*$, and Z_{pq} can be interpreted as the partition function of QCD with a non-zero isospin chemical potential $\mu_u = -\mu_d = \mu_I/2$. The small μ behavior of both the isospin and baryon number theories at $T = 0$ is easily understood. The isospin theory has a second order phase transition at $\mu_I = m_\pi$ which corresponds to the onset of pion condensation. The baryon theory has a first order transition at $\mu_B = m_p - B$, where $B \simeq 15$ MeV is the binding energy of infinite nuclear matter. This implies that for $\mu > m_\pi$ the partition functions Z and Z_{pq} describe very different physical systems, and the sign problem is severe.

The sign problem may manifest itself in different ways. Consider, for example, an attempt to study the correlation function of A nucleons in a QCD ensemble generated at $\mu_B = 0$. For large A this correlation function determines the binding energy of nuclear matter. There are two difficulties with this approach. The first is that the operator contains $3A$ quark fields, so that the correlator has up to $(3A)!$ contractions. This is not prohibitive, because the number of contractions can be reduced using symmetries and iterative algorithms. Indeed, correlators for medium mass nuclei have been computed [49]. The second, more serious, problem is the signal-to-noise ratio. The variance of the correlator C is

$$\text{var}(C) = \langle CC^\dagger \rangle - \langle C \rangle^2 \, . \tag{2.58}$$

The A nucleon correlator C contains $3A$ forward going quark propagators, and $CC^\dagger$ consists of $3A$ forward and $3A$ backward propagators. This implies that $CC^\dagger$ couples to a state of $3A$ mesons. Since the lightest meson is the pion and the lightest baryon is the proton the signal-to-noise of an A nucleon correlation function is

$$\frac{\mathscr{S}}{\mathscr{N}} \sim \exp(-A(m_p - 3m_\pi/2)\tau) \, . \tag{2.59}$$

In order to resolve nuclear binding effects we have to go to distances of order $\tau \sim 1/B \sim 10$ fm. It may be possible to improve on this by using variationally improved sources, but even for $\tau \simeq 2$ fm the signal to noise is extremely poor for $A \gtrsim 4$. This shows that in simulations with fixed A the sign problem manifests itself as a noise problem. This is not surprising. One way to think about the sign problem is to view it as an overlap problem. The configurations that contribute to Z_{pq} have poor overlap with those that contribute to Z. The same phenomenon is at work here. Configurations generated at $\mu_B = 0$ reflect vacuum physics, and the lightest fermionic fluctuation is a pion. Large cancellations are required to explore the physics of multi-baryon states.

There are many attempts to find direct solutions to the sign problem, but at this time the only regime in which controlled calculations are feasible is the regime of small μ and high T. In this region the partition function can be expanded in a Taylor series in μ/T. The corresponding expansion coefficients are generalized susceptibilities that can be determined from lattice simulations at zero chemical potential. The susceptibilities not only determine the equation of state at finite baryon density, but also control fluctuations of conserved charges.

In addition to methods that are restricted to the regime $\mu \lesssim \pi T$, a number of proposals to explore QCD at high baryon density are being pursued. This includes new approaches, like integration over Lefshetz thimbles [73, 74], as well as novel variants of old approaches, like the complex Langevin method [75, 76], or the use of dual variables [77]. The ultimate promise of these methods is still unclear, but the central importance of the sign problem to computational physics continues to attract new ideas.

2.4.5 Real time properties

The basic trick in lattice QCD is the continuation of the path integral to imaginary time. This makes it possible to calculate the path integral by importance sampling, but it implies that we only have direct access to imaginary time correlation functions. For many observables this is not a serious problem. Thermodynamic observables, for example, are static quantities and no analytic continuation is necessary. The ground state contribution to a hadron correlation function is $\Pi(\tau) \sim e^{-m_H \tau}$ which is trivially continued to $\Pi(t) \sim e^{-im_H t}$. However, difficulties arise if one studies excited states, in particular resonances, the interaction between hadrons, or the real time response of many body systems at finite temperature and density.

Significant progress has been made in studying scattering processes, at least in the elastic regime. This is discussed in some of the later chapters of this book. Here, I will concentrate on the calculation of real time response functions. The prototypical example is the calculation of the shear viscosity of a QCD plasma using the retarded correlation function of the stress tensor T_{xy},

$$G_R^{xy,xy}(\omega, \mathbf{k}) = -i \int dt \int d^3x \, e^{i(\omega t - \mathbf{k} \cdot \mathbf{x})} \Theta(t) \langle [T^{xy}(\mathbf{x}, t), T^{xy}(0, 0)] \rangle \,, \tag{2.60}$$

The associated spectral function is defined by $\rho(\omega, \mathbf{k}) = -\operatorname{Im} G_R(\omega, \mathbf{k})$. The imaginary part of the retarded correlator is a measure of dissipation. Fluid dynamics is an effective theory of the response function in the low energy, small momentum limit [78, 79]. The static response is determined by the pressure of the fluid, and the leading energy and momentum dependence is governed by transport coefficients. These relations can be used to derive Kubo formulas, expressions for the transport coefficients in terms of retarded correlation functions. The Kubo relation for the shear viscosity is

$$\eta = \lim_{\omega \to 0} \lim_{k \to 0} \frac{\rho^{xy,xy}(\omega, \mathbf{k})}{\omega} \,, \tag{2.61}$$

and similar results hold for the bulk viscosity, the thermal conductivity, and heavy quark diffusion constants.

The spectral function contains information about the physical excitations that carry the response. The euclidean path integral does not provide direct access to the retarded correlator or the spectral function. Lattice calculations are based on the relation between the spectral function and the imaginary energy (Matsubara) correlation function

$$G_E(i\omega_n) = \int \frac{d\omega}{2\pi} \frac{\rho(\omega)}{\omega - i\omega_n}, \tag{2.62}$$

where $\omega_n = 2\pi n T$ is the Matsubara frequency. The imaginary time correlation function is

$$G_E(\tau) = \int \frac{d\omega}{2\pi} K(\omega, \tau) \rho(\omega), \tag{2.63}$$

where the kernel $K(\omega, \tau)$ is given by

$$K(\omega, \tau) = \frac{\cosh[\omega(\tau - 1/(2T))]}{\sinh[\omega/(2T)]} = [1 + n_B(\omega)] e^{-\omega\tau} + n_B(\omega) e^{\omega\tau}, \tag{2.64}$$

and $n_B(\omega)$ is the Bose distribution function. The imaginary time correlation function equ. (2.63) was studied on the lattice in [80–83]. The basic idea for calculating transport coefficients is to numerically compute $G_E(\tau)$, invert the integral transform in equ. (2.63) to obtain the spectral functions $\rho(\omega)$, and then study the limit $\omega \to 0$.

The problem is that $G_E(\tau)$ is computed on a small number of discrete lattice sites, and that the imaginary time correlator at distances on the order of $\beta/2$ is not very sensitive to the slope of the spectral function at low energy. Recent attempts to to address these problems and to obtain numerically stable spectral functions and reliable error estimates are based on Bayesian methods such as the maximum entropy method mentioned in Sect. 2.2, see [84, 85]. It is also possible to optimize the contribution from the transport peak by measuring the correlation functions of conserved charges, such as energy and momentum density, at non-zero spatial momentum [86, 87]. A possible issue with lattice calculations is that effects of poor resolution tend to favor small values of η/s. The finite temperature spectral function satisfies the sum rule [88]

$$\frac{2}{\pi} \int d\omega \left[\eta(\omega) - \eta_{T=0}(\omega)\right] = \frac{3}{10} sT, \tag{2.65}$$

where $\eta(\omega) = \rho(\omega)/\omega$. On the lattice it is difficult to resolve sharp features in the spectral function. I will therefore assume that the $T \neq 0$ spectral function is a Lorentzian with width πT

$$\eta(\omega) - \eta_{T=0}(\omega) \simeq \frac{\eta(0)(\pi T)^2}{\omega^2 + (\pi T)^2}. \tag{2.66}$$

Then the integral on the lhs is equal to $\eta(0)\pi T$, and the sum rule predicts $\eta/s \sim 3/(10\pi)$, quite close to $\eta/s = 1/(4\pi)$. The lesson is that it is easier to obtain small values of η/s, suggested by holography, and much more difficult to obtain large values of η/s, predicted by perturbative QCD [89].

The first calculation of the shear viscosity on the lattice was performed by Karsch and Wyld [80]. More recently, the problem of computing the shear and and bulk viscosity in a pure gauge plasma near T_c was revisited by Meyer [81, 87]. He obtains $\eta/s = 0.102(56)$ and $\zeta/s = 0.065(17)$ at $T = 1.24 T_c$. Shear viscosity is only weakly dependent on temperature, but bulk viscosity is strongly peaked near T_c. The value of η/s is consistent with experimental results, and with the prediction from holographic duality, $\eta/s = 1/(4\pi)$ [90].
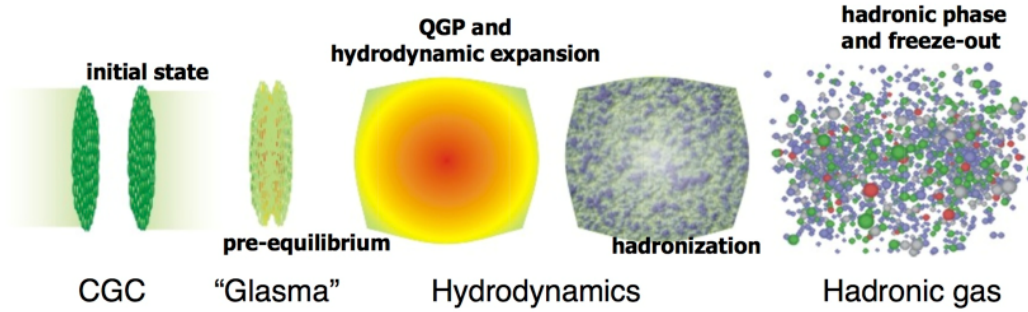
Fig. 2.4 Schematic time evolution of a heavy ion collision. Figure courtesy of S. Bass. CGC refers to the color glass condensate, a semi-classical model of the overpopulated gluon configuration in the initial state of a heavy ion collision. Glasma refers to the non-equilibrium evolution of this state into a locally equilibrated plasma. Hydrodynamics is the theory of the time evolution of a locally equilibrated fireball, and hadronic phase refers to the late time kinetic stage of the collision.

2.5 Nonequilibrium QCD

In the remainder of this chapter I will discuss a number of coarse grained approaches to the non-equilibrium dynamics of QCD. These method are relevant to the study of nuclear collisions, in particular in the ultra-relativistic regime. This regime is explored experimentally at the Relativistic Heavy Ion Collider (RHIC) at Brookhaven National Laboratory and the Large Hadron Collider (LHC) at CERN. A rough time line of a heavy ion collision is shown in Fig. 2.4. Initial nucleon-nucleon collisions release a large number of quarks and gluons. This process is described by the full non-equilibrium quantum field theory, but there are a number of approximate descriptions that may be useful in certain regimes. The first is a classical field theory description in terms of highly occupied classical gluon fields. The second is a kinetic theory in terms of quark and gluon quasi-particles. Finally, there is a new approach, which is a description in terms of a dual gravitational theory.

Theories of the initial state demonstrate that there is a tendency towards local equilibration. If local equilibrium is achieved then a simpler theory, fluid dynamics is applicable. Fluid dynamics is very efficient in the sense that it deals with a small number of variables, the conserved densities of particle number, energy and momentum, and that it has very few parameters, an equation of state and a set of transport coefficients. The fluid dynamic stage of a heavy ion collision has a finite duration. Eventually the density becomes too low and local equilibrium can no longer be maintained. At this point kinetic theory is again relevant, now formulated in terms of hadronic quasi-particles. All the theories we have mentioned, fluid dynamics, kinetic theory, classical field theory, and holography, have reached a high degree of sophistication and I will point to text books and review for detailed introductions. Nevertheless, the basic ideas are quite simple, and I will provide some examples in the following sections.

2.5.1 Fluid Dynamics

I begin with fluid dynamics, because it is the most general and in some ways the simplest non-equilibrium theory. It is important to remember, however, that fluid dynamics is a very rich framework, both mathematically and in terms of the range of phenomena that one may encounter. In the following I will focus on the non-relativistic theory. There is no fundamen-

tal difference between the relativistic and non-relativistic theories, but some simplifications appear in the non-relativistic regime. Non-relativistic fluid dynamics is used in many areas of physics, including the physics of cold atomic Fermi gases and neutron stars. The relativistic theory is relevant to high energy heavy ion collisions and supernova explosions. Introductions to relativistic fluid dynamics can be found in [91–93].

Fluid dynamics reduces the complicated non-equilibrium many-body problem to equations of motion for the conserved charges. The reason that this is possible is the separation of scales between the microscopic collision time τ_{micro}, and the relaxation time τ_{macro} of hydrodynamic variables. A generic perturbation of the system decays on a time scale on the order of τ_{micro}, irrespective of the typical length scale involved. Here, τ_{micro} is determined by microscopic time scales, such as the typical collision time between quasi-particles. A fluctuation of a conserved charge, on the other hand, cannot decay locally and has to relax by diffusion or propagation. The relevant time scale τ_{macro} increases with the length scale of the perturbation. As a consequence, when we focus on sufficiently large scales we can assume $\tau_{macro} \gg \tau_{micro}$, and focus on the evolution of conserved charges.

In a simple non-relativistic fluid the conserved charges are the mass density ρ, the momentum density π, and the energy density $\mathscr{E}$. The momentum density can be used to define the fluid velocity, $\mathbf{u} = \pi/\rho$. By Galilean invariance the energy density can then be written as the sum of the internal energy density and the kinetic energy density, $\mathscr{E} = \mathscr{E}_0 + \frac{1}{2}\rho u^2$. The conservation laws are

$$\frac{\partial \rho}{\partial t} = -\nabla \cdot \pi, \tag{2.67}$$

$$\frac{\partial \pi_i}{\partial t} = -\nabla_j \Pi_{ij}, \tag{2.68}$$

$$\frac{\partial \mathscr{E}}{\partial t} = -\nabla \cdot \mathbf{j}^\varepsilon. \tag{2.69}$$

In order for these equations to close we have to specify constitutive relations for the stress tensor Π_{ij} and the energy current $\mathbf{j}^\varepsilon$. Since fluid dynamics is an effective long wavelength theory we expect that the currents can be systematically expanded in gradients of the hydrodynamic variables ρ, $\mathbf{u}$ and $\mathscr{E}_0$. At leading order the stress tensor contains no derivatives and the structure is completely fixed by rotational symmetry and Galilean invariance. We have

$$\Pi_{ij} = \rho u_i u_j + P\delta_{ij} + \delta\Pi_{ij}, \tag{2.70}$$

where $P = P(\rho, \mathscr{E}_0)$ is the equation of state and $\delta\Pi_{ij}$ contains gradient terms. The approximation $\delta\Pi_{ij} = 0$ is called ideal fluid dynamics, and the equation of motion for π is known as the Euler equation. Ideal fluid dynamics is time reversal invariant and the entropy is conserved. If gradient terms are included then time reversal invariance is broken and the entropy increases. We will refer to $\delta\Pi_{ij}$ as the dissipative stresses. At first order in the gradient expansion $\delta\Pi_{ij}$ can be written as $\delta\Pi_{ij} = -\eta\sigma_{ij} - \zeta\delta_{ij}\langle\sigma\rangle$ with

$$\sigma_{ij} = \nabla_i u_j + \nabla_j u_i - \frac{2}{3}\delta_{ij}\langle\sigma\rangle, \qquad \langle\sigma\rangle = \nabla \cdot \mathbf{u}. \tag{2.71}$$

The dissipative stresses are determined by two transport coefficients, the shear viscosity η and the bulk viscosity ζ. The energy current is given by

$$\mathbf{j}^\varepsilon = \mathbf{u}w + \delta\mathbf{j}^\varepsilon, \tag{2.72}$$

where $w = P + \mathscr{E}$ is the enthalpy. At leading order in the gradient expansion

$$\delta j_i^\varepsilon = u_j\delta\Pi_{ij} - \kappa\nabla_i T, \tag{2.73}$$

where κ is the thermal conductivity. The second law of thermodynamics implies that η, ζ and κ must be positive. The equation of motion for π at first order in gradients is known as the Navier-Stokes equation, and equ. (2.73) is Fourier's law of heat conduction.

It is sometimes useful to rewrite the fluid dynamic equations using the comoving derivatives $D_t = \partial_t + \mathbf{u} \cdot \nabla$. The equations are

$$D_t \rho = -\rho \nabla \cdot \mathbf{u}, \tag{2.74}$$

$$D_t u_i = -\frac{1}{\rho} \nabla_j \left(\delta_{ij} P + \delta \Pi_{ij} \right), \tag{2.75}$$

$$D_t \varepsilon = -\frac{1}{\rho} \nabla_i \left(u_i P + \delta j_i^{\mathscr{E}} \right), \tag{2.76}$$

where $\varepsilon = \mathscr{E}/\rho$ is the energy per mass. This is called the Lagrangian form of the equations, in contrast to the Eulerian form given above. The Eulerian form is more naturally implemented on a fixed space-time lattice, whereas the Lagrangian form lends itself to a discretization where the computational cell is dragged along with the fluid.

2.5.2 Computational fluid dynamics

The fluid dynamic equations form a set of partial differential equations (PDEs) that can be solved in a variety of ways. I will focus here on grid based methods. The main difficulties that numerical method needs to address are: i) The existence of surfaces of discontinuity (shocks), ii) the need to implement global conservation laws exactly, even on a coarse lattice, iii) the existence of instabilities (turbulence), and the need to deal with solutions that involve many different length scales.

In the following I will discuss a numerical scheme that addresses these issues in a fairly efficient way, the PPM algorithm of Collela and Woodward [94], as implemented in the VH1 code by Blondin and Lufkin [95] and extended to viscous fluids in [96]. The first observation is that it is sufficient to construct a 1-d algorithm. Higher dimensional methods can be constructed by combining updates in different directions. Note that the coordinate system can be curvilinear, for example 3-d spherical or cylindrical coordinates, or the Milne coordinate system that is used for longitudinally expanding quark gluon plasmas.

The basic 1-d algorithm consists of a Lagrangian time step followed by a remap onto an Eulerian grid. I will denote the 1-d velocity by u and write the equation of mass conservation in terms of a mass variable m

$$\frac{\partial \tau}{\partial t} - \frac{\partial u}{\partial m} = 0, \tag{2.77}$$

where $\tau = \rho^{-1}$ and

$$m(r) = \int_{r_0}^{r} dr \, \rho(r). \tag{2.78}$$

Here, I restrict myself to flat coordinate systems. In curvilinear coordinates equ. (2.77) and (2.78) contain suitable volume factors. Equ. (2.77) is solved by

$$\frac{dr}{dt} = u \left(m(r), t \right), \tag{2.79}$$

which is the equation for the Lagrange coordinate. In terms of the mass coordinate $m(r)$ the momentum and energy equations are

$$\frac{\partial u}{\partial t} + \frac{\partial P}{\partial m} = 0, \tag{2.80}$$

$$\frac{\partial \varepsilon}{\partial t} + \frac{\partial (uP)}{\partial m} = 0, \tag{2.81}$$

where I have only written down the ideal contributions to the stress tensor and energy current. To put these equations on a grid I focus on the mass integrated quantities

$$U_j^n = \frac{1}{\Delta m_j} \int_{m_{j-1/2}}^{m_{j+1/2}} U(m, t^n) dm \tag{2.82}$$

where U is any of the hydrodynamic variables (τ, u, ε), Δm_j is the mass contained in the cell j, and $m_{j+1/2} = \sum_k^j \Delta m_k$. We can now integrate the conservation laws (2.80,2.77). The result is

$$u_j^{n+1} = u_j^n + \frac{\Delta t}{\Delta m_j} \left(\bar{P}_{j-1/2} - \bar{P}_{j+1/2} \right), \tag{2.83}$$

$$\varepsilon_j^{n+1} = \varepsilon_j^n + \frac{\Delta t}{\Delta m_j} \left(\bar{u}_{j-1/2} \bar{P}_{j-1/2} - \bar{u}_{j+1/2} \bar{P}_{j+1/2} \right), \tag{2.84}$$

where I have introduced the cell face averages $\bar{u}_{j\pm1/2}$ and $\bar{P}_{j\pm1/2}$. These quantities can be obtained by parabolic interpolation from the cell integrated values. The PPM scheme introduced in [94] uses a method for constructing cell face averages which conserves the cell integrated variables.

This scheme addresses the second issue mentioned above. The first issue, the existence of shocks, can be taken into account by refining the method for calculating the cell face averages. The observation is that one can make use of exact solution of the equations of fluid dynamics in the case of piecewise constant one-dimensional flows, known as the Riemann problem. We can view $\bar{u}_{j+1/2}$ and $\bar{P}_{j+1/2}$ as the solution of a Riemann problem with left state u_j, P_j and right state u_{j+1}, P_{j+1}. The PPM code contains a simple iterative Riemann solver described in [94]. Using $\bar{u}_{j\pm1/2}$ and $\bar{P}_{j\pm1/2}$ the Lagrange step is given by:

```
do n = nmin-3, nmax+3

! density evolution. lagrangian code, so all we have to do is watch the
! change in the geometry.

  r(n) = r(n) * ( dvol1(n) / dvol(n) )
  r(n) = max(r(n),smallr)

! velocity evolution due to pressure acceleration and forces.

  uold (n) = u(n)
  u(n) = u(n) - dtbdm(n)*(pmid(n+1)-pmid(n))*0.5*(amid(n+1)+amid(n)) &
       + 0.5*dt*(fict0(n)+fict1(n))

! total energy evolution

  e(n) = e(n) - dtbdm(n)*(amid(n+1)*upmid(n+1) - amid(n)*upmid(n))
  q(n) = e(n) - 0.5*(u(n)**2+v(n)**2+w(n)**2)
  p(n) = max(r(n)*q(n)*gamm,smallp)

enddo
```

Here, $r(n)$ is the density, $u(n)$ is the velocity, and $e(n)$ is the energy per mass. The transverse components of the velocity are $v(n), w(n)$. In cartesian coordinates the volume and area factors $dvol(n), amid(n)$ are equal to unity, and the fictitious forces $fict(n)$ vanish.

After the Lagrange step the hydrodynamic variables have to be remapped onto a fixed Eulerian grid. This can be done using the parabolic interpolation mentioned above. The advantage of the remap step is that it is simple to change the grid resolution in the process. Finally, we have to specify the time step and grid resolution. The grid resolution is determined by the requirement that $(\Delta x)\nabla_x U \ll U$, where Δx is the cell size, and U is any of the hydrodynamic variables. Note that there is no need to worry about discontinuities, because shocks are captured by the Riemann solver. Also note that the PPM scheme has at least second order accuracy, so that relatively coarse grids can be used. The time step is determined by the Courant criterion $c\Delta x \leq \Delta t$, where c is the maximum of the speed of sound and the local flow velocity. This criterion ensures that the domain of dependence of any physical variable does not exceed the cell size.

In general, modern hydro codes are very fast and efficient. The main difficulty is that $3+1$ dimensional simulations may require a lot of memory, and that some physical phenomena, such as turbulent convection and shock instabilities in supernovae, require very high resolution. One of the frontiers of numerical hydrodynamics is the problem of dealing with systems that transition from fluid dynamics to ballistic behavior at either early or late times, or systems in which the density varies by a very large factor. Problems of this type arise in the early and late time dynamics of heavy ion collisions, the dilute corona of cold atomic gases, and the transition from hydrodynamics to free streaming in the neutrino transport in a supernova explosions. Recent progress in this direction includes the development of the anisotropic hydrodynamics method [97–100], and applications of the lattice Boltzmann method to problems in nuclear and atomic physics [101, 102].

2.5.3 Kinetic theory

Fluid dynamics is based on the assumption of local thermal equilibrium and requires the mean free path to be small compared to the characteristic scales of the problem. When this condition is not satisfied a more microscopic approach to the non-equilibrium problem is required. The simplest method of this type is kinetic theory, which is based on the existence of well defined quasi-particles. This implies, in particular, that the width of a quasi-particle has to be small compared to its energy. In this case we can define the phase space density $f(\mathbf{x},\mathbf{p},t)$ of quasi-particles. In general, there can be many different kinds of quasi-particles, labeled by their spin, charge, and other quantum numbers. The phase space distribution determines the conserved densities that enter the hydrodynamic description. For example, the mass density is given by

$$\rho(\mathbf{x},t) = \int d\Gamma\, m f(\mathbf{x},\mathbf{p},t), \qquad (2.85)$$

where $d\Gamma = d^3 p/(2\pi)^3$. The momentum density is

$$\pi(\mathbf{x},t) = \int d\Gamma\, m v_p f(\mathbf{x},\mathbf{p},t), \qquad (2.86)$$

where $v_p = \nabla_p E_p$ is the quasi-particle velocity and E_p is the quasi-particle energy. In general, the quasi-particle energy can be a functional of the phase distribution $f(\mathbf{x},\mathbf{p},t)$. This takes into account possible in-medium modifications of particle properties. If E_p is a functional of $f(\mathbf{x},\mathbf{p},t)$ then the total energy of the system is not just given by the integral of $E_p f(\mathbf{x},\mathbf{p},t)$. Instead, we must construct an energy density functional $\mathscr{E}[f]$ that satisfies [103]

$$E_p = \frac{\delta \mathscr{E}}{\delta f_p}. \qquad (2.87)$$

The equation of motion for the distribution function is the Boltzmann equation

$$(\partial_t + \mathbf{v} \cdot \nabla_x - \mathbf{F} \cdot \nabla_p) f(\mathbf{x}, \mathbf{p}, t) = C[f],\tag{2.88}$$

where $\mathbf{F} = -\nabla_x E_p$ is a force, and $C[f_p]$ is the collision term. For dilute systems the collision term is dominated by binary scattering and

$$C[f_p] = -\prod_{i=2,3,4} \left(\int d\Gamma_i \right) w(1,2;3,4) \left(f_1 f_2 - f_3 f_4 \right),\tag{2.89}$$

where $f_i = f(\mathbf{x}, \mathbf{p}_i, t)$. The transition rate is given by

$$w(1,2;3,4) = (2\pi)^4 \delta \left(\sum_i E_i \right) \delta \left(\sum_i \mathbf{p}_i \right) |\mathscr{A}|^2,\tag{2.90}$$

where $\mathscr{A}$ is the scattering amplitude. For non-relativistic s-wave scattering $\mathscr{A} = 4\pi a/m$, where a is the scattering length.

The Boltzmann equation is a 6+1 dimensional partial integro-differential equation, and direct methods of integration, similar to those used in computational fluid dynamics, are impractical. Standard methods for solving the Boltzmann equation rely on sampling phase space using Monte Carlo methods. In nuclear physics the test particle method for solving the Boltzmann equation was popularized by Bertsch and Das Gupta [104]. Below, I will present a simple non-relativistic algorithm described by Lepers et al. [105].

The main idea is to represent the distribution as a sum of delta functions

$$f(\mathbf{x}, \mathbf{p}, t) = \frac{N}{N_t} \sum_{i=1}^{N_t} (2\pi)^3 \delta(\mathbf{p} - \mathbf{p}_i(t)) \delta(\mathbf{x} - \mathbf{x}_i(t)),\tag{2.91}$$

where N is the number of particles, the integral of $f(\mathbf{x}, \mathbf{p}, t)$ over phase space, and N_t is the number of test particles. In typical applications $N_t \gg N$, but if N is already very large it is possible to run simulations with $N_t < N$. Phase space averages can be computed as averages over test particles

$$\bar{F} = \frac{1}{N} \int d^3 x \int d\Gamma \, f(\mathbf{x}, \mathbf{p}, t) F(\mathbf{x}, \mathbf{p}) = \frac{1}{N_t} \sum_{i=1}^{N_t} F(\mathbf{x}_i, \mathbf{p}_i).\tag{2.92}$$

In practice this requires some smoothing, and the delta functions are replaced by Gaussian distributions

$$\delta(\mathbf{p} - \mathbf{p}_i) \delta(\mathbf{x} - \mathbf{x}_i) \to g_{w_p}(\mathbf{p} - \mathbf{p}_i) g_{w_x}(\mathbf{x} - \mathbf{x}_i),\tag{2.93}$$

where $g_w(\mathbf{x})$ is a normalized Gaussian with width w. The widths w_x and w_p are chosen such that the delta function singularities are smoothed out, but physical structures of the distribution function $f(\mathbf{x}, \mathbf{p}, t)$ are preserved.

If there is no collision term the equation of motion for the distribution function is Hamilton's equation for the test particle positions and momenta

$$\frac{d\mathbf{x}_i}{dt} = \frac{\mathbf{p}_i}{m}, \qquad \frac{d\mathbf{p}_i}{dt} = \mathbf{F}_i.\tag{2.94}$$

These equations can be solved with high accuracy using a staggered leapfrog algorithm

$$\mathbf{v}_i(t_{n+1/2}) = \mathbf{v}_i(t_n) + \mathbf{a}_i(t_n) \Delta t/2,\tag{2.95}$$

$$\mathbf{r}_i(t_{n+1}) = \mathbf{r}_i(t_n) + \mathbf{v}_i(t_{n+1/2}) \Delta t,\tag{2.96}$$

$$\mathbf{v}_i(t_{n+1}) = \mathbf{v}_i(t_{n+1/2}) + \mathbf{a}_i(t_{n+1}) \Delta t/2,\tag{2.97}$$

where $\mathbf{a}_i = \mathbf{F}_i/m$ is the acceleration of particle i, and $\Delta t = t_{n+1} - t_n$ is the time step of the algorithm. The size of the time step depends on the specific problem, but a good check is provided by monitoring conservation of energy.

The collision term is treated stochastically, by allowing the test particles to collide with the scaled cross section $\sigma_t = (N/N_t)\sigma$. To determine whether a collision occurs we go through all pairs of particles and compute the relative distance $\mathbf{r}_{ij} = \mathbf{r}_i - \mathbf{r}_j$ and velocity $\mathbf{v}_{ij} = \mathbf{v}_i - \mathbf{v}_j$. We then determine whether on the current trajectory the time of closest approach will be reached during the next time step. This happens if $t_{min} = t_n - \mathbf{r}_{ij} \cdot \mathbf{v}_{ij}/\mathbf{v}_{ij}^2$ satisfies $|t_{min} - t_n| \leq \Delta t/2$. In that case we compute

$$r_{min}^2 = \mathbf{r}_{ij}^2 - \frac{(\mathbf{r}_{ij} \cdot \mathbf{v}_{ij})^2}{\mathbf{v}_{ij}^2} \tag{2.98}$$

and check if $\pi r_{min}^2 < \sigma_t$. If this condition is satisfied then the collision is allowed to take place. For an s-wave elastic collision we propagate the particles to t_{min}, randomize their relative velocity $\mathbf{v}_{ij}$, and then propagate them back to t_n. Higher partial wave amplitudes are easy to implement by randomizing $\mathbf{v}_{ij}$ with suitable probability distributions. After all pairs have been checked we perform the velocity and position update in equ. (2.95-2.97).

There are a number of refinements that can be included. At low temperature Pauli-blocking has to be taken into account. This can be done by computing the phase space densities $f(\mathbf{r}_i, \mathbf{p}_i, t)$ for the collision products, and accepting the collision with probability $(1 - f_i)(1 - f_j)$. At higher energies relativistic effects are important. Relativistic effects in the particle propagation are easy to incorporate, but the treatment of the collision term is more subtle. The problem is that a finite collision cross section, treated geometrically, will lead to instantaneous interactions at a distance. Additional difficulties arise from the treatment of resonances, pair production and annihilation, n-body processes, etc. There are a number of codes on the market that address these issues, and that have been tuned against existing data on pp, pA and AA interactions in the relativistic regime. Examples include UrQMD [106], GiBUU [107], HSD [108], and others.

At high energies the initial pp collisions are very inelastic, and one has to rely on Monte Carlo generators developed in the high energy physics community. A possible alternative is to use a purely partonic kinetic theory that involves scattering between quark and gluon quasiparticles. There are some subtleties with this approach, having to do with the problem of how to include screening and damping of the exchanged gluons, soft gluon radiation, etc. I will not attempt to discuss these issues here, and I refer the reader to the original literature [109, 110].

2.5.4 Classical field theory

An interesting simplification occurs if the occupation numbers are large, $f \gg 1$. This is argued to happen for the gluons in the initial state of a heavy ion collision [111]. In this limit the classical kinetic theory is equivalent to a classical field theory [112]. Indeed, if the occupations numbers are non-perturbative, $f \gtrsim 1/g$, the kinetic theory no longer applies, and we have to rely on classical field theory. In general the classical action is not known, but in the weak coupling limit the bare QCD action can be used.

Classical QCD simulation have been used to study a number of issues, such as particle production from an overpopulated gluon field, and the possible approach to thermal equilibrium. Instabilities in the classical field evolution may play an important role in speeding up the equilibration process. Here, I will briefly describe a method for solving classical evolution equations on a space-time lattice, following the recent review [113].

In order to construct a Hamiltonian approach to lattice QCD I start from the Wilson action in Minkowski space with separate coupling constants β_0 and β_s in the temporal and spatial direction

$$S[U] = -\frac{\beta_0}{2N_c} \sum_x \sum_{i=1}^3 \text{Tr}\left(W_{0i}(x) + W_{0i}^\dagger(x) - 2\right) + \frac{\beta_s}{2N_c} \sum_x \sum_{i<j} \text{Tr}\left(W_{ij}(x) + W_{ij}^\dagger(x) - 2\right), \qquad (2.99)$$

In the continuum limit, we expect

$$\beta_0 = \frac{2N_c a}{g^2 \Delta t}, \qquad \beta_s = \frac{2N_c \Delta t}{g^2 a}. \qquad (2.100)$$

where a and Δt are spatial and temporal lattice spacings. In order to construct a Hamiltonian we have to fix the gauge freedom of the theory. Here, I will use the temporal axial gauge, $A_0 = 0$. In this case the canonical variables are the spatial gauge potentials and the conjugate momenta are the electric fields. On the lattice the gauge $A_0 = 0$ corresponds to setting all temporal gauge links to the identity, $U_0(x) = 1$. The canonical variables are given by the spatial gauge links $U_j(x)$, and the conjugate momenta are the temporal plaquettes $W_{0j}(x)$. In the continuum limit

$$A_j^a(x) = \frac{2i}{ag} \text{Tr}\left[\lambda^a U_j(x)\right], \qquad (2.101)$$

$$E_j^a(x) = \frac{2i}{ag\Delta t} \text{Tr}\left[\lambda^a W_{0j}(x)\right]. \qquad (2.102)$$

Varying the action equ. (2.99) with respect to $U_j(x)$ gives an equation of motion for E_j

$$E_j^a(t+\Delta t, \mathbf{x}) = E_j^a(t, \mathbf{x}) + \frac{i\Delta t}{ga^3} \sum_k \left\{ \text{Tr}\left[\lambda^a U_j(x) U_k(x+\hat{j}) U_j^\dagger(x+\hat{k}) U_k^\dagger(x)\right] \right.$$
$$\left. + \text{Tr}\left[\lambda^a U_j(x) U_k^\dagger(x+\hat{j}-\hat{k}) U_j^\dagger(x-\hat{k}) U_k(x-\hat{k})\right] \right\}. \qquad (2.103)$$

We note that $E_j^a(t+\Delta t, \mathbf{x})$ is determined by the electric fields and the spatial gauge links at time t. Using equ. (2.102) and the electric field E_j^a at time $t+\Delta t$ we can compute the temporal plaquette $W_{0j}(x)$ at $t+\Delta t$. This result can be used to evolve the spacelike gauge links

$$U_j(t+\Delta t, \mathbf{x}) = W_{0j}(x) U_j(x). \qquad (2.104)$$

Together, equ. (2.103) and equ. (2.104) describe a staggered leapfrog algorithm, similar to equ. (2.95-2.97) above. An important constraint on the numerical evolution is provided by Gauss law. Varying the lattice action with respect to U_0 before imposing temporal axial gauge gives

$$\sum_j \left[E_j^a(x) - U_j^\dagger(x-\hat{j}) E_j^a(x-\hat{j}) U_j(x-\hat{j}) \right] = 0. \qquad (2.105)$$

This constraint is preserved by the evolution equations.

The classical field equations are exactly scale invariant and there is no dependence on the coupling constant g. Physical quantities, like the energy momentum tensor, explicitly depend on g. In practice classical field simulations require a model for the initial conditions and the corresponding coupling. The initial conditions are typically an ensemble of gauge fields distributed according to some distribution, for example an anisotropic Gaussian in momentum space. The anisotropy is assumed to be a consequence of the strong longitudinal expansion of the initial state of a heavy ion collision. Physical observables are determined by averages the evolved fields over the initial ensemble.

Note that a purely classical field evolution does not thermalize. A thermal ensemble of classical fields would satisfy the equipartition law, and the total energy would be dominated by modes near the lattice cutoff. This is the Rayleigh-Jeans UV catastrophe. However, classical field evolution has interesting non-thermal fixed points [114], which may play a role in thermalization.

The classical field framework has been extended in a variety of ways. One direction is the inclusion of quantum fluctuations on top of the classical field [115]. Another problem is the inclusion of modes that are not highly populated. In the hard thermal loop approximation one can show that hard modes can be described as colored particles interacting with the classical field corresponding to the soft modes [116]. The equations of motion for the colored particles are known as Wong's equations [117]. Numerical studies can be found in [118].

2.5.5 Nonequilibrium QCD: Holography

A new approach to quantum fields in and out of equilibrium is provided by the AdS/CFT correspondence [119–123]. The AdS/CFT correspondence is a holographic duality. It asserts that the dynamics of a quantum field theory defined on the boundary of a higher dimensional space is encoded in boundary correlation functions of a gravitational theory in the bulk. The correspondence is simplest if the boundary theory is strongly coupled and contains a large number N of degrees of freedom. In this case the bulk theory is simply classical Einstein gravity. The partition function of the boundary quantum field theory (QFT) is

$$Z_{QFT}[J_i] = \exp\left(-S\left[\phi_i|_{\partial M} = J_i\right]\right), \qquad (2.106)$$

where J_i is a set of sources in the field theory, S is the gravitational action, ϕ_i is a dual set of fields in the gravitational theory, and ∂M is the boundary of AdS_5. The fields ϕ_i satisfy classical equations of motions subject to boundary conditions on ∂M.

The original construction involves a black hole in AdS$_5$ and is dual to a relativistic fluid governed by a generalization of QCD known as $\mathcal{N} = 4$ super Yang-Mills theory. This theory is considered in the limit of a large number of colors N_c. The gravitational theory is Einstein gravity with additional matter fields that are not relevant here. The AdS$_5$ black hole metric is

$$ds^2 = \frac{(\pi T R_a)^2}{u}\left(-f(u)dt^2 + d\mathbf{x}^2\right) + \frac{R_a^2}{4u^2 f(u)}du^2, \qquad (2.107)$$

where $\mathbf{x}, t$ are Minkowski space coordinates, and u is a "radial" coordinate where $u = 1$ is the location of the black hole horizon and $u = 0$ is the boundary. T is the temperature, R_a is the AdS radius, and $f(u) = 1 - u^2$.

It is instructive to check that this metric does indeed provide a solution to the Einstein equations with a negative cosmological constant. This can be done using a simple Mathematica script. I begin by defining the metric and its inverse:

```
(* metric *)
(* ------ *)
n = 5;
coord = {t, x, y, z, u};
f[u_] := 1 - u^2
metric = DiagonalMatrix[{-f[u]/u*(Pi*T*Ra)^2, (Pi*T*Ra)^2/u, (Pi*T*Ra)^2/
   u, (Pi*T*Ra)^2/u, Ra^2/(4*u^2*f[u])}]
inversemetric = Simplify[Inverse[metric]]
```

From the metric I compute the Christoffel symbols

$$\Gamma^{\mu}_{\alpha\beta} = \frac{1}{2}g^{\mu\nu}\left(\partial_{\alpha}g_{\nu\beta} + \partial_{\beta}g_{\nu\alpha} - \partial_{\mu}g_{\alpha\beta}\right),\tag{2.108}$$

the Riemann tensor

$$R^{\mu}_{\nu\alpha\beta} = \partial_{\alpha}\Gamma^{\mu}_{\nu\beta} - \partial_{\beta}\Gamma^{\mu}_{\nu\alpha} + \Gamma^{\rho}_{\nu\beta}\Gamma^{\mu}_{\rho\alpha} - \Gamma^{\rho}_{\nu\alpha}\Gamma^{\mu}_{\rho\beta},\tag{2.109}$$

the Ricci tensor $R_{\alpha\beta} = R^{\mu}_{\alpha\mu\beta}$, and the scalar curvature $R = R^{\mu}_{\mu}$. Finally, I compute the Einstein tensor $G_{\mu\nu} = R_{\mu\nu} - \frac{1}{2}g_{\mu\nu}R$.

```
(* Christoffel Symbols *)
(* ------------------- *)
affine := affine = Simplify[
  Table[(1/2)*
   Sum[(inversemetric[[i, s]])*(D[metric[[s, j]], coord[[k]]] +
      D[metric[[s, k]], coord[[j]]] -
      D[metric[[j, k]], coord[[s]]]), {s, 1, n}], {i, 1, n}, {j, 1,
    n}, {k, 1, n}]]

(* Riemann Tensor *)
(* -------------- *)
riemann := riemann = Simplify[Table[
  D[affine[[i, j, l]], coord[[k]]] -
   D[affine[[i, j, k]], coord[[l]]] +
   Sum[affine[[s, j, l]]*affine[[i, k, s]] -
     affine[[s, j, k]]*affine[[i, l, s]], {s, 1, n}], {i, 1, n}, {j,
    1, n}, {k, 1, n}, {l, 1, n}]]

(* Ricci Tensor *)
(* ------------ *)
ricci := ricci = Simplify[
  Table[Sum[riemann[[i, j, i, l]], {i, 1, n}], {j, 1, n}, {l, 1, n}]]

(* scalar curvature *)
(* ---------------- *)
scalar = Simplify[
 Sum[inversemetric[[i, j]]*ricci[[i, j]], {i, 1, n}, {j, 1, n}]]

(* Einstein tensor *)
(* --------------- *)
einstein = Simplify[ricci - (1/2)*scalar*metric]
```

Now I can check the equation of motion, $G_{\mu\nu} = \frac{\Lambda}{2}g_{\mu\nu}$, where the cosmological constant is determined by the AdS radius R.

```
(* Field equation with cosmological constant *)
(* ----------------------------------------- *)
lam = 12/Ra^2;
Simplify[einstein - lam/2*metric]
```

In the boundary theory the metric couples to the stress tensor $\Pi_{\mu\nu}$. Correlation functions of the stress tensor can be found by linearizing the bulk action around the AdS$_5$ solution, $g_{\mu\nu} = g^0_{\mu\nu} + \delta g_{\mu\nu}$. Small oscillations of the off-diagonal strain δg^y_x are particularly simple, because the equation of motion for $\phi \equiv g^y_x$ is that of a minimally coupled scalar

$$\frac{1}{\sqrt{-g}}\partial_\mu\left(\sqrt{-g}g^{\mu\nu}\partial_\nu\phi\right)=0\,. \tag{2.110}$$

The wave equation can be obtained using the metric coefficients defined above.

```
(* \sqrt{-g} g^{\mu\nu} \partial_{nu} \Phi(t,z,u) *)
(* ---------------------------------------- *)
SqrtG = Simplify[Sqrt[-Det[metric]], {Ra > 0, T > 0, u > 0}]
dnuPhi = Table[D[Phi[t, z, u], coord[[i]]], {i, 1, n}];
DnuPhi = SqrtG*inversemetric.dnuPhi;

(* Laplacian, up to factor \sqrt{-g} *)
(* ------------------------------- *)
DPhi = FullSimplify[Sum[D[DnuPhi[[nu]], coord[[nu]]], {nu, 1, n}]]

(* harmonic space and time dependence *)
(* ------------------------------- *)
DPhiS =
 DPhi /. { D[Phi[t, z, u], {z, 2}] -> -k^2*fp,
   D[Phi[t, z, u], {t, 2}] -> -w^2*fp,
   D[Phi[t, z, u], {u, 2}] -> fpPP, D[Phi[t, z, u], {u, 1}] -> fpP}
```

In the case of harmonic dependence on the Minkowski coordinates $\delta g_x^y=\phi_k(u)e^{ikx-i\omega t}$ the fluctuations are governed by the wave equation

$$\phi_k''(u)-\frac{1+u^2}{uf(u)}\phi_k'(u)+\frac{\omega^2-k^2f(u)}{(2\pi T)^2uf(u)^2}\phi_k(u)=0\,. \tag{2.111}$$

This differential equation has two linearly independent solutions. The retarded correlation function corresponds to picking a solution that is purely infalling at the horizon [120]. The retarded correlation function $G_R(\omega,k)$ defined in equ. (2.60) is determined by inserting the solution into the Einstein-Hilbert action, and then computing the variation with respect to the boundary value of δg_x^y.

The infalling solution can be expressed as

$$\phi_k(u)=(1-u)^{-i\mathfrak{w}/2}F_k(u) \tag{2.112}$$

where $\mathfrak{w}=\omega/(2\pi T)$ and the first factor describes the near horizon behavior. The function $F_k(u)$ can be obtained as an expansion in $\mathfrak{w}$ and $\mathfrak{k}=k/(2\pi T)$. At second order in $O(\mathfrak{w}$ and $\mathfrak{k}$ the solution is [124]

$$F_k(u)=1-\frac{i\mathfrak{w}}{2}\log\left(\frac{1+u}{2}\right)+\frac{\mathfrak{w}^2}{8}\left\{\left[8-\frac{8\mathfrak{k}^2}{\mathfrak{w}^2}+\log\left(\frac{1+u}{2}\right)\right]\log\left(\frac{1+u}{2}\right)-4Li_2\left(\frac{1-u}{2}\right)\right\}\,. \tag{2.113}$$

In the opposite limit, $\mathfrak{w}\gg1$, the wave equation can be solved using a WKB approximation [125]. For $\mathfrak{k}=0$ the result is

$$\phi_k(u)=\pi\mathfrak{w}^2\frac{u}{\sqrt{1-u^2}}\left[iJ_2\left(2\mathfrak{w}\sqrt{u}\right)-Y_2\left(2\mathfrak{w}\sqrt{u}\right)\right]\,. \tag{2.114}$$

In the intermediate regime the wave equation can be solved numerically. A standard method is to start from the near horizon result given in equ. (2.112) and integrate outwards towards the boundary. The retarded correlation function is given by the variation of the boundary action with respect to the field. For this purpose we consider the quadratic part of the Einstein-Hilbert action and use the AdS/CFT correspondence to express Newton's constant in terms of gauge theory parameters. We find
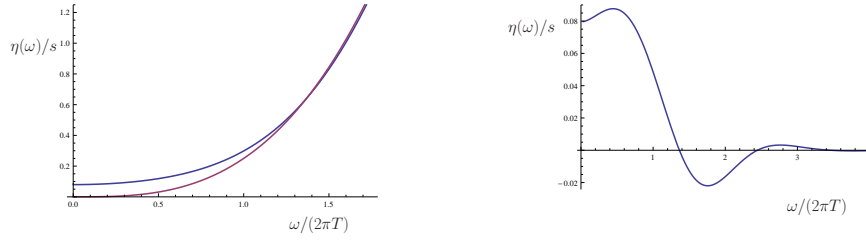
Fig. 2.5 Viscosity spectral function in a $\mathcal{N} = 4$ SUSY Yang Mills plasma. The spectral function is computed in the large N_c limit of a strongly coupled plasma using the AdS/CFT correspondence. The figure in the left panel shows $\eta(\omega)/s$ (blue) and the zero temperature counterpart $\eta_{T=0}(\omega)/s$ (red) as a function of ω. The figure in the right panel shows the finite temperature part $[\eta(\omega) - \eta_{T=0}(\omega)]/s$. The figures were generated using the script described below equ. (2.116).

$$S = -\frac{\pi^2 N^2 T^4}{8} \int du \int d^4x \, \frac{f(u)}{u} \left(\partial_u \phi\right)^2 + \dots . \tag{2.115}$$

The boundary action follows after an integration by parts. The retarded Green function is determined by the second variational derivative with respect to the boundary value of the field [124, 126],

$$G_R(\mathfrak{w}, \mathfrak{k}) = -\frac{\pi^2 N^2 T^4}{4} \left[\frac{f(u)\partial_u \phi_k(u)}{u \phi_k(u)} \right]_{u \to 0} . \tag{2.116}$$

Finally, the spectral function is given by $\eta(\omega, k) = -\omega^{-1} Im\, G_R(\omega, k)$. Below is a short Mathematica script that determines the spectral function numerically.

```
(* equation of motion for minimally coupled scalar *)
(* with harmonic space and time dependence *)
(* --------------------------------------------- *)
f[u_] := 1 - u^2
EomPhi = phi''[u] - (1 + u^2)/(u f[u]) phi'[u]
  + (w^2 - q^2 f[u])/(u f[u]^2) phi[u]

(* boundary solution *)
(* ----------------- *)
phiHorizon[u_] := (1-u)^(-I*w/2)

(* numerically integrate from Horizon to boundary *)
(* ---------------------------------------------- *)
SolPhi[omega_, qq_] := Block[{w = omega, q = qq},
  NDSolve[
    {0 == EomPhi,
     phi[epsH] == phiHorizon[epsH],
```
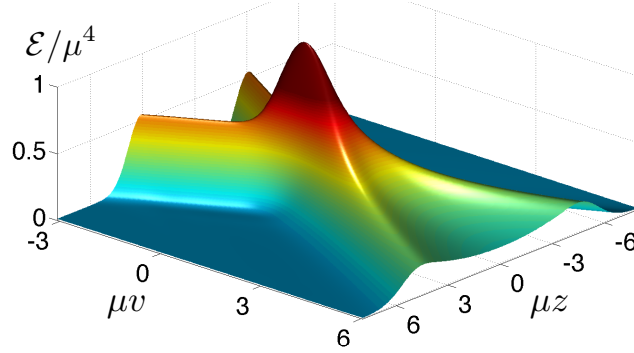
Fig. 2.6 Energy density of colliding shock waves in AdS_5 space [127]. The figure shows the energy density $\mathcal{E}/\mu^4$ on the boundary of AdS_5 as a function of the time coordinate v and the longitudinal direction z. The shocks are infinitely extended in the transverse direction. The parameter μ sets the overall scale.

```
   phi'[epsH] == phiHorizon'[epsH]},
  phi[u],
  {u, epsB, epsH}]][[1, 1, 2]]

(* retarded correlator from boundary action *)
(* --------------------------------------- *)
Gret[omega_, qq_] := (f[u]/u D[solPhi[omega, qq], u]/solPhi[omega, qq] )
 /. {u -> epsB}
```

The spectral function for $k = 0$ is shown in Fig. 2.5. This is an interesting result because it represent a systematic calculation of a real time observable in the strong coupling limit of a quantum field theory. As explained in Sect. 2.4.5 the corresponding lattice calculation is very difficult, and existing results are difficult to improve upon. We also note that the result is quite different from expectations at weak coupling. At weak coupling we expect the spectral function to show a narrow transport peak at zero energy [79].

So far we have only considered calculations very close to equilibrium, corresponding to small perturbations of the AdS_5 Schwarzschild solution. In order to address the problem of initial state dynamics and thermalization we have to consider initial conditions that mimic colliding nuclei. Recent work focuses on colliding shock waves in asymptotically AdS_5 spaces. In the strong coupling limit the evolution of the shock waves is a problem in numerical relativity. Special methods have been developed to deal with problems in AdS space [128]. These methods are quite different from the techniques employed in connection with black hole or neutron star mergers in asymptotically flat Minkowski space time. A typical result is shown in Fig. 2.6. The calculations demonstrate fast "hydrodynamization", that means a rapid decay of non-hydrodynamic modes. At somewhat longer time scales thermal equilibration is achieved. This corresponds to the formation of an event horizon in the bulk. In general, it was realized that there is a fluid-gravity correspondence, an equivalence between dynamic space times containing a horizon and solutions of the Navier-Stokes equation [129]. This correspondence can be used to study, both analytically and numerically, difficult problems in fluid dynamics.

2.6 Outlook and acknowledgments

I hope this brief review provides a flavor of the breadth of computational problems that are related QCD. This includes many issues that are at the forefront of computational physics, like

the sign problem in euclidean QCD at finite baryon density, and the challenge to extract real time correlation functions from the euclidean path integral. It also includes many problems that are of great interest to mathematicians. Both the Yang-Mills existence and mass gap as well as the Navier-Stokes existence and smoothness problems are among the Clay Millenium Prize problems [130, 131]. Interesting work on the Boltzmann equation was recently recognized with a Field medal [132], and gradient flow plays an important role in the proof of the Poincare conjecture [133].

Appendix: Z_2 gauge theory

This is a simple Monte Carlo program for Z_2 gauge theory written by M. Creutz [135].

```c
/* Z_2 lattice gauge simulation */
/* Michael Creutz <creutz@bnl.gov> */
/* http://thy.phy.bnl.gov/~creutz/z2.c */

#include <stdio.h>
#include <stdlib.h>
#include <math.h>

/* the lattice is of dimensions SIZE**4 */
#define SIZE 6
int link[SIZE][SIZE][SIZE][SIZE][4]; /* last index gives link direction */

/* utility functions */
void moveup(int x[],int d) {
 x[d]+=1;
 if (x[d]>=SIZE) x[d]-=SIZE;
 return;
}
void movedown(int x[],int d) {
 x[d]-=1;
 if (x[d]<0) x[d]+=SIZE;
 return;
}
void coldstart(){ /* set all links to unity */
 int x[4],d;
 for (x[0]=0;x[0]<SIZE;x[0]++)
   for (x[1]=0;x[1]<SIZE;x[1]++)
     for (x[2]=0;x[2]<SIZE;x[2]++)
       for (x[3]=0;x[3]<SIZE;x[3]++)
```

```c
      for (d=0;d<4;d++)
    link[x[0]][x[1]][x[2]][x[3]][d]=1;
  return;
}
/* for a random start: call coldstart() and then update once at beta=0 */

/* do a Monte Carlo sweep; return energy */
double update(double beta){
  int x[4],d,dperp,staple,staplesum;
  double bplus,bminus,action=0.0;
  for (x[0]=0; x[0]<SIZE; x[0]++)
    for (x[1]=0; x[1]<SIZE; x[1]++)
      for (x[2]=0; x[2]<SIZE; x[2]++)
        for (x[3]=0; x[3]<SIZE; x[3]++)
          for (d=0; d<4; d++) {
            staplesum=0;
            for (dperp=0;dperp<4;dperp++){
              if (dperp!=d){
                /* move around thusly:
                   dperp     6--5
                   ^         | |
                   |         1--4
                   |         | |
                   -----> d  2--3 */
                /* plaquette 1234 */
                movedown(x,dperp);
                staple=link[x[0]][x[1]][x[2]][x[3]][dperp]
                  *link[x[0]][x[1]][x[2]][x[3]][d];
                moveup(x,d);
                staple*=link[x[0]][x[1]][x[2]][x[3]][dperp];
                moveup(x,dperp);
                staplesum+=staple;
                /* plaquette 1456 */
                staple=link[x[0]][x[1]][x[2]][x[3]][dperp];
                moveup(x,dperp);
                movedown(x,d);
                staple*=link[x[0]][x[1]][x[2]][x[3]][d];
                movedown(x,dperp);
                staple*=link[x[0]][x[1]][x[2]][x[3]][dperp];
                staplesum+=staple;
              }
            }
            /* calculate the Boltzmann weight */
            bplus=exp(beta*staplesum);
            bminus=1/bplus;
            bplus=bplus/(bplus+bminus);
            /* the heatbath algorithm */
            if ( drand48() < bplus ){
              link[x[0]][x[1]][x[2]][x[3]][d]=1;
              action+=staplesum;
            }
            else{
              link[x[0]][x[1]][x[2]][x[3]][d]=-1;
              action-=staplesum;
            }
          }
  action /= (SIZE*SIZE*SIZE*SIZE*4*6);
  return 1.-action;
}

/*****************************/
```

```c
int main(){
 double beta, dbeta, action;
 srand48(1234L); /* initialize random number generator */
 /* do your experiment here; this example is a thermal cycle */
 dbeta=.01;
 coldstart();
 /* heat it up */
 for (beta=1; beta>0.0; beta-=dbeta){
   action=update(beta);
   printf("%g\t%g\n",beta,action);
 }
 printf("\n\n");
 /* cool it down */
 for (beta=0; beta<1.0; beta+=dbeta){
   action=update(beta);
   printf("%g\t%g\n",beta,action);
 }
 printf("\n\n");
 exit(0);
}
```

References

1. R.P. Feynman, A.R. Hibbs, *Quantum Mechanics and Path Integrals* (McGraw-Hill, 1965)
2. N. Metropolis, A.W. Rosenbluth, M.N. Rosenbluth, A.H. Teller, E. Teller, J. Chem. Phys. **21**, 1087 (1953). DOI 10.1063/1.1699114
3. M. Creutz, B. Freedman, Annals Phys. **132**, 427 (1981). DOI 10.1016/0003-4916(81)90074-9
4. E.V. Shuryak, O.V. Zhirov, Nucl. Phys. **B242**, 393 (1984). DOI 10.1016/0550-3213(84)90401-2
5. E.V. Shuryak, Nucl. Phys. **B302**, 621 (1988). DOI 10.1016/0550-3213(88)90191-5
6. T. Schäfer, Instantons and Monte Carlo methods in quantum mechanics (2004). ArXive:hep-lat/0411010
7. M. Jarrell, J.E. Gubernatis, Phys. Rept. **269**, 133 (1996). DOI 10.1016/0370-1573(95)00074-7
8. M. Asakawa, T. Hatsuda, Y. Nakahara, Prog. Part. Nucl. Phys. **46**, 459 (2001). DOI 10.1016/S0146-6410(01)00150-8
9. C. Jarzynski, Physical Review Letters **78**, 2690 (1997). DOI 10.1103/PhysRevLett.78.2690
10. D.J. Gross, F. Wilczek, Phys.Rev.Lett. **30**, 1343 (1973). DOI 10.1103/PhysRevLett.30.1343
11. H.D. Politzer, Phys.Rev.Lett. **30**, 1346 (1973). DOI 10.1103/PhysRevLett.30.1346
12. S.R. Coleman, E.J. Weinberg, Phys.Rev. **D7**, 1888 (1973). DOI 10.1103/PhysRevD.7.1888
13. K. Nakamura, et al., J. Phys. **G37**, 075021 (2010). DOI 10.1088/0954-3899/37/7A/075021
14. M.G. Alford, A. Schmitt, K. Rajagopal, T. Schäfer, Rev. Mod. Phys. **80**, 1455 (2008). DOI 10.1103/RevModPhys.80.1455
15. A. Adams, L.D. Carr, T. Schäfer, P. Steinberg, J.E. Thomas, New J. Phys. **14**, 115009 (2012). DOI 10.1088/1367-2630/14/11/115009
16. P. Braun-Munzinger, V. Koch, T. Schäfer, J. Stachel, Phys. Rept. **621**, 76 (2016). DOI 10.1016/j.physrep.2015.12.003
17. M. Gell-Mann, R.J. Oakes, B. Renner, Phys. Rev. **175**, 2195 (1968). DOI 10.1103/PhysRev.175.2195
18. S.R. Coleman, E. Witten, Phys. Rev. Lett. **45**, 100 (1980). DOI 10.1103/PhysRevLett.45.100
19. G. 't Hooft, NATO Sci. Ser. B **59**, 135 (1980)
20. E.V. Shuryak, Sov. Phys. JETP **47**, 212 (1978). [Zh. Eksp. Teor. Fiz.74,408(1978)]
21. E.V. Shuryak, Phys. Lett. **B78**, 150 (1978). DOI 10.1016/0370-2693(78)90370-2. [Yad. Fiz.28,796(1978)]
22. A.D. Linde, Phys. Lett. **B96**, 289 (1980). DOI 10.1016/0370-2693(80)90769-8
23. R.D. Pisarski, F. Wilczek, Phys. Rev. **D29**, 338 (1984). DOI 10.1103/PhysRevD.29.338
24. Y. Aoki, G. Endrodi, Z. Fodor, S.D. Katz, K.K. Szabo, Nature **443**, 675 (2006). DOI 10.1038/nature05120
25. A. Bazavov, et al., Phys. Rev. **D85**, 054503 (2012). DOI 10.1103/PhysRevD.85.054503
26. Y. Aoki, Z. Fodor, S.D. Katz, K.K. Szabo, Phys. Lett. **B643**, 46 (2006). DOI 10.1016/j.physletb.2006.10.021
27. Y. Aoki, S. Borsanyi, S. Durr, Z. Fodor, S.D. Katz, S. Krieg, K.K. Szabo, JHEP **06**, 088 (2009). DOI 10.1088/1126-6708/2009/06/088
28. A. Bazavov, et al., Phys. Rev. **D90**(9), 094503 (2014). DOI 10.1103/PhysRevD.90.094503
29. M.A. Stephanov, Prog. Theor. Phys. Suppl. **153**, 139 (2004)

30. Z. Fodor, S.D. Katz, JHEP **03**, 014 (2002)
31. C. Allton, S. Ejiri, S. Hands, O. Kaczmarek, F. Karsch, et al., Phys.Rev. **D66**, 074507 (2002). DOI 10.1103/PhysRevD.66.074507
32. F. Karsch, C.R. Allton, S. Ejiri, S.J. Hands, O. Kaczmarek, E. Laermann, C. Schmidt, Nucl. Phys. Proc. Suppl. **129**, 614 (2004). DOI 10.1016/S0920-5632(03)02659-8. [,614(2003)]
33. Z. Fodor, S. Katz, JHEP **0404**, 050 (2004). DOI 10.1088/1126-6708/2004/04/050
34. R.V. Gavai, S. Gupta, Phys. Rev. **D78**, 114503 (2008). DOI 10.1103/PhysRevD.78.114503
35. S. Datta, R.V. Gavai, S. Gupta, Nucl. Phys. **A904-905**, 883c (2013). DOI 10.1016/j.nuclphysa.2013.02. 156
36. P. de Forcrand, O. Philipsen, Phys. Rev. Lett. **105**, 152001 (2010). DOI 10.1103/PhysRevLett.105.152001
37. M.A. Stephanov, K. Rajagopal, E.V. Shuryak, Phys. Rev. Lett. **81**, 4816 (1998)
38. G. Sauer, H. Chandra, U. Mosel, Nucl. Phys. **A264**, 221 (1976). DOI 10.1016/0375-9474(76)90429-2
39. J. Pochodzalla, et al., Phys. Rev. Lett. **75**, 1040 (1995). DOI 10.1103/PhysRevLett.75.1040
40. J.B. Elliott, P.T. Lake, L.G. Moretto, L. Phair, Phys. Rev. **C87**(5), 054622 (2013). DOI 10.1103/PhysRevC. 87.054622
41. M.G. Alford, K. Rajagopal, F. Wilczek, Nucl. Phys. **B537**, 443 (1999). DOI 10.1016/S0550-3213(98) 00668-3
42. T. Schäfer, Nucl. Phys. **B575**, 269 (2000). DOI 10.1016/S0550-3213(00)00063-8
43. T. Schäfer, F. Wilczek, Phys. Rev. Lett. **82**, 3956 (1999). DOI 10.1103/PhysRevLett.82.3956
44. T. Hatsuda, M. Tachibana, N. Yamamoto, G. Baym, Phys. Rev. Lett. **97**, 122001 (2006). DOI 10.1103/ PhysRevLett.97.122001
45. M. Creutz, *Quarks, Gluons, and Lattices* (Cambridge University Press, 1983)
46. I. Montvay, G. Münster, *Quantum Fields on a Lattice* (Cambridge University Press, 1994)
47. J. Smit, *Introduction to Quantum Fields on a Lattice* (Cambridge University Press, 2002)
48. C. Gattringer, C.B. Lang, *Quantum Chromodynamics on the Lattice* (Springer, 2009)
49. H.W. Lin, H.B. Meyer, *Lattice QCD for Nuclear Physics* (Springer, 2014)
50. Z. Fodor, S.D. Katz, The Phase diagram of quantum chromodynamics (2009). ArXiv:0908.3341
51. H.T. Ding, F. Karsch, S. Mukherjee, Thermodynamics of strong-interaction matter from Lattice QCD (2015). ArXiv:1504.05274
52. K.G. Wilson, Phys. Rev. **D10**, 2445 (1974). DOI 10.1103/PhysRevD.10.2445. [,45(1974)]
53. F. Mezzadri, How to generate random matrices from the classical compact groups (2006). ArXiv:math-ph/0609050
54. A. Hasenfratz, P. Hasenfratz, Phys. Lett. **B93**, 165 (1980). DOI 10.1016/0370-2693(80)90118-5. [,241(1980)]
55. G.P. Lepage, in *Strong interactions at low and intermediate energies. Proceedings, 13th Annual Hampton University Graduate Studies, HUGS'98, Newport News, USA, May 26-June 12, 1998* (1998), pp. 49–90
56. U. Wolff, Phys. Rev. Lett. **62**, 361 (1989). DOI 10.1103/PhysRevLett.62.361
57. J.B. Kogut, L. Susskind, Phys. Rev. **D11**, 395 (1975). DOI 10.1103/PhysRevD.11.395
58. D.B. Kaplan, Phys. Lett. **B288**, 342 (1992). DOI 10.1016/0370-2693(92)91112-M
59. H. Neuberger, Phys. Lett. **B417**, 141 (1998). DOI 10.1016/S0370-2693(97)01368-3
60. M. Luscher, in *Modern perspectives in lattice QCD: Quantum field theory and high performance computing. Proceedings, International School, 93rd Session, Les Houches, France, August 3-28, 2009* (2010), pp. 331–399
61. E. Endress, C. Pena, K. Sivalingam, Comput. Phys. Commun. **195**, 35 (2015). DOI 10.1016/j.cpc.2015. 04.017
62. V. Dick, F. Karsch, E. Laermann, S. Mukherjee, S. Sharma, Phys. Rev. **D91**(9), 094504 (2015). DOI 10.1103/PhysRevD.91.094504
63. M. Teper, Phys. Lett. **B171**, 86 (1986). DOI 10.1016/0370-2693(86)91004-X
64. M. Lüscher, JHEP **08**, 071 (2010). DOI 10.1007/JHEP08(2010)071,10.1007/JHEP03(2014)092. [Erratum: JHEP03,092(2014)]
65. A.A. Belavin, A.M. Polyakov, A.S. Schwartz, Yu.S. Tyupkin, Phys. Lett. **B59**, 85 (1975). DOI 10.1016/ 0370-2693(75)90163-X
66. T. Schäfer, E.V. Shuryak, Rev. Mod. Phys. **70**, 323 (1998). DOI 10.1103/RevModPhys.70.323
67. L. Del Debbio, L. Giusti, C. Pica, Phys. Rev. Lett. **94**, 032003 (2005). DOI 10.1103/PhysRevLett.94. 032003
68. M. Ce, C. Consonni, G.P. Engel, L. Giusti, PoS **LATTICE2014**, 353 (2014)
69. E. Poppitz, T. Schäfer, M. Ünsal, JHEP **03**, 087 (2013). DOI 10.1007/JHEP03(2013)087
70. T. Banks, A. Casher, Nucl. Phys. **B169**, 103 (1980). DOI 10.1016/0550-3213(80)90255-2
71. P.H. Ginsparg, K.G. Wilson, Phys. Rev. **D25**, 2649 (1982). DOI 10.1103/PhysRevD.25.2649
72. A. Cherman, T. Schäfer, M. Unsal, Chiral Lagrangian from Duality and Monopole Operators in Compactified QCD (2016). ArXiv:1604.06108

73. M. Cristoforetti, F. Di Renzo, L. Scorzato, Phys. Rev. **D86**, 074506 (2012). DOI 10.1103/PhysRevD.86.074506

74. G. Aarts, L. Bongiovanni, E. Seiler, D. Sexty, JHEP **10**, 159 (2014). DOI 10.1007/JHEP10(2014)159

75. G. Aarts, E. Seiler, I.O. Stamatescu, Phys. Rev. **D81**, 054508 (2010). DOI 10.1103/PhysRevD.81.054508

76. D. Sexty, Phys. Lett. **B729**, 108 (2014). DOI 10.1016/j.physletb.2014.01.019

77. T. Kloiber, C. Gattringer, PoS **LATTICE2013**, 206 (2014)

78. T. Schäfer, D. Teaney, Rept. Prog. Phys. **72**, 126001 (2009). DOI 10.1088/0034-4885/72/12/126001

79. T. Schäfer, Ann. Rev. Nucl. Part. Sci. **64**, 125 (2014). DOI 10.1146/annurev-nucl-102313-025439

80. F. Karsch, H.W. Wyld, Phys. Rev. **D35**, 2518 (1987). DOI 10.1103/PhysRevD.35.2518

81. H.B. Meyer, Phys. Rev. **D76**, 101701 (2007). DOI 10.1103/PhysRevD.76.101701

82. H.B. Meyer, Phys. Rev. Lett. **100**, 162001 (2008). DOI 10.1103/PhysRevLett.100.162001

83. S. Sakai, A. Nakamura, PoS **LAT2007**, 221 (2007). DOI 10.1063/1.2729742. [AIP Conf. Proc.893,5(2007)]

84. G. Aarts, C. Allton, J. Foley, S. Hands, S. Kim, Phys. Rev. Lett. **99**, 022002 (2007). DOI 10.1103/PhysRevLett.99.022002

85. G. Aarts, PoS **LAT2007**, 001 (2007)

86. G. Aarts, C. Allton, J. Foley, S. Hands, S. Kim, Nucl. Phys. **A785**, 202 (2007). DOI 10.1016/j.nuclphysa.2006.11.148

87. H.B. Meyer, JHEP **08**, 031 (2008). DOI 10.1088/1126-6708/2008/08/031

88. P. Romatschke, D.T. Son, Phys. Rev. **D80**, 065021 (2009). DOI 10.1103/PhysRevD.80.065021

89. P.B. Arnold, G.D. Moore, L.G. Yaffe, JHEP **11**, 001 (2000). DOI 10.1088/1126-6708/2000/11/001

90. P. Kovtun, D.T. Son, A.O. Starinets, Phys. Rev. Lett. **94**, 111601 (2005). DOI 10.1103/PhysRevLett.94.111601

91. P. Romatschke, Int. J. Mod. Phys. **E19**, 1 (2010). DOI 10.1142/S0218301310014613

92. L. Rezzolla, O. Zanotti, *Relativistic Hydrodynamics* (Oxford University Press, 2013)

93. S. Jeon, U. Heinz, Int. J. Mod. Phys. **E24**(10), 1530010 (2015). DOI 10.1142/S0218301315300106

94. P. Colella, P.R. Woodward, J. Comp. Phys. **54**, 174 (1984)

95. J.M. Blondin, E.A. Lufkin, Astrophys. J. Supp. Ser. **88**, 589 (1993)

96. T. Schäfer, Phys. Rev. **A82**, 063629 (2010). DOI 10.1103/PhysRevA.82.063629

97. W. Florkowski, R. Ryblewski, Phys. Rev. **C83**, 034907 (2011). DOI 10.1103/PhysRevC.83.034907

98. M. Martinez, M. Strickland, Nucl. Phys. **A848**, 183 (2010). DOI 10.1016/j.nuclphysa.2010.08.011

99. M. Bluhm, T. Schäfer, Phys. Rev. **A92**(4), 043602 (2015). DOI 10.1103/PhysRevA.92.043602

100. M. Bluhm, T. Schäfer, Phys. Rev. Lett. **116**(11), 115301 (2016). DOI 10.1103/PhysRevLett.116.115301

101. P. Romatschke, M. Mendoza, S. Succi, Phys. Rev. **C84**, 034903 (2011). DOI 10.1103/PhysRevC.84.034903

102. J. Brewer, M. Mendoza, R.E. Young, P. Romatschke, Phys. Rev. **A93**(1), 013618 (2016). DOI 10.1103/PhysRevA.93.013618

103. L.P. Kadanoff, G. Baym, *Quantum Statistical Mechanics* (W. A. Benjamin, 1962)

104. G.F. Bertsch, S. Das Gupta, Phys. Rept. **160**, 189 (1988). DOI 10.1016/0370-1573(88)90170-6

105. T. Lepers, D. Davesne, S. Chiacchiera, M. Urban, Phys. Rev. **A82**, 023609 (2010). DOI 10.1103/PhysRevA.82.023609

106. S.A. Bass, et al., Prog. Part. Nucl. Phys. **41**, 255 (1998). DOI 10.1016/S0146-6410(98)00058-1. [Prog. Part. Nucl. Phys.41,225(1998)]

107. O. Buss, T. Gaitanos, K. Gallmeister, H. van Hees, M. Kaskulov, O. Lalakulich, A.B. Larionov, T. Leitner, J. Weil, U. Mosel, Phys. Rept. **512**, 1 (2012). DOI 10.1016/j.physrep.2011.12.001

108. W. Ehehalt, W. Cassing, Nucl. Phys. **A602**, 449 (1996). DOI 10.1016/0375-9474(96)00097-8

109. K. Geiger, B. Muller, Nucl. Phys. **B369**, 600 (1992). DOI 10.1016/0550-3213(92)90280-O

110. Z. Xu, C. Greiner, Phys. Rev. **C71**, 064901 (2005). DOI 10.1103/PhysRevC.71.064901

111. L.D. McLerran, R. Venugopalan, Phys. Rev. **D49**, 2233 (1994). DOI 10.1103/PhysRevD.49.2233

112. A.H. Mueller, D.T. Son, Phys. Lett. **B582**, 279 (2004). DOI 10.1016/j.physletb.2003.12.047

113. S. Mrowczynski, B. Schenke, M. Strickland, (2016)

114. J. Berges, A. Rothkopf, J. Schmidt, Phys. Rev. Lett. **101**, 041603 (2008). DOI 10.1103/PhysRevLett.101.041603

115. K. Dusling, T. Epelbaum, F. Gelis, R. Venugopalan, Nucl. Phys. **A850**, 69 (2011). DOI 10.1016/j.nuclphysa.2010.11.009

116. D.F. Litim, C. Manuel, Phys. Rept. **364**, 451 (2002). DOI 10.1016/S0370-1573(02)00015-7

117. S.K. Wong, Nuovo Cim. **A65**, 689 (1970). DOI 10.1007/BF02892134

118. C.R. Hu, B. Muller, Phys. Lett. **B409**, 377 (1997). DOI 10.1016/S0370-2693(97)00851-4

119. J.M. Maldacena, Int. J. Theor. Phys. **38**, 1113 (1999). DOI 10.1023/A:1026654312961. [Adv. Theor. Math. Phys.2,231(1998)]

120. D.T. Son, A.O. Starinets, Ann. Rev. Nucl. Part. Sci. **57**, 95 (2007). DOI 10.1146/annurev.nucl.57.090506.123120

121. S.S. Gubser, A. Karch, Ann. Rev. Nucl. Part. Sci. **59**, 145 (2009). DOI 10.1146/annurev.nucl.010909.083602

122. J. Casalderrey-Solana, H. Liu, D. Mateos, K. Rajagopal, U.A. Wiedemann, (2011)

123. O. DeWolfe, S.S. Gubser, C. Rosen, D. Teaney, Prog. Part. Nucl. Phys. **75**, 86 (2014). DOI 10.1016/j.ppnp.2013.11.001

124. G. Policastro, D.T. Son, A.O. Starinets, JHEP **09**, 043 (2002). DOI 10.1088/1126-6708/2002/09/043

125. D. Teaney, Phys. Rev. **D74**, 045025 (2006). DOI 10.1103/PhysRevD.74.045025

126. D.T. Son, A.O. Starinets, JHEP **03**, 052 (2006). DOI 10.1088/1126-6708/2006/03/052

127. P.M. Chesler, L.G. Yaffe, Phys. Rev. Lett. **106**, 021601 (2011). DOI 10.1103/PhysRevLett.106.021601

128. P.M. Chesler, L.G. Yaffe, JHEP **07**, 086 (2014). DOI 10.1007/JHEP07(2014)086

129. M. Rangamani, Class. Quant. Grav. **26**, 224003 (2009). DOI 10.1088/0264-9381/26/22/224003

130. A. Jaffe, E. Witten, Quantum Yang Mills Theory, Official Description of Millenium Prize Problems (2000). www.claymath.org

131. C. Fefferman, Existence and smoothness of the Navier-Stokes Equation, Official Description of Millenium Prize Problems (2000). www.claymath.org

132. C. Mouhot, C. Villani, Acta Mathematica **207**, 29 (2011). DOI 10.1007/s11511-011-0068-9

133. G. Perelman, The entropy formula for the Ricci flow and its geometric applications (2002). ArXiv:math/0211159 [math.DG]

134. C. Shen, Z. Qiu, H. Song, J. Bernhard, S. Bass, U. Heinz, Comput. Phys. Commun. **199**, 61 (2016). DOI 10.1016/j.cpc.2015.08.039

135. M. Creutz, Computers in Science & Engineering **March/April 2004**, 80 (2004)

Chapter 3
Lattice quantum chromodynamics approach to nuclear physics

Tetsuo Hatsuda

Abstract Each chapter should be preceded by an abstract (10–15 lines long) that summarizes the content. The abstract will appear *online* at www.SpringerLink.com and be available with unrestricted access. This allows unregistered users to read the abstract as a teaser for the complete chapter. As a general rule the abstracts will not appear in the printed version of your book unless it is the style of your particular book or that of the series to which your book belongs.

Please use the 'starred' version of the new Springer abstract command for typesetting the text of the online abstracts (cf. source file of this chapter template abstract) and include them with the source files of your manuscript. Use the plain abstract command if the abstract is also to appear in the printed version of the book.

3.1 General Introduction

3.2 Continuum quantum chromodynamics: basics

3.3 Lattice quantum chromodynamics: basics

3.4 Lattice quantum chromodynamics: applications

3.5 Hadron interactions: basics

Tetsuo Hatsuda
Name of institution and address, e-mail: name@email.address

Appendix

References

1. First reference

skmattwod()
skvectwod()
subalign[1][]

$$\tag{3.1a}$$

spliteq

$$\tag{3.2}$$

Chapter 4
General aspects of effective field theories and few-body applications

Hans-Werner Hammer and Sebastian König

Abstract Effective field theory provides a powerful framework to exploit a separation of scales in physical systems. In these lectures, we discuss some general aspects of effective field theories and their application to few-body physics. In particular, we consider an effective field theory for non-relativistic particles with resonant short-range interactions where certain parts of the interaction need to be treated nonperturbatively. As an application, we discuss the so-called *pionless effective field theory* for low-energy nuclear physics. The extension to include long-range interactions mediated by photon and pion-exchange is also addressed.

4.1 Introduction: dimensional analysis and the separation of scales

Effective field theory (EFT) provides a general approach to calculate low-energy observables by exploiting scale separation. The origin of the EFT approach can be traced to the development of the renormalization group [1] and the intuitive understanding of ultraviolet divergences in quantum field theory [2]. A concise formulation of the underlying principle was given by Weinberg [3]: If one starts from the most general Lagrangian consistent with the symmetries of the underlying theory, one will get the most general S-matrix consistent with these symmetries. As a rule, such a most general Lagrangian will contain infinitely many terms. Only together with a power counting scheme that orders these terms according to their importance at low energies one obtains a predictive paradigm for a low-energy theory.

The Lagrangian and physical observables are typically expanded in powers of a low-momentum scale $M_{\rm lo}$, which can be a typical external momentum or an internal infrared scale, over a high-momentum scale $M_{\rm hi} \gg M_{\rm lo}$.[1] This expansion provides the basis for the power counting scheme. It depends on the system to which physical scales $M_{\rm hi}$ and $M_{\rm lo}$ correspond to.

As an example, we take a theory that is made of two particle species, two light bosons with mass $M_{\rm lo}$ and heavy bosons with mass $M_{\rm hi} \gg M_{\rm lo}$.[2] We consider now soft processes in which the energies and momenta are of the order of the light particle mass (the so-called soft scale).

Hans-Werner Hammer

Institut für Kernphysik, Technische Universität Darmstadt, 64289 Darmstadt, Germany, e-mail: `Hans-Werner.Hammer@physik.tu-darmstadt.de`,

Sebastian König

Department of Physics, The Ohio State University, Columbus, Ohio 43210, USA e-mail: `koenig.389@osu.edu`

[1] Note there are often more than two scales, which complicates the power counting. Here we focus on the simplest case to introduce the general principle.

[2] For further examples, see the lectures by Kaplan [4, 5].
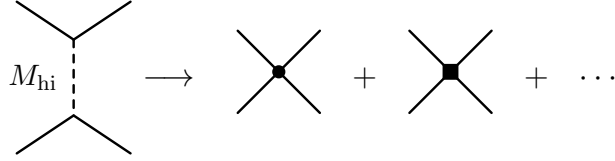
Fig. 4.1 Expansion of heavy-particle exchange between light particles in terms of contact interactions between light particles. The solid and dashed lines denote light and heavy particles, respectively. The circle and square denote contact interactions with zero and two derivatives, in order.

Under such conditions, the short-distance physics related to the heavy particles can never be resolved explicitly. However, it can be represented by light-particle contact interactions with increasing dimension (number of derivatives). To illustrate this, we consider the scattering of the light particles mediated by heavy-particle exchange, with g the heavy-light coupling constant. The corresponding interaction Lagrangian is given by

$$\mathscr{L}_{\text{int}} = g\left(\chi^\dagger \phi\phi + \phi^\dagger\phi^\dagger\chi\right),$$ (4.1)

where ϕ denotes the light boson field and χ is the heavy boson field. As depicted in Fig. 4.1, one can represent such exchange diagrams by a sum of local operators of the light fields with increasing number of derivatives. In a symbolic notation, the leading order scattering amplitude can be written as

$$T \sim \frac{g^2}{M_{\text{hi}}^2 - q^2} = \frac{g^2}{M_{\text{hi}}^2} + \frac{g^2 q^2}{M_{\text{hi}}^4} + \cdots,$$ (4.2)

with q^2 the squared 4-momentum transfer. We will come back to this example in more detail in section 4.2.

In many cases, the corresponding high-energy theory is either not known or can not easily be solved. Still, EFT offers a predictive and systematic framework for performing calculations in the light-particle sector. We denote by Q a typical energy or momentum of the order of M_{lo} and by M_{hi} the hard scale where the EFT will break down. In many cases, this scale is set by the masses of the heavy particles not considered explicitly and thus replaced by contact interactions as in the example above. In such a setting, any matrix element or Green's function admits an expansion in the small parameter Q/M_{hi} [3]

$$\mathscr{M} = \sum_\nu \left(\frac{Q}{M_{\text{hi}}}\right)^\nu \mathscr{F}\left(\frac{Q}{\Lambda}, g_i\right)$$ (4.3)

where $\mathscr{F}$ is a function of order one (this is the naturalness assumption), Λ a regularization scale (related to the UV divergences appearing in the loop graphs) and the g_i denotes a collection of coupling constants, often called low-energy constants (LECs). These parameterize (encode) the unknown high-energy (short-distance) physics and must be determined by a fit to data (or can be directly calculated if the corresponding high-energy theory is known/can be solved). The counting index ν in general depends on the fields in the effective theory, the number of derivatives and the number of loops. This defines the so-called power counting which allows to categorize all contributions to any matrix element at a given order. It is important to stress that ν must be bounded from below to define a sensible EFT. In QCD, *e.g.*, this is a consequence of the spontaneous breaking of chiral symmetry.

The contributions with the lowest possible value of ν define the so-called leading order (LO) contribution, the first corrections with the second smallest allowed value of ν the next-to-leading order (NLO) terms and so on. In contrast to more conventional perturbation theory, the small parameter is not a dimensionless coupling constant (like, *e.g.*, in Quantum Electro-

dynamics) but rather a ratio of two scales. Typically, one expands in the ratio of a small energy or momentum and the hard scale M_{hi}. A prototype of such a perturbative EFT is chiral perturbation theory that exploits the strictures of the spontaneous and explicit chiral symmetry breaking in QCD [6, 7]. Here, the light degrees of freedom are the pions, that are generated through the symmetry violation. Heavier particles like *e.g.* vector mesons only appear indirectly as they generate local four-pion interactions with four, six, *etc.* derivatives.

In these lectures, we also consider EFTs with bound states, where certain contributions need to resummed nonperturbatively. In section 4.2, we start with some general considerations. This is followed by the explicit discussion of an EFT for non-relativistic bosons with short-range interactions and large scattering length in section 4.3. The extension of this framework to low-energy nucleons is presented in section 4.4 Finally, we will discuss the inclusion of long-range interactions mediated by photon and pion exchange in 4.5.

4.2 Theoretical foundations of effective field theory

As mentioned in the introduction, effective field theories are described by writing down Lagrangians with an infinite number of terms, restricted only by symmetry considerations, and ordered by a scheme referred to as "power counting." In this section, we discuss the meaning and importance of all these ingredients.

4.2.1 Top-down vs. bottom-up approaches

Generally, there are two different motivations for working with an EFT. Given a known quantum field theory, which can be solved to compute a given quantity of interest, it can be beneficial to switch to an effective description valid only in a limited energy regime simply because carrying out the calculation is more efficient with the effective theory. With such a solvable underlying theory, the parameters ("low-energy constants") of the effective theory can be computed directly by considering some number of (simple) processes, *i.e.*, one does not need experimental input beyond what was needed to fix the parameters of the underlying theory. This approach, based on a reduction of expressions from the underlying to the effective picture is called a "top-down" approach.

An alternative procedure, somewhat closer to what we described at the outset, is to start "bottom up," *i.e.*, by simply writing down the effective Lagrangian directly—or more precisely only those terms of the infinitely many which are needed to achieve a given desired accuracy. Being able to that of course requires that as a first step one has already figures out which terms are allowed and how they should be ordered.

Our approach here is to work top down in the pedagogical sense, *i.e.*, postpone the discussion of the bottom-up approach and its ingredients until later in this section, and instead dive into the matter starting with examples that show how effective low-energy theories can arise from more fundamental ones. We assume that the reader is familiar the material from a standard (relativistic) quantum field theory course.

4.2.1.1 Integrating out exchange particles: part I

As was also mentioned in the introduction, the very first step in the construction of an EFT is to identify the relevant degrees of freedom to work with, as well as those which are irrelevant

and thus do not need to be kept explicitly (with emphasis on the last word, because *implicitly* the physics of left-out degrees of freedom should and does enter in the effective description).

Let us illustrate this by showing how integrating out a "heavy" particle gives rise to contact interactions between the remaining degrees of freedom (*cf.* the example in section 4.1). We stress that the particles which are integrated out can in fact be lighter than what is left (like it is the case in pionless EFT)—what really matters for the procedure is which particles are assumed to appear in *asymptotic* states, and what is the typical energy/momentum scale between those. In that spirit, we are not making explicit assumptions about the mass hierarchy of the particles in the following. For the illustration here, we consider two scalar fields (complex and relativistic) with Yukawa interactions and start with a Lagrangian for two species:

$$\mathscr{L} = -\phi^\dagger \left(\Box + m_\phi^2\right)\phi - \chi^\dagger \left(\Box + m_\chi^2\right)\chi + g\left(\phi^\dagger \phi^\dagger \chi + \text{h.c.}\right). \tag{4.4}$$

Suppose now we are only interested in interactions between ϕ particles at energy scales much smaller than m_χ, so that the explicit χ exchange generated by the interaction term in Eq. (4.4) cannot be resolved. In that case, we can derive a new effective Lagrangian that only contains ϕ degrees of freedom, a process referred to as "integrating out" the field χ stemming from its implementation in the path-integral formalism. In effect, that amounts to using the equations of motion, which we do here. From the Euler-Lagrange equation for $\chi^\dagger$, we directly get

$$\chi = \left(\Box + m_\chi^2\right)^{-1} g\phi\phi. \tag{4.5}$$

Defining the Klein-Gordon propagator

$$D_\chi(x-y) = \int \frac{\mathrm{d}^4 p}{(2\pi)^4} e^{-\mathrm{i}p(x-y)} \frac{\mathrm{i}}{p^2 - m_\chi^2 + \mathrm{i}\varepsilon}, \tag{4.6}$$

satisfying

$$\left(\Box + m_\chi^2\right) D_\chi(x-y) = -\mathrm{i}\delta^{(4)}(x-y), \tag{4.7}$$

we can write out Eq. (4.5) in configuration space as

$$\chi(x) = \mathrm{i}g \int \mathrm{d}^4 y\, D_\chi(x-y)\phi(y)\phi(y). \tag{4.8}$$

Inserting this back into the Lagrangian (4.4), we obtain

$$\mathscr{L}(x) = -\phi^\dagger(x)\left(\Box + m_\phi^2\right)\phi(x) - \mathrm{i}g^2\phi^\dagger(x)\phi^\dagger(x)\int \mathrm{d}^4 y\, D_\chi(x-y)\phi(y)\phi(y), \tag{4.9}$$

where we have written out the spacetime dependence of all fields and used Eq. (4.7) to cancel the terms involving $\chi^\dagger(x)$. So far, we have made only exact manipulations, but the resulting Lagrangian (4.9) is *non-local*, *i.e.*, it depends on fields evaluated at different spacetime points. To simplify it further, we want to exploit the fact that χ is considered "heavy" compared to the scales we want to describe. Mathematically, this means that $D_\chi(x-y)$ is peaked at distances that are small compared to $1/m_\chi^2$. There are several ways to implement this knowledge. A particularly intuitive version is to expand the propagator (4.6) in momentum space,

$$\frac{\mathrm{i}}{p^2 - m_\chi^2 + \mathrm{i}\varepsilon} = \frac{-\mathrm{i}}{m_\chi^2}\left(1 + \frac{p^2}{m_\chi^2} + \cdots\right), \tag{4.10}$$

and then Fourier-transform back to configuration space. The first term gives a simple delta function, and terms with powers of p^2 induce operators with derivatives acting on $\delta(x-y)$. Inserting the leading term into Eq. (4.9), we arrive at the effective *local* Lagrangian

$$\mathscr{L}_{\text{eff}}(x) = -\phi^\dagger(x)\left(\Box + m_\phi^2\right)\phi(x) - \frac{g^2}{m_\chi^2}\phi^\dagger(x)\phi^\dagger(x)\phi(x)\phi(x) + \cdots. \tag{4.11}$$

The ellipses contain operators with derivatives acting on $\phi(x)$, obtained from those acting on the delta functions from the propagator after integrating by parts. A diagrammatic illustration of the procedure is shown in Fig. 4.2.
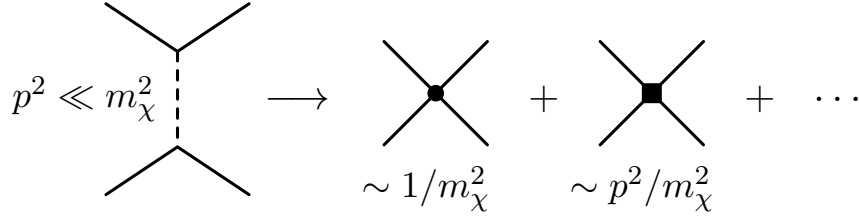
Fig. 4.2 Chain of contact interactions obtained by integrating out an exchange particle.

We note that an alternative derivation of the above result, discussed for example in Ref. [8], is given by Taylor-expanding the field product $\phi(y)\phi(y)$ about $y = x$ under the integral and then using the properties of the propagator. This directly gives terms with an increasing number of derivatives acting on $\phi^\dagger(x)\phi^\dagger(x)$, and those with an odd number of derivatives are found to vanish, in agreement with Eq. (4.10) featuring only even powers of p^2.

4.2.1.2 Emergence of many-body forces

We now add a third field Φ to the Lagrangian:

$$\mathscr{L} = -\phi^\dagger\left(\Box + m_\phi^2\right)\phi - \chi^\dagger\left(\Box + m_\chi^2\right)\chi - \Phi^\dagger\left(\Box + m_\Phi^2\right)\Phi$$
$$+ g\left(\phi^\dagger\phi^\dagger\chi + \text{h.c.}\right) + g'\left(\Phi^\dagger\phi\chi + \text{h.c.}\right). \tag{4.12}$$

The new interaction term is chosen such that Φ can "decay" into a ϕ and a χ, thus acting like a heavier version of the ϕ. In spite of the simplicity of this bosonic toy model, it is useful to think about ϕ and Φ as the nucleon and its Δ excitation, respectively, and about χ as a pion field. If we first integrate out the Φ field following the procedure described in the previous section, we find

$$\Phi(x) = \mathrm{i}g' \int \mathrm{d}^4 y\, D_\Phi(x - y)\phi(y)\chi(y), \tag{4.13}$$

and thus

$$\mathscr{L}_{\text{eff}} = -\phi^\dagger\left(\Box + m_\phi^2\right)\phi - \chi^\dagger\left(\Box + m_\chi^2\right)\chi + g\left(\phi^\dagger\phi^\dagger\chi + \text{h.c.}\right) + \frac{g'^2}{m_\Phi^2}\phi^\dagger\chi^\dagger\phi\chi + \cdots, \tag{4.14}$$

where we have only kept the leading (no derivatives) induced contact interaction. Proceeding as before for the χ field, we now get

$$\left(\Box + m_\chi^2\right)\chi = g\phi\phi + \frac{g'^2}{m_\Phi^2}\phi^\dagger\phi\chi + \cdots. \tag{4.15}$$

This can no longer be solved exactly because we now have a χ on the right-hand side. However, using the general operator identify

$$\left(\hat{A} - \hat{B}\right)^{-1} = \hat{A}^{-1} + \hat{A}^{-1}\hat{B}\hat{A}^{-1} + \cdots, \tag{4.16}$$

we can write down a formal iterative solution:

$$\chi = \left(\Box + m_\chi^2\right)^{-1} g\phi\phi + \left(\Box + m_\chi^2\right)^{-1} \frac{g'^2}{m_\Phi^2}\phi^\dagger\phi \left(\Box + m_\chi^2\right)^{-1} g\phi\phi + \cdots, \tag{4.17}$$

with each of the inverse differential operators giving a propagator when written out. Those, in turn, each give factors of $-\mathrm{i}/m_\Phi^2$ times a delta function, plus additional terms with derivatives.

4.1. *E*xercise: Derive Eq. (4.16).

Inserting the above result back into the Eq. (4.14), we see that in addition to the two-body contact operator $(\phi^\dagger\phi)^2$ obtained previously, we now also get all kinds of higher-body interactions. For example, we get a three-body force through

$$\frac{g'^2}{m_\Phi^2}\phi^\dagger\chi^\dagger\phi\chi \rightarrow \frac{g'^2 g^2}{m_\Phi^2 m_\chi^4}(\phi^\dagger\phi)^3. \tag{4.18}$$

In Fig. 4.3 it is illustrated diagrammatically how such a term arises subsequently, starting from a diagram derived from the original Lagrangian (4.12) with three fields.
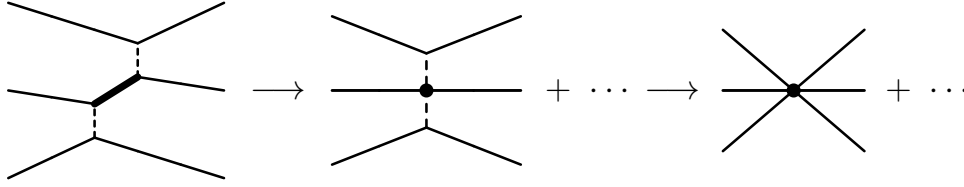
Fig. 4.3 Emergence of a three-body contact interaction.

4.2.2 Nonrelativistic field theory

Relativistic effects and exact Lorentz invariance are not crucial to describe systems at low energies, where "low" means "much smaller than the particles' rest mass." Based on that, one typically starts with a nonrelativistic framework and writes down effective Lagrangians of so-called Schrödinger fields, *e.g.*,

$$\mathscr{L}_{\phi,\text{free}} = \phi^\dagger \left(\mathrm{i}\partial_t + \frac{\nabla^2}{2m}\right)\phi \tag{4.19}$$

for a free scalar particle, where $\phi^\dagger(t,\mathbf{x})$ is the field operator that creates a particle at time t and position $\mathbf{x}$, and $\phi(t,\mathbf{x})$) correspondingly destroys it. Written in terms of momentum-space ladder operators $\hat{a}_\mathbf{p}, \hat{a}_\mathbf{p}^\dagger$ (as they appear in standard many-body quantum mechanics), we have

$$\phi(t,\mathbf{x}) = \int \frac{\mathrm{d}^3 p}{(2\pi)^3}\hat{a}_\mathbf{p}\, \mathrm{e}^{-\mathrm{i}E_\mathbf{p}t}\mathrm{e}^{\mathrm{i}\mathbf{p}\cdot\mathbf{x}}, \tag{4.20}$$

and analogously for $\phi^\dagger(t,\mathbf{x})$. Note that here $E_\mathbf{p} = \mathbf{p}^2/(2m)$ is the kinetic energy alone, and that creation and destruction operators are completely separated. Intuitively, this makes perfect sense: At low energies, virtual particle-antiparticle pairs would be highly off-shell, thus giving rise to very short-range effects that we can simply describe as contact interactions. Other effects, such as self-energy corrections to the particle mass, are automatically accounted for by

using the physical value for m in Eq. (4.19). With this in mind, one can proceed in the bottom-up approach and construct an interacting theory by supplementing the free Lagrangian with all allowed contact operators. In particular, like Eq. (4.19) they should all be invariant under Galilei transformations, the low-energy remnant of the Poincaré group. Before we come back to this, however, we find it instructive to explicitly consider the low-energy limit of a relativistic theory.

4.2.2.1 Nonrelativistic limit of a bosonic field

Let us make the connection of Eq. (4.19) to a relativistic complex Klein–Gordon field Φ, the Lagrangian for which can be written as

$$\mathscr{L}_{\varphi,\text{free}} = -\varphi^\dagger \left(\partial_t^2 - \nabla^2 + m^2 \right) \varphi \,. \tag{4.21}$$

Using integration by parts, this can be shown to be equivalent to the more common form written with $(\partial_\mu \varphi^\dagger)(\partial^\mu \varphi)$. This implies the Klein–Gordon equation for the field operator,

$$\left(\partial_t^2 - \nabla^2 + m^2 \right) \varphi = 0 \,, \tag{4.22}$$

the most general solution of which is typically written as (with a four-vectors $x = (t, \mathbf{x})$, $p = (p_0, \mathbf{p})$, and a Lorentz-invariant integration measure)

$$\varphi(x) = \int \frac{\mathrm{d}^3 p}{(2\pi)^3} \frac{1}{\sqrt{2\omega_\mathbf{p}}} \left(\hat{a}_\mathbf{p} \, \mathrm{e}^{-\mathrm{i} p \cdot x} + \hat{b}_\mathbf{p}^\dagger \, \mathrm{e}^{\mathrm{i} p \cdot x} \right) \bigg|_{p_0 = \omega_\mathbf{p}} \,, \tag{4.23}$$

where $\omega_\mathbf{p} = \sqrt{\mathbf{p}^2 + m^2}$. With this convention where p_0 is chosen positive, modes created by $\hat{a}_\mathbf{p}^\dagger$ correspond to particles (propagating forward in time), whereas $\hat{b}_\mathbf{p}^\dagger$ creates an antiparticle (positive-energy state propagating backwards in time). That we have both stems from the fact that the complex scalar field corresponds to two real ones (completely decoupled in the absence of interactions), each of which comes with its own pair of creation and annihilation operators. To take the nonrelativistic limit, we have to consider the particle and antiparticles separately. Defining

$$\varphi_a(x) = \int \frac{\mathrm{d}^3 p}{(2\pi)^3} \frac{1}{\sqrt{2\omega_\mathbf{p}}} \hat{a}_\mathbf{p} \, \mathrm{e}^{-\mathrm{i} p \cdot x} \bigg|_{p_0 = \omega_\mathbf{p}} \equiv \mathrm{e}^{-\mathrm{i} m t} \phi_a(x) \,, \tag{4.24}$$

and plugging this into the Klein–Gordon equation, we get

$$\mathrm{e}^{-\mathrm{i} m t} \left[\partial_t^2 - 2\mathrm{i} m \partial_t - \nabla^2 \right] \phi_a(x) = 0 \,, \tag{4.25}$$

where the quadratic mass term has canceled. Since $\phi_a(x) = \mathrm{e}^{\mathrm{i} m t} \varphi_a(x)$, we see from Eq. (4.24) that in the Fourier transform each time derivative acting on $\phi_a(x)$ brings down a factor

$$\omega_p - m = \sqrt{\mathbf{p}^2 + m^2} - m \approx \mathbf{p}^2 / (2m) \,, \tag{4.26}$$

i.e., just the kinetic energy $E_\mathbf{p}$ up to corrections of higher order in $1/m$. In the nonrelativistic limit, $E_\mathbf{p} \ll m$, so we see that we can neglect the quadratic time derivative in Eq. (4.25) compared to the other two terms in Eq. (4.25), and then recover the Schrödinger equation for ϕ_a:

$$\left(\mathrm{i}\partial_t + \frac{\nabla^2}{2m}\right)\phi_a(x) = 0.$$ (4.27)

This establishes the connection to our $\phi(t,\mathbf{x})$ in Eq. (4.19) when we insert an additional factor $\sqrt{2m}$ in the field redefinition to account for the otherwise different normalizations. For the antiparticles, we can carry out an analogous procedure, except that we have to choose the opposite sign for the mass-dependent phase in the field redefinition analogous to Eq. (4.24) because the antiparticle part of $\varphi(x)$ comes with a factor $\mathrm{e}^{+\mathrm{i}p\cdot x}$.

4.2.2.2 Nonrelativistic fermions

For relativistic Dirac fermions, the nonrelativistic reduction can be carried out with the help of a so-called Foldy-Wouthuysen transformation. The idea behind the approach is to decouple the particle and antiparticle modes contained together in a four-spinor ψ through a sequence of unitary transformations. In the following, we demonstrate this procedure, using an *interacting* model theory to also illustrate what happens to interaction terms in the nonrelativistic limit. Since it will be useful to motivate the pionless EFT discussed in Sec. 4.4, we start with a Lagrangian of the form

$$\mathscr{L} = \bar{\psi}\left(\mathrm{i}\partial - M_N\right)\psi + \frac{1}{2}(\partial^\mu\pi)\cdot(\partial_\mu\pi) - \frac{1}{2}m_\pi^2\pi^2 + \frac{1}{2}(\partial^\mu\sigma)\cdot(\partial_\mu\sigma) - \frac{1}{2}m_\sigma^2\sigma^2$$
$$- g\bar{\psi}(\sigma - \mathrm{i}\gamma^5\tau\cdot\pi)\psi, \quad (4.28)$$

where the nucleon field ψ is an isospin doublet of Dirac spinors, π is an isospin triplet, and σ is an isoscalar. A Lagrangian of this form (plus additional interaction terms among σ and π), can be obtained from a linear sigma model after spontaneous symmetry breaking (see, for example, [8], Chapter I) and augmented by an explicit mass term for π.[3] We denote the Pauli matrices in spin and isospin space as $\sigma = (\sigma^i)$ and $\tau = (\tau^\lambda)$, respectively. For the gamma matrices we use the standard (Dirac) representation:

$$\gamma^0 = \mathbf{1}00-\mathbf{1} \ , \ \ \gamma^i = 0\sigma^i - \sigma^i 0 \ , \ \ \gamma^5 = 0\mathbf{1}\mathbf{1}0.$$ (4.29)

To perform the nonrelativistic reduction, we start by separating odd and even operators, which are two-by-two block matrices in Dirac space. The result is

$$\mathscr{L}_\psi = \psi^\dagger\left(\hat{E} + \hat{O} - \gamma^0 M_N\right)\psi,$$ (4.30)

where

$$\hat{E} = \mathrm{i}\partial_t - g\sigma 00\mathrm{i}\partial_t + g\sigma \ \ \text{and} \ \ \hat{O} = 0-\mathrm{i}\sigma\cdot\nabla + \mathrm{i}g\tau\cdot\pi - \mathrm{i}\sigma\cdot\nabla - \mathrm{i}g\tau\cdot\pi 0.$$ (4.31)

Rotating the phase of the fermion field,

$$\psi \to \tilde{\psi} = \mathrm{e}^{-\mathrm{i}M_N t}\psi,$$ (4.32)

just like we did for the bosonic field in Eq. (4.24), we can remove the mass term for the upper components:

$$\mathscr{L}_\psi = \tilde{\psi}^\dagger\left(\hat{E} + \hat{O} - (\gamma^0 - \mathbf{1})M_N\right)\tilde{\psi}.$$ (4.33)

The Foldy-Wouthuysen transformation is now constructed to (approximately) decouple the upper from the lower components, *i.e.*, nucleons from their antiparticles. To achieve this, we use a sequence of further unitary redefinitions of the fermion field. The first of these is

---

[3] We stress, however, that this really is a model and not a proper EFT describing QCD.

$$\tilde{\psi} \to \tilde{\psi}' = e^{-i\hat{S}}\tilde{\psi} \quad \text{with} \quad \hat{S} = -\frac{i\gamma^0\hat{O}}{2M_N}. \tag{4.34}$$

Let us consider this transformation up to quadratic order in $1/M_N$. Expanding the exponential, we have

$$\tilde{\psi} = e^{i\hat{S}}\tilde{\psi}' = \left(1 + \frac{\gamma^0\hat{O}}{2M_N} + \frac{(\gamma^0\hat{O})^2}{8M_N^2} + \mathcal{O}(1/M_N^3)\right)\tilde{\psi}' \tag{4.35}$$

and likewise

$$\tilde{\psi}^\dagger = \tilde{\psi}'^\dagger e^{-i\hat{S}} = \tilde{\psi}'^\dagger\left(1 - \frac{\gamma^0\hat{O}}{2M_N} + \frac{(\gamma^0\hat{O})^2}{8M_N^2} + \mathcal{O}(1/M_N^3)\right). \tag{4.36}$$

Inserting this into Eq. (4.33) and collecting contributions up to corrections which are $\mathcal{O}(1/M_N^2)$, we get a number of terms:

$$-\frac{\gamma^0\hat{O}\hat{E}}{2M_N} + \frac{\hat{E}\gamma^0\hat{O}}{2M_N} = \frac{\gamma^0[\hat{O},\hat{E}]}{2M_N} \tag{4.37a}$$

$$\frac{\hat{O}\gamma^0\hat{O}}{2M_N} - (\gamma^0 - \mathbf{1})\frac{(\gamma^0\hat{O})^2}{8M_N} - \frac{\gamma^0\hat{O}^2}{2M_N} + \frac{\gamma^0\hat{O}}{2M_N}(\gamma^0 - \mathbf{1})\frac{\gamma^0\hat{O}}{2M_N} - \frac{(\gamma^0\hat{O})^2}{8M_N}(\gamma^0 - \mathbf{1}) = -\frac{\gamma^0\hat{O}^2}{2M_N}, \tag{4.37b}$$

$$\frac{1}{2}\gamma^0\hat{O}(\gamma^0 - \mathbf{1}) - \frac{1}{2}(\gamma^0 - \mathbf{1})\gamma^0\hat{O} = -\hat{O}. \tag{4.37c}$$

Above we have used that

$$[\gamma_0, \hat{E}] = 0 \quad, \quad \{\gamma_0, \hat{O}\} = 0, \tag{4.38}$$

and $(\gamma^0)^2 = \mathbf{1}$. Collecting everything, we get

$$\mathscr{L}_{\pi N} = \tilde{\psi}'^\dagger\left(\hat{E} - \frac{\gamma^0\hat{O}^2}{2M_N} + \frac{\gamma^0[\hat{O},\hat{E}]}{2M_N} - (\gamma^0 - \mathbf{1})M_N\right)\tilde{\psi}' + \mathcal{O}(1/M_N^2). \tag{4.39}$$

The $\hat{O}^2$ term is even and we see that the original odd operator is canceled, but we have generated a new term $\sim [\hat{O},\hat{E}]$ If we neglect the interaction and consider

$$\hat{E} = \hat{E}_{\text{free}} = i\partial_t 00 i\partial_t \quad \text{and} \quad \hat{O} = \hat{O}_{\text{free}} = 0 - i\sigma\cdot\nabla - i\sigma\cdot\nabla 0, \tag{4.40}$$

we find that $[\hat{O}_{\text{free}}, \hat{E}_{\text{free}}] = 0$ (partial derivatives commute) and thus the desired decoupling up to $\mathcal{O}(1/M_N^2)$. For the interacting case, on the other hand, the commutator does not vanish. We see, however, that the new odd contribution is suppressed by a factor $1/M_N$. To push it to the next higher order, we need another rotation:

$$\tilde{\psi}' \to \tilde{\psi}'' = e^{-i\hat{S}'}\tilde{\psi}', \tag{4.41a}$$

with

$$\hat{S}' = -\frac{i\gamma^0\hat{O}'}{2M_N} \quad \text{with} \quad \hat{O}' = \frac{\gamma^0[\hat{O},\hat{E}]}{2M_N} \tag{4.41b}$$

After a couple of steps, we arrive at

$$\mathscr{L}_\psi = \tilde{\psi}''^\dagger\left(\hat{E} - \frac{\gamma^0\hat{O}^2}{2M_N} - (\gamma^0 - \mathbf{1})M_N\right)\tilde{\psi}'' + \mathcal{O}(1/M_N^2), \tag{4.42}$$

i.e., up to $\mathcal{O}(1/M_N^2)$ there are now no odd terms left and the upper and lower components of $\tilde{\psi}''$ are decoupled at this order.

4.2. *Exercise:* Carry out the steps that lead from the transformation (4.41) to Eq. (4.42). Note that it suffices to expand the exponentials up to first order.

In this Lagrangian, we can now write

$$\tilde{\psi}'' = Nn \tag{4.43}$$

and identify the upper ("large") component N—a doublet in both spin and isospin space—with the particle and the lower ("small") component with the antiparticle states. The term $(\gamma^0 - \mathbf{1})M_N$ in Eq. (4.42) ensures that there is no explicit mass term for the field N, whereas that for n comes with a factor two, corresponding to the Dirac mass gap between particles and antiparticles. Let us now write down the Lagrangian obtained for N, omitting the decoupled small components:

$$\mathscr{L}_\psi = N^\dagger \left(i\partial_t - g\sigma - \frac{1}{2M_N} \left[-i\boldsymbol{\sigma}\cdot\nabla + ig\boldsymbol{\tau}\cdot\boldsymbol{\pi} \right] \left[-i\boldsymbol{\sigma}\cdot\nabla - ig\boldsymbol{\tau}\cdot\boldsymbol{\pi} \right] \right) N + \cdots . \tag{4.44}$$

To simplify this further, we use that[4]

$$(\boldsymbol{\sigma}\cdot\nabla)(\boldsymbol{\sigma}\cdot\nabla) = \nabla^2 \tag{4.45}$$

and, from the product rule,

$$(\boldsymbol{\sigma}\cdot\nabla)(\boldsymbol{\tau}\cdot\boldsymbol{\pi}) = \boldsymbol{\sigma}\cdot(\boldsymbol{\tau}\cdot\nabla\boldsymbol{\pi}) + (\boldsymbol{\tau}\cdot\boldsymbol{\pi})(\boldsymbol{\sigma}\cdot\nabla) = \sigma^i \tau^a (\partial_i \pi^a) + \tau^a \pi^a \sigma^i \partial_i . \tag{4.46}$$

In the last step we have written out all indices to clarify the meaning of the two dot products. Collecting everything, we find that the $(\boldsymbol{\tau}\cdot\boldsymbol{\pi})(\boldsymbol{\sigma}\cdot\nabla)$ terms cancel out and arrive at

$$\mathscr{L} = N^\dagger \left(i\partial_t + \frac{\nabla^2}{2M_N} \right) N - g\,\sigma N^\dagger N + N^\dagger \left(\frac{g}{2M_N}\boldsymbol{\sigma}\cdot(\boldsymbol{\tau}\cdot\nabla\boldsymbol{\pi}) + \frac{g^2}{2M_N}(\boldsymbol{\tau}\cdot\boldsymbol{\pi})^2 \right) N$$
$$+ \frac{1}{2}(\partial^\mu\boldsymbol{\pi})\cdot(\partial_\mu\boldsymbol{\pi}) - \frac{1}{2}m_\pi^2\boldsymbol{\pi}^2 + \frac{1}{2}(\partial^\mu\sigma)\cdot(\partial_\mu\sigma) - \frac{1}{2}m_\sigma^2\sigma^2 + \cdots . \tag{4.47}$$

This includes the expected nonrelativistic kinetic term for the fermion field, as well as various interactions with σ and π. Note that the latter two particles are still relativistic and unchanged by the Foldy-Wouthuysen transformation, so that we could simply reinstate their kinetic terms as in Eq. (4.28).

4.2.2.3 Integrating out exchange particles: part II

With Eq. (4.28) we are now also in a convention situation to illustrate how we end up with only contact interactions between the nonrelativistic fermions if we integrate out the σ and π fields. Their equations of motion are

$$\left(\Box + m_\sigma^2 \right) \sigma = g N^\dagger N \tag{4.48}$$

and

$$\left(\Box + m_\pi^2 \right) \pi^\lambda = -\frac{g}{2M_N}\nabla\cdot\left[N^\dagger \boldsymbol{\sigma}\tau^\lambda N \right] - \frac{g^2}{M_N}N^\dagger(\boldsymbol{\tau}\cdot\boldsymbol{\pi})\tau^\lambda N . \tag{4.49}$$

---

[4] Note that Eq. (4.45) is very simple because we have not included a coupling of ψ to the electromagnetic field. If we had done that, the ∇ would be a covariant derivative, $\mathbf{D} = \nabla + ie\mathbf{A}$, and Eq. (4.45) would generate, among other terms, the magnetic spin coupling $\boldsymbol{\sigma}\cdot\mathbf{B}$.

The σ part can be handled exactly as in Sec. 4.2.1.1, giving a leading four-nucleon contact interaction $\sim g^2/m_\sigma^2$ plus a tower of operators with increasing number of derivatives. The π part is more interesting, but also more complicated due to the derivative in Eq. (4.49). We thus keep the following discussion rather qualitative and leave it as an exercise to work out the details.

In that spirit, we consider only the first term in Eq. (4.49), corresponding to a one-π-exchange operator when substituted back into the Lagrangian. With the propagator $D_\pi(x-y)$ defined in complete analogy to Eq. (4.6), we can write

$$\pi^\lambda(x) = -\frac{\mathrm{i}g}{2M_N}\int \mathrm{d}^4 y\, D_\pi(x-y)\, \partial_j^y\left[N^\dagger(y)\,\sigma^j \tau^\lambda N(y)\right] + \cdots, \tag{4.50}$$

and thus get

$$\mathscr{L}_{\mathrm{int}} \sim \left[N^\dagger(x)\,\sigma^i \tau^\lambda N(x)\right]\partial_i^x \int \mathrm{d}^4 y\, D_\pi(x-y)\, \partial_j^y\left[N^\dagger(y)\,\sigma^j \tau^\lambda N(y)\right] + \cdots, \tag{4.51}$$

where for the time being we omit the prefactor $g^2/(4M_N^2)$. We integrate by parts to have ∂_j^y act on $D_\pi(x-y)$. The ∂_i^x does this already, so, with all indices written out for clarity:

$$\mathscr{L}_{\mathrm{int}} \sim \int \mathrm{d}^4 y\, N_{\alpha a}^\dagger(x)\left(\sigma^i\right)^\alpha{}_\beta\left(\tau^\lambda\right)^a{}_b N^{\beta b}(x)\left[\partial_x^i \partial_y^j D_\pi(x-y)\right]N_{\gamma c}^\dagger(y)\left(\sigma^j\right)^\gamma{}_\delta\left(\tau^\lambda\right)^c{}_d N^{\delta d}(y) + \cdots. \tag{4.52}$$

From the definition of the propagator we find that

$$\partial_i^x \partial_j^y D_\pi(x-y) = \int \frac{\mathrm{d}^4 p}{(2\pi)^4}(\mathrm{i}p_i)(-\mathrm{i}p_j)\mathrm{e}^{-\mathrm{i}p(x-y)}\frac{\mathrm{i}}{p^2 - m_\pi^2 + \mathrm{i}\varepsilon} = -\partial_i^x \partial_j^x D_\pi(x-y), \tag{4.53}$$

so the partial derivatives can be written fully symmetric in i and j. The various fermion field operators can be rearranged with the help of

$$N^{\beta b}(x)N_{\gamma c}^\dagger(y) = -\frac{1}{4}\left[(N^\dagger(y)N(x))\,\delta_\gamma^\beta \delta_c^b + (N^\dagger(y)\tau^\kappa N(x))\,\delta_\gamma^\beta\left(\tau^\kappa\right)^b{}_c\right.$$
$$\left. + (N^\dagger(y)\sigma^k N(x))\left(\sigma^k\right)^\beta{}_\gamma \delta_c^b + (N^\dagger(y)\,\tau^\kappa \sigma^k N(x))\left(\sigma^k\right)^\beta{}_\gamma\left(\tau^\kappa\right)^b{}_c\right]. \tag{4.54}$$

Using also $\sigma^i \sigma^j = \delta^{ij}\mathbf{1} + \mathrm{i}\varepsilon^{ijk}\sigma^k$,
$\sigma^i \sigma^k \sigma^j = \delta^{kj}\sigma^i + \delta^{ki}\sigma^j - \delta^{ij}\sigma^k + \mathrm{i}\varepsilon^{ikj}\mathbf{1}$,
$\sigma^i \sigma^j \sigma^i = -\sigma^j$, we get four terms from Eq. (4.52) decomposed into contributions symmetric and antisymmetric in i and j, with the latter all vanishing upon contraction with $\partial_i^x \partial_j^x$. The simplest symmetric term comes with a δ^{ij}, yielding $\nabla^2 D_\pi(x-y)$. To see what this generates, we Taylor-expand the fermion fields that depend on y about x, e.g., $N(y) = N(x) + (y-x)^\mu \partial_\mu N(x) + \cdots$. This gives as the leading piece a combination of four fermion operators all evaluated at x, times

$$\int \mathrm{d}^4 y \int \frac{\mathrm{d}^4 p}{(2\pi)^4}\mathrm{e}^{-\mathrm{i}p\cdot(x-y)}\frac{\mathrm{i}\mathbf{p}^2}{p^2 - m_\pi^2 + \mathrm{i}\varepsilon} = \int \mathrm{d}^4 y \int \frac{\mathrm{d}^3 p}{(3\pi)^4}\int \frac{\mathrm{d}p_0}{2\pi}\mathrm{e}^{-\mathrm{i}p(x-y)}\frac{\mathrm{i}\mathbf{p}^2}{p_0^2 - \mathbf{p}^2 - m_\pi^2 + \mathrm{i}\varepsilon}. \tag{4.55}$$

The integral over p_0 can be solved via contour integration. Defining $\omega_{\mathbf{p}} = \sqrt{\mathbf{p}^2 + m_\pi^2}$, we get

$$\int \frac{\mathrm{d}p_0}{2\pi}\mathrm{e}^{-\mathrm{i}p_0(x_0-y_0)}\frac{\mathrm{i}}{p_0^2 - \mathbf{p}^2 - m_\pi^2 + \mathrm{i}\varepsilon} = \frac{\mathrm{e}^{-\mathrm{i}\omega_{\mathbf{p}}'|x_0-y_0|}}{2\omega_{\mathbf{p}}'}\quad \text{with}\quad \omega_{\mathbf{p}}' = \omega_{\mathbf{p}} - \frac{\mathrm{i}\varepsilon}{2\omega_{\mathbf{p}}} \equiv \omega_{\mathbf{p}} - \mathrm{i}\varepsilon'. \tag{4.56}$$

It is important here to keep track of the small imaginary part, as it allows us to write

$$\int_{-\infty}^{\infty} \mathrm{d}y_0 \, \frac{\mathrm{e}^{-\mathrm{i}\omega_{\mathbf{p}}'|x_0-y_0|}}{2\omega_{\mathbf{p}}'} = \int_{0}^{\infty} \mathrm{d}y_0 \, \frac{\mathrm{e}^{-\mathrm{i}\omega_{\mathbf{p}}'|y_0|}}{\omega_{\mathbf{p}}'} = -\mathrm{i}/(\omega_{\mathbf{p}}')^2 \,. \tag{4.57}$$

Collecting the results up to this point, we arrive at

$$\int \mathrm{d}^4 y \int \frac{\mathrm{d}^4 p}{(2\pi)^4} \, \mathrm{e}^{-\mathrm{i}p(x-y)} \frac{\mathrm{i}\mathbf{p}^2}{p^2 - m_\pi^2 + \mathrm{i}\varepsilon} = -\int \mathrm{d}^3 y \int \frac{\mathrm{d}^3 p}{(2\pi)^3} \, \mathrm{e}^{\mathrm{i}\mathbf{p}\cdot(\mathbf{x}-\mathbf{y})} \frac{\mathbf{p}^2}{\mathbf{p}^2 + m_\pi^2} \,. \tag{4.58}$$

We finally obtain the desired contact interaction by expanding

$$\frac{\mathbf{p}^2}{\mathbf{p}^2 + m_\pi^2} = \frac{\mathbf{p}^2}{m_\pi^2} \left(1 - \frac{\mathbf{p}^2}{m_\pi^2} + \cdots \right) \,, \tag{4.59}$$

with a leading term $\sim \mathbf{p}^2$, generating a contact interaction $\sim (N^\dagger N)\nabla^2(N^\dagger N)$. This is of course not surprising: after all, the original interaction term in Eq. (4.47) generating the contact operator had a single derivative ∇. Considering other terms coming from Eq. (4.54), one can also find operators like $(N^\dagger \boldsymbol{\sigma} \cdot \nabla N)(N^\dagger \boldsymbol{\sigma} \cdot \nabla N)$, and it is a useful exercise to work this out in detail. But already from our qualitative discussion here we can infer that the resulting effective theory is an expansion in $\mathbf{p}^2/m_\pi^2$, i.e., its range of validity is determined by three-momenta—rather than the energies—being small compared to m_π.[5]

4.2.2.4 The Schrödinger field

We conclude this section by looking at the non-relativistic field theory from a more general perspective, establishing its close connection to the "second quantized" approach to (many-body) quantum mechanics that is used in several later chapters of this volume.

Recall from the beginning of this section that the Lagrangian (4.19) for the free Schrödinger field ϕ is

$$\mathscr{L}_{\phi,\mathrm{free}} = \phi^\dagger \left(\mathrm{i}\partial_t + \frac{\nabla^2}{2m} \right) \phi \,. \tag{4.60}$$

This trivially gives the equation of motion

$$\left(\mathrm{i}\partial_t + \frac{\nabla^2}{2m} \right) \phi = 0 \,, \tag{4.61}$$

which is formally the same as the free Schrödinger equation. However, recall that ϕ here is a field *operator*, i.e., $\phi(x)$ creates a particle at $x = (t, \mathbf{x})$ from the vacuum, so to really get an ordinary Schrödinger equation, we have to act with both sides of Eq. (4.61) on $|0\rangle$, and define the quantum-mechanical one-body state

$$|\phi(t,\mathbf{x})\rangle = \phi(t,\mathbf{x})|0\rangle \,. \tag{4.62}$$

If we add to Eq. (4.60) a term $V(x)\phi^\dagger(x)\phi(x)$, we obtain the Schrödinger equation for a particle in a potential $V(x)$. Exactly as for a relativistic field we can define the propagator

$$D_\phi(x-y) = \int \frac{\mathrm{d}^4 q}{(2\pi)^4} \, \mathrm{e}^{-\mathrm{i}p(x-y)} \frac{\mathrm{i}}{p_0 - \frac{\mathbf{p}^2}{2m} + \mathrm{i}\varepsilon} \,, \tag{4.63}$$

satisfying

---

[5] This is assuming $m_\pi < m_\sigma$.

$$\left(\mathrm{i}\partial_t + \frac{\nabla^2}{2m}\right) D_\phi(x-y) = -\mathrm{i}\delta^{(4)}(x-y)\,. \tag{4.64}$$

Up to a conventional factor i, this is precisely the (retarded) Green's function[6] familiar, for example, from non-relativistic scattering theory (then typically denoted G_0). This will appear again when the Lippmann–Schwinger equation is derived using the field-theory language in Sec. 4.3.

While it is nice and reassuring that we can go back to simple quantum mechanics from the one-body Schrödinger Lagrangian discussed so far, this feature is not very relevant in practice. We can, however, straightforwardly generalize it to the many case. To that end, consider a Lagrangian that includes a two-body interaction, written in terms of a general non-local potential:[7]

$$\mathscr{L}_{\phi,\text{2-body}}(x) = \phi^\dagger(x)\left(\mathrm{i}\partial_t + \frac{\nabla^2}{2m}\right)\phi(x) + \int \mathrm{d}^4 y\, \phi^\dagger(x)\phi(x) V(x,y)\, \phi^\dagger(y)\phi(y)\,. \tag{4.65}$$

Note that this has exactly the structure that we found when we integrated out particles in the preceding sections, before expanding the propagators to get simple contact interactions. Such a Lagrangian (possibly including also higher-body forces) is a convenient starting point for example for many-body perturbation theory used to study quantum systems at finite density.

Coming back to effective field theories, we stress that these are *not* defined by putting a given potential into a Lagrangian; in doing that, one merely gets a model written in a convenient way. The EFT instead makes no assumptions on the interaction (besides symmetry constraints). It is thus much more general and not a model, but to be predictive it requires a number of *a priori* unknown parameters to be fixed and its various terms to be ordered systematically. It is this that we turn to next.

4.2.3 Symmetries and power counting

So far, we have discussed how to obtain effective low-energy Lagrangians by integrating out "heavy" degrees of freedom, leaving only those that we want to describe at low energies or rather, as we showed explicitly with the pseudoscalar pion-nucleon model, low momenta. We found the contact interactions generated this way to come with the integrated-out particle's mass in the denominator, and with an increasing number of derivatives as we keep more and more terms from the expansion. These derivatives will turn into powers of momentum, which is a small scale for external states. We furthermore showed how a nonrelativistic reduction generates a chain of operators with an increasing power of the particle's mass in the denominator, thus also giving a hierarchy of terms that eventually restore the original theory's relativistic structure with coupling between particles and antiparticles.

From these procedures it is clear that the terms in the effective Lagrangian should be ordered in a natural way, with the most important ones being those with the least number of large mass scales in the denominator and the least number of derivatives in the numerator. It is also clear that they are restricted in their structure. For example, if we start with a Lorentz-invariant relativistic theory, after the nonrelativistic reduction we will only get terms

---

[6] Note that in the nonrelativistic case there is no "Feynman propagator." Particles and particles are decoupled, and the denominator in Eq. (4.63) only has a single pole at $p_0 = \mathbf{p}^2/(2m) - \mathrm{i}\varepsilon$. Flipping the sign of the iε term gives the advanced Green's function.

[7] A static (time-independent) potential, as it is more common in quantum mechanics, would be a function only of $\mathbf{x}$ and $\mathbf{y}$, and all fields in the interaction term would be evaluated at the same time t.

that are invariant under "small" Lorentz boosts. More precisely, the nonrelativistic operators should be invariant under Galilean transformations (assuming the original theory had rotational invariance, this simply gets inherited by the effective one), and the form of so-called "relativistic corrections" is determined by the expansion of the dispersion relation:

$$E^2 = m^2 + p^2 \implies E = m + \frac{p^2}{2m} - \frac{p^4}{8m^3} + \cdots. \tag{4.66}$$

We now turn to discussing the bottom-up approach guided by these principles. To that end, consider the effective Lagrangian for a nonrelativistic bosonic field with contact interactions:

$$\begin{aligned}
\mathscr{L} = {}& \phi^\dagger \left(i\partial_t + \frac{\nabla^2}{2m} \right) \phi + \phi^\dagger \frac{\nabla^4}{8m^3} \phi + \cdots \\
& + g_2^{(0)}(\phi^\dagger \phi)^2 + g_2^{(2s/p)} \left((\phi^\dagger \overset{\leftrightarrow}{\nabla} \phi)^2 - (\phi^\dagger \phi)(\phi^\dagger (\overset{\leftrightarrow}{\nabla})^2 \phi) \mp 2(\phi^\dagger \phi)\nabla^2(\phi^\dagger \phi) \right) + \cdots \\
& \hspace{8cm} + g_3^{(0)}(\phi^\dagger \phi)^3 + \cdots. \tag{4.67}
\end{aligned}$$

Here we have used the definition

$$f \overset{\leftrightarrow}{\nabla} g = f(\nabla)g - (\nabla f)g \tag{4.68}$$

and conveniently separated the two-body terms with two derivatives into those which contribute to S-wave ($\sim g_2^{(2s)}$) and P-wave ($\sim g_2^{(2p)}$) interactions, respectively. One can of course choose different linear combinations, but a separation by partial waves is typically a good choice for systems with rotational invariance. It is a useful exercise to work out how the structure for the derivative interactions gives the desired result, working in momentum space and considering contractions with external in and out states that have center-of-mass momenta $\pm \mathbf{k}^2$ and $\pm \mathbf{p}/2$, respectively. The structure of the individual terms is determined by the requirement of Galilean invariance,[8], and the EFT paradigm tells us to write down all possible terms with a given number of derivatives (with odd numbers excluded by parity invariance).

4.2.3.1 The breakdown scale

As mentioned in the introduction, the most important requirement to construct an EFT is the identification of—at least two, but possibly more—separated scales, ratios of which are used to extract a small expansion parameter. The better the scale separation, the smaller this parameter becomes, and consequently the better the more precise (and, provided all contributions have been identified correctly, accurate) the theory becomes at any given order in the expansion. In the simplest case, there is one low scale Q associated with the typical momentum of the physical system that we want to describe, and a single large scale M_{hi}, the "breakdown scale" associated with the physics that our EFT does not take into account—in other words: resolve—explicitly. This is exactly the situation that we constructed when we integrated out exchange particles from a given theory in Secs. 4.2.1.1 and 4.2.2.3. By construction, the EFT is not appropriate to describe processes with momenta of the order of or large than the breakdown scale. To emphasize this meaning, it is sometimes also denoted by the letter Λ (with or possibly without some qualifying subscript).[9]

---

[8] See for example Ref. [9], Sec. 2.1.1 for a rigorous discussion of the required transformation properties.

[9] We alert the reader that in the literature this is sometimes referred to as the "cutoff of the EFT." We do not use that language to avoid confusion with an (arbitrary) momentum cutoff introduced to regularize divergent loop integrals (discussed .

As already mentioned, integrating out degrees of freedom from a given more fundamental theory will naturally give a breakdown scale set by that particle's mass. But it can also be something more general. For example, although in the situations discussed here so far the particles we were ultimately interested in were already present as degrees of freedom in the original theory, such a scenario is merely a special case. The first step in writing down an effective field theory is to identify what the appropriate—literally: effective—degrees of freedom are for the processes one wants to describe, and they can be different from those of the fundamental theory. This is exactly the case in nuclear physics: while the degrees of freedom in quantum chromodynamics (QCD) are quarks and gluons, describing the binding of nuclei with these is, although possible with state-of-the-art lattice QCD calculations, largely inefficient to say the least. It is much more economical to work with nucleons directly as degrees of freedom, as done in most chapters of this volume, because a detailed knowledge of the internal structure of protons and neutrons is not necessary to describe their binding into nuclei; it is only resolved at much higher energies, for example in deep inelastic scattering. The reason for this is color confinement: the low-energy degrees of freedom of QCD are not quarks and gluons, but color-neutral hadrons. Chiral effective field theory, which we will come back to in Sec. 4.5.3, is designed to work at momenta of the order of pion mass, breaking down at the scale of chiral-symmetry breaking (estimated to be roughly a GeV, but possibly lower).

Other examples are halo EFT, constructed to describe nuclear systems that have the structure of a few nucleons weakly bound to a tight core, which can then effective be treated as a structureless particle. Clearly, such a theory will break down at momenta large enough to probe the core's internal structure. Similarly, one can construct an effective theory for systems of ultracold atomic gases, the constituents of which can be treated as pointlike degrees of freedom without using QED to describe their individual structure, and much less QCD to describe their atomic nuclei.

Whatever the breakdown scale is, once identified it can be used to systematically order terms in the effective Lagrangian by powers of $Q/M_{\text{hi}} \ll 1$, and we now turn to discussing how this ordering can be set up.

4.2.3.2 Naïve dimensional analysis

In our units with $\hbar = c = 1$, the action

$$S = \int \mathrm{d}^4x \, \mathscr{L}(x) \tag{4.69}$$

has to be a dimensionless quantity. This, in turn, fixes the dimensions for the individual building blocks in the Lagrangian. In a relativistic theory, mass and energy are equivalent and one would simply express everything in terms of a generic mass dimension. For our nonrelativistic framework, on the other hand, energies are *kinetic* energies because the time dependence associated with the rest mass has been absorbed into the field (*cf.* Secs. 4.2.2.1 and 4.2.2.2). This implies that energy and mass scales—as well as time and space—should be counted separately.[10] In fact, it is more natural to consider powers of momentum. To understand what this means, let us start with the kinetic term in Eq. (4.67): $[\nabla^2/(2m)] = \text{momentum}^2/\text{mass}$. The time derivative has to scale in the same way, implying that for time itself we have $[t] = \text{mass}/\text{momentum}^2$, whereas $[x] = \text{momentum}^{-1}$. Consequently, the integration measure

---

[10] This separation would be quite clear if we had not set $c = 1$, which would in fact be more appropriate for a nonrelativistic system. The reason we still do it that it allows us to still energies and momenta in the same units, *e.g.*, in MeV, following the standard convenient in nuclear physics.

scales like $[\mathrm{d}^4 x = \mathrm{d}t\,\mathrm{d}^3 x] = \mathrm{mass}/\mathrm{momentum}^5$ (to compare, in the relativistic theory one would simply count $[\mathrm{d}^4 x] = \mathrm{mass}^{-4} = \mathrm{energy}^{-4}$).

Since the dimension of $\mathscr{L}$ has to cancel that of the measure to give a dimensionless action,we can now infer that our field has to satisfy $[\phi] = \mathrm{momentum}^{3/2}$, *i.e.*, even though it is a scalar field it scales with a fractional dimension (recall that in the relativistic case a scalar would have dimension energy[1]). Knowing the scaling of the field and the measure, we can now proceed and deduce that of the various coupling constants.

The basic idea is very simple: each term (operator) in the Lagrangian (4.67) has $2n$ fields and $2m$ derivatives, giving it a total dimension of $\mathrm{momentum}^{3n+2m}$. For example, the $(\phi^\dagger \phi)^2$ term with $2n = 4$ and $m = 0$ has dimension $\mathrm{momentum}^6$. Hence, to get the correct overall dimension $\mathrm{momentum}^5/\mathrm{mass}$ for $\mathscr{L}$, the coupling constant $g_2^{(0)}$ has to be $\sim 1/(\mathrm{momentum} \times \mathrm{mass})$. Since it is supposed to describe unresolved short-distance details, the momentum scale in the denominator is should be the breakdown scale, whereas the mass scale, which as we mentioned is a feature of the nonrelativistic framework and common to all operators, is simply associated with m_ϕ. Of course, counting a single operator does not tell us much: it is the relative order of terms that matters, so we proceed to the $g_2^{(2)}$ interactions. These all come with two derivatives, which are associated with the external (small) momentum scale Q. Hence, we have $2n = 4$ and $2m = 2$, and we need to compensate the two additional powers of momentum in the numerator with two more powers of M_{hi} in the denominator, finding that the $g_2^{(2)}$ interactions are down compared to the $g_2^{(0)}$ term by a factor $(Q/M_{\mathrm{hi}})^2$. This is exactly in line with our picture of the contact terms gradually building up the an unresolved particle exchange through a derivative expansion. For higher-body interactions, it is the larger number of fields that gives a suppression by inverse powers of M_{hi} compared to operators with fewer fields.

This kind of analysis can be much improved if something is known about which unresolved physics is supposed to be represented by which operator, and it is generally more complex if the theory involves different fields. For example, in the EFT for halo nuclei there are contact interactions associated with unresolved pion exchange, as well as those systematically accounting for the internal structure of the core field. Instead of merely putting generic powers of M_{hi} in every denominator, it can be necessary to keep track of several high scales separately to figure out the ordering of terms. Also, it is possible that the external momentum is not the only relevant low-momentum scale in the problem.

This rather abstract discussion will become clearer when we finally discuss concrete EFTs in the following sections 4.3 and 4.4. In that context, we will use the scaling of the various terms in the Lagrangian to power-count diagrams as a whole, *i.e.*to estimate the size of individual contributions composed of vertices and loops to a given physical amplitude of interest. We will then also discuss how the actual so-called scaling dimension of a field in the Lagrangian can turn out to deviate from what we estimated here based purely on dimensional grounds.

4.2.3.3 Fine tuning

In connection with the previous comment is another point worth stressing already here: nïve dimensional analysis resides at the beginning of EFT wisdom, not at the end, and in quite a few cases it turns out to be exactly what the name says: naïve. In other words, the actual scaling of a coupling constant can be quite different from what one would infer by counting dimensions, a scenario that is commonly referred to as "fine tuning." To understand why that is consider, for example, our bosonic toy model from Sec. 4.2.1.1, but now assume that there already is a four-ϕ contact interaction present prior to integrating out the χ field:

$$\mathscr{L} = -\phi^\dagger \left(\Box + m_\phi^2\right)\phi - \chi^\dagger \left(\Box + m_\chi^2\right)\chi + g\left(\phi^\dagger\phi^\dagger\chi + \text{h.c.}\right) + h(\phi^\dagger\phi)^2. \tag{4.70}$$

This could, for example, come from unknown (or integrated out) short-distance physics at a yet higher scale. When we now integrate out the χ, the generated non-derivative contact term will combine with the existing one, giving a single operator in the effective low-energy Lagrangian (recall that on dimensional grounds h has to have dimensions of inverse mass squared):

$$\mathscr{L} = -\phi^\dagger \left(\Box + m_\phi^2\right)\phi + \left(h - \frac{g^2}{m_\chi^2}\right)(\phi^\dagger\phi)^2 + \cdots. \tag{4.71}$$

Now suppose we had started in the bottom-up approach and simply written down the four-ϕ contact operator with some coefficient c to be determined. According to NDA, we would assume that its scale is set by two powers of the breakdown scale in the denominator, and assuming we actually know about the more fundamental theory, we might have estimated that breakdown scale to be of the order m_χ. From Eq. (4.71) we see that depending on what values g and h take in the underlying theory, the actual size of c might deviate strongly from the naïve expectation, and it could even be set by a low-energy scale of the effective theory. But for this to happen, there would have to be a delicate cancellation between h and g^2/m_χ^2, which is typically deemed unlikely given the *a priori* vast range of possible values these parameters could take; thus the term "fine tuning." The fact that coupling constants are in fact not simple fixed numbers but get renormalized by loop effects (*i.e.*, depend on a regularization scale with a behavior determined by the renormalization group) justifies this language even more.

4.2.3.4 Loops and renormalization

It is indeed high time we talk about loops. Our considerations in this section so far have been limited to tree level, which is always only a first approximation in a quantum field theory. In a perturbative theory, loop contributions from virtual intermediate states are added to improve the accuracy of the result. To treat a nonperturbative system such as a bound nucleus, on the other hand, they are absolutely crucial: recall that any finite sum of diagrams in perturbation can never produce a bound state (for example, think about poles in the S-matrix, which cannot be generated through a finite sum of terms). In the field-theory language, this means that an infinite number of diagrams with increasing number of loops has to be summed to get the amplitude with the desired physical properties.

This situation is in fact familiar already from the Schrödinger equation written in the form

$$|\psi\rangle = \hat{G}_0(E)\hat{V}|\psi\rangle \quad, \quad \hat{G}_0 = \hat{G}_0(E) = (E - \hat{H}_0)^{-1}, \tag{4.72}$$

which can be iterated to get $|\psi\rangle = \hat{G}_0\hat{V}\hat{G}_0\hat{V}|\psi\rangle = \cdots$. When these operators are written out in momentum space, each propagator $\hat{G}_0$ corresponds to a loop. More closely related to the amplitude written down in a nonrelativistic field theory, this exercise can be repeated with the Lippmann-Schwinger equation for the T-matrix and its formal solution, the infinite Born series. Exactly this will be recovered in Sec. 4.3.

Of course, even in a nonperturbative theory we do not expect that *all* loop diagrams should be summed up to infinity. Generally, we want the power counting to tell us how to estimate the contribution from a given diagram, including loop diagrams. To do that, we need to know not only what which factors we pick up from vertices, but also need an estimate for the integration measure $\mathrm{d}^4 q = \mathrm{d}q_0\, \mathrm{d}^3 q$. Any loop diagram contributing to an amplitude with external momenta of the order Q will have this scale running through it a whole. It is thus natural to count the contribution from the three-momentum as $\mathrm{d}^3 q \sim Q^3$ and, recalling that in the nonrelativistic theory q_0 is a kinetic energy, $\mathrm{d}q_0 \sim Q^2/m$. For each Schrödinger propagator we get, conversely,

a factor m/Q^2, as can be seen from Eq. (4.63). These simple rules combined with those for the vertices give an estimate for any diagram in the theory determined by Eq. (4.67).

What this discussion does not cover is the fact that loops in a quantum field theory can be—and mostly are—divergent. Compared to the loops one gets from integrating the Schrödinger or Lippmann-Schwinger equation in quantum mechanics with a potential $\hat{V}$, which are typically all finite, this is different in the EFT simply because our delta-function (contact) interactions are too singular to make direct sense beyond tree level. Of course, this is no different than in any other quantum field theory, and it just means that divergent loops have to be regularized (for example, by imposing a momentum cutoff or with dimensional regularization), and then suitable renormalization conditions have to be imposed to fix the various coupling constants in the effective Lagrangian. These then become functions of the renormalization scale, with a behavior governed by the renormalization group (RG). In Sec. 4.3 this will be discussed in detail for a bosonic EFT that describes, for example, ultracold atomic systems.

The cutoff

What the regularization of loop integrals does is most transparent with a momentum cutoff. We denote this by Λ and stress again that it has to be distinguished from the EFT breakdown scale M_{hi}. The latter determines the scale beyond which we know our EFT not to be valid. In other words, short-range dynamics corresponding to momenta larger than M_{hi} is, in general, not correctly described by the EFT. Yet from loop integrals we get contributions from states up to the UV cutoff Λ. Renormalization means to adjust the coupling constants in such a way that they compensate the wrong high-momentum loop contributions in such a way that the physics the EFT is supposed to describe comes out correctly. For momenta up to M_{hi}, we trust the EFT, so it makes sense to keep such states in loops. Hence, one should typically choose $\Lambda > M_{\mathrm{hi}}$. Choosing it lower that the breakdown scale is possible, but this can induce corrections of the order $Q/\Lambda > Q/M_{\mathrm{hi}}$, which is not desirable for the power counting. In the renormalized EFT, any cutoff in the interval $[M_{\mathrm{hi}}, \infty)$ is thus an equally good choice—it does not have to be "taken to infinity." Instead, that phrase should be understood to mean adjusting the couplings at any given finite cutoff. If this procedure is carried out numerically, it can be desirable to keep the cutoff small, but one has to make sure that in principle in *can* be varied arbitrarily.

4.2.4 Matching

The determination of the couplings ("low-energy constants") in the effective Lagrangian is done by expressing a given physical quantity (*e.g.*, a scattering amplitude or related) in terms of the couplings and then adjusting them to reproduce a known result. This can be done using experimental input or, when working top-down, by calculating the same amplitude in the more fundamental theory. Generally, this procedure is referred to as "matching." At tree level, this is again exactly what we did by integrating out particles and found the coefficients of the generated contact interactions in terms of the original coupling and mass denominators. Once loop diagrams are involved, the process becomes somewhat more complicated because (a) one has to make sure to use compatible regularization schemes and renormalization scales and (b) loop diagrams with lower-order vertices typically mix with higher-order tree-level diagrams. The latter is a general feature of combined loop and derivative expansions and is thus also important when matching to experimental input. While these comments may sound

a bit cryptic here, they will become much clearer in the next section when we finally work with a concrete EFT.

4.3 Effective field theory for strongly interacting bosons

We will now use the insights from the previous sections to construct a local effective field theory for identical, spinless bosons with short-range S-wave interactions.[11] For the treatment of higher partial wave interactions the reader is referred to the literature [11–13]. The most general effective Lagrangian consistent with Galilei invariance can be written as

$$\mathscr{L} = \phi^\dagger \left(\mathrm{i}\partial_t + \frac{\nabla^2}{2m} \right) \phi - \frac{C_0}{4} \left(\phi^\dagger \phi \right)^2 - \frac{C_2}{4} \left(\nabla(\phi^\dagger \phi) \right)^2 + \frac{D_0}{36} \left(\phi^\dagger \phi \right)^3 + \cdots . \tag{4.73}$$

where m is the mass of the particles and the ellipses denote higher-derivative and/or higher-body interactions. The leading two- and three-body interactions are explicitly written out. The scaling of the coefficients C_0, C_2, D_0, ... depends on the scales of the considered system. Two explicit examples, corresponding natural and unnaturally large scattering length, are discussed below.

4.3.1 EFT for short-range interactions

We start by considering natural system where all interactions are characterized by only one mass scale M_{hi} that we identify with the formal breakdown scale of the EFT introduced in the previous section. We will see below that this is indeed justified. Since the nonrelativistic boson fields have dimension 3/2, the coupling constants must scale as

$$C_0 \sim \frac{1}{mM_{\mathrm{hi}}}, \quad C_2 \sim \frac{1}{mM_{\mathrm{hi}}^3}, \quad \text{and} \quad D_0 \sim \frac{1}{mM_{\mathrm{hi}}^4}, \tag{4.74}$$

such that higher dimension operators are strongly suppressed for small momenta $k \ll M_{\mathrm{hi}}$.[12] We first focus on the two-body system and calculate the contribution of the interaction terms in Eq. (4.73) to the scattering amplitude of two particles in perturbation theory. After renormalization, the result reproduces the low-energy expansion of the scattering amplitude for particles with relative momentum k and total energy $E = k^2/m$:

$$T_2(E) = \frac{8\pi}{m} \frac{1}{k\cot\delta_0(k) - \mathrm{i}k} = -\frac{8\pi a}{m} \left(1 - \mathrm{i}ak + (ar_e/2 - a^2)k^2 + \mathscr{O}(k^3) \right), \tag{4.75}$$

where the effective range expansion for short-range interactions $k\cot\delta_0(k) = -1/a + r_e k^2/2 + \mathscr{O}(k^4)$ has been used.

Since all coefficients of the effective Lagrangian are natural (scaling with inverse powers of M_{hi}), it is sufficient to count the powers of small momenta Q in scattering amplitudes to determine the scaling of the amplitudes with M_{lo}. The correct dimensions are made up with appropriate factors of M_{hi} contained in the coupling constants (*cf.* Eq. (4.74)). For a general

---

[11] See Ref. [10] for a similar discussion with a focus on applications in ultracold atoms.

[12] Note that coupling constants scale with the particle mass as $1/m$ in nonrelativistic theories. This can be seen by rescaling all energies as $q_0 \to \tilde{q}_0/m$ and all time coordinates as $t \to \tilde{t}m$, so that dimensionful quantities are measured in units of momentum. Demanding that the action is independent of m, it follows that the coupling constants must scale as $1/m$.

two-body amplitude with L loops and V_{2i} interaction vertices with $2i$ derivatives, we thus have $T_2 \sim Q^\nu$ where the power ν is given by

$$\nu = 3L + 2 + \sum_i (2i - 2)V_{2i} \geq 0. \tag{4.76}$$

Here we have used that loop integrations contribute a factor k^5 and propagators a factor k^{-2} in nonrelativistic theories. The values of the coupling constants C_0 and C_2 can be determined by matching to Eq. (4.75). In the lowest two orders only C_0 contributes.

4.3. *E*xercise: Derive Eq. (4.76) using the topological identity for Feynman diagrams:

$$L = I - V + 1, \tag{4.77}$$

with L, V, and I the total number of loops, vertices, and internal lines respectively.

The contact interactions in Eq. (4.73) are ill-defined unless an ultraviolet cutoff is imposed on the momenta in loop diagrams. This can be seen by writing down the off-shell amplitude for two-body scattering at second order in perturbation theory:

$$T_2(E) \approx -C_0 - \frac{i}{2}C_0^2 \int \frac{d^3q}{(2\pi)^3} \int \frac{dq_0}{2\pi} \frac{1}{q_0 - q^2/2m + i\varepsilon} \frac{1}{E - q_0 - q^2/2m + i\varepsilon} + \cdots.$$

The two terms correspond to the first two diagrams in Fig. 4.4. The intermediate lines have
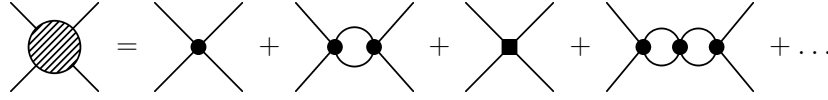
Fig. 4.4 Diagrammatic expression for the two-body scattering amplitude T_2. The circle (square) denotes a C_0 (C_2) interaction, respectively.

momenta $\pm q$. The integral over q_0 in Eq. (4.78) is easily evaluated using contour integration:

$$T_2(E) \approx -C_0 - \frac{1}{2}C_0^2 \int \frac{d^3q}{(2\pi)^3} \frac{1}{E - q^2/m + i\varepsilon} + \cdots. \tag{4.78}$$

The integral over q diverges. It can be regularized by imposing an ultraviolet cutoff $|q| < \Lambda$. Taking the limit $\Lambda \gg |E|^{1/2}$, the amplitude reduces to [13]

$$T_2(E) \approx -C_0 + \frac{mC_0^2}{4\pi^2}\left(\Lambda - \frac{\pi}{2}\sqrt{-mE - i\varepsilon}\right) + \cdots. \tag{4.79}$$

The dependence on the ultraviolet cutoff Λ can be consistently eliminated by a perturbative renormalization procedure. A simple choice is to eliminate the parameter C_0 in favor of the scattering length a, which is given by Eq. (4.75):

$$a \approx \frac{mC_0}{8\pi}\left(1 - \frac{mC_0\Lambda}{4\pi^2} + \cdots\right). \tag{4.80}$$

---

[13] If the calculation was carried out in a frame in which the total momentum of the two scattering particles was nonzero, the simple cutoff $|q| < \Lambda$ would give a result that does not respect Galilean invariance. To obtain a Galilean-invariant result requires either using a more sophisticated cutoff or else imposing the cutoff $|q| < \Lambda$ only after an appropriate shift in the integration variable q.

Inverting this expression to obtain C_0 as a function of a we obtain

$$C_0 \approx \frac{8\pi a}{m} \left(1 + \frac{2a\Lambda}{\pi} + \cdots\right),\tag{4.81}$$

where we have truncated at second order in a. Inserting the expression for C_0 into Eq. (4.79) and expanding to second order in a, we obtain the renormalized expression for the amplitude:

$$T_2(E) \approx -\frac{8\pi a}{m} \left(1 + a\sqrt{-mE - i\varepsilon} + \cdots\right) = -\frac{8\pi a}{m} \left(1 - iak + \cdots\right).\tag{4.82}$$

If we evaluate this at the on-shell point $E = k^2/m$ and insert it into Eq. (4.79), we find that it reproduces the first two terms in the expansion of the universal scattering amplitude in Eq. (4.75) in powers of ka. By calculating $T_2(E)$ to higher order in perturbation theory, we can reproduce the low-momentum expansion of Eq. (4.75) to higher order in ka. At the next order, the C_2 term will contribute at tree level while C_0 will contribute at the two-loop level. Thus a perturbative treatment of the EFT reproduces the low-momentum expansion of the two-body scattering amplitude. The perturbative approximation is valid only if the momentum satisfies $k \ll 1/a$.

A more interesting case occurs when the scattering length is large, but all other effective range coefficients are still determined by the scale M_{hi}: $k \sim 1/|a| \sim M_{\mathrm{lo}} \ll M_{\mathrm{hi}} \sim 1/r_e$. This scenario is able to support shallow bound states with binding momentum of order $1/a$ and is relevant to ultracold atoms close to a Feshbach resonance and very low-energy nucleons. The scaling of the operators is then modified to:

$$C_0 \sim \frac{1}{mM_{\mathrm{lo}}}, \quad C_2 \sim \frac{1}{mM_{\mathrm{lo}}^2 M_{\mathrm{hi}}}, \quad \text{and} \quad D_0 \sim \frac{1}{mM_{\mathrm{lo}}^4}.\tag{4.83}$$

The factors of M_{lo} in amplitudes can now come from small momenta and from the coupling constants. Above we adjusted the scaling of the three-body coupling D_0 as well, foreclosing a result discussed below Eq. (4.96).

With the scaling as in Eq. (4.83), the power counting expression in Eq. (4.76) is therefore modified to

$$v = 3L + 2 + \sum_i (i - 3)V_{2i} \geq -1.\tag{4.84}$$

If we are interested in two-body observables involving energy $E \sim 1/a^2$, such as shallow bound or virtual states, we must resum the diagrams involving only C_0 interactions to all orders [14, 15]. Without this resummation, our EFT would break down not at M_{hi}, but already at the much smaller scale $1/|a| \sim M_{\mathrm{lo}}$. In the scenario assumed here, all higher-derivative two-body interactions (C_2 and beyond) still involve inverse powers of M_{hi} and are thus perturbative.

The resummation of C_0 interactions is most easily accomplished by realizing that the corresponding Feynman diagrams in Fig. 4.4 form a geometric series. Summing the geometric series, the exact expression for the amplitude is

$$T_2(E) = -C_0 \left[1 + \frac{mC_0}{4\pi^2} \left(\Lambda - \frac{\pi}{2}\sqrt{-mE - i\varepsilon}\right)\right]^{-1}.\tag{4.85}$$

Alternatively, we can use the fact that summing the C_0 diagrams in Fig. 4.4 is equivalent to solving the following integral equation:

$$T_2(E) = -C_0 - \frac{i}{2}C_0 \int \frac{d^3 q}{(2\pi)^3} \int \frac{dq_0}{2\pi} \frac{1}{q_0 - q^2/2m + i\varepsilon} \frac{1}{E - q_0 - q^2/2m + i\varepsilon} T_2(E).\tag{4.86}$$

The integral equation is expressed diagrammatically in Fig. 4.5. Since the function $T_2(E)$ is
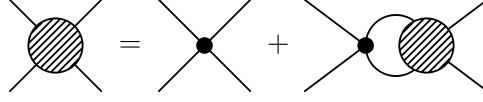
Fig. 4.5 Integral equation for the two-body scattering amplitude T_2 at leading order in the case of large scattering length. Notation as in Fig. 4.4.

independent of q and q_0, it can be pulled outside of the integral in Eq. (4.86). The integral can be regularized by imposing an ultraviolet cutoff Λ. The integral equation is now trivial to solve and the solution is given in Eq. (4.85).

The expression for the resummed two-body amplitude in Eq. (4.85) depends on the parameter C_0 in the Lagrangian and on the ultraviolet cutoff Λ. As in the perturbative case, renormalization can be implemented by eliminating C_0 in favor of a low-energy observable, such as the scattering length a. Matching the resummed expression to the effective range expansion for T_2, we obtain

$$C_0 = \frac{8\pi a}{m} \left(1 - \frac{2a\Lambda}{\pi} \right)^{-1} . \tag{4.87}$$

Given a fixed ultraviolet cutoff Λ, this equation prescribes how the parameter C_0 must be tuned in order to give the scattering length a. Note that for $\Lambda \gg 1/|a|$, the coupling constant C_0 is always negative regardless of the sign of a. Eliminating C_0 in Eq. (4.85) in favor of a, we find that the resummed amplitude reduces to

$$T_2(E) = \frac{8\pi}{m} \frac{1}{-1/a + \sqrt{-mE - i\varepsilon}} , \tag{4.88}$$

which reproduces the effective range expansion of the scattering amplitude by construction. In this simple case, we find that our renormalization prescription eliminates the dependence on Λ completely. In general, we should expect it to only be suppressed by powers of $1/(a\Lambda)$ or mE/Λ^2. A final step of taking the limit $\Lambda \to \infty$ would then be required to obtain results that are completely independent of Λ. The first correction to Eq. (4.88) is given by the C_2 interaction. The corresponding diagrams are shown in Fig. 4.6. After the matching, the final result for the
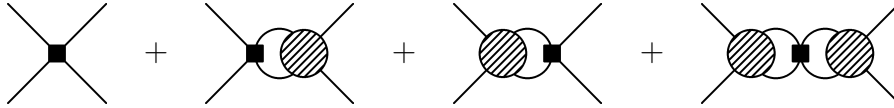
Fig. 4.6 Next-to-leading order correction to T_2. Notation as in Fig. 4.4.

scattering amplitude at next-to-leading order is

$$T_2(E) = \frac{8\pi}{m} \left(\frac{1}{-1/a + \sqrt{-mE - i\varepsilon}} + \frac{r_e mE/2}{(-1/a + \sqrt{-mE - i\varepsilon})^2} \right) , \tag{4.89}$$

where r_e is the effective range. The derivation of this expression will be left as an exercise.

4.4. *Exercise:* Derive the next-to-leading order correction in Eq. (4.89) by calculating the loop diagrams in Fig. 4.6. Neglect all terms that vanish as $\Lambda \to \infty$. Introduce a next-to-leading order piece of C_0 to cancel the cubic divergence.

4.3.2 Dimer field formalism

In applications to systems with more than two particles, it is often useful to rewrite the EFT for short-range interactions specified by the Lagrangian (4.73) using so-called dimer fields d [16]: $L = \phi^\dagger \left(i\partial_t + \frac{\nabla^2}{2m} \right) \phi + g_0 d^\dagger d + g_2 d^\dagger \left(i\partial_t + \frac{\nabla^2}{4m} \right) d + \cdots$
$- y \left(d^\dagger \phi^2 + \phi^{\dagger 2} d \right) - d_0 d^\dagger d \phi^\dagger \phi + \cdots$. One important feature of this Lagrangian is that there is no direct two-body contact interaction term $(\phi^\dagger \phi)^2$. All interactions between ϕ particles are mediated via exchange of a dimer field d, *i.e.*, we have effectively performed a Hubbard–Stratonovich transformation. Eliminating the dimer field d by using its equations of motion, it can be shown that the physics of this EFT is equivalent to the Lagrangian (4.73).

Note that the Lagrangian (4.3.2) contains one more free parameter than the Lagrangian (4.73). Thus some parameters are redundant. For the leading-order case ($g_n = 0$ for $n \geq 2$), *e.g.*, we find explicitly,

$$C_0 = \frac{4y^2}{g_0},$$ (4.90)

such that y and g_0 are not independent. Higher-order corrections can be obtained by including a kinetic-energy term for the dimer field. The constants g_0 and y then become independent and can be related to combinations of C_0 and C_2 in the theory without dimers. Here, we only discuss the leading-order case.

4.5. *E*xercise: Derive Eq. (4.90) using the classical equation of motion for d.
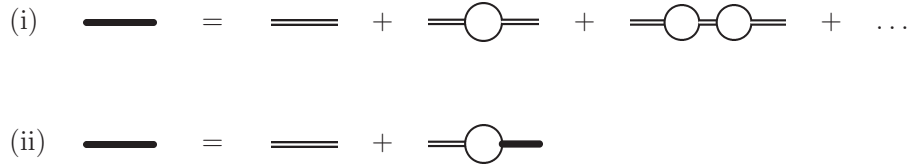
Fig. 4.7 Diagrammatic equations for the full dimer propagator $iD(P_0,P)$. Thin (thick) solid lines represent particle (full dimer) propagators. Double lines indicate bare dimer propagators. (i) perturbative expansion in powers of y, (ii) integral equation summing the geometric series in (i).

The bare propagator for the dimer field is simply the constant i/g_0, which corresponds to no propagation in space or time. However, there are corrections to the dimer propagator from the diagrams in Fig. 4.7(i) which allow the dimer to propagate. This is completely analogous to the geometric series we found we had to sum to obtain the leading-order scattering amplitude. In Feynman diagrams, we represent the full dimer propagator $iD(P_0,P)$ by a thick solid line. We can calculate the full dimer propagator by solving the simple integral equation shown in Fig. 4.7(ii). The loop on the right side is just the integral in Eq. (4.78), with E replaced by $P_0 - P^2/(4m)$, where P_0 and P are the energy and momentum of the dimer. The solution for the full dimer propagator is

$$iD(P_0,P) = \frac{2\pi i}{y^2 m} \left[\frac{2\pi g_0}{y^2 m} + \frac{2}{\pi}\Lambda - \sqrt{-mP_0 + P^2/4 - i\varepsilon} \right]^{-1},$$ (4.91)

where as before Λ is a cutoff on the loop momentum in the bubbles. Using Eq. (4.90) and making the substitution given in Eq. (4.87), the expression for the complete dimer propagator is

$$\mathrm{i}D(P_0,P) = -\frac{2\pi\mathrm{i}}{y^2 m}\left[-1/a + \sqrt{-mP_0 + P^2/4 - \mathrm{i}\varepsilon}\right]^{-1}. \tag{4.92}$$

Note that all the dependence on the ultraviolet cutoff is now in the multiplicative factor $1/y^2$. The complete dimer propagator differs from the off-shell two-body amplitude T_2 in Eq. (4.88) only by a multiplicative constant. For $a > 0$, it has a pole at $P_0 = -1/(ma^2) + P^2/4$ corresponding to a dimer of momentum P and binding energy $B_2 = 1/(ma^2)$. As P_0 approaches the dimer pole, the limiting behavior of the propagator is

$$D(P_0,P) \longrightarrow \frac{Z_D}{P_0 - (-1/(ma^2) + P^2/4) + \mathrm{i}\varepsilon}, \tag{4.93}$$

where the residue factor is

$$Z_D = \frac{4\pi}{am^2 y^2}. \tag{4.94}$$

If we regard the composite operator d as a quantum field that annihilates and creates dimers, then Z_D is the wave function renormalization constant for that field. The renormalized propagator $Z_D^{-1}D(P_0,P)$ is completely independent of the ultraviolet cutoff.

4.3.3 Three-body system

We now study the amplitude for particle-dimer scattering T_3. The simplest diagram we can write down involving only two-body interactions is the exchange of a particle between in- and outgoing dimers. With the scaling of low-energy constants as in Eq. (4.83), the power counting implies that all diagrams that are chains of such exchanges are equally important, *i.e.*, they have to be summed up nonperturbatively. Just like in the two-body case, this can be written as an integral equation. Also including the three-body interaction (note $D_0 \to d_0$ in the Lagrangian with dimer fields), we get the result that is shown diagrammatically in Fig. 4.8.[14]

Omitting the three-body interaction, this is exactly the well-known Skorniakov-Ter-Martirosian (STM) integral equation [17], which the EFT with Lagrangian (4.3.2) reproduces by construction. In addition, EFT provides a clear method to renormalize this equation with a three-body interaction and thus remove its pathologies (discussed below).

In Fig. 4.8, all external lines are understood to be amputated. It simply gives the non-perturbative solution of the three-body problem for the interaction terms proportional to g_0, y, and d_0 in Eq. (4.3.2).

The two tree diagrams on the right side of Fig. 4.8 constitute the inhomogeneous term in the integral equation. An iterative ansatz for the solution of this equation shows that all diagrams with the g_0, y, and d_0 interactions are generated by the iteration. Note also that the thick black lines in Fig. 4.8 represent the full dimer propagator given in Eq. (4.92).

In the center-of-mass frame, we can take the external momenta of the particle and dimer to be $-p$ and $+p$ for the incoming lines and $-k$ and $+k$ for the outgoing lines. We take their energies to be E_A and $E - E_A$ for the incoming lines and E_A' and $E - E_A'$ for the outgoing lines. The amplitude T_3 is then a function of the momenta p and k and the energies E, E_A and E_A'. The integral equation involves a loop over the momentum $-q$ and energy q_0 of a virtual particle. Using the Feynman rules encoded in the Lagrangian (4.3.2), we obtain

---

[14] Note that this amplitude is well defined even if $a < 0$ and there is no two-body bound state. In this case particle lines must be attached to the external dimer propagators to obtain the 3-particle scattering amplitude.
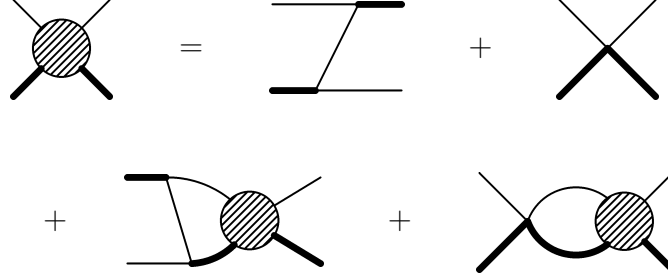
Fig. 4.8 The integral equation for the three-body amplitude T_3. Thin (thick) solid lines represent particle (full dimer) propagators. External lines are amputated.

$$
T_3(p,k;E,E_A,E_A') = -\left[\frac{4y^2}{E - E_A - E_A' - (p+k)^2/(2m) + i\varepsilon} + d_0\right]
$$
$$
+ \frac{2\pi i}{my^2} \int \frac{dq_0}{2\pi} \int \frac{d^3q}{(2\pi)^3} \left[\frac{4y^2}{E - E_A - q_0 - (p+q)^2/(2m) + i\varepsilon} + d_0\right]
$$
$$
\times \frac{1}{q_0 - q^2/(2m) + i\varepsilon} \frac{T_3(q,k;E,q_0,E_A')}{1/a - \sqrt{-m(E - q_0) + q^2/4 - i\varepsilon}}. \quad (4.95)
$$

The integral over q_0 can be evaluated by contour integration. This sets $q_0 = q^2/(2m)$, so the amplitude T_3 inside the integral has the incoming particle on-shell.

We obtain a simpler integral equation if we also set the energies of both the initial and final particles in T_3 on-shell: $E_A = p^2/(2m)$, $E_A' = k^2/(2m)$. Thus only the dimer lines have energies that are off-shell. The resulting integral equation is

$$
T_3\left(p,k;E,\frac{p^2}{2m},\frac{k^2}{2m}\right) = -4my^2\left[\frac{1}{mE - (p^2 + p\cdot k + k^2) + i\varepsilon} + \frac{d_0}{4my^2}\right]
$$
$$
- 8\pi \int \frac{d^3q}{(2\pi)^3} \left[\frac{1}{mE - (p^2 + p\cdot q + q^2) + i\varepsilon} + \frac{d_0}{4my^2}\right]
$$
$$
\times \frac{T_3(q,k;E,q^2/(2m),k^2/(2m))}{-1/a + \sqrt{-mE + 3q^2/4 - i\varepsilon}}. \quad (4.96)
$$

This is an integral equation with three integration variables for an amplitude T_3 that depends explicitly on seven independent variables. There is also an additional implicit variable provided by an ultraviolet cutoff $|q| < \Lambda$ on the loop momentum.

If we set $d_0 = 0$ and ignore the ultraviolet cutoff, the integral equation in Eq. (4.96) is equivalent to the Skorniakov-Ter-Martirosian (STM) equation, an integral equation for three particles interacting via zero-range two-body forces derived by Skorniakov and Ter-Martirosian in 1957 [17]. It was shown by Danilov that the STM equation has no unique solution in the case of identical bosons [18]. He also pointed out that a unique solution could be obtained if one three-body binding energy is fixed. Kharchenko was the first to solve the STM equation with a finite ultraviolet cutoff that was tuned to fit observed three-body data. Thus the cutoff was treated as an additional parameter [19]. When we discuss the running of d_0, we will see that this *ad hoc* procedure is indeed justified and emerges naturally when the three-body equation is renormalized [20].

Here we restrict our attention to the sector of the three-body problem with total orbital angular momentum $L = 0$ where the three-body interaction contributes. For higher L, the original STM equation has a unique solution and can be solved numerically without complication.

The projection onto $L = 0$ can be accomplished by averaging the integral equation over the cosine of the angle between p and k: $x = p \cdot k/(pk)$. It is also convenient to multiply the amplitude T_3 by the wave function renormalization factor Z_D given in Eq. (4.94). We will denote the resulting amplitude by T_3^0:

$$T_3^0(p,k;E) \equiv Z_D \int_{-1}^{1} \frac{dx}{2} T_3\left(p,k;E,p^2/(2m),k^2/(2m)\right). \tag{4.97}$$

Furthermore, it is convenient to express the three-body coupling constant in the form

$$d_0 = -\frac{4my^2}{\Lambda^2} H(\Lambda). \tag{4.98}$$

Since H is dimensionless, it can only be a function of the dimensionless variables $a\Lambda$ and Λ/Λ_*, where Λ_* is a three-body parameter defined below. We will find that H is a function of Λ/Λ_* only.

The resulting integral equation is:

$$T_3^0(p,k;E) = \frac{16\pi}{ma}\left[\frac{1}{2pk}\ln\left(\frac{p^2+pk+k^2-mE-i\varepsilon}{p^2-pk+k^2-mE-i\varepsilon}\right) + \frac{H(\Lambda)}{\Lambda^2}\right]$$
$$+ \frac{4}{\pi}\int_0^{\Lambda} dq\, q^2 \left[\frac{1}{2pq}\ln\left(\frac{p^2+pq+q^2-mE-i\varepsilon}{p^2-pq+q^2-mE-i\varepsilon}\right) + \frac{H(\Lambda)}{\Lambda^2}\right]$$
$$\times \frac{T_3^0(q,k;E)}{-1/a+\sqrt{3q^2/4-mE-i\varepsilon}}. \tag{4.99}$$

Note that the ultraviolet cutoff Λ on the integral over q has been made explicit. A change in the endpoint Λ of the loop integral should be compensated by the Λ-dependence of the function H in Eq. (4.99). More specifically, H must be tuned as a function of Λ so that the cutoff dependence of the solution $T_3^0(p,k;E)$ of Eq. (4.99) decreases as a power of Λ. This will guarantee that $T_3^0(p,k;E)$ has a well-behaved limit as $\Lambda \to \infty$. The renormalization group behavior of H will be discussed in detail below. In the next subsection, we show how different three-body observables can be obtained from the solution $T_3^0(p,k;E)$ of Eq. (4.99).

4.6. Fill in the gaps in the above derivation of Eq. (4.99) and generalize the derivation to general angular momentum L.

4.3.4 Three-body observables

The solution $T_3^0(p,k;E)$ to the three-body integral equation (4.99) encodes all information about three-body observables in the sector with total orbital angular momentum quantum number $L = 0$. In particular, it contains information about the binding energies $B_3^{(n)}$ of the three-body bound states [21]. For a given ultraviolet cutoff Λ, the amplitude $T_3^0(p,k;E)$ has a finite number of poles in E corresponding to the bound states whose binding energies are less than about Λ^2. As Λ increases, new poles emerge corresponding to deeper bound states. In the limit $\Lambda \to \infty$, the locations of these poles approach the energies $-B_3^{(n)}$ of the three-body bound states. The residues of the poles of $T_3^0(p,k;E)$ factor into functions of p and functions of k:

$$T_3^0(p,k;E) \longrightarrow \frac{\mathscr{B}^{(n)}(p)\mathscr{B}^{(n)}(k)}{E+B_3^{(n)}}, \qquad \text{as } E \to -B_3^{(n)}. \tag{4.100}$$

Matching the residues of the poles on both sides of Eq. (4.99), we obtain the bound-state equation $B^{(n)}(p) = \frac{4}{\pi} \int_0^{\Lambda} dq\, q^2 \left[\frac{1}{2pq} \ln \frac{p^2+pq+q^2-mE-i\varepsilon}{p^2-pq+q^2-mE-i\varepsilon} + \frac{H(\Lambda)}{\Lambda^2} \right]$

$\times \left[-1/a + \sqrt{3q^2/4 - mE - i\varepsilon} \right]^{-1} \mathscr{B}^{(n)}(q)$. The values of E for which this homogeneous integral equation has solutions are the energies $-B_3^{(n)}$ of the three-body states. For a finite ultraviolet cutoff Λ, the spectrum of $B_3^{(n)}$ is cut off around Λ^2.
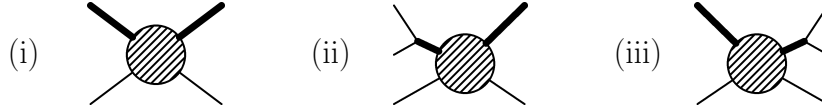
Fig. 4.9 Amplitudes for (i) particle-dimer scattering, (ii) three-body recombination, and (iii) three-body breakup. Diagrams (ii) [(iii)] should be summed over the three pairs of particles that can interact first [last]. Notation as in Fig. 4.8.

The S-wave phase shifts for particle-dimer scattering can be determined from the solution $T_3^0(p,k;E)$ to the integral equation (4.99). The T-matrix element for the elastic scattering of an particle and a dimer with momenta k is given by the amplitude T_3^0 evaluated at the on-shell point $p = k$ and $E = -B_2 + 3k^2/(4m)$ and multiplied by a wave function renormalization factor $Z_D^{1/2}$ for each dimer in the initial or final state. It can be represented by the Feynman diagram in Fig. 4.9(i). The blob represents the amplitude T_3 or equivalently $Z_D^{-1} T_3^0$. The external double lines are amputated and correspond to asymptotic dimers and are associated with factors $Z_D^{1/2}$

The S-wave contribution to the T-matrix element is

$$T_{PD\to PD}^0 = T_3^0(k,k;3k^2/(4m) - 1/(ma^2)),\tag{4.101}$$

where $B_2 = 1/(ma^2)$ has been used. Note that the factors of Z_D multiplying T_3^0 cancel. The differential cross section for elastic particle-dimer scattering is

$$d\sigma_{PD\to PD} = \frac{2m}{3k} |T_{PD\to PD}(k)|^2 \frac{km}{6\pi^2} d\Omega.\tag{4.102}$$

The flux factor $2m/(3k)$ is the inverse of the relative velocity of the particle and the dimer. The phase space factor $kmd\Omega/(6\pi^2)$ takes into account energy and momentum conservation and the standard normalization of momentum eigenstates:

$$\int \frac{d^3 p_A}{(2\pi)^3} \frac{d^3 p_D}{(2\pi)^3} (2\pi)^4 \delta^3(p_A + p_D) \delta(p_A^2/(2m) + p_D^2/(4m) - E) = \frac{m}{6\pi^2} (4mE/3)^{1/2} \int d\Omega.\tag{4.103}$$

The S-wave phase shift for particle-dimer scattering is related to the T-matrix element via

$$\frac{1}{k\cot\delta_0^{PD}(k) - ik} = \frac{m}{3\pi} T_3^0(k,k;3k^2/(4m) - 1/(ma^2)).\tag{4.104}$$

In particular, the particle-dimer scattering length is given by

$$a_{PD} = -\frac{m}{3\pi} T_3^0(0,0;-1/(ma^2)).\tag{4.105}$$

The threshold rate for three-body recombination can also be obtained from the solution $T_3^0(p,k;E)$ to the three-body integral equation in Eq. (4.99). This is possible only at threshold, because a 3-particle scattering state becomes pure $L = 0$ only in the limit that the energies

of the particles go to zero. The T-matrix element for the recombination process can be represented by the Feynman diagram in Fig. 4.9(ii) summed over the three pairs of particle lines that can attach to the dimer line. The blob represents the amplitude $Z_D^{-1} T_3^0$ evaluated at the on-shell point $p = 0$ $k = 2/(\sqrt{3}a)$, and $E = 0$. The solid line represents the dimer propagator $iD(0,0)$ evaluated at zero energy and momentum $2/(\sqrt{3}a)$, which is given by Eq. (4.91). The factor for the particle-dimer vertex is $-i2y$. The wave function renormalization factor $Z_D^{1/2}$ for the final-state dimer is given by Eq. (4.94). In the product of factors multiplying T_3^0, the dependence on y and Λ can be eliminated in favor of the scattering length a. Taking into account a factor of 3 from the three Feynman diagrams, the T-matrix element is

$$T_{PD \to PPP} = 6\sqrt{\pi a^3}\, T_3^0(0, 2/(\sqrt{3}a); 0)\,. \tag{4.106}$$

The differential rate dR for the recombination of three particles with energies small compared to the dimer binding energy can be expressed as

$$dR = |T_{PPP \to PD}|^2\, \frac{km}{6\pi^2}\, d\Omega\,, \tag{4.107}$$

where $k = 2/(\sqrt{3}a)$. The threshold rate for three-body breakup can be obtained in a similar way from the Feynman diagram in Fig. 4.9(iii)

The inhomogeneous integral equation for the off-shell particle dimer amplitude, Eq. (4.99), and the homogeneous equation, Eq. (4.3.4), for the three-body binding energies afford no analytical solution. They are usually solved by discretizing the integrals involved and solving the resulting matrix problems numerically.

4.3.5 Renormalization group limit cycle

The form of the full renormalized dimer propagator in Eq. (4.92) is consistent with the continuous scaling symmetry

$$a \longrightarrow \lambda a\,, \qquad E \longrightarrow \lambda^{-2} E\,, \tag{4.108}$$

for any positive real number λ. In the integral equation (4.99), this scaling symmetry is broken by the ultraviolet cutoff on the integral and by the three-body terms proportional to H/Λ^2. To see that the cutoff and the three-body terms are essential, we set $H = 0$ and take $\Lambda \to \infty$. The resulting integral equation has exact scaling symmetry. We should therefore expect its solution $T_3^0(p,k;E)$ to behave asymptotically as $p \to \infty$ like a pure power of p. Neglecting the inhomogeneous term, neglecting E and $1/a^2$ compared to q^2, and setting $T_3^0 \approx p^{s-1}$, the integral equation reduces to [18]

$$p^{s-1} = \frac{4}{\sqrt{3}\pi p} \int_0^\infty dq\, q^{s-1} \ln \frac{p^2 + pq + q^2}{p^2 - pq + q^2}\,. \tag{4.109}$$

Making the change of variables $q = xp$, the dependence on p drops out, and we obtain

$$1 = \frac{4}{\sqrt{3}\pi} \int_0^\infty dx\, x^{s-1} \ln \frac{1 + x + x^2}{1 - x + x^2}\,. \tag{4.110}$$

The integral is a Mellin transform that can be evaluated analytically. The resulting equation for s is

$$1 = \frac{8}{\sqrt{3}s} \frac{\sin(\pi s/6)}{\cos(\pi s/2)}\,. \tag{4.111}$$

The solutions with the lowest values of $|s|$ are purely imaginary: $s = \pm i s_0$, where $s_0 \approx 1.00624$. The most general asymptotic solution therefore has two arbitrary constants:

$$T_3^0(p,k;E) \longrightarrow A_+ \, p^{-1+is_0} + A_- \, p^{-1-is_0}, \qquad \text{as } p \to \infty. \tag{4.112}$$

The inhomogeneous term in the integral equation (4.99) will determine one of the constants. The role of the three-body term in the integral equation is to determine the other constant, thus giving the integral equation a unique solution.

By demanding that the solution of the integral equation (4.99) has a well-defined limit as $\Lambda \to \infty$, Bedaque *et al.*deduced the Λ-dependence of H and therefore of d_0 [20]. The leading dependence on Λ on the right side of the three-body integral equation in Eq. (4.99) as $\Lambda \to \infty$ is a log-periodic term of order Λ^0 that comes from the region $q \sim \Lambda$. There are also contributions of order $1/\Lambda$ from the region $|a|^{-1}, k, |E|^{1/2} \ll q \ll \Lambda$, which have the form

$$\frac{8}{\pi\sqrt{3}} \int^\Lambda dq \left(\frac{1}{q^2} + \frac{H(\Lambda)}{\Lambda^2} \right) (A_+ \, q^{+is_0} + A_- \, q^{-is_0}). \tag{4.113}$$

The sum of the two terms will decrease even faster as $1/\Lambda^2$ if we choose the function H to have the form

$$H(\Lambda) = \frac{A_+ \Lambda^{is_0}/(1-is_0) + A_- \Lambda^{-is_0}/(1+is_0)}{A_+ \Lambda^{is_0}/(1+is_0) + A_- \Lambda^{-is_0}/(1-is_0)}. \tag{4.114}$$

The tuning of H that makes the term in Eq. (4.113) decrease like $1/\Lambda^2$ also suppresses the contribution from the region $q \sim \Lambda$ by a power of $1/\Lambda$ so that it goes to 0 in the limit $\Lambda \to \infty$. By choosing $A_\pm = (1+s_0^2)^{1/2} \Lambda_*^{\mp is_0}/2$ in Eq. (4.114), we obtain [20]

$$H(\Lambda) \approx \frac{\cos[s_0 \ln(\Lambda/\Lambda_*) + \arctan s_0]}{\cos[s_0 \ln(\Lambda/\Lambda_*) - \arctan s_0]}. \tag{4.115}$$

This equation defines a three-body scaling-violation parameter Λ_* with dimensions of momentum. The value of Λ_* can be fixed from a three-body datum. All other three-body observables can then be predicted. If Eq. (4.115) is substituted back into the three-body equation (4.99) for numerical calculations, it must be multiplied by a normalization factor $b \approx 1$ whose precise value depends on the details of the regularization [22].

Note that H is a π-periodic function of $s_0 \ln(\Lambda/\Lambda_*)$, so Λ_* is defined only up to a multiplicative factor of $(e^{\pi/s_0})^n$, where n is an integer. Thus the scaling symmetry of Eq. (4.108) is broken to the discrete subgroup of scaling transformations with multiples of the preferred scaling factor $\lambda = e^{\pi/s_0}$. This discrete scaling symmetry is, *e.g.*, evident in the geometric spectrum of three-body Efimov states [21] in the unitary limit ($1/a = 0$) that naturally emerge in this EFT:

$$B_3^{(n)} \approx 0.15 \lambda^{2(n_*-n)} \frac{\Lambda_*^2}{m}, \tag{4.116}$$

where n_* an integer labeling the state with binding energy $0.15 \Lambda_*^2/m$.[15] The discrete scaling symmetry becomes also manifest in the log-periodic dependence of three-body observables on the scattering length. This log-periodic behavior is the hallmark signature of a renormalization group limit cycle. It has been observed experimentally in the three-body recombination spectra of ultracold atomic gases close to a Feshbach resonance [23, 24].

The physics of the renormalization procedure is illustrated in Fig. 4.10 where we show the unrenormalized three-body binding energies B_3 in the case of positive scattering length as a function of the cutoff Λ (solid line). As the cutoff Λ is increased, B_3 increases asymptotically as Λ^2. At a certain cutoff (indicated by the dotted line), a new bound state appears at the

---

[15] For a detailed discussion of the Efimov effect for finite scattering length and applications to ultracold atoms, see Ref. [10].
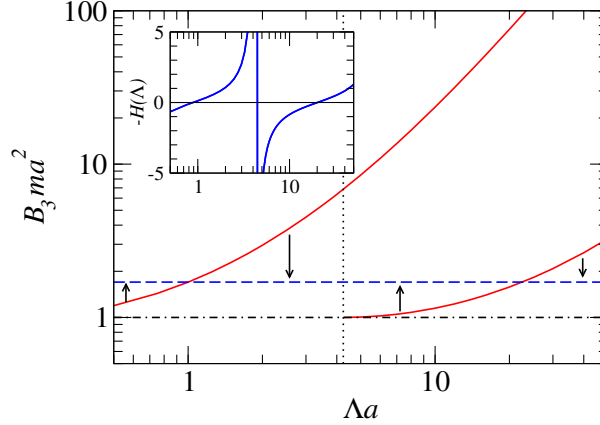
Fig. 4.10 Unrenormalized three-body energies B_3 as a function of the momentum cutoff Λ (solid lines). The dotted line indicates the cutoff where a new three-body state appears at the particle-dimer threshold (dash-dotted line). The dashed line shows a hypothetical renormalized energy. The inset shows the running of the three-body force $d_0(\Lambda) \sim -H(\Lambda)$ with Λ.

boson-dimer threshold. This pattern repeats every time the cutoff increases by the discrete scaling factor $\exp(\pi/s_0)$. Now assume that we adopt the renormalization condition that the shallowest state should have a constant energy given by the dashed line. At small values of the cutoff, we need an attractive three-body force to increase the binding energy of the shallowest state as indicated by the arrow. As the cutoff is increased further, the required attractive contribution becomes smaller and around $\Lambda a = 1.1$ a repulsive three-body force is required (downward arrow). Around $\Lambda a = 4.25$, a new three-body state appears at threshold and we cannot satisfy the renormalization condition by keeping the first state at the required energy anymore. The number of bound states has changed and there is a new shallow state in the system. At this point the three-body force turns from repulsive to attractive to move the new state to the required energy. The corresponding running of the three-body force with the cutoff Λ is shown in the inset. After renormalization, the first state is still present as a deep state with large binding energy, but for threshold physics its presence can be ignored. This pattern goes on further and further as the cutoff is increased [25].

4.4 Effective field theory for nuclear few-body systems

4.4.1 Overview

Depending on the physics one wishes to describe, there are several effective field theories for low-energy nuclear physics to choose from. They differ in the set of effective degrees of freedom, their expansion point (typical low-energy scale) and range of applicability. Chiral effective field theory includes nucleons and pions and is designed as an expansion about the so-called "chiral limit," *i.e.*, the scenario where the quark masses are exactly zero such that the pions emerge as exactly massless Goldstone bosons from the spontaneous breaking of chiral symmetry. In reality, the quark-masses are nonzero such that the pions become "pseudo-Goldstone" bosons with a small (compared to typical QCD scales like m_ρ or M_N) mass m_π. Chiral EFT takes this as a typical low scale so that its power counting is designed for momenta of the order $Q \sim m_\pi$; we come back to this in Sec. 4.5.3.

For momenta much smaller than m_π, explicit pion exchange cannot be resolved such that these can be regarded as integrated out, much like we did explicitly for the pseudoscalar toy model in Sec. 4.2.2.3. The resulting "pionless" theory has, up to long-range forces that we consider in Sec. 4.5.1) only contact interactions between nucleons left. These contact interactions parameterize not only unresolved pion exchange, but also that of heavier mesons, for which contact terms already exist in Chiral EFT. Pionless EFT is formally very similar to the few-boson EFT discussed in Sec. 4.3, and it despite its simplicity it gives rise to surprisingly rich physics, as we will show in this section.

4.4.2 Pionless effective field theory

The neutron-proton S-wave scattering lengths are experimentally determined to be about 5.4 fm in the $^3S_1$ channel, and -23.7 fm in the $^1S_0$ channel. What is special about these numbers is that they are large compared to the typical nuclear length scale determined by the pion Compton wavelength, $m_\pi^{-1} \sim 1.4$ fm. This estimate comes from the long-range component of the nuclear interaction being determined by one-pion exchange. Naïvely, if we consider the low-energy limit (NN center-of-mass momentum going to zero) we expect that we can integrate out the pions and end up with a contact interaction scaling with the inverse pion mass, and thus a perturbative EFT reproducing natural-sized scattering lengths. The fact that this is not the case is typically interpreted as nature "choosing" the fine-tuned scenario outlined in Sec. 4.2.3.3. In this case, pion exchange[16] combines with shorter range interactions to yield the large S-wave scattering lengths (and the deuteron as an unnaturally shallow bound state), implying that nuclear physics is a strongly coupled and thus nonperturbative system at low energies. This is what allows us to write down an EFT that is closely related to the one that describes strongly interacting bosons. What governs the physics of low-energy observables is to a good appropriation just the fact that the scattering lengths are large, so we end up with a short-range EFT much like the one for bosons encountered in Sec. 4.3. Some rather technical new features arise from the fact that nucleons are fermions with spin and isospin.

4.4.3 The two-nucleon S-wave system

The leading-order Lagrangian for pionless EFT can be written as

$$\mathcal{L} = N^\dagger \left(i\partial_0 + \frac{\nabla^2}{2M_N} + \cdots \right) N - C_{0,s}(N^T \hat{P}_s N)^\dagger (N^T \hat{P}_s N) - C_{0,t}(N^T \hat{P}_t N)^\dagger (N^T \hat{P}_t N) + \cdots , \qquad (4.117)$$

with projectors

$$(\hat{P}_t)^i = \sigma^2 \sigma^i \tau^2 / \sqrt{8} \ , \ (\hat{P}_s)^\lambda = \sigma^2 \tau^2 \tau^\lambda / \sqrt{8} \qquad (4.118)$$

such that $C_{0,s}$ and $C_{0,t}$ refer to the $^1S_0$ and $^3S_1$ NN channels, respectively. As in previous sections of this chapter, we use σ^i to denote the Pauli matrices in spin space, and write $(\sigma^i)^\alpha{}_\beta$ to refer to their individual entries (with the upper index referring to the row). Conversely, we use the notation $(\tau^\lambda)^a{}_b$ in isospin space.

With the usual cartesian indices $i, \lambda = 1, 2, 3$ the projectors for given i or λ give somewhat unusual combinations of individual states. For example, np configurations are completely

---

[16] As discussed in Sec. 4.5.3 this actually has to be the exchange of two or more pions, as one-pion exchange does not contribute to S-wave scattering at zero energy.

contained in the $\lambda = 3$ isospin component, whereas nn and pp are obtained from linear combinations $1 \pm i2$, In other words, in order to separate the physical states (and likewise to get spin-1 states with $m = 0, \pm 1$ quantum numbers) one should work instead with a spherical basis. For example, if one wants to include isospin-breaking terms, it is convenient to work with the projectors

$$(\tilde{P}_s)^{-1} = \frac{1}{\sqrt{2}} \left[(\hat{P}_s)^1 - i(\hat{P}_s)^2 \right] \quad , \quad (\tilde{P}_s)^0 = (\hat{P}_s)^3 \quad , \quad (\tilde{P}_s)^{+1} = -\frac{1}{\sqrt{2}} \left[(\hat{P}_t)^1 + i(\hat{P}_s)^2 \right] . \qquad (4.119)$$

Otherwise, since the difference is a unitary rotation, the choice of basis is arbitrary.

4.4.3.1 Spin and isospin projection

To understand why the projectors have been defined as in Eq. (4.118), it is instructive to calculate the tree-level contribution to the amplitude in a given channel. With all spin and isospin vertices written out, the Feynman rule for the four-nucleon vertex in the $^3S_1$ channel is

$$\sim i\frac{C_{0,t}}{8} (\sigma^i \sigma^2)^\alpha{}_\beta (\tau^2)^a{}_b (\sigma^2 \sigma^i)^\gamma{}_\delta (\tau^2)^c{}_d, \qquad (4.120)$$

which is obtained by simply writing out the $(\hat{P}_t)^i$ from Eq. (4.118). Furthermore, this diagram has an associated combinatorial factor 4 because there are two possibilities each to contract the in- and outgoing legs with external nucleon fields.

In order to calculate the T-matrix, we have to write out the Lippmann–Schwinger equation with all indices (and symmetry factors) and then apply the appropriate projectors. For $^3S_1$ and isospin 0, the result should have two free spin-1 indices, which we label k and j for the in- and outgoing side, respectively. The inhomogeneous term is just the vertex (4.120) with an additional factor 4. Applying the projectors, we get

$$\frac{1}{\sqrt{8}} (\sigma^2 \sigma^j)^\beta{}_\alpha (\tau^2)^b{}_a \times 4 \times i\frac{C_{0,t}}{8} (\sigma^i \sigma^2)^\alpha{}_\beta (\tau^2)^a{}_b (\sigma^2 \sigma^i)^\gamma{}_\delta (\tau^2)^c{}_d \times \frac{1}{\sqrt{8}} (\tau^2)^d{}_c (\sigma^k \sigma^2)^\delta{}_\gamma$$

$$= i\frac{C_{0,t}}{16} \text{Tr}(\sigma^j \sigma^i) \text{Tr}(\tau^2 \tau^2) \text{Tr}(\sigma^i \sigma^k) \text{Tr}(\tau^2 \tau^2) = iC_{0,t} \delta^{jk}, \quad (4.121)$$

where we have used the well-known of the Pauli matrices. This is exactly the expected result: the projectors (4.118) have been constructed to give this. The projection of other, more complicated diagram works in the same way. Albeit somewhat tedious, it is technically straightforward. For higher partial waves, one of course has to take into account the coupling of spin and orbital angular momentum.

4.4.3.2 Dibaryon fields

Just like for bosons, it is convenient to introduce auxiliary dimer—now called dibaryon—field for each of the NN S-wave states. This is done by rewriting the Lagrangian (4.117) as

$$\mathscr{L} = N^\dagger \left(\mathrm{i}\partial_0 + \frac{\nabla^2}{2M_N} + \cdots \right) - t^{i\dagger} \left[g_t + \left(\mathrm{i}\partial_0 + \frac{\nabla^2}{4M_N} \right) \right] t^i + y_t \left[t^{i\dagger} \left(N^T P_t^i N \right) + \mathrm{h.c.} \right]$$

$$- s^{\lambda\dagger} \left[g_s \left(\mathrm{i}\partial_0 + \frac{\nabla^2}{4M_N} \right) \right] s^\lambda + y_s \left[s^{\lambda\dagger} \left(N^T P_s^\lambda N \right) + \mathrm{h.c.} \right] + \cdots, \quad (4.122)$$

where t (s) denotes a $^3S_1$($^1S_0$) dibaryon field and the projection operators $P_{s,t}$ are as defined in Eq. (4.118). The "bare" dibaryon propagators are just $\mathrm{i}/g_{s,t}$, while the full leading-order expressions are obtained by summing up all nucleon bubble insertions. This resummation, which without dibaryon fields gives the *NN* T-matrix as a bubble chain, reflects the fact we need to generate shallow states (the bound deuteron and the virtual $^1S_0$ state) to account for the unnaturally large *NN* scattering lengths. Pionless EFT is designed to capture this feature.

Omitting spin-isospin factors for simplicity, the resummed propagators are

$$\mathrm{i}\Delta_{s,t}(p_0, \mathbf{p}) = \frac{-\mathrm{i}}{g_{s,t} + y_{s,t}^2 I_0(p_0, \mathbf{p})}, \quad (4.123)$$

where

$$I_0(p_0, \mathbf{p}) = M_N \int^\Lambda \frac{\mathrm{d}^3 q}{(2\pi)^3} \frac{1}{M_N p_0 - \mathbf{p}^2/4 - \mathbf{q}^2 + \mathrm{i}\varepsilon} = -\frac{M_N}{4\pi} \left(\frac{2\Lambda}{\pi} - \sqrt{\frac{\mathbf{p}^2}{4} - M_N p_0 - \mathrm{i}\varepsilon} \right) + \mathcal{O}(1/\Lambda) \quad (4.124)$$

is the familiar bubble integral regularized with a momentum cutoff. The cutoff dependence is absorbed into the parameters $y_{s,t}$ and $g_{s,t}$ to obtain the renormalized propagators. Attaching external nucleon legs gives the *NN* T-matrix,

$$\mathrm{i}T_{s,t}(k) = (\mathrm{i}y_{s,t})^2 \, \mathrm{i}\Delta_{s,t}\left(p_0 = k^2/M_N, \mathbf{p} = \mathbf{0} \right) = \frac{4\pi}{M_N} \frac{\mathrm{i}}{k\cot\delta_{s,t}(k) - \mathrm{i}k}, \quad (4.125)$$

so we can match to the effective range expansions for $k\delta_{s,t}(k)$. At leading order, the renormalization condition is to reproduce $k\cot\delta_{s,t}(k) = -1/a_{s,t} + \mathcal{O}(k^2)$, which gives

$$\frac{4\pi g_{s,t}}{M_N y_{s,t}^2} = -\frac{1}{a_{s,t}} + \frac{2\Lambda}{\pi}. \quad (4.126)$$

Instead of this standard choice of the expansion around the zero-energy threshold, it is convenient to expand the $^3S_1$ channel around the deuteron pole.[17] This is

$$k\cot\delta_t(k) = \gamma_t + \frac{\rho_t}{2}\left(k^2 + \gamma_t^2 \right) + \cdots, \quad (4.127)$$

where $\gamma_t = \sqrt{M_N B_d} \simeq 45.7$ is the deuteron binding momentum and $\rho_t \simeq 1.765$ is the "deuteron effective range." This choice, which sets

$$\frac{4\pi g_t}{M_N y_t^2} = -\gamma_t + \frac{2\Lambda}{\pi}, \quad (4.128)$$

gets the exact deuteron pole position right at leading order, but is equivalent to the choice in Eq. (4.126) up to range corrections.

---

[17] The shallow deuteron bound-state pole is within the radius of convergence of the effective range expansion. The deuteron binding momentum is $\gamma_t = 1a_t + \cdots$, where the ellipses include corrections from the effective range (and higher-order shape parameters).

Wavefunction renormalization

The residue at the deuteron pole gives the deuteron wavefunction renormalization. We find

$$Z_t^{-1} = i\frac{\partial}{\partial p_0} \left.\frac{1}{i\Delta_t(p_0,\mathbf{p})}\right|_{p_0=-\frac{\gamma_t^2}{M_N},\mathbf{p}=0} = \frac{M_N^2 y_t^2}{8\pi\gamma_t} \Rightarrow \sqrt{Z_t} = \frac{1}{y_t}\frac{\sqrt{8\pi\gamma_t}}{M_N} \tag{4.129}$$

for the renormalization as in Eq. (4.128). If we directly consider the (off-shell) T-matrix near the pole, we find $\quad \mathrm{T(E)} = 4\pi\dfrac{1}{M_N\frac{1}{-\gamma_t+\sqrt{-M_N E - i\varepsilon}}=-\frac{4\pi}{M_N}\frac{\sqrt{-M_N E - i\varepsilon}+\gamma_t}{-M_N E - \gamma_t^2}\quad\text{for }\varepsilon\to 0\ \sim -\frac{8\pi\gamma_t}{M_N^2}\frac{1}{E+\dfrac{\gamma_t^2}{M_N}}\quad\text{as }E\to-\gamma_t^2/M_N}\quad .$

Comparing to the standard factorization at the pole,[18]

$$T(k,p;E) = -\frac{B^\dagger(k)B(p)}{E+E_B} + \text{terms regular at } E = -E_B\,, \tag{4.130}$$

we can read off from Eq. (4.4.3.2) that

$$B(p) = \sqrt{\frac{8\pi\gamma_t}{M_N^2}} = y_t\sqrt{Z_t}\,, \tag{4.131}$$

independent of momentum at this order.

4.4.4 Three nucleons: scattering and bound states

As done in Sec. 4.3.3 for bosons, the dimer/dibaryon formalism allows for a particularly intuitive and simple description of the three-body system. Looking at nucleon-deuteron S-wave scattering[19], we find that the spin 1 of the deuteron can couple with the spin $1/2$ of the nucleon to a total spin of either $3/2$ or $1/2$. These two cases are referred to as the quartet and doublet channel, respectively.

4.4.4.1 Quartet channel
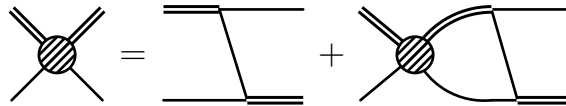
Fig. 4.11 *Nd* quartet-channel integral equation. Nucleons and deuterons are represented as single and double lines, respectively. The blob represents the T-matrix.

In the quartet-channel, the spins of all three nucleons have to be aligned to produce the total spin $3/2$. This means that only the deuteron field can appear in intermediate states, and the Pauli principle excludes a three-body contact interaction without derivatives. The resulting integral equation for the *Nd* T-matrix is shown diagrammatically in Fig. 4.11. Compared to Fig. 4.8, we use a different convention here were the T-matrix blob is drawn to the left of the

---

[18] The minus sign in Eq. (4.130) is a consequence of the convention we use here for the T-matrix.

[19] We work in the isospin-symmetric theory here, but in the absence of electromagnetic interactions (discussed in Sec. 4.5.1), the nucleon here should be thought of as a neutron.

nucleon exchange, and we denote in- and outgoing momenta (in the Nd center-of-mass frame) by $\pm\mathbf{k}$ and $\pm\mathbf{p}$, respectively.[20] The energy and momentum dependence are exactly the same as for bosons, but we have to include the additional spin-isospin structure from the vertices. Doing this, the result in its full glory reads:

$$\left(\mathrm{i}T_q^{ij}\right)^{\beta b}{}_{\alpha a}(\mathbf{k},\mathbf{p};E) = -\frac{\mathrm{i}M_N y_t^2}{2}\left(\sigma^j\sigma^i\right)^{\beta}{}_{\alpha}\delta_a^b\,\frac{1}{\mathbf{k}^2+\mathbf{k}\cdot\mathbf{p}+\mathbf{p}^2-M_N E-\mathrm{i}\varepsilon}$$
$$+\int\frac{\mathrm{d}^3q}{(2\pi)^3}\,\Delta_t\left(E-\frac{\mathbf{q}^2}{2M_N},\mathbf{q}\right)\left(\mathrm{i}T_q^{ik}\right)^{\gamma c}{}_{\alpha a}(E;\mathbf{k},\mathbf{q})$$
$$\times\frac{M_N y_t^2}{2}\,\frac{\left(\sigma^j\sigma^k\right)^{\beta}{}_{\gamma}\delta_c^b}{\mathbf{q}^2+\mathbf{q}\cdot\mathbf{p}+\mathbf{p}^2-M_N E-\mathrm{i}\varepsilon}\,. \quad (4.132)$$

This unprojected amplitude carries spin and isospin indices for the various fields in the initial and final states. To select the overall spin $3/2$ contribution, we take linear combinations as in Eq. (4.119) to select the maximal projections for the in- and outgoing deuterons and $\alpha=\beta=1$ to get nucleons with spin orientation $+1/2$. We also set $a=b=2$ to select neutrons. Altogether, this gives

$$\left(\sigma^j\sigma^i\right)^{\beta}{}_{\alpha}\delta_a^b\to 2\,, \quad (4.133)$$

in the inhomogeneous term, and the same factor for the integral part. The fully projected quartet-channel amplitude is

$$T_q = \frac{1}{2}\left(T_q^{11}+\mathrm{i}\left(T_q^{12}-T_q^{21}\right)+T_q^{22}\right)^{12}_{12}\,. \quad (4.134)$$

4.7. *Exercise:* Work out the details leading to Eq. (4.134).

Finally, the S-wave projection of Eq. (4.132) is done by applying the operator $\frac{1}{2}\int_{-1}^{1}\mathrm{d}\cos\theta$, where θ is the angle between $\mathbf{k}$ and $\mathbf{p}$. Introducing a momentum cutoff Λ, the resulting equation can be solved numerically by discretizing the remaining one-dimensional integral. From the result, which we denote by T_q^0, we can calculate observables like scattering phase shifts,

$$\delta_q(k) = \frac{1}{2\mathrm{i}}\ln\left(1+\frac{2\mathrm{i}kM_N}{3\pi}Z_t T_q^0(k,k;E_k)\right)\quad,\quad E_k = \frac{3k^2}{4M_N}-\frac{\gamma_t^2}{M_N}\,, \quad (4.135)$$

or the Nd scattering length:

$$a_q = \frac{M_N}{3\pi}\lim_{k\to 0}Z_t T_q^0(k,k;E_k)\,. \quad (4.136)$$

Note that we have not absorbed the wavefunction renormalization Z_t into T_q^0 but instead chose to keep it explicit in Eqs. (4.135) and (4.136)

4.4.4.2 Doublet channel

The doublet channel (total spin $1/2$) has a richer structure, since now also the $^1S_0$ dibaryon can appear as an intermediate state. The result is a coupled channel integral equation, shown diagrammatically in Fig. 4.12. We skip here the technicalities of the spin-isospin projection (for details, see Ref. [26] and earlier references therein) and merely quote the result in a compact notation:

---

[20] Unlike what is done in Sec. 4.3, we also read diagrams from left (incoming particles) to right (outgoing particles). Both conventions can be found in the literature.
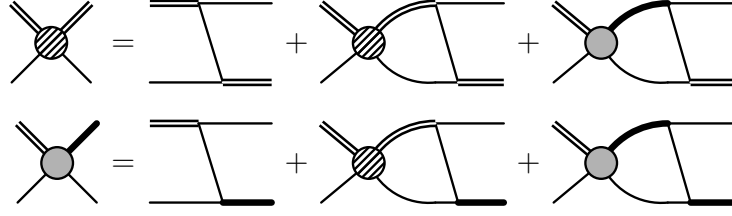
Fig. 4.12 *Nd* doublet-channel integral equation. As in Fig. 4.11, nucleons and deuterons are drawn as single and double lines, respectively. Additionally, we represent the $^1S_0$dibaryon as a thick line. The hatched and shaded blobs are the two components of the doublet-channel $Nd \to Nd$ T-matrix.

$$T^0_{d,1} T^0_{d,2} = M_N y_t^2/2 - 3M_N y_t y_s/2K + D_t 00 D_s - M_N y_t^2/2 3M_N y_t y_s/2 3M_N y_s y_t/2 - M_N y_s^2/2K \otimes T^0_{d,1} T^0_{d,2}, \tag{4.137}$$

where K is the "kernel" function

$$K(k,p;E) = \frac{1}{2kp} \ln\left(\frac{k^2 + p^2 + kp - M_N E - i\varepsilon}{k^2 + p^2 - kp - M_N E - i\varepsilon}\right), \tag{4.138}$$

$$D_{s,t}(q;E) = \Delta_{s,t}\left(E - \frac{q^2}{2M_N};q\right), \tag{4.139}$$

and the integral operation

$$A \otimes B \equiv \frac{1}{2\pi^2} \int_0^\Lambda \mathrm{d}q\, q^2 A(\ldots,q)B(q,\ldots) \tag{4.140}$$

has to be applied within each block. Just like the quartet-channel equation, Eq. (4.137) can be solved numerically by discretizing the integrals, with the additional complication that we now have a 2×2 block matrix. The T-matrix likewise becomes a 2-block vector, the upper part of which is gives the physical $Nd \to Nd$ amplitude.[21]

4.8. *Exercise:* Express the fully projected integral equation for the quartet channel amplitude T_q^0 using the compact notation based on Eqs. (4.138), (4.139), and (4.140).

Leading-order three-nucleon force

Studying the doublet-channel solution as a function of increasing UV cutoff Λ, one finds that there is no stable limit as $\Lambda \to \infty$. Instead, the amplitude changes wildly as Λ is varied. This is much unlike the quartet-channel case, which shows a rapid convergence with Λ.

The origin of this behavior was explained by Bedaque *et al.* [27]. The behavior for large Λ is governed by large momenta, which means that infrared scales like the scattering lengths do not matter. Indeed, one finds that $D_t(E;q)$ and $D_s(E;q)$ have the same leading behavior as $q \to \infty$. To analyze the asymptotic behavior of the amplitude we can thus go to the $SU(4)$ spin-isospin symmetric limit and set $D_t = D_t \equiv D$ as well as $y_t = y_s \equiv y$. In this limit, the two integral equations in Eq. (4.137) can be decoupled by defining $T_{d,\pm} = T_{d,1} \pm T_{d,2}$. For $T_{d,+}$ we find the integral equation

$$T^0_{d,+}(k,p;E) = -M_N y^2 K(k,p;E) + M_N y^2 \int_0^\Lambda \frac{\mathrm{d}q}{2\pi^2}\, q^2 K(k,q;E)D(q;E)T^0_{d,+}(q,p;E), \tag{4.141}$$

---

[21] Note that this vector is one part of the more general full off-shell amplitude, which is a 2×2 block matrix including the two combinations of dibaryon legs that do not appear in Fig. 4.12.

which is formally exactly the same as the three-boson integral equation, Eq. (4.99), in the absence of a three-body force. As discussed in Sec. 4.3.3, this equation does not have a unique solution in the limit $\Lambda \to \infty$. Since $T_{d,1/2}$ are linear combinations of involving $T_{d,+}$, they inherit the same behavior. But the cure is now obvious: a three-nucleon force, which by naïve counting would only enter at higher orders, has to be promoted to leading order in order to make Eq. (4.137) well defined. This three-nucleon force, like the asymptotic amplitudes, is $SU(4)$ symmetric (invariant under arbitrary spin-isospin rotations) and can be written as

$$\mathscr{L}_3 = \frac{h_0}{3} N^\dagger \left[y_t^2 \, t^{i\dagger} t^j \sigma^i \sigma^j + y_s^2 \, s^{A\dagger} s^B \tau^A \tau^B - y_t y_s \left(t^{i\dagger} s^A \sigma^i \tau^A + \text{h.c.} \right) \right] N , \tag{4.142}$$

where the cutoff-running of the three-nucleon coupling is analogous to what we derived for bosons:

$$h_0 = \frac{M_N H(\Lambda)}{\Lambda^2} . \tag{4.143}$$

Including this, the coupled doublet-channel integral equation becomes

$$T_{d,1}^0 T_{d,2}^0 = M_N y_t^2 / 2 - 3 M_N y_t y_s / 2 K + D_t 00 D_s - M_N y_t^2 / 2 (K + h_0) 3 M_N y_t y_s / 2 (K + h_0) 3 M_N y_s y_t / 2 (K + h_0) - M_N y_s^2 / 2 (K + h_0) \otimes T_{d,1}^0 T_{d,2}^0 . \tag{4.144}$$

We stress that the requirement to include this three-body force at leading-order is a feature of the nonperturbative physics that can be traced back to the large NN scattering lengths. All loop diagrams obtained by iterating the integral equation are individually finite as $\Lambda \to \infty$, yet their infinite sum does not exist in that limit unless the h_0 contact interaction is included.

The Phillips line

The form of $H(\Lambda)$ is given by Eq. (4.115), but since there is a prefactor that depends on the details of the regularization scheme, in practice one has to determine the appropriate value numerically after choosing a cutoff Λ. This requires a three-body datum as input, which is conveniently chosen to be the triton binding energy—the ^{3}Hbound state corresponds to a pole in T_d at $E = -E_B(^3\text{H})$, cf. Sec. 4.3.4—or the doublet-channel nd scattering length (or, in principle, a phase shift at some fixed energy). Once one of these is fixed, the rest can be predicted. In particular, this means that the existence of a single three-body parameter in pionless EFT at leading order provides a natural explanation of the Phillips line, i.e., the observation that various phenomenological potentials, which were all tuned to produce the same NN phase shifts, gave different results for the triton binding energy and doublet S-wave scattering length, which however are strongly correlated. In our framework, we can obtain the line shown in Fig. 4.13 by fitting $H(\Lambda)$ to different values of the scattering length and then calculating $E_B(^3\text{H})$ (or vice versa). Alternatively, one can find the same curve by setting h_0 to zero and varying Λ to move along the line.

With this, we conclude our discussion the three-nucleon system. For more details, like calculations beyond leading order, we encourage the reader to encourage the literature.

4.5 Beyond short-range interactions: adding photons and pions

4.5.1 Electromagnetic interactions

So far, we have studied only effective theories where the particles (atoms of nucleons) interact solely via short-range force (regulated contact interactions). While this is, as we have argued,
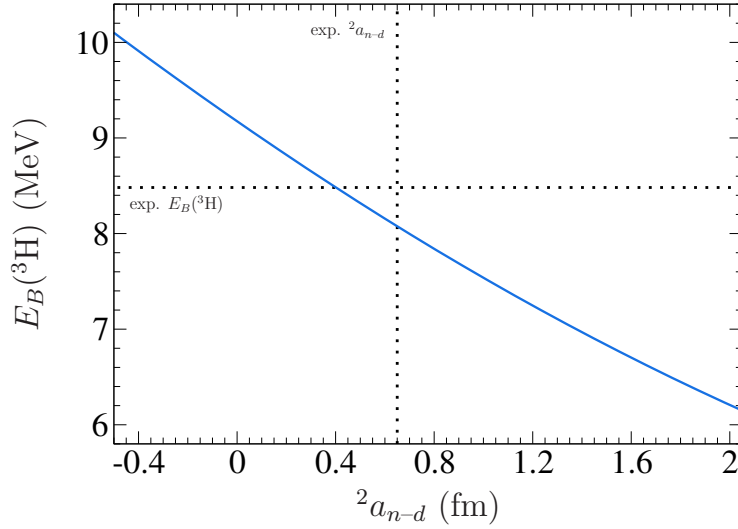
Fig. 4.13 Correlation (Phillips line) between ^{3}Hbinding energy (in MeV) and doublet *nd* scattering length (in fm) in leading-order pionless EFT.

sufficient to describe the strong nuclear interactions at (sufficiently low) energies where the EFT is valid, the electromagnetic interaction does not fit in this scheme. Nevertheless, since almost all systems of interest in low-energy nuclear physics involve more than one proton, the inclusion of such effects is of course important.

Any coupling of photons to charged particles has to be written down in a gauge-invariant way. A natural way to ensure gauge invariance is to replace all derivatives in the effective Lagrangian with covariant ones, *i.e.*,

$$\partial_\mu \to D_\mu = \partial_\mu + ieA_\mu \hat{Q}, \tag{4.145}$$

where $\hat{Q}$ is the charge operator (for nucleons, for example, $\hat{Q}_N = (\mathbf{1} + \tau_3)/2$). Moreover $e^2 = 4\pi\alpha$ defines the electric unit charge in terms of the fine structure constant $\alpha \approx 1/137$.

Since in the EFT there is an infinite tower of contact interactions with an increasing number of derivatives, we also get an infinite number of photon vertices. Still, merely plugging in the covariant derivative is not enough (after all, this is called *minimal* substitution); it is possible to write down terms which are gauge invariant by themselves, and for the EFT to be complete these have to be included as well. Before we come back to this in Sec. 4.5.1.4, let us first see what we get from gauging the derivatives in the nucleon kinetic term:

$$N^\dagger \left(i\partial_t + \frac{\nabla^2}{2M_N} + \cdots \right) N \to N^\dagger \left(iD_t + \frac{D^2}{2M_N} + \cdots \right) N. \tag{4.146}$$

In addition to this, we also have to include the photon kinetic and gauge fixing terms to complete the electromagnetic sector. A convenient choice for the our nonrelativistic framework is Coulomb gauge, *i.e.*, demanding that $\nabla \cdot \mathbf{A} = 0$. A covariant way to write is condition is

$$\partial_\mu A^\mu - \eta_\mu \eta_\nu \partial^\nu A^\mu = 0 \tag{4.147}$$

with the timelike unit vector $\eta^\mu = (1,0,0,0)$. Hence, we add to our effective Lagrangian the term

$$\mathscr{L}_{\text{photon}} = -\frac{1}{4} F_{\mu\nu} F^{\mu\nu} - \frac{1}{2\xi} \left(\partial_\mu A^\mu - \eta_\mu \eta_\nu \partial^\nu A^\mu \right)^2. \tag{4.148}$$

4.5.1.1 The Coulomb force

From Eq. (4.148) we get the equation of motion for the photon field as

$$\left[\Box g^{\mu\nu} - \partial^\mu \partial^\nu + \frac{1}{\xi} \left(\partial^\mu \partial^\nu - \eta^\nu \eta_\kappa \partial^\mu \partial^\kappa - \eta^\mu \eta_\lambda \partial^\lambda \partial^\nu + \eta^\mu \eta^\nu \eta_\lambda \eta_\kappa \partial^\lambda \partial^\kappa \right) \right] A_\nu(x) = 0. \quad (4.149)$$

The photon propagator is defined as the Feynman Green's function for the differential operator acting on $A_\nu(x)$. Writing down the general solution in momentum space and choosing $\xi = 0$ at the end (recall that it is an artificial parameter introduced through enforcing the gauge condition in the path integral [28]), we get

$$D_\gamma^{\mu\nu}(k) = \frac{-i}{k^2 + i\varepsilon} \left(g^{\mu\nu} + \frac{k^\mu k^\nu + k^2 \eta^\mu \eta^\nu - (k \cdot \eta)(k^\mu \eta^\nu + \eta^\mu k^\nu)}{(k \cdot \eta)^2 - k^2} \right). \quad (4.150)$$

A simple inspection of which shows that it vanishes if μ or $\nu = 0$. In other words, A_0 photons do not propagate. Correspondingly, their equation of motion becomes time independent and we can use it to remove A_0 from the effective Lagrangian (the nuclear part plus $\mathscr{L}_{\text{photon}}$). We find

$$\nabla^2 A_0 = -e N^\dagger \hat{Q} N, \quad (4.151)$$

which is just the Poisson equation with the nucleon charge density on the right-hand side. Solving this in Fourier space, where ∇^2 turns into the squared three-momentum, we eventually get a term

$$\mathscr{L}_{\text{Coulomb}}(x_0, \mathbf{x}) = -e^2 \int \mathrm{d}^3 y\, N^\dagger(x_0, \mathbf{x}) N(x_0, \mathbf{x}) \frac{e^{-i\mathbf{q} \cdot (\mathbf{x} - \mathbf{y})}}{\mathbf{q}^2} \left(\frac{1 + \tau^3}{2} \right) N^\dagger(x_0, \mathbf{y}) N(x_0, \mathbf{y}), \quad (4.152)$$

i.e., static Coulomb potential ($\sim 1/r$ in configuration space) between charged nucleons. This is a non-local interaction that really should be kept in the Lagrangian as a whole. Still, to calculate Feynman diagrams it is convenient to split it up into a vertex

$$\beta, b, \mathbf{q} \underline{\hspace{2cm}} \alpha, a, \mathbf{q} + \mathbf{k} \\ \Big\{ \qquad\qquad \sim -ie \left(\frac{1 + \tau^3}{2} \right)^a_b \delta^\alpha_\beta, \quad (4.153) \\ 0, \mathbf{k}$$

and a factor $i/\mathbf{k}^2$ for each "Coulomb-photon propagator," which is really just an expression for the static potential in momentum space. Note that the sign in Eq. (4.153) is arbitrary because these vertices really only come in pairs; we have chosen it here to coincide with what one would naïvely read off from the $N^\dagger i D_0 N$ term.

Finding that A_0 photons only appear as static internal exchanges goes well in line that physical photons in external states have to be transverse. Still, one might wonder how to treat diagrams with virtual photons coupled to a nuclear system (e.g., electrodisintegration), which should have A_0 contributions. The answer is that the proper way to treat these is to add appropriate external currents to the Lagrangian, which then, in turn, appear on the right-hand side of Eq. (4.151).

4.5.1.2 Coulomb enhancement and divergences

The Coulomb force is a long-range interaction: it only falls off like a power law ($\sim 1/r$) in configuration space. In momentum space, it correspondingly has a pole at vanishing momentum transfer ($\mathbf{q}^2 = 0$), i.e., it gives rise to an infrared divergence. There are standard

techniques for dealing with this, for example defining so-called Coulomb-modified scattering phase shifts and effective-range expansions well-known from quantum-mechanical scattering theory. These are based on treating Coulomb effects fully nonperturbatively, *i.e.*, resumming to exchange of Coulomb photons to all orders. In the EFT power counting, the need for this resummation is reflected in the fact dressing a given two-body scattering diagram with external momenta of order Q by an additional Coulomb photon gives a factor $\alpha M_N/Q$, *i.e.*, an *enhancement* if $Q \lesssim \alpha M_N$. In Figure 4.14 we show this for two-photon exchange compared to the single-photon diagram.

Fig. 4.14 Infrared enhancement of Coulomb-photon exchange.

If a problem with Coulomb interactions is solved numerically, the IR divergence has to be regularized in some way to have all quantities well defined. One way to do this "screening" the potential with a photon mass λ, *i.e.*, replacing $\mathbf{q}^2$ with $\mathbf{q}^2 + \lambda^2$ in the Coulomb-photon propagator. If this is done, λ should be kept as small as possible and be extrapolated to zero for all physical observables at the end of the calculation.
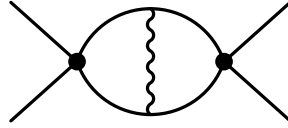
Fig. 4.15 Single photon insertion in a proton-proton bubble diagram.

In contrast to what one might naïvely expect, Coulomb contributions can also modify the UV behavior of diagrams. Consider, for example the insertion of a single photon within a bubble contributing to proton-proton scattering, as shown in Fig. 4.15. Power counting momenta in this diagram (with C_0 vertices) gives a factor $(Q^5/M_N)^2$ from the two loops, $(M_N/Q^2)^4$ from the nucleon propagators, and an obvious α/Q^2 from the photon, meaning that overall we have Q^0, corresponding to a superficial logarithmic divergence of this diagram (which one can confirm with an explicit calculation). This is a new feature compared to the theory with only short-range interactions, where this particular divergence is absent (all divergences are of power-law type there). Without going into any details, we stress that this divergence has to be accounted for when the theory with Coulomb contributions is renormalized. In particular, this example teaches us that in the EFT the Coulomb force is not merely an "add-on potential" that slightly shifts results, but that it has to be treated consistently along with the short-range interactions.

4.5.1.3 Transverse photons

Transverse photons come from the quadratic spatial derivative:

$$\mathbf{D}^2 = (\partial^i + \mathrm{i}eA^i\hat{Q})(\partial^i + \mathrm{i}eA^i\hat{Q}) = \nabla^2 + \mathrm{i}e(A^i\hat{Q}\,\partial^i + \partial^i A^i\hat{Q}) - e^2 A^2\hat{Q}. \qquad (4.154)$$

We can rewrite this using

$$\partial^i\left(A^i\hat{Q}N\right) = (\partial^i A^i)\hat{Q}N + A^i\hat{Q}\,\partial^i N, \qquad (4.155)$$

where the first term vanishes in Coulomb gauge. Hence, we get the vertex

$$\sim -\frac{e}{M_N}\left(\frac{\mathbf{1}+\tau^3}{2}\right)^a_b \delta^\alpha{}_\beta (\mathrm{i}\mathbf{q})^n, \qquad (4.156)$$

with the momentum dependence coming from the derivative. We leave it as an exercise to write down the Feynman rule for the two-photon term $\sim A^2 \hat{Q}$.

Comparing Eq. (4.156) with Eq. (4.153) that a diagram with the exchange of a transverse photon is suppressed by a factor Q^2/M_N^2 compared to the same topology with a Coulomb photon. Transverse photons also have a more complicated propagator than the simple $\mathrm{i}/\mathbf{k}^2$ that we found for Coulomb photons. From Eq. (4.150) we find that

$$\sim \frac{\mathrm{i}}{k_0^2 - \mathbf{k}^2 + \mathrm{i}\varepsilon}\left(\delta^{mn} - \frac{k^m k^n}{\mathbf{k}^2}\right). \qquad (4.157)$$

which now depends on the energy k_0 and thus gives rise to poles in Feynman diagrams. Note that the structure is somewhat different from what one typically sees in QED textbooks that use Lorenz/Feynman gauge.

4.5.1.4 Other external currents

The covariant derivative alone only gives us photons coupled to the proton's charge. However, as mentioned previously, minimal substitution only gives a subset of all possible electromagnetic terms. For example, the magnetic coupling of photons to the nucleons (both protons and neutrons in this case) is given by

$$\mathscr{L}_{\mathrm{mag}} = \frac{e}{2M_N}N^\dagger(\kappa_0 + \kappa_1\tau^3)\,\boldsymbol{\sigma}\cdot\mathbf{B}N. \qquad (4.158)$$

where κ_0 and κ_1 are the isoscalar and isovector nucleon magnetic moments, respectively. That is, the low-energy constant of this operator has been fixed directly to the associated single-nucleon observable (similarly to how the nucleon mass is fixed immediately in the nonrelativistic theory). With $\mathbf{B} = \nabla \times \mathbf{A}$ and all indices written out, this is

$$\mathscr{L}_{\mathrm{mag}} = \frac{e}{2M_N}N^\dagger_{\alpha a}\left(\kappa_0\mathbf{1} + \kappa_1\tau^3\right)^a_b\left(\sigma^i\right)^\alpha{}_\beta\,\varepsilon_{ijm}\partial^j A^m N^{\beta b}. \qquad (4.159)$$

and it gives rise to the Feynman rule

$$\sim \frac{\mathrm{i}e}{2M_N}\left(\kappa_0\mathbf{1} + \kappa_1\tau^3\right)^a_b\,\varepsilon_{ijm}\left(\sigma^i\right)^\alpha{}_\beta(\mathrm{i}\mathbf{k})^j. \qquad (4.160)$$

We point out that Eq. (4.159) only gives the leading magnetic coupling. In traditional nuclear physics language, it corresponds to a one-body operator. At higher orders in the EFT, there are additional operators, like a four-nucleon contact interaction with an additional photon. Such many-body terms correspond to what phenomenological approaches model as "meson exchange currents."

4.5.2 Example: deuteron breakup

As an application of the things discussed in the previous sections, we now consider the low-energy reaction $d\gamma \leftrightarrow np$. By time-reversal symmetry, the amplitudes for the processes corresponding to the two possible directions of the arrow are the same. For definiteness, we show the simplest diagram for the breakup reaction in Fig. 4.16.
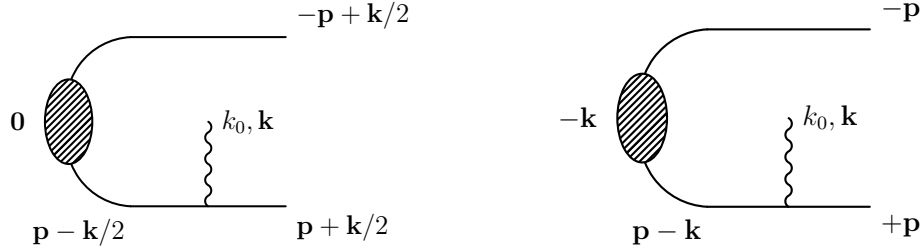
Fig. 4.16 Deuteron breakup diagram in two different kinematic frames. **Left:** lab frame, deuteron at rest. **Right:** center-of-mass frame of the outgoing nucleons.

The reaction can be considered in different reference frames. In the lab frame (left panel of Fig. 4.16), the deuteron is initially at rest and then gets hits by a photon with four-momentum $(k_0,\mathbf{k})$. For our theoretical discussion here it is more convenient to take the two outgoing nucleons in their center-of-mass frame, as shown in the right panel of Fig. 4.16). To first order, we can translate between the two frames by boosting all nucleons lines with a momentum $\mathbf{k}/2$. A more careful analysis would keep track of relativistic kinematics (the external photon is never nonrelativistic), but this is not essential for the illustration here, so we can get away with interpreting $(k_0,\mathbf{k})$ to mean different things in the two frames.

In the *NN* center-of-mass frame, the initial and final-state energies are $E_i = k_0 + \frac{k^2}{4M_N} - \frac{\gamma_t^2}{M_N}$, $E_f = \frac{p^2}{2M_N} + \frac{p^2}{2M_N} = \frac{p^2}{M_N}$, where we have neglected the small deuteron binding energy by setting $M_d = 2M_N$. Conservation of energy implies that

$$p = \sqrt{M_N k_0 - \gamma_t^2 + k^2/4} \Leftrightarrow k_0 = \frac{p^2}{M_N} - \frac{k^2}{4M_N} + \frac{\gamma_t^2}{M_N}, \tag{4.161}$$

and the energy assigned to the internal nucleon propagator has to be $-\frac{k_0}{2} - \frac{\gamma_t^2}{2M_N} + \frac{k^2}{8M_N}$.

The blob in Fig. 4.16 represents the deuteron vertex function calculated in Sec. **??**. Taking the result found there and adding the spin-isospin structure, we find

$$i \quad \sim i\frac{1}{\sqrt{8}}\frac{\sqrt{8\pi\gamma_t}}{M_N}\left(\sigma^i\sigma^2\right)^\alpha{}_\beta\left(\tau_2\right)^a{}_b. \tag{4.162}$$

With this, we can finally write down the amplitude. For an E1 transition, the photon couples to the nucleon charge via the Feynman rule given in Eq. (4.156). Combining this with the ingredients above, we get

$\mathrm{i}\mathscr{M}_{\mathrm{E1}}$

$$= 2 \times \frac{-e}{M_N} \left(\frac{\mathbf{1}+\tau^3}{2}\right)^c_a \delta^\gamma_\alpha \mathrm{i}(\mathbf{p}-\mathbf{k})^j \frac{\mathrm{i}}{-\dfrac{k_0}{2}-\dfrac{\gamma_t^2}{2M_N}+\dfrac{k^2}{8M_N}-\dfrac{(\mathbf{p}-\mathbf{k})^2}{2M_N}+\mathrm{i}\varepsilon} \frac{\mathrm{i}}{\sqrt{8}} \frac{\sqrt{8\pi\gamma_t}}{M_N} \left(\sigma^2 \sigma^i\right)^\beta_\gamma \left(\tau_2\right)^b_c$$

$$\times (\varepsilon^*_{s_\gamma})^j (\varepsilon^*_{s_d})^i (N_{s_p})^{\alpha a} (N_{s_n})_{\beta b}. \quad (4.163)$$

We have included a factor 2 to account for the fact that in drawing the diagram, the photon could be coupled to either nucleon (the isospin projection operator ensures of course that only the proton charge gives a contribution). Moreover, in the second line we have included polarization vectors and spinors for all external particles, the spins of which we denote as s_γ, s_d, s_p, and s_n, respectively. From the amplitude in Eq. 4.163 one can proceed to calculate the corresponding cross section by summing/averaging over the various initial and final states and integrating over the available phase space. We skip these details and close by noting that the isospin part is of course completely fixed ("polarized") by the experimental setup. Hence, the spinor-isospinors are

$$(N_{s_p})^{\alpha a} = N^\alpha_{s_p} 1 0^a \quad , \quad (N_{s_n})_{\beta b} = N^\alpha_{s_p} 1 0_b, \quad (4.164)$$

i.e., we can directly set $a = 1$ (isospin "up", proton) and $b = 2$ (isospin "down", neutron) in the amplitude.

4.9. *Exercise:* Write down the analog of Eq. (4.163) with a magnetically-coupled (M1) photon.

4.5.3 Chiral effective field theory

Pionless EFT provides a simple yet powerful framework to describe few-nucleon systems at very low energies, but its name implies its natural limitation, *i.e.*, the inability to describe physics at energy scales where pion exchange can be resolved. Certainly this becomes important for scattering calculations at momentum scales larger than the pion mass. But nuclear binding also generally increases with increasing number A of bound nucleons, which translates to larger typical momentum scales within the nucleus. There are indications that pionless EFT still converges for $A = 4$, but the question is not fully settled.

The construction of an effective field theory of nucleons and pions was pioneered by Weinberg in the early 1990s [29, 30], proposing a scheme to construct a nuclear potential based on Feynman diagrams from chiral perturbation theory. This theory, which is constructed as an expansion around the so-called "chiral limit," in which the pions are exactly massless Goldstone bosons. The resulting theory, which has been applied with great success in the purely pionic and single-nucleon sector, treats the pion mass as a *small* scale and thus has a power counting designed for typical momenta $Q \sim m_\pi$.

For two or more nucleons, the theory is highly nonperturbative, which motivated Weinberg to develop a scheme where the power counting is applied to the *potential* instead of the amplitude, as we have otherwise done throughout this section. Kaplan *et al.* [15, 31, 32] proposed a different scheme where pions are included perturbatively on top of a leading order given by pionless EFT. This approach has, however, been found not to converge in channels where pion exchange generates a singular attractive interaction [33]. It is thus understood today that pions in general have to be treated nonperturbatively, in a framework generally referred to as "chiral effective field theory." How exactly this should be implemented, however, is still a matter of debate. Instead of summarizing this here, we refer the reader to the literature (see, e.g., Refs. [11, 34–41]).

4.5.3.1 Leading-order pion-nucleon Lagrangian

For an thorough introduction to the field of chiral perturbation theory, we recommend the reader to study the lecture notes of Scherer and Schindler [42] as well as the vast original literature cited therein. It uses an elaborate formalism to construct the most general pion-nucleon Lagrangian that is invariant under chiral transformations (individual rotations of left- and right-handed nucleon fields) plus terms implementing the explicit breaking of chiral symmetry due to finite quark masses. In the conventions of Ref. [42], the leading-order pion-nucleon Lagrangian is

$$\mathscr{L}_{\pi N}^{(1)} + \mathscr{L}_2^{\pi} = \bar{\psi} \left(iD - M_N + \frac{g_A}{2} \gamma^\mu \gamma^5 u_\mu \right) \psi + \frac{f_\pi^2}{4} \mathrm{Tr} \left[(\partial^\mu U)^\dagger (\partial_\mu U) + \chi U^\dagger + U \chi^\dagger \right]. \qquad (4.165)$$

Here, ψ is the nucleon Dirac field, and the matrix-valued field

$$U \equiv = \exp\left(i \frac{\tau \cdot \pi}{f_\pi} \right) \qquad (4.166)$$

collects the pion fields in an exponential representation. D_μ here is the so-called chiral covariant derivative that couples the pion field to the nucleons. The matrix

$$\chi = 2B_0 \, \mathrm{diag}(m_q, m_q), \qquad (4.167)$$

where m_q is the light quark mass (in the exact isospin limit, $m_u = m_d = m_q$) contains the effect from explicit chiral symmetry breaking. Via the Gell-Mann–Oakes–Renner relation,

$$m_\pi^2 = 2B_0 m_q, \qquad (4.168)$$

one can show that χ generates a mass term for the pion field.

4.10. *Exercise:* Expand the exponential in Eq. (4.166) to show that $\frac{f_\pi^2}{4} \mathrm{Tr} \left[(\partial^\mu U)^\dagger (\partial_\mu U) \right]$ generates a kinetic term for the pion field π plus higher-order pion self interactions.

After a couple of steps, which we encourage the reader to follow based on the definitions given in Ref. [42], the leading terms in the Lagrangian are found to be

$$\mathscr{L}_{\pi N}^{(1)} + \mathscr{L}_2^{\pi} = \bar{\psi} (i\partial - M_N) \psi + \frac{1}{2} (\partial^\mu \pi) \cdot (\partial_\mu \pi) - \frac{1}{2} m_\pi^2 \pi^2$$
$$- \frac{g_A}{2f_\pi} \bar{\psi} \gamma^\mu \gamma^5 (\tau \cdot \partial_\mu \pi) \psi + \frac{i}{8f_\pi^2} \bar{\psi} \gamma^\mu (\tau \cdot \pi)(\tau \cdot \partial_\mu \pi) \psi + \cdots. \qquad (4.169)$$

Comparing this to our pseudoscalar model (4.28) in Sec. 4.2.2.2, we see that the pion-nucleon coupling now comes with explicit derivatives, as required by chiral symmetry. After a Foldy-Wouthuysen transformation, however, one-pion-exchange in the nonrelativistic limit gives the same structure as in Eq. (4.49). There is no explicit σ field in Eq. (4.169); in the chiral theory, this particle only appears as a resonance generated by two-pion exchange.

References

1. K.G. Wilson, Rev. Mod. Phys. **55**, 583 (1983)

2. G.P. Lepage, *From Actions to Answers (TASI-89)* (World Scientific, Singapore, 1989), chap. What is Renormalization?, pp. 133–269. URL http://arxiv.org/abs/hep-ph/0506330
3. S. Weinberg, Physica A **96**, 327 (1979)
4. D.B. Kaplan, (1995). URL http://arxiv.org/abs/nucl-th/9506035
5. D.B. Kaplan, (2005)
6. J. Gasser, H. Leutwyler, Annals Phys. **158**, 142 (1984)
7. J. Gasser, H. Leutwyler, Nucl. Phys. B **250**, 465 (1985)
8. J.F. Donoghue, E. Golowich, B.R. Holstein, (1992)
9. P.R. Hagen, Effective field theory for halo nuclei. Ph.D. thesis, Bonn University (2014)
10. E. Braaten, H.W. Hammer, Phys. Rept. **428**, 259 (2006). DOI 10.1016/j.physrep.2006.03.001
11. S.R. Beane, P.F. Bedaque, W.C. Haxton, D.R. Phillips, M.J. Savage, *At The Frontier of Particle Physics* (World Scientific, 2001), *Handbook of QCD*, vol. 1, chap. From hadrons to nuclei: Crossing the border, pp. 133–269
12. C.A. Bertulani, H.W. Hammer, U. van Kolck, Nucl. Phys. A **712**, 37 (2002)
13. P.F. Bedaque, H.W. Hammer, U. van Kolck, Phys. Lett. B **569**, 159 (2003)
14. U. van Kolck, Nucl. Phys. A **645**, 273 (1999)
15. D.B. Kaplan, M.J. Savage, M.B. Wise, Nucl. Phys. **B534**, 329 (1998). DOI 10.1016/S0550-3213(98)00440-4
16. D.B. Kaplan, Nucl. Phys. B **494**, 471 (1997)
17. G.V. Skorniakov, K.A. Ter-Martirosian, Sov. Phys. JETP **4**, 648 (1957)
18. G. Danilov, Sov. Phys. JETP **13**, 349 (1961)
19. V.F. Kharchenko, Sov. J. Nucl. Phys. **16**, 173 (1973)
20. P.F. Bedaque, H.W. Hammer, U. van Kolck, Phys. Rev. Lett. **82**, 463 (1999). DOI 10.1103/PhysRevLett.82.463
21. V. Efimov, Phys. Lett. B **33**(8), 563 (1970)
22. E. Braaten, D. Kang, L. Platter, Phys. Rev. Lett. **106**, 153005 (2011)
23. F. Ferlaino, R. Grimm, Physics **3**, 9 (2010)
24. J. Ulmanis, S. Häfner, R. Pires, F. Werner, D.S. Petrov, E.D. Kuhnle, M. Weidemüller, Phys. Rev. A **93**, 022707 (2016)
25. P.F. Bedaque, H.W. Hammer, U. van Kolck, Nucl. Phys. **A646**, 444 (1999). DOI 10.1016/S0375-9474(98)00650-2
26. S. König, H.W. Grießhammer, H.W. Hammer, J. Phys. G **42**, 045101 (2015)
27. P.F. Bedaque, H.W. Hammer, U. van Kolck, Nucl. Phys. A **676**, 357 (2000)
28. M.E. Peskin, D.V. Schroeder, *An Introduction to Quantum Field Theory* (Westview Press, 1995)
29. S. Weinberg, Phys. Lett. **B251**, 288 (1990). DOI 10.1016/0370-2693(90)90938-3
30. S. Weinberg, Nucl. Phys. **B363**, 3 (1991). DOI 10.1016/0550-3213(91)90231-L
31. D.B. Kaplan, M.J. Savage, M.B. Wise, Nucl. Phys. **B478**, 629 (1996). DOI 10.1016/0550-3213(96)00357-4
32. D.B. Kaplan, M.J. Savage, M.B. Wise, Phys. Lett. **B424**, 390 (1998). DOI 10.1016/S0370-2693(98)00210-X
33. S. Fleming, T. Mehen, I.W. Stewart, Nucl. Phys. **A677**, 313 (2000). DOI 10.1016/S0375-9474(00)00221-9
34. P.F. Bedaque, U. van Kolck, Ann. Rev. Nucl. Part. Sci. **52**, 339 (2002)
35. A. Nogga, R.G.E. Timmermans, U. van Kolck, Phys. Rev. C **72**, 054006 (2005)
36. M.C. Birse, Phys. Rev. C **74**, 014003 (2006)
37. E. Epelbaum, H.W. Hammer, U.G. Meissner, Rev. Mod. Phys. **81**, 1773 (2009). DOI 10.1103/RevModPhys.81.1773
38. R. Machleidt, D.R. Entem, Phys. Rept. **503**, 1 (2011). DOI 10.1016/j.physrep.2011.02.001
39. E. Epelbaum, U.G. Meißner, Few Body Syst. **54**, 2175 (2013)
40. H.W. Hammer, A. Nogga, A. Schwenk, Rev. Mod. Phys. **85**, 197 (2013)
41. B. Long, Y. Mei, Phys. Rev. C **93**(4), 044003 (2016)
42. S. Scherer, M.R. Schindler, Lect. Notes Phys. **830**, 1 (2012)

Chapter 5
Lattice methods and effective field theory

Amy Nicholson

Abstract Lattice field theory is a non-perturbative tool for studying properties of strongly interacting field theories, which is particularly amenable to numerical calculations and has quantifiable systematic errors. In these lectures we apply these techniques to nuclear Effective Field Theory (EFT), a non-relativistic theory for nuclei involving the nucleons as the basic degrees of freedom. The lattice formulation of [1, 2] for so-called pionless EFT is discussed in detail, with portions of code included to aid the reader in code development. Systematic and statistical uncertainties of these methods are discussed at length, and extensions beyond pionless EFT are introduced in the final Section.

5.1 Introduction

Quantitative understanding of nuclear physics at low energies from first principles remains one of the most challenging programs in contemporary theoretical physics research. While physicists have for decades used models combined with powerful numerical techniques to successfully reproduce known nuclear structure data and make new predictions, currently the only tools available for tackling this problem that have direct connections to the underlying theory, Quantum Chromodynamics (QCD), as well as quantifiable systematic errors, are Lattice QCD and Effective Field Theory (EFT). Combined, these techniques may be used to not only quantify any bias introduced when altering QCD in order to make it computationally tractable, but also to better understand the connection between QCD and nuclear physics.

The lattice is a tool for discretizing a field theory in order to reduce the path integral, with an infinite number of degrees of freedom, to a finite-dimensional ordinary integral. By rendering the dimension finite (though extremely large), the integral may then be estimated on a computer using Monte Carlo methods. Errors introduced through discretization and truncation of the region of spacetime sampled are controlled through the spatial and temporal lattice spacings, b_s, b_τ, and the spatial and temporal lengths, L, β. Thus, these errors may be quantified through the lattice spacing dependence of the observables, and often may be removed through extrapolation to the continuum and infinite volume limits.

LQCD is a powerful and advanced tool for directly calculating low-energy properties of QCD. However, severe computational issues exist when calculating properties of systems with nucleons. Unfortunately, these problems grow rapidly with the number of nucleons in the system.

Amy Nicholson

Department of Physics, University of California, Berkeley, Berkeley CA 94720, USA, e-mail: `anicholson@berkeley.edu`

The first issue is the large number of degrees of freedom involved when using quark fields to create nucleons. In order to calculate a correlation function for a single nucleon in LQCD using quarks (each of which has twelve internal degrees of freedom given by spin and color), one has to perform all possible Wick contractions of the fields in order to build in fermion antisymmetrization. For example, to create a proton using three valence quark operators requires the calculation of two different terms corresponding to interchanging the two up quark sources. The number of contractions involved for a nuclear correlation function grows with atomic number Z and mass number A as $(A+Z)!(2A-Z)!$. For He_4 this corresponds to $\sim 5 \times 10^5$ terms[1]!

The second major problem occurs when performing a stochastic estimate of the path integral. A single quark propagator calculated on a given gauge field configuration may be a part of either a light meson or a heavy nucleon. However, the difference cannot be determined until correlations with the other quark fields present are built in by summing over a sufficiently large number of these field configurations[2]. This leads to large fluctuations from configuration to configuration, and a stochastic signal-to-noise ratio, $\mathscr{R}$, which degrades exponentially with the number of nucleons in the system,

$$\mathscr{R} \sim e^{-A(M-3/2m_\pi)\tau} , \tag{5.1}$$

where M is the nucleon mass and m_π is the pion mass [3]. This is currently the major limiting factor for the size of nuclear which can be probed using LQCD. The best calculations we have from LQCD using multiple nucleons to date are in the two-nucleon sector [4–29], while fewer calculations have been performed for three and four nucleon systems [9, 11, 12, 14, 17–21, 30, 31]; however, even for two nucleon systems unphysically large pion masses must be used in order to reduce the noise problem. We will discuss signal-to-noise problems in more detail in Sec. 5.3.1.

Starting from an EFT using nucleons as the fundamental degrees of freedom greatly reduces the consequences from both of these issues. EFTs also enjoy the same benefit as the lattice over traditional model techniques of having quantifiable systematic errors, this time controlled by the cutoff of the EFT compared to the energy regime studied. For chiral EFTs this scale is generally $\Lambda_\chi \sim m_\rho \sim 700$ MeV. Systematic errors can be reduced by going to higher orders in an expansion of p/Λ_χ, where p is the momentum scale probed, with the remaining error given by the size of the first order which is not included. In a potential model there is no controlled expansion, and it is generally unknown how much the results will be affected by leaving out any given operator. In addition, field theories provide a rigorous mathematical framework for calculating physical processes, and can be directly translated into a lattice scheme.

Our discussion will begin with understanding a very basic nuclear EFT, pionless EFT, at leading order. We will then proceed to discretize this theory and set up a framework for performing Monte Carlo calculations of our lattice theory. We will then discuss how to calculate observables using the lattice theory, and how to understand their associated statistical uncertainties. Next we will discuss quantifying and reducing systematic errors. Then we will begin to add terms to our theory going beyond leading order pionless EFT. Finally, we will discuss remaining issues and highlight some successes of the application of these methods by several different groups.

---

[1] This is a very naïve estimate; far more sophisticated algorithms exist with power-law scaling.

[2] This interpretation of the signal-to-noise problem has been provided by David B. Kaplan.

5.2 Basics of Effective Field Theory and Lattice Effective Field Theory

5.2.1 Pionless Effective Field Theory

The EFT philosophy that we will follow is to write down all possible operators involving the relevant degrees of freedom within some energy range (determined by the cutoff) that are consistent with the symmetries of the underlying theory. Each operator will be multiplied by an unknown low-energy constant which may be fixed by comparing an observable with experiment or lattice QCD. In order to reduce this generally infinite number of operators to a finite number we must also establish a power-counting rule for neglecting operators that do not contribute within some desired accuracy. This is a notoriously difficult problem for nuclear physics, and is in general observable and renormalization scheme dependent. Here, we will only briefly touch upon two common power-counting schemes, the so-called Weinberg and KSW expansions [32–36]. For reviews of these and other power-counting schemes, see [37–39].

The simplest possible nuclear EFT involves non-relativistic nucleon fields interacting via delta functions. This is known as a pionless EFT, and is only relevant for energy scales up to a cutoff $\Lambda \sim m_\pi$. Below this scale, the finite range of pion exchange cannot be resolved, and all interactions appear to be point-like. In this discussion we will closely follow that of Ref. [40]. For the moment, let's just consider a theory of two-component (spin up/down) fermion fields, ψ, with the following Lagrangian,

$$\mathscr{L}_{\text{eff}} = \psi^\dagger \left(i\partial_\tau + \frac{\nabla^2}{2M} \right) \psi + g_0 \left(\psi^\dagger \psi \right)^2 + \frac{g_2}{8} \left[\left(\psi\psi \right)^\dagger \left(\psi \overleftrightarrow{\nabla}^2 \psi \right) + \text{h.c.} \right] + \cdots , \tag{5.2}$$

where

$$\overleftrightarrow{\nabla}^2 \equiv \overleftarrow{\nabla}^2 - 2\overleftarrow{\nabla} \cdot \overrightarrow{\nabla} + \overrightarrow{\nabla}^2 , \tag{5.3}$$

M represents the nucleon mass, $g_0, g_2, \ldots$ are unknown, low-energy constants (LECs) which may be fixed by comparing to experimental or LQCD results, and all spin indices are suppressed. Because the effective theory involves dynamical degrees of freedom that are only relevant up to a certain scale, we must define a cutoff, Λ, above which the theory breaks down. In general, the LECs scale as $\Lambda^{-\dim(\mathscr{O})}$, where $\dim(\mathscr{O})$ represents the dimension of the operator associated with the LEC. According to naïve power counting, the g_2 term in Eq. (5.2) should be suppressed relative to the g_0 term, because adding a derivative to an operator increases its dimension. One should be careful in practice, however, because naïve power counting does not always hold, as we will see several times throughout these lectures.

5.2.1.1 Two particle scattering amplitude

In order to set the coefficients $g_0, g_2, \ldots$, we may look to experimental scattering data. In particular, if we wish to set the g_0 coefficient we should consider two-particle s-wave scattering because the operator associated with g_0 contains no derivatives. g_2 and other LECs may be set using p- and higher-wave scattering data. Recall that the S-matrix for non-relativistic scattering takes the following form:

$$S = 1 + \frac{iMp}{2\pi} A , \tag{5.4}$$

where p is the scattering momentum and A is the scattering amplitude. For s-wave scattering the amplitude may be written as,

$$A = \frac{4\pi}{M} \frac{1}{p\cot\delta - ip} ,$$ (5.5)

where δ is the s-wave scattering phase shift. Given a short-range two-body potential, the scattering phase shift has a well-known expansion for low momenta, called the effective range expansion,

$$p\cot\delta = -\frac{1}{a} + \frac{1}{2}r_0 p^2 + r_1 p^4 + \cdots ,$$ (5.6)

where a is the scattering length, r_0 is the effective range, and r_1 and higher order terms are referred to as shape parameters. The effective range and shape parameters describe the short-range details of the potential, and are generally of order of the appropriate power of the cutoff in a naturally tuned scenario.

The scattering length may be used to describe the asymptotic behavior of the radial wavefunction. In particular, consider two-particles interacting via an attractive square-well potential. If the square-well is sufficiently strongly attractive, the wavefunction turns over and goes to zero at some finite characteristic length. This means the system is bound and the size of the bound state is given by the scattering length, a. On the other hand, if the wavefunction extends over infinite space, then the system is in a scattering state and the scattering length may be determined as the distance from the origin where the asymptote of the wavefunction intersects the horizontal axis (see Fig. 5.1). This implies that the scattering length in the case of a scattering state is negative. If the potential is tuned to give a system which is arbitrarily close to the crossover point from a bound state to a scattering state, corresponding to infinite scattering length, the state is described as being near unitarity, because the unitarity bound on the scattering cross section is saturated at this point. Note that this implies that the scattering length may be any size and is not necessarily associated with the scale set by the cutoff. However, such a scenario requires fine-tuning of the potential. Such fine-tuning is well-known to occur in nuclear physics, with the deuteron and neutron-neutron s-wave scattering being notable examples.

Fig. 5.1 Sketches of two-body radial wavefunctions vs. r corresponding to various scattering lengths. From left to right: $a < 0$, $a \to \infty$, $a > 0$.
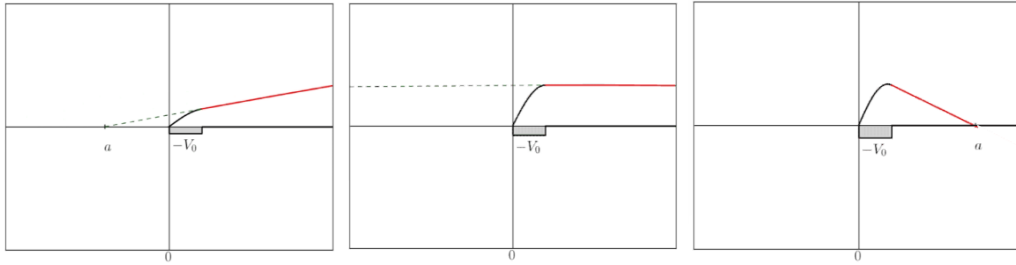
A many-body system composed of two-component fermions with an attractive interaction is known to undergo pairing between the species (higher N-body interactions are prohibited by the Pauli exclusion principle), such as in neutron matter, found in the cores of neutron stars, which is composed of spin up and spin down neutrons. At low temperature, these bosonic pairs condense into a coherent state. If the interaction is only weakly attractive, the system will form a BCS state composed of widely separated Cooper pairs, where the average pair size is much larger than the average interparticle spacing. On the other hand, if the inter-

action is strongly attractive then the pairs form bosonic bound states which condense into a Bose-Einstein condensate. The crossover between these two states corresponds to the unitary regime, and has been studied extensively in ultracold atom experiments, where the interaction between atoms may be tuned using a Feschbach resonance. In this regime, the average pair size is equal to the interparticle spacing (given by the inverse density), which defines the only scale for the system. Thus, all dimensionful observables one wishes to calculate for this system are determined by the appropriate power of the density times some dimensionless constant.

5.2.1.2 Two-body LECs

Returning to our task of setting the couplings using scattering parameters as input, we might consider comparing Eq. (5.2) and Eq. (5.6), to determine the LEC g_0 using the scattering length, g_2 using the effective range, and so forth. To see how this is done in practice we may compute the scattering amplitude A in the effective theory, and match the coefficients to the effective range expansion. Let's begin using only the first interaction term in the effective theory, corresponding to g_0. Diagrammatically, the scattering amplitude may be written as the sum of all possible bubble diagrams (see Fig. 5.2). Because the scattering length may take on any value, as mentioned previously, we cannot assume that the coupling g_0 is small, so we should sum all diagrams non-perturbatively. The first diagram in the sum is given by the tree level result, g_0. If we assume that the system carries energy $E = p^2/M$, then the second diagram may be labeled as in Fig. 5.3, and gives rise to the loop integral,

$$I_0 = i \int \frac{d^4q}{(2\pi)^4} \frac{1}{\left(E/2 + q_0 - \frac{q^2}{2M} - i\varepsilon\right)\left(E/2 - q_0 - \frac{q^2}{2M} + i\varepsilon\right)} \ . \tag{5.7}$$

Performing the integral over q_0 and the solid angle gives

$$I_0 = \frac{1}{2\pi^2} \int^{\pi\Lambda/2} dq \frac{q^2}{\left(E - \frac{q^2}{M}\right)} \tag{5.8}$$

$$= \frac{M}{2\pi^2} \left[\frac{\pi\Lambda}{2} - \sqrt{ME}\tanh^{-1}\left(\frac{\Lambda}{\sqrt{ME}}\right)\right] \ , \tag{5.9}$$

where I have introduced a hard momentum cutoff, Λ. Removing the cutoff by taking it to infinity results in

$$I_0 \xrightarrow[\Lambda\to\infty]{} \frac{M}{4\pi}\left[\Lambda + ip\right] \ . \tag{5.10}$$

Because the interaction is separable, the nth bubble diagram is given by n products of this loop function. Thus, the scattering amplitude is factorizable, and may be written

$$A = g_0 \left[1 + \sum_n (g_0 I_0)^n\right] \tag{5.11}$$

$$= \frac{g_0}{1 - g_0 I_0} \ . \tag{5.12}$$

We may now compare Eqs. (5.5,5.6) and Eq. (5.11) to relate the coupling g_0 to the scattering phase shift. This is easiest to do by equating the inverse scattering amplitudes,

$$\frac{1}{A} = \frac{1}{g_0} - \frac{M}{4\pi}\Lambda - \frac{iMp}{4\pi} = -\frac{M}{4\pi a} - \frac{iMp}{4\pi} \ , \tag{5.13}$$

where I have used Eq. (5.6) cut off at leading order. We now have the relation

$$g_0 = \frac{4\pi}{M} \frac{1}{\Lambda - 1/a}$$ (5.14)

between the coupling and the physical scattering length.

Fig. 5.2 Two-body scattering amplitude represented as a sum of bubble diagrams corresponding to a single contact interaction with coupling g_0.

Fig. 5.3 Feynman diagram for a single bubble in Fig. 5.2, giving rise to the loop integral Eq. (5.7).
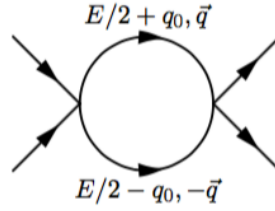
Note that the coupling runs with the scale Λ; the particular dependence is determined by the regularization and renormalization scheme chosen. In order to understand the running of the coupling we may examine the beta function. To do so we first define a dimensionless coupling,

$$\hat{g}_0 \equiv -\frac{M\Lambda}{4\pi} g_0 \,,$$ (5.15)

then calculate

$$\beta(\hat{g}_0) \equiv \Lambda \frac{\partial \hat{g}_0}{\partial \Lambda} = -\frac{a\Lambda}{(a\Lambda - 1)^2} = -\hat{g}_0(\hat{g}_0 - 1) \,.$$ (5.16)

This function is a simple quadratic that is plotted in Fig. 5.4. The beta function has two zeroes, $\hat{g}_0 = 0, 1$, corresponding to fixed points of the theory. At a fixed point, the coupling no longer runs with the scale Λ, and the theory is said to be scale-invariant (or conformal, given some additional conditions). This means that there is no intrinsic scale associated with the theory. The fixed point at $\hat{g}_0 = 0$ is a trivial fixed point, and corresponds to a non-interacting, free field theory (zero scattering length). The other, non-trivial fixed point at $\hat{g}_0 = 1$ corresponds to a strongly interacting theory with infinite scattering length; this is the unitary regime mentioned previously. Here, not only does the scattering length go to infinity, as does the size of the radial wavefunction, but the energy of the bound state (as approached from $\hat{g}_0 > 1$) goes to zero and all relevant scales have vanished. Note that this is an unstable fixed point; the potential must be finely tuned to this point or else the theory flows away from unitarity as $\Lambda \to 0$ (IR limit).

Generally perturbation theory is an expansion around free field theory, corresponding to a weak coupling expansion. This is the approach used as part of the Weinberg power counting

Fig. 5.4 Beta function (Eq. (5.16)) for the two-body contact interaction. Arrows represent the direction of flow toward the IR.
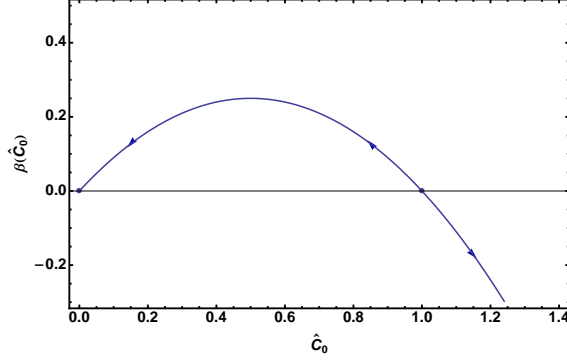
scheme for nuclear EFT [32,33]. However, in some scattering channels of interest for nuclear theory the scattering length is indeed anomalously large, such as the $^1S_0$ and $^3S_1$ nucleon-nucleon scattering channels, where

$$a_{^1S_0} \sim -24 \text{ fm} , \tag{5.17}$$

$$a_{^3S_1} \sim 5 \text{ fm} . \tag{5.18}$$

Such large scattering lengths suggest that an expansion around the strongly coupled fixed-point of unitarity may be a better starting point and lead to better convergence. This approach was taken by Kaplan, Savage, and Wise and led to the KSW power-counting scheme [34–36]. Unfortunately, nuclear physics consists of many scales of different sizes and a consistent power-counting framework with good convergence for all observables has yet to be developed; in general the convergence of a given scheme depends on the scattering channels involved.

Because nuclear physics is not weakly coupled in all channels, non-perturbative methods, such as lattice formulations, will be favorable for studying few- and many-body systems, where two-body pairs may interact through any combination of channels simultaneously. Due to the scale-invariant nature of the unitary regime, it provides a far simpler testbed for numerical calculations of strongly-interacting theories, so we will often use it as our starting point for understanding lattice EFT methods.

5.2.2 Lattice Effective Field Theory

Our starting point for building a lattice EFT will be the path integral formulation of quantum field theory in Euclidean spacetime. The use of Euclidean time allows the exponent of the path integral to be real (in certain cases), a property which will be essential to our later use of stochastic methods for its evaluation. Given a general theory for particles $\psi, \psi^\dagger$ obeying a Lagrangian density

$$\mathscr{L}(\psi^\dagger, \psi) = \psi^\dagger \left(\partial_\tau - \mu \right) \psi + \mathscr{H} \left[\psi^\dagger, \psi \right] , \tag{5.19}$$

where τ is the Euclidean time, μ the chemical potential, and $\mathscr{H}$ is the Hamiltonian density, the Euclidean path integral is given by

$$Z = \int \mathscr{D}\psi^\dagger \mathscr{D}\psi e^{-\int d\tau d^3x \left[\mathscr{L}(\psi^\dagger, \psi) \right]} . \tag{5.20}$$

If the integral over Euclidean time is compact, then the finite time extent β acts as an inverse temperature, and we may draw an analogy with the partition function in statistical mechanics, $Z = tr\left[e^{-H\beta}\right]$. This analogy is often useful when discussing lattice formulations of the path integral. In this work we will generally consider $\mu = 0$ and create non-zero particle density by introducing sources and sinks for particles and calculating correlation functions.

We discretize this theory on a square lattice consisting of $L^3 \times N_\tau$ points, where L is the number of points in all spatial directions, and N_τ is the number of temporal points. We will focus on zero temperature physics, corresponding to large N_τ[3]. We must also define the physical distance between points, the lattice spacings b_s, b_τ, where $b_\tau = b_s^2/M$ by dimensional analysis for non-relativistic theories. The fields are now labeled by discrete points, $\psi(\mathbf{x}, \tau) \to \psi_{\mathbf{n},\tau}$, and continuous integrals are replaced by discrete sums, $\int d^3x \to \sum_{\mathbf{n},\tau}^{L,N_\tau}$.

5.2.2.1 Free field theory

To discretize a free field theory, we must discuss discretization of derivatives. The simplest operator which behaves as a single derivative in the continuum limit is a finite difference operator,

$$\partial_{\hat{k}}^{(L)} f_j = \frac{1}{b_s}\left[f_{j+\hat{k}} - f_j\right] \,, \tag{5.21}$$

where $\hat{k}$ is a unit vector in the k-direction. The discretized second derivative operator must involve two hops, and should be a symmetric operator to behave like the Laplacian. A simple possibility is

$$\nabla_L^2 f_j = \sum_k \frac{1}{b_s^2}\left[f_{j+\hat{k}} + f_{j-\hat{k}} - 2f_j\right] \,. \tag{5.22}$$

We can check the continuum limit by inspecting the corresponding kinetic term in the action,

$$S_{\text{KE}} \propto \sum_j \psi_j^\dagger \nabla_L^2 \psi_j \,. \tag{5.23}$$

The fields may be expanded in a plane wave basis,

$$\psi_j = \sum_{k=-L/2}^{L/2} \psi_k e^{-\frac{2\pi i}{L} jk} \,, \tag{5.24}$$

for spatial indices, j, leading to

$$\sum_j \psi_j^\dagger \nabla_L^2 \psi_j = \frac{1}{b_s^2}\sum_j\sum_{k'}\sum_k \psi_{k'}^\dagger \psi_k \left[e^{\frac{2\pi i}{L} jk'} e^{\frac{-2\pi i}{L} jk}\right]\left[e^{\frac{-2\pi i}{L} k} + e^{\frac{2\pi i}{L} k} - 2\right] \,. \tag{5.25}$$

After performing the sum over j the first piece in brackets gives $\delta_{kk'}$, while the second is proportional to $\sin^2(k\pi/L)$, resulting in,

$$\sum_j \psi_j^\dagger \nabla_L^2 \psi_j = -\frac{4}{b_s^2}\sum_k \psi_k^\dagger \psi_k \sin^2\left(\frac{k\pi}{L}\right) \,. \tag{5.26}$$

Finally, expanding the sine function for small k/L gives,

---

[3] The explicit condition on N_τ required for extracting zero temperature observables will be discussed in Sec. 10.2.6

$$\sum_j \psi_j^\dagger \nabla_L^2 \psi_j = \sum_k \psi_k^\dagger \psi_k \underbrace{\left[-\left(\frac{2\pi k}{b_s L}\right)^2 + \frac{b_s^2}{12}\left(\frac{2\pi k}{b_s L}\right)^4 + \cdots \right]}_{-p^2 + \frac{b_s^2}{12}p^4 + \cdots \xrightarrow{b_s \to 0} -p^2} , \qquad (5.27)$$

where I've used the finite volume momentum $p = \frac{2\pi k}{b_s L}$ to rewrite the expression in square brackets. Thus, we have the correct continuum limit for the kinetic operator. Note that for larger momenta, approaching the continuum limit requires smaller b_s. However, this is only one possibility for a kinetic term. We can always add higher dimension operators (terms with powers of b_s in front of them), in order to cancel leading order terms in the expansion Eq. (5.27). This is a form of what's called improvement of the action, and will be discussed in more detail in Sec. 5.4.

Adding a temporal derivative term,

$$\partial_\tau^{(L)} \psi_{\mathbf{x},\tau} = \frac{1}{b_\tau}\left[\psi_{\mathbf{n},\tau} - \psi_{\mathbf{n},\tau-1} \right] , \qquad (5.28)$$

we can now write down a simple action for a non-relativistic free-field theory,

$$S_{\text{free}} = \sum_{\tau,\tau'} \frac{1}{b_\tau} \psi_{\tau'}^\dagger [K_0]_{\tau,\tau'} \psi_\tau , \qquad (5.29)$$

where I've defined a matrix K_0 whose entries are $L^3 \times L^3$ blocks,

$$K_0 \equiv \begin{pmatrix} D & -1 & 0 & 0 & \ldots \\ 0 & D & -1 & 0 & \ldots \\ 0 & 0 & D & -1 & \ldots \\ . & . & . & . & . \\ . & . & . & . & . \\ 1 & . & . & . & . \end{pmatrix} \qquad (5.30)$$

where $D \equiv 1 - \frac{b_s^2 \nabla_L^2}{2}$ contains the spatial Laplacian, and therefore connects fields on the same time slice (corresponding to diagonal entries of the matrix K_0), while the temporal derivative contributes the off-diagonal pieces. Note that the choice of "1" in the lower left corner corresponds to anti-periodic boundary conditions, appropriate for fermionic fields. For zero temperature calculations the temporal boundary conditions are irrelevant, and it will often be useful to choose different temporal boundary conditions for computational or theoretical ease.

5.2.2.2 Interactions

Now let's discuss adding interactions to the theory. We'll focus on the first term in a nuclear EFT expansion, the four-fermion interaction:

$$\mathscr{L}_{\text{int}} = g_0 \psi_{n,\uparrow} \psi_{n,\uparrow} \psi_{n,\downarrow} \psi_{n,\downarrow} , \qquad (5.31)$$

where $(\uparrow,\downarrow)$ now explicitly label the particles' spins (or alternatively, flavors). Because anti-commuting fields cannot easily be accommodated on a computer, they must be integrated out analytically. The only Grassmann integral we know how to perform analytically is a Gaussian, so the action must be bilinear in the fields. One trick for doing this is called a Hubbard-Stratonovich (HS) transformation, in which auxiliary fields are introduced to mediate the

interaction. The key is to use the identity,

$$e^{b_\tau g_0 \psi_\uparrow^\dagger \psi_\uparrow \psi_\downarrow^\dagger \psi_\downarrow} = \frac{1}{\sqrt{2\pi}} \int_{-\infty}^{\infty} d\phi \, e^{-\phi^2/2 - \phi\sqrt{b_\tau g_0}\left(\psi_\uparrow^\dagger \psi_\uparrow + \psi_\downarrow^\dagger \psi_\downarrow\right)} \, , \tag{5.32}$$

where I have dropped the spacetime indices for brevity. This identity may be verified by completing the square in the exponent on the right hand side and performing the Gaussian integral over the auxiliary field ϕ. This form of HS transformation has the auxiliary field acting in what is called the density channel $\left(\psi_\uparrow^\dagger \psi_\uparrow + \psi_\downarrow^\dagger \psi_\downarrow\right)$. It is also possible to choose the so-called BCS channel, $\left(\psi_\uparrow^\dagger \psi_\downarrow^\dagger + \psi_\uparrow \psi_\downarrow\right)$, the usual formulation used in BCS models, however this causes a so-called sign problem when performing Monte Carlo sampling, as will be discussed in detail in Sec. 5.3.1.1. Transformations involving non-Gaussian auxiliary fields may also be used, such as

$$\begin{aligned} Z_2 \text{ field:} \quad & \frac{1}{2} \sum_{\phi=\pm 1} e^{-\phi\sqrt{b_\tau g_0}\left(\psi_\uparrow^\dagger \psi_\uparrow + \psi_\downarrow^\dagger \psi_\downarrow\right)} \\ \text{compact continuous:} \quad & \frac{1}{2\pi} \int_{-\pi}^{\pi} e^{-\sin\phi\sqrt{b_\tau g_0}\left(\psi_\uparrow^\dagger \psi_\uparrow + \psi_\downarrow^\dagger \psi_\downarrow\right)} \, . \end{aligned} \tag{5.33}$$

These formulations may have different pros and cons in terms of computational and theoretical ease for a given problem, and should be chosen accordingly. For example, the Z_2 interaction is conceptually and computationally the simplest interaction, however, it also induces explicit $4-$ and higher-body interactions in systems involving more than two-components which may not be desired.

5.2.2.3 Importance sampling

The action may now be written with both kinetic and interaction terms,

$$S = \frac{1}{b_\tau} \sum_{\tau,\tau'} \psi_{\tau'}^\dagger \left[K(\phi)\right]_{\tau'\tau} \psi_\tau \, , \tag{5.34}$$

where the matrix K includes blocks which depend on the auxiliary field ϕ, and also contains non-trivial spin structure that has been suppressed. The partition function can be written

$$Z = \int \mathscr{D}\phi \mathscr{D}\psi^\dagger \mathscr{D}\psi \rho[\phi] e^{-S[\phi,\psi^\dagger\psi]} \, , \tag{5.35}$$

where the integration measure for the ϕ field, $\rho[\phi]$, depends on the formulation chosen,

$$\rho[\phi] = \begin{cases} \prod_n e^{-\phi_n^2/2} & \text{Gaussian} \\ \prod_n \frac{1}{2}\left(\delta_{\phi_n,1} + \delta_{\phi_n,-1}\right) & Z_2 \\ \prod_n \left(\theta(-\pi+\phi_n)\theta(\pi-\phi_n)\right) & \text{compact continuous} \end{cases} \, . \tag{5.36}$$

With the action in the bilinear form of Eq. (5.34), the ψ fields can be integrated out analytically, resulting in

$$Z_\phi = \int \mathscr{D}\phi P[\phi] \qquad P[\phi] \equiv \rho[\phi] \det K[\phi] \, . \tag{5.37}$$

Observables take the form

$$\langle \mathscr{O} \rangle = \frac{1}{Z} \int \mathscr{D}\phi P[\phi] \mathscr{O}[\phi] \, . \tag{5.38}$$

Through the use of discretization and a finite volume, the path integral has been converted into a standard integral with finite dimension. However, the dimension is still much too large to imagine calculating it on any conceivable computer, so we must resort to Monte Carlo methods for approximation. The basic idea is to generate a finite set of ϕ field configurations of size N_{cfg} according to the probability measure $P[\phi]$, calculate the observable on each of these configurations, then take the mean as an approximation of the full integral,

$$\langle \mathscr{O} \rangle \approx \frac{1}{N_{\text{cfg}}} \sum_n^{N_{\text{cfg}}} \mathscr{O}(\phi_n) \ . \tag{5.39}$$

Assuming the central limit theorem holds, for N_{cfg} large enough (a non-trivial condition, as will be discussed in Sec. 5.3.2), the distribution of the mean approaches a Gaussian, and the error on the mean falls off with the square root of the sample size.

There are several algorithms on the market for generating field configurations according to a given probability distribution, and I will only briefly mention a few. Lattice calculations are particularly tricky due to the presence of the determinant in Eq. (5.37), which is a highly non-local object and is very costly to compute. One possible algorithm to deal with this is called determinantal Monte Carlo, which implements local changes in ϕ, followed by a simple Metropolis accept/reject step. This process can be rather inefficient due to the local updates. An alternative possibility is Hybrid Monte Carlo, commonly used for lattice QCD calculations, in which global updates of the field are produced using molecular dynamics as a guiding principle. Note that the field ϕ must be continuous in order to use this algorithm due to the use of classical differential equations when generating changes in the field. Also common in lattice QCD calculations is the use of pseudofermion fields as a means for estimating the fermion determinant. Here the determinant is rewritten in terms of a Gaussian integral over bosonic fields, χ,

$$\det K[\phi] \propto \int \mathscr{D}\chi^\dagger \mathscr{D}\chi\, e^{-\chi^\dagger K^{-1}[\phi]\chi} \ . \tag{5.40}$$

This integral is then evaluated stochastically. These are just a sample of the available algorithms. For more details on these and others in the context of non-relativistic lattice field theory, see [41].

5.2.2.4 Example formulation

Now that we have developed a general framework for lattice EFT, let's be explicit and make a few choices in order to further our understanding and make calculations simpler. The first choice I'm going to make is to use a Z_2 ϕ field, so that $\rho[\phi]$ is trivial. The next simplification I'm going to make is to allow the ϕ fields to live only on temporal links,

$$\mathscr{L}_{\text{int}} = \sqrt{b_\tau g_0}\, \phi_{x,\tau} \psi_{x,\tau}^\dagger \psi_{x,\tau-1} \ . \tag{5.41}$$

Note that we are free to make this choice, so long as the proper four-fermion interaction is regained in the continuum limit. This choice renders the interaction separable, as it was in our continuum effective theory. This means we may analytically sum two-body bubble chain diagrams as we did previously in order to set the coupling g_0 using some physical observable (see Fig. 5.5).

With this choice we can now write the K-matrix explicitly as

$$K[\phi,N_\tau] \equiv \begin{pmatrix} D & -X(\phi_{N_\tau-1}) & 0 & 0 & \cdots & \cdot \\ 0 & D & -X(\phi_{N_\tau-2}) & 0 & \cdots & \cdot \\ \cdot & \cdot & \cdot & \cdot & & \\ \cdot & \cdot & \cdot & \cdot & & \\ \cdot & \cdot & \cdot & & D & X(\phi_0) \\ X(\phi_{N_\tau}) & \cdot & & \cdot & 0 & D \end{pmatrix} , \tag{5.42}$$

where $X(\phi_\tau) \equiv 1 - \sqrt{g_0}\phi_\tau$. Now the ϕ-dependence exists only on the upper diagonal, as well as the lower left due to the boundary condition. This block will be eliminated through our final choice: open boundary conditions in time for the ψ fields, $X(\phi_{N_\tau}) = 0$. As mentioned previously, we are free to choose the temporal boundary conditions as we please, so long as we only consider zero temperature (and zero chemical potential) observables.

Fig. 5.5 Two-body scattering amplitude of Fig. 5.2, where the contact interaction has been replaced in the second line by exchange of a dimer auxiliary field via a Hubbard-Stratonovich transformation.
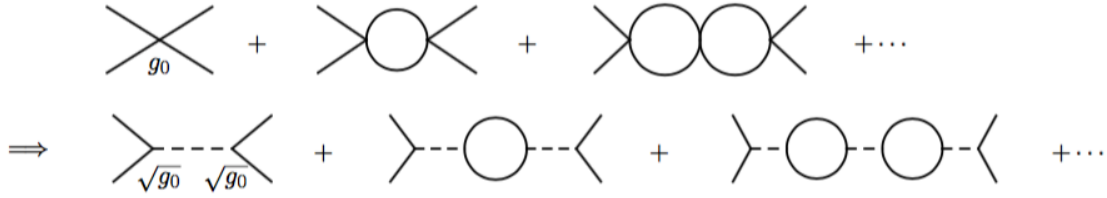
With this set of choices the matrix K consists purely of diagonal elements, D, and upper diagonal elements, $X(\phi_\tau)$. One property of such a matrix is that the determinant, which is part of the probability distribution, is simply the product of diagonal elements, $\det K = \prod_\tau D$. Note that D is completely independent of the field ϕ. This means that the determinant in this formulation has no impact on the probability distribution $P[\phi]$, and therefore never needs to be explicitly computed, greatly reducing the computational burden. Thus in all of our calculations, performing the path integral over ϕ simply amounts to summing over $\phi = \pm 1$ at each lattice site.

Finally, this form of K also makes the calculation of propagators very simple. The propagator from time 0 to τ may be written,

$$\begin{aligned} K^{-1}(\tau,0) &= D^{-1}X(\phi_{\tau-1})D^{-1}X(\phi_{\tau-2})D^{-1}\cdots X(\phi_0)D^{-1} \\ &= D^{-1}X(\phi_{\tau-1})K^{-1}(\tau-1,0) , \end{aligned} \tag{5.43}$$

where $K^{-1}(0,0) = D^{-1}$, and all entries are $V \times V$, $(V = L^3)$ matrices which may be projected onto the desired state. This form suggests a simple iterative approach to calculating propagators: start with a source (a spatial vector projecting onto some desired quantum numbers and interpolating wavefunction), hit it with the kinetic energy operator corresponding to free propagation on the time slice, then hit it with the ϕ field operator on the next time link, then another free kinetic energy operator, and so on, finally projecting onto a chosen sink vector.

As will be discussed further in Secsystematic, it is often preferable to calculate the kinetic energy operator in momentum space, while the auxiliary field in $X(\phi)$ must be generated in position space. Thus, Fast Fourier Transforms (FFTs) may be used between each operation to quickly translate between the bases. Example code for generating source vectors, kinetic operators, and interaction operators will be provided in later Sections.

A cartoon of this process on the lattice is shown in Fig. 5.6. The choice of Z_2 auxiliary fields also simplifies the understanding of how four-fermion interactions are generated. On every

time link, imagine performing the sum over $\phi = \pm 1$. Clearly, if there is only a single fermion propagator on a given link this gives zero contribution because the term is proportional to $\sum_{\phi=\pm 1} \sqrt{g_0} \phi = 0$. However, on time slices where two propagators overlap, we have instead $\sum_{\phi=\pm 1} g_0 \phi^2 = 2g_0$. In sum, anywhere two fermions exist at the same spacetime point of a factor of g_0 contributes, corresponding to an interaction.

Fig. 5.6 Schematic of a lattice calculation for a two-particle correlation function. The two particles (red and blue lines) propagate through the lattice between source $\psi(0)$ and sink $\psi(\tau)$, seeing particular values of the auxiliary field, ϕ, on each time link. If two particles occupy the same temporal link, then upon summation over all possible values of ϕ at each link, a non-zero contribution is generated by the interaction term because $\langle \phi^2 \rangle \neq 0$.
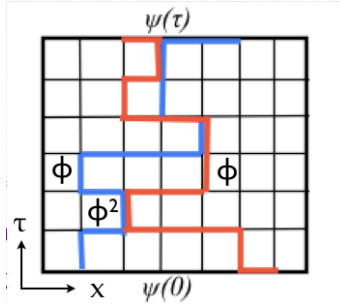
5.2.2.5 Tuning the two-body interaction

There are several ways to set the two-body coupling. Here we will explore two methods, using different two-body observables. The first involves calculating the two-particle scattering amplitude, and tuning the coupling to reproduce known scattering parameters, to make a connection with our previous calculation for the effective theory. The second method uses instead the energy spectrum of a two-particle system in a box. This powerful method will be useful later when we begin to improve the theory in order to reduce systematic errors.

We have calculated the scattering amplitude previously for our effective theory using a momentum cutoff. For the first method for tuning the coupling, we will calculate it again using our lattice theory with the lattice cutoff as a regulator. First we need the single particle free propagator:

$$
G_0(\tau, \mathbf{p}) = \langle \mathbf{p}, \tau | \left(D^{-1} \right)^{\tau+1} | \mathbf{p}, 0 \rangle = \left(1 + \frac{\Delta(p)}{M} \right)^{-(\tau+1)} ,
$$
$$
\Delta(p) \equiv -\frac{1}{2} \langle \mathbf{p} | \nabla_L^2 | \mathbf{p} \rangle
$$
$$
= \sum_i \sin^2 \frac{p_i}{2} , \tag{5.44}
$$

where I've set $b_s = 1$ (we will use this convention from now on until we begin to discuss systematic errors), and have used the previously defined discretized Laplacian operator. I've written the propagator in a mixed $\mathbf{p}, \tau$ representation, as this is often useful in lattice calculations for calculating correlation functions in time when the kinetic operator, D, is diagonal in momentum space.

The diagrammatic two-particle scattering amplitude is shown on the bottom line in Fig. 5.5. Because we have chosen the interaction to be separable, the amplitude can be factorized:

$$A = g_0 \left[1 + \sum_n (g_0 \hat{L})^n \right] = \frac{g_0}{1 - g_0 \hat{L}} \ , \tag{5.45}$$

where the one loop integral, $\hat{L}$, will be defined below. As before, in order to set a single coupling we need one observable, so we use the effective range expansion for the scattering phase shift to leading order,

$$A = \frac{4\pi}{M} \frac{1}{p \cot \delta - i p} \approx -\frac{4\pi a}{M} \ . \tag{5.46}$$

Relating Eqs. (5.45,5.46), we find

$$\frac{1}{g_0} = -\frac{M}{4\pi a} + \hat{L} \ . \tag{5.47}$$

We will now evaluate the loop integral using the free single particle propagators, Eq. (5.44),

$$\begin{aligned}
\hat{L} &= \frac{1}{V} \sum_{\mathbf{p}} \sum_{\tau=0}^{\infty} [G_0(\tau, \mathbf{p})]^2 \\
&= \frac{1}{V} \sum_{\mathbf{p}} \sum_{\tau=0}^{\infty} \frac{1}{\left(1 + \frac{\Delta(p)}{M} \right)^{2\tau+2}} \\
&= \frac{1}{V} \sum_{\mathbf{p}} \frac{1}{\left(1 + \frac{\Delta(p)}{M} \right)^2} \left[1 + \sum_{\tau=0}^{\infty} \frac{1}{\left[\left(1 + \frac{\Delta(p)}{M} \right)^2 \right]^{\tau}} \right] \\
&= \frac{1}{V} \sum_{\mathbf{p}} \frac{M}{2} \frac{1}{\Delta(p) \left(1 + \frac{\Delta(p)}{2M} \right)} \ .
\end{aligned} \tag{5.48}$$

This final sum may be calculated numerically for a given M and L (governing the values of momenta included in the sum), as well as for different possible definitions of the derivative operators contained in Δ, giving the desired coupling, g_0, via Eq. (5.47).

The second method for setting the coupling utilizes the calculation of the ground state energy of two particles. We start with the two-particle correlation function,

$$C_2(\tau) = \frac{1}{Z} \int \mathscr{D}\phi \mathscr{D}\psi^\dagger \mathscr{D}\psi e^{-S[\psi^\dagger, \psi, \phi]} \Psi_{\text{src},2}^\dagger \Psi_{\text{snk},2} \ , \tag{5.49}$$

where $\Psi_{\text{src},2(\text{snk},2)}$ is a source (sink) wavefunction involving one spin up and one spin down particle. Integrating out the fermion fields gives,

$$\begin{aligned}
C_2(\tau) &= \frac{1}{Z_\phi} \int \mathscr{D}\phi P[\phi] \langle \Psi_{\text{snk},2} | K^{-1}(\tau,0) \otimes K^{-1}(\tau,0) | \Psi_{\text{src},2} \rangle \\
&= \frac{1}{4\tau} \sum_{\phi=\pm 1} \langle \Psi_{\text{snk},2} | D^{-1} \otimes D^{-1} X(\phi_\tau) \otimes X(\phi_\tau) D^{-1} \otimes D^{-1} X(\phi_{\tau-1}) \otimes X(\phi_{\tau-1}) \cdots | \Psi_{\text{src},2} \rangle \ .
\end{aligned}$$
$$\tag{5.50}$$

I will now write out the components of the matrices explicitly:

$$\begin{aligned}
C_2(\tau) = \frac{1}{4\tau} \sum_{x_1 x_2 x_1' x_2' \cdots y_1 y_2} \sum_{\phi_{x_1} \phi_{x_1'} \cdots = \pm 1} \langle \Psi_{\text{snk},2} | x_1 x_2 \rangle D_{x_1 x_1'}^{-1} D_{x_2 x_2'}^{-1} (\delta_{x_1 x_1'} + \sqrt{g_0} \phi_{x_1} \delta_{x_1 x_1'}) (\delta_{x_2 x_2'} + \sqrt{g_0} \phi_{x_2} \delta_{x_2 x_2'}) \\
\times D_{x_1' x_1''}^{-1} D_{x_2' x_2''}^{-1} \cdots \langle y_1 y_2 | \Psi_{\text{src},2} \rangle \ .
\end{aligned} \tag{5.51}$$

The first (last) piece in angle brackets represents the position space wavefunction created by the sink (source). All ϕ fields in Eq. (5.51) are uncorrelated, so we can perform the sum for each time slice independently. One such sum is given by,

$$
\frac{1}{4} \sum_{x_1 x_1' x_2 x_2'} \sum_{\phi_{x_1} \phi_{x_2}} \delta_{x_1 x_1'} \delta_{x_2 x_2'} ('1 + \sqrt{g_0} \phi_{x_1} + \sqrt{g_0} \phi_{x_2} + g_0 \phi_{x_1} \phi_{x_2})
$$
$$
= \sum_{x_1 x_2} (1 + g_0 \delta_{x_1 x_2}) , \tag{5.52}
$$

where the cross terms vanish upon performing the sum. If we make the following definitions,

$$
\langle x_1 x_1' | \mathscr{D}^{-1} | x_2 x_2' \rangle \equiv D_{x_1 x_1'}^{-1} D_{x_2 x_2'}^{-1} , \qquad \langle x_1 x_2 | \mathscr{V} | x_1' x_2' \rangle \equiv g_0 \delta_{x_1 x_1'} \delta_{x_2 x_2'} \delta_{x_1 x_2} , \tag{5.53}
$$

then we can write the two-particle correlation function as,

$$
C_2(\tau) = \langle \Psi_{\text{snk},2} | \mathscr{D}^{-1}(1+\mathscr{V}) \mathscr{D}^{-1}(1+\mathscr{V}) \cdots \mathscr{D}^{-1}(1+\mathscr{V}) \mathscr{D}^{-1} | \Psi_{\text{src}} \rangle
$$
$$
= \langle \Psi_{\text{snk}} | \mathscr{D}^{-1/2} \mathscr{T} \mathscr{D}^{-1/2} | \Psi_{\text{src},2} \rangle , \tag{5.54}
$$

where I have made the definition

$$
\mathscr{T} \equiv \mathscr{D}^{-1/2} (1+\mathscr{V}) \mathscr{D}^{-1/2} . \tag{5.55}
$$

Recall from statistical mechanics that correlation functions may be written as τ insertions of the transfer matrix, e^{-H}, acting between two states,

$$
C(\tau) = \langle \Psi_{\text{snk},2} | e^{-H\tau} | \Psi_{\text{src},2} \rangle
$$
$$
= \langle \Psi_{\text{snk},2} | [e^{-H}]^\tau | \Psi_{\text{src},2} \rangle . \tag{5.56}
$$

Then we may identify $\mathscr{T}$ in Eq. (5.55) as the transfer matrix of the theory, $\mathscr{T} = e^{-H}$. This in turn implies that the logarithm of the eigenvalues of $\mathscr{T}$ give the energies of the two-particle system.

We will now evaluate the transfer matrix in momentum space:

$$
\langle pq | \mathscr{T} | p'q' \rangle = \sum_{kk'll'} \langle pq | \mathscr{D}^{-1/2} | kl \rangle \langle kl | 1 + \mathscr{V} | k'l' \rangle \langle k'l' | \mathscr{D}^{-1/2} | p'q' \rangle
$$
$$
= \sum_{kk'll'} \delta_{k'p'} \delta_{l'q'} \delta_{pk} \delta_{ql} \left(\delta_{kk'} \delta_{ll'} + \delta_{k+l,k'+l'} \frac{g_0}{V} \right)
$$
$$
\times \left[\frac{1}{\left(1 + \frac{\Delta(p)}{M}\right) \left(1 + \frac{\Delta(q)}{M}\right) \left(1 + \frac{\Delta(p')}{M}\right) \left(1 + \frac{\Delta(q')}{M}\right)} \right]^{1/2}
$$
$$
= \frac{\delta_{pp'} \delta_{qq'} + \frac{g_0}{V} \delta_{p+q,p'+q'}}{\sqrt{\xi(p)\xi(q)\xi(q')\xi(p')}} , \tag{5.57}
$$

where I have made the definition,

$$
\xi(p) \equiv 1 + \frac{\Delta(q)}{M} . \tag{5.58}
$$

The eigenvalues of the matrix $\mathscr{T}$ may be evaluated numerically to reproduce the entire two-particle spectrum. However, for the moment we only need to set a single coupling, g_0, so one eigenvalue will be sufficient. The largest eigenvalue of the transfer matrix, corresponding to the ground state, may be found using a simple variational analysis[4]. Choosing a simple trial state wavefunction,

---

[4] Many thanks to Michael Endres for the following variational argument.

$$\langle pq|\Psi\rangle = \frac{\psi(p)}{\sqrt{V}}\delta_{p,-q} \, , \tag{5.59}$$

subject to the normalization constraint,

$$\frac{1}{V}\sum_p |\psi(p)|^2 = 1 \, , \tag{5.60}$$

we now need to maximize the following functional:

$$\langle \Psi|\mathscr{T}|\Psi\rangle = \left[\frac{1}{V}\sum_p \frac{|\psi(p)|^2}{\xi^2(p)} + \frac{g_0}{V^2}\left|\sum_p \frac{\psi(p)}{\xi(p)}\right|^2 + \lambda\left(1 - \frac{1}{V}\sum_p |\psi(p)|^2\right)\right] \, , \tag{5.61}$$

where λ is a Lagrange multiplier enforcing the normalization constraint, and I have used the fact that $\xi(p)$ is symmetric in p to simplify the expression. Taking a functional derivative with respect to $\psi^\dagger(q)$ on both sides gives

$$-\lambda\psi(q) + \frac{\psi(q)}{\xi^2(q)} + \frac{g_0}{V}\sum_p \frac{\psi(p)}{\xi(p)\xi(q)} = 0 \, , \tag{5.62}$$

where I have set the expression equal to zero in order to locate the extrema. Rearranging this equation, then taking a sum over q on both sides gives

$$\sum_q \frac{\psi(q)}{\xi(q)} = \sum_q \frac{g_0}{V}\frac{1}{\lambda\xi^2(q)-1}\sum_p \frac{\psi(p)}{\xi(p)} \, , \tag{5.63}$$

finally resulting in

$$1 = \frac{g_0}{V}\sum_q \frac{1}{\lambda\xi^2(q)-1} \, . \tag{5.64}$$

We now have an equation involving two unknowns, λ and g_0. We need a second equation in order to determine these two parameters. We may use the constraint equation to solve for $\psi(p)$, giving

$$\psi(p) = \mathscr{N}\frac{\xi(p)}{\lambda\xi^2(p)-1} \, , \qquad \frac{1}{\mathscr{N}^2} = \frac{1}{V}\sum_p \frac{\xi^2(p)}{[\lambda\xi^2(p)-1]^2} \, . \tag{5.65}$$

Plugging this back in to our transfer matrix we find,

$$\langle\Psi|\mathscr{T}|\Psi\rangle = \lambda \, . \tag{5.66}$$

This tells us that λ is equivalent to the eigenvalue we sought, $E_0 = -\ln\lambda(g_0)$. As a check, we can compare Eqs. (5.47,5.64) in the unitary limit: $a \to \infty, \lambda \to 1$, giving

$$\frac{1}{g_0} = \frac{M}{2V}\sum_p \frac{1}{\Delta\left(1+\frac{\Delta}{2M}\right)} \tag{5.67}$$

for both Equations.

In Sec. 5.2.2.5 we will discuss a simple formalism for determining the exact two particle spectrum in a box for any given scattering phase shift. This will allow us to eliminate certain finite volume systematic errors automatically. The transfer matrix method is also powerful because it gives us access to the entire two particle, finite-volume spectrum. When we discuss improvement in Sec. 5.4.2, we will add more operators and couplings to the interaction

in order to match not only the ground state energy we desire, but higher eigenvalues as well. This will allow us to control the interaction between particles with non-zero relative momentum. To gain access to higher eigenvalues, the transfer matrix must be solved numerically, however, this may be accomplished quickly and easily for a finite volume system.

5.3 Calculating observables

Perhaps the simplest observable to calculate using lattice (or any imaginary time) methods is the ground-state energy. While the two-body system may be solved exactly and used to set the couplings for two-body interactions, correlation functions for N-body systems can then be used to make predictions. However, the transfer matrix for $N \gtrsim 4$ cannot in general be solved exactly, because the dimension of the matrix increases with particle number. For this reason we form instead N-body correlation functions,

$$C_N(\tau) = \frac{1}{Z} \int \mathscr{D}\phi \, \mathscr{D}\psi^\dagger \mathscr{D}\psi \, e^{-S[\psi^\dagger, \psi, \phi]} \Psi^{(b)}_{b_1 \cdots b_N}(\tau) \Psi^{\dagger(a)}_{a_1 \cdots a_N}(0) \ , \tag{5.68}$$

where

$$\Psi^{(a)\dagger}_{a_1 \cdots a_N}(\tau) = \int dx_1 \cdots dx_N A^{(a)}(x_1 \cdots x_N) \psi_{a_1}(x_1, \tau) \cdots \psi_{a_N}(x_N, \tau) \tag{5.69}$$

is a source for N particles with spin/flavor indices $a_1 \cdots a_N$, and a spatial wavefunction $A^{(a)}(x_1 \cdots x_N)$. For the moment the only requirement we will make of the wavefunction is that it has non-zero overlap with the ground-state wavefunction (i.e. it must have the correct quantum numbers for the state of interest).

Recall that a correlation function consists of τ insertions of the transfer matrix between source and sink. We can then expand the correlation function in a basis of eigenstates,

$$\begin{aligned} C_N(\tau) &= \frac{1}{Z} \langle \tilde{\Psi}^{(a)}_{a_1 \cdots a_N} | e^{-H\tau} | \tilde{\Psi}^{(b)}_{b_1 \cdots b_N} \rangle = \frac{1}{Z} \sum_{m,n} \langle \tilde{\Psi}^{(a)}_{a_1 \cdots a_N} | m \rangle \langle m | e^{-H\tau} | n \rangle \langle n | \tilde{\Psi}^{(b)}_{b_1 \cdots b_N} \rangle \\ &= \sum_m Z^{(a)}_m Z^{*(b)}_m e^{-E_n \tau} \ , \end{aligned} \tag{5.70}$$

where $Z^{(a)}_m$ is the overlap of wavefunction a with the energy eigenstate m, and E_n is the nth eigenvalue of the Hamiltonian. In the limit of large Euclidean time (zero temperature), the ground state dominates,

$$C_N(\tau) \xrightarrow[\tau \to \infty]{} Z^{(a)}_0 Z^{*(b)}_0 e^{-E_0 \tau} \ , \tag{5.71}$$

with higher excited states exponentially suppressed by $\sim e^{-\Delta_{n0}\tau}$, where $\Delta_{n0} \equiv E_n - E_0$ is the energy splitting between the nth state and the ground state. It should be noted that for a non-relativistic theory the rest masses of the particles do not contribute to these energies, so the ground state energy of a single particle at rest is $E_0 = 0$, in contrast to lattice QCD formulations.

In this way, we can think of the transfer matrix as acting as a filter for the ground state, removing more excited state contamination with each application in time. A common method for determining the ground state energy from a correlation function is to construct the so-called effective mass function,

$$M_{\text{eff}}(\tau) \equiv \ln \frac{C(\tau)}{C(\tau+1)} \xrightarrow[\tau \to \infty]{} E_0 \ , \tag{5.72}$$

and look for a plateau at long times, whose value corresponds to the ground-state energy.

Once the ground state has been isolated, we can calculate matrix elements with the ground state as follows,

$$
\begin{aligned}
\langle \Psi^{(a)}_{a_1 \cdots a_N} | A(\tau') | \Psi^{(b)}_{b_1 \cdots b_N} \rangle &= \sum_{lmnq} \langle \Psi^{(a)}_{a_1 \cdots a_N} | l \rangle \langle l | e^{-H(\tau-\tau')} | m \rangle \langle m | A | n \rangle \langle n | e^{-H\tau'} | q \rangle \langle q | \Psi^{(b)}_{b_1 \cdots b_N} \rangle \\
&= \sum_{ln} Z^{(a)}_l Z^{*(b)}_n e^{-E_l(\tau-\tau')} e^{-E_n \tau'} \langle m | A | n \rangle \; .
\end{aligned}
\tag{5.73}
$$

To filter out the ground state, the matrix element insertion A must be placed sufficiently far in time from both source and sink, $\{ \Delta_{l0}(\tau - \tau'), \Delta_{n0}\tau' \} \gg 1$,

$$
\xrightarrow[\tau,\tau'\to\infty]{} Z^{(a)}_0 Z^{*(b)}_0 e^{-E_0\tau} \langle 0 | A | 0 \rangle \; .
\tag{5.74}
$$

In order to isolate the matrix element and remove unknown Z factors and ground state energies, ratios may be formed with correlation functions at various times, similar to the effective mass function.

Another observable one may calculate using lattice methods is the scattering phase shift between interacting particles. Because all lattice calculations are performed in a finite volume, which cannot accommodate true asymptotic scattering states, direct scattering measurements are not possible. However, a method has been devised by Lüscher which uses finite volume energy shifts to infer the interaction, and therefore, the infinite volume scattering phase shift. The Lüscher method will be discussed further in Sec. 5.4.2.1. Because the inputs into the Lüscher formalism are simply energies, correlation functions may be used in the same way as described above to produce this data.

5.3.1 Signal-to-noise

Recall that we must use Monte Carlo methods to approximate the partition function using importance sampling,

$$
C(\tau) \approx \frac{1}{N_{\text{cfg}}} \sum_{i=1}^{N_{\text{cfg}}} C(\phi_i, \tau) \xrightarrow[\tau\to\infty]{} Z_0 e^{-E_0\tau} \; ,
\tag{5.75}
$$

where ϕ is generated according to the appropriate probability distribution. In the long Euclidean time limit we expect that this quantity will give us an accurate value for the ground state energy. As stated previously, if the ensemble is large enough for the central limit theorem to hold, then the error on the mean (noise) will be governed by the sample standard deviation,

$$
\sigma^2_C(\tau) = \frac{1}{N_{\text{cfg}}} \left[\sum_{i=1}^{N_{\text{cfg}}} |C(\phi_i, \tau)|^2 - \left| \sum_{i=1}^{N_{\text{cfg}}} C(\phi_i, \tau) \right|^2 \right] \; .
\tag{5.76}
$$

As an example of how to estimate the size of the fluctuations relative to the signal, let's consider a single particle correlation function, consisting of a single propagator,

$$
\frac{1}{Z_\phi} \int \mathscr{D}\phi P(\phi) \langle \Psi_a | K^{-1}(\phi, \tau) | \Psi_b \rangle \approx \frac{1}{N_{\text{cfg}}} \sum_{i=1}^{N_{\text{cfg}}} K^{-1}_{ab}(\phi_i, \tau) \; ,
\tag{5.77}
$$

where the indices $\{ab\}$ indicate projection onto the states specified by the source/sink. In the large Euclidean time limit, this object will approach a constant, Z_0, because the ground state energy for a single particle is $E_0 = 0$. For the non-relativistic theory as we have set it up, the matrix K is real so long as $g_0 > 0$ (attractive interaction). The standard deviation is then given by

$$\sigma_{C_1}^2(\tau) = \frac{1}{N_{\text{cfg}}} \left[\sum_{i=1}^{N_{\text{cfg}}} \left(K_{ab}^{-1}(\phi_i, \tau) \right)^2 - \left(\sum_{i=1}^{N_{\text{cfg}}} K_{ab}^{-1}(\phi_i, \tau) \right)^2 \right] . \tag{5.78}$$

The second term on the right hand side of the above equation is simply the square of the single particle correlation function, and will therefore also go to a constant, Z_0^2, for large Euclidean time. To gain an idea of how large the first term of $\sigma_{C_1}^2$ is, let's take a look at a correlation function for one spin up and one spin down particle,

$$C_2(\tau) = \frac{1}{Z} \int \mathscr{D}\phi \mathscr{D}\psi^\dagger \mathscr{D}\psi e^{-S[\psi^\dagger, \psi, \phi]} \psi_\uparrow^{(b)}(\tau) \psi_\downarrow^{(b)}(\tau) \psi_\uparrow^{\dagger(a)}(0) \psi_\downarrow^{\dagger(a)}(0) , \tag{5.79}$$

where I have chosen the same single particle source (sink), $\psi^{(a)}$ ($\psi^{(b)}$), for both particles (this is only allowed for bosons or for fermions with different spin/flavor labels). After integrating out the ψ fields we have

$$C_2(\tau) = \frac{1}{Z_\phi} \int \mathscr{D}\phi P(\phi) K_{ab}^{-1}(\phi, \tau) K_{ab}^{-1}(\phi, \tau) , \tag{5.80}$$

which is approximately given by

$$C_2(\tau) \approx \frac{1}{N_{\text{cfg}}} \sum_{i=1}^{N_{\text{cfg}}} \left[K_{ab}^{-1}(\phi_i, \tau) \right]^2 . \tag{5.81}$$

This is precisely what we have for the first term on the right hand side of Eq. (5.78). Therefore, this term should be considered a two-particle correlation function, whose long Euclidean time behavior is known. Note that we must interpret this quantity as a two-particle correlation function whose particles are either bosons or fermions with different spin/flavor labels due to the lack of anti-symmetrization.

We may now write the long-time dependence of the variance of the single particle correlator as

$$\sigma_{C_1}^2(\tau) \approx C_2(\tau) - (C_1(\tau))^2 \xrightarrow[\tau \to \infty]{} Z_2 e^{-E_0^{(2)}\tau} - Z_1^2 , \tag{5.82}$$

where $E_0^{(2)}$ is the ground state energy of the two-particle system. For a two-body system with an attractive interaction in a finite volume, $E_0^{(2)} < 0$, and we may write

$$\sigma_{C_1}^2(\tau) \xrightarrow[\tau \to \infty]{} Z_2 e^{E_B^{(2)}\tau} - Z_1^2 , \tag{5.83}$$

where I've defined $E_B^{(2)} \equiv -E_0^{(2)}$. This tells us that $\sigma_{C_1}^2$, and therefore the noise, grows exponentially with time. We can write the signal-to-noise ratio $\mathscr{R}_{C_1}(\tau)$ as

$$\mathscr{R}_{C_1}(\tau) \equiv \frac{C_1(\tau)}{\frac{1}{\sqrt{N_{\text{cfg}}}} \sigma_{C_1}(\tau)} \xrightarrow[\tau \to \infty]{} \sqrt{N_{\text{cfg}}} \frac{Z_1}{\sqrt{Z_2} e^{E_B^{(2)}\tau/2}} = \sqrt{N_{\text{cfg}}} \frac{Z_1}{\sqrt{Z_2}} e^{-E_B^{(2)}\tau/2} , \tag{5.84}$$

where I've dropped the constant term in $\sigma^2_{C_1}$, because it is suppressed in time relative to the exponentially growing term. This expression indicates that the signal-to-noise ratio itself grows exponentially with time, and therefore an exponentially large N_{cfg} will be necessary to extract a signal at large Euclidean time. Unfortunately, large Euclidean time is necessary in order to isolate the ground state.

This exponential signal-to-noise problem is currently the limiting factor in system size for the use of any lattice method for nuclear physics. Here, we will discuss it in some detail because in many cases understanding the physical basis behind the problem can lead to methods for alleviation. One method we can use is to employ knowledge of the wavefunction of the signal and/or the wavefunction of the undesired noise in order to maximize the ratio of Z-factors, $Z_1/\sqrt{Z_2}$. For example, choosing a plane wave source for our single particle correlator gives perfect overlap with the desired signal, but will give poor overlap with the bound state expected in the noise. This leads to what has been referred to as a "golden window" in time where the ground-state dominates before the noise begins to turn on [42]. In general, choosing a perfect source for the signal is not possible, however, a proposal for simultaneously maximizing the overlap with the desired state as well as reducing the overlap with the noise using a variational principle has been proposed in [43, 44]. We will discuss other methods for choosing good interpolating fields in Sec. 5.3.3, in order to allow us to extract a signal at earlier times where the signal-to-noise problem is less severe.

Another situation where understanding of the noise may allow us to reduce the noise is when the auxiliary fields and couplings used to generate the interactions can often be introduced in different ways, for instance, via the density channel vs. the BCS channel as mentioned previously. While different formulations can give the same effective interaction, they may lead to different sizes of the fluctuations. Understanding what types of interactions generate the most noise is therefore crucial. This will become particularly relevant when we discuss adding interactions beyond leading order to our EFT in Sec. 5.5, where different combinations of interactions can be tuned to give the same physical observables.

Let's now discuss what happens to $\sigma^2_{C_1}$ if we have a repulsive interaction ($g_0 < 0$). Because nuclear potentials have repulsive cores, such a scenario occurs for interactions at large energy. Since the auxiliary-field-mediated interaction is given by $\sqrt{g_0}\phi\psi^\dagger\psi$, this implies that the interaction is complex. Our noise is now given by

$$\sigma^2_{C_1}(\tau) = \frac{1}{N_{\text{cfg}}}\sum_{i=1}^{N_{\text{cfg}}} K^{-1}_{ab}(\phi_i,\tau)\left[K^{-1}_{ab}(\phi_i,\tau)\right]^\dagger - |C_1(\tau)|^2 \; . \tag{5.85}$$

Recall that the single particle propagator can be written

$$K^{-1}(\phi_i,\tau) = D^{-1}X(\phi_{i,\tau})D^{-1}X(\phi_{i,\tau-1})\cdots \qquad X(\phi_{i,\tau}) = 1 + \sqrt{g_0}\phi_{i,\tau} \; . \tag{5.86}$$

The complex conjugate of the propagator then corresponds to taking $\phi \to -\phi$,

$$\left[K^{-1}(\phi_i,\tau)\right]^\dagger = D^{-1}X(-\phi_{i,\tau})D^{-1}X(-\phi_{i,\tau-1}) \; . \tag{5.87}$$

Again, ϕ fields on different time slices are independent, so we may perform each sum over $\phi = \pm 1$ separately. Each sum that we will encounter in the two-particle correlator consists of the product of $X(\phi_\tau)X(-\phi_\tau)$,

$$\sum_\phi (1 + \sqrt{g_0}\phi)(1 - \sqrt{g_0}\phi) = 1 - g_0^2 = 1 + |g_0|^2 \; , \tag{5.88}$$

which is exactly the same as we had for the attractive interaction. This implies that even though the interaction in the theory we're using to calculate the correlation function is repulsive, the noise is controlled by the energy of two particles with an attractive interaction,

which we have already investigated. In this particular case for a single particle propagator, the signal-to-noise ratio is the same regardless of the sign of the interaction[5].

In general, however, signal-to-noise problems for systems with repulsive interactions are exponentially worse than those for attractive interactions. This is because generically the signal-to-noise ratio falls off as,

$$\mathcal{R} \sim e^{-(E_S - E_N/2)\tau} \, , \tag{5.89}$$

where $E_{S(N)}$ is the ground-state energy associated with the signal (noise). Because the signal corresponds to a repulsive system while the noise corresponds to an attractive system, the energy difference in the exponential will be greater than for a signal corresponding to an attractive system.

5.3.1.1 Sign Problems

A related but generally more insidious problem can occur in formulations having fermion determinants in the probability measure, known as a sign problem. A sign problem occurs when the determinant is complex, for example, in our case of a repulsive interaction. While we were able to eliminate the fermion determinant in one particular formulation, there are situations when having a fermion determinant in the probability measure may be beneficial, for example, when using forms of favorable reweighting, as will be discussed later on, or may be necessary, such as for non-zero chemical potential or finite temperature, when the boundary conditions in time may not be altered. For these reasons, we will now briefly discuss sign problems.

The basic issue behind a sign problem is that a probability measure, by definition, must be real and positive. Therefore, a complex determinant cannot be used for importance sampling. Methods to get around the sign problem often result in exponentially large fluctuations of the observable when calculated on a finite sample, similar to the signal-to-noise problem (the two usually result from the same physical mechanism). One particular method is called reweighting, in which a reshuffling occurs between what is considered the "observable" and what is considered the "probability measure". For example, when calculating an observable,

$$\langle \mathcal{O} \rangle = \frac{1}{Z_\phi} \int \mathcal{D}\phi P(\phi) \mathcal{O}(\phi) \, , \tag{5.90}$$

when $P(\phi)$ is complex, we can multiply and divide by the magnitude of $P(\phi)$ in both numerator and denominator,

$$\langle \mathcal{O} \rangle = \frac{\int \mathcal{D}\phi |P(\phi)| \frac{P(\phi)\mathcal{O}(\phi)}{|P(\phi)|}}{\int \mathcal{D}\phi |P(\phi)| \frac{P(\phi)}{|P(\phi)|}} \, , \tag{5.91}$$

as well as multiply and divide by $\tilde{Z}_\phi \equiv \int \mathcal{D}\phi |P(\phi)|$,

---

[5] This argument is somewhat simplified by our particular lattice setup in which we have no fermion determinant as part of the probability measure. For cases where there is a fermion determinant, there will be a mismatch between the interaction that the particles created by the operators see (attractive) and the interaction specified by the determinant used in the probability measure (repulsive). This is known as a partially quenched theory, and is unphysical. However, one may calculate a spectrum using an effective theory in which valence (operator) and sea (determinant) particles are treated differently. Often it is sufficient to ignore the effects from partial quenching because any differences contribute only to loop diagrams and may be suppressed.

$$\langle \mathcal{O} \rangle = \frac{\int \mathscr{D}\phi \, |P(\phi)| \frac{P(\phi)\mathcal{O}(\phi)}{|P(\phi)|}}{\tilde{Z}_\phi} \bigg/ \frac{\int \mathscr{D}\phi \, |P(\phi)| \frac{P(\phi)}{|P(\phi)|}}{\tilde{Z}_\phi} = \langle \mathcal{O}' \rangle_{|P|} \big/ \langle \mathcal{O}'' \rangle_{|P|} \quad , \tag{5.92}$$

where

$$\mathcal{O}' \equiv \frac{P(\phi)\mathcal{O}(\phi)}{|P(\phi)|} \, , \qquad \mathcal{O}'' \equiv \frac{P(\phi)}{|P(\phi)|} \, , \tag{5.93}$$

and $\langle \cdots \rangle_{|P|}$ implies that the path integrals in the expectation values use the measure $|P(\phi)|$. The advantage is that now the probability measure used for sampling is real and positive, at the cost of having to calculate two observables, $\mathcal{O}', \mathcal{O}''$. The real disadvantage, however, is that the second observable, $\mathcal{O}''$ corresponds to the complex phase of the original measure, $P(\phi)$, which is highly oscillatory from field configuration to field configuration.

We can measure the size of the fluctuations of the phase of $P(\phi) = [\det K(\phi)]^2$, corresponding to a two-spin (or flavor) theory with a repulsive interaction,

$$\langle \mathcal{O}'' \rangle_{|P|} = \frac{\int \mathscr{D}\phi \, \det K(\phi) \det K^*(\phi)}{\int \mathscr{D}\phi \, [\det K(\phi)]^2} \, . \tag{5.94}$$

The denominator of the above ratio corresponds to the partition function of the original theory which has two spins of particles interacting via a repulsive interaction. The numerator also corresponds to the partition function of a two-spin theory. However, recall that $K^*(\phi)$ corresponds to a propagator with the opposite sign on the interaction term. Because fermions of the same spin don't interact (Pauli principle), the only interaction in this theory is that between two particles of opposite spin, which we established previously will be an attractive interaction due to the sign flip on $K^*(\phi)$. Thus, the numerator corresponds to the partition function of a two-spin theory with an attractive interaction.

A partition function is simply the logarithm of the free energy, $Z = e^{-\beta F}$. For a system in a finite volume at zero temperature this becomes $Z = e^{-V\mathscr{E}_0}$, where $\mathscr{E}_0$ is the energy density of the ground state of the theory. This implies that

$$\langle \mathcal{O}'' \rangle_{|P|} \underset{\tau \to \infty}{\sim} e^{-V(\mathscr{E}_0^{(\mathrm{rep})} - \mathscr{E}_0^{(\mathrm{att})})} \, , \tag{5.95}$$

where $\mathscr{E}_0^{(\mathrm{rep})}$ ($\mathscr{E}_0^{(\mathrm{att})}$) is the energy density of the ground state of the repulsive (attractive) theory. Generically, $\mathscr{E}_0^{(\mathrm{att})} \leq \mathscr{E}_0^{(\mathrm{rep})}$, for theories which are identical up to the sign of their interaction. This may be shown using the Cauchy-Schwarz theorem,

$$\langle |\det K(\phi)| \rangle \leq |\langle \det K(\phi) \rangle| \, . \tag{5.96}$$

Therefore, $\langle \mathcal{O}'' \rangle_{|P|}$ will be exponentially small for large Euclidean times so long as $\mathscr{E}_0^{(\mathrm{rep})} \neq \mathscr{E}_0^{(\mathrm{att})}$. The variance, on the other hand, is

$$\langle |\mathcal{O}''|^2 \rangle_{|P|} - |\langle \mathcal{O}'' \rangle_{|P|}|^2 = \langle 1 \rangle - |\langle \mathcal{O}'' \rangle_{|P|}|^2 \underset{\tau \to \infty}{\sim} 1 - e^{-2V(\mathscr{E}_0^{(\mathrm{rep})} - \mathscr{E}_0^{(\mathrm{att})})} \sim 1 \, . \tag{5.97}$$

So again, we have an exponentially small signal-to-noise ratio at large Euclidean time for the observable $\mathcal{O}''$. This argument is very similar to our signal-to-noise argument for correlation functions. In general, if a theory has a sign problem there will be a corresponding signal-to-noise problem for correlation functions. The reverse is not always true, however, because reweighting is only necessary when the integration measure is complex, so even if there is a signal-to-noise problem in calculating correlation functions (as there is for an attractive interaction), a sign problem may not arise. Sign problems are in general far more problematic due to the exponential scaling with the volume, and because correlation functions give us

the additional freedom of choosing interpolating fields in order to try to minimize the noise. In some cases, however, it may be possible to use knowledge learned from signal-to-noise problems in order to solve or reduce sign problems, and vice-versa [45–47].

5.3.1.2 Noise in Many-Body Systems

Let us now discuss signal-to-noise ratios for N-body correlation functions. First, we'll look at the two-particle case. We have already defined the correlation function for two particles with different spin/flavor labels,

$$C_2(\tau) = \langle \left[K_{ab}^{-1}(\phi_i, \tau) \right]^2 \rangle . \tag{5.98}$$

The variance is given by

$$\sigma_{C_2}^2(\tau) = \langle \left[K_{ab}^{-1}(\phi_i, \tau) \right]^4 \rangle - (C_2(\tau))^2 . \tag{5.99}$$

It is simple to see that the first term in this expression corresponds to a four-particle correlation function, where each particle has a different flavor/spin index (because there is no anti-symmetrization of the fermion fields). Thus, we can write,

$$\sigma_{C_2}^2(\tau) = C_4(\tau) - (C_2(\tau))^2 , \tag{5.100}$$

where $C_4(\tau)$ corresponds to a correlator with four particles having different flavors. This is much like a correlator for an alpha particle in the spin/flavor $SU(4)$ limit, thus, it will be dominated at large times by the binding energy, $E_B^{(4)}$, of a state with a large amount of binding energy per particle. Our signal-to-noise ratio is then,

$$\mathcal{R}_{C_2}(\tau) \underset{\tau \to \infty}{\sim} \frac{e^{E_B^{(2)}\tau}}{e^{E_B^{(4)}\tau/2}} , \tag{5.101}$$

where, $E_B^{(4)}/2 > E_B^{(2)}$. Therefore, the signal-to-noise ratio is again falling off exponentially in time; this problem clearly becomes worse as the coupling becomes stronger. Finally, we can consider a many-body correlator composed of a Slater determinant over N single-particle states in a two spin/flavor theory,

$$C_{2N}(\tau) = \langle \left[\det K^{-1}(\phi_i, \tau) \right]^2 \rangle . \tag{5.102}$$

The ground state of this correlator will be either a BEC or BCS state, as discussed earlier in Sec. 5.2.1.1. The noise, on the other hand, will be dominated by a system of alpha-like clusters, since the number of flavors in the noise is always double that of the signal, which can bind to form nuclei. The ground-state energy of this bound state will clearly be much lower than that of a dilute BEC/BCS state, and our signal-to-noise ratio will be exponentially small in the large time limit.

In general this pattern continues for fermion correlators with any number of particles, spins, and flavors. This is because doubling the number of flavors reduces the amount of Pauli repulsion in the resulting expression for the variance. Even for bosonic systems signal-to-noise can be a problem, simply as a result of the Cauchy-Schwarz triangle inequality, which tells you that, at best, your signal-to-noise ratio can be 1, corresponding to a non-interacting system. Turning on interactions then generally leads to exponential decay of the signal-to-noise ratio. Signal-to-noise problems also generally scale exponentially with the system size,

leading to limitations on system size based on computational resources. Thus, understanding and combatting signal-to-noise problems is paramount to further development in the field.

5.3.2 Statistical Overlap

For the lattice formulations we have thus far explored one generates configurations according to the probability distribution associated with the vacuum. One then introduces sources to create particles, which are considered part of the "observable". However, the configurations which are the most important for creating the vacuum may not necessarily be the most important for the observable one wishes to calculate.

We can look to lattice QCD for a pedagogical example. In QCD, the fermion determinant encodes vacuum bubbles created by quark/anti-quark pairs. According to the tenets of confinement, bubbles with large spacetime area require a large energy to produce, and are therefore highly suppressed in the partition function. When doing importance sampling, small vacuum bubbles will dominate. On the other hand, if we now calculate an observable which introduces particle sources, a configuration involving a large vacuum bubble may become very important to the calculation. This is because the total relevant spacetime area of the given configuration, taking into account the particles created by the sources, can in fact be small (see Fig. 5.7). However, by sampling according to the vacuum probability, this configuration will be missed, skewing the calculation in an unknown manner. The farther the observable takes us from the vacuum, the worse this problem becomes, making this a particularly troublesome issue for many-body calculations.

Fig. 5.7 A schematic of an example configuration in LQCD which may lead to a statistical overlap problem. Red propagators correspond to valence quarks (quarks created by the sources/sinks in the operator), while blue corresponds to sea quarks (vacuum bubbles generated via Monte Carlo). Due to confinement, large bubbles (determined by the area enclosed by the blue propagator) are suppressed in the QCD vacuum and thus will likely be thrown out during importance sampling. In the presence of quark sources, however, these configurations are very important in the calculation of the observable (due to the small area enclosed between the red and blue propagators).
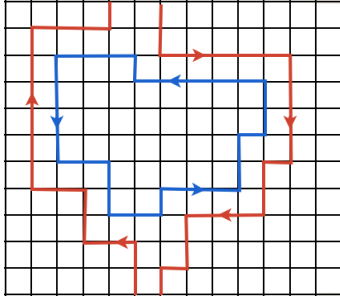
Such problems are referred to as statistical overlap problems. Another situation where these overlap problems can often occur is when doing reweighting to evade a sign problem, as discussed in Sec. 5.3.1.1. For example, if the distribution being sampled corresponds to a theory with an attractive interaction, but the desired observable has a repulsive interaction, the Monte Carlo sampling will be unlikely to pick up the most relevant configurations, affecting the numerator of Eq. (5.92).

We can understand the problem further by studying probability distributions of observables. While the distribution of the sampled field, ϕ in our case, may be peaked around the mean value of ϕ, the distribution of the observable as calculated over the sample may

not be peaked near the true mean of the observable. Such a distribution necessarily has a long tail. Plotting histograms of the values of the observable as calculated over the sample, $\{C(\phi_1), C(\phi_2), \cdots C(\phi_{N_{\text{cfg}}})\}$, can allow us to gain an idea of the shape of the distribution for that observable. An example of a distribution with a statistical overlap problem is plotted in Fig. 5.8. In this case, the peak of the distribution is far from the true mean. Values in the tail of the distribution have small weight, and are likely to be thrown out during importance sampling, skewing the sample mean without a corresponding increase in the error bar. The error bar is instead largely set by the width of the distribution near the peak. One way to determine whether there is an overlap problem is to recalculate the observable on a different sample size; if the mean value fluctuates significantly outside the original error bar this indicates an overlap problem.

Fig. 5.8 Schematic drawing of a long-tailed probability distribution (blue) which leads to an overlap problem. Monte Carlo sampling leads to a sample distribution which is centered around the peak of the underlying distribution (red), far from the mean. The ideal probability distribution one would like to sample is narrow and centered around the mean (green).
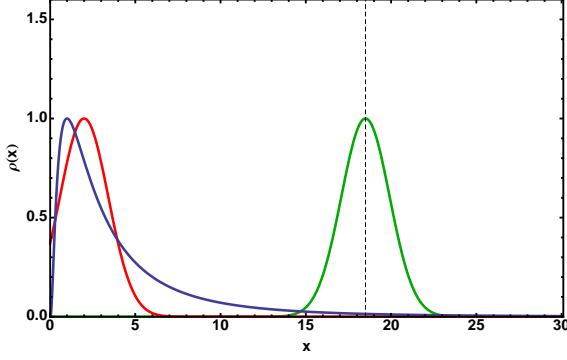
The central limit theorem tells us that regardless of the initial distribution we pull from, the distribution of the mean should approach a Gaussian for a large enough sample size, so in principle we should be able to combat an overlap problem by brute force. However, what constitutes a "large enough" sample size is dictated by the shape of the original distribution. The Berry-Esseen theorem [48, 49] can be used to determine that the number of configurations necessary to assume the central limit theorem applies is governed by

$$\sqrt{N_{\text{cfg}}} \sim \frac{\langle x^3 \rangle}{\langle x^2 \rangle^{3/2}} \ , \tag{5.103}$$

where $\langle x^n \rangle$ is the nth moment of the distribution of the observable. Thus, a large skewness, or long tail, increases the number of configurations necessary before the central limit theorem applies, and therefore, to trust an error bar determined by the standard deviation of the distribution of the mean.

One could imagine repeating an argument similar to that made for estimating the variance of our correlation functions in order to estimate the third moment. For example, if our observable is the two-particle correlation function, $C_2(\tau)$, then the third moment will be

$$\langle [K_{ab}(\phi_i, \tau)]^6 \rangle \ , \tag{5.104}$$

corresponding to a correlation function containing six particles of different flavors. Again, increasing the number of flavors generally increases the binding energy per particle of the system, leading to a third moment which is exponentially large compared to the appropriately scaled second moment. This implies that an exponentially large number of configurations

will be necessary before the central limit theorem applies to the distribution of the mean of correlation functions calculated using this formulation.

While we mentioned that using reweighting to avoid a sign problem is one situation where overlap problems often occur, it is also possible to use reverse reweighting in order to lessen an overlap problem. Here instead we would like to reweight in order to make the distribution of ϕ have <u>more</u> overlap with the configurations that are important for the observable. An example that is commonly used is to include the desired correlation function itself, calculated at some fixed time, to be part of the probability measure. This may be accomplished using ratios of correlators at different times,

$$\frac{C_N(\tau' + \tau)}{C_N(\tau')} = \frac{\int \mathscr{D}\phi \tilde{P}(\phi)\tilde{\mathscr{O}}(\phi,\tau)}{\int \mathscr{D}\phi \tilde{P}(\phi)} \ , \tag{5.105}$$

where

$$\tilde{P}(\phi) \equiv P(\phi)C_N(\tau',\phi) \ , \qquad \tilde{\mathscr{O}}(\phi,\tau) \equiv \frac{C_N(\tau'+\tau,\phi)}{C_N(\tau',\phi)} \ . \tag{5.106}$$

Now the probability distribution incorporates an N-body correlator at one time, τ', and will therefore do a much better job of generating configurations relevant for the N-body correlator at different times. A drawback of this method is that it is much more computationally expensive to require the calculation of propagators for the generation of eaach configuration. Furthermore, the configurations that are generated will be operator-dependent, so that calculating the correlator C_{N+1} will require the generation of a whole new set of field configurations.

Another method for overcoming a statistical overlap problem is to try to get a more faithful estimate of the mean from the long-tailed distribution itself. To try to better understand the distribution, let's use our signal-to-noise argument to estimate higher moments of the distribution. We can easily estimate the Nth moment of the correlation function for a single particle,

$$\mathscr{M}_N \sim C_N \underset{\tau \to \infty}{\sim} e^{-E_0^{(N)}\tau} \ , \tag{5.107}$$

where $E_0^{(N)}$ is the ground-state energy of N particles with different flavors. Let's consider the theory to be weakly coupled (small scattering length, $a/L \ll 1$). In this case the two-body interaction dominates and we can use perturbation theory to estimate the energy of two particles in a box: $E_0^{(2)} \approx \frac{4\pi a}{ML^3}$. A weakly coupled system of N particles interacting via the two-body interaction is given by simply counting the number of possible pairs of interacting particles, $E_0^{(N)} \approx N(N-1)\frac{4\pi a}{ML^3}$, leading to the following expression for the moments [50]:

$$\mathscr{M}_N \sim e^{-N(N-1)\frac{4\pi a}{ML^3}} \ . \tag{5.108}$$

Distributions with the particular N dependence seen in Eq. (5.108) are called log-normal distributions, so named because the distribution of the logarithm of a log-normally distributed quantity is normal. While we derived this expression for theories near weak coupling, there is also evidence that the log-normal distribution occurs for correlators near unitarity as well [51, 52].

The central limit theorem implies that normal distributions occur generically for large sums of random numbers; the same argument leads to the conclusion that log-normal distributions occur for large products of random numbers. Let's think about how correlation functions are calculated on the lattice: particles are created, then propagate through random fields from one time slice to the next until reaching a sink. Each application of the random

field is multiplied by the previous one,

$$K^{-1}(\tau) = D^{-1}X(\tau)D^{-1}X(\tau-1)\cdots ,$$ (5.109)

and then products of these propagators may be used to form correlation functions for multiple particles. Thus, one might expect that in the $\tau \to \infty$ limit (or for large numbers of particles), the distributions of these correlation functions might flow toward the log-normal distribution. More precisely though, each block $X(\tau)$ is actually a matrix of random numbers, and products of random matrices are far less well understand than products of random numbers. Nonetheless, products of random link variables are used to form most observables in nearly all lattice calculations, and approximately log-normal distributions appear to be ubiquitous as well, including in lattice QCD calculations.

If it is $\ln C$ that is nearly Gaussian rather than C, then it may be better to sample $\ln C$ as our observable instead. Without asserting any assumptions about the actual form of the distribution, we can expand around the log-normal distribution using what is known as a cumulant expansion,

$$\ln\langle \mathscr{O} \rangle = \sum_{n=1}^{\infty} \frac{1}{n!} \kappa_n (\ln \mathscr{O}) ,$$ (5.110)

where κ_n is the nth cumulant, or connected moment. The cumulants may be calculated using the following recursion relation:

$$\kappa_n(x) = \langle x^n \rangle - \sum_{m=1}^{n-1} \binom{n-1}{m-1} \kappa_m(x)\langle x^{n-m} \rangle .$$ (5.111)

Note that the expansion in Eq. (5.110) is an exact equality for an observable obeying any distribution. We may now expand the correlation function as

$$\ln\langle C \rangle \xrightarrow[\tau \to \infty]{} -E_0\tau = \langle \ln C \rangle + \frac{1}{2}\left(\langle (\ln C)^2 \rangle - \langle \ln C \rangle^2\right) + \frac{1}{6}\kappa_3(\ln C) + \cdots .$$ (5.112)

Again, this expansion is true for a correlation function obeying any distribution. However, if the distribution of $\ln C$ is exactly log-normal, then $\kappa_{n\geq 3}(\ln C) = 0$. If the distribution is approximately log-normal, then the third and higher cumulants are small corrections, further suppressed in the cumulant expansion by $1/n!$. This suggests that we may cut off the expansion after including a finite number of cumulants without significantly affecting the result (see Fig. 5.9). We may also include the next higher order cumulant in order to estimate any systematic error associated with our cutoff.

The benefit of using the cumulant expansion to estimate the mean rather than using the standard method is that for a finite sample size, high-order cumulants of $\ln C$ are poorly measured, which is the culprit behind the overlap problem. However, for approximately log-normal distributions these high-order cumulants should be small in the infinite statistics limit. Thus, by not including them in the expansion we do a better job at estimating the true mean on a finite sample size. In other words, by sampling $\ln C$ rather than C, we have shifted the overlap problem into high, irrelevant moments which we may neglect.

The cumulant expansion avoids some of the drawbacks of reweighting, such as greatly increased computational effort in importance sampling. However, the farther the distribution is from log-normal, the higher one must go in the cumulant expansion, which can be particularly difficult to do with noisy data. Thus, for some observables it may be difficult to show convergence of the series on a small sample. Which method is best given the competition between the computational effort used in generating samples via the reweighting method versus the

Fig. 5.9 Results for the energy of 50 two-component fermions at unitarity using the cumulant expansion (Eq. (5.110)) cut off at $\mathscr{O}(N_k)$. Figure from [2].
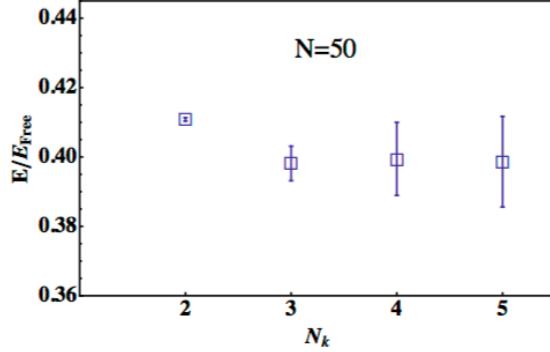
large number of samples which may be required to show convergence of the cumulant expansion is unclear and probably observable dependent.

5.3.3 Interpolating Fields

The previous section highlights the importance of gaining access to the ground state as early in time as possible, since the number of configurations required grows exponentially with time. Returning to our expression for the expansion of a correlation function in terms of energy eigenstates,

$$
\begin{aligned}
C(\tau) &= Z_0 e^{-E_0 \tau} + Z_1 e^{-E_1 \tau} + \cdots \\
&= Z_0 e^{-E_0 \tau} \left[1 + \frac{Z_1}{Z_0} e^{-(E_1 - E_0)\tau} + \cdots \right] ,
\end{aligned}
\tag{5.113}
$$

we see that the condition that must be met in order to successfully suppress the leading contribution from excited state contamination is

$$
\tau \gg \frac{\ln\left(\frac{Z_1}{Z_0 E_0}\right)}{E_1 - E_0} ,
\tag{5.114}
$$

where E_0, Z_0 (E_1, Z_1) are the ground (first excited) state energy and wavefunction overlap factor, respectively. Assuming we have properly eliminated excited states corresponding to unwanted quantum numbers through the choice of our source/sink, we have no further control over the energy difference $E_1 - E_0$ in the denominator, because this is set by the theory. Unfortunately, this makes the calculation of many-body observables extremely difficult as this energy splitting can become arbitrarily small due to collective excitations. Therefore, our only recourse is to choose excellent interpolating fields in order to reduce the numerator of Eq. (5.114).

The simplest possible choice for a many-body interpolating field is composed of non-interacting single particle states. A Slater determinant over the included states takes care of fermion antisymmetrization. For example, a correlation function for $N_\uparrow$ ($N_\downarrow$) spin up (spin down) particles can be written,

$$
C_{N_\uparrow, N_\downarrow}(\tau) = \langle \det S^\downarrow(\tau) \det S^\uparrow(\tau) \rangle ,
\tag{5.115}
$$

where

$$S_{ij}^{\sigma}(\tau) \equiv \langle \alpha_i^{\sigma} | K^{-1}(\tau,0) | \alpha_j^{\sigma} \rangle \, , \tag{5.116}$$

and $\langle \alpha_j^{\sigma} |$ corresponds to single particle state i with spin σ. As an example, we may use a plane wave basis for the single particle states,

$$| \alpha_j^{\uparrow} \rangle = | \mathbf{p}_j \rangle \, , \qquad | \alpha_j^{\downarrow} \rangle = | -\mathbf{p}_j \rangle \, , \tag{5.117}$$

where I've chosen equal and opposite momenta for the different spin labels in order to enforce zero total momentum (this condition may be relaxed to attain boosted systems).

Though the interpolating field chosen in Eq. (5.115) has non-zero overlap with the ground state of interest, if the overlap is small it may take an inordinately long time to remove excited state contributions. Consider a system involving only two-particle correlations, as in our two-spin fermion system, and make the simplification that the ground state consists of non-interacting two-body pairs having wavefunction $\Psi_{2\text{-body}}$, and overlap with a product of two non-interacting single particle states given by

$$\langle \Psi_{2\text{-body}} | \left(| \mathbf{p} \rangle \otimes | -\mathbf{p} \rangle \right) = \varepsilon < 1. \tag{5.118}$$

Then the corresponding overlap of the Slater determinant in Eq. (5.115) with the ground state wavefunction scales as

$$\left(\langle \Psi_{2\text{-body}} | \otimes \cdots \otimes \langle \Psi_{2\text{-body}} | \right) \left(| \mathbf{p}_1 \rangle \otimes | -\mathbf{p}_1 \rangle \otimes \cdots \otimes | \mathbf{p}_N \rangle \otimes | -\mathbf{p}_N \rangle \right) \sim \varepsilon^N \, . \tag{5.119}$$

Thus the overlap of single-particle states with an interacting $2N$-body state is exponentially small with N. This condition worsens for systems with 3- and higher-body correlations.

In order to do a better job we can incorporate two-body correlations into the sinks as follows: first, we construct a two particle propagator,

$$\begin{aligned} S_{ij}^{\uparrow\downarrow}(\tau) &= \langle \Psi_2 | K^{-1}(\tau,0) \otimes K^{-1}(\tau,0) \left(| \alpha_i^{\uparrow} \rangle \otimes | \alpha_j^{\downarrow} \rangle \right) \\ &= \sum_{\mathbf{p}} \Psi(\mathbf{p}) \langle \mathbf{p} | K^{-1}(\tau,0) | \alpha_i^{\uparrow} \rangle \langle -\mathbf{p} | K^{-1}(\tau,0) | \alpha_j^{\downarrow} \rangle \, , \end{aligned} \tag{5.120}$$

where $\Psi_2(\mathbf{p})$ is some two-body wavefunction (this process could equally well be performed in position space). As an example, to incorporate BCS pairing, we may use a wavefunction of the form:

$$\Psi_2(\mathbf{p}) \sim \frac{e^{-b|\mathbf{p}|}}{|\mathbf{p}|^2} \, , \tag{5.121}$$

where b is some parameter which may be tuned to maximize the overlap of the wavefunction. We may also use the wavefunction derived in Eq. (5.65) for a lattice version of such a wavefunction. An example code fragment for implementing such wavefunctions is given in Fig. 5.10.

To ensure Pauli exclusion, it is sufficient to antisymmetrize only the sources, $| \alpha_i \rangle$, leading to the following many-body correlation function,

$$C_{N_{\uparrow},N_{\downarrow}}(\tau) = \langle \det S^{\uparrow\downarrow}(\tau) \rangle \, , \tag{5.122}$$

where the determinant runs over the two sink indices. For correlation functions having an odd number of particles, one may replace a row i of $S^{\uparrow\downarrow}$ with the corresponding row of the single particle object, $S^{\uparrow}$. The benefit of folding the wavefunction in at the sinks only is an $\mathscr{O}(V^2)$ savings in computational cost: to fold a two-body wavefunction in at both source and

Fig. 5.10 Portion of c++ code for implementing two types of two-body source vector: Eq. (5.65) (GND) and Eq. (5.121) (PAIR2). Note that these vectors are computed in momentum space. The first operator applied to a source is the kinetic operator, D^{-1}, which is also computed in momentum space.

```cpp
if (two_body_arg.wavefunc_type==WAVEFUNC_TYPE_GND) {

  Dispersion dispersion1(two_body_arg.dispersion_type1, two_body_arg.mass1, CUTOFF_TYPE_HARD);
  Dispersion dispersion2(two_body_arg.dispersion_type2, two_body_arg.mass2, CUTOFF_TYPE_HARD);

  double xi1;
  double xi2;
  double lambda = two_body_arg.lambda;

  for (int i=0; i<vol; i++) {
    xi1 = 1.0 + dispersion1.Get(i);
    xi2 = 1.0 + dispersion2.Get(i);

    // Note that psi(p) = xi(p)/(lambda*xi(p)^2-1) is the eigenstate of the transfer matrix.
    // The correlation function, however, is given by <final| D^{-1/2} T^N D^{-1/2} |initial>
    // Hence <p|final> = xi(p) psi(p), where xi is the same as D^{1/2} in momentum space).
    //
    // wavefunc[i] = xi^2/(lambda*xi^2-1.0);
    wavefunc[i] = 1.0;                        // This way avoids NAN when dispersion type is QUADRATIC, or PERFECT
    wavefunc[i] /= lambda - 1.0/(xi1*xi2);    // so do it this way instead:
  }
}

if (two_body_arg.wavefunc_type==WAVEFUNC_TYPE_PAIR2) {

  Dispersion dispersion(DISPERSION_TYPE_QUADRATIC, 1.0, CUTOFF_TYPE_HARD);
  double b = two_body_arg.lambda;
  double psq;

  for (int i=0; i<vol; i++) {
    psq = 2.0*dispersion.Get(i);
    if (psq < 1e-15) {
      wavefunc[i] = 0.0; // Omit divergent contribution to wave funcion--must be treated separately
    } else {
      wavefunc[i] = exp(- b*sqrt(psq) )/psq;
    }
  }

}
```

sink requires the calculation of propagators from all possible spatial points on the lattice to all possible spatial points in order to perform the resulting double sum.

Higher-body correlations may also be important and can be incorporated using similar methods. However, these will lead to further $\mathcal{O}(V)$ increases in computation time. Finally, the entire system should be projected onto the desired parity, lattice cubic irreducible representation (which we will now briefly discuss), etc. in order to eliminate any contamination from excited states having different quantum numbers.

5.3.3.1 Angular momentum in a box

The projection onto the cubic irreps is the lattice equivalent of a partial wave decomposition in infinite volume (and the continuum limit). The cubic group is finite, and therefore has a finite number of irreps, reflecting the reduced rotational symmetry of the box. The eigenstates of the systems calculated on the lattice will have good quantum numbers corresponding to the cubic irreps. When mapping these states onto angular momenta associated with infinite volume, there will necessarily be copies of the same irrep corresponding to the same angular momentum due to the reduced symmetry. This means that the box mixes angular momenta, as displayed in Table 5.3.3.1. For example, an energy level calculated in a finite volume that has been projected onto the positive parity A_1 irrep will have overlap with $j = 0, 4, \cdots$. For low energies it may be possible to argue that contributions from high partial waves are kinematically suppressed, since the scattering amplitude scales with p^{2l+1}, but in general the different partial wave contributions must be disentangled using multiple data points from different cubic irreps.

A pedagogical method for projecting two-particle states onto the desired cubic irrep involves first projecting the system onto a particular spin state: for example, a two nucleon sys-

j	cubic irreps
0	A_1
1	T_1
2	$E + T_2$
3	$A_2 + T_1 + T_2$
4	$A_1 + E + T_1 + T_2$

Table 5.1 Decomposition of the cubic group onto total angular momentum, j.

tem may be projected onto either a spin singlet (symmetric) or spin triplet (anti-symmetric) state. The wavefunctions may then be given an "orbital angular momentum" label by performing a partial projection using spherical harmonics confined to only the allowed rotations in the box. For example, we could fix the position of one of the particles at the origin $(0,0,0)$, then displace the second particle to a position (x_0, y_0, z_0). This configuration will be labeled by the wavefunction $\psi_{s,m_s}[(x_0, y_0, z_0)]$, where s, m_s are the total and z-component of the spin. We can then perform the partial projection,

$$\tilde{\psi}_{l,m_l;s,m_s} = \sum_i Y_{l,m_l}[R_i(x_0, y_0, z_0)] \, \psi_{s,m_s}[R_i(x_0, y_0, z_0)] \ , \tag{5.123}$$

where the R_i are cubic rotation matrices. Essentially, the set $R_i(x, y, z)$ correspond to all possible lattice vectors of the same magnitude. For example, if our original vector was $(1, 0, 0)$, then we would sum over the set of displacements $\{(\pm 1, 0, 0), (0, \pm 1, 0), (0, 0, \pm 1)\}$. I want to emphasize that the l, m_l are only wavefunction labels and do not correspond to good quantum numbers due to the reduced rotational symmetry.

Now that the wavefunctions have spin and orbital momentum labels, these may be combined into total angular momentum labels j, m_j using the usual Clebsch-Gordan coefficients. Finally, these wavefunctions are projected onto cubic irreps using so-called subduction matrices [53]. As an example, a wavefunction labeled with $j = 2$ (having five possible m_j labels) will have overlap with two cubic irreps, T_2, E. The subduction matrices are:

$$T_2 : \overbrace{\begin{pmatrix} 0 & 1 & 0 & 0 & 0 \\ 1/\sqrt{2} & 0 & 0 & 0 & -1/\sqrt{2} \\ 0 & 0 & 0 & 1 & 0 \end{pmatrix}}^{m_j = -2, -1, 0, 1, 2} \ , \qquad E : \begin{pmatrix} 0 & 0 & 1 & 0 & 0 \\ 1/\sqrt{2} & 0 & 0 & 0 & 1/\sqrt{2} \end{pmatrix} \ . \tag{5.124}$$

Note that the T_2 irrep has three degenerate states, while the E irrep has two, matching the total of five degenerate states for $j = 2$ in infinite volume.

Using this method for projection onto the cubic irreps has several benefits, including ease of bookkeeping and extension to higher-body systems using pairwise combinations onto a given j, m_j, followed by subduction of the total resulting wavefunction. Furthermore, in cases where more than one partial wave has overlap onto the chosen cubic irrep, wavefunctions with different partial wave labels may have different overlap onto the ground- and excited states of the system. Therefore, they can be used as a handle for determining the best source for the state of interest. We will discuss methods for using multiple sources for disentangling low-lying states and allowing for measurements at earlier times in the next subsection.

5.3.4 Analysis methods

Having done our best to come up with interpolating wavefunctions, we can attempt to extract the ground state energy (and possibly excited state energies) earlier in time by performing

multiple exponential fits to take into account any remaining excited state contamination. Using the known functional form for the correlator,

$$y(\tau) = \sum_n^\Lambda Z_n e^{-E_n \tau} , \tag{5.125}$$

where Λ is a cutoff in the number of exponentials included in the fit, we may perform a correlated χ^2 minimization,

$$\chi_\Lambda^2 = \sum_{\tau,\tau'} [C(\tau) - y(\tau)] \left(\mathscr{C}^{-1}\right)_{\tau\tau'} [C(\tau') - y(\tau')] , \tag{5.126}$$

where $\mathscr{C}$ is the covariance matrix taking into account the correlation between different time steps. Because the correlation function at a given time is built directly upon the correlation function for the previous time step, there is large correlation between times that must be taken into account.

We can go further by noting that correlation functions formed using different sources, but having the same quantum numbers, will lead to the same spectrum in Eq. (5.125), but with different overlap factors, Z_n. Thus, the χ^2 minimization can be expanded to include different sources s, with only a modest increase in the number of parameters to be fit. Different sources may be produced, for example, by varying some parameter in the wavefunction, such as b in Eq. (5.121), through a different basis of non-interacting single particle states, such as plane waves vs. harmonic oscillator states, or through different constructions of the same cubic irrep, as discussed in the previous subsection. The resulting χ^2 minimization is

$$y_s(\tau) = \sum_n^\Lambda Z_n^{(s)} e^{-E_n \tau} , \qquad \chi_\Lambda^2 = \sum_{\tau,\tau',s,s'} [C_s(\tau) - y_s(\tau)] \left(\mathscr{C}^{-1}\right)_{\tau\tau'}^{ss'} [C_{s'}(\tau') - y_{s'}(\tau')] , \tag{5.127}$$

where the covariance matrix now takes into account the correlation between different sources calculated on the same ensembles.

In general, multiple parameter fits require high precision from the data in order to extract several parameters. The use of priors through Bayesian analysis techniques may be beneficial in some circumstances when performing multi-exponential fits to noisy data.

A more elegant approach using a set of correlation functions created using different operators is based on a variational principle [54, 55]. A basic variational argument proceeds as follows [56]: starting with some set of operators $\mathscr{O}_i$ which produce states $|\phi_i\rangle = \mathscr{O}_i|0\rangle$ from the vacuum, we can evolve the state to some time τ_0, $|\tilde{\phi}_i\rangle = e^{-\tau_0 H/2}|\phi_i\rangle$ in order to eliminate the highest excited states, but leaving a finite set of states contributing to the correlation function. We would like to find some wavefunction $|\psi\rangle = \sum_{i=1}^N \alpha_i |\tilde{\phi}_i\rangle$ which is a linear combination of our set of operators parameterized by $\{\alpha_i\}$, that maximizes the following quantity for $\tau > \tau_0$:

$$\lambda_0(\tau,\tau_0) = \underset{\{\alpha_i\}}{\text{Max}} \frac{\langle\psi|e^{-(\tau-\tau_0)H}|\psi\rangle}{\langle\psi|\psi\rangle} , \tag{5.128}$$

so that

$$\lambda_0(\tau,\tau_0) \approx e^{-E_0(\tau-\tau_0)} . \tag{5.129}$$

A powerful method for finding the appropriate linear combination of states satisfying the variational principle uses a generalized eigenvalue problem (GEVP). For this method we form a matrix of correlation functions using all combinations of sources and sinks formed from a set of operators,

$$C_{ij}(\tau) = \langle \mathcal{O}_i(\tau)\mathcal{O}_j^*(0)\rangle = \sum_n e^{-E_n\tau} Z_i^{(n)} Z_j^{(n)} \ . \tag{5.130}$$

The GEVP may be stated as:

$$C(\tau)v_n(\tau, \tau_0) = \lambda_n(\tau, \tau_0)C(\tau_0)v_n(\tau, \tau_0) \ , \tag{5.131}$$

where v_n (λ_n) are a set of eigenvectors (eigenvalues) to be determined as follows: assume we choose τ_0 to be far out enough in time such that only N states contribute to the correlation function,

$$C_{ij}(\tau) = \sum_n^N e^{-E_n\tau} Z_i^{(n)} Z_j^{(n)} \ . \tag{5.132}$$

Let's introduce a set of dual vectors $u_i^{(n)}$ such that

$$\sum_i u_i^{(n)} Z_i^{(m)} = \delta_{mn} \ . \tag{5.133}$$

Applying u_i to C_{ij} gives

$$\sum_j C_{ij}(\tau)u_j^{(m)} = \sum_j \sum_n e^{-E_n\tau} Z_i^{(n)} Z_j^{(n)} u_j^{(m)} = e^{-E_m\tau} Z_i^{(m)} \ . \tag{5.134}$$

Going back to our original GEVP, Eq. (5.131),

$$C(\tau)u^{(m)} = \lambda_m(\tau, \tau_0)C(\tau_0)u^{(m)} \ , \tag{5.135}$$

we can now identify,

$$\lambda_m(\tau, \tau_0) = e^{-E_m(\tau-\tau_0)} \ . \tag{5.136}$$

Thus, the energies may be found from the eigenvalues of the matrix, $C^{-1}(\tau_0)C(\tau)$. Solving this GEVP gives us access to not only the ground state, but some of the lowest excited states as well.

Any remaining contributions from states corresponding to $E_n, n > N$ can be shown to be exponentially suppressed as $e^{-(E_{N+1}-E_n)\tau_0}$, where E_{N+1} is the first state neglected in the analysis. We should define a new effective mass function to study the time dependence of each of the extracted states,

$$E_n^{(\text{eff})}(\tau, \tau_0) \equiv \ln \frac{\lambda_n(\tau, \tau_0)}{\lambda_n(\tau+1, \tau_0)} \ , \tag{5.137}$$

and look for a plateau,

$$\lim_{\tau\to\infty} E_n^{(\text{eff})}(\tau, \tau_0) = E_n \ , \tag{5.138}$$

to indicate convergence to the desired state. The reference time τ_0 may be chosen to optimize this convergence, and should generally be close to the beginning of the plateau of the standard effective mass.

The GEVP method works very well in many situations and has been used extensively for LQCD spectroscopy. The main determining factor on the applicability of the method is whether one is able to construct a basis of operators which encapsulates the full low-lying spectrum sufficiently well. One major drawback is that the GEVP assumes a symmetric correlator matrix, meaning that the same set of operators must be used at both source and sink.

As discussed in Sec. 5.3.3, this may be difficult to do numerically due to increases in computational time which scale with the volume when projecting onto a given wavefunction (unless the wavefunction is simply a delta function; however, this operator generally has extremely poor overlap with any physical states of interest). This is particularly a problem for noisy systems where large amounts of statistics are necessary.

There are a few alternatives to the GEVP which do not require a symmetric correlator matrix, such as the generalized pencil of functions (GPof) method [57–59], and the matrix Prony method [60, 61]. We will now briefly discuss the latter, following the discussion of [60].

The Prony method uses the idea of a generalized effective mass,

$$M_{\tau_0}^{(\text{eff})}(\tau) = \frac{1}{\tau_0} \ln \frac{C(\tau)}{C(\tau + \tau_0)} \xrightarrow{\tau \to \infty} E_0 \ , \tag{5.139}$$

for some, in principle arbitrary, offset τ_0. Because the correlator $C(\tau)$ is a sum of exponentials, it follows certain recursion relations. As an example, for times where only a single exponential contributes we have,

$$C(\tau + \tau_0) + \alpha C(\tau) = 0 \ . \tag{5.140}$$

Plugging in our single exponential for the correlator we can solve for α, then plug it back in to our original expression,

$$e^{-E_0 \tau_0} + \alpha = 0$$
$$\longrightarrow C(\tau - \tau_0) - e^{E_0 \tau_0} C(\tau) = 0 \ . \tag{5.141}$$

Solving for the ground state energy gives us the same expression as the generalized effective mass at large times,

$$E_0 = \frac{1}{\tau_0} \ln \frac{C(\tau)}{C(\tau + \tau_0)} \ . \tag{5.142}$$

This recursion relation may be generalized for times with contributions from multiple states using the correlation function at different time separations,

$$C(\tau + \tau_0 k) + \alpha_k C(\tau + \tau_0(k-1)) + \cdots + \alpha_1 C(\tau) = 0 \ . \tag{5.143}$$

We can now generalize this method for a set of correlation functions produced using different operators. Let $C_i(\tau)$ be an N-component vector of correlation functions corresponding to different sources and/or sinks. The correlators then obey the following matrix recursion relation,

$$MC(\tau + \tau_0) - VC(\tau) = 0 \ , \tag{5.144}$$

for some matrices, M, V, to be determined. Assume the correlator has contributions from Λ states,

$$C(\tau) = \sum_n^\Lambda \alpha_n u_n \lambda_n^{-\tau} \ , \tag{5.145}$$

where $\lambda_n = e^{E_n}$, and u_n is a normalized vector, then we have the following modified GEVP,

$$Mu = \lambda^{\tau_0} Vu \ . \tag{5.146}$$

A solution for M and V may be found by applying $\sum_{t=\tau}^{\tau+t_W} C(t)^T$ to both sides of Eq. (5.144),

$$M \sum_{t=\tau}^{\tau+t_W} C(t+\tau_0)C(t)^T - V \sum_{t=\tau}^{\tau+t_W} C(t)C(t)^T = 0 \;, \qquad (5.147)$$

leading to the solution,

$$M = \left[\sum_{t=\tau}^{\tau+t_W} C(t+\tau_0)C(t)^T \right]^{-1} \;, \qquad V = \left[\sum_{t=\tau}^{\tau+t_W} C(t)C(t)^T \right] \;. \qquad (5.148)$$

The parameter t_W is essentially free and may be tuned for optimization, but must obey $t_W \geq \Lambda - 1$ in order to ensure that the matrices are full rank. The λ_n may then be found from the eigenvalues of $V^{-1}M$.

Here we have only used a single recursion relation, which is useful for finding the ground state at earlier times than traditional methods. However, this method is generally less effective for calculating excited states than the symmetric GEVP described previously. It may be possible to construct higher order recursion relations for the matrix Prony method in order to get more reliable access to excited states.

5.4 Systematic errors and improvement

5.4.1 Improving the kinetic energy operator

The first systematic effect we will examine comes from the discretization of the kinetic operator, first discussed in Sec. 5.2.2. In this section I will show the lattice spacing dependence explicitly so that we may see how discretization errors scale. The kinetic term depends on the definition of the Laplacian operator, which we originally defined to be,

Note 5.1. check units/lattice spacings

$$\nabla_L^2 f_j = \sum_{k=1,2,3} \frac{1}{b_s^2} \left[f_{j+\hat{k}} + f_{j-\hat{k}} - 2f_j \right] \;, \qquad (5.149)$$

leading to the following kinetic term in momentum space,

$$\Delta(p) = \frac{1}{b_s^2} \sum_i \sin^2 \frac{b_s p_i}{2} \approx -\frac{p^2}{2} + \frac{p^4}{24} b_s^2 + \cdots \;. \qquad (5.150)$$

The transfer matrix for the non-interacting system is given by

$$\mathscr{T} = e^{-b_\tau H} = 1 + b_\tau \frac{\Delta(p)}{M} \;, \qquad (5.151)$$

leading to the energy,

$$E = \frac{p^2}{2M} + \mathscr{O}\left(\frac{p^4}{M} b_s^2 \right) \;. \qquad (5.152)$$

Therefore, discretization errors in this observable appear at $\mathscr{O}\left(b_s^2\right)$ using this particular discretization. To be more precise, the errors scale with the dimensionless combination $(pb_s)^2$, reflecting the fact that the errors grow as higher momentum scales are probed. As we will discuss in Sec. 5.5, small lattice spacings can lead to computational difficulties beyond the obvious scaling with the number of lattice sites, and taking the continuum limit may prove to be quite difficult. Therefore, it would be beneficial to have an improved operator whose

discretization errors come in at a higher order in pb_s. One way to determine such an operator is to examine the relation between the finite difference and the continuum derivative in more detail using a Taylor expansion of the finite difference operator acting on a generic function, $f(x)$,

$$f(x+b_s) - f(x) = b_s f'(x) + \frac{b_s^2}{2} f''(x) + \frac{b_s^3}{6} f'''(x) + \frac{b_s^4}{24} f''''(x) + \cdots . \tag{5.153}$$

Using this expansion, the expression we used previously for the discretized Laplacian can be written,

$$\nabla_L^2 f(x) = \frac{1}{b_s^2} \left(f(x+b_s) + f(x-b_s) - 2f(x) \right) = f''(x) + \frac{b_s^2}{12} f''''(x) + \cdots . \tag{5.154}$$

We see that the leading error comes in at $\mathcal{O}(b_s^2)$, as expected. One method for eliminating the leading error is to add terms involving multiple hops,

$$\tilde{\nabla}_L^2 f(x) = \frac{1}{b_s^2} \left(f(x+b_s) + f(x-b_s) - 2f(x) + c_1 f(x+2b_s) + c_2 f(x-2b_s) \right) , \tag{5.155}$$

where c_1, c_2 must be fixed in such a way as to eliminate the leading error. From symmetry, we must have $c_1 = c_2$. We can then Taylor expand these new terms in our action, and determine the resulting energy as a function of c_1,

$$E(c_1) = \frac{p^2}{2M} + h(c_1) \frac{p^4}{M} b_s^2 + \cdots . \tag{5.156}$$

By solving $h(c_1) = 0$ for c_1, discretization errors will only enter at $\mathcal{O}(b_s^4)$, implying a faster approach to the continuum as b_s is decreased. Perhaps more importantly, in cases where decreasing the lattice spacing is difficult or impossible, the resulting systematic errors at finite lattice spacing will be significantly reduced.

This is our first, very simple, example of improvement. A more general method for improving the action in order to reduce discretization effects utilizes an EFT-like approach [2,62–65]: we add higher dimension operators consistent with the symmetries of the theory and having unknown coefficients. The coefficients are then fixed by matching onto known physical quantities. The dimension of the operator added determines the order at which discretization errors have been eliminated.

In principle, one would need an infinite number of operators in order to eliminate all discretization errors. We are, of course, limited in the number of displacements we can add, as in Eq. (5.155), by the number of lattice sites. Therefore, the best possible kinetic operator, utilizing all possible spatial hops allowed by the lattice, may still only exactly reproduce the non-interacting spectrum up to the momentum cutoff set by the edge of the first Brillouin zone. Because the kinetic operator Δ is diagonal in momentum space, we may determine this "perfect" operator directly by setting the transfer matrix,

$$\mathscr{T} = 1 + \frac{b_\tau \Delta(p)}{M} = e^{-\frac{b_\tau p^2}{2M}} , \tag{5.157}$$

up to a cutoff, leading to the operator,

$$\Delta_{\text{perf}}(p) = M \left(e^{\frac{b_\tau p^2}{2M}} - 1 \right) , \qquad p < \frac{\pi}{b_s} . \tag{5.158}$$

While this operator is simple in momentum space, it is highly non-local in position space, as expected, and would be unwieldy to use in a typical lattice calculation. However, another

benefit of having a non-relativistic formulation with a separable interaction is that the form of the propagator,

$$K^{-1}(\tau) = D^{-1}X(\tau)D^{-1}X(\tau-1)\cdots D^{-1}$$
$$= D^{-1}X(\tau)K^{-1}(\tau-1) , \tag{5.159}$$

suggests that the kinetic (D^{-1}) and interaction (X) operators may each be applied separately in whatever basis is most convenient. So, we may choose to start with a source in momentum space (which is often preferable), then apply an exact kinetic operator, D^{-1}, also in momentum space, perform a FFT to position space, hit the resulting vector with the X operator, which is most easily specified in position space, FFT again back to momentum space to perform a kinetic operation, and so on until finally the sink is applied. Example code for calculating various forms of inverse kinetic operator in momentum space is shown in Fig. 5.11.

Fig. 5.11 Example c++ code fragment for computing various lattice Laplacian operators: Eq. (5.150) (STAN-DARD), Eq. (5.158) (PERFECT), as well as a simple quadratic in momentum (QUADRATIC). Note that these are computed in momentum space, and they may be used to calculate the kinetic operator D^{-1}, then directly applied to the momentum space vectors computed in Fig. 5.10.

```cpp
for(int i=0; i<GJP.Vol(); i++) {

  z = i%z_sites;
  Y = i/z_sites;
  y = Y%y_sites;
  x = Y/y_sites;

  if (dispersion_type==DISPERSION_TYPE_STANDARD) {
    //
    // \Delta(p) = 2 \sum_j \sin^2(p_j/2)
    //
    sx = sin( x * PI / x_sites );
    sy = sin( y * PI / y_sites );
    sz = sin( z * PI / z_sites );
    dispersion[i] = 2.0 * ( sx*sx + sy*sy + sz*sz );
    dispersion[i] /= mass;
  }

  if ( (dispersion_type==DISPERSION_TYPE_QUADRATIC)||(dispersion_type==DISPERSION_TYPE_PERFECT) ) {

    sx = x / (double)x_sites;
    sy = y / (double)y_sites;
    sz = z / (double)z_sites;
    psq = (sx*sx + sy*sy + sz*sz)*4.0*PISQ;

    //---- Cutoff, beyond which we take psq = infinity
    if ( (cutoff_type==CUTOFF_TYPE_HARD)&&(psq > GJP.CutoffSq() ) ) {
      dispersion[i] = numeric_limits<double>::infinity();
    } else {
      if (dispersion_type==DISPERSION_TYPE_QUADRATIC) { dispersion[i] = psq/(2.0*mass); }
      if (dispersion_type==DISPERSION_TYPE_PERFECT) { dispersion[i] = ( exp( psq/(2.0*mass) ) -1.0 ); }
    }


  }

}
```

The benefit to using the FFT repeatedly rather than simply converting the kinetic operator into position space is that modern FFT libraries are highly optimized and cheap to use. For comparison, if we used the "perfect" kinetic operator in position space it would be a dense $V \times V$ matrix. The operation of applying such an object to a V-dimensional vector,

$$D^{-1}(x)|\psi(x)\rangle , \tag{5.160}$$

scales like V^2. On the other hand, using the FFT to convert the V-dimensional vector to momentum space, then applying a diagonal matrix to it,

$$D^{-1}(p)\,(\mathrm{FFT}|\psi(x)\rangle = |\tilde{\psi}(p)\rangle) , \tag{5.161}$$

scales like $V \log V$. This is a method referred to as "Fourier acceleration" (see e.g. [66–69]).

For formulations lacking separability of the kinetic and interaction operations, this method cannot generally be applied. In such cases, the kinetic operator should be kept relatively sparse in position space. Such a condition disfavors the use of Eq. (5.158) for a more modestly improved operator, composed of only a few spatial displacements, using the method outlined in the beginning of this Section.

5.4.2 Improving the interaction

To discuss systematic errors and improvement of the interaction, we will focus on systems tuned to unitarity. Because unitarity corresponds to a conformal fixed-point, the systems we will study only depend on a single scale, the density, n. The finite lattice spacing necessarily breaks this conformal symmetry, and we can consider dependence on any new scales to stem from systematic errors. Systems having multiple intrinsic scales contain more complicated dependences of systematic errors, and will be discussed later on.

Recall that the scattering phase shift for two particles at unitarity is,

$$p \cot \delta = 0 \ , \tag{5.162}$$

implying that the inverse scattering length, effective range, and all other shape parameters vanish. In Sec. 5.2.2.5, we discussed how to tune the two-particle coupling in order to reproduce infinite scattering length. The lattice, however, naturally induces an effective range for the interactions, which have been generated via auxiliary fields extending across a lattice link, of size b_s. In order to improve the interaction and eliminate the unwanted effective range contribution stemming from discretization, we may add a higher-order interaction operator,

$$\sqrt{g_2} \phi \psi^\dagger \nabla_L^2 \psi \ , \tag{5.163}$$

recalculate the scattering amplitude, A, as a function of g_0, g_2, and tune g_2 to eliminate the r_0 term in the effective range expansion. In principle, one may further generalize the interaction operator,

$$\mathscr{L}_{\text{int}} = \sum_n \sqrt{g_{2n}} \phi \psi^\dagger \nabla_L^{2n} \psi \ , \tag{5.164}$$

and use the g_{2n} to tune away successive terms in the effective range expansion. In practice this may be difficult because the interaction is generally no longer separable, so that loops can't be summed analytically. An easier method may be to use the transfer matrix, as we did in Sec. 5.2.2, to determine the two particle energy spectrum in a box, then tune the couplings in order to reproduce the desired energies. The target energies may be determined for systems obeying any known physical scattering phase shift using an approach known as the Lüscher method, which we will now briefly review.

5.4.2.1 Lüscher's method

Lüscher's method ([70, 71]) was originally developed as a tool for extracting physical scattering phase shifts from finite volume, Euclidean space observables produced by lattice QCD. The concept of asymptotic "in" and "out" scattering states does not exist in a finite volume, making direct scattering "experiments" impossible on the lattice. Furthermore, the issue of analytic continuation from Euclidean to Minkowski time is a tricky one, particularly when

utilizing stochastic techniques. Thus, Lüscher proposed utilizing a different observable, finite volume energy shifts, and inferring the infinite volume scattering phase shift that would lead to the observed finite volume spectrum. In this section, we will largely follow the discussion in [72].

First let's recap how to calculate the infinite volume s-wave scattering phase shift in our effective theory assuming the following generic tree-level interaction: $\mathscr{L}_2 = \sum_n g_{2n} p^{2n}$. The scattering amplitude is given by,

$$A_\infty = \frac{\sum_n g_{2n} p^{2n}}{1 - \sum_n g_{2n} p^{2n} I_0^\infty} = \frac{4\pi}{M} \frac{1}{p \cot\delta - ip} \, , \tag{5.165}$$

where I will now include the super/subscript "∞" to indicate infinite volume quantities, and I_0^∞ is defined as,

$$I_0^\infty = \int \frac{d^3q}{(2\pi)^3} \frac{1}{E - q^2/M} \, . \tag{5.166}$$

Note that I have assumed that the interaction is separable in deriving Eq. (5.165). This would not be possible using a momentum cutoff as a regulator, so we will use dimensional regularization for this integral. By investigating the inverse scattering amplitude,

$$A_\infty^{-1} = \frac{1}{\sum_n g_{2n} p^{2n}} - I_0^\infty = \frac{M}{4\pi}(p \cot\delta - ip) \, , \tag{5.167}$$

we can identify

$$\sum_n g_{2n} p^{2n} = \left[I_0^\infty + \frac{M}{4\pi}(p \cot\delta - ip) \right]^{-1} \, . \tag{5.168}$$

the quantity on the right can be expanded using the effective range expansion; the couplings are then determined by the scattering parameters, as we have seen previously.

Now that we have a relation between the couplings and the physical scattering parameters, let's now use this same effective theory to determine its finite volume spectrum. In a finite volume, there is no continuum of scattering states, but rather a discrete spectrum corresponding to poles in the finite volume analogue of the scattering amplitude, A_{FV},

$$\text{Re}\left[A_{\text{FV}}^{-1} \right] = 0 \, . \tag{5.169}$$

Because the imposition of a finite volume can affect only the IR behavior of the theory, the interactions, and therefore the couplings, g_{2n}, remain unchanged. Any differences come from loops, where intermediate particles may go on shell and explore the finite boundary. Therefore, our finite volume analogue of the scattering amplitude may be written, where

$$A_{\text{FV}}^{-1} = \frac{1}{\sum_n g_{2n} p^{2n}} - I_0^{\text{FV}} \, , \tag{5.170}$$

where the loop integral has been replaced by a finite volume sum over the allowed quantized momenta in a box,

$$I_0^{\text{FV}} = \frac{1}{L^3} \sum_{\mathbf{n}}^{\Lambda} \frac{1}{E - \left(\frac{2\pi n}{L}\right)^2 /M} \, . \tag{5.171}$$

Again, because the couplings are unchanged by the finite volume we are free to use Eq. (5.168) to replace them with the physical infinite volume phase shift, resulting in,

$$A_{\text{FV}}^{-1} = \frac{M}{4\pi}(p\cot\delta - ip) + I_0^\infty - I_0^{\text{FV}} \ . \tag{5.172}$$

This leads to the eigenvalue equation,

$$\text{Re}\left[A_{\text{FV}}^{-1}\right] = \frac{M}{4\pi}p\cot\delta + \text{Re}\left[I_0^\infty - I_0^{\text{FV}}\right] = 0 \ . \tag{5.173}$$

I have specified taking the real part of the inverse amplitude merely for calculational simplicity; this quantity is, in fact, already purely real because there are no integrals, and therefore, no $i\varepsilon$ prescription. Furthermore, the difference between the infinite volume integral and the finite volume sum must be finite because the two encode the same UV behavior. Finally, we have the result,

$$p\cot\delta = \frac{4\pi}{M}\left[-\frac{M}{4\pi^2 L}\sum_{\mathbf{n}}^{\Lambda}\frac{1}{\left(\frac{pL}{2\pi}\right)^2 - n^2} - \frac{M\Lambda}{\pi L}\right] = \frac{1}{\pi L}S(\eta) \ , \tag{5.174}$$

where $\eta \equiv \left(\frac{pL}{2\pi}\right)^2$, and

$$S(\eta) \equiv \sum_{\mathbf{n}}^{\Lambda}\frac{1}{n^2 - \eta} - 4\pi\Lambda \ , \tag{5.175}$$

is related to the Riemann zeta function. The cutoff on the sum, Λ, may be interpreted as an upper limit on the allowed momenta due to the finite lattice spacing, however, in practice it is taken to ∞ so that discretization and finite volume effects may be separately accounted for (note that we haven't used our lattice propagators in this derivation, which would be necessary for a proper treatment of discretization effects). Values of momenta which solve this eigenvalue equation for a given phase shift and volume correspond to the predicted finite volume spectrum. This is illustrated in Fig. 5.12, where the function $S(\eta)$ has been plotted, along with several representative phase shifts, corresponding to positive and negative scattering lengths. The locations of the intersections give the energy eigenvalues for that volume. The poles of the S function give the locations of the energies of a non-interacting system in a box, while the zeroes give the energies for systems at unitarity.

Many extensions of Lüscher's method exist for more complicated systems, such as multi-channel processes [73–80], higher partial waves [81–83], moving frames [84, 85], moving bound states [86, 87], asymmetric boxes [88, 89], and three-body systems [90–93], as well as perturbative expansions for many-boson systems [94–96]. Formulations for general systems involving two nucleons may be found in [97, 98]. These formulations have been successfully applied in Lattice QCD for the determination of scattering phase shifts of nucleon-nucleon [4, 7–10, 14, 15, 18, 21, 25, 99], meson-meson [100–118], meson-baryon [119–122], and hyperon-nucleon [16, 123, 124] systems.

5.4.2.2 Applying Lüscher's method to tune the two-body couplings

The prescription for a lattice QCD calculation of nucleon-nucleon phase shifts is to start with quark interpolating fields to create a two nucleon correlation function, measure a set of finite volume energies, then use the eigenvalue equation, Eq. (5.174), to infer the infinite volume two nucleon phase shift that produces those energies. For our lattice EFT, however, two nucleon phase shifts are used as input into the coefficients in the Lagrangian. Thus, we can use the Lüscher method in reverse to calculate what we expect the two nucleon energies in a box to be given a known phase shift, then tune the couplings to reproduce those same

Fig. 5.12 $S(\eta)$ (solid red) and $\pi L p \cot \delta$ (dashed) as a function of $\eta \equiv \left(\frac{pL}{2\pi}\right)^2$. The $\pi L p \cot \delta$ correspond to $r_0/a = -0.1$, for the following volumes: $L/|a| = 2$ (blue), $L/|a| = 4$ (pink), $L/|a| = 8$ (yellow), $L/|a| = 10$ (green). The energy eigenstates for the corresponding volumes are given by the intercepts of $S(\eta)$ with the dashed lines. Figure from [41].
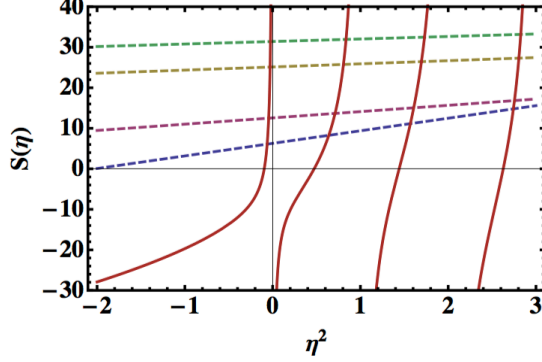
energies in our lattice calculations. Having tuned the two-body sector, we can then make predictions about 3- and higher-body systems.

Our prescription for tuning the coefficients will be to construct the two-body transfer matrix with some set of operators,

$$C(\mathbf{p}) = \sum_{n}^{\Lambda_n} g_{2n} \mathscr{O}_{2n}(\mathbf{p}) \,, \tag{5.176}$$

which satisfy the low energy expansion $\mathscr{O}_{2n}(\mathbf{p}) = \mathbf{p}^{2n}\left[1 + \mathscr{O}(\mathbf{p}^2)\right]$ at low momenta, and should be chosen to depend only on the relative momentum of the two particle system in order to ensure Galilean invariance. This is important so that once the interaction is tuned boosted pairs of particles will see the same interaction. A convenient choice for the operators is given by,

$$\mathscr{O}_{2n}(\mathbf{p}) = M^n \left(1 - e^{-\hat{\mathbf{p}}^2/M}\right)^n \,, \tag{5.177}$$

where $\hat{\mathbf{p}}$ is taken to be a periodic function of $\mathbf{p}$ and satisfies the relation $\hat{\mathbf{p}}^2 = \mathbf{p}^2 \theta(\Lambda - |\mathbf{p}|) + \Lambda^2 \theta(|\mathbf{p}| - \Lambda)$ for $\mathbf{p}$ in the first Brillouin zone. Sample code for calculating this interaction operator is shown in Fig. 5.13.

The transfer matrix may then be diagonalized numerically to determine the energy eigenvalues. The g_{2n} should then be tuned until the energies match the first Λ_n eigenvalues given by the Lüscher method. This process serves a dual purpose: tuning multiple couplings helps reduce lattice spacing effects like the effective range, as we discussed previously, and also takes into account finite volume effects by correctly translating the exact infinite volume phase shifts into a finite volume. The process of tuning for the case of unitarity is illustrated in Fig. 5.14. Here, $N_{\mathscr{O}}$ coefficients have been tuned to correctly reproduce the first $N_{\mathscr{O}}$ Lüscher eigenvalues. The entire two-body spectrum is then calculated using these coefficients, and the resulting energies are plugged back into Eq. (5.174) to determine the effective phase shift seen by pairs of particles with different momenta. To be truly at unitarity, we should have $p \cot \delta = 0$ for all momenta. Clearly, tuning more coefficients brings us closer to unitarity for larger and larger momenta. This is particularly important for calculations involving many-body systems, where the average momentum grows with the density, $\langle p \rangle \sim n^{1/3}$.

A quantitative prediction can be made for the error remaining in higher, untuned two-body energy levels [1]. Assuming $N_{\mathscr{O}}$ terms in the effective range expansion have been tuned to

Fig. 5.13 C++ code fragment for calculating the interaction given in Eq. (5.176), using the operators Eq. (5.177), given some set of input coefficients interaction_arg.couplings[Λ_n]. Note that this operator is calculated in momentum space. It may be applied directly to the momentum space vector resulting from the first operation of the kinetic operator, D^{-1}. A FFT must then be performed before applying the random auxiliary field, ϕ_x. A final FFT must then be performed to return to momentum space before applying the next operation of D^{-1} in order to propagate the system forward in time.

```cpp
double xi1;
double xi2;

double psq;
double mass = 2.0 * kinetic_arg1.mass * kinetic_arg2.mass; // reduced mass
mass /= kinetic_arg1.mass + kinetic_arg2.mass; // reduced mass

double PSQ = GJP.Cutoff(); PSQ *= PSQ;
double XI1 = exp( PSQ/(2.0*kinetic_arg1.mass));
double XI2 = exp( PSQ/(2.0*kinetic_arg2.mass));

for(int i=0; i<vol; i++) {

  xi1 = 1.0 + dispersion1.Get(i);
  if (xi1 > XI1) { xi1 = XI1; }
  xi2 = 1.0 + dispersion2.Get(i);
  if (xi2 > XI2) { xi2 = XI2; }

  psq = 1.0 - 1.0 /(xi1*xi2);
  psq *= mass;

  //---- Evaluate the interaction as a Taylor series in p^2: O(p) = sum_n C_n p^(2n)
  interaction[i] = 0.0;
  for (int j=0; j<interaction_arg.num_couplings; j++) {
    interaction[i] += interaction_arg.couplings[j]*pow(psq,j);
  }

  //---- Make sure O(p) is non-negative before taking the square root!
  if (interaction[i]<0.0) {
    ERR.General(fname, "Interaction is less the zero; cannot take square root.");
  }

  //---- Normalize operator, etc..
  interaction[i] *= 2.0 * TWOPI / mass;  // Just a convention
  interaction[i] = sqrt(interaction[i]); // Division by vol because FFT is not normalized
  interaction[i] /= vol; // Division by vol because FFT is not normalized
  interaction[i] *= dt; // Controls overall sign and step size of the interaction

}
```

Fig. 5.14 Effective scattering phase shifts $p \cot \delta$ vs. η produced by a set of contact interactions of the form in Eq. (5.176), with $N_{\mathscr{O}}$ coefficients tuned to unitarity. Figure from [1].
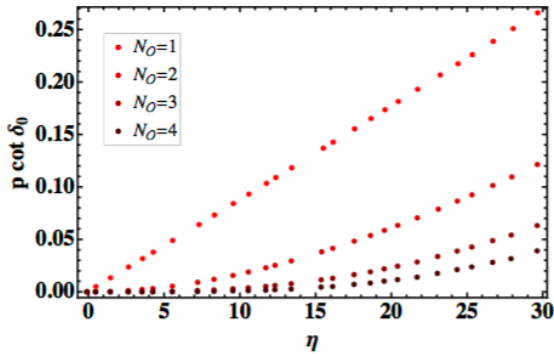
zero,

$$p \cot \delta \sim r_{N_{\mathcal{O}}-1} p^{2N_{\mathcal{O}}} = \left(\frac{2\pi}{L}\right)^{2N_{\mathcal{O}}} r_{N_{\mathcal{O}}-1} \eta^{N_{\mathcal{O}}} \, , \tag{5.178}$$

we can then use Lüscher's relation for the first untuned eigenvalue η_k,

$$\left(\frac{2\pi}{L}\right)^{2N_{\mathcal{O}}} r_{N_{\mathcal{O}}-1} \eta_k^{N_{\mathcal{O}}} = \frac{1}{\pi L} S(\eta_k) \, . \tag{5.179}$$

Let's suppose η_k^* is the eigenvalue one would expect in the true unitary limit. We can then Taylor expand the function $S(\eta_k)$ around η_k^*,

$$S(\eta_k) \approx c_k(\eta_k - \eta_k^*) \, , \tag{5.180}$$

where c_k is the slope near η_k^*. The error is then estimated as,

$$\frac{\eta_k}{\eta_k^*} - 1 \approx \frac{\pi L}{\eta_k^* c_k} \left(\frac{2\pi}{L}\right)^{2N_{\mathcal{O}}} r_{N_{\mathcal{O}}-1} (\eta_k^*)^{N_{\mathcal{O}}} \sim \mathcal{O}\left(L^{1-2N_{\mathcal{O}}}\right) \sim \mathcal{O}\left((b_s n^{1/3})^{2N_{\mathcal{O}}-1}\right) \, , \tag{5.181}$$

where on the right I have rewritten the scaling with the volume as a scaling with the density to remind you that though the errors scale with the volume, these are not actually finite volume errors we are investigating, but discretization effects scaling with the dimensionless quantity $b_s n^{1/3} \sim b_s/L_{phys} = 1/L$ for systems at unitarity. The Lüscher method takes into account finite volume effects automatically.

5.4.3 Scaling of discretization errors for many-body systems

Having tuned our two-body interaction, we can now also predict the scaling of errors that we should expect to find in an N-body calculation. Let us suppose that the first untuned operator contains at most $2N_{\mathcal{O}}$ derivatives,

$$\mathcal{O}_{2N_{\mathcal{O}}} \sim (\psi\psi)^\dagger \psi \nabla^{2N_{\mathcal{O}}} \psi \, . \tag{5.182}$$

The leading error results when any pair of particles interacts via this operator, and should scale with the dimension of this operator.

To determine the operator dimension, first let me briefly recap how scaling dimensions are determined in a non-relativistic theory (see [40] for more details). We expect the action, S, to be a dimensionless quantity, so we will consider the action for a non-interacting theory to determine how the fields and derivatives must scale,

$$S = \int d\tau d^3x \psi^\dagger \left(\partial_\tau - \frac{\nabla^2}{2M}\right) \psi \, . \tag{5.183}$$

First, note that the mass, M, carries zero scaling dimension in a non-relativistic theory because it is considered to be much larger than any scale of interest. Then, from the expression in parentheses, we see that time and space must scale differently, $[\partial_\tau] = 2[\nabla]$. Using the convention $[\nabla] = 1$, we can then determine that the dimension of the fermion field must be $[\psi] = 3/2$.

Now let us return to the operator, Eq. (5.182), and determine its scaling dimension relative to the energy,

$$\left[(\psi\psi)^{\dagger}\, \psi\nabla^{2N_{\mathscr{O}}}\psi \right] - \left[\psi^{\dagger}\partial_{\tau}\psi \right] = (6 + 2N_{\mathscr{O}}) - (5) = 1 + 2N_{\mathscr{O}}\ . \tag{5.184}$$

This indicates that the error from such an operator will scale as $\sim \mathscr{O}(b_s p)^{1+2N_{\mathscr{O}}}$, or $\sim \mathscr{O}\left((b_s n^{1/3})^{1+2N_{\mathscr{O}}}\right)$ for unitary fermions. This is similar scaling that we saw for higher two-body states, however, here the dependence on the number of particles is also important.

One may in principle tune as many operators as possible in order to perfect the interaction for higher energies. In practice, however, as more and more operators are tuned, the coefficients in front of higher dimensional operators which are still untuned can become very large. This can cause interactions seen by pairs of particles far in the tail of the momentum distribution to generate large errors. Thus, similar to the case of the kinetic operator, there is a limit to how "perfect" the interaction can be made.

On the other hand, these s-wave two-body interactions are not the only possible errors that are induced by the lattice, so we should not expect to see much improvement by tuning more operators corresponding to errors which are higher order than the leading operator which is not accounted for. For example, an unfortunate consequence of our tuning program is the introduction of interactions in the p-wave channel, as well as in higher partial waves. While a simple interaction which is point-like in space has no p-wave contribution, the introduction of spatial derivatives in our tuning operators gives rise to these new p-wave interactions. The leading p-wave operator has the form,

$$\mathscr{O}_{p\text{-wave}} \sim \psi^{\dagger}\nabla\psi \cdot \psi^{\dagger}\nabla\psi\ , \tag{5.185}$$

and induces errors at $\mathscr{O}\left(b_s n^{1/3}\right)^3$. In order to cancel this operator we could in principle add a ϕ field which carries momentum and carry out a similar program for tuning the coefficients as we used for the s-wave interaction. This destroys the separability of our interaction, however, and may be difficult to implement, in addition to introducing a new source of noise.

In general, we can determine all possible sources of discretization error as well as their scaling using a method referred to as the Symanzik effective action [2, 62–65]. The basic procedure begins through considering any possible operators (that have not been explicitly tuned) which are allowed by the symmetry of the theory. Because these operators may only be induced through discretization and must disappear in the continuum limit, they should be multiplied by the lattice spacing raised to the appropriate scaling dimension of the operator. We can then determine at what order in b_s, relative to the energy, we can expect systematic errors to arise.

Let's take a look another interesting operator which arises due to discretization, corresponding to a three-body interaction. While there can be no point-like 3-body interaction in the continuum limit for 2-component fermions due to the Pauli exclusion principle, three particles separated by a lattice spacing may interact via ϕ-field exchange because they don't all lie on the same spacetime point. Thus, we should include in our Symanzik effective action an operator,

$$\mathscr{O}_{3\text{-body}} \sim (\psi\psi\psi)^{\dagger}\, \psi\psi\psi\ . \tag{5.186}$$

Naïvely, the dimension of this operator is 9, and therefore should contribute errors of $\mathscr{O}\left((b_s n^{1/3})^4\right)$. So far, all of the operators we've discussed obey this simple scaling, corresponding to naïve dimensional analysis. However, our theory is strongly interacting, which can in general lead to large anomalous dimensions of certain operators.

As an example, let's consider the scaling dimension of a very basic operator, the field ϕ. The canonical (non-interacting) dimension for a generic bosonic field in a non-relativistic theory can be deduced by looking at the kinetic term in the action,

$$S_{\text{kin}} = \int d\tau d^3x \nabla^2 \phi^2 \ , \tag{5.187}$$

leading to a scaling dimension, $[\phi] = 3/2$. However, once interactions with the ψ fields are included, the ϕ propagator is renormalized through loop diagrams (see Fig. 5.15). For a non-perturbative interaction, we must sum all possible loop diagrams. However, there is a simpler way to determine the scaling dimension of the strongly interacting ϕ field. The key is to recognize that near unitarity the ϕ field represents a bound state of two ψ fields at threshold. We can therefore write ϕ as a local operator,

$$\phi(x) = \lim_{x \to y} |x - y| \psi^\dagger(x) \psi(y) \ , \tag{5.188}$$

where $|x - y|$ must be included to ensure that matrix elements of the operator are finite (the wavefunction for two particles at unitarity must scale as $|x - y|^{-1}$ at short distances [125]). Using our previous analysis for the scaling dimension of the ψ field, we find,

$$[\phi]_{\text{int}} = 2 \ , \tag{5.189}$$

which implies a very strong wavefunction renormalization.

Fig. 5.15 Propagator for the bosonic field ϕ, dressed by fermionic loops.
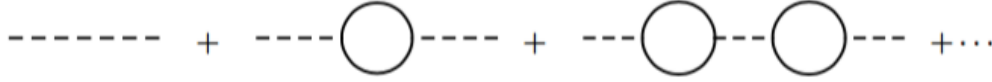
In general it can be very difficult to calculate anomalous dimensions directly in a non-perturbative fashion. However, for non-relativistic conformal field theories (CFT), there exists an operator-state correspondence (similar to an ADS/CFT correspondence), which relates the scaling dimension of an operator in the CFT (e.g. for unitary fermions) to the energy of the corresponding state in a harmonic potential [125]. For example, we have already determined the dimension of the field ψ to be 3/2, and the energy of a single fermion in a harmonic potential with oscillator frequency ω is $3/2\omega$. The energy of two unitary fermions in a harmonic potential is 2ω, corresponding to the dimension of the ϕ field, $[\phi] = 2$.

Returning now to our 3-body operator, we can use numerical results for the energy of three fermions in a total $l = 0$ state in a harmonic potential [126, 127] to determine that,

$$[\psi\psi\psi] = 4.67 \ . \tag{5.190}$$

The error-inducing operator in the Symanzik effective action both creates and destroys this 3-body state, resulting in

$$\left[(\psi\psi\psi)^\dagger \psi\psi\psi \right] = 9.34 \ . \tag{5.191}$$

The relative error in the energy will then be $\mathcal{O}\left(L^{-(9.34-5)}\right) = \mathcal{O}\left(L^{-4.34}\right)$.

It turns out that the ground state of three fermions in a harmonic potential is actually not the s-wave state, but a p-wave state with energy $\sim 4.27\omega$. Thus, we should expect an additional systematic error corresponding to a 3-body p-wave operator that contributes at $\mathcal{O}\left(L^{-3.55}\right)$ [128]. Finally, at approximately the same order as the 3-body s-wave there is a 2-body d-

wave operator (four derivatives) with zero anomalous dimension, and therefore contributing at $\mathscr{O}\left(L^{-5}\right)$.

While certainly only the leading error ($\mathscr{O}\left(L^{-3}\right)$) will dominate very close to the continuum limit, at a finite lattice spacing we have just demonstrated that there are several sources of error scaling with very similar powers of the lattice spacing. If we wish to eliminate discretization errors through extrapolation to the continuum limit, we must include all possible non-negligible contributions in our extrapolation function. For example, we could employ the following function:

$$E(L) = E_0 \left[1 + aL^{-3} + bL^{-3.55} + cL^{-4.34} + dL^{-5} + \cdots \right] , \qquad (5.192)$$

and fit the coefficients $\{a,b,c,d\}$ using data at several volumes, in order to extract the continuum energy, E_0 [2].

5.4.4 Additional sources of systematic error

It should be pretty clear by now that understanding and controlling systematic errors can be quite complicated, even for conformal systems! For more complex systems with contributions from multiple scales, such as nucleii, things become even messier. As a simple example of a system with more than one scale we can consider trapping our unitary fermions in a harmonic potential, which will allow us to discuss finite volume errors that are not accounted for by the Lüscher method. This is clearly relevant for cold atom experiments, which utilize traps, but may also be useful for calculating the energies needed to use the operator-state correspondence discussed in the previous subsection.

The new characteristic length scale contributed by the introduction of the harmonic trap is given by the size of the trap, L_0. We now have two different dimensionless quantities which determine the scaling of systematic errors due to discretization, b_s/L_0, and finite volume, L_0/L_{phys}, individually. To determine the size of discretization errors we may use the Symanzik effective action method as previously described, with the average momentum scale replaced by $n^{1/3} \to N^{1/3}/L_0$. Finite volume errors may be estimated by examining the long distance behavior of the wavefunction of the system of interest, where distortions due to the finite boundary can occur. For a system in a harmonic trap with local interactions, wavefunctions behave as Gaussians at large distance, so we might consider using a function $E(L_{\mathrm{phys}}) = E_0 \left(1 + ae^{-(L_0/L_{\mathrm{phys}})^2} \right)$ to extrapolate to the infinite volume limit.

For the case of nuclei, which are bound states whose wavefunctions fall off exponentially at long distance, we might expect systematic errors to scale as $e^{-R/L_{\mathrm{phys}}}$, where R is the characteristic size of the bound state. In general, one may also need to consider effects from interactions between images produced due to the periodic boundary conditions. For example, if the interaction between images is mediated at long distances by the exchange of a light particle, such as a pion, then we might expect systematic errors to fall off exponentially with $\sim (m_\pi L_{\mathrm{phys}})$. Note that this type of finite volume effect is not accounted for by the Lüscher formalism; this is because in order to derive Eq. (5.174) we had to assume that all interactions were point-like.

Finally, we should briefly discuss systematic errors associated with temporal discretization. These tend to be far less worrisome for zero temperature results for several reasons. The first is due to the relation $b_\tau = \frac{b_s^2}{M}$ for non-relativistic theories, indicating that temporal discretization errors are of lower order than spatial discretization errors. Furthermore, our tuning method for improving the kinetic and interaction operators also translates into an improved temporal derivative operator. The lattice temporal derivative is given by the finite

difference,

$$\partial_\tau \psi \sim \psi_{\tau+1} - \psi_\tau \sim (\mathcal{T} - 1)\, \psi_\tau \;, \tag{5.193}$$

where on the right hand side I have used the knowledge that the transfer matrix $\mathcal{T}$ is our time-translation operator. By perfecting the transfer matrix with our tuning method, we are in turn perfecting the single time hop operation, thereby reducing temporal discretization errors.

We also have the freedom to use the anisotropy parameter M to tune the temporal lattice spacing to be intrinsically smaller than the spatial lattice spacing. However, it should be noted that because the temperature is controlled by the physical Euclidean time length, $1/(b_\tau N_\tau)$, increasing the anisotropy parameter M will necessitate an increase in the number of temporal lattice points to reach the zero temperature limit. On the other hand, having a finer temporal lattice spacing may also help to better resolve plateaus occurring within a short "golden window" before the noise begins to set in, due to the increase in the number of points available for fitting. For this reason, anisotropic lattices are sometimes used in lattice QCD for noisy systems. However, points corresponding to a finer temporal lattice spacing are also more correlated, so it is currently unclear whether anisotropic lattices are actually beneficial for resolving noisy signals.

5.5 Beyond leading order EFT

The first step away from unitarity and toward real nuclear physics that we can easily take is to introduce a four-component nucleon field, N, containing two flavors of spin up and spin down fermions. The nucleons have two allowed s-wave scattering channels, $^1S_0$ and $^3S_1$, which should be tuned independently (breaking the approximate $SU(4)$ symmetry between the nucleons) to give the physical nucleon-nucleon scattering lengths. One possible way to achieve this is to introduce two four-fermion interactions corresponding to,

$$\mathscr{L}_{\text{int}} = -\frac{1}{2}C_S \left(N^\dagger N\right)^2 - \frac{1}{2}C_T \left(N^\dagger \sigma N\right)^2 \;, \tag{5.194}$$

where σ_i is a Pauli matrix acting on the spin indices, and C_S, C_T are couplings for the spin singlet and spin triplet channel, respectively. The lattice version of this interaction requires the introduction of two independent auxiliary fields, ϕ_S, ϕ_T. One possibility is,

$$\mathscr{L}_{\text{int}}^{(L)} = \sqrt{C_S}\phi_S N^\dagger N + \sqrt{C_T}\phi_T \sigma \cdot N^\dagger \sigma N \;. \tag{5.195}$$

There are, in fact, many ways to implement the same interactions, and the different implementations will affect the signal-to-noise ratios of observables. For example, one could imagine having one of the ϕ fields couple to both channels equally (the $SU(4)$ limit), tuned to give the scattering length of the more attractive channel, $^3S_1$, then adding a second auxiliary field coupling only to the $^1S_0$ channel and tuning this coupling to be repulsive, making this channel more weakly attractive as desired. As we learned in Sec. 5.3.1, repulsive interactions cause severe sign and noise problems, so this would clearly be a poor choice of implementation.

Let's look at the signal-to-noise ratio for a two-particle correlator in the $^1S_0$ channel using the interaction shown above, Eq. (5.195), where neither interaction is repulsive, but their relative strengths are different. The signal goes like,

$$\langle K_n^{\uparrow -1}(\tau) K_n^{\downarrow -1}(\tau) \rangle \sim e^{-E_0^{(^1S_0)}\tau} \;. \tag{5.196}$$

while the noise is given by,

$$\sigma^2 \sim \langle K_n^{\uparrow -1}(\tau) K_n^{\downarrow -1}(\tau) \rangle K_{n'}^{\uparrow -1}(\tau) K_{n'}^{\downarrow -1}(\tau) \rangle \sim e^{E_B^{(4)} \tau} \; , \tag{5.197}$$

where n' denotes a particle of different flavor from n, and $E_B^{(4)}$ is the binding energy of a four particle, four flavor state. This causes a signal-to-noise problem which is similar to our original two-body correlator, however, in this case the problem is exacerbated by the fact that particles in Eq. (5.197) having different flavor index interact through the most attractive channel, $^3S_1$. This results in a greater disparity between the energies governing the signal and the noise, leading to more severe exponential decay of the signal-to-noise ratio. Unequal interactions can also lead to problems with reweighting methods designed to alleviate an overlap problem if the desired reweighting factor is no longer real or positive.

One method, devised by the Bonn-Raleigh group (for a review, see e.g. [129]), for avoiding the extra noise caused by unequal interactions in the two s-wave channels, is to use an $SU(4)$ symmetric transfer matrix, $\mathscr{T}_{SU(4)}$, to evolve the system for several time steps before applying the full asymmetric transfer matrix. This process may be thought of as utilizing several applications of $\mathscr{T}_{SU(4)}$ in order to produce a better interpolating wavefunction from some initial guess wavefunctions, $\Psi_{i,f}$, which is then used as a source for the correlation function,

$$C(\tau) = \langle \Psi_f | \mathscr{T}_{SU(4)}^{\tau'} \mathscr{T}^\tau \mathscr{T}_{SU(4)}^{\tau'} | \Psi_i \rangle = \langle \tilde{\Psi}_f | \mathscr{T}^\tau | \tilde{\Psi}_i \rangle \; , \tag{5.198}$$

where $|\tilde{\Psi}_i\rangle \equiv \mathscr{T}_{SU(4)}^{\tau'} |\Psi_i\rangle$. Using this method reduces the number of times the noisier $\mathscr{T}$ must be used because the system begins in a state that is already closer to the true ground state.

Another method used by the same group to reduce noise is to perform a Fierz transformation on the four-fermion interactions in order to define interactions with more symmetric couplings [130]. Using the identity,

$$\left(N^\dagger N\right)^2 = -\frac{1}{2}\left(N^\dagger \sigma N\right)^2 - \frac{1}{2}\left(N^\dagger \tau N\right)^2 \; , \tag{5.199}$$

we can rewrite the four-fermion interactions, Eq. (5.194), to give the following,

$$\tilde{\mathscr{L}}_{\text{int}} = -\frac{1}{2} g_0 \left(N^\dagger N\right)^2 - \frac{1}{2} g_I \left(N^\dagger \tau N\right)^2 \; , \tag{5.200}$$

where τ_i is a Pauli matrix acting on the flavor components of N, and the couplings $g_{0,I}$ are related to the original couplings by,

$$g_0 = g_S - 2g_T \; , \qquad g_I = -g_T \; . \tag{5.201}$$

5.5.1 Tuning the effective range

The method outlined in Sec. 5.2.2.5 was devised as a way to allow us to tune our couplings to reproduce any physical scattering phase shift using the Lüscher finite volume method. We were able to successfully tune the system to unitarity, where the effective range and all higher shape parameters vanish. For nucleon scattering, the effective ranges in the s-wave channels are given roughly by the Compton wavelength of the pion, so the next logical step in our quest toward nuclear physics should be to try to tune our coefficients to give the physical effective ranges. Unfortunately, a problem arises for producing a non-zero effective range non-perturbatively using point-like interactions in combination with a lattice regulator.

The choice of regulator is relevant when attempting to perform non-perturbative calculations because EFTs in general are non-renormalizable. However, they should be renormalizable order by order in perturbation theory, because at each order we introduce a new operator having the correct dimensions and symmetries to act as a counterterm, absorbing infinities from loops containing lower order interactions. Lattice methods incorporate the Lagrangian of the theory non-perturbatively, effectively summing the entire subset of diagrams for each interaction. In principle, such a formulation may also require the introduction of an infinite number of counterterms to absorb the divergences from all loop diagrams.

In certain cases, however, this situation can be avoided. An example is our non-perturbative tuning of the scattering length. Recall that all bubble diagrams involving only the coupling g_0 were separable; this allowed us to write the non-perturbative scattering amplitude as a geometric sum, and we were able to absorb all loop divergences into the single coupling, g_0. The condition of separability for loop diagrams containing interactions which carry momenta is dependent on the choice of regulator. Our choice of a lattice regulator, which is similar to a momentum cutoff, leads to a bound, known as the Wigner bound, on the allowed effective ranges one can access non-perturbatively [131–133].

Because the general tuning method introduced in Sec. 5.2.2.5 involves the numerical calculation of the transfer matrix, understanding the Wigner bound in this context is difficult. To better illustrate the issue, let's attempt to tune the effective range instead using the first method for tuning, outlined in Sec. 5.2.1.2. This method involves calculating the scattering amplitude and tuning the couplings to match the desired scattering parameters directly from the effective range expansion.

We will again calculate a sum of bubble diagrams, however, we must now include an interaction of the form $\mathscr{L}_{\text{int}} \sim g_2 \psi^\dagger \nabla^2 \psi$, which we would like to use to tune the effective range. We will largely follow the discussion of [134]. A generic integral from one of these diagrams will have the form,

$$I_{2n} = \frac{1}{2\pi^2} \int dq \frac{q^{2+2n}}{E - q^2/M} \ , \tag{5.202}$$

where $n = 0, 1, 2$, depending on which of the two interactions we have at the two vertices. Since we are interested in the renormalizability of the scattering amplitude, we will separate out the divergent pieces of such an integral by expanding around $q \to \infty$,

$$I_{2n} = \frac{1}{2\pi^2} \int dq \left[Mq^{2n} - EM \int dq \frac{q^{2n-2}}{E - q^2/M} \right] \ , \tag{5.203}$$

and investigate the integrals using different regularization schemes. The above relation may be iterated for a given n until the remaining integral is finite. The lowest order integral that we will need is given by,

$$I_0 = -\frac{1}{2\pi^2} \int dq \frac{q^2}{E - q^2/M} \ . \tag{5.204}$$

We evaluated this integral previously using a cutoff, $\pi\Lambda/2$, to find,

$$I_0 = \frac{M}{4\pi} [\Lambda + iME] \qquad \text{(cutoff)} \ . \tag{5.205}$$

Using dimensional regularization (dim reg), on the other hand, eliminates power-law divergences, so the result becomes,

$$I_0 = \frac{M}{4\pi} iME \qquad \text{(dim reg)} \ . \tag{5.206}$$

The other two integrals we will need have two and four additional powers of the momentum. Using our relation, Eq. (5.203), we can write,

$$I_2 = MEI_0 - \lambda_2 \,, \tag{5.207}$$

where

$$\lambda_2 = \frac{M}{2\pi^2} \int dq\, q^2 = \begin{cases} -\frac{M\pi}{48}\Lambda^3 & \text{cutoff} \\ 0 & \text{dim reg} \end{cases} \,, \tag{5.208}$$

and

$$I_4 = MEI_2 - \lambda_4 \,, \tag{5.209}$$

where

$$\lambda_4 = \frac{M}{2\pi^2} \int dq\, q^4 = \begin{cases} -\frac{M\pi^3}{320}\Lambda^5 & \text{cutoff} \\ 0 & \text{dim reg} \end{cases} \,. \tag{5.210}$$

From these results we see that dim reg leads to a separable interaction because each of the integrals can be written in terms of I_0 times some overall factor. On the other hand, the cutoff introduces new terms which cannot be factorized.

In order to evaluate the scattering amplitude more generally for a non-separable interaction we must solve a matrix equation. We will set this up by noting that the interaction can be written,

$$V(p,p') = \sum_{i,j=0}^{1} p'^{2i} v_{ij} p^{2j} \,, \tag{5.211}$$

where

$$v = \begin{pmatrix} g_0 & g_2 \\ g_2 & 0 \end{pmatrix} \,. \tag{5.212}$$

The amplitude is then,

$$A = -\sum_{i,j=0}^{1} (ME)^{i+j} a_{ij} \,, \tag{5.213}$$

where

$$a = v + v\mathscr{I}a \,, \qquad \mathscr{I} = \begin{pmatrix} I_0 & I_2 \\ I_2 & I_4 \end{pmatrix} \,. \tag{5.214}$$

We can now solve for a,

$$a = [1 - v\mathscr{I}]^{-1} v = \frac{1}{\lambda} \begin{pmatrix} g_0 + g_2^2 I_4 & g_2(1 - g_2 I_2) \\ g_2(1 - g_2 I_2) & g_2^2 I_0 \end{pmatrix} \,, \tag{5.215}$$

where

$$\lambda \equiv 1 - g_0 I_0 - 2g_2 I_2 + g_2^2(I_2^2 - I_0 I_4) \,. \tag{5.216}$$

Finally, we have

$$\frac{1}{A} = -\frac{(g_2\lambda_2 - 1)^2}{g_0 + g_2[ME(2 - g_2\lambda_2) + g_2\lambda_4]} + I_0$$
$$= \frac{M}{4\pi}\left(-1/a + 1/2r_0ME - i\sqrt{ME}\right) , \tag{5.217}$$

where I have used the effective range expansion for the inverse scattering amplitude on the right hand side.

This expression may be used to determine the couplings $g_{0,2}$ in terms of the effective range parameters, a, r_0, by expanding the left hand side in powers of ME, and comparing the resulting coefficients to the corresponding parameters in the effective range expansion. The leading order is,

$$\frac{1}{A}\bigg|_{E=0} = -\frac{(g_2\lambda_2 - 1)^2}{g_0 + g_2^2\lambda_4} + I_0|_{E=0} = -\frac{M}{4\pi a} , \tag{5.218}$$

while the next order gives,

$$\left[\frac{\partial}{\partial(ME)}\frac{1}{A}\right]_{E=0} \frac{g_2\left(I_0|_{E=0} + \frac{M}{4\pi a}\right)^2)(2 - g_2\lambda_2)}{(g_2\lambda_2 - 1)^2} = \frac{M}{8\pi}r_0 . \tag{5.219}$$

Using these two expressions and the above relations for λ_n and I_0, we can derive the following dependence of the effective range on the couplings for a theory regularized using dim reg,

$$r_0 = \frac{Mg_2}{\pi a^2} . \tag{5.220}$$

Because the effective range is proportional to the coupling g_2, it can be tuned arbitrarily. Thus, as expected from the separability of the interaction, there are no issues with renormalizability when using dim reg.

Let us now see what happens for the case of a cutoff. The relation becomes,

$$r_0 = \frac{8\pi}{M}\left(\frac{M}{4\pi a} + I_0|_{E=0}\right)^2 \left[\frac{1}{(g_2\lambda_2 - 1)^2\lambda_2} - \frac{1}{\lambda_2}\right]$$
$$= \frac{M}{2\pi}(1/a + \Lambda)^2 \left[-\frac{1}{\left(g_2\frac{M\pi}{48}\Lambda^3 - 1\right)^2 \frac{M\pi}{48}\Lambda^3} + \frac{48}{M\pi\Lambda^3}\right] . \tag{5.221}$$

We should now attempt to remove the cutoff by taking, $\Lambda \to \infty$,

$$r_0 \xrightarrow[\Lambda \to \infty]{} -\frac{\frac{M}{2\pi}\Lambda^2}{\left(g_2\frac{M\pi}{48}\Lambda^3 - 1\right)^2 \frac{M\pi}{48}\Lambda^3} , \tag{5.222}$$

where I have kept the first term in square brackets in Eq. (5.221) because there g_2 may be renormalized to absorb factors of Λ. Because g_2 must be real to ensure a Hermitian Hamiltonian, this expression shows that if we attempt to remove the cutoff of the theory, we are only allowed to tune $r_0 \leq 0$.

More generally, Wigner showed that for any potential which obeys $V(r, r') \to 0$ for $r, r' > R$ sufficiently quickly for some characteristic radius R, then

$$r_0 \leq 2\left(R - \frac{R^2}{a} + \frac{R^3}{3a^2}\right) . \tag{5.223}$$

For a potential generated using delta function interactions and a momentum cutoff, $R \sim 1/\Lambda$, and we arrive at our expression $r_0 \leq 0$.

In our lattice formulation the interactions are generated by an auxiliary field extending across a single time link, so that $R \sim b_s$. Therefore, if we try to tune r_0 non-perturbatively via the inclusion of such interactions in the Lagrangian, we are limited to $r_0 \lesssim b_s$. This was not a problem when we considered unitarity, since at this point $r_0 = 0$. For nuclear physics, this bound restricts us to tuning the effective range to be smaller than the lattice spacing, implying that there is no continuum limit to the theory. On the other hand, the theory we are attempting to simulate is only an effective theory of nucleons, valid up to a physical cutoff. Thus, so long as we do not attempt to probe physics beyond scales of order $\sim 1/r_0$ there will be no inconsistencies. This is clearly a limitation, however, and also restricts our ability to vary the lattice spacing when studying discretization effects.

One possibility for avoiding this restriction is to include the effective range contribution to observables perturbatively, keeping the renormalizability of the effective theory intact. Perturbative corrections may be added by expanding the transfer matrix,

$$\mathscr{T} \approx e^{-H_0 b_\tau} - b_\tau \delta H e^{-H_0 b_\tau} \,, \tag{5.224}$$

where $H = H_0 + \delta H$ is the full Hamiltonian and δH is the piece we wish to treat perturbatively. Multiple insertions of δH may be included to reach higher orders in the effective theory.

5.5.2 Including pions
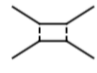
If we wish to probe energies of order the pion mass we must include pions explicitly into the effective theory. Unfortunately, pions are notoriously difficult to include in a consistent power counting scheme. Here, we will only briefly outline some of the issues related to power counting for pion contributions.

The KSW expansion proposed that pion exchange be treated as a series of perturbative corrections to the leading order pionless EFT [34–36]. In this case, a tree level one pion exchange (1PE) diagram may be given by [135],

$$\sim \frac{g_A^2}{2 f_\pi^2} f\left(\frac{p}{m_\pi}\right) \,, \tag{5.225}$$

where g_A is the axial coupling, f_π is the pion decay constant, and $f(p/m_\pi)$ is a dimensionless function. By comparison, at one loop there is a box diagram,

$$\sim \left(\frac{g_A^2}{2 f_\pi^2}\right)^2 \frac{M m_\pi}{4\pi} \tilde{f}\left(\frac{p}{m_\pi}\right) \,. \tag{5.226}$$

Note that the factor of the nucleon mass, a large energy scale for the effective theory, comes from diagrams in which intermediate nucleons can go on-shell. This implies that an expansion parameter for the set of ladder diagrams is approximately,

$$\frac{g_A^2 M m_\pi}{8\pi f_\pi^2} \sim 0.5 \,, \tag{5.227}$$

and that the expansion may converge very slowly. In practice, the convergence for this formulation might be acceptable in the $^1S_0$ scattering channel, but is poor in the spin triplet channel. This is likely due to the singular tensor force contribution to the two-nucleon potential in this channel, which we will discuss in a moment [135].

Weinberg's formulation for nuclear EFT involves summing a subset of diagrams non-perturbatively, then using the resulting nucleon-nucleon potential to solve the Schrodinger equation. In doing so we can take into account higher orders in a perturbative expansion that breaks down or converges slowly. For the pions we can iterate all possible tree level pion exchange diagrams to give the following 1PE potential [38],

$$V_{\text{1PE}}(\mathbf{r} = \left(\frac{g_A}{2f_\pi}\right)^2 \boldsymbol{\tau}_1 \cdot \boldsymbol{\tau}_2 \left[m_\pi^2 \frac{e^{-m_\pi r}}{12\pi r}\left(S_{12}(\hat{r})\left(1 + \frac{3}{m_\pi r} + \frac{3}{(m_\pi r)^2}\right) + \boldsymbol{\sigma}_1 \cdot \boldsymbol{\sigma}_2\right) - \frac{1}{3}\boldsymbol{\sigma}_1 \cdot \boldsymbol{\sigma}_2 \delta^3(r)\right],$$
(5.228)

where $S_{12} = 3\boldsymbol{\sigma}_1 \cdot \hat{r}\boldsymbol{\sigma}_2 \cdot \hat{r} - \boldsymbol{\sigma}_1 \cdot \boldsymbol{\sigma}_2$.

The most divergent part of this potential, scaling like $\sim 1/r^2$, comes from the tensor force in the spin triplet channel. Attractive potentials which scale as r^{-n} for $n \geq 2$ are referred to as singular potentials. Particles sitting in a singular potential eventually fall toward the center with infinite velocity, which is clearly unphysical. Thus, singular potentials can only be defined with an explicit cutoff that cannot be removed. Particles generally sit near this cutoff, rendering the system sensitive to the short-range details of the choice of boundary condition. Therefore, systems involving singular potentials are generally model dependent and we can no longer have a true effective theory because the cutoff cannot be removed.

The reason such a singular potential arises is similar to that which led to the Wigner bound in the previous section. Again, we are attempting to sum a subset of diagrams in an effective theory non-perturbatively, which cannot in general be assumed to be a renormalizable process. In practice, nuclear theorists using so-called chiral potentials are generally able to demonstrate that the cutoff dependence is small so long as the cutoff is only varied within a particular range, typically $\Lambda \sim 300 - 1000$ MeV. Therefore, if we wish to include pions non-perturbatively in our lattice theory we should keep this in mind as it implies a restriction on the allowed lattice spacings, just as we found for the non-perturbative inclusion of effective range contributions.

Pion fields may be added directly to our lattice Lagrangian in a straightforward way. The incorporation of dynamical pions, however, will likely complicate importance sampling by introducing noise and/or sign problems, and adds complexity to the Monte Carlo algorithms. Fortunately fully dynamical pions are unnecessary; all we actually seek is the addition of a term in the Lagrangian which generates the tree level diagrams between a single pion and two nucleons. The lattice formulation then non-perturbatively accounts for all possible loop diagrams involving this pion-nucleon interaction. Diagrams involving vacuum pion loops, pion self-energies, etc. are higher order in our chiral expansion and can be included perturbatively if necessary.

One possible implementation utilized by the Bonn-Raleigh group is to use static pion auxiliary fields, $\pi_{\mathbf{x},\tau}^{(I)}$, with isospin I, and the following action [129, 130]:

$$S_{\pi\pi} = \left(\frac{m_\pi^2}{2} + 3\right) \sum_{\mathbf{x},\tau,I} \pi_{\mathbf{x},\tau}^{(I)}\pi_{\mathbf{x},\tau}^{(I)} - \sum_{\mathbf{x},\tau,I,k} \pi_{\mathbf{x},\tau}^{(I)}\pi_{\mathbf{x}+\hat{k},\tau}^{(I)} .$$
(5.229)

Because the pions are derivatively coupled to the nucleons, the interaction term should behave like,

$$S_{\pi NN} \sim \frac{g_A}{2f_\pi} \sum_{I,k} \left[\pi_{\mathbf{x}+\hat{k}}^{(I)} - \pi_{\mathbf{x}-\hat{k}}^{(I)}\right] \psi_{\mathbf{x}}^\dagger \psi_{\mathbf{x}} ,$$
(5.230)

(see [129] for more details on the particular interaction chosen). The pions have been chosen to only couple to the nucleons through spatial displacements. This simplifies the analysis by

eliminating the renormalization of the nucleon mass through nucleon self-energy diagrams such as:
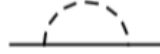
Then we can simply utilize the physical value, $M \sim 938$ MeV, for the nucleon mass. These pions therefore act instantaneously, much the same way as they do in a pion potential picture.

5.5.3 3- and higher-body interactions

Naïve dimensional analysis dictates that the leading three-body interaction should be suppressed relative to the two-body interaction by $\mathcal{O}(L^3)$. We should be more cautious by this point, since we have seen dimensional analysis fail in previous cases for strongly interacting systems. For that reason, we will now inspect the three-body system more carefully.

To begin, we will consider a system of three particles interacting via only the simplest, leading order two-body contact interaction. We will follow the discussion of [136]. Let us assume that all three particles carry different quantum numbers, as they do for the triton and ^{3}He, and that all pairs of particles interact via the same two-body coupling, g_0. To calculate the three-particle scattering amplitude for a strongly coupled system we must iterate this interaction non-perturbatively, as we did for the two-particle system.

A useful trick for calculating this quantity is the addition of a bosonic dimer field, ϕ, coupling to two fermion particles, ψ. This allows us to rewrite the three-particle scattering amplitude in the form of a two-particle scattering amplitude. The dimer propagator must be fully dressed by fermion loop bubbles and can be written diagrammatically as shown in Fig. 5.16. This bubble sum is essentially the same as the one we have encountered several times before in these lectures. However, we must now allow external momentum, $(p_0, \mathbf{p})$ to flow through the diagrams, leading to the following dressed propagator for the dimer field,

$$D_0(p_0, \mathbf{p}) = \frac{1}{1 - g_0 \, I_0|_{E=p_0-p^2/M}} = \frac{1/a - \Lambda}{1/a + i\sqrt{Mp_0 - p^2 - i\varepsilon}} \ , \tag{5.231}$$

where I've used the results from Sec. 5.2.1.2 to rewrite the coupling in terms of the scattering length, a, and the cutoff, Λ. We see that the dimer propagator has a pole at $p_0 = \frac{p^2}{M} - \frac{1}{Ma^2}$, corresponding to a (virtual) bound state for (negative) positive scattering length with energy $E_B = \frac{1}{Ma^2}$.

Fig. 5.16 Dressed propagator for the bosonic dimer field, ϕ.

Using this dimer field, we can write the full three-body scattering amplitude, A_3, as an integral equation, shown in Fig. 5.17. To simplify the expression, we can set the ψ fields to be on-shell, so that all off-shell properties are absorbed into the dimer propagator. The amplitude can then be written,

$$A_3(p, k; E, p^2/M) = -\frac{g_0}{E - p^2/M - k^2/M - (p+k)^2/M + i\varepsilon}$$

$$+ \frac{8\pi i}{g_0} \int \frac{d^4q}{(2\pi)^4} \left(\frac{g_0}{E - p^2/M - q_0 - (p+q)^2/M + i\varepsilon} \right)$$
$$\times \left(\frac{1}{q_0 - q^2/M + i\varepsilon} \right) \left(\frac{A_3(q,k;E,q_0)}{1/a + i\sqrt{M(E - q_0) + q^2 - i\varepsilon}} \right) , \qquad (5.232)$$

known as the Skorniakov-Ter-Martirosian (STM) integral equation. Integrating over q_0 and projecting the system onto the s-wave channel gives (see [136] for more details),

$$\tilde{A}_3(p,k;E) = \frac{1}{apk} \ln \left(\frac{p^2 + pk + k^2 - ME - i\varepsilon}{p^2 - pk + k^2 - ME - i\varepsilon} \right)$$
$$+ \frac{1}{4\pi^2} \int^\Lambda dq \frac{q}{p} \ln \left(\frac{p^2 + pq + q^2 - ME - i\varepsilon}{p^2 - pq + q^2 - ME - i\varepsilon} \right) \frac{\tilde{A}_3(q,k;E)}{-1/a + \sqrt{3q^2 - ME - i\varepsilon}} . \quad (5.233)$$

For large scattering length (strong interaction) we have,

$$\tilde{A}_3(p,k;E) \xrightarrow[a\to\infty]{} \frac{1}{4\pi^2} \int^\Lambda dq \frac{q}{p} \ln \left(\frac{p^2 + pq + q^2 - ME - i\varepsilon}{p^2 - pq + q^2 - ME - i\varepsilon} \right) \frac{\tilde{A}_3(q,k;E)}{\sqrt{3q^2 - ME - i\varepsilon}} \qquad (5.234)$$

Fig. 5.17 Full three-particle scattering amplitude written in terms of a two-particle amplitude for a fermion scattering with a dimer field. Here we have only included two-body interactions, with no explicit three-body contact interaction.
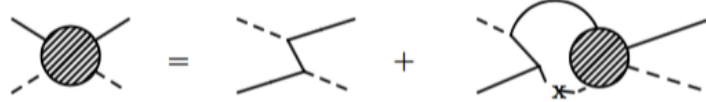
This integral contains divergences, which may be renormalized by adding an explicit three-body coupling, H. To absorb the divergences, the coupling must have the following dependence on the momentum cutoff, Λ [137–139]:

$$H(\Lambda) = \frac{\cos \left[s_0 \ln(\Lambda/\Lambda_*) + \tan^{-1} s_0 \right]}{\cos \left[s_0 \ln(\Lambda/\Lambda_*) - \tan^{-1} s_0 \right]} , \qquad (5.235)$$

where $s_0 \sim 1.006$ is a constant, and Λ_* is some reference scale which may be set by a three-body observable, such as the triton binding energy, or the neutron-deuteron scattering length.

There are two remarkable things to note here: the first is that this result for the scattering amplitude is only a leading order result, yet we had to introduce a three-body coupling in order to renormalize the theory. This illustrates another case where naïve dimensional analysis does not work, because the three-body coupling contributes at the same order as the two-body coupling. The second is the running of the coupling $H(\Lambda)$, plotted on a logarithmic scale in Fig. 5.18. We see that the coupling, and therefore also observables depending on the coupling, displays a log-periodic discrete scaling symmetry, related to the so-called Efimov effect. This property arises for systems obeying a potential at the threshold of singularity, $\sim 1/r^2$, as can be shown to occur for our three-body system using hyperspherical coordinates [140, 141].

Because the three-body interaction has been demonstrated to be relevant at leading order, we should in general include it non-perturbatively to our lattice theory by adding an interaction term to the Lagrangian such as,

$$C_3 \phi_3 \psi_\tau^\dagger \psi_{\tau+1} , \qquad (5.236)$$

where C_3 is tuned to reproduce some three-body observable, and $\phi_3 \in Z_3$ (cube roots of 1). However, ϕ_3 is necessarily a complex field, will induce severe noise and/or sign problems.

Fig. 5.18 Running of the three-body contact interaction $H(\Lambda)$ at unitarity vs. the momentum cutoff, Λ, showing log-periodicity.
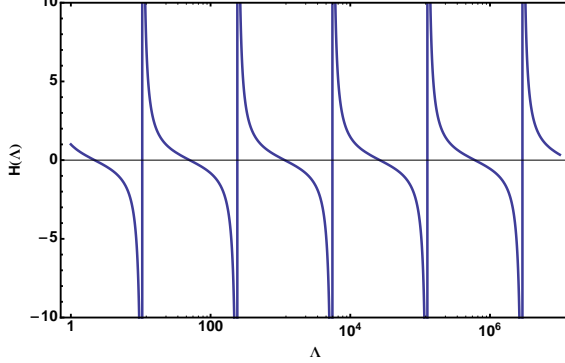
The interaction may alternatively be introduced via multiple Z_2 interactions, but the noise problem remains.

Fig. 5.18 is important for our discussion because it shows how the three-body coupling runs as we change the lattice spacing. The larger the coupling, the worse the noise/sign problem will be. The solution chosen by the Bonn-Raleigh group is to tune the ratio b_τ/b_s until a chosen three-body observable is sufficiently well-described by tuning only the two-body interactions. This implies that the three-body interaction is small at this point, and can then be regarded as a higher-order correction and included perturbatively. A drawback to this approach is that we can no longer use the anisotropy parameter as a knob for probing temporal discretization errors. Because the spatial lattice spacing may also already be restricted by the condition of renormalizability of any pion or effective range contributions to the Lagrangian, we have forfeited most of our ability to demonstrate that discretization errors are under control.

Another possibility for reducing the contribution from the three-body interaction might be to change the short-distance behavior of the two-body sector in another way. For example, tuning different numbers of two-body interaction coefficients (Sec. 5.2.2.5) or changing the discretization of the kinetic operator will shift the reference scale Λ^*, giving us a different value for $H(\Lambda)$ at a fixed lattice spacing.

Finally, given that the three-body sector required a reshuffling of the orders in perturbation theory at strong coupling, should we expect the same for higher N-body interactions? Fortunately it has been fairly well established that four- and higher body operators are not necessary to renormalize the theory at leading order and are therefore irrelevant. This means that we may treat four- and higher-body interactions as perturbative corrections.

This is observed via the so-called Tjon line (see, e.g. [142]). Recall that while the two-body system at unitarity has no intrinsic scale, in order to describe the three-body system we had to introduce a single scale, Λ_*, to be set by some three-body observable. Once this scale is set, all other three-body observables may then be predicted. If four- and higher-body operators appear only at higher orders, then this three-body scale remains the only relevant scale in the problem, and observables must be proportional to Λ_* [6]. This implies that varying the three-body parameter Λ_*, in a plot of the binding energy for the four-body system versus the binding energy of the three-body system, will result in a straight line. Any non-linear dependence on

---

[6] This single scale is also critical for the appearance of the log-normal distribution in correlators near unitarity, where the moments are given by

$$\mathcal{M}_N \sim e^{-E_{\text{N-body}}\tau} \sim e^{-f(N)\Lambda_*\tau} \ . \tag{5.237}$$

Numerical evidence was shown in [51] that $f(N)$ has the expected form for the log-normal distribution.

higher-order N-body operators contributes only within the error band predicted at this order in perturbation theory.

5.5.4 Final considerations

Perhaps the most worrisome issue we have discussed is the inability to take the continuum limit due to interactions that are included non-pertubatively and which generate new non-zero scales beyond the scattering length. The lattice spacing must also be kept reasonably large for another reason mentioned previously, related to numerical stability: if the lattice spacing becomes too small, the system will begin to probe the repulsive core of the two-body potential, leading to sign and/or signal-to-noise problems.

Though we may not have the ability to vary the lattice spacing by significant amounts, we must still prove that our results do not depend strongly on the short-distance details of the action. This can be demonstrated instead by changing the discretization of derivatives in the action, using more or less improvement of the interaction, etc., and showing that the results do not change significantly [129].

Showing convergence of the EFT for the lattice results is also a major concern, particularly since we have no single power-counting scheme that is known to converge in all channels even in the continuum theory. One possible indication of issues with convergence in the current Bonn-Raleigh method is the need for a significant repulsive four-body interaction in order to stabilize four- and higher-body systems, which seem prone to forming four-body clusters on a single lattice site. This is akin to the particles falling to the bottom of a singular potential, and may be related to the particular tuning of the three-body interaction. However, once this interaction has been set the convergence of the results appears to be relatively stable.

Possibly the biggest open issues to be resolved are the sign/noise problems and proving convergence to the ground (or desired excited) state. Noise problems have restricted most calculations of nuclear systems to nuclei in (or near) the alpha ladder, where approximate $SU(4)$ symmetry applies. New theories and/or algorithms would be enormously helpful in this arena. The engineering of better sources or methods for extracting the desired states might be particularly beneficial for both the reduction of noise and to eliminate the need for performing long temporal extrapolations.

Despite these limitations there have been enormous successes for lattice EFT for few- and many-body states both for systems at unitarity and nuclei. As an example, at unitarity the energies of up to 50 two-component fermions have been calculated with errors comparable to state-of-the-art Green's Function Monte Carlo calculations [1, 2, 143–146]. The Raleigh-Bonn group has calculated properties of nuclei up to $A = 28$ [147–151]. Particularly exciting is their investigation of the structure of the Hoyle state, a key component of the triple alpha process necessary for Carbon production in stars [152–156].

5.6 Reading assignments and Exercises

5.1. Write a simple lattice code to evaluate a two-particle correlation function as a function of Euclidean time using a Z_2 auxiliary field. Simple sources for two-particle states may be delta functions in position or momentum space. Use the long time behavior of the effective mass function, $\ln \frac{C_2(\tau)}{C_2(\tau+1)} \xrightarrow[\tau\to\infty]{} E_0$ (see Sec. 10.2.6), to determine the ground state energy for your choice of coupling, g. Compare this with what you expect from Eq. (5.64), using the relation $\lambda = e^{-E_0}$, as the number of lattice points is increased.

5.2. Much of these lecture notes follow this review: arXiv:1208.6556. There you will also find more information about algorithms. The following is an excellent pedagogical introduction to EFT's by David B. Kaplan: arXiv:nucl-th/0510023.

5.3. Construct sources for three fermions in an $l = 0$, $l = 1$ state and find the lowest energies corresponding to each state at unitarity. Which l corresponds to the true ground state of this system?

5.4. Explore the cumulant expansion using a toy model [143]:

$$C(\tau, \phi) = \prod_{i=1}^{\tau} (1 + g\phi_i) \,, \tag{5.238}$$

for $0 \leq g \leq 1$ and $\phi \in [-1, 1]$. The true mean of the correlator should be $\langle C(\tau, \phi) \rangle = 1$, corresponding to $E_0 = 0$. Compare the cumulant expansion cut off at various orders on a finite sample size to the mean calculated using standard methods as the sample size is varied.

5.5. Reading: D. Lee: arXiv:0804.3501 [129] G.P. Lepage: Analysis of algorithms for lattice field theory [3]

5.6. Add a term

$$c\psi_\tau^\dagger \nabla_L^2 \psi_{\tau-1} \tag{5.239}$$

to the simple interaction, Eq. (5.41), and derive an analytic expression for tuning the couplings, g_0, c in order to eliminate the effective range contribution. You may use either the scattering amplitude or the transfer matrix method.

5.7. Write numerical code (Mathematica will suffice) to solve the transfer matrix for two particles for a chosen set of coefficients, g_{2n} (Eq. (5.176)), using $L = 32$, $M = 5$, and tune your coefficients to match the first few expected Lüscher eigenvalues at unitarity. Compare your results with those in Table II of Ref. [1].

5.8. Add a harmonic potential to your code by modifying the interaction: $X(\tau) \to e^{-U/2}X(\tau)e^{-U/2}$, with the matrix U given by $U_{x,x'} = 1/2\kappa x^2 \delta_{x,x'}$. Find the energies of two unitary fermions in a harmonic trap, exploring and removing finite volume and discretization effects by varying the parameters, $L, L_0 = (\kappa M)^{-1/4}, \omega = \sqrt{\kappa/M}$, and performing extrapolations in these quantities if necessary. Compare your result to the expected value of 2ω.

References

1. M.G. Endres, D.B. Kaplan, J.W. Lee, A.N. Nicholson, Phys. Rev. A **84**, 043644 (2011)
2. M.G. Endres, D.B. Kaplan, J.W. Lee, A.N. Nicholson, Phys.Rev. **A87**(2), 023615 (2013). DOI 10.1103/PhysRevA.87.023615
3. G.P. Lepage, From Actions to Answers, Proceedings of the 1989 Theoretical Advanced Study Institute (TASI) (1989)
4. E. Berkowitz, T. Kurth, A. Nicholson, B. Joo, E. Rinaldi, M. Strother, P.M. Vranas, A. Walker-Loud, (2015)
5. T. Kurth, E. Berkowitz, E. Rinaldi, P. Vranas, A. Nicholson, M. Strother, A. Walker-Loud, (2015)
6. A. Nicholson, E. Berkowitz, E. Rinaldi, P. Vranas, T. Kurth, B. Joo, M. Strother, A. Walker-Loud, in *Proceedings, 33rd International Symposium on Lattice Field Theory (Lattice 2015)* (2015). URL `http://inspirehep.net/record/1403559/files/arXiv:1511.02262.pdf`

7. K. Orginos, A. Parreno, M.J. Savage, S.R. Beane, E. Chang, W. Detmold, Phys. Rev. **D92**(11), 114512 (2015). DOI 10.1103/PhysRevD.92.114512

8. W. Detmold, K. Orginos, A. Parreno, M.J. Savage, B.C. Tiburzi, S.R. Beane, E. Chang, Phys. Rev. Lett. **116**(11), 112301 (2016). DOI 10.1103/PhysRevLett.116.112301

9. E. Chang, W. Detmold, K. Orginos, A. Parreno, M.J. Savage, B.C. Tiburzi, S.R. Beane, Phys. Rev. **D92**(11), 114502 (2015). DOI 10.1103/PhysRevD.92.114502

10. S.R. Beane, E. Chang, W. Detmold, K. Orginos, A. Parreño, M.J. Savage, B.C. Tiburzi, Phys. Rev. Lett. **115**(13), 132001 (2015). DOI 10.1103/PhysRevLett.115.132001

11. S.R. Beane, E. Chang, S.D. Cohen, W. Detmold, H.W. Lin, K. Orginos, A. Parreño, M.J. Savage, Phys. Rev. **D91**(11), 114503 (2015). DOI 10.1103/PhysRevD.91.114503

12. S.R. Beane, E. Chang, S. Cohen, W. Detmold, H.W. Lin, K. Orginos, A. Parreno, M.J. Savage, B.C. Tiburzi, Phys. Rev. Lett. **113**(25), 252001 (2014). DOI 10.1103/PhysRevLett.113.252001

13. S.R. Beane, et al., Phys. Rev. **C88**(2), 024003 (2013). DOI 10.1103/PhysRevC.88.024003

14. S.R. Beane, E. Chang, S.D. Cohen, W. Detmold, H.W. Lin, T.C. Luu, K. Orginos, A. Parreno, M.J. Savage, A. Walker-Loud, Phys. Rev. **D87**(3), 034506 (2013). DOI 10.1103/PhysRevD.87.034506

15. S.R. Beane, E. Chang, W. Detmold, H.W. Lin, T.C. Luu, K. Orginos, A. Parreno, M.J. Savage, A. Torok, A. Walker-Loud, Phys. Rev. **D85**, 054511 (2012). DOI 10.1103/PhysRevD.85.054511

16. S.R. Beane, W. Detmold, H.W. Lin, T.C. Luu, K. Orginos, M.J. Savage, A. Torok, A. Walker-Loud, Phys. Rev. **D81**, 054505 (2010). DOI 10.1103/PhysRevD.81.054505

17. T. Yamazaki, in *Proceedings, 33rd International Symposium on Lattice Field Theory (Lattice 2015)* (2015). URL `http://inspirehep.net/record/1407162/files/arXiv:1511.09179.pdf`

18. T. Yamazaki, K.i. Ishikawa, Y. Kuramashi, A. Ukawa, Phys. Rev. **D92**(1), 014501 (2015). DOI 10.1103/PhysRevD.92.014501

19. T. Yamazaki, K.I. Ishikawa, Y. Kuramashi, A. Ukawa, PoS **LATTICE2013**, 230 (2014)

20. T. Yamazaki, K.i. Ishikawa, Y. Kuramashi, A. Ukawa, PoS **LATTICE2012**, 143 (2012)

21. T. Yamazaki, K.i. Ishikawa, Y. Kuramashi, A. Ukawa, Phys. Rev. **D86**, 074514 (2012). DOI 10.1103/PhysRevD.86.074514

22. T. Doi, et al., in *12th International Conference on Hypernuclear and Strange Particle Physics (HYP 2015) Sendai, Japan, September 7-12, 2015* (2015). URL `http://inspirehep.net/record/1409502/files/arXiv:1512.04199.pdf`

23. T. Doi, et al., in *Proceedings, 33rd International Symposium on Lattice Field Theory (Lattice 2015)* (2015). URL `http://inspirehep.net/record/1408519/files/arXiv:1512.01610.pdf`

24. N. Ishii, S. Aoki, T. Hatsuda, Phys. Rev. Lett. **99**, 022001 (2007). DOI 10.1103/PhysRevLett.99.022001

25. K. Murano, N. Ishii, S. Aoki, T. Doi, T. Hatsuda, Y. Ikeda, T. Inoue, H. Nemura, K. Sasaki, Phys. Lett. **B735**, 19 (2014). DOI 10.1016/j.physletb.2014.05.061

26. S. Aoki, PoS **Hadron2013**, 020 (2013)

27. K. Murano, Few Body Syst. **54**, 1105 (2013). DOI 10.1007/s00601-013-0692-3

28. N. Ishii, S. Aoki, T. Doi, T. Hatsuda, Y. Ikeda, T. Inoue, K. Murano, H. Nemura, K. Sasaki, Phys. Lett. **B712**, 437 (2012). DOI 10.1016/j.physletb.2012.04.076

29. T. Inoue, N. Ishii, S. Aoki, T. Doi, T. Hatsuda, Y. Ikeda, K. Murano, H. Nemura, K. Sasaki, Prog. Theor. Phys. **124**, 591 (2010). DOI 10.1143/PTP.124.591

30. S.R. Beane, W. Detmold, T.C. Luu, K. Orginos, A. Parreno, M.J. Savage, A. Torok, A. Walker-Loud, Phys. Rev. **D80**, 074501 (2009). DOI 10.1103/PhysRevD.80.074501

31. T. Doi, S. Aoki, T. Hatsuda, Y. Ikeda, T. Inoue, N. Ishii, K. Murano, H. Nemura, K. Sasaki, Prog. Theor. Phys. **127**, 723 (2012). DOI 10.1143/PTP.127.723

32. S. Weinberg, Phys. Lett. **B251**, 288 (1990). DOI 10.1016/0370-2693(90)90938-3

33. S. Weinberg, Nucl. Phys. **B363**, 3 (1991). DOI 10.1016/0550-3213(91)90231-L

34. D.B. Kaplan, M.J. Savage, M.B. Wise, Nucl. Phys. **B478**, 629 (1996). DOI 10.1016/0550-3213(96)00357-4

35. D.B. Kaplan, M.J. Savage, M.B. Wise, Phys. Lett. **B424**, 390 (1998). DOI 10.1016/S0370-2693(98)00210-X

36. D.B. Kaplan, M.J. Savage, M.B. Wise, Nucl. Phys. **B534**, 329 (1998). DOI 10.1016/S0550-3213(98)00440-4

37. E. Epelbaum, H.W. Hammer, U.G. Meissner, Rev. Mod. Phys. **81**, 1773 (2009). DOI 10.1103/RevModPhys.81.1773

38. E. Epelbaum, (2010). URL `http://inspirehep.net/record/843247/files/arXiv:1001.3229.pdf`

39. R. Machleidt, D.R. Entem, Phys. Rept. **503**, 1 (2011). DOI 10.1016/j.physrep.2011.02.001

40. D.B. Kaplan, (2005)

41. J.E. Drut, A.N. Nicholson, J. Phys. **G40**, 043101 (2013). DOI 10.1088/0954-3899/40/4/043101

42. S.R. Beane, W. Detmold, K. Orginos, M.J. Savage, Prog. Part. Nucl. Phys. **66**, 1 (2011). DOI 10.1016/j.ppnp.2010.08.002

43. W. Detmold, M.G. Endres, Phys. Rev. **D90**(3), 034503 (2014). DOI 10.1103/PhysRevD.90.034503

44. W. Detmold, M.G. Endres, PoS **LATTICE2014**, 170 (2015)

45. D. Grabowska, D.B. Kaplan, A.N. Nicholson, Phys. Rev. **D87**(1), 014504 (2013). DOI 10.1103/PhysRevD. 87.014504
46. A.N. Nicholson, D. Grabowska, D.B. Kaplan, (2012). DOI 10.1088/1742-6596/432/1/012032. [J. Phys. Conf. Ser.432,012032(2013)]
47. M.G. Endres, D.B. Kaplan, J.W. Lee, A.N. Nicholson, PoS **LATTICE2011**, 017 (2011)
48. A.C. Berry, Transactions of the American Mathematical Society **49**(1), 122 (1941)
49. C.G. Esseen, Arkiv fåŮů matematik, astronomi och fysik **A28**, 1 (1942)
50. T. DeGrand, Phys.Rev. **D86**, 014512 (2012). DOI 10.1103/PhysRevD.86.014512
51. A.N. Nicholson, Phys. Rev. Lett. **109**, 073003 (2012). DOI 10.1103/PhysRevLett.109.073003. URL `http://link.aps.org/doi/10.1103/PhysRevLett.109.073003`
52. A.N. Nicholson, EPJ Web Conf. **113**, 03019 (2016). DOI 10.1051/epjconf/201611303019
53. J.J. Dudek, R.G. Edwards, M.J. Peardon, D.G. Richards, C.E. Thomas, Phys. Rev. **D82**, 034508 (2010). DOI 10.1103/PhysRevD.82.034508
54. C. Michael, I. Teasdale, Nuclear Physics B **215**(3), 433 (1983). DOI http://dx.doi.org/10.1016/0550-3213(83)90674-0. URL `http://www.sciencedirect.com/science/article/pii/0550321383906740`
55. M. Lüscher, U. Wolff, Nucl.Phys. **B339**, 222 (1990). DOI 10.1016/0550-3213(90)90540-T
56. B. Blossier, M. Della Morte, G. von Hippel, T. Mendes, R. Sommer, JHEP **04**, 094 (2009). DOI 10.1088/1126-6708/2009/04/094
57. C. Aubin, K. Orginos, PoS **LATTICE2011**, 148 (2011)
58. Y. Hua, T. Sarkar, IEEE Transactions on antennas and propagation **37**, 229 (1989)
59. T. Sarkar, O. Pereira, IEEE Antennas and Propagation Magazine **37**, 48 (1995)
60. S.R. Beane, W. Detmold, T.C. Luu, K. Orginos, A. Parreno, et al., Phys.Rev. **D79**, 114502 (2009). DOI 10.1103/PhysRevD.79.114502
61. G.T. Fleming, S.D. Cohen, H.W. Lin, V. Pereyra, Phys. Rev. **D80**, 074506 (2009). DOI 10.1103/PhysRevD.80.074506
62. K.S. in, *Recent Developments in Gauge Theories* (Plenum, New York, 1980). Edited by G. 't Hooft *et al.*
63. K.S. in, *Mathematical Problems in Theoretical Physics* (Springer, New York, 1982). Edited by R. Schrader *et al.*
64. K. Symanzik, Nuclear Physics B **226**(1), 187 (1983). DOI 10.1016/0550-3213(83)90468-6. URL `http://www.sciencedirect.com/science/article/pii/0550321383904686`
65. K. Symanzik, Nuclear Physics B **226**(1), 205 (1983). DOI 10.1016/0550-3213(83)90469-8. URL `http://www.sciencedirect.com/science/article/pii/0550321383904698`
66. G. Batrouni, A. Hansen, M. Nelkin, Phys. Rev. Lett. **57**, 1336 (1986)
67. C. Davies, G. Batrouni, G. Katz, A. Kronfeld, P. Lepage, P. Rossi, B. Svetitsky, K. Wilson, J. Stat. Phys. **43**, 1073 (1986)
68. C.T.H. Davies, G.G. Batrouni, G.R. Katz, A.S. Kronfeld, G.P. Lepage, K.G. Wilson, P. Rossi, B. Svetitsky, Phys. Rev. D **37**, 1581 (1988)
69. G. Katz, G. Batrouni, C. Davies, A. Kronfeld, P. Lepage, P. Rossi, B. Svetitsky, K. Wilson, Phys. Rev. D **37**, 1589 (1988)
70. M. Lüscher, Commun. Math. Phys. **105**, 153 (1986). DOI 10.1007/BF01211097
71. M. Lüscher, Nucl. Phys. **B354**, 531 (1991). DOI 10.1016/0550-3213(91)90366-6
72. S. Beane, P. Bedaque, A. Parreno, M. Savage, Phys.Lett. **B585**, 106 (2004). DOI 10.1016/j.physletb.2004.02.007
73. R.A. Briceno, Z. Davoudi, (2012)
74. M.T. Hansen, S.R. Sharpe, Phys.Rev. **D86**, 016007 (2012). DOI 10.1103/PhysRevD.86.016007
75. N. Li, S.Y. Li, C. Liu, Phys. Rev. **D90**(3), 034509 (2014). DOI 10.1103/PhysRevD.90.034509
76. R.A. Briceno, Phys. Rev. **D89**(7), 074507 (2014). DOI 10.1103/PhysRevD.89.074507
77. R.A. Briceño, M.T. Hansen, (2015)
78. R.A. Briceño, M.T. Hansen, Phys. Rev. **D92**(7), 074509 (2015). DOI 10.1103/PhysRevD.92.074509
79. R.A. Briceño, M.T. Hansen, A. Walker-Loud, PoS **LATTICE2014**, 095 (2015)
80. R.A. Briceño, M.T. Hansen, A. Walker-Loud, Phys. Rev. **D91**(3), 034501 (2015). DOI 10.1103/PhysRevD.91.034501
81. T. Luu, M.J. Savage, Phys.Rev. **D83**, 114508 (2011). DOI 10.1103/PhysRevD.83.114508
82. S. Koenig, D. Lee, H.W. Hammer, Phys.Rev.Lett. **107**, 112001 (2011)
83. S. Koenig, D. Lee, H.W. Hammer, Annals Phys. **327**, 1450 (2012)
84. K. Rummukainen, S.A. Gottlieb, Nucl.Phys. **B450**, 397 (1995). DOI 10.1016/0550-3213(95)00313-H
85. C. Kim, C. Sachrajda, S.R. Sharpe, Nucl.Phys. **B727**, 218 (2005)
86. S. Bour, S. Koenig, D. Lee, H.W. Hammer, U.G. Meissner, Phys.Rev. **D84**, 091503 (2011). DOI 10.1103/PhysRevD.84.091503
87. Z. Davoudi, M.J. Savage, Phys.Rev. **D84**, 114502 (2011). DOI 10.1103/PhysRevD.84.114502
88. X. Li, C. Liu, Phys.Lett. **B587**, 100 (2004). DOI 10.1016/j.physletb.2004.02.068

89. X. Feng, X. Li, C. Liu, Phys.Rev. **D70**, 014505 (2004). DOI 10.1103/PhysRevD.70.014505
90. M.T. Hansen, S.R. Sharpe, Phys. Rev. **D93**(9), 096006 (2016). DOI 10.1103/PhysRevD.93.096006
91. M.T. Hansen, S.R. Sharpe, Phys. Rev. **D92**(11), 114509 (2015). DOI 10.1103/PhysRevD.92.114509
92. M.T. Hansen, S.R. Sharpe, Phys. Rev. **D90**(11), 116003 (2014). DOI 10.1103/PhysRevD.90.116003
93. R.A. Briceno, Z. Davoudi, Phys. Rev. **D87**(9), 094507 (2013). DOI 10.1103/PhysRevD.87.094507
94. S.R. Beane, W. Detmold, M.J. Savage, Phys.Rev. **D76**, 074507 (2007). DOI 10.1103/PhysRevD.76.074507
95. W. Detmold, M.J. Savage, Phys.Rev. **D77**, 057502 (2008). DOI 10.1103/PhysRevD.77.057502
96. B. Smigielski, J. Wasem, Phys.Rev. **D79**, 054506 (2009). DOI 10.1103/PhysRevD.79.054506
97. R.A. Briceno, Z. Davoudi, T.C. Luu, Phys. Rev. **D88**(3), 034502 (2013). DOI 10.1103/PhysRevD.88.034502
98. R.A. Briceño, Z. Davoudi, T. Luu, M.J. Savage, Phys. Rev. **D88**(11), 114507 (2013). DOI 10.1103/PhysRevD.88.114507
99. S.R. Beane, P.F. Bedaque, K. Orginos, M.J. Savage, Phys. Rev. Lett. **97**, 012001 (2006). DOI 10.1103/PhysRevLett.97.012001
100. D.J. Wilson, J.J. Dudek, R.G. Edwards, C.E. Thomas, (2014)
101. D.J. Wilson, R.A. Briceno, J.J. Dudek, R.G. Edwards, C.E. Thomas, (2015)
102. J.J. Dudek, R.G. Edwards, C.E. Thomas, Phys.Rev. **D86**, 034031 (2012). DOI 10.1103/PhysRevD.86.034031
103. J.J. Dudek, R.G. Edwards, C.E. Thomas, Phys.Rev. **D87**(3), 034505 (2013). DOI 10.1103/PhysRevD.87.034505,10.1103/PhysRevD.90.099902
104. J.J. Dudek, R.G. Edwards, C.E. Thomas, D.J. Wilson, Phys.Rev.Lett. **113**(18), 182001 (2014). DOI 10.1103/PhysRevLett.113.182001
105. S.R. Beane, E. Chang, W. Detmold, H.W. Lin, T.C. Luu, K. Orginos, A. Parreno, M.J. Savage, A. Torok, A. Walker-Loud, Phys. Rev. **D85**, 034505 (2012). DOI 10.1103/PhysRevD.85.034505
106. S. Aoki, et al., Phys. Rev. **D76**, 094506 (2007). DOI 10.1103/PhysRevD.76.094506
107. S. Aoki, et al., Phys. Rev. **D84**, 094505 (2011). DOI 10.1103/PhysRevD.84.094505
108. C. Pelissier, A. Alexandru, Phys. Rev. **D87**(1), 014503 (2013). DOI 10.1103/PhysRevD.87.014503
109. X. Feng, K. Jansen, D.B. Renner, Phys. Rev. **D83**, 094505 (2011). DOI 10.1103/PhysRevD.83.094505
110. A. Martínez Torres, E. Oset, S. Prelovsek, A. Ramos, JHEP **05**, 153 (2015). DOI 10.1007/JHEP05(2015)153
111. D.R. Bolton, R.A. Briceno, D.J. Wilson, (2015)
112. R.A. Briceno, J.J. Dudek, R.G. Edwards, C.J. Shultz, C.E. Thomas, D.J. Wilson, Phys. Rev. Lett. **115**, 242001 (2015). DOI 10.1103/PhysRevLett.115.242001
113. C.B. Lang, L. Leskovec, D. Mohler, S. Prelovsek, Phys. Rev. **D86**, 054508 (2012). DOI 10.1103/PhysRevD.86.054508
114. S. Prelovsek, L. Leskovec, C.B. Lang, D. Mohler, Phys. Rev. **D88**(5), 054508 (2013). DOI 10.1103/PhysRevD.88.054508
115. C.B. Lang, L. Leskovec, D. Mohler, S. Prelovsek, R.M. Woloshyn, Phys. Rev. **D90**(3), 034510 (2014). DOI 10.1103/PhysRevD.90.034510
116. C.B. Lang, D. Mohler, S. Prelovsek, R.M. Woloshyn, Phys. Lett. **B750**, 17 (2015). DOI 10.1016/j.physletb.2015.08.038
117. C.B. Lang, D. Mohler, S. Prelovsek, M. Vidmar, Phys. Rev. **D84**(5), 054503 (2011). DOI 10.1103/PhysRevD.89.059903,10.1103/PhysRevD.84.054503. [Erratum: Phys. Rev.D89,no.5,059903(2014)]
118. R.A. Briceño, J.J. Dudek, R.G. Edwards, C.J. Shultz, C.E. Thomas, D.J. Wilson, (2016)
119. V. Verduci, C.B. Lang, PoS **LATTICE2014**, 121 (2014)
120. C.B. Lang, V. Verduci, Phys. Rev. **D87**(5), 054502 (2013). DOI 10.1103/PhysRevD.87.054502
121. A. Torok, S.R. Beane, W. Detmold, T.C. Luu, K. Orginos, et al., Phys.Rev. **D81**, 074506 (2010). DOI 10.1103/PhysRevD.81.074506
122. W. Detmold, A. Nicholson, (2015)
123. S.R. Beane, E. Chang, S.D. Cohen, W. Detmold, H.W. Lin, T.C. Luu, K. Orginos, A. Parreno, M.J. Savage, A. Walker-Loud, Phys. Rev. Lett. **109**, 172001 (2012). DOI 10.1103/PhysRevLett.109.172001
124. S.R. Beane, P.F. Bedaque, T.C. Luu, K. Orginos, E. Pallante, A. Parreno, M.J. Savage, Nucl. Phys. **A794**, 62 (2007). DOI 10.1016/j.nuclphysa.2007.07.006
125. Y. Nishida, D.T. Son, Phys. Rev. D **76**, 086004 (2007)
126. D. Blume, J. von Stecher, C.H. Greene, Physical Review Letters **99**(23), 233201 (2007). DOI 10.1103/PhysRevLett.99.233201
127. D. Blume, K.M. Daily, Comptes Rendus Physique **12**, 86 (2011)
128. F. Werner, Y. Castin, Phys. Rev. Lett. **97**(15), 150401 (2006). DOI 10.1103/PhysRevLett.97.150401
129. D. Lee, Prog. Part. Nucl. Phys. **63**, 117 (2009). DOI 10.1016/j.ppnp.2008.12.001
130. B. Borasoy, E. Epelbaum, H. Krebs, D. Lee, U.G. Meissner, Eur. Phys. J. **A31**, 105 (2007). DOI 10.1140/epja/i2006-10154-1
131. E.P. Wigner, Phys. Rev. **98**, 145 (1955). DOI 10.1103/PhysRev.98.145. URL http://link.aps.org/doi/10.1103/PhysRev.98.145

132. D.R. Phillips, T.D. Cohen, Phys. Lett. **B390**, 7 (1997). DOI 10.1016/S0370-2693(96)01411-6
133. T.D. Cohen, Phys. Rev. **C55**, 67 (1997). DOI 10.1103/PhysRevC.55.67
134. D.R. Phillips, S.R. Beane, T.D. Cohen, Annals Phys. **263**, 255 (1998). DOI 10.1006/aphy.1997.5771
135. S. Fleming, T. Mehen, I.W. Stewart, Nucl. Phys. **A677**, 313 (2000). DOI 10.1016/S0375-9474(00)00221-9
136. E. Braaten, H.W. Hammer, Phys. Rept. **428**, 259 (2006). DOI 10.1016/j.physrep.2006.03.001
137. P.F. Bedaque, H.W. Hammer, U. van Kolck, Nucl. Phys. **A646**, 444 (1999). DOI 10.1016/S0375-9474(98)00650-2
138. P.F. Bedaque, H.W. Hammer, U. van Kolck, Phys. Rev. Lett. **82**, 463 (1999). DOI 10.1103/PhysRevLett.82.463
139. S.R. Beane, P.F. Bedaque, L. Childress, A. Kryjevski, J. McGuire, U. van Kolck, Phys. Rev. **A64**, 042103 (2001). DOI 10.1103/PhysRevA.64.042103
140. V.N. Efimov, Physics Letters B **33**(8), 563 (1970). DOI 10.1016/0370-2693(70)90349-7
141. V.N. Efimov, Sov. J. Nucl. Phys. **12**, 589 (1971)
142. H.W. Hammer, L. Platter, Ann. Rev. Nucl. Part. Sci. **60**, 207 (2010). DOI 10.1146/annurev.nucl.012809.104439
143. M.G. Endres, D.B. Kaplan, J.W. Lee, A.N. Nicholson, Phys. Rev. Lett. **107**, 201601 (2011)
144. M.G. Endres, D.B. Kaplan, J.W. Lee, A.N. Nicholson, PoS **Lattice 2010**, 182 (2010)
145. J.W. Lee, M.G. Endres, D.B. Kaplan, A.N. Nicholson, PoS **Lattice 2010**, 197 (2010)
146. A.N. Nicholson, M.G. Endres, D.B. Kaplan, J.W. Lee, PoS **Lattice 2010**, 206 (2010)
147. E. Epelbaum, H. Krebs, D. Lee, U.G. Meissner, Eur. Phys. J. **A45**, 335 (2010). DOI 10.1140/epja/i2010-11009-x
148. E. Epelbaum, H. Krebs, D. Lee, U.G. Meissner, Phys. Rev. Lett. **104**, 142501 (2010). DOI 10.1103/PhysRevLett.104.142501
149. E. Epelbaum, H. Krebs, T.A. Lahde, D. Lee, U.G. MeiSSner, G. Rupak, Phys. Rev. Lett. **112**(10), 102501 (2014). DOI 10.1103/PhysRevLett.112.102501
150. T.A. Lahde, E. Epelbaum, H. Krebs, D. Lee, U.G. MeiSSner, G. Rupak, (2013). [PoSLAT-TICE2013,231(2014)]
151. T.A. Lahde, E. Epelbaum, H. Krebs, D. Lee, U.G. MeiSSner, G. Rupak, Phys. Lett. **B732**, 110 (2014). DOI 10.1016/j.physletb.2014.03.023
152. E. Epelbaum, H. Krebs, D. Lee, U.G. Meissner, Phys. Rev. Lett. **106**, 192501 (2011). DOI 10.1103/PhysRevLett.106.192501
153. E. Epelbaum, H. Krebs, T.A. Lahde, D. Lee, U.G. Meissner, Phys. Rev. Lett. **109**, 252501 (2012). DOI 10.1103/PhysRevLett.109.252501
154. E. Epelbaum, H. Krebs, T.A. Lahde, D. Lee, U.G. MeiSSner, Phys. Rev. Lett. **110**(11), 112502 (2013). DOI 10.1103/PhysRevLett.110.112502
155. E. Epelbaum, H. Krebs, T.A. Lahde, D. Lee, U.G. MeiSSner, Eur. Phys. J. **A49**, 82 (2013). DOI 10.1140/epja/i2013-13082-y
156. T.A. Lahde, E. Epelbaum, H. Krebs, D. Lee, U.G. MeiSSner, G. Rupak, Pramana **83**(5), 651 (2014). DOI 10.1007/s12043-014-0861-z

Chapter 6
Lattice methods and the nuclear few- and many-body problem

Dean Lee

Abstract This chapter builds upon the review of lattice methods and effective field theory of the previous chapter. We begin with a brief overview of lattice calculations using chiral effective field theory. We then describe several methods for computing scattering on the lattice. After that we focus on the main goal, explaining the theory and algorithms relevant to lattice simulations of nuclear few- and many-body systems. We discuss the exact equivalence of four different lattice formalisms, the Grassmann path integral, transfer matrix operator, Grassmann path integral with auxiliary fields, and transfer matrix operator with auxiliary fields. Along with our analysis we include several coding examples and a number of exercises for the calculations of few- and many-body systems at leading order in chiral effective field theory.

6.1 Introduction

Effective field theory (EFT) provides a theoretical framework for organizing low-energy interactions in powers of particle momenta. Chiral effective field theory applies this framework to the low-energy interactions of protons and neutrons while explicitly including the interactions of pions [1–9]. Pions are qualitatively different from other mesons since they become massless in the limit of massless quarks, thereby producing long-range exchange interactions. The low-energy expansion of chiral EFT is organized in powers of Q, where Q denotes the typical momentum of the nucleons as well as explicit factors of the pion mass. The most important interactions are called leading order (LO) or $O(Q^0)$. The next most important contributions are next-to-leading order (NLO) or $O(Q^2)$. The terms after this are next-to-next-to-leading order (NNLO) or $O(Q^3)$, and so on.

Lattice EFT refers generally to lattice simulations based upon the framework of effective field theory. There are a few reviews in the literature which discuss current methods used in lattice effective field theory [10, 11] as well as the discussion in the previous chapter of this volume. Many different phenomena can be studied in lattice EFT using the same lattice action. In principle all systematic errors are introduced up front when defining the low-energy effective theory, as opposed to the particular computational scheme used to calculate observables.

Lattice EFT has been aided by efficient lattice methods developed for lattice QCD and condensed matter applications. The methods include Markov Chain Monte Carlo techniques,

Dean Lee

Department of Physics, North Carolina State University, Raleigh, NC 27695, USA, e-mail: `dean_lee@nscu.edu`

auxiliary fields [12, 13], pseudofermion methods [14], and non-local updating schemes such as the hybrid Monte Carlo algorithm [15–17]. Lattice EFT was first used in studies of infinite nuclear matter [18] and infinite neutron matter with and without explicit pions [19–22]. The method has also been used to study light nuclei in pionless EFT [23] and chiral EFT at leading order [24]. There have been further studies of neutron matter [25–27] and light nuclei [28,29], and there have been several applications to nuclear structure and nuclear clustering [30–35] as well as recent work on nuclear scattering and reactions [36–38].

6.2 Scattering on the lattice

At any given order in the chiral EFT expansion, there will be short-range interaction coefficients which depend on the chosen regularization of the large-momentum divergences. On the lattice this regularization is provided by the lattice spacing, unless some additional regularization is applied to the lattice interactions. In order to set the values of the short-range two-nucleon interaction coefficients, we make a comparison of nucleon-nucleon scattering on the lattice with experimental scattering data. The extension to three-nucleon interaction coefficients is also required at NNLO, and that procedure on the lattice has been discussed in Ref. [28]

As discussed in the previous chapter, Lüscher [39–41] has shown that the finite-volume energy levels for a two-body system in a periodic cubic box are related to the infinite-volume scattering matrix. While the method is very useful at low momenta, it can become less accurate at higher momenta and higher orbital angular momenta. Also spin-orbit coupling and partial-wave mixing are difficult to measure accurately using Lüscher's method due to scattering artifacts produced by the cubic periodic boundary. An alternative approach has been developed to measure phase shifts for particles on the lattice using a spherical wall boundary [42, 43].

In this approach, a hard spherical wall boundary is imposed on the relative separation between the two particles. This wall is placed at some chosen radius R_{wall}, and it removes copies of the interactions produced by the periodic lattice. Working in the center-of-mass frame, we solve the time-independent Schrödinger equation as a function of the relative separation between the particles and compute spherical standing waves which vanish at $r = R_{\text{wall}}$. At values of r beyond the range of the interaction, the spherical standing waves can be written as a superposition of products of spherical harmonics and spherical Bessel functions,

$$[\cos \delta_\ell \cdot j_\ell(kr) - \sin \delta_\ell \cdot y_\ell(kr)] Y_{\ell,\ell_z}(\theta, \phi). \tag{6.1}$$

Here k is the relative momentum between the scattering particles, and δ_ℓ is the phase shift for partial wave L. We can extract k from the energy of the standing wave, and the phase shift δ_ℓ is determined by setting the wave function in Eq. (6.1) to zero at the wall boundary.

When the total intrinsic spin of the two nucleons is nonzero, spin-orbit coupling generates mixing between partial waves. In this case the standing wave at the wall boundary is decomposed into spherical harmonics and coupled-channel equations are solved to extract the phase shifts and mixing angles. The spherical wall method was used to calculate phase shifts and mixing angle for low-energy nucleon-nucleon scattering [25]. Recently the spherical wall approach has been improved in accuracy and computational efficiency [44]. In the improved approach one projects onto spherical harmonics Y_{ℓ,ℓ_z} with angular momentum quantum numbers ℓ, ℓ_z. In this manner one constructs radial position states for a given partial wave,

$$|r\rangle^{\ell,\ell_z} = \sum_{\mathbf{r}'} Y_{\ell,\ell_z}(\hat{\mathbf{r}}') \delta_{r,|\mathbf{r}'|} |\mathbf{r}'\rangle. \tag{6.2}$$

We require that r is less than half the box length $L/2$. Using this technique we are essentially constructing a radial lattice Hamiltonian for each partial wave.

It is also useful to introduce auxiliary potentials in the region lying just in front of the spherical wall boundary [44]. We use the auxiliary potential to tune the energy of the scattering wave. This auxiliary potential is a spherical attractive well positioned in front of the spherical wall boundary. We can tune to any scattering energy by adjusting the depth of the well. For systems with partial wave mixing due to spin-orbit coupling, we also include a Hermitian but imaginary off-diagonal auxiliary potential for the two coupled channels. This breaks time reversal symmetry, and the resulting standing wave solutions now have both real and imaginary parts that are linearly independent. From the real and imaginary solutions one can determine the scattering phase shifts and mixing angle at any given value of the scattering energy.

This spherical wall approach has been used together with a technique called the adiabatic projection method to study nuclear scattering and reactions on the lattice. The adiabatic projection method [35,38,45–47] is a general framework that produces a low-energy effective theory for clusters of particles which becomes exact in the limit of large projection time. For the case of two-cluster scattering, we consider a set of two cluster states $|\mathbf{R}\rangle$ labeled by the spatial separation vector $\mathbf{R}$. The initial wave functions are wave packets which, for large $|\mathbf{R}|$, factorize into a product of two individual clusters,

$$|\mathbf{R}\rangle = \sum_{\mathbf{r}} |\mathbf{r} + \mathbf{R}\rangle_1 \otimes |\mathbf{r}\rangle_2. \tag{6.3}$$

The summation over $\mathbf{r}$ is required to produce states with total momentum equal to zero. We bin the initial cluster states together according to radial distance and angular momentum. In this manner, we form radial position states with projected angular momentum quantum numbers, which we label $|R\rangle^{J,J_z}$.

The next step is to multiply by powers of the transfer matrix in order to form "dressed" cluster states. This produces states that approximately span the set of low-energy cluster-cluster scattering states in our periodic box. We discuss the transfer matrix formalism in detail later in this chapter. After n_t time steps, we have the dressed cluster states

$$|R\rangle^{J,J_z}_{n_t} = M^{n_t} |R\rangle^{J,J_z}. \tag{6.4}$$

These dressed cluster states are then used to compute matrix elements of the transfer matrix M,

$$[M_{n_t}]^{J,J_z}_{R',R} = {}^{J,J_z}_{n_t}\langle R'|M|R\rangle^{J,J_z}_{n_t}. \tag{6.5}$$

Since such states are not orthogonal, we also compute a norm matrix

$$[N_{n_t}]^{J,J_z}_{R',R} = {}^{J,J_z}_{n_t}\langle R'|R\rangle^{J,J_z}_{n_t}. \tag{6.6}$$

The "radial adiabatic transfer matrix" is defined as the matrix product

$$\left[M^a_{n_t}\right]^{J,J_z}_{R',R} = \left[N^{-\frac{1}{2}}_{n_t} M_{n_t} N^{-\frac{1}{2}}_{n_t}\right]^{J,J_z}_{R',R}, \tag{6.7}$$

and the scattering phase shifts can then be determined from the standing waves of the radial adiabatic transfer matrix.

6.3 Lattice formalisms

Throughout our discussion of the lattice formalism we use dimensionless parameters and operators corresponding with physical values times the appropriate power of the spatial lattice spacing a. In our notation the three-component integer vector $\mathbf{n}$ labels the lattice sites of a three-dimensional periodic lattice with dimensions L^3. The spatial lattice unit vectors are denoted $\hat{\mathbf{l}} = \hat{1}, \hat{2}, \hat{3}$. We use n_t to label lattice steps in the temporal direction, and L_t denotes the total number of lattice time steps. The temporal lattice spacing is given by a_t, and $\alpha_t = a_t/a$ is the ratio of the temporal to spatial lattice spacing. We also define $h = \alpha_t/(2m)$, where m is the nucleon mass in lattice units. In Fig. 6.1 we show a diagram of the four different but exactly equivalent lattice formulations that we discuss, the Grassmann path integral, transfer matrix operator, Grassmann path integral with auxiliary fields, and transfer matrix operator with auxiliary fields.

6.3.1 Grassmann path integral

We define the lattice action starting from the lattice Grassmann path integral action without auxiliary fields. This is the simplest formulation in which to derive the lattice Feynman rules. We let c and c^* be anticommuting Grassmann fields for the nucleons. In our notation c is a column vector composed of the spin-isospin nucleon degrees of freedom c_i, while c^* is a row vector of the components c_i^*. The Grassmann fields are periodic with respect to the spatial extent of the L^3 lattice,

$$c_i(\mathbf{n}+L\hat{1},n_t) = c_i(\mathbf{n}+L\hat{2},n_t) = c_i(\mathbf{n}+L\hat{3},n_t) = c_i(\mathbf{n},n_t), \tag{6.8}$$

$$c_i^*(\mathbf{n}+L\hat{1},n_t) = c_i^*(\mathbf{n}+L\hat{2},n_t) = c_i^*(\mathbf{n}+L\hat{3},n_t) = c_i^*(\mathbf{n},n_t), \tag{6.9}$$

and antiperiodic along the temporal direction,

$$c_i(\mathbf{n},n_t+L_t) = -c_i(\mathbf{n},n_t), \tag{6.10}$$

$$c_i^*(\mathbf{n},n_t+L_t) = -c_i^*(\mathbf{n},n_t). \tag{6.11}$$

We write $DcDc^*$ as shorthand for the integral measure,

Grassmann path integral $\exp[-S(c,c^*)]$	$=$	Transfer matrix operator M
$\parallel$		$\parallel$
Grassmann path integral with auxiliary field $\exp[-S(c,c^*,s)]$	$=$	Transfer matrix operator with auxiliary field $M^{(n_t)}(s)$
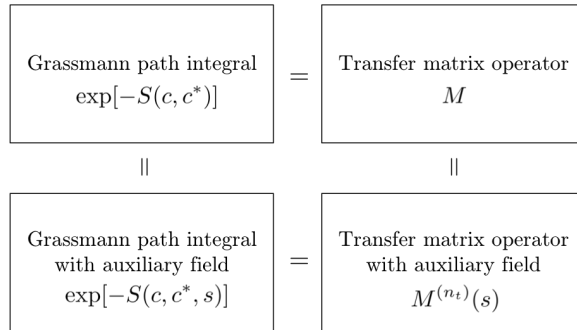
Fig. 6.1 A schematic diagram of the different lattice formulations, namely, the Grassmann path integral, transfer matrix operator, Grassmann path integral with auxiliary fields, and transfer matrix operator with auxiliary fields.

$$DcDc^* = \prod_{\mathbf{n},n_t,i} dc_i(\mathbf{n},n_t)dc_i^*(\mathbf{n},n_t). \tag{6.12}$$

We use the usual convention for Grassmann integration,

$$\int dc_i(\mathbf{n},n_t) = \int dc_i^*(\mathbf{n},n_t) = 0, \tag{6.13}$$

$$\int dc_i(\mathbf{n},n_t)c_i(\mathbf{n},n_t) = \int dc_i^*(\mathbf{n},n_t)c_i^*(\mathbf{n},n_t) = 1 \quad \text{(no sum on } i\text{)}. \tag{6.14}$$

We consider the Grassmann path integral

$$\mathscr{Z} = \int DcDc^* \exp\left[-S(c^*,c)\right], \tag{6.15}$$

where the lattice action can be broken into a free part and interacting part,

$$S(c^*,c) = S_{\text{free}}(c^*,c) + S_{\text{int}}(c^*,c). \tag{6.16}$$

The free part is the free non-relativistic nucleon action, which is

$$S_{\text{free}}(c^*,c) = \sum_{\mathbf{n},n_t} c^*(\mathbf{n},n_t)\left[c(\mathbf{n},n_t+1) - c(\mathbf{n},n_t)\right] + \alpha_t \sum_{n_t} K^{(n_t)}(c^*,c), \tag{6.17}$$

where

$$K^{(n_t)}(c^*,c) = \sum_{k=0,1,2,\cdots} (-1)^k \frac{w_k}{2m} \sum_{\mathbf{n},\hat{\mathbf{l}}} c^*(\mathbf{n},n_t)\left[c(\mathbf{n}+k\hat{\mathbf{l}},n_t) + c(\mathbf{n}-k\hat{\mathbf{l}},n_t)\right], \tag{6.18}$$

and the hopping coefficients w_k correspond to a hopping parameter expansion of the squared momentum,

$$P^2(\mathbf{p}) = 2 \sum_{k=0,1,2,\cdots} \sum_{l=1,2,3} (-1)^k w_k \cos\left(kp_l\right). \tag{6.19}$$

The hopping coefficients can be chosen to match the continuum relation

$$P^2(\mathbf{p}) = \mathbf{p}^2, \tag{6.20}$$

up to some chosen level of lattice discretization error. The hopping coefficients w_k for a few different lattice actions are shown in Table 6.1.

Table 6.1 Hopping coefficients w_k for several lattice actions

coefficient	standard	$O(a^2)$-improved	$O(a^4)$-improved
w_0	1	5/4	49/36
w_1	1	4/3	3/2
w_2	0	1/12	3/20
w_3	0	0	1/90

6.3.2 Transfer matrix operator

Let $a_i(\mathbf{n})$ and $a_i^\dagger(\mathbf{n})$ denote fermion annihilation and creation operators for the nucleon component i at lattice site $\mathbf{n}$. The shorthand $a(\mathbf{n})$ represents a column vector of nucleon components $a_i(\mathbf{n})$, and $a^\dagger(\mathbf{n})$ represents a row vector of components $a_i^\dagger(\mathbf{n})$. We can write any Grassmann path integral with instantaneous interactions as the trace of a product of operators using the identity [48, 49]

$$
\mathrm{Tr}\left\{\,:F_{L_t-1}\left[a^\dagger(\mathbf{n}'),a(\mathbf{n})\right]:\,\times\cdots\times:F_0\left[a^\dagger(\mathbf{n}'),a(\mathbf{n})\right]:\,\right\}
$$
$$
=\int DcDc^*\exp\left\{\sum_{n_t=0}^{L_t-1}\sum_{\mathbf{n},i}c_i^*(\mathbf{n},n_t)\left[c_i(\mathbf{n},n_t)-c_i(\mathbf{n},n_t+1)\right]\right\}
$$
$$
\times\prod_{n_t=0}^{L_t-1}F_{n_t}\left[c^*(\mathbf{n}',n_t),c(\mathbf{n},n_t)\right],
\tag{6.21}
$$

where $c_i(\mathbf{n},L_t)=-c_i(\mathbf{n},0)$.

Let us define the free non-relativistic lattice Hamiltonian

$$
H_{\mathrm{free}}(a^\dagger,a)=\sum_{k=0,1,2,\cdots}(-1)^k\frac{w_k}{2m}\sum_{\mathbf{n},\hat{\mathbf{l}}}a^\dagger(\mathbf{n})\left[a(\mathbf{n}+k\hat{\mathbf{l}})+a(\mathbf{n}-k\hat{\mathbf{l}})\right].
\tag{6.22}
$$

We write the interaction term as $H_{\mathrm{int}}(a^\dagger,a)$, so that our total Hamiltonian is

$$
H(a^\dagger,a)=H_{\mathrm{free}}(a^\dagger,a)+H_{\mathrm{int}}(a^\dagger,a).
\tag{6.23}
$$

Using the correspondence Eq. (6.21), we can rewrite the path integral $\mathscr{Z}$ defined in Eq. (6.15) as a transfer-matrix partition function,

$$
\mathscr{Z}=\mathrm{Tr}\left(M^{L_t}\right),
\tag{6.24}
$$

where M is the normal-ordered transfer matrix operator

$$
M=:\exp\left[-H(a^\dagger,a)\alpha_t\right]:.
\tag{6.25}
$$

Roughly speaking, the transfer matrix operator is the exponential of the Hamiltonian operator over one Euclidean lattice time step. In order to satisfy the identity Eq. (6.21), the exact definition of the transfer matrix is the normal-ordered exponential as defined in Eq. (6.25).

In this transfer matrix formalism, one can do simulations of nucleons using Monte Carlo, and this would essentially be a lattice version of diffusion or Green's function Monte Carlo [50]. Visually one can view the nucleons as interacting with each other while diffusing in space with each time step, as indicated in Fig. 6.2. At leading order in chiral effective field theory, the interactions include two independent S-wave contact interactions and the exchange of pions. We discuss these interactions in detail in the following.

6.3.3 Grassmann path integral with auxiliary field

We now assume that there exists an integral relation that allows us to write $\exp\left[-S_{\mathrm{int}}(c^*,c)\right]$ as an integral over auxiliary fields. The purpose of the auxiliary field transformation is to decouple the interactions among the nucleons. Instead the interactions will be between the nucleons and the auxiliary fields.
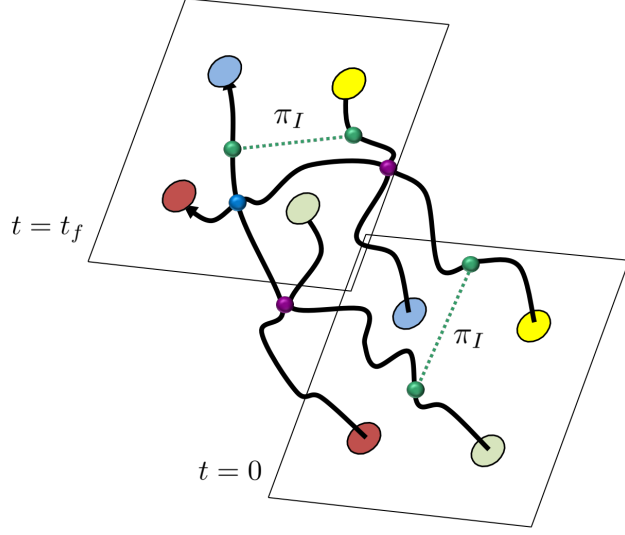
Fig. 6.2 A sketch showing nucleons which evolve with each time step. At leading order in chiral effective field theory, the interactions include two contact interactions and the exchange of pions.

We now illustrate using the interactions that appear at leading order in chiral effective field theory. For pedagogical purposes we discuss the simplest possible implementation of the leading order action on the lattice. We first consider a zero-range contact interaction which is independent of nucleon spin and isospin. The action has the form

$$S_{\text{int}}^{C}(c^*,c) = \alpha_t \frac{C}{2} \sum_{\mathbf{n},n_t} [c^*(\mathbf{n},n_t)c(\mathbf{n},n_t)]^2 . \tag{6.26}$$

We can write this as

$$\exp\left[-S_{\text{int}}^{C}(c^*,c)\right] = \int Ds \, \exp\left[-S_{ss}(s) - S_s(c^*,c,s)\right] \tag{6.27}$$

for auxiliary field $s(\mathbf{n},n_t)$, where

$$S_{ss}(s) = \frac{1}{2} \sum_{\mathbf{n},n_t} s^2(\mathbf{n},n_t), \tag{6.28}$$

$$S_s(c^*,c,s) = \sqrt{-C\alpha_t} \sum_{\mathbf{n},n_t} s(\mathbf{n},n_t)c^*(\mathbf{n},n_t)c(\mathbf{n},n_t). \tag{6.29}$$

In our definition of the integration measure Ds, we include a factor of $1/\sqrt{2\pi}$ for each degree of freedom.

Next we consider an isospin-dependent contact interaction

$$S_{\text{int}}^{C'}(c^*,c) = \alpha_t \frac{C'}{2} \sum_{\mathbf{n},n_t,I} [c^*(\mathbf{n},n_t)\tau_I c(\mathbf{n},n_t)]^2 , \tag{6.30}$$

where τ_I for $I = 1,2,3$ are the Pauli matrices in isospin space. Then we can use

$$\exp\left[-S_{\text{int}}^{C'}(c^*,c)\right] = \int \prod_I Ds_I \exp\left[-S_{s_I s_I}(s_I) - S_{s_I}(c^*,c,s_I)\right] \tag{6.31}$$

for auxiliary fields $s_I(\mathbf{n},n_t)$ where

$$S_{S_I S_I}(s_I) = \frac{1}{2} \sum_{\mathbf{n},n_t,I} s_I^2(\mathbf{n},n_t), \tag{6.32}$$

$$S_{S_I}(c^*,c,s_I) = \sqrt{-C'\alpha_t} \sum_{\mathbf{n},n_t,I} s_I(\mathbf{n},n_t) c^*(\mathbf{n},n_t) \tau_I c(\mathbf{n},n_t). \tag{6.33}$$

Finally we work with the one-pion exchange potential (OPEP). In this case the pion acts much like the auxiliary fields. However there are also spatial correlations in the quadratic part of the pion action and a gradient coupling between the pions and nucleons. The one-pion exchange interaction on the lattice can written as

$$\exp\left[-S_{\text{int}}^{\text{OPEP}}(c^*,c)\right] = \int \prod_I D\pi_I \exp\left[-S_{\pi_I \pi_I}(\pi_I) - S_{\pi_I}(c^*,c,\pi_I)\right]. \tag{6.34}$$

The free pion action is

$$S_{\pi_I \pi_I}(\pi_I) = \frac{1}{2}\alpha_t m_\pi^2 \sum_{\mathbf{n},n_t,I} \pi_I^2(\mathbf{n},n_t) \tag{6.35}$$

$$+ \frac{1}{2}\alpha_t \sum_{k=0,1,2,\cdots} (-1)^k w_k \sum_{\mathbf{n},n_t,I,\hat{\mathbf{l}}} \pi_I(\mathbf{n},n_t)\left[\pi_I(\mathbf{n}+k\hat{\mathbf{l}},n_t) + \pi_I(\mathbf{n}-k\hat{\mathbf{l}},n_t)\right], \tag{6.36}$$

with the coefficient w_k as defined in Table 6.1 and m_π is the pion mass. At leading order we do not consider any isospin-breaking effects. The pion coupling to the nucleon is

$$S_{\pi_I}(c^*,c,\pi_I) = \frac{g_A \alpha_t}{2f_\pi} \sum_{\mathbf{n},n_t,l,I} \Delta_k \pi_I(\mathbf{n},n_t) c^*(\mathbf{n},n_t) \sigma_k \tau_I c(\mathbf{n},n_t), \tag{6.37}$$

where σ_l for $l = 1,2,3$ are the Pauli matrices in spin space and

$$\Delta_l \pi_I(\mathbf{n},n_t) = \frac{1}{2} \sum_{k=1,2,\cdots} (-1)^{k-1} o_k \left[\pi_I(\mathbf{n}+k\hat{\mathbf{l}},n_t) - \pi_I(\mathbf{n}-k\hat{\mathbf{l}},n_t)\right], \tag{6.38}$$

with coefficients o_k corresponding to a hopping parameter expansion of the momentum,

$$P(p_l) = \sum_{k=1,2,\cdots} (-1)^{k-1} o_k \sin(k p_l). \tag{6.39}$$

Here g_A is the axial-vector coupling constant, and f_π is the pion decay constant. The hopping coefficients can be chosen to match the continuum result

$$P(p_l) = p_l. \tag{6.40}$$

The hopping coefficients o_k for a few different lattice actions are shown in Table 6.2.

Table 6.2 Hopping coefficients o_k for several lattice actions.

coefficent	standard	$O(a^2)$-improved	$O(a^4)$-improved
o_1	1	4/3	3/2
o_2	0	1/6	3/10
o_3	0	0	1/30

6.3.4 Transfer matrix operator with auxiliary field

Using the equivalence in Eq. (6.21), we can write $\mathscr{Z}$ as the trace of a product of transfer matrix operators which depend on the auxiliary field,

$$\mathscr{Z} = \int Ds \prod_I (Ds_I D\pi_I) \, \exp\left[-S_{ss}(s) - S_{s_I s_I}(s_I) - S_{\pi_I \pi_I}(\pi_I)\right] \mathrm{Tr}\left\{M^{(L_t-1)} \cdots M^{(0)}\right\}. \tag{6.41}$$

The transfer matrix at time step n_t is given by

$$M^{(n_t)} =: \, \exp\left[-H^{(n_t)}(a^\dagger, a, s, s_I, \pi_I)\alpha_t\right] : \, , \tag{6.42}$$

where

$$H^{(n_t)}(a^\dagger, a, s, s_I, \pi_I)\alpha_t = H_{\text{free}}(a^\dagger, a)\alpha_t + S_s^{(n_t)}(a^\dagger, a, s) + S_{s_I}^{(n_t)}(a^\dagger, a, s_I) + S_{\pi_I}^{(n_t)}(a^\dagger, a, \pi_I), \tag{6.43}$$

and

$$S_s^{(n_t)}(a^\dagger, a, s) = \sqrt{-C\alpha_t} \sum_{\mathbf{n}} s(\mathbf{n}, n_t) a^\dagger(\mathbf{n}) a(\mathbf{n}), \tag{6.44}$$

$$S_{s_I}^{(n_t)}(a^\dagger, a, s_I) = \sqrt{-C'\alpha_t} \sum_{\mathbf{n}, I} s_I(\mathbf{n}, n_t) a^\dagger(\mathbf{n}) \tau_I a(\mathbf{n}), \tag{6.45}$$

$$S_{\pi_I}^{(n_t)}(a^\dagger, a, \pi_I) = \frac{g_A \alpha_t}{2 f_\pi} \sum_{\mathbf{n}, k, I} \Delta_k \pi_I(\mathbf{n}, n_t) a^\dagger(\mathbf{n}) \sigma_k \tau_I a(\mathbf{n}). \tag{6.46}$$

6.4 Projection Monte Carlo

Let us consider a system with A nucleons. We can create a general single-nucleon state using creation operators acting on the vacuum with coefficient function $f(\mathbf{n})$. We write $f(\mathbf{n})$ as a column vector in the space of nucleon spin and isospin components, and the single-nucleon state can be written as

$$|f\rangle = \sum_{\mathbf{n}} a^\dagger(\mathbf{n}) f(\mathbf{n}) |0\rangle. \tag{6.47}$$

For our projection Monte Carlo calculation we take our A-body initial state to be a Slater determinant of single nucleon states,

$$|f_1, \cdots, f_A\rangle = \left[\sum_{\mathbf{n}} a^\dagger(\mathbf{n}) f_1(\mathbf{n})\right] \cdots \left[\sum_{\mathbf{n}} a^\dagger(\mathbf{n}) f_A(\mathbf{n})\right] |0\rangle. \tag{6.48}$$

We use the same construction for the *A*-body final state.

For the purposes of coding the projection Monte Carlo calculation, it is convenient to view the identical nucleons as having a hidden index $j = 1, \cdots, A$ that makes all of the nucleons distinguishable. If we antisymmetrize all physical states over this extra index then all physical observables are exactly recovered. So our initial state $|f_1, \cdots, f_A\rangle$ becomes

$$\frac{1}{\sqrt{A!}} \sum_P \left[\sum_{\mathbf{n}} a^\dagger_{[P(1)]}(\mathbf{n}) f_1(\mathbf{n})\right] \cdots \left[\sum_{\mathbf{n}} a^\dagger_{[P(A)]}(\mathbf{n}) f_A(\mathbf{n})\right] |0\rangle$$

$$= \frac{1}{\sqrt{A!}} \sum_{P'} \mathrm{sgn}(P') \left[\sum_{\mathbf{n}} a^\dagger_{[1]}(\mathbf{n}) f_{P'(1)}(\mathbf{n})\right] \cdots \left[\sum_{\mathbf{n}} a^\dagger_{[A]}(\mathbf{n}) f_{P'(A)}(\mathbf{n})\right] |0\rangle, \tag{6.49}$$
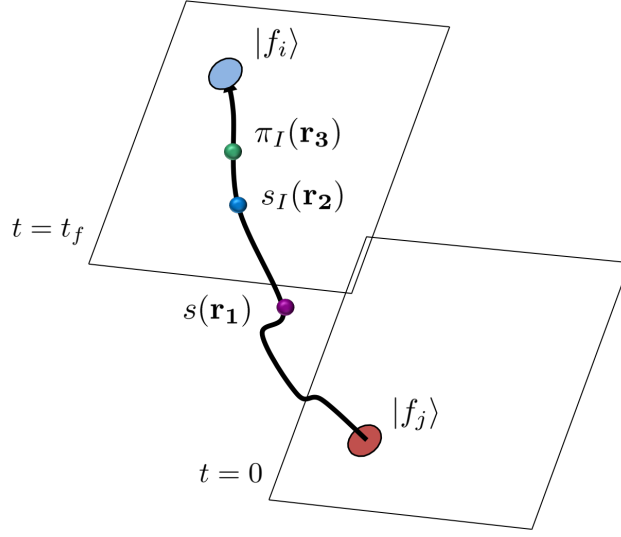
Fig. 6.3 A sketch showing the worldline for a single nucleon with a background of pion fields and auxiliary fields.

where the summations are over all permutations P, and sgn is the sign of the permutation. With these hidden indices our normal-ordered auxiliary-field transfer matrix $M^{(n_t)}$ becomes

$$\left[1 - H^{(n_t)}(a^\dagger_{[1]}, a_{[1]}, s, s_I, \pi_I)\alpha_t\right] \cdots \left[1 - H^{(n_t)}(a^\dagger_{[A]}, a_{[A]}, s, s_I, \pi_I)\alpha_t\right] \tag{6.50}$$

We see that the higher-order powers of the exponential vanish due to normal ordering.

In the projection Monte Carlo calculation we compute the amplitude

$$Z(n_t) = \langle f_1, \cdots, f_A | M^{(n_t-1)} \cdots M^{(0)} | f_1, \cdots, f_A \rangle \tag{6.51}$$

for $n_t = L_t$ and $n_t = L_t - 1$. In the limit of large L_t the amplitudes will be dominated by the state with the lowest energy E_0 and nonzero overlap with $|f_1, \cdots, f_A\rangle$. In this limit the ratio $Z(n_t)/Z(n_t - 1)$ will converge to $\exp(-E_0\alpha_t)$ from above.

Each nucleon evolves as a particle in a fluctuating background of auxiliary fields and pion fields. The original interactions are reproduced after integrating over the fluctuating auxiliary and pion fields. For a simulation with A nucleons, the amplitude for a given configuration of pion and auxiliary fields is proportional to the determinant of an $A \times A$ matrix $\mathbf{M}$. The entries of $\mathbf{M}_{ij}$ are single nucleon worldline amplitudes for a nucleon starting at state $|f_j\rangle$ at $t = 0$ and ending at state $|f_i\rangle$ at $t = t_f = L_t\alpha_t$. This is shown in Fig. 6.3.

In Fig. 6.4, we show a sample code which calculates the auxiliary-field transfer matrix multiplications on the left starting from the single-nucleon initial states. We only show the terms which arise from the free-nucleon transfer matrix and the auxiliary field s. Similarly, in Fig. 6.5, we show a sample code which calculates the auxiliary-field transfer matrix multiplications on the right starting from the single-nucleon final states. Again we present only the terms arising from the free-nucleon transfer matrix and the auxiliary field s. In Fig. 6.6 we show how these transfer matrix product multiplications are implemented as functions or subroutines (specific to Fortran as programming language) and used to compute the determinant and inverse of the matrix of single-nucleon amplitudes $\mathbf{M}$.

6.5 Importance sampling

We do importance sampling according to the positive measure

```
DO nt = nt1+1, nt2
  DO np = 0,num-1
    DO nz = 0,L-1; DO ny = 0,L-1; DO nx = 0,L-1
      DO ni = 0,1; DO ns = 0,1

        zvecs(nx,ny,nz,nt,ns,ni,np) = zvecs(nx,ny,nz,nt-1,ns,ni,np) &
            * (1.D0-6.D0*w0_N*h+CDSQRT(-c0*atovera*(1.D0,0.D0)))*s(nx,ny,nz,nt-1))

        zvecs(nx,ny,nz,nt,ns,ni,np) = zvecs(nx,ny,nz,nt,ns,ni,np) &
            + w1_N*h*zvecs(MOD(nx+1,L),ny,nz,nt-1,ns,ni,np) &
            + w1_N*h*zvecs(MOD(nx-1+L,L),ny,nz,nt-1,ns,ni,np) &
            + w1_N*h*zvecs(nx,MOD(ny+1,L),nz,nt-1,ns,ni,np) &
            + w1_N*h*zvecs(nx,MOD(ny-1+L,L),nz,nt-1,ns,ni,np) &
            + w1_N*h*zvecs(nx,ny,MOD(nz+1,L),nt-1,ns,ni,np) &
            + w1_N*h*zvecs(nx,ny,MOD(nz-1+L,L),nt-1,ns,ni,np)

        IF (improveN >= 1) THEN
          zvecs(nx,ny,nz,nt,ns,ni,np) = zvecs(nx,ny,nz,nt,ns,ni,np) &
              - w2_N*h*zvecs(MOD(nx+2,L),ny,nz,nt-1,ns,ni,np) &
              - w2_N*h*zvecs(MOD(nx-2+L,L),ny,nz,nt-1,ns,ni,np) &
              - w2_N*h*zvecs(nx,MOD(ny+2,L),nz,nt-1,ns,ni,np) &
              - w2_N*h*zvecs(nx,MOD(ny-2+L,L),nz,nt-1,ns,ni,np) &
              - w2_N*h*zvecs(nx,ny,MOD(nz+2,L),nt-1,ns,ni,np) &
              - w2_N*h*zvecs(nx,ny,MOD(nz-2+L,L),nt-1,ns,ni,np)
        END IF

        IF (improveN == 2) THEN
          zvecs(nx,ny,nz,nt,ns,ni,np) = zvecs(nx,ny,nz,nt,ns,ni,np) &
              + w3_N*h*zvecs(MOD(nx+3,L),ny,nz,nt-1,ns,ni,np) &
              + w3_N*h*zvecs(MOD(nx-3+L,L),ny,nz,nt-1,ns,ni,np) &
              + w3_N*h*zvecs(nx,MOD(ny+3,L),nz,nt-1,ns,ni,np) &
              + w3_N*h*zvecs(nx,MOD(ny-3+L,L),nz,nt-1,ns,ni,np) &
              + w3_N*h*zvecs(nx,ny,MOD(nz+3,L),nt-1,ns,ni,np) &
              + w3_N*h*zvecs(nx,ny,MOD(nz-3+L,L),nt-1,ns,ni,np)
        END IF

      END DO; END DO
    END DO; END DO; END DO
  END DO
END DO
```

Fig. 6.4 Sample code which calculates the auxiliary-field transfer matrix multiplications on the left starting from the single-nucleon initial states. We only show the terms which arise from the free-nucleon transfer matrix and the auxiliary field s.

$$|Z(L_t)|\exp\left[-S_{ss}(s)-S_{s_I s_I}(s_I)-S_{\pi_I \pi_I}(\pi_I)\right], \tag{6.52}$$

and use hybrid Monte Carlo to do global updates of the auxiliary and pion fields. The hybrid Monte Carlo (HMC) algorithm [15–17] is efficient in quickly generating decorrelated configurations for each auxiliary and pion field. Here we describe the updating algorithm for the s field. The updating of the s_I and π_I fields proceed in a very similar fashion. In general terms, the HMC algorithm can be described by means of a probability weight $P(s)$

$$P(s) \propto \exp[-V(s)], \tag{6.53}$$

where $V(s)$ is in general a non-local function of the field $s(\mathbf{n},n_t)$, and a molecular dynamics (MD) Hamiltonian,

$$H(s,p) \equiv \frac{1}{2}\sum_{\mathbf{n},n_t}[p_s(\mathbf{n},n_t)]^2 + V(s). \tag{6.54}$$

Classical Hamiltonian dynamics is introduced by defining the momentum $p_s(\mathbf{n},n_t)$ conjugate to $s(\mathbf{n},n_t)$.

```
DO nt = nt2,nt1+1,-1

   DO np = 0,num-1
      DO nz = 0,L-1; DO ny = 0,L-1; DO nx = 0,L-1
         DO ni = 0,1; DO ns = 0,1

            zdualvecs(nx,ny,nz,nt-1,ns,ni,np) = zdualvecs(nx,ny,nz,nt,ns,ni,np) &
               * (1.D0-6.D0*w0_N*h+CDSQRT(-c0*atovera*(1.D0,0.D0)))*s(nx,ny,nz,nt-1))

            zdualvecs(nx,ny,nz,nt-1,ns,ni,np) = zdualvecs(nx,ny,nz,nt-1,ns,ni,np) &
                + w1_N*h*zdualvecs(MOD(nx+1,L),ny,nz,nt,ns,ni,np) &
                + w1_N*h*zdualvecs(MOD(nx-1+L,L),ny,nz,nt,ns,ni,np) &
                + w1_N*h*zdualvecs(nx,MOD(ny+1,L),nz,nt,ns,ni,np) &
                + w1_N*h*zdualvecs(nx,MOD(ny-1+L,L),nz,nt,ns,ni,np) &
                + w1_N*h*zdualvecs(nx,ny,MOD(nz+1,L),nt,ns,ni,np) &
                + w1_N*h*zdualvecs(nx,ny,MOD(nz-1+L,L),nt,ns,ni,np)

            IF (improveN >= 1) THEN
               zdualvecs(nx,ny,nz,nt-1,ns,ni,np) = zdualvecs(nx,ny,nz,nt-1,ns,ni,np) &
                   - w2_N*h*zdualvecs(MOD(nx+2,L),ny,nz,nt,ns,ni,np) &
                   - w2_N*h*zdualvecs(MOD(nx-2+L,L),ny,nz,nt,ns,ni,np) &
                   - w2_N*h*zdualvecs(nx,MOD(ny+2,L),nz,nt,ns,ni,np) &
                   - w2_N*h*zdualvecs(nx,MOD(ny-2+L,L),nz,nt,ns,ni,np) &
                   - w2_N*h*zdualvecs(nx,ny,MOD(nz+2,L),nt,ns,ni,np) &
                   - w2_N*h*zdualvecs(nx,ny,MOD(nz-2+L,L),nt,ns,ni,np)
            END IF

            IF (improveN == 2) THEN
               zdualvecs(nx,ny,nz,nt-1,ns,ni,np) = zdualvecs(nx,ny,nz,nt-1,ns,ni,np) &
                   + w3_N*h*zdualvecs(MOD(nx+3,L),ny,nz,nt,ns,ni,np) &
                   + w3_N*h*zdualvecs(MOD(nx-3+L,L),ny,nz,nt,ns,ni,np) &
                   + w3_N*h*zdualvecs(nx,MOD(ny+3,L),nz,nt,ns,ni,np) &
                   + w3_N*h*zdualvecs(nx,MOD(ny-3+L,L),nz,nt,ns,ni,np) &
                   + w3_N*h*zdualvecs(nx,ny,MOD(nz+3,L),nt,ns,ni,np) &
                   + w3_N*h*zdualvecs(nx,ny,MOD(nz-3+L,L),nt,ns,ni,np)
            END IF

         END DO; END DO
      END DO; END DO; END DO
   END DO
```

Fig. 6.5 Sample code which calculates auxiliary-field transfer matrix multiplications on the right starting from the single-nucleon final states. We only show terms involving the free-nucleon transfer matrix and the auxiliary field s.

Fig. 6.6 Sample code showing how the transfer matrix product multiplications are called as functions or subroutines and used to compute the determinant and inverse of the matrix of single-nucleon amplitudes.

```
CALL getzvecs(s,sI,zvecs,zwave,Lt,0, &
     pion,ztau2x2,n_f)
CALL getzdualvecs(s,sI,zdualvecs,zdualwave, &
     Lt,0,pion,ztau2x2,n_f)
CALL getinvcorr(zvecs,zdualvecs,zldeter, &
     zcorrmatrix,zcorrinv,Lt)
aldeterabs = DBLE(zldeter)
zdeterphase = CDEXP((0.D0,1.D0)*DIMAG(zldeter))
act = bose - aldeterabs
```

Given an arbitrary initial configuration $s^0(\mathbf{n}, n_t)$, the conjugate momentum is chosen from a random Gaussian distribution according to

$$P[p_s^0(\mathbf{n}, n_t)] \propto \exp\left\{ -\frac{1}{2}\left[p_s^0(\mathbf{n}, n_t)\right]^2 \right\}, \tag{6.55}$$

after which the Hamiltonian equations of motion are integrated numerically with a small but nonzero step size $\varepsilon_{\text{step}}$. This method begins with a "half-step" forward in the conjugate momentum,

$$\tilde{p}_s^0(\mathbf{n},n_t) = p_s^0(\mathbf{n},n_t) - \frac{\varepsilon_{\text{step}}}{2}\left[\frac{\partial V(s)}{\partial s(\mathbf{n},n_t)}\right]_{s=s^0}, \tag{6.56}$$

followed by repeated updates of s and $\tilde{p}_s$ according to

$$s^{i+1}(\mathbf{n},n_t) = s^i(\mathbf{n},n_t) + \varepsilon_{\text{step}}\tilde{p}_s^i(\mathbf{n},n_t), \qquad \tilde{p}_s^{i+1}(\mathbf{n},n_t) = \tilde{p}_s^i(\mathbf{n},n_t) - \varepsilon_{\text{step}}\left[\frac{\partial V(s)}{\partial s(\mathbf{n},n_t)}\right]_{s=s^{i+1}}, \tag{6.57}$$

for a specified number of steps N_{step}. This is followed by an additional half-step backward in $\tilde{p}_s$ given by

$$p_s^{N_{\text{step}}}(\mathbf{n},n_t) = \tilde{p}_s^{N_{\text{step}}}(\mathbf{n},n_t) + \frac{\varepsilon_{\text{step}}}{2}\left[\frac{\partial V(s)}{\partial s(\mathbf{n},n_t)}\right]_{s=s^0}. \tag{6.58}$$

The length of such an MD "trajectory" should be taken large enough to ensure significant decorrelation between successive configurations of the auxiliary field. The evolved configuration is then subjected to a "Metropolis test" against a random number $r \in [0,1)$. The new configuration is accepted if

$$r < \exp\left[-H(s^{N_{\text{step}}}, p_s^{N_{\text{step}}}) + H(s^0, p_s^0)\right]. \tag{6.59}$$

It should be noted that although H is in principle conserved in the MD evolution, the truncation error of the leapfrog method introduces a systematic error. The Metropolis test eliminates the need for extrapolation in $\varepsilon_{\text{step}}$.

In our case $\exp[-V(s)]$ has the form

$$|Z(L_t)|\exp\left[-S_{ss}(s) - S_{s_I s_I}(s_I) - S_{\pi_I \pi_I}(\pi_I)\right], \tag{6.60}$$

where $Z(L_t)$ is the determinant of an $A \times A$ matrix of single-nucleon amplitudes $\mathbf{M}$. The derivative of V is then computed using

$$\begin{aligned}
\frac{\partial V(s)}{\partial s(\mathbf{n},n_t)} &= \frac{\partial S_{ss}(s)}{\partial s(\mathbf{n},n_t)} - \frac{\partial \text{Re}\left[\ln\left(\det\mathbf{M}\right)\right]}{\partial s(\mathbf{n},n_t)} \\
&= \frac{\partial S_{ss}(s)}{\partial s(\mathbf{n},n_t)} - \text{Re}\left[\frac{1}{\det\mathbf{M}}\sum_{k,l}\frac{\partial\det\mathbf{M}}{\partial\mathbf{M}_{kl}}\frac{\partial\mathbf{M}_{kl}}{\partial s(\mathbf{n},n_t)}\right] \\
&= \frac{\partial S_{ss}(s)}{\partial s(\mathbf{n},n_t)} - \text{Re}\left[\sum_{k,l}\mathbf{M}_{lk}^{-1}\frac{\partial\mathbf{M}_{kl}}{\partial s(\mathbf{n},n_t)}\right].
\end{aligned} \tag{6.61}$$

In Fig. 6.7 we show a sample code calculating the quadratic part of the action due to the auxiliary fields and pion fields,

$$\frac{1}{2}\sum_{\mathbf{n},n_t}[p_s(\mathbf{n},n_t)]^2 + \frac{1}{2}\sum_{\mathbf{n},n_t,I}[p_{s_I}(\mathbf{n},n_t)]^2 + \frac{1}{2}\sum_{\mathbf{n},n_t,I}[p_{\pi_I}(\mathbf{n},n_t)]^2 + S_{ss}(s) + S_{s_I s_I}(s_I) + S_{\pi_I \pi_I}(\pi_I). \tag{6.62}$$

In the code we have found it convenient to rescale the pion field by a factor of $\sqrt{q_\pi}$ where

$$q_\pi = \alpha_t\left(m_\pi^2 + 6w_0\right). \tag{6.63}$$

In Fig. 6.8 we show a sample code which calculates

$$\left[\frac{\partial V(s)}{\partial s(\mathbf{n},n_t)}\right]_{s=s^0} \tag{6.64}$$

and uses it to compute the half-step forward in the conjugate momentum,

```
bose = 0.D0
DO nt = 0,Lt−1
   DO nz = 0,L−1; DO ny = 0,L−1; DO nx = 0,L−1
      bose = bose &
            + s(nx,ny,nz,nt)**2.D0/2.D0 &
            + p_s(nx,ny,nz,nt)**2.D0/2.D0
      DO iso = 1,3
         bose = bose &
               + sI(nx,ny,nz,nt,iso)**2.D0/2.D0 &
               + p_sI(nx,ny,nz,nt,iso)**2.D0/2.D0 &
               + pion(nx,ny,nz,nt,iso)**2.D0/2.D0 &
               + atovera/qpi3*pion(nx,ny,nz,nt,iso)*( &
               − w1_P*pion(MOD(nx+1,L),ny,nz,nt,iso) &
               − w1_P*pion(nx,MOD(ny+1,L),nz,nt,iso) &
               − w1_P*pion(nx,ny,MOD(nz+1,L),nt,iso) &
               + w2_P*pion(MOD(nx+2,L),ny,nz,nt,iso) &
               + w2_P*pion(nx,MOD(ny+2,L),nz,nt,iso) &
               + w2_P*pion(nx,ny,MOD(nz+2,L),nt,iso) &
               − w3_P*pion(MOD(nx+3,L),ny,nz,nt,iso) &
               − w3_P*pion(nx,MOD(ny+3,L),nz,nt,iso) &
               − w3_P*pion(nx,ny,MOD(nz+3,L),nt,iso)) &
               + p_pion(nx,ny,nz,nt,iso)**2.D0/2.D0
      END DO
   END DO; END DO; END DO
END DO
```

Fig. 6.7 Sample code calculating the quadratic part of the action due to the auxiliary fields and pion fields.

```
DO npart1 = 0,n_f−1; DO npart2 = 0,n_f−1
   zdcorrmatrix(npart2,npart1) = 0.D0
   DO ni = 0,1; DO ns = 0,1
      zdcorrmatrix(npart2,npart1) = &
            zdcorrmatrix(npart2,npart1) + &
            zdualvecs(nx,ny,nz,nt+1,ns,ni,npart2) &
            *zvecs(nx,ny,nz,nt,ns,ni,npart1) &
            *CDSQRT(−c0*atovera*(1.D0,0.D0))/L**3
   END DO; END DO
END DO; END DO

dVds(nx,ny,nz,nt) = s(nx,ny,nz,nt)
DO npart1 = 0,n_f−1; DO npart2 = 0,n_f−1
   dVds(nx,ny,nz,nt) = dVds(nx,ny,nz,nt) &
         − DBLE(zdcorrmatrix(npart2,npart1) &
         *zcorrinv(npart1,npart2))
END DO; END DO

p_sHMC(nx,ny,nz,nt,0) = &
      p_s(nx,ny,nz,nt) − 0.5D0*eHMC*dVds(nx,ny,nz,nt)
```

Fig. 6.8 Sample code which computes the derivative of the potential $V(s)$ with respect to the auxiliary field $s(\mathbf{n}, n_t)$ and uses it to compute the half-step forward in the conjugate momentum.

$$\tilde{p}_s^0(\mathbf{n}, n_t) = p_s^0(\mathbf{n}, n_t) - \frac{\varepsilon_{\text{step}}}{2} \left[\frac{\partial V(s)}{\partial s(\mathbf{n}, n_t)} \right]_{s=s^0}. \tag{6.65}$$

In Fig. 6.9 we show an example code which performs the Metropolis test against a random number $r \in [0, 1)$, with the new configuration being accepted if

$$r < \exp\left[-H(s^{N_{\text{step}}}, p_s^{N_{\text{step}}}) + H(s^0, p_s^0) \right]. \tag{6.66}$$

Although importance sampling uses only the absolute volume, the complex phase of the determinant is treated as an observable and is collected with each configuration of the auxiliary and pion fields.

```
IF (ntrial .eq. 1 .or. grnd() .lt. DEXP(-actnew+act)) THEN

   accept = accept + 1.

   DO nt = 0,Lt-1
      DO nz = 0,L-1; DO ny = 0,L-1; DO nx = 0,L-1
         s(nx,ny,nz,nt) = snew(nx,ny,nz,nt)
      END DO; END DO; END DO
   END DO
   DO nt = 0,Lt-1
      DO nz = 0,L-1; DO ny = 0,L-1; DO nx = 0,L-1
         DO iso = 1,3
            sI(nx,ny,nz,nt,iso) = sInew(nx,ny,nz,nt,iso)
            pion(nx,ny,nz,nt,iso) = pionnew(nx,ny,nz,nt,iso)
         END DO
      END DO; END DO; END DO
   END DO
   aldeterabs = aldeternewabs
   zdeterphase = zdeternewphase

END IF
```

Fig. 6.9 Sample code showing the Metropolis condition used to determine whether the new configuration is accepted or rejected.

6.6 Exercises

6.1. Write a lattice hybrid Monte Carlo code involving only the quadratic part of the action due to the auxiliary fields and pions,

$$\frac{1}{2}\sum_{\mathbf{n},n_t}[p_s(\mathbf{n},n_t)]^2 + \frac{1}{2}\sum_{\mathbf{n},n_t,I}[p_{s_I}(\mathbf{n},n_t)]^2 + \frac{1}{2}\sum_{\mathbf{n},n_t,I}[p_{\pi_I}(\mathbf{n},n_t)]^2 + S_{ss}(s) + S_{s_I s_I}(s_I) + S_{\pi_I \pi_I}(\pi_I). \qquad (6.67)$$

Verify that the change in the action produced by the hybrid Monte Carlo update is scaling quadratically in the step size, $\varepsilon_{\text{step}}$, in the limit $\varepsilon_{\text{step}} \to 0$ with $N_{\text{step}}\varepsilon_{\text{step}}$ held fixed.

6.2. Write a function (subroutine) that generates the single-nucleon states on the lattice corresponding to the Slater-determinant state of four nucleons — proton spin-up, proton spin-down, neutron spin-up, and neutron spin-down — each with zero momentum.

6.3. Write a (function) subroutine that extends the sample code in Fig. 6.4 to repeatedly multiply the auxiliary-field transfer matrix on the left starting from some initial single-nucleon wave functions. Include the contributions from the auxiliary fields s and s_I as well as the pion field π_I.

6.4. Write a function (subroutine) that extends the sample code in Fig. 6.5 to repeatedly multiply the auxiliary-field transfer matrix on the right starting from some final single-nucleon wave functions. Include the contributions from the auxiliary fields s and s_I as well as the pion field π_I.

6.5. Use the Slater-determinant state constructed in Prob. 6.2 as the initial and final states. Apply the functions (subroutines) written in Prob. 6.3 and Prob. 6.4 with all coupling constants set to zero. Verify that this state is the ground state of the non-interacting system with energy equal to zero.

6.6. Use the Slater-determinant state constructed in Prob. 6.2 as the initial and final states. Then implement the functions (subroutines) written in Prob. 6.3 and Prob. 6.4 and extend the sample code in Fig. 6.8 to compute the derivatives of $V(s)$ with respect to $s(\mathbf{n},n_t)$, $s_I(\mathbf{n},n_t)$, and $\pi_I(\mathbf{n},n_t)$.

6.7. Take the code you have written for Prob. 6.6 and complete the remaining steps needed to do hybrid Monte Carlo updates for s, s_I, and π_I. Verify that the change in the action produced

by the hybrid Monte Carlo update is scaling quadratically in ε_{step} in the limit $\varepsilon_{step} \to 0$ with $N_{step}\varepsilon_{step}$ held fixed.

6.8. Take the code you have written for Prob. 6.7 and complete the remaining steps needed to calculate the energy of the four-nucleon ground state by computing the ratio of the amplitudes $Z(L_t)/Z(L_t-1)$.

References

1. S. Weinberg, Phys. Lett. **B251**, 288 (1990). DOI 10.1016/0370-2693(90)90938-3
2. S. Weinberg, Nucl. Phys. **B363**, 3 (1991). DOI 10.1016/0550-3213(91)90231-L
3. C. Ordonez, U. van Kolck, Phys. Lett. **B291**, 459 (1992)
4. C. Ordonez, L. Ray, U. van Kolck, Phys. Rev. Lett. **72**, 1982 (1994)
5. U. van Kolck, Phys. Rev. **C49**, 2932 (1994)
6. E. Epelbaum, W. Glöckle, U.G. Meißner, Phys. Lett. **B439**, 1 (1998)
7. E. Epelbaum, W. Glöckle, U.G. Meißner, Nucl. Phys. **A637**, 107 (1998)
8. P.F. Bedaque, U. van Kolck, Ann. Rev. Nucl. Part. Sci. **52**, 339 (2002)
9. E. Epelbaum, H.W. Hammer, U.G. Meissner, Rev. Mod. Phys. **81**, 1773 (2009). DOI 10.1103/RevModPhys.81.1773
10. D. Lee, Prog. Part. Nucl. Phys. **63**, 117 (2009). DOI 10.1016/j.ppnp.2008.12.001
11. J.E. Drut, A.N. Nicholson, J. Phys. G: Nucl. Part. Phys. **40**(4), 043101 (2013). DOI 10.1088/0954-3899/40/4/043101
12. J. Hubbard, Phys. Rev. Lett. **3**, 77 (1959)
13. R.L. Stratonovich, Soviet Phys. Doklady **2**, 416 (1958)
14. D.H. Weingarten, D.N. Petcher, Phys. Lett. **B99**, 333 (1981)
15. R.T. Scalettar, D.J. Scalapino, R.L. Sugar, Phys. Rev. **B34**, 7911 (1986)
16. S. Gottlieb, W. Liu, D. Toussaint, R.L. Renken, R.L. Sugar, Phys. Rev. **D35**, 2531 (1987)
17. S. Duane, A.D. Kennedy, B.J. Pendleton, D. Roweth, Phys. Lett. **B195**, 216 (1987)
18. H.M. Müller, S.E. Koonin, R. Seki, U. van Kolck, Phys. Rev. **C61**, 044320 (2000)
19. D. Lee, B. Borasoy, T. Schäfer, Phys. Rev. **C70**, 014007 (2004)
20. D. Lee, T. Schäfer, Phys. Rev. **C72**, 024006 (2005)
21. D. Lee, T. Schäfer, Phys. Rev. **C73**, 015201 (2006)
22. D. Lee, T. Schäfer, Phys. Rev. **C73**, 015202 (2006)
23. B. Borasoy, H. Krebs, D. Lee, U.G. Meißner, Nucl. Phys. **A768**, 179 (2006)
24. B. Borasoy, E. Epelbaum, H. Krebs, D. Lee, U.G. Meissner, Eur. Phys. J. **A31**, 105 (2007). DOI 10.1140/epja/i2006-10154-1
25. B. Borasoy, E. Epelbaum, H. Krebs, D. Lee, U.G. Meißner, Eur. Phys. J. **A35**, 343 (2008)
26. B. Borasoy, E. Epelbaum, H. Krebs, D. Lee, U.G. Meißner, Eur. Phys. J. **A35**, 357 (2008)
27. G. Wlazłowski, J.W. Holt, S. Moroz, A. Bulgac, K.J. Roche, Phys. Rev. Lett. **113**(18), 182503 (2014). DOI 10.1103/PhysRevLett.113.182503
28. E. Epelbaum, H. Krebs, D. Lee, U.G. Meißner, Eur. Phys. J. **A41**, 125 (2009)
29. E. Epelbaum, H. Krebs, D. Lee, U.G. Meissner, Phys. Rev. Lett. **104**, 142501 (2010). DOI 10.1103/PhysRevLett.104.142501
30. E. Epelbaum, H. Krebs, D. Lee, U.G. Meissner, Phys. Rev. Lett. **106**, 192501 (2011). DOI 10.1103/PhysRevLett.106.192501
31. E. Epelbaum, H. Krebs, T.A. Lahde, D. Lee, U.G. Meissner, Phys. Rev. Lett. **109**, 252501 (2012). DOI 10.1103/PhysRevLett.109.252501
32. E. Epelbaum, H. Krebs, T.A. Lahde, D. Lee, U.G. MeiSSner, Phys. Rev. Lett. **110**(11), 112502 (2013). DOI 10.1103/PhysRevLett.110.112502
33. T.A. Lahde, E. Epelbaum, H. Krebs, D. Lee, U.G. MeiSSner, G. Rupak, Phys. Lett. **B732**, 110 (2014). DOI 10.1016/j.physletb.2014.03.023

34. E. Epelbaum, H. Krebs, T.A. Lahde, D. Lee, U.G. MeiSSner, G. Rupak, Phys. Rev. Lett. **112**(10), 102501 (2014). DOI 10.1103/PhysRevLett.112.102501
35. S. Elhatisari, et al., (2016)
36. G. Rupak, D. Lee, Phys. Rev. Lett. **111**(3), 032502 (2013). DOI 10.1103/PhysRevLett.111.032502
37. G. Rupak, P. Ravi, Phys. Lett. **B741**, 301 (2014). DOI 10.1016/j.physletb.2014.12.055
38. S. Elhatisari, D. Lee, G. Rupak, E. Epelbaum, H. Krebs, T.A. Lähde, T. Luu, U.G. Meißner, Nature **528**, 111 (2015). DOI 10.1038/nature16067
39. M. Lüscher, Commun. Math. Phys. **104**, 177 (1986)
40. M. Lüscher, Commun. Math. Phys. **105**, 153 (1986). DOI 10.1007/BF01211097
41. M. Lüscher, Nucl. Phys. **B354**, 531 (1991)
42. B. Borasoy, E. Epelbaum, H. Krebs, D. Lee, U.G. Meissner, Eur.Phys.J. **A34**, 185 (2007). DOI 10.1140/epja/i2007-10500-9
43. J. Carlson, V. Pandharipande, R. Wiringa, Nucl. Phys. A **424**(1), 47 (1984). DOI http://dx.doi.org/10.1016/0375-9474(84)90127-1. URL http://www.sciencedirect.com/science/article/pii/0375947484901271
44. B.N. Lu, T.A. Lähde, D. Lee, U.G. Meißner, (2015)
45. M. Pine, D. Lee, G. Rupak, Eur. Phys. J. **A49**, 151 (2013). DOI 10.1140/epja/i2013-13151-3
46. S. Elhatisari, D. Lee, Phys. Rev. **C90**(6), 064001 (2014). DOI 10.1103/PhysRevC.90.064001
47. A. Rokash, M. Pine, S. Elhatisari, D. Lee, E. Epelbaum, et al., (2015)
48. M. Creutz, Phys. Rev. **D38**, 1228 (1988)
49. M. Creutz, Found. Phys. **30**, 487 (2000)
50. J. Carlson, S. Gandolfi, F. Pederiva, S.C. Pieper, R. Schiavilla, K.E. Schmidt, R.B. Wiringa, Rev. Mod. Phys. **87**, 1067 (2015). DOI 10.1103/RevModPhys.87.1067

Chapter 7

From few to many nucleons and methods for nuclear reactions

Giuseppina Orlandini

Abstract Each chapter should be preceded by an abstract (10–15 lines long) that summarizes the content. The abstract will appear *online* at www.SpringerLink.com and be available with unrestricted access. This allows unregistered users to read the abstract as a teaser for the complete chapter. As a general rule the abstracts will not appear in the printed version of your book unless it is the style of your particular book or that of the series to which your book belongs.

Please use the 'starred' version of the new Springer abstract command for typesetting the text of the online abstracts (cf. source file of this chapter template abstract) and include them with the source files of your manuscript. Use the plain abstract command if the abstract is also to appear in the printed version of the book.

7.1 The Nuclear few- and many-body problem

7.2 Methods for bound states based on the variational principle I:The No Core Shell Model (NCSM)

7.3 Methods for bound states based on the variational principle II:The Hyperspherical Harmonics (HH) method

7.4 Methods for reactions involving continuum states I:Perturbation induced reactions and integral transforms

7.5 Methods for reactions involving continuum states II:The continuum state problem reduced to a bound state problem

Giuseppina Orlandini
Name of institution and address, e-mail: name@email.address

Chapter 8
High-performance computing Many-body methods and infinite nuclear matter

Justin G. Lietz, Samuel Novario, Gustav R. Jansen, Gaute Hagen, and Morten Hjorth-Jensen,

Abstract We present a computational approach to infinite nuclear matter employing Hartree-Fock theory, many-body perturbation theory and coupled cluster theory. These lectures are closely linked with those in chapters 9.5.4, 10.4 and 11.1 and serve as input for the correlation functions employed in Monte Carlo calculations in chapter 9.5.4, the in-medium similarity renormalization group theory of dense fermionic systems of chapter chapter 10.4 and the Green's function approach in chapter 11.1. We provide extensive code examples and benchmark calculations, allowing thereby an eventual reader to start writing her/his own codes. We start with an object-oriented serial code and end with in-depth discussions on strategies for porting the code to present and planned high-performance computing facilities.

8.1 Introduction

Studies of dense baryonic matter are of central importance to our basic understanding of the stability of nuclear matter, spanning from matter at high densities and temperatures to matter as found within dense astronomical objects like neutron stars. An object like a neutron star offers an intriguing interplay between nuclear processes and astrophysical observables, spanning many orders of magnitude in density and several possible compositions of matter, from the crust of the star to a possible quark matter phase in its interior, see for example Refs. [1–5] for discussions. A central issue in studies of infinite nuclear matter is the deter-

Justin G. Lietz
Department of Physics and Astronomy and National Superconducting Cyclotron Laboratory, Michigan State University, East Lansing, Michigan, USA, e-mail: `lietz@nscl.msu.edu`,

Samuel Novario
Department of Physics and Astronomy and National Superconducting Cyclotron Laboratory, Michigan State University, East Lansing, Michigan, USA, e-mail: `novarios@nscl.msu.edu`,

Gustav R. Jansen
Oak Ridge National Laboratory, Physics Division, Oak Ridge, Tennessee, USA and Department of Physics and Astronomy, University of Tennessee, Knoxville, Tennessee, USA, e-mail: `jansen@ornl.gov`,

Gaute Hagen
Oak Ridge National Laboratory, Physics Division, Oak Ridge, Tennessee, USA and Department of Physics and Astronomy, University of Tennessee, Knoxville, Tennessee, USA, e-mail: `hageng@ornl.gov`,

Morten Hjorth-Jensen
Department of Physics and Astronomy and National Superconducting Cyclotron Laboratory, Michigan State University, East Lansing, Michigan, USA and Department of Physics, University of Oslo, Oslo, Norway, e-mail: `hjensen@msu.edu`

mination of the equation of state (EoS), which can in turn be used to determine properties like the mass range, the mass-radius relationship, the thickness of the crust and the rate by which a neutron star cools down over time. The EoS is also an important ingredient in studies of the energy release in supernova explosions.

The determination and our understanding of the EoS for dense nuclear matter is intimately linked with our capability to solve the nuclear many-body problem. In particular, to be able to provide precise constraints on the role of correlations beyond the mean field, is crucial for improved and controlled calculations of the EoS of nucleonic matter. In recent years, there has been a considerable algorithmic development of first principle (or *ab initio*) methods for solving the nuclear many-body problem. Linked with a similar progress in the derivation of nuclear forces based on effective field theory (EFT), see chapters four, five and six of the present text and Refs. [6–8], we are now in a situation where reliable results can be provided at different levels of approximation. The nuclear Hamiltonians which are now used routinely in nuclear structure and nuclear matter calculations, include both *NN* and 3NFs derived from EFT, see for example Refs. [9–18]. Parallel to the development of nuclear forces from EFT, which employs symmetries of quantum chromodynamics, there are recent and promising approaches to derive the EoS using forces constrained from lattice quantum chromodynamics calculations [19], see chapters 2 and 3 of the present text.

Theoretical studies of nuclear matter and the pertinent EoS span back to the very early days of nuclear many-body physics. These early developments are nicely summarized in for example the review of Day [20] from 1967. These early state-of-the-art calculations were performed using what is known as Brueckner-Bethe-Goldstone theory [21, 22], see for example Refs. [5, 23, 24] for recent reviews and developments. In these calculations, mainly particle-particle correlations were summed to infinite order. Other correlations were often included in a perturbative way. A systematic inclusion of other correlations in a non-perturbative way are nowadays accounted for in many-body methods like coupled cluster theory [25, 26], various Monte Carlo methods [27, 28], Green's function approaches [18, 24, 29] and density functional theories [30], just to mention a few of the actual many-body methods which are used for nuclear matter studies.

The aim of this part of the lectures (comprising this chapter and the three subsequent ones) is to provide the necessary ingredients for perfoming studies of neutron star matter (or matter in β-equilibrium) and symmetric nuclear matter. We will mainly focus on pure neutron matter, but the framework and formalism can easily be extended to other dense and homogeneous fermionic systems such as the electron gas in two and three dimensions. The introductory material we present here forms also the basis for the next three chapters, starting with the definition of the single-particle basis and our Hamiltonians as well as Hartree-Fock theory. For infinite matter, due to the translational invariance of the Hamiltonian, the single-particle basis, in terms of plane waves, is unchanged under Hartree-Fock calculations.

Neutron star matter at densities of 0.1 fm^{-3} and greater, is often assumed to be made of mainly neutrons, protons, electrons and muons in beta equilibrium. However, other baryons like various hyperons may exist, as well as possible mesonic condensates and transitions to quark degrees of freedom at higher densities [5]. In these notes we limit ourselves to matter composed of neutrons only. Furthermore, we will also consider matter at temperatures much lower than the typical Fermi energies.

In the next section we present some of the basic quantities that enter the different many-body methods discussed in this and the three subsequent chapters. All these methods start with some single-particle basis states, normally obtained via the solution of mean-field approaches like Hartree-Fock theory. Contributions from correlations beyond such a mean-field basis to selected observables, are then obtained via a plethora of many-body methods. These methods represent different mathematical algorithms used to solve either Schrödinger's or Dirac's equations for many interacting fermions. After the definitions of our basis states, we

derive the Hartree-Fock equations in the subsequent section and move on with many-body perturbation theory, full configuration interaction theory and coupled cluster theory. Monte Carlo methods, Green's function theory approaches and Similarity Renormlization group approaches are discussed in the subsequent three chapters.

The strengths and weaknesses of these methods are discussed throughout these chapters, with applications to either a simple pairing model and/or pure neutron matter. Our focus will be on pure neutron matter, starting with a simple model for the interaction between nucleons. This allows us to focus on the pedagogical and algorithmic aspects of the various many-body methods, avoiding thereby the full complexity of nuclear forces. If properly written however, the codes can easily be extended to include models of the nuclear interactions based on effective field theory (see chapters four, five and six of the present text) and other baryon species than just neutrons. In our conclusions we point back to models for nuclear forces and their links to the underlying theory of the strong interaction discussed in the first chapters of this book, bridging thereby the gap between the theory of nuclear Hamiltonians and many-body methods.

8.2 Single-particle basis, Hamiltonians and models for the nuclear force

8.2.1 Introduction to nuclear matter and Hamiltonians

Although our focus here and in the coming chapters is on neutron matter only, our formalism lends itself easily to studies of nuclear matter with a given proton fraction and electrons. In this section we outline some of the background details, with a focus on the calculational basis and the representation of a nuclear Hamiltonian.

Neutron star matter is not composed of only neutrons. Rather, matter is composed of various baryons and leptons in chemical and charge equilibrium. The equilibrium conditions are governed by the weak processes (normally referred to as the processes for β-equilibrium)

$$b_1 \rightarrow b_2 + l + \bar{\nu}_l \qquad b_2 + l \rightarrow b_1 + \nu_l, \tag{8.1}$$

where b_1 and b_2 refer to different types of baryons, for example a neutron and a proton. The symbol l is either an electron or a muon and $\bar{\nu}_l$ and ν_l their respective anti-neutrinos and neutrinos. Leptons like muons appear at a density close to nuclear matter saturation density, the latter being

$$n_0 \approx 0.16 \pm 0.02 \text{ fm}^{-3},$$

with a corresponding energy per baryon $\mathscr{E}_0$ for symmetric nuclear matter at saturation density of

$$\mathscr{E}_0 = B/A = -15.6 \pm 0.2 \text{ MeV}.$$

The energy per baryon is the central quantity in the present studies. From the energy per baryon, we can define the pressure P which counteracts the gravitional forces and hinders the gravitational collapse of neutron start. The pressure is defined through the relation

$$P = n^2 \frac{\partial \mathscr{E}}{\partial n} = n \frac{\partial \varepsilon}{\partial n} - \varepsilon, \tag{8.2}$$

where ε is the energy density. Similarly, the chemical potential for particle species i is given by

$$\mu_i = \left(\frac{\partial \varepsilon}{\partial n_i}\right). \tag{8.3}$$

In calculations of properties of neutron star matter in β-equilibrium, we need to calculate the energy per baryon $\mathscr{E}$ for e.g. several proton fractions x_p. The proton fraction corresponds to the ratio of protons as compared to the total nucleon number (Z/A). It is defined as

$$x_p = \frac{n_p}{n}, \tag{8.4}$$

where $n = n_p + n_n$ is the total baryonic density if neutrons and protons are the only baryons present. If this is the case, the total Fermi momentum k_F and the Fermi momenta k_{Fp}, k_{Fn} for protons and neutrons are related to the total nucleon density n by

$$\begin{aligned} n &= \frac{2}{3\pi^2} k_F^3 \\ &= x_p n + (1 - x_p) n \\ &= \frac{1}{3\pi^2} k_{Fp}^3 + \frac{1}{3\pi^2} k_{Fn}^3. \end{aligned} \tag{8.5}$$

The energy per baryon will thus be labelled as $\mathscr{E}(n, x_p)$. The quantity $\mathscr{E}(n, 0)$ refers then to the energy per baryon for pure neutron matter (PNM) while $\mathscr{E}(n, \frac{1}{2})$ is the corresponding value for SNM. Furthermore, in this work, subscripts n, p, e, μ will always refer to neutrons, protons, electrons and muons, respectively.

Since the mean free path of a neutrino in a neutron star is bigger than the typical radius of such a star (~ 10 km), we will throughout assume that neutrinos escape freely from the neutron star, see for example Ref. [?] for a discussion on trapped neutrinos. Eq. (8.1) yields then the following conditions for matter in β equilibrium with for example nucleonic degrees freedom only

$$\mu_n = \mu_p + \mu_e, \tag{8.6}$$

and

$$n_p = n_e, \tag{8.7}$$

where μ_i and n_i refer to the chemical potential and number density in fm^{-3} of particle species i. If muons are present as well, we need to modify the equation for charge conservation, Eq. (8.7), to read

$$n_p = n_e + n_\mu,$$

and require that $\mu_e = \mu_\mu$.

An important ingredient in the discussion of the EoS and the criteria for matter in β-equilibrium is the so-called symmetry energy $\mathscr{S}(n)$, defined as the difference in energy for symmetric nuclear matter and pure neutron matter

$$\mathscr{S}(n) = \mathscr{E}(n, x_p = 0) - \mathscr{E}(n, x_p = 1/2). \tag{8.8}$$

If we expand the energy per baryon in the case of nucleonic degrees of freedom only in the proton concentration x_p about the value of the energy for SNM ($x_p = \frac{1}{2}$), we obtain,

$$\mathscr{E}(n, x_p) = \mathscr{E}(n, x_p = \frac{1}{2}) + \frac{1}{2} \frac{d^2 \mathscr{E}}{dx_p^2}(n)(x_p - 1/2)^2 + \ldots, \tag{8.9}$$

where the term $d^2\mathscr{E}/dx_p^2$ is to be associated with the symmetry energy $\mathscr{S}(n)$ in the empirical mass formula. If we assume that higher order derivatives in the above expansion are small, then through the conditions for β-equilbrium of Eqs. (8.6) and (8.7) and Eq. (8.3) we can define the proton fraction by the symmetry energy as

$$\hbar c \left(3\pi^2 n x_p\right)^{1/3} = 4\mathscr{S}(n)\left(1 - 2x_p\right), \tag{8.10}$$

where the electron chemical potential is given by $\mu_e = \hbar c k_F$, i.e. ultrarelativistic electrons are assumed. Thus, the symmetry energy is of paramount importance for studies of neutron star matter in β-equilibrium. One can extract information about the value of the symmetry energy at saturation density n_0 from systematic studies of the masses of atomic nuclei. However, these results are limited to densities around n_0 and for proton fractions close to $\frac{1}{2}$, see for example the various contributions in Ref. [?]. Typical values for $\mathscr{S}(n)$ at n_0 are in the range $27 - 38$ MeV. For densities greater than n_0 it is more difficult to get a reliable information on the symmetry energy, and thereby the related proton fraction.

With this background, we are now ready to define our basic inputs and approximations to the various many-body theories discussed in this chapter the three subsequent ones. We will assume that the interacting part of the Hamiltonian can be approximated by a two-body interaction. This means that our Hamiltonian is written as the sum of some one-body part and a two-body part

$$\hat{H} = \hat{H}_0 + \hat{H}_I = \sum_{i=1}^{A} \hat{h}_0(x_i) + \sum_{i<j}^{A} \hat{v}(r_{ij}), \tag{8.11}$$

with

$$H_0 = \sum_{i=1}^{A} \hat{h}_0(x_i). \tag{8.12}$$

The one-body operator is defined as

$$\hat{h}_0(x_i) = \hat{t}(x_i) + \hat{u}_{\text{ext}}(x_i),$$

where $\hat{t}$ represents the kinetic energy and x_i represents both spatial and spin degrees of freedom. For many-body calculations of finite nuclei, the external potential $u_{\text{ext}}(x_i)$ is normally approximated by a harmonic oscillator or Woods-Saxon potential. For atoms, the external potential is defined by the Coulomb interaction an electron feels from the atomic nucleus. However, other potentials are fully possible, such as one derived from the self-consistent solution of the Hartree-Fock equations to be discussed below. Since we will work with plane waves, the one-body operator is simply given by the kinetic energy operator.

Our Hamiltonian is invariant under the permutation (interchange) of two particles. Since we deal with fermions however, the total wave function is anti-symmetric. Let $\hat{P}$ be an operator which interchanges two particles. Due to the symmetries we have ascribed to our Hamiltonian, this operator commutes with the total Hamiltonian,

$$[\hat{H}, \hat{P}] = 0,$$

meaning that a many-body eigenstate $\Psi_\lambda(x_1, x_2, \ldots, x_A)$ of $\hat{H}$ is an eigenfunction of $\hat{P}$ as well.

In our case we assume that we can approximate the exact eigenfunction for say the ground state with a Slater determinant

$$\Phi_0(x_1, x_2, \ldots, x_A, \alpha, \beta, \ldots, \sigma) = \frac{1}{\sqrt{A!}} \begin{vmatrix} \psi_\alpha(x_1) & \psi_\alpha(x_2) & \ldots & \ldots & \psi_\alpha(x_A) \\ \psi_\beta(x_1) & \psi_\beta(x_2) & \ldots & \ldots & \psi_\beta(x_A) \\ \ldots & \ldots & \ldots & \ldots & \ldots \\ \ldots & \ldots & \ldots & \ldots & \ldots \\ \psi_\sigma(x_1) & \psi_\sigma(x_2) & \ldots & \ldots & \psi_\sigma(x_A) \end{vmatrix}, \tag{8.13}$$

where x_i stand for the coordinates and spin values of a particle i and $\alpha, \beta, \ldots, \gamma$ are quantum numbers needed to describe remaining quantum numbers.

The single-particle function $\psi_\alpha(x_i)$ are eigenfunctions of the one-body Hamiltonian h_0, that is

$$\hat{h}_0(x_i)\psi_\alpha(x_i) = (\hat{t}(x_i) + \hat{u}_{\text{ext}}(x_i))\,\psi_\alpha(x_i) = \varepsilon_\alpha\psi_\alpha(x_i).$$

The energies ε_α are the so-called non-interacting single-particle energies, or unperturbed energies. The total energy is in this case the sum over all single-particle energies, if no two-body or more complicated many-body interactions are present.

The properties of the determinant lead to a straightforward implementation of the Pauli principle since no two particles can be at the same place (two columns being the same in the above determinant) and no two particles can be in the same state (two rows being the same). As a practical matter, however, Slater determinants beyond $N = 4$ quickly become un-wieldy. Thus we turn to the **occupation representation** or **second quantization** to simplify calculations. For a good introduction to second quantization see for examples Ref. [26].

We start thus with a set of orthonormal single-particle states $\{\psi_\alpha(x)\}$. To each single-particle state $\psi_\alpha(x)$ we associate a creation operator $a_\alpha^\dagger$ and an annihilation operator a_α. When acting on the vacuum state $|0\rangle$, the creation operator $a_\alpha^\dagger$ causes a particle to occupy the single-particle state $\psi_\alpha(x)$

$$\psi_\alpha(x) \rightarrow a_\alpha^\dagger|0\rangle$$

But with multiple creation operators we can occupy multiple states:

$$\psi_\alpha(x)\psi_\beta(x')\psi_\delta(x'') \rightarrow a_\alpha^\dagger a_\beta^\dagger a_\delta^\dagger|0\rangle.$$

Now we impose anti-symmetry, by having the fermion operators satisfy the anti-commutation relations

$$a_\alpha^\dagger a_\beta^\dagger + a_\beta^\dagger a_\alpha^\dagger = \left\{a_\alpha^\dagger, a_\beta^\dagger\right\} = 0,$$

so that

$$a_\alpha^\dagger a_\beta^\dagger = -a_\beta^\dagger a_\alpha^\dagger.$$

Because of this property, with obtain $a_\alpha^\dagger a_\alpha^\dagger = 0$, enforcing the Pauli exclusion principle. Thus we can represent a Slater determinant using creation operators as

$$a_\alpha^\dagger a_\beta^\dagger a_\delta^\dagger \ldots |0\rangle$$

each index $\alpha, \beta, \delta, \ldots$ must be unique.

We will now find it convenient to define a Fermi level and introduce a new reference vacuum. The Fermi level is defined in terms of all occupied single-particle states below a certain excitation single-particle energy. With the definition of a Fermi level, we can in turn define our ansatz for the ground state, represented by a Slater determinant as Φ_0. We will through-out the rest of this text using creation and annihilation operators to represent quantum mechanical operators and states. It means that our compact representation of a given Slater determinant in Fock space [26] is

$$\Phi_0 = |i_1 \ldots i_A\rangle = a_{i_1}^\dagger \ldots a_{i_A}^\dagger|0\rangle$$

where $|0\rangle$ is the true vacuum and we have defined the creation and annihilation operators as

$$a_p^\dagger|0\rangle = |p\rangle, \quad a_p|q\rangle = \delta_{pq}|0\rangle$$

with the anti-commutation relations

$$\delta_{pq} = \left\{a_p, a_q^\dagger\right\},$$

and

$$\{a_p^\dagger, a_q\} = \{a_p, a_q\} = \{a_p^\dagger, a_q^\dagger\} = 0.$$

We can rewrite the ansatz for the ground state as

$$|\Phi_0\rangle = \prod_{i \leq F} a_i^\dagger |0\rangle,$$

where we have introduced the shorthand labels for states below the Fermi level F as $i, j, \ldots \leq F$. For single-particle states above the Fermi level we reserve the labels $a, b, \ldots > F$, while the labels $p, q, \ldots$ represent any possible single particle state, that is states below and above the Fermi level.

Since our focus is on infinite systems, the one-body part of the Hamiltonian is given by the kinetic energy operator only. In second quantization it is defined as

$$\hat{H}_0 = \hat{T} = \sum_{pq} \langle p|\hat{t}|q\rangle a_p^\dagger a_q,$$

where the matrix elements $\langle p|\hat{t}|q\rangle$ are defined in Eq. **(??)**. The two-body interaction reads

$$\hat{H}_I = \hat{V} = \frac{1}{4} \sum_{pqrs} \langle pq|\hat{v}|rs\rangle_{AS} a_p^\dagger a_q^\dagger a_s a_r,$$

where we have defined the anti-symmetrized matrix elements

$$\langle pq|\hat{v}|rs\rangle_{AS} = \langle pq|\hat{v}|rs\rangle - \langle pq|\hat{v}|sr\rangle.$$

We can also define a three-body operator

$$\hat{V}_3 = \frac{1}{36} \sum_{pqrstu} \langle pqr|\hat{v}_3|stu\rangle_{AS} a_p^\dagger a_q^\dagger a_r^\dagger a_u a_t a_s,$$

with the anti-symmetrized matrix element

$$\langle pqr|\hat{v}_3|stu\rangle_{AS} = \langle pqr|\hat{v}_3|stu\rangle + \langle pqr|\hat{v}_3|tus\rangle + \langle pqr|\hat{v}_3|ust\rangle - \langle pqr|\hat{v}_3|sut\rangle - \langle pqr|\hat{v}_3|tsu\rangle - \langle pqr|\hat{v}_3|uts\rangle.$$
(8.14)

In this and the forthcoming chapters we will limit ourselves to two-body interactions at most.

Using the ansatz for the ground state $|\Phi_0$ as new reference vacuum state, we need to redefine the anticommutation relations to

$$\{a_p^\dagger, a_q\} = \delta_{pq}, p, q \leq F,$$

and

$$\{a_p, a_q^\dagger\} = \delta_{pq}, \ p, q > F.$$

It is easy to see then that

$$a_i|\Phi_0\rangle = |\Phi_i\rangle \neq 0, \quad a_a^\dagger|\Phi_0\rangle = |\Phi^a\rangle \neq 0,$$

and

$$a_i^\dagger|\Phi_0\rangle = 0 \quad a_a|\Phi_0\rangle = 0.$$

With the new reference vacuum state the Hamiltonian can be rewritten as, see problem 8.1

$$\hat{H} = E_{\text{Ref}} + \hat{H}_N,$$

with the reference energy defined as the expectation value of the Hamiltonian using the reference state Φ_0

$$E_{\text{Ref}} = \langle \Phi_0 | \hat{H} | \Phi_0 \rangle = \sum_{i \leq F} \langle i | \hat{h}_0 | i \rangle + \frac{1}{2} \sum_{ij \leq F} \langle ij | \hat{v} | ij \rangle,$$

and the new normal-ordered Hamiltonian defined as

$$\hat{H}_N = \sum_{pq} \langle p | \hat{h}_0 | q \rangle \left\{ a_p^\dagger a_q \right\} + \frac{1}{4} \sum_{pqrs} \langle pq | \hat{v} | rs \rangle \left\{ a_p^\dagger a_q^\dagger a_s a_r \right\} + \sum_{pq, i \leq F} \langle pi | \hat{v} | qi \rangle \left\{ a_p^\dagger a_q \right\},$$

where the curly brackets represent normal-ordering with respect to the new reference vacuum state. The normal-ordered Hamiltonian can be rewritten in terms of a new one-body operator and a two-body operator as

$$\hat{H}_N = \hat{F}_N + \hat{V}_N,$$

with

$$\hat{F}_N = \sum_{pq} \langle p | \hat{f} | q \rangle \left\{ a_p^\dagger a_q \right\},$$

where

$$\langle p | \hat{f} | q \rangle = \langle p | \hat{h}_0 | q \rangle \sum_{i \leq F} \langle pi | \hat{v} | qi \rangle.$$

The last term on the right hand side represents a medium modification to the single-particle Hamiltonian due to the two-body interaction. Finally, the two-body interaction is given by

$$\hat{V}_N = \frac{1}{4} \sum_{pqrs} \langle pq | \hat{v} | rs \rangle \left\{ a_p^\dagger a_q^\dagger a_s a_r \right\}.$$

8.2.2 Single-particle basis for infinite matter

Infinite nuclear or neutron matter is a homogeneous system and the one-particle wave functions are given by plane wave functions normalized to a volume Ω for a box with length L (the limit $L \to \infty$ is to be taken after we have computed various expectation values)

$$\psi_{\mathbf{k}\sigma}(\mathbf{r}) = \frac{1}{\sqrt{\Omega}} \exp{(i\mathbf{k}\mathbf{r})} \xi_\sigma$$

where $\mathbf{k}$ is the wave number and ξ_σ is the spin function for either spin up or down nucleons

$$\xi_{\sigma=+1/2} = \begin{pmatrix} 1 \\ 0 \end{pmatrix} \qquad \xi_{\sigma=-1/2} = \begin{pmatrix} 0 \\ 1 \end{pmatrix}.$$

We focus first on the kinetic energy operator. We assume that we have periodic boundary conditions which limit the allowed wave numbers to

$$k_i = \frac{2\pi n_i}{L} \quad i = x, y, z \quad n_i = 0, \pm 1, \pm 2, \ldots$$

The operator for the kinetic energy can be written as, see problem **??**,

$$\hat{T} = \sum_{\mathbf{p}\sigma_p} \frac{\hbar^2 k_P^2}{2m} a_{\mathbf{p}\sigma}^\dagger a_{\mathbf{p}\sigma_p}.$$

When using periodic boundary conditions, the discrete-momentum single-particle basis functions (excluding spin and/or isospin degrees of freedom) result in the following single-particle energy

$$\varepsilon_{n_x,n_y,n_z} = \frac{\hbar^2}{2m}\left(\frac{2\pi}{L}\right)^2 \left(n_x^2 + n_y^2 + n_z^2\right) = \frac{\hbar^2}{2m}\left(k_{n_x}^2 + k_{n_y}^2 + k_{n_z}^2\right),$$ (8.15)

for a three-dimensional system with

$$k_{n_i} = \frac{2\pi n_i}{L} \ n_i = 0, \pm 1, \pm 2, \dots,$$

We will select the single-particle basis such that both the occupied and unoccupied single-particle spaces have a closed-shell structure. This means that all single-particle states corresponding to energies below a chosen cutoff are included in the basis. We study only the unpolarized spin phase, in which all orbitals are occupied with one spin-up and one spin-down fermion (neutrons and protons in our case). With the kinetic energy rewritten in terms of the discretized momenta we can set up a similar table and obtain (assuming identical particles one and including spin up and spin down solutions) for energies less than or equal to $n_x^2 + n_y^2 + n_z^2 \leq 3$, as shown in Table 8.1

Table 8.1 Total number of particle filling $N_{\uparrow\downarrow}$ for various $n_x^2 + n_y^2 + n_z^2$ values for one spin-1/2 fermion species. Borrowing from nuclear shell-model terminology, filled shells corresponds to all single-particle states for one $n_x^2 + n_y^2 + n_z^2$ value being occupied. For matter with both protons and neutrons, the filling degree increased with a factor of 2.

$n_x^2+n_y^2+n_z^2$	n_x	n_y	n_z	$N_{\uparrow\downarrow}$
0	0	0	0	2
1	-1	0	0	
1	1	0	0	
1	0	-1	0	
1	0	1	0	
1	0	0	-1	
1	0	0	1	14
2	-1	-1	0	
2	-1	1	0	
2	1	-1	0	
2	1	1	0	
2	-1	0	-1	
2	-1	0	1	
2	1	0	-1	
2	1	0	1	
2	0	-1	-1	
2	0	-1	1	
2	0	1	-1	
2	0	1	1	38
3	-1	-1	-1	
3	-1	-1	1	
3	-1	1	-1	
3	-1	1	1	
3	1	-1	-1	
3	1	-1	1	
3	1	1	-1	
3	1	1	1	54

Continuing in this way we get for $n_x^2 + n_y^2 + n_z^2 = 4$ a total of 22 additional states, resulting in 76 as a new magic number. For the lowest six energy values the degeneracy in energy gives

us 2, 14, 38, 54, 76 and 114 as magic numbers. These numbers will then define our Fermi level when we compute the energy in a Cartesian basis. When performing calculations based on many-body perturbation theory, Coupled cluster theory or other many-body methods, we need then to add states above the Fermi level in order to sum over single-particle states which are not occupied.

If we wish to study infinite nuclear matter with both protons and neutrons, the above magic numbers become $4, 28, 76, 108, 132, 228, \ldots$.

Every number of particles for filled shells defines also the number of particles to be used in a given calculation. The number of particles can in turn be used to define the density n (or the Fermi momentum) of the system via

$$n = g \frac{k_F^3}{6\pi^2},$$

where k_F is the Fermi momentum and the degeneracy g, which is two for one type of spin-$1/2$ particles and four for symmetric nuclear matter. With the density defined, having fixed the number of particles A and the Fermi momentum k_F, we can define the length L of the box used with periodic boundary contributions via the relation

$$V = L^3 = \frac{A}{n}.$$

We can then can use L to define the spacing between various k-values, that is

$$\Delta k = \frac{2\pi}{L}.$$

Here, A can be the number of nucleons. If we deal with the electron gas only, this needs to be replaced by the number of electrons N. Exercise 8.4 deals with setting up a program that establishes the single-particle basis for nuclear matter calculations with input a given number of nucleons and a user specificied density or Fermi momentum.

8.2.3 Two-body interaction

As mentioned above, we will employ a plane wave basis for our calculations of infinite matter properties. With a cartesian basis it means that we can calculate directly the various matrix elements, as discussed in the previous subsection. However, a cartesian basis represents an approximation to the thermodynamical limit. In order to compare the stability of our basis with results from the thermodynamical limit, it is convenient to rewrite the nucleon-nucleon interaction in terms of a partial wave expansion. This will allow us to compute the Hartree-Fock energy of the ground state in the thermodynamical limit (with the caveat that we need to limit the number of partial waves). In order to find the expressions for the Hartree-Fock energy in a partial wave basis, we will find it convenient to rewrite our two-body force in terms of the relative and center-of-mass motion momenta.

The direct matrix element, with single-particle three-dimensional momenta $\mathbf{k}_p$, spin σ_p and isospin τ_p, is defined as

$$\langle \mathbf{k}_p \sigma_p \tau_p \mathbf{k}_q \sigma_q \tau_q | \hat{v} | \mathbf{k}_r \sigma_r \tau_r \mathbf{k}_s \sigma_s \tau_s \rangle,$$

or in a more compact form as $\langle \mathbf{pq} | \hat{v} | \mathbf{rs} \rangle$ where the boldfaced letters $\mathbf{p}$ etc represent the relevant quantum numbers, here momentum, spin and isospin. Introducing the relative momentum

$$\mathbf{k} = \frac{1}{2} \left(\mathbf{k}_p - \mathbf{k}_q \right),$$

and the center-of-mass momentum

$$\mathbf{K} = \mathbf{k}_p + \mathbf{k}_q,$$

we have

$$\langle \mathbf{k}_p \sigma_p \tau_p \mathbf{k}_q \sigma_q \tau_q | \hat{v} | \mathbf{k}_r \sigma_r \tau_r \mathbf{k}_s \sigma_s \tau_s \rangle = \langle \mathbf{k} \mathbf{K} \sigma_p \tau_p \sigma_q \tau_q | \hat{v} | \mathbf{k}' \mathbf{K}' \sigma_r \tau_r \sigma_s \tau_s \rangle.$$

The nucleon-nucleon interaction conserves the total momentum and charge, implying that the above uncoupled matrix element reads

$$\langle \mathbf{k} \mathbf{K} \sigma_p \tau_p \sigma_q \tau_q | \hat{v} | \mathbf{k}' \mathbf{K}' \sigma_r \tau_r \sigma_s \tau_s \rangle = \delta_{T_z,T_z'} \delta(\mathbf{K} - \mathbf{K}') \langle \mathbf{k} T_z S_z = (\sigma_a + \sigma_b) | \hat{v} | \mathbf{k}' T_z S_z' = (\sigma_c + \sigma_d) \rangle,$$

where we have defined the isospin projections $T_z = \tau_p + \tau_q$ and $T_z' = \tau_r + \tau_s$. Defining $\hat{v} = \hat{v}(\mathbf{k}, \mathbf{k}')$, we can rewrite the previous equation in a more compact form as

$$\delta_{T_z,T_z'} \delta(\mathbf{K} - \mathbf{K}') \langle \mathbf{k} T_z S_z = (\sigma_p + \sigma_q) | \hat{v} | \mathbf{k}' T_z S_z' = (\sigma_r + \sigma_s) \rangle = \delta_{T_z,T_z'} \delta(\mathbf{K} - \mathbf{K}') \langle T_z S_z | \hat{v}(\mathbf{k}, \mathbf{k}') | T_z S_z' \rangle.$$

These matrix elements can in turn be rewritten in terms of the total two-body quantum numbers for the spin S of two spin-1/2 fermions as

$$\langle \mathbf{k} T_z S_z | \hat{v}(\mathbf{k}, \mathbf{k}') | \mathbf{k}' T_z S_z' \rangle = \sum_{SS'} \langle \frac{1}{2} \sigma_p \frac{1}{2} \sigma_q | S S_z \rangle \langle \frac{1}{2} \sigma_r \frac{1}{2} \sigma_s | S' S_z' \rangle \langle \mathbf{k} T_z S S_z | \hat{v}(\mathbf{k}, \mathbf{k}') | \mathbf{k}' T_z S' S_z' \rangle$$

The coefficients $\langle \frac{1}{2} \sigma_p \frac{1}{2} \sigma_q | S S_z \rangle$ are so-called Clebsch-Gordan recoupling coefficients. We will assume that our interactions break charge and isospin symmetry. We will refer to $T_z = 0$ as the *pn* (proton-neutron) channel, $T_z = -1$ as the *pp* (proton-proton) channel and $T_z = 1$ as the *nn* (neutron-neutron) channel.

The nucleon-nucleon force is often derived and analyzed theoretically in terms of a partial wave expansion. A state with linear momentum $\mathbf{k}$ can be written as

$$|\mathbf{k}\rangle = \sum_{l=0}^{\infty} \sum_{l_l=-l}^{L} \iota^l Y_l^{m_l}(\hat{k}) |klm_l\rangle.$$

In terms of the relative and center-of-mass momenta $\mathbf{k}$ and $\mathbf{K}$, the potential in momentum space is related to the nonlocal operator $V(\mathbf{r}, \mathbf{r}')$ by

$$\langle \mathbf{k}' \mathbf{K}' | \hat{v} | \mathbf{k}' \mathbf{K} \rangle = \int d\mathbf{r} d\mathbf{r}' e^{-\iota \mathbf{k}' \mathbf{r}'} V(\mathbf{r}', \mathbf{r}) e^{\iota \mathbf{k} \mathbf{r}} \delta(\mathbf{K}, \mathbf{K}'). \tag{8.16}$$

We will assume that the interaction is spherically symmetric and use the partial wave expansion of the plane waves in terms of spherical harmonics. This means that we can separate the radial part of the wave function from its angular dependence. The wave function of the relative motion is described in terms of plane waves as

$$e^{\iota \mathbf{k} \mathbf{r}} = \langle \mathbf{r} | \mathbf{k} \rangle = 4\pi \sum_{lm} \iota^l j_l(kr) Y_{lm}^*(\hat{\mathbf{k}}) Y_{lm}(\hat{\mathbf{r}}), \tag{8.17}$$

where j_l is a spherical Bessel function and Y_{lm} the spherical harmonic. This partial wave basis is useful for defining the operator for the nucleon-nucleon interaction, which is symmetric with respect to rotations, parity and isospin transformations. These symmetries imply that the interaction is diagonal with respect to the quantum numbers of total angular momentum J, spin S and isospin T. Using the above plane wave expansion, and coupling to final J, S and T we get

$$\langle \mathbf{k}' | V | \mathbf{k} \rangle = (4\pi)^2 \sum_{JM} \sum_{lm} \sum_{l'm'} \iota^{l+l'} Y_{lm}^*(\hat{\mathbf{k}}) Y_{l'm'}(\hat{\mathbf{k}}') \mathscr{C}_{m'M_S M}^{l'SJ} \mathscr{C}_{mM_S M}^{lSJ} \langle k'l'STJM | V | klSTJM \rangle, \tag{8.18}$$

where we have defined

$$\langle k'l'STJM|V|klSTJM\rangle = \int j_{l'}(k'r')\langle l'STJM|V(r',r)|lSTJM\rangle j_l(kr)r'^2 dr' r^2 dr. \tag{8.19}$$

We have omitted the momentum of the center-of-mass motion $\mathbf{K}$ and the corresponding orbital momentum L, since the interaction is diagonal in these variables. The potentials we will employ in this work, like those of the Bonn group, are all non-local potentials defined in momentum space, and we will therefore not need the last equation.

The interaction we will use for these calculations is a semirealistic nucleon-nucleon potential known as the Minnesota potential [?] which has the form, $V_\alpha(r) = V_\alpha \exp-(\alpha r^2)$. The spin and isospin dependence of the Minnesota potential is given by,

$$V(r) = \frac{1}{2}\left(V_R + \frac{1}{2}(1 + P_{12}^\sigma)V_T + \frac{1}{2}(1 - P_{12}^\sigma)V_S\right)(1 - P_{12}^\sigma P_{12}^\tau), \tag{8.20}$$

where $P_{12}^\sigma = \frac{1}{2}(1 + \sigma_1 \cdot \sigma_2)$ and $P_{12}^\tau = \frac{1}{2}(1 + \tau_1 \cdot \tau_2)$ are the spin and isospin exchange operators, respectively. A Fourier transform to momentum space of the radial part $V_\alpha(r)$ is rather simple, see problem 8.5, since the radial depends only on the magnitude of the relative distance and thereby the relative momentum $\mathbf{q} = \frac{1}{2}(\mathbf{k}_p - \mathbf{k}_q - \mathbf{k}_r + \mathbf{k}_s)$. Omitting spin and isospin dependencies, the momentum space version of the interaction reads

$$\langle \mathbf{k}_p \mathbf{k}_q |V_\alpha| \mathbf{k}_r \mathbf{k}_s\rangle = \frac{V_\alpha}{L^3}\left(\frac{\pi}{\alpha}\right)^{3/2}\exp\left(\frac{-q^2}{4\alpha}\right)\delta_{\mathbf{k}_p + \mathbf{k}_q, \mathbf{k}_r + \mathbf{k}_s} \tag{8.21}$$

The various parameters defining the interaction model used in this work are listed in Table 8.2.

Table 8.2 Parameters used to define the Minnesota interaction model [?].

α	V_α	κ_α
R	200 MeV	1.487 fm^{-2}
T	178 MeV	0.639 fm^{-2}
S	91.85 MeV	0.465 fm^{-2}

8.2.4 Models from Effective field theory for the two- and three-nucleon interactions

During the past two decades, it has been demonstrated that chiral effective field theory represents a powerful tool to deal with hadronic interactions at low energy in a systematic and model-independent way (see Refs. [?,?,?,?,?,?,7,8,31]). EFTs are defined in terms of effective Lagrangians which are given by an infinite series of terms with increasing number of derivatives and/or nucleon fields, with the dependence of each term on the pion field prescribed by the rules of broken chiral symmetry. Applying this Lagrangian to a particular process, an unlimited number of Feynman graphs can be drawn. Therefore, a scheme is needed that makes the theory manageable and calculable. This scheme which tells us how to distinguish between large (important) and small (unimportant) contributions is chiral perturbation theory (ChPT). ChPT allows for an expansion in terms of $(Q/\Lambda_\chi)^\nu$, where Q is generic for an external momentum (nucleon three-momentum or pion four-momentum) or a pion mass, and $\Lambda_\chi \sim 1$ GeV
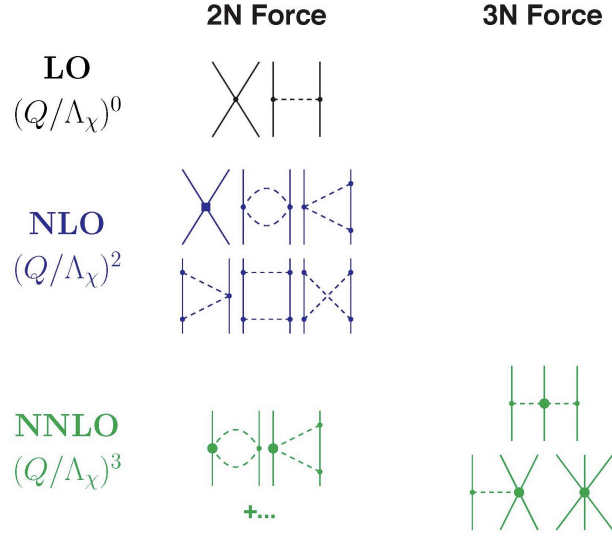
Fig. 8.1 Nuclear forces in ChPT up to NNLO. Solid lines represent nucleons and dashed lines pions. Small dots, large solid dots, and solid squares denote vertices of index $\Delta_i = 0$, 1, and 2, respectively.

is the chiral symmetry breaking scale. Determining the power ν has become known as power counting.

Nuclear potentials are defined as sets of irreducible graphs up to a given order. The power ν of a few-nucleon diagram involving A nucleons is given in terms of naive dimensional analysis by:

$$\nu = -2 + 2A - 2C + 2L + \sum_i \Delta_i , \qquad (8.22)$$

with

$$\Delta_i \equiv d_i + \frac{n_i}{2} - 2 , \qquad (8.23)$$

where C denotes the number of separately connected pieces and L the number of loops in the diagram; d_i is the number of derivatives or pion-mass insertions and n_i the number of nucleon fields (nucleon legs) involved in vertex i; the sum runs over all vertices contained in the diagram under consideration. Note that $\Delta_i \geq 0$ for all interactions allowed by chiral symmetry. In this work we will focus on optimized two- and three-nucleon forces at order NNLO, as indicated in Fig. 8.1. Studies of the convergence of chiral perturbation theory for the quantities studied here, will be presented in a future work.

Below we revisit briefly the formalism and results presented in Refs. [**?**]. For further details on chiral effective field theory and nuclear interactions, see for example Refs. [7, 8, 31] For an irreducible NN diagram ("two-nucleon potential", $A = 2$, $C = 1$), Eq. (8.22) collapses to

$$\nu = 2L + \sum_i \Delta_i . \qquad (8.24)$$

Thus, in terms of naive dimensional analysis or "Weinberg counting" [**?**,**?**], the various orders of the irreducible graphs which define the chiral NN potential are given by (cf. Fig. 8.1)

$$V_{\text{LO}} = V_{\text{ct}}^{(0)} + V_{1\pi}^{(0)} \qquad (8.25)$$

$$V_{\text{NLO}} = V_{\text{LO}} + V_{\text{ct}}^{(2)} + V_{1\pi}^{(2)} + V_{2\pi}^{(2)} \qquad (8.26)$$

$$V_{\text{NNLO}} = V_{\text{NLO}} + V_{1\pi}^{(3)} + V_{2\pi}^{(3)} \qquad (8.27)$$

where the superscript denotes the order ν of the low-momentum expansion. LO stands for leading order, NLO for next-to-leading order and NNLO stands for next-to-next-to leading order. Contact potentials carry the subscript "ct" and pion-exchange potentials can be identified by an obvious subscript.

The charge-independent one-pion-exchange (1PE) potential reads

$$V_{1\pi}(\mathbf{k}',\mathbf{k}) = -\frac{g_A^2}{4f_\pi^2}\,\tau_1\cdot\tau_2\,\frac{\sigma_1\cdot\mathbf{q}\,\sigma_2\cdot\mathbf{q}}{q^2+m_\pi^2}\,, \tag{8.28}$$

where $\mathbf{k}'$ and $\mathbf{k}$ represent the final and initial nucleon momenta in the center-of-mass system (CMS) and $\mathbf{q} \equiv \mathbf{k}' - \mathbf{k}$ is the momentum transfer; $\sigma_{1,2}$ and $\tau_{1,2}$ are the spin and isospin operators of nucleon 1 and 2; g_A, f_π, and m_π denote axial-vector coupling constant, the pion decay constant, and the pion mass, respectively. Since higher order corrections contribute only to mass and coupling constant renormalizations and since, on shell, there are no relativistic corrections, the on-shell 1PE has the form of Eq. (8.28) to all orders.

It is well known that, for high-precision NN potentials, charge dependence is important. Therefore, we will take the charge dependence of the 1PE into account. Defining a pion-mass dependent 1PE by

$$V_{1\pi}(m_\pi) \equiv -\frac{g_A^2}{4f_\pi^2}\,\frac{\sigma_1\cdot\mathbf{q}\,\sigma_2\cdot\mathbf{q}}{q^2+m_\pi^2}\,,$$

the 1PE for proton-proton (pp) and neutron-neutron (nn) scattering is

$$V_{1\pi}^{(pp)}(\mathbf{k}',\mathbf{k}) = V_{1\pi}^{(nn)}(\mathbf{k}',\mathbf{k}) = V_{1\pi}(m_{\pi^0})\,,$$

while for neutron-proton (np) scattering we have

$$V_{1\pi}^{(np)}(\mathbf{k}',\mathbf{k}) = -V_{1\pi}(m_{\pi^0}) + (-1)^{T+1}\,2V_{1\pi}(m_{\pi^\pm})\,,$$

where T denotes the isospin of the two-nucleon system. We use $m_{\pi^0} = 134.9766$ MeV and $m_{\pi^\pm} = 139.5702$ MeV. For the leading-order, next-to-leading order and NNLO, we refer the reader to Refs. [?, 7]. The final interaction at order NNLO is multiplied with the following factors [7],

$$\widehat{V}(\mathbf{k}',\mathbf{k}) \equiv \frac{1}{(2\pi)^3}\sqrt{\frac{M_N}{E_{p'}}}\,V(\mathbf{p}',\mathbf{p})\,\sqrt{\frac{M_N}{E_p}} \tag{8.29}$$

with $E_p = \sqrt{M_N^2 + p^2}$ and where the factor $1/(2\pi)^3$ is just added for convenience. The potential $\widehat{V}$ satisfies the nonrelativistic Lippmann-Schwinger (LS) equation,

$$\widehat{T}(\mathbf{k}',\mathbf{k}) = \widehat{V}(\mathbf{k}',\mathbf{k}) + \int d^3p''\,\widehat{V}(\mathbf{k}',\mathbf{k}'')\,\frac{M_N}{k^2-k''^2+i\varepsilon}\,\widehat{T}(\mathbf{k}'',\mathbf{k})\,. \tag{8.30}$$

In pp scattering, we use $M_N = M_p = 938.2720$ MeV, and in nn scattering, $M_N = M_n = 939.5653$ MeV. Moreover, the on-shell momentum is simply

$$p^2 = \frac{1}{2}M_N T_{\text{lab}}\,, \tag{8.31}$$

where T_{lab} denotes the kinetic energy of the incident nucleon in the laboratory system ("Lab. Energy"). For np scattering, we have

$$M_N = \frac{2M_p M_n}{M_p + M_n} = 938.9182 \text{ MeV, and} \tag{8.32}$$

$$p^2 = \frac{M_p^2 T_{\text{lab}}(T_{\text{lab}} + 2M_n)}{(M_p + M_n)^2 + 2T_{\text{lab}}M_p}, \tag{8.33}$$

which is based upon relativistic kinematics.

Iteration of $\widehat{V}$ in the LS equation, Eq. (8.30), requires cutting $\widehat{V}$ off for high momenta to avoid infinities. This is consistent with the fact that ChPT is a low-momentum expansion which is valid only for momenta $Q \ll \Lambda_\chi \approx 1$ GeV. Therefore, the potential $\widehat{V}$ is multiplied with the regulator function $f(k',k)$,

$$\widehat{V}(\mathbf{k}', \mathbf{k}) \longmapsto \widehat{V}(\mathbf{k}', \mathbf{k}) f(k', k) \tag{8.34}$$

with

$$f(p', p) = \exp[-(p'/\Lambda)^{2n} - (p/\Lambda)^{2n}]. \tag{8.35}$$

Up to NNLO in chiral perturbation theory there are, in addition to the two-body interaction diagrams discussed above, also a few three-body interaction diagrams, see Fig. 8.1. In chiral perturbation theory, the orders are generated systematically, and at a given chiral order the number of Feynman diagrams is finite. Consistency requires that a calculation includes all diagrams which are present at the chosen order. In this work we employ chirally consistent many-body calculations including all NNLO nuclear interactions.

There are in total five contact terms that determine the strength of the NNLO three-nucleon force (3NF); c_1, c_3, and c_4 are associated with the three-body two-pion-exchange (2PE) diagram, c_D and c_E determine the strength of the one-pion-exchange plus contact (1PE) diagram and the pure contact (CNT) diagram, respectively. Following the notation of Ref. [32] the three-body diagrams are given by

$$V_{ijk}^{2PE} = \sum_{i \neq j \neq k} \frac{1}{2} \left(\frac{g_A}{f_\pi}\right)^2 \frac{(\boldsymbol{\sigma_i} \cdot \mathbf{q_i})(\boldsymbol{\sigma_j} \cdot \mathbf{q_j})}{(\mathbf{q_i}^2 + m_\pi^2)(\mathbf{q_j}^2 + m_\pi^2)} F_{ijk}^{\alpha\beta} \tau_i^\alpha \tau_j^\beta, \tag{8.36}$$

where q_i denotes the momentum transfer associated with nucleon i, and

$$F_{ijk}^{\alpha\beta} = \delta^{\alpha\beta} \left[-\frac{4c_1 m_\pi^2}{f_\pi^2} + \frac{2c_3}{f_\pi^2} \mathbf{q_i} \cdot \mathbf{q_j} \right] \tag{8.37}$$

$$+ \sum_\gamma \frac{c_4}{f_\pi^2} \varepsilon^{\alpha\beta\gamma} \tau_k^\gamma \boldsymbol{\sigma_k} \cdot [\mathbf{q_i} \times \mathbf{q_j}]. \tag{8.38}$$

For this diagram, no new parameters are introduced since the c_1, c_3, c_4 appear already in the 2PE two-nucleon interaction. The remaining two three-body terms are given by

$$V_{ijk}^{1PE} = -\sum_{i \neq j \neq k} \frac{g_A}{8f_\pi^2} \frac{c_D}{f_\pi^2 \Lambda_\chi} \frac{(\boldsymbol{\sigma_j} \cdot \mathbf{q_j})}{(\mathbf{q_j}^2 + m_\pi^2)} (\tau_i \cdot \tau_j)(\boldsymbol{\sigma_i} \cdot \boldsymbol{\sigma_j}) \tag{8.39}$$

and

$$V_{ijk}^{CNT} = \frac{1}{2} \sum_{i \neq j \neq k} \frac{c_E}{f_\pi^4 \Lambda_\chi} (\tau_i \cdot \tau_j) \tag{8.40}$$

with $\Lambda_\chi = 700$ MeV. Following [33], we use a regulator depending on the momentum-transfer q,

$$f(q) = \exp[-q^4/\Lambda] \tag{8.41}$$

and thus obtain a local three-body force.

8.3 Hartree-Fock theory

Hartree-Fock (HF) theory is an algorithm for finding an approximative expression for the ground state of a given Hamiltonian. The basic ingredients contain a single-particle basis $\{\psi_\alpha\}$ defined by the solution of the following eigenvalue problem

$$\hat{h}^{\mathrm{HF}} \psi_\alpha = \varepsilon_\alpha \psi_\alpha,$$

with the Hartree-Fock Hamiltonian defined as

$$\hat{h}^{\mathrm{HF}} = \hat{t} + \hat{u}_{\mathrm{ext}} + \hat{u}^{\mathrm{HF}}.$$

The term $\hat{u}^{\mathrm{HF}}$ is a single-particle potential to be determined by the HF algorithm. The HF algorithm means to choose $\hat{u}^{\mathrm{HF}}$ in order to have

$$\langle \hat{H} \rangle = E^{\mathrm{HF}} = \langle \Phi_0^{HF} | \hat{H} | \Phi_0^{HF} \rangle,$$

that is to find a local minimum with a Slater determinant Φ_0^{HF} being the ansatz for the ground state. The variational principle ensures that $E^{\mathrm{HF}} \geq E_0$, with E_0 the exact ground state energy.

We will show that the Hartree-Fock Hamiltonian $\hat{h}^{\mathrm{HF}}$ equals our definition of the operator $\hat{f}$ discussed in connection with the new definition of the normal-ordered Hamiltonian, that is we have, for a specific matrix element

$$\langle p | \hat{h}^{\mathrm{HF}} | q \rangle = \langle p | \hat{f} | q \rangle = \langle p | \hat{t} + \hat{u}_{\mathrm{ext}} | q \rangle + \sum_{i \leq F} \langle pi | \hat{V} | qi \rangle_{AS},$$

meaning that

$$\langle p | \hat{u}^{\mathrm{HF}} | q \rangle = \sum_{i \leq F} \langle pi | \hat{V} | qi \rangle_{AS}.$$

The so-called Hartree-Fock potential $\hat{u}^{\mathrm{HF}}$ brings an explicit medium dependence due to the summation over all single-particle states below the Fermi level F. It brings also in an explicit dependence on the two-body interaction (in nuclear physics we can also have complicated three- or higher-body forces). The two-body interaction, with its contribution from the other bystanding fermions, creates an effective mean field in which a given fermion moves, in addition to the external potential $\hat{u}_{\mathrm{ext}}$ which confines the motion of the fermion. For systems like nuclei or infinite nuclear matter, there is no external confining potential. Nuclei and nuclear matter are examples of self-bound systems, where the binding arises due to the intrinsic nature of the strong force. For nuclear systems thus, there would be no external one-body potential in the Hartree-Fock Hamiltonian.

Another possibility is to expand the single-particle functions in a known basis and vary the coefficients, that is, the new single-particle wave function is written as a linear expansion in terms of a fixed chosen orthogonal basis (for example the well-known harmonic oscillator functions or the hydrogen-like functions etc). We define our new Hartree-Fock single-particle basis by performing a unitary transformation on our previous basis (labelled with greek indices) as

$$\psi_p^{HF} = \sum_\lambda C_{p\lambda} \phi_\lambda. \tag{8.42}$$

In this case we vary the coefficients $C_{p\lambda}$. If the basis has infinitely many solutions, we need to truncate the above sum. We assume that the basis ϕ_λ is orthogonal. A unitary transformation keeps the orthogonality, as discussed in problem **??** below.

It is normal to choose a single-particle basis defined as the eigenfunctions of parts of the full Hamiltonian. The typical situation consists of the solutions of the one-body part of the Hamiltonian, that is we have

$$\hat{h}_0 \phi_\lambda = \varepsilon_\lambda \phi_\lambda.$$

For infinite nuclear matter $\hat{h}_0$ is given by the kinetic energy operator and the states are given by plane wave functions. Due to the translational invariance of the two-body interaction, the Hartree-Fock single-particle eigenstates are also given by the same functions. For infinite matter thus, it is only the single-particle energies that change when we solve the Hartree-Fock equations.

The single-particle wave functions $\phi_\lambda(\mathbf{r})$, defined by the quantum numbers λ and $\mathbf{r}$ are defined as the overlap

$$\phi_\lambda(\mathbf{r}) = \langle \mathbf{r} | \lambda \rangle.$$

In our discussions we will use our definitions of single-particle states above and below the Fermi (F). Levels given by the labels $ijkl\cdots \le F$ refer to single-hole states and $abcd\cdots > F$ for so-called particle states. For general single-particle states we employ the labels $pqrs\ldots$.

We use greek letters to refer to our original single-particle basis. The expectation value for the energy with the ansatz Φ_0 for the ground state reads (see problem 8.7, with application to infinite nuclear matter)

$$E[\Phi_0] = \sum_{\mu=1}^{A} \langle \mu | h | \mu \rangle + \frac{1}{2} \sum_{\mu=1}^{A} \sum_{\nu=1}^{A} \langle \mu\nu | \hat{v} | \mu\nu \rangle_{AS}.$$

Now we are interested in defining a new basis defined in terms of a chosen basis as defined in Eq. (8.42). We can then rewrite the energy functional as

$$E[\Phi^{HF}] = \sum_{i=1}^{A} \langle i | h | i \rangle + \frac{1}{2} \sum_{ij=1}^{A} \langle ij | \hat{v} | ij \rangle_{AS}, \tag{8.43}$$

where Φ^{HF} is the new Slater determinant defined by the new basis of Eq. (8.42).

Using Eq. (8.42) we can rewrite Eq. (8.43) as

$$E[\Psi] = \sum_{i=1}^{A} \sum_{\alpha\beta} C_{i\alpha}^* C_{i\beta} \langle \alpha | h | \beta \rangle + \frac{1}{2} \sum_{ij=1}^{A} \sum_{\alpha\beta\gamma\delta} C_{i\alpha}^* C_{j\beta}^* C_{i\gamma} C_{j\delta} \langle \alpha\beta | \hat{v} | \gamma\delta \rangle_{AS}. \tag{8.44}$$

We wish now to minimize the above functional. We introduce a set of Lagrange multipliers, noting that since $\langle i | j \rangle = \delta_{i,j}$ and $\langle \alpha | \beta \rangle = \delta_{\alpha,\beta}$, the coefficients $C_{i\gamma}$ obey the relation

$$\langle i | j \rangle = \delta_{i,j} = \sum_{\alpha\beta} C_{i\alpha}^* C_{i\beta} \langle \alpha | \beta \rangle = \sum_{\alpha} C_{i\alpha}^* C_{i\alpha},$$

which allows us to define a functional to be minimized that reads

$$F[\Phi^{HF}] = E[\Phi^{HF}] - \sum_{i=1}^{A} \varepsilon_i \sum_{\alpha} C_{i\alpha}^* C_{i\alpha}. \tag{8.45}$$

Minimizing with respect to $C_{i\alpha}^*$ (the equations for $C_{i\alpha}^*$ and $C_{i\alpha}$ can be written as two independent equations) we obtain

$$\frac{d}{dC_{i\alpha}^*} \left[E[\Phi^{HF}] - \sum_j \varepsilon_j \sum_\alpha C_{j\alpha}^* C_{j\alpha} \right] = 0,$$

which yields for every single-particle state i and index α (recalling that the coefficients $C_{i\alpha}$ are matrix elements of a unitary matrix, or orthogonal for a real symmetric matrix) the following Hartree-Fock equations

$$\sum_\beta C_{i\beta} \langle \alpha|h|\beta \rangle + \sum_{j=1}^{A} \sum_{\beta\gamma\delta} C_{j\beta}^* C_{j\delta} C_{i\gamma} \langle \alpha\beta|\hat{v}|\gamma\delta \rangle_{AS} = \varepsilon_i^{HF} C_{i\alpha}.$$

We can rewrite this equation as (changing dummy variables)

$$\sum_\beta \left\{ \langle \alpha|h|\beta \rangle + \sum_{j}^{A} \sum_{\gamma\delta} C_{j\gamma}^* C_{j\delta} \langle \alpha\gamma|\hat{v}|\beta\delta \rangle_{AS} \right\} C_{i\beta} = \varepsilon_i^{HF} C_{i\alpha}.$$

Note that the sums over greek indices run over the number of basis set functions (in principle an infinite number).

Defining

$$h_{\alpha\beta}^{HF} = \langle \alpha|h|\beta \rangle + \sum_{j=1}^{A} \sum_{\gamma\delta} C_{j\gamma}^* C_{j\delta} \langle \alpha\gamma|\hat{v}|\beta\delta \rangle_{AS},$$

we can rewrite the new equations as

$$\sum_\gamma h_{\alpha\beta}^{HF} C_{i\beta} = \varepsilon_i^{HF} C_{i\alpha}. \tag{8.46}$$

The latter is nothing but a standard eigenvalue problem. Our Hartree-Fock matrix is thus

$$\hat{h}_{\alpha\beta}^{HF} = \langle \alpha|\hat{h}_0|\beta \rangle + \sum_{j=1}^{A} \sum_{\gamma\delta} C_{j\gamma}^* C_{j\delta} \langle \alpha\gamma|\hat{v}|\beta\delta \rangle_{AS}.$$

The Hartree-Fock equations are solved in an iterative way starting with a guess for the coefficients $C_{j\gamma} = \delta_{j,\gamma}$ and solving the equations by diagonalization till the new single-particle energies ε_i^{HF} do not change anymore by a prefixed quantity.

Normally we assume that the single-particle basis $|\beta\rangle$ forms an eigenbasis for the operator $\hat{h}_0$, meaning that the Hartree-Fock matrix becomes

$$\hat{h}_{\alpha\beta}^{HF} = \varepsilon_\alpha \delta_{\alpha,\beta} + \sum_{j=1}^{A} \sum_{\gamma\delta} C_{j\gamma}^* C_{j\delta} \langle \alpha\gamma|\hat{v}|\beta\delta \rangle_{AS}.$$

8.3.1 Hartree-Fock algorithm with simple Python code

The equations are often rewritten in terms of a so-called density matrix, which is defined as

$$\rho_{\gamma\delta} = \sum_{i=1}^{N} \langle \gamma|i \rangle \langle i|\delta \rangle = \sum_{i=1}^{N} C_{i\gamma} C_{i\delta}^*. \tag{8.47}$$

It means that we can rewrite the Hartree-Fock Hamiltonian as

$$\hat{h}_{\alpha\beta}^{HF} = \varepsilon_\alpha \delta_{\alpha,\beta} + \sum_{\gamma\delta} \rho_{\gamma\delta} \langle \alpha\gamma|V|\beta\delta \rangle_{AS}.$$

It is convenient to use the density matrix since we can precalculate in every iteration the product of the eigenvector components C.

The Hartree-Fock equations are, in their simplest form, solved in an iterative way, starting with a guess for the coefficients $C_{i\alpha}$. We label the coefficients as $C_{i\alpha}^{(n)}$, where the superscript n stands for iteration n. To set up the algorithm we can proceed as follows.

1. We start with a guess $C_{i\alpha}^{(0)} = \delta_{i,\alpha}$. Alternatively, we could have used random starting values as long as the vectors are normalized. Another possibility is to give states below the Fermi level a larger weight. We construct then the density matrix and the Hartree-Fock Hamiltonian.

2. The Hartree-Fock matrix simplifies then to

$$\hat{h}_{\alpha\beta}^{HF}(0) = \varepsilon_\alpha \delta_{\alpha,\beta} + \sum_{\gamma\delta} \rho_{\gamma\delta}^{(0)} \langle \alpha\gamma | V | \beta\delta \rangle_{AS}.$$

Solving the Hartree-Fock eigenvalue problem yields then new eigenvectors $C_{i\alpha}^{(1)}$ and eigenvalues $\varepsilon_i^{HF}(1)$.

3. With the new eigenvectors we can set up a new Hartree-Fock potential

$$\sum_{\gamma\delta} \rho_{\gamma\delta}^{(1)} \langle \alpha\gamma | V | \beta\delta \rangle_{AS}.$$

The diagonalization with the new Hartree-Fock potential yields new eigenvectors and eigenvalues.

4. This process is continued till a user defined test is satisfied. As an example, we can require that

$$\frac{\sum_p |\varepsilon_i^{(n)} - \varepsilon_i^{(n-1)}|}{m} \leq \lambda,$$

where λ is a small number defined by the user ($\lambda \sim 10^{-8}$ or smaller) and p runs over all calculated single-particle energies and m is the number of single-particle states.

The following simple Python program implements the above algorithm using the density matrix formalism outlined above. We have omitted the functions that set up the single-particle basis and the anti-symmetrized two-body interaction matrix elements. These have to be provided.

```python
import numpy as np
from decimal import Decimal
# We skip here functions that set up the one- and two-body parts of the Hamiltonian
# These functions need to be defined by the user. The two-body interaction below is
# calculated by calling the function TwoBodyInteraction(alpha,gamma,beta,delta)
# Similalry, the one-body part is computed by the function singleparticleH(alpha)
# We have omitted specific quantum number tests as well (isopsin conservation,
# momentum conservation etc)

if __name__ == '__main__':

  """ Star HF-iterations, preparing variables and density matrix """

      """ Coefficients for setting up density matrix, assuming only one along the diagonals
          """
  C = np.eye(spOrbitals) # HF coefficients
      DensityMatrix = np.zeros([spOrbitals,spOrbitals])
      for gamma in range(spOrbitals):
          for delta in range(spOrbitals):
              sum = 0.0
              for i in range(Nparticles):
                  sum += C[gamma][i]*C[delta][i]
              DensityMatrix[gamma][delta] = Decimal(sum)
      maxHFiter = 100
      epsilon = 1.0e-5
      difference = 1.0
  hf_count = 0
```

```python
oldenergies = np.zeros(spOrbitals)
newenergies = np.zeros(spOrbitals)
while hf_count < maxHFiter and difference > epsilon:
  print "############## Iteration %i ##############" % hf_count
        HFmatrix = np.zeros([spOrbitals,spOrbitals])
  for alpha in range(spOrbitals):
    for beta in range(spOrbitals):
                  """ Setting up the Fock matrix using the density matrix and
                      antisymmetrized two-body interaction """
              sumFockTerm = 0.0
                  for gamma in range(spOrbitals):
                      for delta in range(spOrbitals):
                          sumFockTerm +=
                              DensityMatrix[gamma][delta]*TwoBodyInteraction(alpha,gamma,beta,delta)
                  HFmatrix[alpha][beta] = Decimal(sumFockTerm)
                  """ Adding the one-body term """
                  if beta == alpha: HFmatrix[alpha][alpha] += singleparticleH(alpha)
  spenergies, C = np.linalg.eigh(HFmatrix)
          """ Setting up new density matrix """
          DensityMatrix = np.zeros([spOrbitals,spOrbitals])
          for gamma in range(spOrbitals):
              for delta in range(spOrbitals):
                  sum = 0.0
                  for i in range(Nparticles):
                      sum += C[gamma][i]*C[delta][i]
                  DensityMatrix[gamma][delta] = Decimal(sum)
  newenergies = spenergies
          """ Brute force computation of difference between previous and new sp HF
              energies """
          sum =0.0
          for i in range(spOrbitals):
              sum += (abs(newenergies[i]-oldenergies[i]))/spOrbitals
          difference = sum
          oldenergies = newenergies
          print "Single-particle energies, ordering may have changed "
          for i in range(spOrbitals):
              print('{0:4d} {1:.4f}'.format(i, Decimal(oldenergies[i])))
  hf_count += 1
```

We end this section by rewriting the ground state energy by adding and subtracting $\hat{u}^{HF}(x_i)$

$$E_0^{HF} = \langle \Phi_0 | \hat{H} | \Phi_0 \rangle = \sum_{i \leq F}^{A} \langle i | \hat{h}_0 + \hat{u}^{HF} | j \rangle + \frac{1}{2} \sum_{i \leq F}^{A} \sum_{j \leq F}^{A} [\langle ij | \hat{v} | ij \rangle - \langle ij | \hat{v} | ji \rangle] - \sum_{i \leq F}^{A} \langle i | \hat{u}^{HF} | i \rangle,$$

which results in

$$E_0^{HF} = \sum_{i \leq F}^{A} \varepsilon_i^{HF} + \frac{1}{2} \sum_{i \leq F}^{A} \sum_{j \leq F}^{A} [\langle ij | \hat{v} | ij \rangle - \langle ij | \hat{v} | ji \rangle] - \sum_{i \leq F}^{A} \langle i | \hat{u}^{HF} | i \rangle.$$

Our single-particle states $ijk\dots$ are now single-particle states obtained from the solution of the Hartree-Fock equations.

Using our definition of the Hartree-Fock single-particle energies we obtain then the following expression for the total ground-state energy

$$E_0^{HF} = \sum_{i \leq F}^{A} \varepsilon_i - \frac{1}{2} \sum_{i \leq F}^{A} \sum_{j \leq F}^{A} [\langle ij | \hat{v} | ij \rangle - \langle ij | \hat{v} | ji \rangle].$$

This equation demonstrates that the total energy is not given as the sum of the individual single-particle energies.

8.4 Full Configuration Interaction Theory

Full configuration theory (FCI), which represents a discretized variant of the continuous eigenvalue problem, allows for, in principle, a numerical exact solution of Schrödinger's equation for many interacting fermions or bosons with a given basis set. This basis set defines an effective Hilbert space. For fermionic problems, the standard approach is to define an upper limit for the set of singel-particle states. As an example, if we use the harmonic oscillator one-body Hamiltonian to generate an orthogonal single-particle basis, truncating the basis at some oscillator excitation energy provides thereby an upper limit. Similarly, truncating the maximum values of $n_{x,y,z}$ for plane wave states with periodic boundary conditions, yields a similar upper limit. Table 8.1 lists several possible truncations to the basis set in terms of the single-particle energies as functions of $n_{x,y,z}$. This single-particle basis is then used to define all possible Slater determinants which can be constructed with a given number of fermions A. The total number of Slater determinants determines thereafter the dimensionality of the Hamiltonian matrix and thereby an effective Hilbert space. truncation errors If we are able to set up the Hamiltonian matrix and solve the pertinent eigenvalue problem within this basis set, FCI provides numerically exact solutions to all states of interest for a given many-body problem. The dimensionality of the problem explodes however quickly. To see this it suffices to consider that the total number of Slater determinants which can be built with say N neutrons distributed among n single-particle states is

$$\binom{n}{N} = \frac{n!}{(n-N)!N!}.$$

As an example, for a model space which comprises the first four major harmonic oscillator shells only, that is the $0s$, $0p$, $1s0d$ and $1p0f$ shells we have 40 single particle states for neutrons and protons. For the eight neutrons of oxygen-16 we would then have

$$\binom{40}{8} = \frac{40!}{(32)!8!} \sim 8 \times 10^7,$$

possible Slater determinants and multiplying this with the number of proton Slater determinants we end up with approximately $d \sim 10^{15}$ possible Slater determinants and a Hamiltonian matrix of dimension $10^{15} \times 10^{15}$, and intractable problem if we wish to diagonalize the Hamiltonian matrix. The dimensionality can be reduced if we look at specific symmetries, however these symmetries will never reduce the problem to dimensionalities which can be handled by standard eigenvalue solvers. These are normally lumped into two main categories, direct solvers for matrices of dimensionalities which are smaller than $d \sim 10^5$, and iterative eigenvalue solvers (when only selected states are being sought after) for dimensionalities up to $10^{10} \times 10^{10}$.

Due to its discreteness thus, the effective Hilbert space will always represent an approximation to the full continuous problem. However, with a given Hamiltonian matrix and effective Hilbert space, FCI provides us with true benchmarks that can convey important information on correlations beyond Hartree-Fock theory and various approximative many-body methods like many-body perturbation theory, coupled cluster theory, Green's function theory and the Similarity Renormalization Group approach. These methods are all discussed in this text. Assuming that we can diagonalize the Hamiltonian matrix, and thereby obtain

the exact solutions, this section serves the aim to link the exact solution obtained from FCI with various approximative methods, hoping thereby that eventual differences can shed light on which correlations play a major role and should be included in the above approximative methods. The simple pairing model discussed in problem 8.9 is an example of a system that allows us to compare exact solutions with those defined by many-body perturbation theory to a given order in the interaction, coupled cluster theory, Green's function theory and the Similarity Renormalization Group (SRG). Many-body perturbation theory and coupled cluster theory are discussed in this chapter, while various SRG approaches are discussed in Chapter 10. Green's function theory is discussed in Chapter 11.

In order to familiarize the reader with these approximative many-body methods, we start with the general definition of the full configuration interaction problem.

We have defined the ansatz for the ground state as

$$|\Phi_0\rangle = \left(\prod_{i\leq F}\hat{a}_i^\dagger\right)|0\rangle,$$

where the index i defines different single-particle states up to the Fermi level. We have assumed that we have A nucleons and that the chosen single-particle basis are eigenstates of the one-body Hamiltonian $\hat{h}_0$ (defining thereby an orthogonal basis set). A given one-particle-one-hole ($1p1h$) state can be written as

$$|\Phi_i^a\rangle = \hat{a}_a^\dagger\hat{a}_i|\Phi_0\rangle,$$

while a $2p2h$ state can be written as

$$|\Phi_{ij}^{ab}\rangle = \hat{a}_a^\dagger\hat{a}_b^\dagger\hat{a}_j\hat{a}_i|\Phi_0\rangle,$$

and a general $ApAh$ state as

$$|\Phi_{ijk...}^{abc...}\rangle = \hat{a}_a^\dagger\hat{a}_b^\dagger\hat{a}_c^\dagger\ldots\hat{a}_k\hat{a}_j\hat{a}_i|\Phi_0\rangle.$$

We use letters $ijkl\ldots$ for states below the Fermi level and $abcd\ldots$ for states above the Fermi level. A general single-particle state is given by letters $pqrs\ldots$.

We can then expand our exact state function for the ground state as

$$|\Psi_0\rangle = C_0|\Phi_0\rangle + \sum_{ai}C_i^a|\Phi_i^a\rangle + \sum_{abij}C_{ij}^{ab}|\Phi_{ij}^{ab}\rangle + \cdots = (C_0+\hat{C})|\Phi_0\rangle,$$

where we have introduced the so-called correlation operator

$$\hat{C} = \sum_{ai}C_i^a\hat{a}_a^\dagger\hat{a}_i + \sum_{abij}C_{ij}^{ab}\hat{a}_a^\dagger\hat{a}_b^\dagger\hat{a}_j\hat{a}_i + \ldots$$

Since the normalization of Ψ_0 is at our disposal and since C_0 is by hypothesis non-zero, we may arbitrarily set $C_0 = 1$ with corresponding proportional changes in all other coefficients. Using this so-called intermediate normalization we have

$$\langle\Psi_0|\Phi_0\rangle = \langle\Phi_0|\Phi_0\rangle = 1,$$

resulting in

$$|\Psi_0\rangle = (1+\hat{C})|\Phi_0\rangle.$$

We rewrite

$$|\Psi_0\rangle = C_0|\Phi_0\rangle + \sum_{ai}C_i^a|\Phi_i^a\rangle + \sum_{abij}C_{ij}^{ab}|\Phi_{ij}^{ab}\rangle + \ldots,$$

in a more compact form as

$$|\Psi_0\rangle = \sum_{PH} C_H^P \Phi_H^P = \left(\sum_{PH} C_H^P \hat{A}_H^P \right) |\Phi_0\rangle,$$

where H stands for $0,1,\ldots,n$ hole states and P for $0,1,\ldots,n$ particle states. The operator $\hat{A}_H^P$ represents a given set of particle-hole excitations. For a two-particle-to-hole excitation this operator is given by $\hat{A}_{2h}^{2p} = \hat{a}_a^\dagger \hat{a}_b^\dagger \hat{a}_j \hat{a}_i$. Our requirement of unit normalization gives

$$\langle \Psi_0 | \Psi_0 \rangle = \sum_{PH} |C_H^P|^2 = 1,$$

and the energy can be written as

$$E = \langle \Psi_0 | \hat{H} | \Psi_0 \rangle = \sum_{PP'HH'} C_H^{*P} \langle \Phi_H^P | \hat{H} | \Phi_{H'}^{P'} \rangle C_{H'}^{P'}.$$

The last equation is normally solved by diagonalization, with the Hamiltonian matrix defined by the basis of all possible Slater determinants. A diagonalization is equivalent to finding the variational minimum of

$$\langle \Psi_0 | \hat{H} | \Psi_0 \rangle - \lambda \langle \Psi_0 | \Psi_0 \rangle,$$

where λ is a variational multiplier to be identified with the energy of the system.

The minimization process results in

$$\delta \left[\langle \Psi_0 | \hat{H} | \Psi_0 \rangle - \lambda \langle \Psi_0 | \Psi_0 \rangle \right] =$$

$$\sum_{P'H'} \left\{ \delta[C_H^{*P}] \langle \Phi_H^P | \hat{H} | \Phi_{H'}^{P'} \rangle C_{H'}^{P'} + C_H^{*P} \langle \Phi_H^P | \hat{H} | \Phi_{H'}^{P'} \rangle \delta[C_{H'}^{P'}] - \lambda \left(\delta[C_H^{*P}] C_{H'}^{P'} + C_H^{*P} \delta[C_{H'}^{P'}] \right) \right\} = 0.$$

Since the coefficients $\delta[C_H^{*P}]$ and $\delta[C_{H'}^{P'}]$ are complex conjugates it is necessary and sufficient to require the quantities that multiply with $\delta[C_H^{*P}]$ to vanish.

This leads to

$$\sum_{P'H'} \langle \Phi_H^P | \hat{H} | \Phi_{H'}^{P'} \rangle C_{H'}^{P'} - \lambda C_H^P = 0,$$

for all sets of P and H.

If we then multiply by the corresponding C_H^{*P} and sum over PH we obtain

$$\sum_{PP'HH'} C_H^{*P} \langle \Phi_H^P | \hat{H} | \Phi_{H'}^{P'} \rangle C_{H'}^{P'} - \lambda \sum_{PH} |C_H^P|^2 = 0,$$

leading to the identification $\lambda = E$. This means that we have for all PH sets

$$\sum_{P'H'} \langle \Phi_H^P | \hat{H} - E | \Phi_{H'}^{P'} \rangle = 0. \tag{8.48}$$

An alternative way to derive the last equation is to start from

$$(\hat{H} - E)|\Psi_0\rangle = (\hat{H} - E) \sum_{P'H'} C_{H'}^{P'} | \Phi_{H'}^{P'} \rangle = 0,$$

and if this equation is successively projected against all Φ_H^P in the expansion of Ψ, we end up with Eq. (8.48).

If we are able to solve this equation by numerical diagonaliztion in a large Hilbert space (it will be truncated in terms of the number of single-particle states included in the definition of Slater determinants), it can then serve as a benchmark for other many-body methods which approximate the correlation operator $\hat{C}$. Our pairing model discussed in problem **??** is an

example of a system which can be diagonalized numerically, providing thereby benchmarks for different approximative methods.

To better understand the meaning of possible configurations and the derivation of a Hamiltonian matrix, we consider here a simple example of six fermions. We assume we can make an ansatz for the ground state with all six fermions below the Fermi level. We will label this state as a zero-particle-zero-hole state $0p - 0h$. With six nucleons we can make at most $6p - 6h$ excitations. If we have an infinity of single particle states above the Fermi level, we will obviously have an infinity of say $2p - 2h$ excitations. Each such way to configure the particles represents a configuration. We will always have to truncate in the basis of single-particle states. This gives us a finite number of possible Slater determinants. Our Hamiltonian matrix would then look like (where each block which is marked with x can contain a large quantity of non-zero matrix elements) as shown here if the Hamiltonian contains at most a two-body interaction, as

	$0p-0h$	$1p-1h$	$2p-2h$	$3p-3h$	$4p-4h$	$5p-5h$	$6p-6h$
$0p-0h$	x	x	x	0	0	0	0
$1p-1h$	x	x	x	x	0	0	0
$2p-2h$	x	x	x	x	x	0	0
$3p-3h$	0	x	x	x	x	x	0
$4p-4h$	0	0	x	x	x	x	x
$5p-5h$	0	0	0	x	x	x	x
$6p-6h$	0	0	0	0	x	x	x

demonstrated in problem **??**. If we use a Hartree-Fock basis, this corresponds to a particular unitary transformation where matrix elements of the type $\langle 0p - 0h|\hat{H}|1p - 1h\rangle = \langle \Phi_0|\hat{H}|\Phi_i^a\rangle = 0$ and our Hamiltonian matrix becomes If we do not make any truncations in the possible sets

	$0p-0h$	$1p-1h$	$2p-2h$	$3p-3h$	$4p-4h$	$5p-5h$	$6p-6h$
$0p-0h$	$\tilde{x}$	0	$\tilde{x}$	0	0	0	0
$1p-1h$	0	$\tilde{x}$	$\tilde{x}$	$\tilde{x}$	0	0	0
$2p-2h$	$\tilde{x}$	$\tilde{x}$	$\tilde{x}$	$\tilde{x}$	$\tilde{x}$	0	0
$3p-3h$	0	$\tilde{x}$	$\tilde{x}$	$\tilde{x}$	$\tilde{x}$	$\tilde{x}$	0
$4p-4h$	0	0	$\tilde{x}$	$\tilde{x}$	$\tilde{x}$	$\tilde{x}$	$\tilde{x}$
$5p-5h$	0	0	0	$\tilde{x}$	$\tilde{x}$	$\tilde{x}$	$\tilde{x}$
$6p-6h$	0	0	0	0	$\tilde{x}$	$\tilde{x}$	$\tilde{x}$

of Slater determinants (many-body states) we can make by distributing A nucleons among n single-particle states, we call such a calculation for a full configuration interaction (FCI) approach. If we make truncations, we have different possibilities

- The standard nuclear shell-model. Here we define an effective Hilbert space with respect to a given core. The calculations are normally then performed for all many-body states that can be constructed from the effective Hilbert spaces. This approach requires a properly defined effective Hamiltonian.
- We can truncate in the number of excitations. For example, we can limit the possible Slater determinants to only $1p - 1h$ and $2p - 2h$ excitations. This is called a configuration interaction calculation at the level of singles and doubles excitations. If we truncate at the level of three-particle-three-hole excitations we end up with singles, doubles and triples excitations. Such truncations reduce considerably the size of the Hamiltonian matrices to be diagonalized, but can lead to so-called unlinked contributions, and thereby wrong results, for a given expectation value [**?**].

- We can limit the number of excitations in terms of the excitation energies. If we do not define a core, this defines normally what is called the no-core shell-model approach [34].

8.4.1 A non-practical way of solving the eigenvalue problem

For reasons to come (links with coupled cluster theory and many-body perturbation theory), we will rewrite Eq. (8.48) as a set of coupled non-linear equations in terms of the unknown coefficients C_H^P. To obtain the eigenstates and eigenvalues in terms of non-linear equations is, from a computational perspective, as a inefficient as finding the roots (and thereby eigenvalues) of the characteristic polynomial. However, this digression serves the scope of linking full configuration interaction theory with approximative solutions to the many-body problem.

To see this, we look at the contributions arising from

$$\langle \Phi_H^P | = \langle \Phi_0 |$$

in Eq. (8.48), that is we multiply with $\langle \Phi_0 |$ from the left in

$$(\hat{H} - E) \sum_{P'H'} C_{H'}^{P'} | \Phi_{H'}^{P'} \rangle = 0.$$

If we assume that we have a two-body operator at most, the Slater-Condon rule for a two-body interaction, see problem **??**, results in an expression for the correlation energy in terms of C_i^a and C_{ij}^{ab} only

$$\langle \Phi_0 | \hat{H} - E | \Phi_0 \rangle + \sum_{ai} \langle \Phi_0 | \hat{H} - E | \Phi_i^a \rangle C_i^a + \sum_{abij} \langle \Phi_0 | \hat{H} - E | \Phi_{ij}^{ab} \rangle C_{ij}^{ab} = 0,$$

or

$$E - E_{\text{Ref}} = \Delta E = \sum_{ai} \langle \Phi_0 | \hat{H} | \Phi_i^a \rangle C_i^a + \sum_{abij} \langle \Phi_0 | \hat{H} | \Phi_{ij}^{ab} \rangle C_{ij}^{ab},$$

where the energy E_{Ref} is the reference energy and ΔE defines the so-called correlation energy. The single-particle basis functions could be the results of a Hartree-Fock calculation or just the eigenstates of the non-interacting part of the Hamiltonian.

In our notes on Hartree-Fock calculations, we have already computed the matrix $\langle \Phi_0 | \hat{H} | \Phi_i^a \rangle$ and $\langle \Phi_0 | \hat{H} | \Phi_{ij}^{ab} \rangle$. If we are using a Hartree-Fock basis, $\langle \Phi_0 | \hat{H} | \Phi_i^a \rangle = 0$ and we are left with a *correlation energy* given by

$$E - E_{\text{Ref}} = \Delta E^{HF} = \sum_{abij} \langle \Phi_0 | \hat{H} | \Phi_{ij}^{ab} \rangle C_{ij}^{ab}.$$

Inserting the various matrix elements we can rewrite the previous equation as

$$\Delta E = \sum_{ai} \langle i | \hat{f} | a \rangle C_i^a + \sum_{abij} \langle ij | \hat{v} | ab \rangle C_{ij}^{ab}.$$

This equation determines the correlation energy but not the coefficients C. We need more equations. Our next step is to set up

$$\langle \Phi_i^a | \hat{H} - E | \Phi_0 \rangle + \sum_{bj} \langle \Phi_i^a | \hat{H} - E | \Phi_j^b \rangle C_j^b + \sum_{bcjk} \langle \Phi_i^a | \hat{H} - E | \Phi_{jk}^{bc} \rangle C_{jk}^{bc} + \sum_{bcdjkl} \langle \Phi_i^a | \hat{H} - E | \Phi_{jkl}^{bcd} \rangle C_{jkl}^{bcd} = 0,$$

as this equation will allow us to find an expression for the coefficents C_i^a since we can rewrite this equation as

$$\langle i|\hat{f}|a\rangle + \langle \Phi_i^a|\hat{H}|\Phi_i^a\rangle C_i^a + \sum_{bj\neq ai}\langle \Phi_i^a|\hat{H}|\Phi_j^b\rangle C_j^b + \sum_{bcjk}\langle \Phi_i^a|\hat{H}|\Phi_{jk}^{bc}\rangle C_{jk}^{bc} + \sum_{bcdjkl}\langle \Phi_i^a|\hat{H}|\Phi_{jkl}^{bcd}\rangle C_{jkl}^{bcd} = EC_i^a.$$

We see that on the right-hand side we have the energy E. This leads to a non-linear equation in the unknown coefficients. These equations are normally solved iteratively (that is we can start with a guess for the coefficients C_i^a). A common choice is to use perturbation theory for the first guess, setting thereby

$$C_i^a = \frac{\langle i|\hat{f}|a\rangle}{\varepsilon_i - \varepsilon_a}.$$

The observant reader will however see that we need an equation for C_{jk}^{bc} and C_{jkl}^{bcd} as well. To find equations for these coefficients we need then to continue our multiplications from the left with the various Φ_H^P terms.

For C_{jk}^{bc} we need then

$$\langle \Phi_{ij}^{ab}|\hat{H}-E|\Phi_0\rangle + \sum_{kc}\langle \Phi_{ij}^{ab}|\hat{H}-E|\Phi_k^c\rangle C_k^c +$$

$$\sum_{cdkl}\langle \Phi_{ij}^{ab}|\hat{H}-E|\Phi_{kl}^{cd}\rangle C_{kl}^{cd} + \sum_{cdeklm}\langle \Phi_{ij}^{ab}|\hat{H}-E|\Phi_{klm}^{cde}\rangle C_{klm}^{cde} + \sum_{cdefklmn}\langle \Phi_{ij}^{ab}|\hat{H}-E|\Phi_{klmn}^{cdef}\rangle C_{klmn}^{cdef} = 0,$$

and we can isolate the coefficients C_{kl}^{cd} in a similar way as we did for the coefficients C_i^a. A standard choice for the first iteration is to set

$$C_{ij}^{ab} = \frac{\langle ij|\hat{v}|ab\rangle}{\varepsilon_i + \varepsilon_j - \varepsilon_a - \varepsilon_b}.$$

At the end we can rewrite our solution of the Schrödinger equation in terms of a series coupled equations for the coefficients C_H^P. This is a very cumbersome way of solving a many-body problem. However, by using this iterative scheme we can illustrate how we can compute the various terms in the wave operator or correlation operator $\hat{C}$. We will later identify the calculation of the various terms C_H^P as parts of different many-body approximations to full configuration interaction theory.

8.4.2 Short summary

If we can diagonalize large matrices, full configuration uteraction theory is the method of choice since

- It gives all eigenvalues, ground state and excited states.
- The eigenvectors are obtained directly from the coefficients C_H^P which result from the diagonalization.
- We can compute easily expectation values of other operators, as well as transition probabilities.
- Correlations are easy to understand in terms of contributions to a given operator beyond the Hartree-Fock contribution. This is the standard approach in many-body theory.

The correlation energy is defined as, with a two-body Hamiltonian,

$$\Delta E = \sum_{ai}\langle i|\hat{f}|a\rangle C_i^a + \sum_{abij}\langle ij|\hat{v}|ab\rangle C_{ij}^{ab}.$$

The coefficients C result from the solution of the eigenvalue problem. The energy of say the ground state is then

$$E = E_{\text{Ref}} + \Delta E,$$

where the so-called reference energy is the energy we can obtain from a Hartree-Fock calculation However, as we have seen, even for a small case like the four first major shells and a nucleus like oxygen-16, the dimensionality becomes quickly intractable. If we wish to include single-particle states that reflect weakly bound systems, we need a much larger single-particle basis. We need thus approximative methods that sum specific correlations to infinite order. All these methods start normally with a Hartree-Fock basis as the calculational basis. In the next section we discuss one of these possible approximative methods, namely many-body perturbation theory.

8.5 Many-body perturbation theory

We assume here that we are only interested in the non-degenerate ground state of a given system and expand the exact wave function in term of a series of Slater determinants

$$|\Psi_0\rangle = |\Phi_0\rangle + \sum_{m=1}^{\infty} C_m |\Phi_m\rangle,$$

where we have assumed that the true ground state is dominated by the solution of the unperturbed problem, that is

$$\hat{H}_0 |\Phi_0\rangle = W_0 |\Phi_0\rangle.$$

The state $|\Psi_0\rangle$ is not normalized, rather we have used an intermediate normalization $\langle \Phi_0|\Psi_0\rangle = 1$ since we have $\langle \Phi_0|\Phi_0\rangle = 1$.

The Schrödinger equation is

$$\hat{H}|\Psi_0\rangle = E|\Psi_0\rangle,$$

and multiplying the latter from the left with $\langle \Phi_0|$ gives

$$\langle \Phi_0|\hat{H}|\Psi_0\rangle = E\langle \Phi_0|\Psi_0\rangle = E,$$

and subtracting from this equation

$$\langle \Psi_0|\hat{H}_0|\Phi_0\rangle = W_0\langle \Psi_0|\Phi_0\rangle = W_0,$$

and using the fact that the both operators $\hat{H}$ and $\hat{H}_0$ are hermitian results in

$$\Delta E = E - W_0 = \langle \Phi_0|\hat{H}_I|\Psi_0\rangle,$$

which is an exact result. We call this quantity the correlation energy.

This equation forms the starting point for all perturbative derivations. However, as it stands it represents nothing but a mere formal rewriting of Schrödinger's equation and is not of much practical use. The exact wave function $|\Psi_0\rangle$ is unknown. In order to obtain a perturbative expansion, we need to expand the exact wave function in terms of the interaction $\hat{H}_I$.

Here we have assumed that our model space defined by the operator $\hat{P}$ is one-dimensional, meaning that

$$\hat{P} = |\Phi_0\rangle\langle \Phi_0|,$$

and

$$\hat{Q} = \sum_{m=1}^{\infty} |\Phi_m\rangle\langle \Phi_m|.$$

We can thus rewrite the exact wave function as

$$|\Psi_0\rangle = (\hat{P} + \hat{Q})|\Psi_0\rangle = |\Phi_0\rangle + \hat{Q}|\Psi_0\rangle.$$

Going back to the Schrödinger equation, we can rewrite it as, adding and a subtracting a term $\omega|\Psi_0\rangle$ as

$$\left(\omega - \hat{H}_0\right)|\Psi_0\rangle = \left(\omega - E + \hat{H}_I\right)|\Psi_0\rangle,$$

where ω is an energy variable to be specified later.

We assume also that the resolvent of $\left(\omega - \hat{H}_0\right)$ exits, that is it has an inverse which defined the unperturbed Green's function as

$$\left(\omega - \hat{H}_0\right)^{-1} = \frac{1}{\left(\omega - \hat{H}_0\right)}.$$

We can rewrite Schrödinger's equation as

$$|\Psi_0\rangle = \frac{1}{\omega - \hat{H}_0}\left(\omega - E + \hat{H}_I\right)|\Psi_0\rangle,$$

and multiplying from the left with $\hat{Q}$ results in

$$\hat{Q}|\Psi_0\rangle = \frac{\hat{Q}}{\omega - \hat{H}_0}\left(\omega - E + \hat{H}_I\right)|\Psi_0\rangle,$$

which is possible since we have defined the operator $\hat{Q}$ in terms of the eigenfunctions of $\hat{H}$.

These operators commute meaning that

$$\hat{Q}\frac{1}{\left(\omega - \hat{H}_0\right)}\hat{Q} = \hat{Q}\frac{1}{\left(\omega - \hat{H}_0\right)} = \frac{\hat{Q}}{\left(\omega - \hat{H}_0\right)}.$$

With these definitions we can in turn define the wave function as

$$|\Psi_0\rangle = |\Phi_0\rangle + \frac{\hat{Q}}{\omega - \hat{H}_0}\left(\omega - E + \hat{H}_I\right)|\Psi_0\rangle.$$

This equation is again nothing but a formal rewrite of Schrödinger's equation and does not represent a practical calculational scheme. It is a non-linear equation in two unknown quantities, the energy E and the exact wave function $|\Psi_0\rangle$. We can however start with a guess for $|\Psi_0\rangle$ on the right hand side of the last equation.

The most common choice is to start with the function which is expected to exhibit the largest overlap with the wave function we are searching after, namely $|\Phi_0\rangle$. This can again be inserted in the solution for $|\Psi_0\rangle$ in an iterative fashion and if we continue along these lines we end up with

$$|\Psi_0\rangle = \sum_{i=0}^{\infty}\left\{\frac{\hat{Q}}{\omega - \hat{H}_0}\left(\omega - E + \hat{H}_I\right)\right\}^i|\Phi_0\rangle,$$

for the wave function and

$$\Delta E = \sum_{i=0}^{\infty}\langle\Phi_0|\hat{H}_I\left\{\frac{\hat{Q}}{\omega - \hat{H}_0}\left(\omega - E + \hat{H}_I\right)\right\}^i|\Phi_0\rangle,$$

which is now a perturbative expansion of the exact energy in terms of the interaction $\hat{H}_I$ and the unperturbed wave function $|\Psi_0\rangle$.

In our equations for $|\Psi_0\rangle$ and ΔE in terms of the unperturbed solutions $|\Phi_i\rangle$ we have still an undetermined parameter ω and a dependecy on the exact energy E. Not much has been gained thus from a practical computational point of view.

In Brilluoin-Wigner perturbation theory it is customary to set $\omega = E$. This results in the following perturbative expansion for the energy ΔE

$$\Delta E = \sum_{i=0}^{\infty} \langle \Phi_0 | \hat{H}_I \left\{ \frac{\hat{Q}}{\omega - \hat{H}_0} \left(\omega - E + \hat{H}_I \right) \right\}^i | \Phi_0 \rangle = \tag{8.49}$$

$$\langle \Phi_0 | \left(\hat{H}_I + \hat{H}_I \frac{\hat{Q}}{E - \hat{H}_0} \hat{H}_I + \hat{H}_I \frac{\hat{Q}}{E - \hat{H}_0} \hat{H}_I \frac{\hat{Q}}{E - \hat{H}_0} \hat{H}_I + \dots \right) | \Phi_0 \rangle. \tag{8.50}$$

This expression depends however on the exact energy E and is again not very convenient from a practical point of view. It can obviously be solved iteratively, by starting with a guess for E and then solve till some kind of self-consistency criterion has been reached.

Actually, the above expression is nothing but a rewrite again of the full Schrödinger equation.

Defining $e = E - \hat{H}_0$ and recalling that $\hat{H}_0$ commutes with $\hat{Q}$ by construction and that $\hat{Q}$ is an idempotent operator $\hat{Q}^2 = \hat{Q}$. Using this equation in the above expansion for ΔE we can write the denominator

$$\hat{Q} \frac{1}{\hat{e} - \hat{Q}\hat{H}_I\hat{Q}} = \hat{Q} \left[\frac{1}{\hat{e}} + \frac{1}{\hat{e}} \hat{Q}\hat{H}_I\hat{Q} \frac{1}{\hat{e}} + \frac{1}{\hat{e}} \hat{Q}\hat{H}_I\hat{Q} \frac{1}{\hat{e}} \hat{Q}\hat{H}_I\hat{Q} \frac{1}{\hat{e}} + \dots \right] \hat{Q}.$$

Inserted in the expression for ΔE leads to

$$\Delta E = \langle \Phi_0 | \hat{H}_I + \hat{H}_I \hat{Q} \frac{1}{E - \hat{H}_0 - \hat{Q}\hat{H}_I\hat{Q}} \hat{Q}\hat{H}_I | \Phi_0 \rangle.$$

In RS perturbation theory we set $\omega = W_0$ and obtain the following expression for the energy difference

$$\Delta E = \sum_{i=0}^{\infty} \langle \Phi_0 | \hat{H}_I \left\{ \frac{\hat{Q}}{W_0 - \hat{H}_0} \left(\hat{H}_I - \Delta E \right) \right\}^i | \Phi_0 \rangle \tag{8.51}$$

$$\langle \Phi_0 | \left(\hat{H}_I + \hat{H}_I \frac{\hat{Q}}{W_0 - \hat{H}_0} (\hat{H}_I - \Delta E) + \hat{H}_I \frac{\hat{Q}}{W_0 - \hat{H}_0} (\hat{H}_I - \Delta E) \frac{\hat{Q}}{W_0 - \hat{H}_0} (\hat{H}_I - \Delta E) + \dots \right) | \Phi_0 \rangle. \tag{8.52}$$

Recalling that $\hat{Q}$ commutes with $\hat{H}_0$ and since ΔE is a constant we obtain that

$$\hat{Q}\Delta E | \Phi_0 \rangle = \hat{Q}\Delta E | \hat{Q}\Phi_0 \rangle = 0.$$

Inserting this results in the expression for the energy results in

$$\Delta E = \langle \Phi_0 | \left(\hat{H}_I + \hat{H}_I \frac{\hat{Q}}{W_0 - \hat{H}_0} \hat{H}_I + \hat{H}_I \frac{\hat{Q}}{W_0 - \hat{H}_0} (\hat{H}_I - \Delta E) \frac{\hat{Q}}{W_0 - \hat{H}_0} \hat{H}_I + \dots \right) | \Phi_0 \rangle.$$

We can now this expression in terms of a perturbative expression in terms of $\hat{H}_I$ where we iterate the last expression in terms of ΔE

$$\Delta E = \sum_{i=1}^{\infty} \Delta E^{(i)}.$$

We get the following expression for $\Delta E^{(i)}$

$$\Delta E^{(1)} = \langle \Phi_0 | \hat{H}_I | \Phi_0 \rangle,$$

which is just the contribution to first order in perturbation theory,

$$\Delta E^{(2)} = \langle \Phi_0 | \hat{H}_I \frac{\hat{Q}}{W_0 - \hat{H}_0} \hat{H}_I | \Phi_0 \rangle,$$

which is the contribution to second order and

$$\Delta E^{(3)} = \langle \Phi_0 | \hat{H}_I \frac{\hat{Q}}{W_0 - \hat{H}_0} \hat{H}_I \frac{\hat{Q}}{W_0 - \hat{H}_0} \hat{H}_I \Phi_0 \rangle - \langle \Phi_0 | \hat{H}_I \frac{\hat{Q}}{W_0 - \hat{H}_0} \langle \Phi_0 | \hat{H}_I | \Phi_0 \rangle \frac{\hat{Q}}{W_0 - \hat{H}_0} \hat{H}_I | \Phi_0 \rangle,$$

being the third-order contribution.

8.5.1 Interpreting the correlation energy and the wave operator

In the FCI section we showed that we could rewrite the exact state function for the ground state as a linear expansion in terms of all possible Slater determinants. We expanded then (as an example) our exact state function for the ground state as

$$|\Psi_0\rangle = C_0 |\Phi_0\rangle + \sum_{ai} C_i^a |\Phi_i^a\rangle + \sum_{abij} C_{ij}^{ab} |\Phi_{ij}^{ab}\rangle + \cdots = (C_0 + \hat{C}) |\Phi_0\rangle,$$

where we introduced the so-called correlation operator

$$\hat{C} = \sum_{ai} C_i^a \hat{a}_a^\dagger \hat{a}_i + \sum_{abij} C_{ij}^{ab} \hat{a}_a^\dagger \hat{a}_b^\dagger \hat{a}_j \hat{a}_i + \dots$$

Using intermediate normalization we have

$$\langle \Psi_0 | \Phi_0 \rangle = \langle \Phi_0 | \Phi_0 \rangle = 1,$$

which results in

$$|\Psi_0\rangle = (1 + \hat{C}) |\Phi_0\rangle.$$

In a shell-model calculation, the unknown coefficients in $\hat{C}$ are the eigenvectors that result from the diagonalization of the Hamiltonian matrix.

How can we use perturbation theory to determine the same coefficients? Let us study the contributions to second order in the interaction, namely

$$\Delta E^{(2)} = \langle \Phi_0 | \hat{H}_I \frac{\hat{Q}}{W_0 - \hat{H}_0} \hat{H}_I | \Phi_0 \rangle.$$

This contribution will also be discussed in connection with the development of a many-body program for nuclear matter, as well as the simple pairing model of problem **??**. The intermediate states given by $\hat{Q}$ can at most be of a $2p - 2h$ nature if we have a two-body Hamiltonian. This means that to second order in perturbation theory we can at most have $1p - 1h$ and $2p - 2h$ excitations as intermediate states. When we diagonalize, these contributions are included to infinite order. This means that in order to include such correlations to higher order in the interaction, we need to go to higher-orders in perturbation theory.

If we limit the attention to a Hartree-Fock basis, we have that $\langle \Phi_0 | \hat{H}_I | 2p - 2h \rangle$ is the only contribution since matrix elements involving $\langle \Phi_0 | \hat{H}_I | 1p - 1h \rangle$ are zero and the contribution to the energy from second order in Rayleigh-Schrödinger perturbation theory reduces to

$$\Delta E^{(2)} = \frac{1}{4} \sum_{abij} \langle ij | \hat{v} | ab \rangle \frac{\langle ab | \hat{v} | ij \rangle}{\varepsilon_i + \varepsilon_j - \varepsilon_a - \varepsilon_b}.$$

If we compare this to the correlation energy obtained from full configuration interaction theory with a Hartree-Fock basis, we found that

$$E - E_{\mathrm{Ref}} = \Delta E = \sum_{abij} \langle ij|\hat{v}|ab \rangle C_{ij}^{ab},$$

where the energy E_{Ref} is the reference energy and ΔE defines the so-called correlation energy.

We see that if we set

$$C_{ij}^{ab} = \frac{1}{4} \frac{\langle ab|\hat{v}|ij \rangle}{\varepsilon_i + \varepsilon_j - \varepsilon_a - \varepsilon_b},$$

we have a perfect agreement between FCI and many-body perturbation theory. However, FCI includes $2p - 2h$ (and more complicated ones as well) correlations to infinite order. In order to make a meaningful comparison we would at least need to sum such correlations to infinite order in perturbation theory. The last equation serves however as a very useful comparison between FCI and many-body perturbation theory. Furthermore, for our nuclear matter studies, one-particle-one-hole intermediate excitations are zero due to the requirement of momentum conservation in infinite systems. These two-particle-two-hole correlations can also be summed to infinite order and a particular class of such excitations are given by two-particle excitations only. These can easily be summed to infinite order, and represent in case of nuclear interactions which are strongly repulsive at short interparticle distances, a physically intuitive way to understand the renomalization of nuclear forces. Such correlations are easily computed by simple matrix inversion techniques and have been widely employed in nuclear many-body theory. Summing up two-particle excitations to infinite order leads to an effective two-body interaction which renomalizes the short-range part of the nuclear interactions. We will discuss the summation of such correlations in our section on the so-called G-matrix 8.5.2.

Summing up, we can see that

- MBPT introduces order-by-order specific correlations and we make comparisons with exact calculations like FCI
- At every order, we can calculate all contributions since they are well-known and either tabulated or calculated on the fly.
- MBPT is a non-variational theory and there is no guarantee that higher orders will improve the convergence.
- However, since FCI calculations are limited by the size of the Hamiltonian matrices to diagonalize (today's most efficient codes can attach dimensionalities of ten billion basis states, MBPT can function as an approximative method which gives a straightforward (but tedious) calculation recipe.
- MBPT has been widely used to compute effective interactions for the nuclear shell-model.
- But there are better methods which sum to infinite order important correlations. Coupled cluster theory is one of these methods and will be discussed in section 8.6.

8.5.2 The Breuckner G-matrix

The Brueckner G-matrix has historically been an important ingredient in many-body calculations of nuclear systems. In this section, we will briefly survey the philosophy behind the G-matrix.

Historically, the G-matrix was developed in microscopic nuclear matter calculations using realistic nucleon-nucleon (NN) interactions. It is an ingenuous as well as an interesting method to overcome the difficulties caused by the strong, short-range repulsive core con-

tained in all modern models for the NN interaction. The *G*-matrix method was originally developed by Brueckner, and further developed by Goldstone and Bethe, Brandow and Petschek. In the literature it is generally referred to as the Brueckner theory or the Brueckner-Bethe-Goldstone theory.

Suppose we want to calculate the nuclear matter ground-state energy E_0 using the non-relativistic Schrödinger equation

$$H\Psi_0(A) = E_0(A)\Psi_0(A), \tag{8.53}$$

with $H = T + V$ where A denotes the number of particles, T is the kinetic energy and V is the nucleon-nucleon (NN) potential. Models for the NN interaction are discussed in the chapter on nuclear forces. The corresponding unperturbed problem is

$$H_0\psi_0(A) = W_0(A)\psi_0(A). \tag{8.54}$$

Here H_0 is just kinetic energy T and ψ_0 is a Slater determinant representing the Fermi sea, where all orbits through the Fermi momentum k_F are filled. We write

$$E_0 = W_0 + \Delta E_0, \tag{8.55}$$

where ΔE_0 is the ground-state energy shift or correlation energy as it was defined in many-body perturbation theory. If we know how to calculate ΔE_0, then we know E_0, since W_0 is easily obtained. In the limit $A \to \infty$, the quantities E_0 and ΔE_0 themselves are not well defined, but the ratios E_0/A and $\Delta E_0/A$ are. The nuclear-matter binding energy per nucleon is commonly denoted by BE/A, which is just $-E_0/A$. In passing, we note that the empirical value for symmetric nuclear matter (proton number Z=neutron number N) is ≈ 16 MeV. There exists a formal theory for the calculation of ΔE_0. According to the well-known Goldstone linked-diagram theory, the energy shift ΔE_0 is given exactly by the diagrammatic expansion shown in Fig. **??**. This theory, is a linked-cluster perturbation expansion for the ground state energy of a many-body system, and applies equally well to both nuclear matter and closed-shell nuclei such as the doubly magic nucleus ^{40}Ca. We will not discuss the Goldstone expansion, but rather discuss briefly how it is used in calculations.

Using the standard diagram rules (see the discussion on coupled cluster theory and many-body perturbation theory), the various diagrams contained in the above figure can be readily calculated (in an uncoupled scheme)

$$(i) = \frac{(-)^{n_h+n_l}}{2^{n_{ep}}} \sum_{ij \leq k_F} \langle ij|\hat{v}|ij\rangle_{AS}, \tag{8.56}$$

with $n_h = n_l = 2$ and $n_{ep} = 1$. As discussed in connection with the diagram rules in the many-body perturbation theory chapter, n_h denotes the number of hole lines, n_l the number of closed fermion loops and n_{ep} is the number of so-called equivalent pairs. The factor $1/2^{n_{ep}}$ is needed since we want to count a pair of particles only once. We will carry this factor $1/2$ with us in the equations below. The subscript AS denotes the anti-symmetrized and normalized matrix element

$$\langle ij|\hat{v}|ij\rangle_{AS} = \langle ij|\hat{v}|ij\rangle - \langle ji|\hat{v}|ij\rangle. \tag{8.57}$$

Similarly, diagrams (ii) and (iii) read

$$(ii) = \frac{(-)^{2+2}}{2^2} \sum_{ij \leq k_F} \sum_{ab > k_F} \frac{\langle ij|\hat{v}|ab\rangle_{AS}\langle ab|\hat{v}|ij\rangle_{AS}}{\varepsilon_i + \varepsilon_j - \varepsilon_a - \varepsilon_b}, \tag{8.58}$$

and

$$(iii) = \frac{(-)^{2+2}}{2^3} \sum_{k_i, k_j \le k_F} \sum_{abcd k_F} \frac{\langle ij|\hat{v}|ab\rangle_{AS} \langle ab|\hat{v}|cd\rangle_{AS} \langle cd|\hat{v}|ij\rangle_{AS}}{(\varepsilon_i + \varepsilon_j - \varepsilon_a - \varepsilon_b)(\varepsilon_i + \varepsilon_j - \varepsilon_c - \varepsilon_d)}. \tag{8.59}$$

In the above, ε denotes the single-particle energies defined by H_0. The steps leading to the above expressions for the various diagrams are rather straightforward. Though, if we wish to compute the matrix elements for the interaction v, a serious problem arises. Typically, the matrix elements will contain a term (see the next section for the formal details) $V(|\mathbf{r}|)$, which represents the interaction potential V between two nucleons, where $\mathbf{r}$ is the internucleon distance. All modern models for V have a strong short-range repulsive core. Hence, matrix elements involving $V(|\mathbf{r}|)$, will result in large (or infinitely large for a potential with a hard core) and repulsive contributions to the ground-state energy. Thus, the diagrammatic expansion for the ground-state energy in terms of the potential $V(|\mathbf{r}|)$ becomes meaningless.

One possible solution to this problem is provided by the well-known Brueckner theory or the Brueckner G-matrix, or just the G-matrix. In fact, the G-matrix is an almost indispensable tool in almost every microscopic nuclear structure calculation. Its main idea may be paraphrased as follows. Suppose we want to calculate the function $f(x) = x/(1+x)$. If x is small, we may expand the function $f(x)$ as a power series $x + x^2 + x^3 + \dots$ and it may be adequate to just calculate the first few terms. In other words, $f(x)$ may be calculated using a low-order perturbation method. But if x is large (or infinitely large), the above power series is obviously meaningless. However, the exact function $x/(1+x)$ is still well defined in the limit of x becoming very large.

These arguments suggest that one should sum up the diagrams (i), (ii), (iii) in fig. **??** and the similar ones to all orders, instead of computing them one by one. Denoting this all-order sum as $1/2\tilde{G}_{ijij}$, where we have introduced the shorthand notation $\tilde{G}_{ijij} = \langle k_i k_j|\tilde{G}|k_i k_j\rangle_{AS}$ (and similarly for $\tilde{v}$), we have that

$$\frac{1}{2}\tilde{G}_{ijij} = \frac{1}{2}\hat{v}_{ijij} + \sum_{ab > k_F} \frac{1}{2}\hat{v}_{ijab} \frac{1}{\varepsilon_i + \varepsilon_j - \varepsilon_a - \varepsilon_b}$$
$$\times \left[\frac{1}{2}\hat{v}_{abij} + \sum_{cd > k_F} \frac{1}{2}\hat{v}_{abcd} \frac{1}{\varepsilon_i + \varepsilon_j - \varepsilon_c - \varepsilon_d} \frac{1}{2}V_{cdij} + \dots \right]. \tag{8.60}$$

The factor $1/2$ is the same as that discussed above, namely we want to count a pair of particles only once. The quantity inside the brackets is just $1/2\tilde{G}_{mnij}$ and the above equation can be rewritten as an integral equation

$$\tilde{G}_{ijij} = \tilde{V}_{ijij} + \sum_{ab > F} \frac{1}{2}\hat{v}_{ijab} \frac{1}{\varepsilon_i + \varepsilon_j - \varepsilon_a - \varepsilon_b}\tilde{G}_{abij}. \tag{8.61}$$

Note that $\tilde{G}$ is the anti-symmetrized G-matrix since the potential $\tilde{v}$ is also anti-symmetrized. This means that $\tilde{G}$ obeys

$$\tilde{G}_{ijij} = -\tilde{G}_{jiij} = -\tilde{G}_{ijji}. \tag{8.62}$$

The $\tilde{G}$-matrix is defined as

$$\tilde{G}_{ijij} = G_{ijij} - G_{jiij}, \tag{8.63}$$

and the equation for G is

$$G_{ijij} = V_{ijij} + \sum_{ab > k_F} V_{ijab} \frac{1}{\varepsilon_i + \varepsilon_j - \varepsilon_a - \varepsilon_b}G_{abij}, \tag{8.64}$$

which is the familiar G-matrix equation. The above matrix is specifically designed to treat a class of diagrams contained in ΔE_0, of which typical contributions were shown in fig. **??**. In fact the sum of the diagrams in fig. **??** is equal to $1/2(G_{ijij} - G_{jiij})$.

Let us now define a more general G-matrix as

$$G_{ijij} = V_{ijij} + \sum_{mn>0} V_{ijmn} \frac{Q(mn)}{\omega - \varepsilon_m - \varepsilon_n} G_{mnij},\qquad(8.65)$$

which is an extension of Eq. (8.64). Note that Eq. (8.64) has $\varepsilon_i + \varepsilon_j$ in the energy denominator, whereas in the latter equation we have a general energy variable ω in the denominator. Furthermore, in Eq. (8.64) we have a restricted sum over mn, while in Eq. (8.65) we sum over all ab and we have introduced a weighting factor $Q(ab)$. In Eq. (8.65) $Q(ab)$ corresponds to the choice

$$Q(a,b) = \begin{cases} 1, & min(a,b) > k_F \\ 0, & \text{else.} \end{cases},\qquad(8.66)$$

where $Q(ab)$ is usually referred to as the G-matrix Pauli exclusion operator. The role of Q is to enforce a selection of the intermediate states allowed in the G-matrix equation. The above Q requires that the intermediate particles a and b must be both above the Fermi surface defined by F. We may enforce a different requirement by using a summation over intermediate states different from that in Eq. (8.65). An example is the Pauli operator for the model-space Brueckner-Hartree-Fock method discussed below.

Before ending this section, let us rewrite the G-matrix equation in a more compact form. The sp energies ε and wave functions are defined by the unperturbed hamiltonian H_0 as

$$H_0 |\psi_a \psi_b = (\varepsilon_a + \varepsilon_b)|\psi_a \psi_b.\qquad(8.67)$$

The G-matrix equation can then be rewritten in the following compact form

$$G(\omega) = V + V \frac{\hat{Q}}{\omega - H_0} G(\omega),\qquad(8.68)$$

with $\hat{Q} = \sum_{ab} |\psi_a \psi_b\rangle\langle\langle\psi_a \psi_b|$. In terms of diagrams, G corresponds to an all-order sum of the "ladder-type" interactions between two particles with the intermediate states restricted by Q.

The G-matrix equation has a very simple form. But its calculation is rather complicated, particularly for finite nuclear systems such as the nucleus ^{18}O. There are a number of complexities. To mention a few, the Pauli operator Q may not commute with the unperturbed hamiltonian H_0 and we have to make the replacement

$$\frac{Q}{\omega - H_0} \to Q \frac{1}{\omega - QH_0Q} Q.$$

The determination of the starting energy ω is also another problem.

In a medium such as nuclear matter we must account for the fact that certain states are not available as intermediate states in the calculation of the G-matrix. Following the discussion above this is achieved by introducing the medium dependent Pauli operator Q. Further, the energy ω of the incoming particles, given by a pure kinetic term in a scattering problem between two unbound particles (for example two colliding protons), must be modified so as to allow for medium corrections. How to evaluate the Pauli operator for nuclear matter is, however, not straightforward. Before discussing how to evaluate the Pauli operator for nuclear matter, we note that the G-matrix is conventionally given in terms of partial waves and the coordinates of the relative and center-of-mass motion. If we assume that the G-matrix is diagonal in α (α is a shorthand notation for J, S, L and T), we write the equation for the G-matrix as a coupled-channels equation in the relative and center-of-mass system

$$G_{ll'}^{\alpha}(kk'K\omega) = V_{ll'}^{\alpha}(kk') + \sum_{l''} \int \frac{d^3q}{(2\pi)^3} V_{ll''}^{\alpha}(kq) \frac{Q(q,K)}{\omega - H_0} G_{l''l'}^{\alpha}(qk'K\omega). \tag{8.69}$$

This equation is similar in structure to the scattering equations discussed in connection with nuclear forces (see the chapter on models for nuclear forces), except that we now have introduced the Pauli operator Q and a medium dependent two-particle energy ω. The notations in this equation follow those of the chapter on nuclear forces where we discuss the solution of the scattering matrix T. The numerical details on how to solve the above G-matrix equation through matrix inversion techniques are discussed below Note however that the G-matrix may not be diagonal in α. This is due to the fact that the Pauli operator Q is not diagonal in the above representation in the relative and center-of-mass system. The Pauli operator depends on the angle between the relative momentum and the center of mass momentum. This angle dependence causes Q to couple states with different relative angular momentua $\mathscr{J}$, rendering a partial wave decomposition of the G-matrix equation rather difficult. The angle dependence of the Pauli operator can be eliminated by introducing the angle-average Pauli operator, where one replaces the exact Pauli operator Q by its average $\bar{Q}$ over all angles for fixed relative and center-of-mass momenta. The choice of Pauli operator is decisive to the determination of the sp spectrum. Basically, to first order in the reaction matrix G, there are three commonly used sp spectra, all defined by the solution of the following equations

$$\varepsilon_m = \varepsilon(k_m) = t_m + u_m = \frac{k_m^2}{2M_N} + u_m, \tag{8.70}$$

and

$$u_m = \sum_{h \leq k_F} \langle mh| G(\omega = \varepsilon_m + \varepsilon_h) |mh\rangle_{AS} \quad k_m \leq k_M, \tag{8.71}$$

$$\tag{8.72}$$

$$u_m = 0, k_m > k_M. \tag{8.73}$$

For notational economy, we set $|\mathbf{k}_m| = k_m$. Here we employ anti-symmetrized matrix elements (AS), and k_M is a cutoff on the momentum. Further, t_m is the sp kinetic energy and similarly u_m is the sp potential. The choice of cutoff k_M is actually what determines the three commonly used sp spectra. In the conventional BHF approach one employs $k_M = k_F$, which leads to a Pauli operator Q_{BHF} (in the laboratory system) given by

$$Q_{\text{BHF}}(k_m, k_n) = \begin{cases} 1, & min(k_m, k_n) > k_F \\ 0, & \text{else.} \end{cases}, \tag{8.74}$$

or, since we will define an angle-average Pauli operator in the relative and center-of-mass system, we have

$$\bar{Q}_{\text{BHF}}(k, K) = \begin{cases} 0, & k \leq \sqrt{k_F^2 - K^2/4} \\ 1, & k \geq k_F + K/2 \\ \frac{K^2/4 + k^2 - k_F^2}{kK} & \text{else,} \end{cases} \tag{8.75}$$

with k_F the momentum at the Fermi surface.

The BHF choice sets $u_k = 0$ for $k > k_F$, which leads to an unphysical, large gap at the Fermi surface, typically of the order of $50 - 60$ MeV. To overcome the gap problem, Mahaux and collaborators introduced a continuous sp spectrum for all values of k. The divergencies which then may occur in Eq. (8.69) are taken care of by introducing a principal value integration in Eq. (8.69), to retain only the real part contribution to the G-matrix.

To define the energy denominators we will also make use of the angle-average approximation. The angle dependence is handled by the so-called effective mass approximation. The single-particle energies in nuclear matter are assumed to have the simple quadratic form

$$
\varepsilon(k_m) = \frac{\hbar^2 k_m^2}{2M_N^*} + \Delta, \quad k_m \leq k_F
$$
$$
= \frac{\hbar^2 k_m^2}{2M_N}, \quad k_m > k_F,
$$
(8.76)

where M_N^* is the effective mass of the nucleon and M_N is the bare nucleon mass. For particle states above the Fermi sea we choose a pure kinetic energy term, whereas for hole states, the terms M_N^* and Δ, the latter being an effective single-particle potential related to the G-matrix, are obtained through the self-consistent Brueckner-Hartree-Fock procedure. The sp potential is obtained through the same angle-average approximation

$$
U(k_m) = \sum_{l\alpha}(2T+1)(2J+1)\left\{ \frac{8}{\pi}\int_0^{(k_F-k_m)/2} k^2 dk G_{ll}^\alpha(k, \bar{K}_1) \right.
$$
(8.77)
$$
\left. + \frac{1}{\pi k_m}\int_{(k_F-k_m)/2}^{(k_F+k_m)/2} kdk(k_F^2 - (k_m-2k)^2)G_{ll}^\alpha(k, \bar{K}_2) \right\},
$$

where we have defined
$$
\bar{K}_1^2 = 4(k_m^2 + k^2),
$$
(8.78)

and
$$
\bar{K}_2^2 = 4(k_m^2 + k^2) - (2k + k_m - k_F)(2k + k_1 + k_F).
$$
(8.79)

This self-consistency scheme consists in choosing adequate initial values of the effective mass and Δ. The obtained G-matrix is in turn used to obtain new values for M_N^* and Δ. This procedure continues until these parameters vary little.

8.6 Coupled cluster theory

.

8.6.1 Introduction

Coester and Kummel first developed the ideas that led to coupled cluster theory in the late 1950s. The basic idea is that the correlated wave function of a many-body system $|\Psi\rangle$ can be formulated as an exponential of correlation operators T acting on a reference state $|\Phi\rangle$

$$
|\Psi\rangle = \exp\left(-\hat{T}\right)|\Phi\rangle .
$$

We will discuss how to define the operators later in this work. This simple ansatz carries enormous power. It leads to a non-perturbative many-body theory that includes summation of ladder diagrams , ring diagrams, and an infinite-order generalization of many-body perturbation theory..

Developments and applications of coupled cluster theory took different routes in chemistry and nuclear physics. In quantum chemistry, coupled cluster developments and applications

have proven to be extremely useful, see for example the review by Barrett and Musial as well as the recent textbook by Shavitt and Bartlett [26].

Many previous applications to nuclear physics struggled with the repulsive character of the nuclear forces and limited basis sets used in the computations. Most of these problems have been overcome during the last decade and coupled-cluster theory is one of the computational methods of preference for doing nuclear physics, with applications ranging from light nuclei to medium-heavy nuclei, see for example the recent review by Hagen,Papenbrock, Hjorth-Jensen and Dean.

8.6.2 A quick tour of Coupled Cluster theory

The ansatz for the wavefunction (ground state) is given by

$$|\Psi\rangle = |\Psi_{CC}\rangle = e^{\hat{T}}|\Phi_0\rangle = \left(\sum_{n=1}^{A} \frac{1}{n!}\hat{T}^n\right)|\Phi_0\rangle,$$

where A represents the maximum number of particle-hole excitations and $\hat{T}$ is the cluster operator defined as

$$\hat{T} = \hat{T}_1 + \hat{T}_2 + \ldots + \hat{T}_A$$

$$\hat{T}_n = \left(\frac{1}{n!}\right)^2 \sum_{\substack{i_1,i_2,\ldots i_n \\ a_1,a_2,\ldots a_n}} t_{i_1 i_2 \ldots i_n}^{a_1 a_2 \ldots a_n} a_{a_1}^\dagger a_{a_2}^\dagger \ldots a_{a_n}^\dagger a_{i_n} \ldots a_{i_2} a_{i_1}.$$

The energy is given by

$$E_{\text{CC}} = \langle\Phi_0|\overline{H}|\Phi_0\rangle,$$

where $\overline{H}$ is a similarity transformed Hamiltonian

$$\overline{H} = e^{-\hat{T}}\hat{H}_N e^{\hat{T}}$$

$$\hat{H}_N = \hat{H} - \langle\Phi_0|\hat{H}|\Phi_0\rangle.$$

The coupled cluster energy is a function of the unknown cluster amplitudes $t_{i_1 i_2 \ldots i_n}^{a_1 a_2 \ldots a_n}$, given by the solutions to the amplitude equations

$$0 = \langle\Phi_{i_1 \ldots i_n}^{a_1 \ldots a_n}|\overline{H}|\Phi_0\rangle.$$

The similarity transformed Hamiltonian $\overline{H}$ is expanded using the Baker-Campbell-Hausdorff expression,

$$\overline{H} = \hat{H}_N + \left[\hat{H}_N, \hat{T}\right] + \frac{1}{2}\left[\left[\hat{H}_N, \hat{T}\right], \hat{T}\right] + \ldots$$

$$\frac{1}{n!}\left[\ldots\left[\hat{H}_N, \hat{T}\right], \ldots \hat{T}\right] + \ldots$$

and simplified using the connected cluster theorem

$$\overline{H} = \hat{H}_N + \left(\hat{H}_N\hat{T}\right)_c + \frac{1}{2}\left(\hat{H}_N\hat{T}^2\right)_c + \cdots + \frac{1}{n!}\left(\hat{H}_N\hat{T}^n\right)_c + \ldots$$

A much used approximation is to truncate the cluster operator $\hat{T}$ at the $n = 2$ level. This defines the so-called singes and doubles approximation to the Coupled Cluster wavefunction, normally shortened to CCSD..

The coupled cluster wavefunction is now given by

$$|\Psi_{CC}\rangle = e^{\hat{T}_1 + \hat{T}_2}|\Phi_0\rangle$$

where

$$\hat{T}_1 = \sum_{ia} t_i^a a_a^\dagger a_i$$

$$\hat{T}_2 = \frac{1}{4}\sum_{ijab} t_{ij}^{ab} a_a^\dagger a_b^\dagger a_j a_i.$$

The amplutudes t play a role similar to the coefficients C in the shell-model calculations. They are obtained by solving a set of non-linear equations similar to those discussed above in connection withe FCI discussion.

If we truncate our equations at the CCSD level, it corresponds to performing a transformation of the Hamiltonian matrix of the following type for a six particle problem (with a two-body Hamiltonian):

	$0p-0h$	$1p-1h$	$2p-2h$	$3p-3h$	$4p-4h$	$5p-5h$	$6p-6h$
$0p-0h$	$\tilde{x}$	$\tilde{x}$	$\tilde{x}$	0	0	0	0
$1p-1h$	0	$\tilde{x}$	$\tilde{x}$	$\tilde{x}$	0	0	0
$2p-2h$	0	$\tilde{x}$	$\tilde{x}$	$\tilde{x}$	$\tilde{x}$	0	0
$3p-3h$	0	$\tilde{x}$	$\tilde{x}$	$\tilde{x}$	$\tilde{x}$	$\tilde{x}$	0
$4p-4h$	0	0	$\tilde{x}$	$\tilde{x}$	$\tilde{x}$	$\tilde{x}$	$\tilde{x}$
$5p-5h$	0	0	0	$\tilde{x}$	$\tilde{x}$	$\tilde{x}$	$\tilde{x}$
$6p-6h$	0	0	0	0	$\tilde{x}$	$\tilde{x}$	$\tilde{x}$

In our FCI discussion the correlation energy is defined as, with a two-body Hamiltonian,

$$\Delta E = \sum_{ai}\langle i|\hat{f}|a\rangle C_i^a + \sum_{abij}\langle ij|\hat{v}|ab\rangle C_{ij}^{ab}.$$

In Coupled cluster theory it becomes (irrespective of level of truncation of T)

$$\Delta E = \sum_{ai}\langle i|\hat{f}|a\rangle t_i^a + \sum_{abij}\langle ij|\hat{v}|ab\rangle t_{ij}^{ab}.$$

Coupled cluster theory has several interesting computational features and is the method of choice in quantum chemistry. The method was originally proposed by Coester and Kummel, two nuclear physicists (way back in the fifties). It came back in full strength in nuclear physics during the last decade.

There are several interesting features:

• With a truncation like CCSD or CCSDT, we can include to infinite order correlations like $2p-2h$.
• We can include a large basis of single-particle states, not possible in standard FCI calculations

However, Coupled Cluster theory is

• non-variational

- if we want to find properties of excited states, additional calculations via for example equation of motion methods are needed
- if correlations are strong, a single-reference ansatz may not be the best starting point
- we cannot quantify properly the error we make when truncations are made in the cluster operator

8.6.3 The CCD approximation

We will now approximate the cluster operator $\hat{T}$ to include only $2p - 2h$ correlations. This leads to the so-called CCD approximation, that is

$$\hat{T} \approx \hat{T}_2 = \frac{1}{4} \sum_{abij} t_{ij}^{ab} a_a^\dagger a_b^\dagger a_j a_i,$$

meaning that we have

$$|\Psi_0\rangle \approx |\Psi_{CCD}\rangle = \exp\left(\hat{T}_2\right)|\Phi_0\rangle.$$

Inserting these equations in the expression for the computation of the energy we have, with a Hamiltonian defined with respect to a general vacuum (see the exercises in the second quantization part)

$$\hat{H} = \hat{H}_N + E_{\text{ref}},$$

with

$$\hat{H}_N = \sum_{pq}\langle p|\hat{f}|q\rangle a_p^\dagger a_q + \frac{1}{4}\sum_{pqrs}\langle pq|\hat{v}|rs\rangle a_p^\dagger a_q^\dagger a_s a_r,$$

we obtain that the energy can be written as

$$\langle \Phi_0|\exp-\left(\hat{T}_2\right)\hat{H}_N\exp\left(\hat{T}_2\right)|\Phi_0\rangle = \langle \Phi_0|\hat{H}_N(1+\hat{T}_2)|\Phi_0\rangle = E_{CCD}.$$

This quantity becomes

$$E_{CCD} = E_{\text{ref}} + \frac{1}{4}\sum_{abij}\langle ij|\hat{v}|ab\rangle t_{ij}^{ab},$$

where the latter is the correlation energy from this level of approximation of CC theory. Similarly, the expression for the amplitudes reads

$$\langle \Phi_{ij}^{ab}|\exp-\left(\hat{T}_2\right)\hat{H}_N\exp\left(\hat{T}_2\right)|\Phi_0\rangle = 0.$$

These equations can be reduced to (after several applications of Wick's theorem) to, for all $i > j$ and all $a > b$,

$$0 = \langle ab|\hat{v}|ij\rangle + (\varepsilon_a + \varepsilon_b - \varepsilon_i - \varepsilon_j)t_{ij}^{ab}$$

$$+\frac{1}{2}\sum_{cd}\langle ab|\hat{v}|cd\rangle t_{ij}^{cd} + \frac{1}{2}\sum_{kl}\langle kl|\hat{v}|ij\rangle t_{kl}^{ab} + \hat{P}(ij|ab)\sum_{kc}\langle kb|\hat{v}|cj\rangle t_{ik}^{ac}$$

$$+\frac{1}{4}\sum_{klcd}\langle kl|\hat{v}|cd\rangle t_{ij}^{cd} t_{kl}^{ab} + \hat{P}(ij)\sum_{klcd}\langle kl|\hat{v}|cd\rangle t_{ik}^{ac} t_{jl}^{bd}$$

$$-\frac{1}{2}\hat{P}(ij)\sum_{klcd}\langle kl|\hat{v}|cd\rangle t_{ik}^{dc} t_{lj}^{ab} - \frac{1}{2}\hat{P}(ab)\sum_{klcd}\langle kl|\hat{v}|cd\rangle t_{lk}^{ac} t_{ij}^{db}, \qquad (8.80)$$

where we have defined

$$\hat{P}(ab) = 1 - \hat{P}_{ab},$$

where $\hat{P}_{ab}$ interchanges two particles occupying the quantum numbers a and b. The operator $\hat{P}(ij|ab)$ is defined as

$$\hat{P}(ij|ab) = (1 - \hat{P}_{ij})(1 - \hat{P}_{ab}).$$

Recall also that the unknown amplitudes t_{ij}^{ab} represent anti-symmetrized matrix elements, meaning that they obey the same symmetry relations as the two-body interaction, that is

$$t_{ij}^{ab} = -t_{ji}^{ab} = -t_{ij}^{ba} = t_{ji}^{ba}.$$

The two-body matrix elements are also anti-symmetrized, meaning that

$$\langle ab|\hat{v}|ij\rangle = -\langle ab|\hat{v}|ji\rangle = -\langle ba|\hat{v}|ij\rangle = \langle ba|\hat{v}|ji\rangle.$$

The non-linear equations for the unknown amplitudes t_{ij}^{ab} are solved iteratively. We discuss the implementation of these equations below.

Approximations to the full CCD equations.

It is useful to make approximations to the equations for the amplitudes. The standard method for solving these equations is to set up an iterative scheme where method's like Newton's method or similar root searching methods are used to find the amplitudes. Itreative solvers need a guess for the amplitudes. A good starting point is to use the correlated wave operator from perturbation theory to first order in the interaction. This means that we define the zeroth approximation to the amplitudes as

$$t^{(0)} = \frac{\langle ab|\hat{v}|ij\rangle}{(\varepsilon_i + \varepsilon_j - \varepsilon_a - \varepsilon_b)},$$

leading to our first approximation for the correlation energy at the CCD level to be equal to second-order perturbation theory without $1p - 1h$ excitations, namely

$$\Delta E_{\text{CCD}}^{(0)} = \frac{1}{4} \sum_{abij} \frac{\langle ij|\hat{v}|ab\rangle \langle ab|\hat{v}|ij\rangle}{(\varepsilon_i + \varepsilon_j - \varepsilon_a - \varepsilon_b)}.$$

With this starting point, we are now ready to solve Eq. (8.80) iteratively. Before we attack the full equations, it is however instructive to study a truncated version of the equations. We will first study the following approximation where we take away all terms except the linear terms that involve the single-particle energies and the the two-particle intermediate excitations, that is

$$0 = \langle ab|\hat{v}|ij\rangle + (\varepsilon_a + \varepsilon_b - \varepsilon_i - \varepsilon_j) t_{ij}^{ab} + \frac{1}{2} \sum_{cd} \langle ab|\hat{v}|cd\rangle t_{ij}^{cd}. \tag{8.81}$$

Setting the single-particle energies for the hole states equal to an energy variable $\omega = \varepsilon_i + \varepsilon_j$, Eq. (8.81) reduces to the well-known equations for the so-called G-matrix, widely used in infinite matter and finite nuclei studies [5]. The equation can then be reordered and solved by matrix inversion. To see this let us define the following quantity

$$\tau_{ij}^{ab} = (\omega - \varepsilon_a - \varepsilon_b) t_{ij}^{ab},$$

and inserting

$$1 = \frac{(\omega - \varepsilon_c - \varepsilon_d)}{(\omega - \varepsilon_c - \varepsilon_d)},$$

in the intermediate sums over cd in Eq. (8.81), we can rewrite the latter equation as

$$\tau_{ij}^{ab}(\omega) = \langle ab|\hat{v}|ij\rangle + \frac{1}{2}\sum_{cd}\langle ab|\hat{v}|cd\rangle \frac{1}{\omega - \varepsilon_c - \varepsilon_d}\tau_{ij}^{cd}(\omega),$$

where we have indicated an explicit energy dependence. This equation, transforming a two-particle configuration into a single index, can be transformed into a matrix inversion problem. Solving the equations for a fixed energy ω allows us to compare directly with results from Green's function theory when only two-particle intermediate states are included.

To solve Eq. (8.81), we would thus start with a guess for the unknown amplitudes, typically using the wave operator defined by first order in perturbation theory, leading to a zeroth approximation to the energy given by second-order perturbation theory for the correlation energy. A simple approach to the solution of Eq. (8.81), is to thus to

1. Start with a guess for the amplitudes and compute the zeroth approximation to the correlation energy
2. Use the ansatz for the amplitudes to solve Eq. (8.81) via for example your root-finding method of choice (Newton's method or modifications thereof can be used) and continue these iterations till the correlation energy does not change more than a prefixed quantity λ; $\Delta E_{\text{CCD}}^{(i)} - \Delta E_{\text{CCD}}^{(i-1)} \leq \lambda$.
3. It is common during the iterations to scale the amplitudes with a parameter α, with $\alpha \in (0,1]$ as $t^{(i)} = \alpha t^{(i)} + (1-\alpha)t^{(i-1)}$.

The next approximation is to include the two-hole term in Eq. (8.80), a term which allow us to make a link with Green's function theory with two-particle and two-hole correlations. This means that we solve

$$0 = \langle ab|\hat{v}|ij\rangle + (\varepsilon_a + \varepsilon_b - \varepsilon_i - \varepsilon_j)\, t_{ij}^{ab} + \frac{1}{2}\sum_{cd}\langle ab|\hat{v}|cd\rangle t_{ij}^{cd} + \frac{1}{2}\sum_{kl}\langle kl|\hat{v}|ij\rangle t_{kl}^{ab}. \tag{8.82}$$

This equation is solved the same way as we would do for Eq. (8.81). The final step is then to include all terms in Eq. (8.80).

8.7 Developing a numerical project

This section will focus on writing a working CCD code from scratch. If you are familiar with writing quantum many-body physics codes, feel free to skip ahead as we are going to go into some detail about implementing CCD as a computer code now. As we saw earlier, the CCD equations can be written as

$$(\varepsilon_i + \varepsilon_j - \varepsilon_a - \varepsilon_b)\, t_{ij}^{ab} = \langle ab|\hat{v}|ij\rangle$$

$$+\frac{1}{2}\sum_{cd}\langle ab|\hat{v}|cd\rangle t_{ij}^{cd} + \frac{1}{2}\sum_{kl}\langle kl|\hat{v}|ij\rangle t_{kl}^{ab} + \hat{P}(ij|ab)\sum_{kc}\langle kb|\hat{v}|cj\rangle t_{ik}^{ac}$$

$$+\frac{1}{4}\sum_{klcd}\langle kl|\hat{v}|cd\rangle t_{ij}^{cd} t_{kl}^{ab} + \hat{P}(ij)\sum_{klcd}\langle kl|\hat{v}|cd\rangle t_{ik}^{ac} t_{jl}^{bd}$$

$$-\frac{1}{2}\hat{P}(ij)\sum_{klcd}\langle kl|\hat{v}|cd\rangle t_{ik}^{dc} t_{lj}^{ab} - \frac{1}{2}\hat{P}(ab)\sum_{klcd}\langle kl|\hat{v}|cd\rangle t_{lk}^{ac} t_{ij}^{db}, \tag{8.83}$$

for all $i < j$ and all $a < b$, using the standard notation that $a,b,\dots$ are particle states and $i,j,\dots$ are hole states. With the CCD correlation energy given by

$$\Delta E_{CCD} = \frac{1}{4} \sum_{ijab} \langle ij|\hat{v}|ab\rangle t_{ij}^{ab}. \tag{8.84}$$

One way to solve these equations, is to write equation (8.83) as a series of iterative nonlinear algebraic equations.

$$t_{ij}^{ab(n+1)} = \frac{1}{\varepsilon_{ij}^{ab}} \Bigg(\langle ab|\hat{v}|ij\rangle$$

$$+\frac{1}{2}\sum_{cd}\langle ab|\hat{v}|cd\rangle t_{ij}^{cd(n)} + \frac{1}{2}\sum_{kl}\langle kl|\hat{v}|ij\rangle t_{kl}^{ab(n)} + \hat{P}(ij|ab)\sum_{kc}\langle kb|\hat{v}|cj\rangle t_{ik}^{ac(n)}$$

$$+\frac{1}{4}\sum_{klcd}\langle kl|\hat{v}|cd\rangle t_{ij}^{cd(n)}t_{kl}^{ab(n)} + \hat{P}(ij)\sum_{klcd}\langle kl|\hat{v}|cd\rangle t_{ik}^{ac(n)}t_{jl}^{bd(n)}$$

$$-\frac{1}{2}\hat{P}(ij)\sum_{klcd}\langle kl|\hat{v}|cd\rangle t_{ik}^{dc(n)}t_{lj}^{ab(n)} - \frac{1}{2}\hat{P}(ab)\sum_{klcd}\langle kl|\hat{v}|cd\rangle t_{lk}^{ac(n)}t_{ij}^{db(n)}\Bigg), \tag{8.85}$$

for all $i < j$ and all $a < b$, where $\varepsilon_{ij}^{ab} = (\varepsilon_i + \varepsilon_j - \varepsilon_a - \varepsilon_b)$, and $t_{ij}^{ab(n)}$ is the t amplitude for the nth iteration of the series. This way, given some starting guess $t_{ij}^{ab(0)}$, we can generate subsequent t amplitudes that converges to some value. Discussion of the mathematical details regarding convergence will be tabled for later; for now we will talk about implementing these equations into a computer program and assume convergence. In pseudocode, the function that updates the t amplitudes looks like

```
CCD_Update()
for i ∈ {0,N_fermi − 1} do
  for j ∈ {0,N_fermi − 1} do
    for a ∈ {N_fermi,N_sp − 1} do
      for b ∈ {N_fermi,N_sp − 1} do
        sum ← TBME[index(a,b,i,j)]
        for c ∈ {N_fermi,N_sp − 1} do
          for d ∈ {N_fermi,N_sp − 1} do
            sum ← sum + 0.5 ∗ ME[index(a,b,c,d)] ∗ t_amplitudes_old[index(c,d,i,j)]
          end for
        end for
        ...
        sum ← sum + (all other terms)
        ...
        energy_denom = SP_energy[i]+SP_energy[j]-SP_energy[a]-SP_energy[b]
        t_amplitudes[index(a,b,i,j)] = sum/energy_denom
      end for
    end for
  end for
end for
```

Where N_{fermi} is the fermi level and N_{sp} is the total number of single particle (s.p.) states, indexed from 0 to $N_{sp} − 1$. At the most basic level, the CCD equations are just the addition of many products containing t_{ij}^{ab} amplitudes and two-body matrix elements (TBMEs) $\langle ij|\hat{v}|ab\rangle$, so a lot of care should be placed into how we store these objects. These are both objects with four indices, so a sensible first implementation of the CCD equations would be to create two 4-D arrays to store the objects. However, it is often more convenient to work with simple 1-D arrays instead. *index*() is a function that maps the four indices onto one index so that a 1-D array can be used. An example of such a function is:

function index(p,q,r,s)

      return $p * N_{sp}^3 + q * N_{sp}^2 + r * N_{sp} + s$
  end function

Because elements with repeated indices vanish, $t_{ii}^{ab} = t_{ij}^{aa} = 0$ and $\langle pp|\hat{v}|rs \rangle = \langle pq|\hat{v}|rr \rangle = 0$, data structures using this index function will contain many elements that are automatically zero, so we will discuss more efficient storage strategies later. Notice also that we are looping over all i, j, a, b, rather than the restricted indices. This means that we are doing redundant work, but it is simpler to code up, and we will want to unrestrict these indices later anyways.

    The goal of this code is to calculate the correlation energy, ΔE_{CCD}, so after each iteration of our equation, we use our newest t amplitudes to update this value,

$$\Delta E_{CCD}^{(n)} = \frac{1}{4} \sum_{ijab} \langle ij|\hat{v}|ab \rangle t_{ij}^{ab(n)}. \tag{8.86}$$

We check that our result is converged by checking that to see if the most recent iteration has changed the correlation energy by less than some tolerance threshold η,

$$\eta > |\Delta E_{CCD}^{(n+1)} - \Delta E_{CCD}^{(n)}|. \tag{8.87}$$

The basic structure of the iterative process will look like:

  while (abs(energy_Diff) > tolerance) **do**
    CCD_Update()
    correlation_Energy ← CCD_Corr_Energy()
    energy_Diff ← correlation_Energy - correlation_Energy_old
    correlation_Energy_old ← correlation_Energy
    t_amplitudes_old ← t_amplitudes
  end while

    Prior to this algorithm, the t amplitudes should be initalized, $t_{ij}^{ab(0)}$. A particularly convenient choice is to set $t_{ij}^{ab(0)} = 0$. Notice that if this starting point is used, then

$$t_{ij}^{ab(1)} = \frac{\langle ab|\hat{v}|ij \rangle}{\varepsilon_{ij}^{ab}}$$

$$\tag{8.88}$$

$$\Delta E_{CCD}^{(1)} = \frac{1}{4} \sum_{ijab} \frac{\langle ab|\hat{v}|ij \rangle}{\varepsilon_{ij}^{ab}}, \tag{8.89}$$

    which is the result from MBPT2. This is a useful, as one iteration of the CCD equations can be ran, and checked against MBPT2 to give some confidence that everything is working so far. To check that everything is working, it is useful to run the code using a minimal example. A simple pairing model Hamiltonian is a nice place to start.

$$\hat{H}_0 = \xi \sum_{p\sigma} (p-1) a_{p\sigma}^\dagger a_{p\sigma} \tag{8.90}$$

$$\hat{V} = -\frac{1}{2} g \sum_{pq} a_{p+}^\dagger a_{p-}^\dagger a_{q-} a_{q+} \tag{8.91}$$

which represents a basic pairing model with p levels each with a spin degeneracy of 2. The form of the coupled cluster equations in (Eq) uses single-particle states that are eigenstates of the Hartree-Fock operator, $(\hat{u} + \hat{u}_{HF}|p\rangle = \varepsilon_p|p\rangle$. In the pairing model, this condition is already fulfilled. All we have to do is define the lowest N_{fermi} states as holes then redefine the single-particle energies,

$$\varepsilon_q = h_{qq} + \sum_i \langle qi||qi\rangle . \qquad (8.92)$$

To be more specific, let's look at this pairing model with 4 particles and 8 single-particle states. These states (with $\xi = 1.0$) could be labeled as such with

State Label	p	$2s_z$	E	type
0	1	1	-g/2	hole
1	1	-1	-g/2	hole
2	2	1	1-g/2	hole
3	2	-1	1-g/2	hole
4	3	1	2	particle
5	3	-1	2	particle
6	4	1	3	particle
7	4	-1	3	particle

Here are some more results for specific values of g that can be used for benchmarking.

g	E_{ref}	ΔE_{MBPT2}	ΔE_{CCD}
-1.0	3	-0.46667	-0.21895*
-0.5	2.5	-0.08874	-0.06306
0.0	2	0	0
0.5	1.5	-0.06239	-0.08336
1.0	1	-0.21905	-0.36956

The $g = -1.0$ case diverges without implementing iterative mixing. Sometimes iterative solvers run into oscillating solutions, and mixing can help the iterations break this cycle.

$$t^{(i)} = \alpha t^{(i)}_{no\_mixing} + (1-\alpha)t^{(i-1)} \qquad (8.93)$$

In the case of this simple pairing model, it is easy to calculate ΔE_{MBPT2} by hand, which is useful to check the code's calcuation of this value, as well as the first CCD iteration.

$$\Delta E_{MBPT2} = \frac{1}{4}\sum_{abij}\frac{\langle ij||ab\rangle \langle ab||ij\rangle}{\varepsilon^{ab}_{ij}} = \sum_{a<b,i<j}\frac{\langle ij||ab\rangle \langle ab||ij\rangle}{\varepsilon^{ab}_{ij}} \qquad (8.94)$$

For our pairing example:

$$\Delta E_{MBPT2} = \frac{\langle 01||45\rangle^2}{\varepsilon^{45}_{01}} + \frac{\langle 01||67\rangle^2}{\varepsilon^{67}_{01}} + \frac{\langle 23||45\rangle^2}{\varepsilon^{45}_{23}} + \frac{\langle 23||67\rangle^2}{\varepsilon^{67}_{23}}$$

$$\Delta E_{MBPT2} = -\frac{g^2}{4}\left(\frac{1}{4+g} + \frac{1}{6+g} + \frac{1}{2+g} + \frac{1}{4+g}\right),$$

which is a nice expression which can be used to check the results for any value of g.

Once a working pairing model has been implemented, improvements can start to be made, all the while using the pairing model to make sure that the code is still working and giving correct answers. Realistic systems will be much larger than this small pairing example.

One limitation that will be ran into while trying to do realistic CCD calculations is that of memory. The 4-indexed TBMEs and t-amplitudes have to store a lot of elements, and the size of these arrays can quite become larger than that of the available memory on the machine. If calculation wants to use 500 s.p. basis states, then a structure like $\langle pq|v|rs\rangle$ will have length 500 for each of its four indices, which means it will have $500^4 = 625*10^8$ elements. To get a handle on how much memory is used, consider the elements as double-precision floating point type. One double takes up 8 bytes of memory. So this array would take up $8*625*10^8$

bytes $= 5000 * 10^8$ bytes $= 500$ Gbytes of memory. Most personal computers in 2016 have 4-8 Gbytes of RAM, so this calculation would be way out of reach. There are supercomputers that can handle applications using 500 Gbytes of memory, but we can quickly reduce the total memory required by applying some physical arguments. In addition to vanishing elements with repeated indices, mentioned above, elements that do not obey certain symmetries are also zero. Almost all realistic two-body forces preserve some quantities due to symmetries in the interaction. For example, an interaction with rotational symmetry will conserve angular momentum. This means that a two-body ket state $|rs\rangle$, which has some set of quantum numbers, will retain quantum numbers corresponding to the interaction symmetries after being acted on by $\hat{v}$. This state is then projected onto $|pq\rangle$ with its own set of quantum numbers. Thus $\langle pq|v|rs\rangle$ is only non-zero if $|pq\rangle$ and $|rs\rangle$ share the same quantum numbers that are preserved by $\hat{v}$. In addition, because the cluster operators represent excitations due to the interaction, t_{ij}^{ab} is only non-zero if $|ij\rangle$ has the same relevant quantum numbers as $|ab\rangle$.

To take advantage of this, these two-body ket states can be organized into "channels" of shared quantum numbers. In the case of the pairing model, the interaction preserves the total spin projection of a two-body state, $S_z = s_{z1} + s_{z2}$. The single particle states can have spin of $+1/2$ or $-1/2$, so there can be three two-body channels with $S_z = -1, 0, +1$. These channels can then be indexed with a unique label in a similar way to the single particle index scheme. In more complicated systems, there will be many more channels involving multiple symmetries, so it is useful to create a data structure that stores the relevant two-body quantum numbers to keep track of the labeling scheme.

Now it is more efficient to use two-dimensional array data structures, where the first index refers to the channel number and the second refers to the element withing that channel. So to access matrix elements or t amplitudes, you can loop over the channels first, then the indices within that channel. To get an idea of the savings using this block diagonal structure, let's look at a case with a plane wave basis, with three momentum and one spin quantum numbers, with an interaction that conserves linear momentum in all three dimensions, as well as the total spin projection. Using 502 basis states, the TBME's require about 0.23 Gb of memory in block diagonal form, which is an enormous saving from the 500 Gb mentions earlier in the naïve storage scheme.

Since the calculation of all of these zeros can now be avoided, improvements in speed as memory will now follow. To get a handle on how example these CCD calculations are we need only to look at the most expensive sum in equation 8.83. This corresponds to the sum over $klcd$. Since this sum is repeated for all $i < j$ and $a < b$, that means these equations will scale as $\mathcal{O}(n_p^4 n_h^4)$. However, (as we saw earlier?), they can be rewritten using intermediates as

$$0 = \langle ab|\hat{v}|ij\rangle + \hat{P}(ab)\sum_c \langle b|\chi|c\rangle \langle ac|t|ij\rangle - \hat{P}(ij)\sum_k \langle k|\chi|j\rangle \langle ab|t|ik\rangle$$

$$+\frac{1}{2}\sum_{cd} \langle ab|\chi|cd\rangle \langle cd|t|ij\rangle + \frac{1}{2}\sum_{kl} \langle ab|t|kl\rangle \langle kl|\chi|ij\rangle \qquad (8.95)$$

$$+\hat{P}(ij)\hat{P}(ab)\sum_{kc} \langle ac|t|ik\rangle \langle kb|\chi|cj\rangle$$

for all i, j, a, b, the reason why these indices are now unrestricted will be explained later. Where the intermediates χ are

$$\langle b|\chi|c\rangle = \langle b|f|c\rangle - \frac{1}{2}\sum_{kld} \langle bd|t|kl\rangle \langle kl|v|cd\rangle \qquad (8.96)$$

$$\langle k|\chi|j\rangle = \langle k|f|j\rangle + \frac{1}{2}\sum_{cdl} \langle kl|v|cd\rangle \langle cd|t|jl\rangle \qquad (8.97)$$

$$\langle kl|\chi|ij\rangle = \langle kl|v|ij\rangle + \frac{1}{2}\sum_{cd}\langle kl|v|cd\rangle\,\langle cd|t|ij\rangle \tag{8.98}$$

$$\langle kb|\chi|cj\rangle = \langle kb|v|cj\rangle + \frac{1}{2}\sum_{dl}\langle kl|v|cd\rangle\,\langle db|t|lj\rangle \tag{8.99}$$

$$\langle ab|\chi|cd\rangle = \langle ab|v|cd\rangle \tag{8.100}$$

Maybe demonstrate how these equations are equal here?

Now the CCD equations will scale as $\mathcal{O}(n_h^2 n_p^4)$ which is quite a bit better than before. This is of course at the cost of computing the intermediates at the beginning of each iteration, which the most expensive one, $\langle kb|\chi|cj\rangle$, will scale as $\mathcal{O}(n_h^3 n_p^3)$. To further speed these computations up, we see that these sums can be written as matrix-matrix multiplication. It is not obvious how to write all of these sums in such a way, but it is useful to first remember that to write out the multiplication of matices $\hat{C} = \hat{A} * \hat{B}$ is

$$C_{ij} = \sum_{k} A_{ik} * B_{kj}. \tag{8.101}$$

Notice that equation (8.98) can be written as

$$\langle K|\chi|I\rangle = \langle K|v|I\rangle + \frac{1}{2}\sum_{C}\langle K|v|C\rangle\,\langle C|t|I\rangle$$

by mapping the two index pairs $kl \to K, ij \to I, cd \to C$. So now the sum looks like a matrix-matrix multiplication. This is useful because there are packages like BLAS (Basic Linear Algebra Subprograms) which have extremely fast implementations of matrix-matrix multiplication.

Now that we have a working CCD program, we can move on to more realistic cases. One such case is infinite nuclear matter using a plane-wave basis. These states are solutions to the free-particle Hamiltonian,

$$\frac{-\hbar^2}{2m}\nabla^2\phi(\mathbf{x}) = \varepsilon\,\phi(\mathbf{x}). \tag{8.102}$$

For a finite basis, we approximate the problem by constructing a box with sides of length L, which quantizes the momentum, and impose periodic boundary conditions in each direction.

$$\phi(x_i) = \phi(x_i + L) \tag{8.103}$$

$$\phi_{\mathbf{k}}(\mathbf{x}) = \frac{1}{\sqrt{L^3}}e^{i\mathbf{k}\cdot\mathbf{x}}, \quad \mathbf{k} = \frac{2\pi\mathbf{n}}{L}, \quad n_i \tag{8.104}$$

The first step in calculating infinite matter is to construct a model space by finding every single-particle state relevant to a given problem. In our case, this amounts to looping over the quantum numbers for spin, isospin, and the three momentum directions. To control the model space size, the momentum can be truncated to give a cubic space, where $n_i \le n_{\max}$, or a spherical space, where $n_x^2 + n_y^2 + n_z^2 \le N_{\max}$. The number of single-particle states in a cubic space increases rapidly with $n_{\max}$ compared to the spherical case with $N_{\max}$. For example, in pure neutron matter a cubic space with $n_{\max} = 3$ has 668 states while the spherical space with $N_{\max} = 17$ has 610 states. Therefore, the spherical case will be used for the rest of the calculations here. The loop increases in energy by counting the number of shells, so states can be 'filled' by labeling the first P proton and N neutron states as holes. The following loop is for pure neutron matter and requires the number of neutrons, N and density, $\rho = N/L^3$, as input. Symmetric nuclear matter requires an extra loop over isospin.

$n = 0$

for shell $\in \{0, ..., N_{\max}\}$ **do**

for $-\sqrt{N_{\max}} \leq n_x \leq \sqrt{N_{\max}}$ **do**
  for $-\sqrt{N_{\max}} \leq n_y \leq \sqrt{N_{\max}}$ **do**
    for $-\sqrt{N_{\max}} \leq n_z \leq \sqrt{N_{\max}}$ **do**
      for $s_z \in \{-\frac{1}{2}, \frac{1}{2}\}$ **do**
        if $n_x^2 + n_y^2 + n_z^2 = \text{shell}$ **then**
          $\text{Energy} = \frac{4\pi^2 \hbar^2}{2m} \times \text{shell}$
          if $n < N$ **then**
            $\text{type} = \text{"hole"}$
          else
            $\text{type} = \text{"particle"}$
          end if
          $\text{STATES} \leftarrow (n, n_x, n_y, n_z, s_z, \text{Energy}, \text{type})$
          $n \leftarrow n + 1$
        end if
      end for
    end for
  end for
end for

The next step is to build every two-body state in the model space and separate them by their particle/hole character and combined quantum numbers. While each single-particle state was unique, two-body states can share quantum numbers with members of a particular two-body channel. These channels allow us to remove matrix elements and cluster amplitudes that violate the symmetries of the interaction and greatly reduces the size and speed of the calculation. Our structures will depend on direct two-body channels, T, where the quantum numbers are added and cross two-body channels, X, where the quantum numbers are subtracted. Before filling the channels, it's helpful to order them with an index function which returns a unique index for a given set of two-body quantum numbers. Without an index function, one has to loop over all the channels for each two-body state which adds a substantial amount of time to this algorithm. An example of an index function for the direct channels in symmetric nuclear matter is, for $N_x = n_{x,1} + n_{x,2}$, $N_y = n_{y,1} + n_{y,2}$, $N_z = n_{z,1} + n_{z,2}$, $S_z = s_{z,1} + s_{z,2}$, $T_z = t_{z,1} + t_{z,2}$, $m = 2\lfloor \sqrt{N_{\max}} \rfloor$, and $M = 2m + 1$,

$$\text{Ind}(N_x, N_y, N_z, S_z, T_z) = 2(N_x + m)M^3 + 2(N_y + m)M^2 + 2(N_z + m)M + 2(S_z + 1) + (T_z + 1). \quad (8.105)$$

This function, which can also be used for the cross-channel index function, is well suited for a cubic model space but can be applied in either case. An additional restriction for two-body states is that they must be composed of two different states to satisfy the Pauli-exclusion principle.

for $\text{sp1} \in STATES$ **do**
  for $\text{sp2} \in STATES$ **do**
    if $sp1 \neq sp2$ **then**
      $N_i \leftarrow n_{i,1} + n_{i,2}$
      $S_z \leftarrow s_{z,1} + s_{z,2}$
      $T_z \leftarrow t_{z,1} + t_{z,2}$
      $\text{i\_dir} \leftarrow \text{Ind}(N_x, N_y, N_z, S_z, T_z)$
      $T \leftarrow (\text{sp1, sp2, i\_dir})$
      $N_i' \leftarrow n_{i,1} - n_{i,2}$
      $S_z' \leftarrow s_{z,1} - s_{z,2}$
      $T_z' \leftarrow t_{z,1} - t_{z,2}$
      $\text{i\_cross} \leftarrow \text{Ind}(N_x', N_y', N_z', S_z', T_z')$

          $X \leftarrow$ (sp1, sp2, i_cross)
      end if
    end for
  end for

From the cross channels, one can construct the cross channel compliments, X', where $X(pq) \equiv X'(qp)$. Also from the direct channels, one can construct one-body, and correspondint three-body, channels for each single-particle state, K by finding every combination of two two-body states within a direct channel that contains that single particle state, $T(pq) = T(rs) \Rightarrow K_p \leftarrow (qrs)$.

  for Chan $\in T$ **do**
    for tb1 $\in$ Chan **do**
      for tb2 $\in$ Chan **do**
        $K \leftarrow \text{tb1}_1$
        $K_{\text{tb1}_1} \leftarrow \text{tb1}_2, \text{tb2}_1, \text{tb2}_2$
      end for
    end for
  end for

These different sctructures can be further categorized by a two-body state's particle-hole character, $\langle pp|t|hh \rangle, \langle hh|v|hh \rangle, \langle pp|v|pp \rangle, \langle hh|v|pp \rangle$, and $\langle hp|v|hp \rangle$, which greatly simplifies the matrix-matrix multiplications of the CCD iterations by indexing the summed variables in a systematic way. Summations are constructed by placeing two structures next to each other in such a way that the inner, summed indices are of the same channel. The resulting structure is indexed by the outer channels.

$$\langle b|\chi|c\rangle = \langle b|f|c\rangle - \frac{1}{2}\sum_{kld}\langle bd|t|kl\rangle\langle kl|v|cd\rangle \to f_c^b\left(K(b),K(c)\right) - \frac{1}{2}t_{kl}^{bd}\left(K(b),K_b(kld)\right)\cdot v_{cd}^{kl}\left(K_c(kld),K(c)\right)$$
(8.106)

$$\langle k|\chi|j\rangle = \langle k|f|j\rangle + \frac{1}{2}\sum_{cdl}\langle kl|v|cd\rangle\langle cd|t|jl\rangle \to f_j^k\left(K(k),K(j)\right) + \frac{1}{2}v_{cd}^{kl}\left(K(k),K_k(cdl)\right)\cdot t_{jl}^{cd}\left(K_j(cdl),K(j)\right)$$
(8.107)

$$\langle kl|\chi|ij\rangle = \langle kl|v|ij\rangle + \frac{1}{2}\sum_{cd}\langle kl|v|cd\rangle\langle cd|t|ij\rangle \to v_{ij}^{kl}\left(T(kl),T(ij)\right) + \frac{1}{2}v_{cd}^{kl}\left(T(kl),T(cd)\right)\cdot t_{ij}^{cd}\left(T(cd),T(ij)\right)$$
(8.108)

$$\langle kb|\chi|cj\rangle = \langle kb|v|cj\rangle + \frac{1}{2}\sum_{dl}\langle kl|v|cd\rangle\langle db|t|lj\rangle \to v_{cj}^{kb}\left(X(kc),X(jb)\right) + \frac{1}{2}v_{cd}^{kl}\left(X(kc),X(dl)\right)\cdot t_{lj}^{db}\left(X(dl),X(jb)\right)$$
(8.109)

$$\langle ab|\chi|cd\rangle = \langle ab|v|cd\rangle \to v_{cd}^{ab}\left(T(ab),T(cd)\right)$$
(8.110)

$$\sum_c \langle b|\chi|c\rangle\langle ac|t|ij\rangle \to \chi_c^b\left(K(b),K(c)\right)\cdot t_{ij}^{ac}\left(K(c),K_c(ija)\right)$$
(8.111)

$$\sum_k \langle k|\chi|j\rangle\langle ab|t|ik\rangle \to \chi_j^k\left(K(j),K(k)\right)\cdot t_{ik}^{ab}\left(K(c),K_c(ija)\right)$$
(8.112)

$$\sum_{cd} \langle ab|\chi|cd\rangle\langle cd|t|ij\rangle \to \chi_{cd}^{ab}\left(T(ab),T(cd)\right)\cdot t_{ij}^{cd}\left(T(cd),T(ij)\right)$$
(8.113)

$$\sum_{kl} \langle ab|t|kl\rangle\langle kl|\chi|ij\rangle \to t_{kl}^{ab}\left(T(ab),T(kl)\right)\cdot \chi_{ij}^{kl}\left(T(kl),T(ij)\right)$$
(8.114)

$$\sum_{kc} \langle ac|t|ik\rangle\langle kb|\chi|cj\rangle = \sum_{kc}\langle ai^{-1}|t|kc^{-1}\rangle\langle kc^{-1}|\chi|jb^{-1}\rangle \to t_{ik}^{ac}\left(X(ia),X(kc)\right)\cdot \chi_{cj}^{kb}\left(X(kc),X(jb)\right)$$
(8.115)

We approximated our problem with periodic boundary conditions, $\phi(x_i) = \phi(x_i + L)$, but we could have chosen anti-periodic boundary conditions, $\phi(x_i) = -\phi(x_i + L)$. The difference between these two shows how the correlation energy contains finite-size effects. One solution to this problem is by integrating over solutions between periodic and anti-periodic conditions, known as twist-averaging. First, we multiply the single-particle states by a phase for each direction, characterized by a twist-angle, θ_i.

$$\phi_{\mathbf{k}}(\mathbf{x}+\mathbf{L}) \to e^{i\theta}\phi_{\mathbf{k}}(\mathbf{x})$$
(8.116)

$\theta_i = 0$ for PBC and $\theta_i = \pi$ for APBC

$$\mathbf{k} \to \mathbf{k} + \frac{\theta}{L}$$
(8.117)

$$\varepsilon_{\mathbf{k}} \to \varepsilon_{\mathbf{k}} + \frac{\pi}{L}\mathbf{k}\cdot\theta + \frac{\pi^2}{L^2}$$
(8.118)

Adding these phases changes the single-particle energies, the correction of which disappear as $L \to \infty$, depending on θ and thus changes the shell structure so that hole states can jump up to particle states and vis a versa. So it's necessary to fill hole states separately for each θ. Integration over some quantitiy is approximated by a weighted sum, such as Gauss-Legendre quadrature, over the quantity for each set of twist angles.

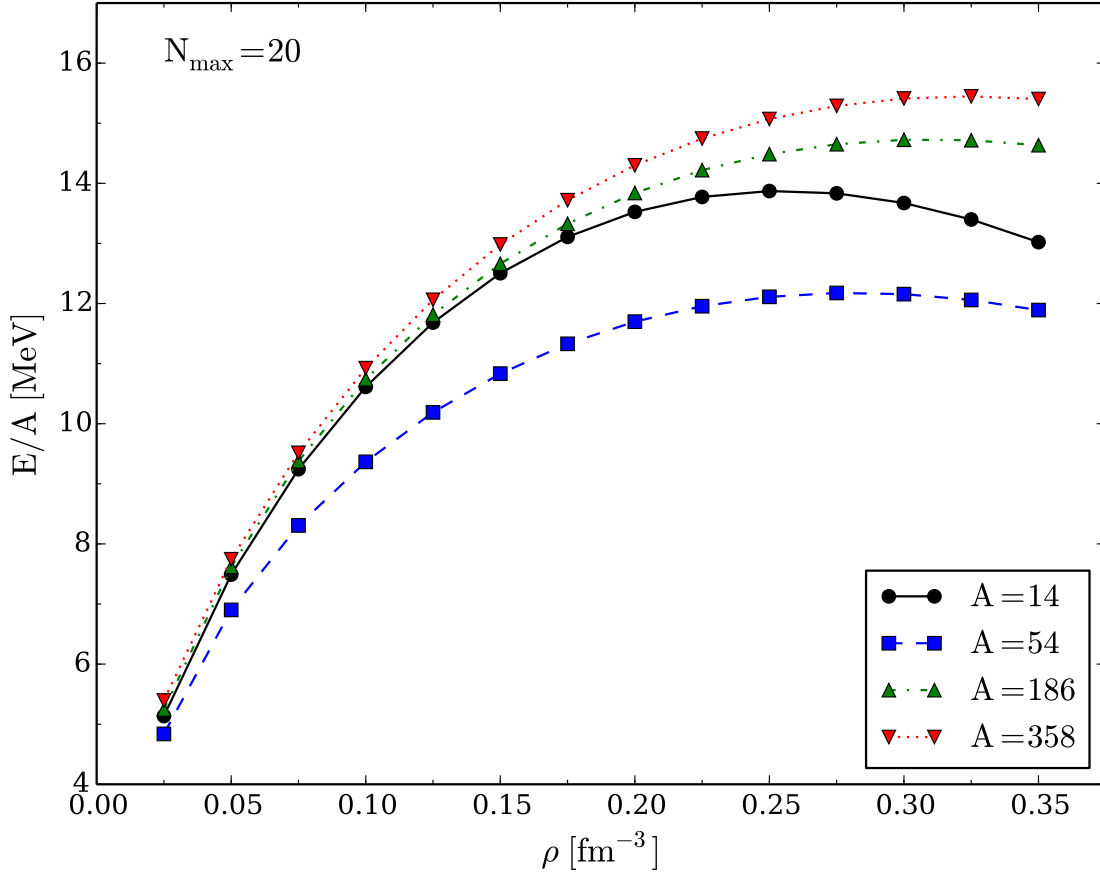Build mesh points and weights for each direction i: $\{\theta_i, w_i\}$

Fig. 8.2 Energy per particle of pure neutron matter computed in the CCD approximation with the Minnesota potential for different numbers of particles with $N_{max} = 20$.

$E_{twist} = 0$
for $(\theta_x, w_x) \in \{\theta_x, w_x\}$ **do**
    for $(\theta_y, w_y) \in \{\theta_y, w_y\}$ **do**
        for $(\theta_z, w_z) \in \{\theta_z, w_z\}$ **do**
            Build Basis States with $k_i \rightarrow k_i + \frac{\theta_i}{L}$
            Order States by Energy and Fill Holes
            Get Result E (T,HF,CCD)
            $E_{twist} = E_{twist} + \frac{1}{\pi^3} w_x w_y w_z E$
        end for
    end for
end for

This technique gives results which depend much less on the particle number, but requires a full calculation for each set of twist angles, which can grow very quickly. For example, using 10 twist angles in each direction requires 1000 calculations. To see the effects of twist averaging, it's easy to calculate the kinetic energy per particle and the Hartree-Fock energy per particle, which avoids the full CCD calculation. These calculations can be compared to the exact values for infinite matter, which are calculated by integrating the the relevent values up to the fermi surface.
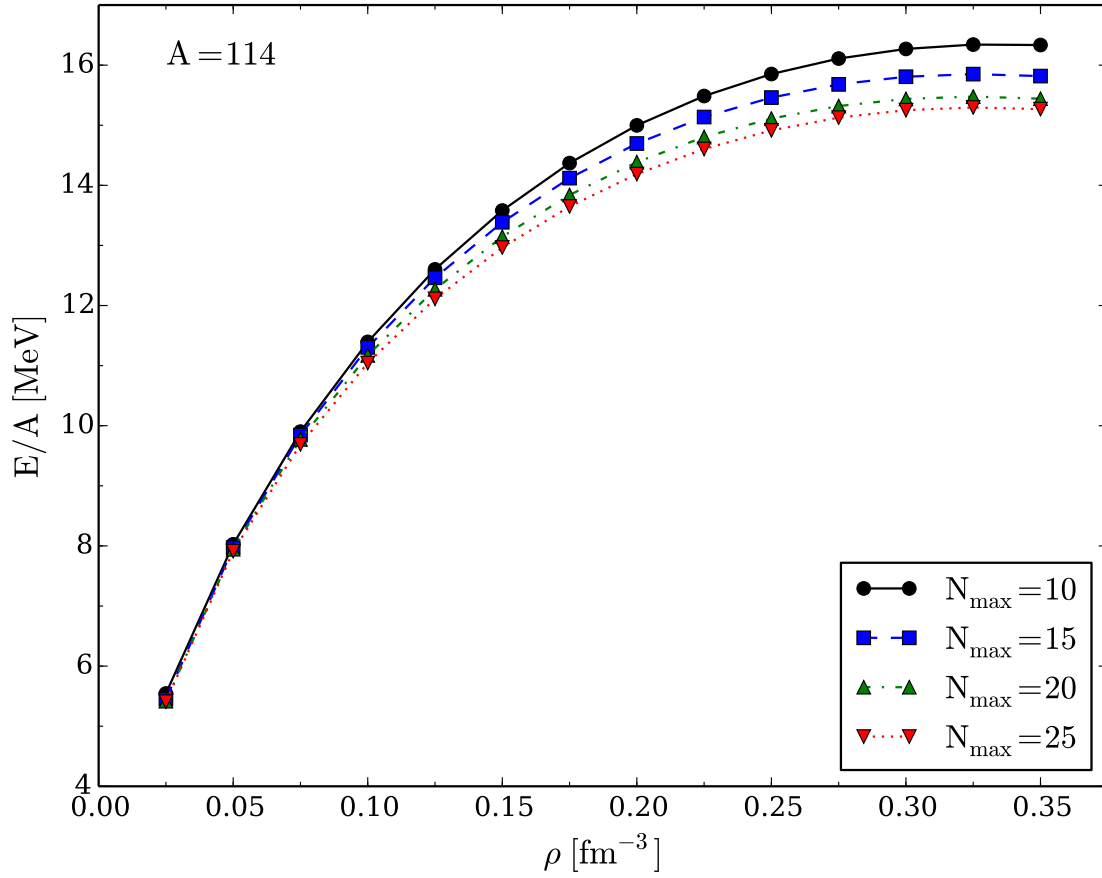
Fig. 8.3 Energy per particle of pure neutron matter computed in the CCD approximation with the Minnesota potential for different model space sizes with A = 20.

$$T_{\text{inf}} = \frac{3\hbar^2 k_f^2}{10m} \tag{8.119}$$

$$HF_{\text{inf}} = \frac{1}{(2\pi)^6} \frac{L^3}{2\rho} \int_0^{k_f} d\mathbf{k}_1 \int_0^{k_f} d\mathbf{k}_2 \, \langle \mathbf{k}_1 \mathbf{k}_2 | \hat{v} | \mathbf{k}_1 \mathbf{k}_2 \rangle \tag{8.120}$$

8.8 Conclusions

8.9 Exercises

8.1. Show that the one-body part of the Hamiltonian

$$\hat{H}_0 = \sum_{pq} \langle p | \hat{h}_0 | q \rangle \, a_p^\dagger a_q$$

can be written, using standard annihilation and creation operators, in normal-ordered form as

$$\hat{H}_0 = \sum_{pq} \langle p | \hat{h}_0 | q \rangle \left\{ a_p^\dagger a_q \right\} + \sum_i \langle i | \hat{h}_0 | i \rangle$$

Fig. 8.4 Finite-size effects in the kinetic energy of pure neutron matter computed with the Minnesota potential as a function of the number of particles for both periodic boundary conditions and twist-averaged boundary conditions.

Explain the meaning of the various symbols. Which reference vacuum has been used?

8.2. Show that the two-body part of the Hamiltonian

$$\hat{H}_I = \frac{1}{4} \sum_{pqrs} \langle pq | \hat{v} | rs \rangle a_p^\dagger a_q^\dagger a_s a_r$$

can be written, using standard annihilation and creation operators, in normal-ordered form as

$$
\begin{aligned}
\hat{H}_I &= \frac{1}{4} \sum_{pqrs} \langle pq | \hat{v} | rs \rangle a_p^\dagger a_q^\dagger a_s a_r \\
&= \frac{1}{4} \sum_{pqrs} \langle pq | \hat{v} | rs \rangle \{ a_p^\dagger a_q^\dagger a_s a_r \} + \sum_{pqi} \langle pi | \hat{v} | qi \rangle \{ a_p^\dagger a_q \} + \frac{1}{2} \sum_{ij} \langle ij | \hat{v} | ij \rangle
\end{aligned}
$$

Explain again the meaning of the various symbols.

8.3. Derive the normal-ordered form of the threebody part of the Hamiltonian.

$$\hat{H}_3 = \frac{1}{36} \sum_{\substack{pqr \\ stu}} \langle pqr | \hat{v}_3 | stu \rangle a_p^\dagger a_q^\dagger a_r^\dagger a_u a_t a_s,$$
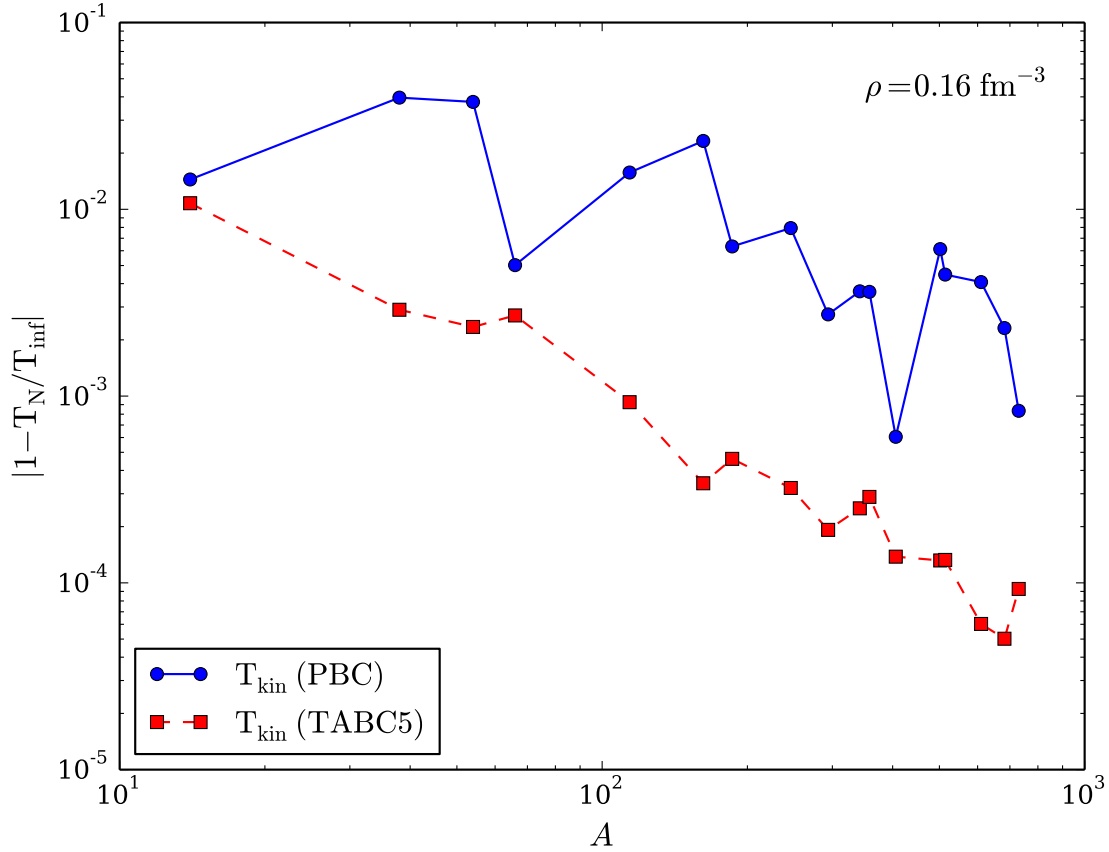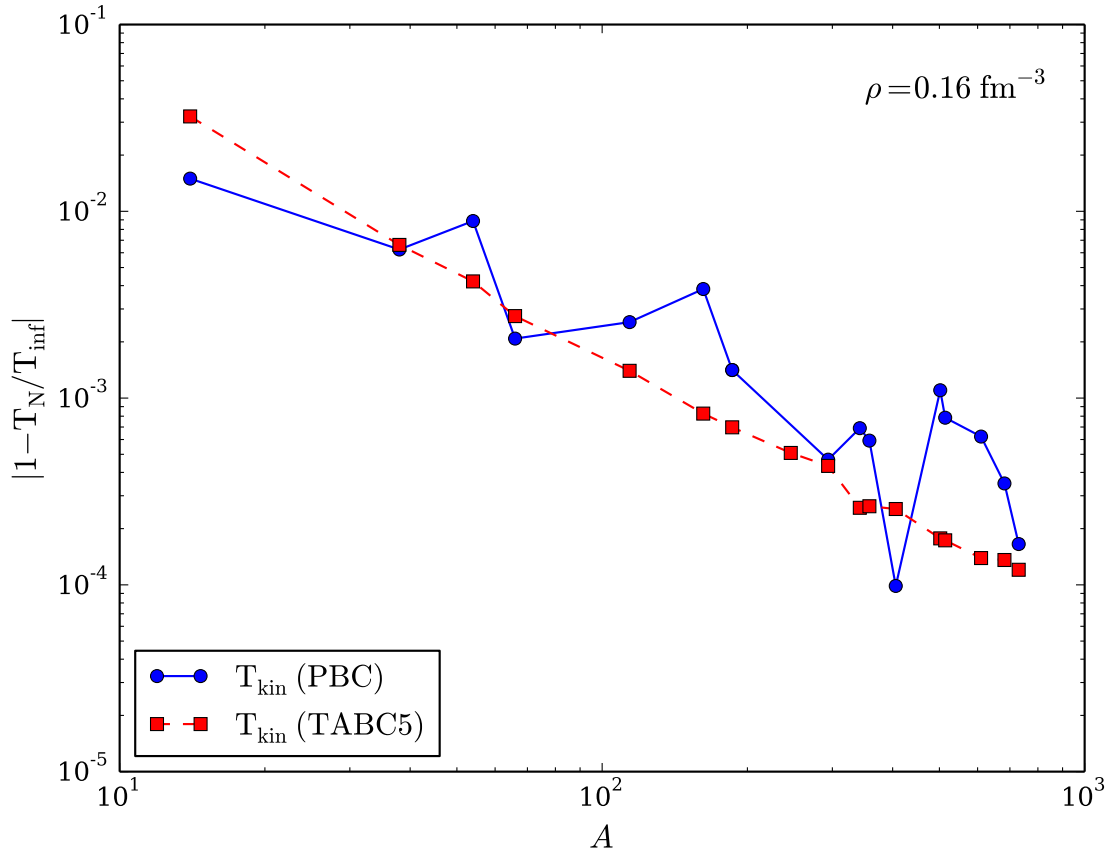
Fig. 8.5 Finite-size effects in the Hartree-Fock energy of pure neutron matter computed with the Minnesota potential as a function of the number of particles for both periodic boundary conditions and twist-averaged boundary conditions.

and specify the contributions to the two-body, one-body and the scalar part.

8.4. Develop a program which sets up a single-particle basis for nuclear matter calculations with input a given number of nucleons and a user specificied density or Fermi momentum. Follow the setup discussed in Table 8.1. You need to define the number of particles A and the density of the system using

$$n = g\frac{k_F^3}{6\pi^2}.$$

Here you can either define the density itself or the Fermi momentum k_F. With the density/Fermi momentum and a fixed number of nucleons A, we can define the length L of the box used with our periodic boundary contributions via the relation

$$V = L^3 = \frac{A}{n}.$$

We can then can use L to define the spacing between various k-values, that is

$$\Delta k = \frac{2\pi}{L}.$$

8.5. The interaction we will use for these calculations is a semirealistic nucleon-nucleon potential known as the Minnesota potential [?] which has the form, $V_\alpha(r) = V_\alpha \exp-(\alpha r^2)$. The

spin and isospin dependence of the Minnesota potential is given by,

$$V(r) = \frac{1}{2}\left(V_R + \frac{1}{2}(1 + P_{12}^\sigma)V_T + \frac{1}{2}(1 - P_{12}^\sigma)V_S\right)(1 - P_{12}^\sigma P_{12}^\tau),$$

where $P_{12}^\sigma = \frac{1}{2}(1 + \sigma_1 \cdot \sigma_2)$ and $P_{12}^\tau = \frac{1}{2}(1 + \tau_1 \cdot \tau_2)$ are the spin and isospin exchange operators, respectively. Show that a Fourier transform to momentum space results in

$$\langle \mathbf{k}_p \mathbf{k}_q | V_\alpha | \mathbf{k}_r \mathbf{k}_s \rangle = \frac{V_\alpha}{L^3}\left(\frac{\pi}{\alpha}\right)^{3/2} \exp\frac{-q^2}{4\alpha} \delta_{\mathbf{k}_p + \mathbf{k}_q, \mathbf{k}_r + \mathbf{k}_s}.$$

Write thereafter a function which sets up the full anty-symmetrized matrix elements for the Minnesota potential using the parameters listed in Table 8.2.

8.6. Consider a Slater determinant built up of orthogonal single-particle orbitals ψ_λ, with $\lambda = 1, 2, \ldots, A$.

The unitary transformation

$$\psi_a = \sum_\lambda C_{a\lambda}\phi_\lambda,$$

brings us into the new basis. The new basis has quantum numbers $a = 1, 2, \ldots, A$. Show that the new basis is orthogonal.

a) Show that the new Slater determinant constructed from the new single-particle wave functions can be written as the determinant based on the previous basis and the determinant of the matrix C.

b) Show that the old and the new Slater determinants are equal up to a complex constant with absolute value unity. Hint: C is a unitary matrix.

8.7. Use the ansatz for the ground state in second quantization

$$|\Phi_0\rangle = \left(\prod_{i \leq F} \hat{a}_i^\dagger\right)|0\rangle,$$

where the index i defines different single-particle states up to the Fermi level, to calculate using Wick's theorem (see the appendix) the expectation value

$$E[\Phi_0] = E_{\text{Ref}} = \sum_{i \leq F}^A \langle i|\hat{h}_0|i\rangle + \frac{1}{2}\sum_{ij \leq F}^A \langle ij|\hat{v}|ij\rangle_{AS}.$$

Insert thereafter the plane wave function basis for the various single-particle states and show that the above energy can be written as

$$E[\Phi_0] = \sum_{i \leq F}^A \langle k_i|\hat{t}|k_i\rangle + \frac{1}{2}\sum_{ij \leq F}^A \langle k_i k_j|\hat{v}|k_i k_j\rangle_{AS},$$

where we use the shorthand $|k_i\rangle = |\mathbf{k}_i, \sigma_i, \tau_{z_i}\rangle$ for the single-particle states in three dimensions.

Replace then the discrete sums with integrals, that is

$$\sum_i \rightarrow \sum_{\sigma_i}\sum_{\tau_{z_i}} \frac{L^3}{(2\pi)^3}\int_0^{\mathbf{k}_F} d\mathbf{k},$$

and show that the energy per particle A can be written as (for symmetric nuclear matter)

$$\frac{E_{\text{Ref}}}{A} = \frac{3\hbar^2 k_F^2}{10M_N} + \frac{1}{2n}\frac{L^3}{(2\pi)^6}\sum_{\sigma_i \sigma_j}\sum_{\tau_{z_i}\tau_{z_j}}\int_0^{\mathbf{k}_F} d\mathbf{k}_i \int_0^{\mathbf{k}_F} d\mathbf{k}_j \langle k_i k_j|\hat{v}|k_i k_j\rangle_{AS},$$

with the density $n = V/A = L^3/A$.

Find the following expression for pure neutron matter. Use the Minnesota interaction and try to simplify the above six-dimensional integral for pure neutron matter (Hint: the interaction depends only the momentum transfer squared and fix one of the momentum integrations along the z-axis. Integrate out the dependence on the various angles).

Finally, write a program which computes the above energy for pure nuetron matter using the Minnesota potential.

8.8. We will assume that we can build various Slater determinants using an orthogonal single-particle basis ψ_λ, with $\lambda = 1, 2, \ldots, A$.

The aim of this exercise is to set up specific matrix elements that will turn useful when we start our discussions of different many-body methods. In particular you will notice, depending on the character of the operator, that many matrix elements will actually be zero.

Consider three A-particle Slater determinants $|\Phi_0\rangle$, $|\Phi_i^a\rangle$ and $|\Phi_{ij}^{ab}\rangle$, where the notation means that Slater determinant $|\Phi_i^a\rangle$ differs from $|\Phi_0\rangle$ by one single-particle state, that is a single-particle state ψ_i is replaced by a single-particle state ψ_a. It will later be interpreted as a so-called one-particle-one-hole excitation. Similarly, the Slater determinant $|\Phi_{ij}^{ab}\rangle$ differs by two single-particle states from $|\Phi_0\rangle$ and is normally thought of as a two-particle-two-hole excitation.

Define a general one-body operator $\hat{F} = \sum_i^A \hat{f}(x_i)$ and a general two-body operator $\hat{G} = \sum_{i>j}^A \hat{g}(x_i, x_j)$ with g being invariant under the interchange of the coordinates of particles i and j.

a)
$$\langle \Phi_0 | \hat{F} | \Phi_0 \rangle,$$

and
$$\langle \Phi_0 | \hat{G} | \Phi_0 \rangle.$$

b) Find thereafter
$$\langle \Phi_0 | \hat{F} | \Phi_i^a \rangle,$$

and
$$\langle \Phi_0 | \hat{G} | \Phi_i^a \rangle,$$

c) Finally, find
$$\langle \Phi_0 | \hat{F} | \Phi_{ij}^{ab} \rangle,$$

and
$$\langle \Phi_0 | \hat{G} | \Phi_{ij}^{ab} \rangle.$$

d) What happens with the two-body operator if we have a transition probability of the type

$$\langle \Phi_0 | \hat{G} | \Phi_{ijk}^{abc} \rangle,$$

where the Slater determinant to the right of the operator differs by more than two single-particle states?

e) With an orthogonal basis of Slater determinants Φ_λ, we can now construct an exact many-body state as a linear expansion of Slater determinants, that is, a given exact state

$$\Psi_i = \sum_{\lambda=0}^{\infty} C_{i\lambda} \Phi_\lambda.$$

In all practical calculations the infinity is replaced by a given truncation in the sum.
If you are to compute the expectation value of (at most) a two-body Hamiltonian for the above exact state

$$\langle \Psi_i | \hat{H} | \Psi_i \rangle,$$

based on the calculations above, which are the only elements which will contribute? (there is no need to perform any calculation here, use your results from exercises a), b), and c)). These results simplify to a large extent shell-model calculations.

8.9. We present a simplified Hamiltonian consisting of an unperturbed Hamiltonian and a so-called pairing interaction term. It is a model which to a large extent mimicks some central features of atomic nuclei, certain atoms and systems which exhibit superfluiditity or superconductivity. To study this system, we will use a mix of many-body perturbation theory (MBPT), Hartree-Fock (HF) theory and full configuration interaction (FCI) theory. The latter will also provide us with the exact answer. When setting up the Hamiltonian matrix you will need to solve an eigenvalue problem.

We define first the Hamiltonian, with a definition of the model space and the single-particle basis. Thereafter, we present the various exercises (some of them are solved).

The Hamiltonian acting in the complete Hilbert space (usually infinite dimensional) consists of an unperturbed one-body part, $\hat{H}_0$, and a perturbation $\hat{V}$.

We limit ourselves to at most two-body interactions and our Hamiltonian is represented by the following operators

$$\hat{H} = \sum_{\alpha\beta} \langle \alpha | h_0 | \beta \rangle a_\alpha^\dagger a_\beta + \frac{1}{4} \sum_{\alpha\beta\gamma\delta} \langle \alpha\beta | V | \gamma\delta \rangle a_\alpha^\dagger a_\beta^\dagger a_\delta a_\gamma,$$

where $a_\alpha^\dagger$ and a_α etc. are standard fermion creation and annihilation operators, respectively, and $\alpha\beta\gamma\delta$ represent all possible single-particle quantum numbers. The full single-particle space is defined by the completeness relation

$$\hat{\mathbf{1}} = \sum_{\alpha=1}^{\infty} |\alpha\rangle\langle\alpha|.$$

In our calculations we will let the single-particle states $|\alpha\rangle$ be eigenfunctions of the one-particle operator $\hat{h}_0$. Note that the two-body part of the Hamiltonian contains anti-symmetrized matrix elements.

The above Hamiltonian acts in turn on various many-body Slater determinants constructed from the single-basis defined by the one-body operator $\hat{h}_0$. As an example, the two-particle model space $\mathscr{P}$ is defined by an operator

$$\hat{P} = \sum_{\alpha\beta=1}^{m} |\alpha\beta\rangle\langle\alpha\beta|,$$

where we assume that $m = \dim(\mathscr{P})$ and the full space is defined by

$$\hat{P} + \hat{Q} = \hat{\mathbf{1}},$$

with the projection operator

$$\hat{Q} = \sum_{\alpha\beta=m+1}^{\infty} |\alpha\beta\rangle\langle\alpha\beta|,$$

being the complement of $\hat{P}$.

Our specific model consists of N doubly-degenerate and equally spaced single-particle levels labelled by $p = 1, 2, \ldots$ and spin $\sigma = \pm 1$. These states are schematically portrayed in Fig. 10.1. The first two single-particle levels define a possible model space, indicated by the label $\mathscr{P}$. The remaining states span the excluded space $\mathscr{Q}$.

We write the Hamiltonian as

$$\hat{H} = \hat{H}_0 + \hat{V},$$

where

$$\hat{H}_0 = \xi \sum_{p\sigma}(p-1)a^\dagger_{p\sigma}a_{p\sigma}$$

and

$$\hat{V} = -\frac{1}{2}g\sum_{pq}a^\dagger_{p+}a^\dagger_{p-}a_{q-}a_{q+}.$$

Here, H_0 is the unperturbed Hamiltonian with a spacing between successive single-particle states given by ξ, which we will set to a constant value $\xi = 1$ without loss of generality. The two-body operator $\hat{V}$ has one term only. It represents the pairing contribution and carries a constant strength g.

The indices $\sigma = \pm$ represent the two possible spin values. The interaction can only couple pairs and excites therefore only two particles at the time.

a) Show that the unperturbed Hamiltonian $\hat{H}_0$ and $\hat{V}$ commute with both the spin projection $\hat{S}_z$ and the total spin $\hat{S}^2$, given by

$$\hat{S}_z := \frac{1}{2}\sum_{p\sigma}\sigma a^\dagger_{p\sigma}a_{p\sigma}$$

and

$$\hat{S}^2 := \hat{S}_z^2 + \frac{1}{2}(\hat{S}_+\hat{S}_- + \hat{S}_-\hat{S}_+),$$

where

$$\hat{S}_\pm := \sum_p a^\dagger_{p\pm}a_{p\mp}.$$

This is an important feature of our system that allows us to block-diagonalize the full Hamiltonian. We will focus on total spin $S = 0$. In this case, it is convenient to define the so-called pair creation and pair annihilation operators

$$\hat{P}_p^+ = a^\dagger_{p+}a^\dagger_{p-},$$

and

$$\hat{P}_p^- = a_{p-}a_{p+},$$

respectively.

b) Show that you can rewrite the Hamiltonian (with $\xi = 1$) as

$$\hat{H} = \sum_{p\sigma}(p-1)a^\dagger_{p\sigma}a_{p\sigma} - \frac{1}{2}g\sum_{pq}\hat{P}_p^+\hat{P}_q^-.$$

c) Show also that Hamiltonian commutes with the product of the pair creation and annihilation operators. This model corresponds to a system with no broken pairs. This means that the Hamiltonian can only link two-particle states in so-called spin-reversed states.

d) Construct thereafter the Hamiltonian matrix for a system with no broken pairs and total spin $S = 0$ for the case of the four lowest single-particle levels indicated in the Fig. 10.1. Our system consists of four particles only. Our single-particle space consists of only the four lowest levels $p = 1,2,3,4$. You need to set up all possible Slater determinants. Find all eigenvalues by diagonalizing the Hamiltonian matrix. Vary your results for values of $g \in [-1,1]$. We refer to this as the exact calculation. Comment the behavior of the ground state as function of g.

8.10. a) We will now set up the Hartree-Fock equations by varying the coefficients of the single-particle functions. The single-particle basis functions are defined as

$$\psi_p = \sum_\lambda C_{p\lambda} \psi_\lambda.$$

where in our case $p = 1, 2, 3, 4$ and $\lambda = 1, 2, 3, 4$, that is the first four lowest single-particle orbits of Fig. 10.1. Set up the Hartree-Fock equations for this system by varying the coefficients $C_{p\lambda}$ and solve them for values of $g \in [-1, 1]$. Comment your results and compare with the exact solution. Discuss also which diagrams in Fig. **??** that can be affected by a Hartree-Fock basis. Compute the total binding energy using a Hartree-Fock basis and comment your results.

b) We will now study the system using non-degenerate Rayleigh-Schrödinger perturbation theory to third order in the interaction. If we exclude the first order contribution, all possible diagrams (so-called anti-symmetric Goldstone diagrams) are shown in Fig. **??**.

Based on the form of the interaction, which diagrams contribute to the binding energy of the ground state? Write down the expressions for the diagrams that contribute and find the contribution to the ground state energy as function $g \in [-1, 1]$. Comment your results. Compare these results with those you obtained from the exact diagonalization with and without the $4p - 4h$ state. Discuss your results for a canonical Hartree-Fock basis and a non-canonical Hartree-Fock basis.

Diagram 1 in Fig. **??** represents a second-order contribution to the energy and a so-called $2p - 2h$ contribution to the intermediate states. Write down the expression for the wave operator in this case and compare the possible contributions with the configuration interaction calculations without the $4p - 4h$ Slater determinant. Comment your results for various values of $g \in [-1, 1]$.

We limit now the discussion to the canonical Hartree-Fock case only. To fourth order in perturbation theory we can produce diagrams with $1p - 1h$ intermediate excitations as shown in Fig. **??**, $2p - 2h$ excitations, see Fig. **??**, $3p - 3h$ excitations as shown in Fig. **??** and finally so-called diagrams with intermediate four-particle-four-hole excitations, see Fig. **??**. Define first linked and unlinked diagrams and explain briefly Goldstone's linked diagram theorem. Based on the linked diagram theorem and the form of the pairing Hamiltonian, which diagrams will contribute to fourth order?

Calculate the energy to fourth order with a canonical Hartree-Fock basis for $g \in [-1, 1]$ and compare with the full diagonalization case in exercise b). Discuss the results.

8.11. This project serves as a continuation of the pairing model with the aim being to solve the same problem but now by developing a program that implements the coupled cluster method with double excitations only. In doing so you will find it convenient to write classes which define the single-particle basis and the Hamiltonian. Your functions that solve the coupled cluster equations will then just need to set up variables which point to interaction elements and single-particle states with their pertinent quantum numbers. Use for example the setup discussed in the FCI lectures for the pairing model.

a) Explain why no single excitations are involved in this model.
b) Set up the coupled cluster equations for doubles excitations and convince yourself about their meaning and correctness.
c) Write a class which holds single-particle data like specific quantum numbers, single-particle Hamiltonian etc. Write also a class which sets up and stores two-body matrix elements defined by the single-particle states. Write thereafter functions/classes which implement the coupled cluster method with doubles only.
d) Compare your results with those from the exact diagonalization with and without the $4p4h$ excitation. Compare also your results to perturbation theory at different orders, in particular to second order. Discuss your results. If other students are solving the same problem using Green's function theory, you can also compare your results with those obtained from

Green's function theory. The aim is to finalize this part during the first week. The codes you will develop can be used as a starting point for the second part of the project.

8.10 Solutions to selected exercises

8.1 To solve this problem, we start by introducing the shorthand label for single-particle states below the Fermi level F as $i, j, \ldots \leq F$. For single-particle states above the Fermi level we reserve the labels $a, b, \ldots > F$, while the labels $p, q, \ldots$ represent any possible single particle state. Using the ansatz for the ground state $|\Phi_0$ as new reference vacuum state, the anticommutation relations are

$$\{a_p^\dagger, a_q\} = \delta_{pq}, p, q \leq F,$$

and

$$\{a_p, a_q^\dagger\} = \delta_{pq}, \ p, q > F.$$

It is easy to see then that

$$a_i|\Phi_0\rangle = |\Phi_i\rangle \neq 0, \quad a_a^\dagger|\Phi_0\rangle = |\Phi^a\rangle \neq 0,$$

and

$$a_i^\dagger|\Phi_0\rangle = 0 \quad a_a|\Phi_0\rangle = 0.$$

We can then rewrite the one-body Hamiltonian as

$$\hat{H}_0 = \sum_{pq} \langle p|\hat{h}_0|q\rangle a_p^\dagger a_q$$
$$= \sum_{pq} \langle p|\hat{h}_0|q\rangle \{a_p^\dagger a_q\} + \delta_{pq\in i} \sum_{pq} \langle p|\hat{h}_0|q\rangle$$
$$= \sum_{pq} \langle p|\hat{h}_0|q\rangle \{a_p^\dagger a_q\} + \sum_i \langle i|\hat{h}_0|i\rangle,$$

where the curly brackets represent normal-ordering with respect to the new vacuum state. Withe respect to the new vacuum reference state, the

8.2 Using our anti-commutation rules, Wick's theorem discussed in the appendix and the definition of the creation and annihilation operators from the previous problem, we can rewrite the set of creation and annihilation operators of

$$\hat{H}_I = \frac{1}{4} \sum_{pqrs} \langle pq|\hat{v}|rs\rangle a_p^\dagger a_q^\dagger a_s a_r$$

as

$$a_p^\dagger a_q^\dagger a_s a_r = \{a_p^\dagger a_q^\dagger a_s a_r\}$$
$$+ \left\{a_p^\dagger \overbrace{a_q^\dagger a_s} a_r\right\} + \left\{a_p^\dagger \overbrace{a_q^\dagger a_s a_r}\right\} + \left\{\overbrace{a_p^\dagger a_q^\dagger} a_s a_r\right\}$$
$$+ \left\{\overbrace{a_p^\dagger a_q^\dagger a_s} a_r\right\} + \left\{\overbrace{a_p^\dagger a_q^\dagger a_s a_r}\right\} + \left\{\overbrace{a_p^\dagger a_q^\dagger a_s a_r}\right\}$$
$$= \{a_p^\dagger a_q^\dagger a_s a_r\} + \delta_{qs\in i}\{a_p^\dagger a_r\} - \delta_{qr\in i}\{a_p^\dagger a_s\} - \delta_{ps\in i}\{a_q^\dagger a_r\}$$
$$+ \delta_{pr\in i}\{a_q^\dagger a_s\} + \delta_{pr\in i}\delta_{qs\in i} - \delta_{ps\in i}\delta_{qr\in i}.$$

Inserting the redefinition of the creation and annihilation operators with respect to the new vacuum state, we have

$$\hat{H}_I = \frac{1}{4} \sum_{pqrs} \langle pq| \hat{v} |rs\rangle a_p^\dagger a_q^\dagger a_s a_r$$

$$= \frac{1}{4} \sum_{pqrs} \langle pq| \hat{v} |rs\rangle \{a_p^\dagger a_q^\dagger a_s a_r\} + \frac{1}{4} \sum_{pqrs} \Big(\delta_{qs\in i} \langle pq| \hat{v} |rs\rangle \{a_p^\dagger a_r\}$$

$$- \delta_{qr\in i} \langle pq| \hat{v} |rs\rangle \{a_p^\dagger a_s\} - \delta_{ps\in i} \langle pq| \hat{v} |rs\rangle \{a_q^\dagger a_r\}$$

$$+ \delta_{pr\in i} \langle pq| \hat{v} |rs\rangle \{a_q^\dagger a_s\} + \delta_{pr\in i} \delta_{qs\in i} - \delta_{ps\in i} \delta_{qr\in i} \Big)$$

$$= \frac{1}{4} \sum_{pqrs} \langle pq| \hat{v} |rs\rangle \{a_p^\dagger a_q^\dagger a_s a_r\}$$

$$+ \frac{1}{4} \sum_{pqi} \Big(\langle pi| \hat{v} |qi\rangle - \langle pi| \hat{v} |iq\rangle - \langle ip| \hat{v} |qi\rangle + \langle ip| \hat{v} |iq\rangle \Big) \{a_p^\dagger a_q\}$$

$$+ \frac{1}{4} \sum_{ij} \Big(\langle ij| \hat{v} |ij\rangle - \langle ij| \hat{v} |ji\rangle \Big)$$

$$= \frac{1}{4} \sum_{pqrs} \langle pq| \hat{v} |rs\rangle \{a_p^\dagger a_q^\dagger a_s a_r\} + \sum_{pqi} \langle pi| \hat{v} |qi\rangle \{a_p^\dagger a_q\} + \frac{1}{2} \sum_{ij} \langle ij| \hat{v} |ij\rangle .$$

Summing up, we obtain a two-body part defined as

$$\hat{V}_N = \frac{1}{4} \sum_{pqrs} \langle pq| \hat{v} |rs\rangle \{a_p^\dagger a_q^\dagger a_s a_r\} ,$$

a one-body part given by

$$\hat{F}_N = \sum_{pqi} \langle pi| \hat{v} |qi\rangle \{a_p^\dagger a_q\} ,$$

and finally the so-called reference energy

$$E_{\text{ref}} = \frac{1}{2} \sum_{ij} \langle ij| \hat{v} |ij\rangle .$$

which is the energy expectation value for the reference state. Thus, our normal-ordered Hamiltonian with at most a two-body nucleon-nucleon interaction is defined as

$$\hat{H}_N = \frac{1}{4} \sum_{pqrs} \langle pq| \hat{v} |rs\rangle \{a_p^\dagger a_q^\dagger a_s a_r\} + \sum_{pq} f_q^p \{a_p^\dagger a_q\} = \hat{V}_N + \hat{F}_N,$$

with

$$\hat{F}_N = \sum_{pq} f_q^p \{a_p^\dagger a_q\} ,$$

and

$$\hat{V}_N = \frac{1}{4} \sum_{pqrs} \langle pq| \hat{v} |rs\rangle \{a_p^\dagger a_q^\dagger a_s a_r\} ,$$

where

$$f_q^p = \langle p| \hat{h}_0 |q\rangle + \sum_i \langle pi| \hat{v} |qi\rangle$$

8.4 The following python code sets up the quantum numbers for both infinite nuclear matter and neutron matter emeploying a cutoff in the value of n.

```
from numpy import *

nmax =2 nshell = 3*nmax*nmax count = 1 tzmin = 1

print "Symmetric nuclear matter:" print "a, nx, ny, nz, sz, tz, nx^2
```

```
+ ny^2 + nz^2" for n in range(nshell): for nx in
range(-nmax,nmax+1): for ny in range(-nmax,nmax+1): for nz in
range(-nmax, nmax+1): for sz in range(-1,1+1): tz = 1 for tz in
range(-tzmin,tzmin+1): e = nx*nx + ny*ny + nz*nz if e == n: if sz !=
0: if tz != 0: print count, " ",nx," ",ny, " ",nz," ",sz," ",tz,"
",e count += 1


nmax =1 nshell = 3*nmax*nmax count = 1 tzmin = 1 print
"----------------------------------" print "Neutron matter:" print
"a, nx, ny, nz, sz, nx^2 + ny^2 + nz^2" for n in range(nshell): for
nx in range(-nmax,nmax+1): for ny in range(-nmax,nmax+1): for nz in
range(-nmax, nmax+1): for sz in range(-1,1+1): e = nx*nx + ny*ny +
nz*nz if e == n: if sz != 0: print count, " ",nx," ",ny, " ",sz,"
",tz," ",e count += 1
```

?? We give first the final Hamiltonian matrix !bt

$$
H = \begin{pmatrix}
2\delta - g & -g/2 & -g/2 & -g/2 & -g/2 & 0 \\
-g/2 & 4\delta - g & -g/2 & -g/2 & -0 & -g/2 \\
-g/2 & -g/2 & 6\delta - g & 0 & -g/2 & -g/2 \\
-g/2 & -g/2 & 0 & 6\delta - g & -g/2 & -g/2 \\
-g/2 & 0 & -g/2 & -g/2 & 8\delta - g & -g/2 \\
0 & -g/2 & -g/2 & -g/2 & -g/2 & 10\delta - g
\end{pmatrix}
$$

The following python program diagonalizes the above Hamiltonian matrix for a given span of interaction strength values, performing both a full configuration interaction calculation and a truncated one. For the truncated case we leave out the $4p4h$ state. This means that in addition to the ground state we include the four possible $2p2h$ states. Such a calculation is normally called a configuration interaction calculation.

```python
from numpy import * from sympy import * from matplotlib.pyplot
import *

g_array = linspace(-1, 1, 1001) e1_array = [] e2_array = []

for g in g_array: H1 = matrix([[2-g , -g/2., -g/2., -g/2., -g/2.,
    0], [-g/2., 4-g, -g/2., -g/2., 0., -g/2.], [-g/2., -g/2., 6-g,
    0, -g/2., -g/2.], [-g/2., -g/2., 0, 6-g, -g/2., -g/2.], [-g/2.,
    0, -g/2., -g/2., 8-g, -g/2.], [0 , -g/2., -g/2., -g/2., -g/2.,
    10-g]])

    H2 = matrix([[2-g , -g/2., -g/2., -g/2., -g/2.], [-g/2.,
        4-g, -g/2., -g/2., 0.], [-g/2., -g/2., 6-g, 0, -g/2.],
      [-g/2., -g/2., 0, 6-g, -g/2.], [-g/2., 0, -g/2., -g/2.,
        8-g]])


    u1, v1 = linalg.eig(H1) u2, v2 = linalg.eig(H2)

    if g == 1./2: print argmin(u1)

            for i in range(5): print " %.3f " % v2[i,0],


    e1_array.append(min(u1)) e2_array.append(min(u2))
```

```
plot(g_array, e1_array, linewidth=2.0) #plot(g_array, e2_array,
linewidth=2.0) plot(g_array, (2-g_array), linewidth=2.0) grid()
xlabel(r"Strength of interaction, $g$", fontsize=16) ylabel(r'Ground
state energy', fontsize=16) #axis([-1,1,-0.4,0.05]) legend(['FCI --
 Exact', 'Reference energy']) savefig("pairing.pdf") show()
```

The eigenvalues and eigenvectors result from the diagonalization of the above Hamiltonian matrix. In the discussions below and in connection with the first stage of the numerical project, we will use these results to benchmark various approximative methods. The lowest eigenvalue corresponds to the ground state energy and we will refer to it as the *exact energy* when no truncations in the space of possible Slater determinants are made..

From our results, we note some important differences between the full configuration interaction (FCI) calculation and the truncated configuration interaction calculation (CI). Full configuration interaction is an exact method, but is only possible if and only if we have a complete and finite SD basis for our system. In practice, we usually don't have this. Non-complete CI however, is always possible, but yiels approximative results only. The method is however still variational however, meaning that we guaranteed that the approximation will be equal or bigger to the true result. Perturbation theory however, is non-variational and there is no guarantee that including higher orders in the perturbation gives an improved result, as we will see below.

In an FCI case, we are including all possible excitations to infinite order, meaning we have all possible $1p1h$, $2p2h$ etc configurations, up to $4p4h$ excitations for our selected model. Due to the nature of the pairing interaction and our selection of specific quantum numbers for the many-body states, we do not have any $1p1h$ or $3p3h$ excitations. In the above CI case, we truncate those excitations somewhere. If we were to draw the diagrams of the interactions that contribute to this CI case, there would be an infinite number of them, as we can have arbitrarily long chains of operators that still only have at most 2p2h intermediate states.

8.10 To fourth order in the interaction there are several diagrams to consider. Fortunately, due to the character of the pairing Hamiltonian, several of these contributions are zero. We limit our discussions also to include the canonical HF-case only. All of the diagrams in the canonical case are shown in figures 3, 4, 5 and 6 above. Using also the linked diagram theorem, where a diagram is called unlinked if and only if it has a disconnected part that is closed, we can eliminate some further diagrams. Goldstones linked-diagram theorem states that all unliked diagrams will cancel against the renormalization terms in Rayleigh-Schrödinger perturbation theory, meaning that we can define the energy to each order as a sum of linked diagrams only. We can then disregard diagram 33 and 41.

Let us now go through all the diagrams and find those that vanish due to having broken pairs, i.e., the diagrams that vanish due to our specific interaction. Take for example diagram 1, which vanishes due to having a term $\langle ab|\hat{v}|ci\rangle$. From this argument, we see that all four diagrams from figure 3 vanish. Similar arguments shows that most diagrams in figure 4 also dissapear. Going through all the diagrams, we see that 5, 6, 14 and 15 are the ones that do not vanish in figure 4. For figure 5 we actually see that all diagrams vanish again. For figure 6 we already found that 33 and 41 vanished due to being unlinked—the rest contribute to the perturbative expansion of the energy. The diagrams of figures 3 and 5 vanish since they involve $1p1h$ and $3p3h$ excitations, respectively.

The expressions for these diagrams can easily be written in terms of a simple Python program. Note however that for every diagram we do actually perform loops over every single-particle state. As we will see later, this is extremely inefficient from a computational point of view. In our discussions of the projects below, we will rewrite the computations of most diagrams in terms of efficient matrix-matrix multiplications or matrix-vector multiplications. The following Python program gives us the final results for perturbation theory to fourth order in

the interaction. The resulting figures include also plots of the relative error in the correlation energy. That is, we compare the computed correlation in perturbation theory with the result from the exact diagonalization discussed above.

```python
from sympy import * from pylab import *

below_fermi = (0,1,2,3) above_fermi = (4,5,6,7)

states = [(1,1),(1,-1),(2,1),(2,-1),(3,1),(3,-1),(4,1),(4,-1)] N = 8
g = Symbol('g')



def h0(p,q): if p == q: p1, s1 = states[p] return (p1 - 1) else:
return 0

def f(p,q): if p == q: return 0

    s = h0(p,q) for i in below_fermi: s += assym(p,i,q,i) return
    s


def assym(p,q,r,s): p1, s1 = states[p] p2, s2 = states[q] p3, s3 =
states[r] p4, s4 = states[s]

    if p1 != p2 or p3 != p4: return 0 if s1 == s2 or s3 == s4:
    return 0 if s1 == s3 and s2 == s4: return -g/2. if s1 == s4
    and s2 == s3: return g/2.

def eps(holes, particles): E = 0 for h in holes: p, s = states[h] E
+= (p-1) for p in particles: p, s = states[p] E -= (p-1) return E


# Diagram 3 s = 0 for a in above_fermi: for b in above_fermi: for c
# in above_fermi: for i in below_fermi: for j in below_fermi: for k
# in below_fermi: s +=
# assym(i,j,a,b)*assym(a,c,j,k)*assym(b,k,c,i)/eps((i,j),(a,b))/eps((k,j),(a,c))
# print s


# ga = linspace(-1,1,101) corr2 = [] corr3 = [] corrx = []


# Diagram 1 s1 = 0 for a in above_fermi: for b in above_fermi: for i
in below_fermi: for j in below_fermi: s1 +=
0.25*assym(a,b,i,j)*assym(i,j,a,b)/eps((i,j),(a,b))

# Diagram 4 s4 = 0 for a in above_fermi: for b in above_fermi: for c
in above_fermi: for d in above_fermi: for i in below_fermi: for j in
below_fermi: s4 +=
0.125*assym(i,j,a,b)*assym(a,b,c,d)*assym(c,d,i,j)/eps((i,j),(a,b))/eps((i,j),(c,d))

# Diagram 5 s5 = 0 for a in above_fermi: for b in above_fermi: for i
in below_fermi: for j in below_fermi: for k in below_fermi: for l in
below_fermi: s5 +=
0.125*assym(i,j,a,b)*assym(k,l,i,j)*assym(a,b,k,l)/eps((i,j),(a,b))/eps((k,l),(a,b))

# Diagram 8 (simplified) s8 = 0 for a in above_fermi: for b in
above_fermi: for i in below_fermi: for j in below_fermi: for k in
below_fermi: s8 -=
0.5*assym(i,j,a,b)*assym(a,b,i,k)*f(k,j)/eps((i,j),(a,b))/eps((i,k),(a,b))
```

```python
# Diagram 9 (simplified) s9 = 0 for a in above_fermi: for b in
above_fermi: for c in above_fermi: for i in below_fermi: for j in
below_fermi: s9 +=
0.5*assym(i,j,a,b)*assym(a,c,i,j)*f(b,c)/eps((i,j),(a,b))/eps((i,j),(a,c))


print s1 print s4 print s5 print s8 print s9

s_5 = -0.0291521990740741*g**4 s14 = -0.0308883101851853*g**4 s34 =
0.0163049768518519*g**4 s36 = -0.0145760995370371*g**4 s38 =
-0.0201099537037037*g**4 s39 = 0.0176938657407407*g**4

ga = linspace(-1,1,10001) e1 = [] corr2 = [] corr3 = [] corr4 = []
for g_val in ga: H1 = matrix([[2-g_val , -g_val/2., -g_val/2.,
    -g_val/2., -g_val/2., 0], [-g_val/2., 4-g_val, -g_val/2.,
    -g_val/2., 0., -g_val/2.], [-g_val/2., -g_val/2., 6-g_val, 0,
    -g_val/2., -g_val/2.], [-g_val/2., -g_val/2., 0, 6-g_val,
    -g_val/2., -g_val/2.], [-g_val/2., 0, -g_val/2., -g_val/2.,
    8-g_val, -g_val/2.], [0 , -g_val/2., -g_val/2., -g_val/2.,
    -g_val/2., 10-g_val]])

    u1, v1 = linalg.eig(H1) e1.append(min(u1))

    corr2.append((s1).subs(g,g_val))
    corr3.append((s1+s4+s5).subs(g,g_val))
    corr4.append((s1+s4+s5+2*s_5+2*s14+2*s34+2*s36+s38+2*s39).subs(g,g_val))

exact = e1 - (2-ga)

plot(ga, exact, linewidth=2.0) plot(ga, corr2, linewidth=2.0)
plot(ga, corr3, linewidth=2.0) plot(ga, corr4, linewidth=2.0)
xlabel(r'Interaction strength, $g$', fontsize=16)
ylabel(r'Correlation energy', fontsize=16) axis([-1,1,-0.5,0.05])
grid() legend(["Exact", "2. order MPBT", "3. order MPBT", "4. order
  MPBT"], 'lower left') savefig("perturbationtheory.pdf") show()
error1 = zeros(len(exact)) error2 = zeros(len(exact)) error3 =
zeros(len(exact))

for i in range(len(exact)): error1[i] =
abs(float(exact[i]-corr2[i])) error2[i] =
abs(float(exact[i]-corr3[i])) error3[i] =
abs(float(exact[i]-corr4[i]))

error1 = array(error1) error2 = array(error2) error3 = array(error3)
print type(error1)

plot(ga, log10(error1)) plot(ga, log10(error2)) plot(ga,
log10(error3)) xlabel(r"Strength of interaction, $g$", fontsize=16)
ylabel(r"Error, $\log_{\rm 10}({\rm abs}({\rm error})$",
fontsize=16) legend(["2. order MPBT", "3. order MPBT", "4. order
  MPBT"], 'lower left') grid() savefig("logerror.pdf") show()
```

Running the Python program shows us that the approximation to both second and third order are very good when the interaction strength is small and contained in the interval $g \in [-0.5, 0.5]$, but as the interaction gets stronger the approximation worsens. We also note that the third-order result is actually worse than the second order result for larger values of the interaction strength, indicating that there is no guarantee that higher orders in many-body perturbation theory may reduce the relative error in a systematic way. This is seen in particular for the results to fourth order. For negative interaction strengths fourth order gives

a better result than second and third order, while for $g > 0$ the relative error is worse. We note also the non-variational character of many-body perturbation theory, with results at different undershooting the true ground state correlation energy

Appendix, Wick's theorem

Wick's theorem is based on two fundamental concepts, namely *normal ordering* and *contraction*. The normal-ordered form of $\hat{A}\hat{B}..\hat{X}\hat{Y}$, where the individual terms are either a creation or annihilation operator, is defined as

$$\left\{\hat{A}\hat{B}..\hat{X}\hat{Y}\right\} \equiv (-1)^p \left[\text{creation operators}\right] \cdot \left[\text{annihilation operators}\right]. \tag{8.121}$$

The p subscript denotes the number of permutations that is needed to transform the original string into the normal-ordered form. A contraction between to arbitrary operators $\hat{X}$ and $\hat{Y}$ is defined as

$$\overbrace{\hat{X}\hat{Y}} \equiv \langle 0|\hat{X}\hat{Y}|0\rangle. \tag{8.122}$$

It is also possible to contract operators inside a normal ordered products. We define the original relative position between two operators in a normal ordered product as p, the so-called permutation number. This is the number of permutations needed to bring one of the two operators next to the other one. A contraction between two operators with $p \neq 0$ inside a normal ordered is defined as

$$\left\{\overbrace{\hat{A}\hat{B}..\hat{X}}\hat{Y}\right\} = (-1)^p \left\{\overbrace{\hat{A}\hat{B}}..\hat{X}\hat{Y}\right\}. \tag{8.123}$$

In the general case with m contractions, the procedure is similar, and the prefactor changes to

$$(-1)^{p_1 + p_2 + .. + p_m}. \tag{8.124}$$

Wick's theorem states that every string of creation and annihilation operators can be written as a sum of normalordered products with all possible ways of contractions,

$$\hat{A}\hat{B}\hat{C}\hat{D}..\hat{R}\hat{X}\hat{Y}\hat{Z} = \left\{\hat{A}\hat{B}\hat{C}\hat{D}..\hat{R}\hat{X}\hat{Y}\hat{Z}\right\} \tag{8.125}$$

$$+ \sum_{[1]} \left\{\overbrace{\hat{A}\hat{B}}\hat{C}\hat{D}..\hat{R}\hat{X}\hat{Y}\hat{Z}\right\} \tag{8.126}$$

$$+ \sum_{[2]} \left\{\overbrace{\hat{A}\hat{B}\hat{C}\hat{D}}..\hat{R}\hat{X}\hat{Y}\hat{Z}\right\} \tag{8.127}$$

$$+ ... \tag{8.128}$$

$$+ \sum_{\left[\frac{N}{2}\right]} \left\{\overbrace{\hat{A}\hat{B}\hat{C}\hat{D}}.. \overbrace{\hat{R}\hat{X}\hat{Y}\hat{Z}}\right\}. \tag{8.129}$$

The $\sum_{[m]}$ means the sum over all terms with m contractions, while $\left[\frac{N}{2}\right]$ means the largest integer that not do not exceeds $\frac{N}{2}$ where N is the number of creation and annihilation operators. When N is even,

$$\left[\frac{N}{2}\right] = \frac{N}{2}, \tag{8.130}$$

and the last sum in Eq. (8.125) is over fully contracted terms. When N is odd,

$$\left[\frac{N}{2}\right] \neq \frac{N}{2}, \tag{8.131}$$

and none of the terms in Eq. (8.125) are fully contracted.

An important extension of Wick's theorem allow us to define contractions between normal-ordered strings of operators. This is the so-called generalized Wick's theorem,

$$\{\hat{A}\hat{B}\hat{C}\hat{D}..\}\{\hat{R}\hat{X}\hat{Y}\hat{Z}..\} = \{\hat{A}\hat{B}\hat{C}\hat{D}..\hat{R}\hat{X}\hat{Y}\hat{Z}\} \tag{8.132}$$

$$+ \sum_{[1]} \left\{ \overbrace{\hat{A}\hat{B}\hat{C}\hat{D}..\hat{R}}\hat{X}\hat{Y}\hat{Z} \right\} \tag{8.133}$$

$$+ \sum_{[2]} \left\{ \overbrace{\hat{A}\hat{B}\hat{C}\hat{D}..\hat{R}\hat{X}}\hat{Y}\hat{Z} \right\} \tag{8.134}$$

$$+ ... \tag{8.135}$$

Turning back to the many-body problem, the vacuum expectation value of products of creation and annihilation operators can be written, according to Wick's theorem in Eq. (8.125), as a sum over normal ordered products with all possible numbers and combinations of contractions,

$$\langle 0|\hat{A}\hat{B}\hat{C}\hat{D}..\hat{R}\hat{X}\hat{Y}\hat{Z}|0\rangle = \langle 0| \{\hat{A}\hat{B}\hat{C}\hat{D}..\hat{R}\hat{X}\hat{Y}\hat{Z}\} |0\rangle \tag{8.136}$$

$$+ \sum_{[1]} \langle 0| \left\{ \overbrace{\hat{A}\hat{B}}\hat{C}\hat{D}..\hat{R}\hat{X}\hat{Y}\hat{Z} \right\} |0\rangle \tag{8.137}$$

$$+ \sum_{[2]} \langle 0| \left\{ \overbrace{\hat{A}\hat{B}\hat{C}\hat{D}}..\hat{R}\hat{X}\hat{Y}\hat{Z} \right\} |0\rangle \tag{8.138}$$

$$+ ... \tag{8.139}$$

$$+ \sum_{[\frac{N}{2}]} \langle 0| \left\{ \overbrace{\hat{A}\hat{B}\hat{C}\hat{D}}.. \overbrace{\hat{R}\hat{X}\hat{Y}\hat{Z}} \right\} |0\rangle. \tag{8.140}$$

All vacuum expectation values of normal ordered products without fully contracted terms are zero. Hence, the only contributions to the expectation value are those terms that *is* fully contracted,

$$\langle 0|\hat{A}\hat{B}\hat{C}\hat{D}..\hat{R}\hat{X}\hat{Y}\hat{Z}|0\rangle = \sum_{[all]} \langle 0| \left\{ \overbrace{\hat{A}\hat{B}\hat{C}\hat{D}}.. \overbrace{\hat{R}\hat{X}\hat{Y}\hat{Z}} \right\} |0\rangle \tag{8.141}$$

$$= \sum_{[all]} \overbrace{\hat{A}\hat{B}\hat{C}\hat{D}}.. \overbrace{\hat{R}\hat{X}\hat{Y}\hat{Z}}. \tag{8.142}$$

To obtain fully contracted terms, Eq. (8.130) must hold. When the number of creation and annihilation operators is odd, the vacuum expectation value can be set to zero at once. When the number is even, the expectation value is simply the sum of terms with all possible combinations of fully contracted terms. Observing that the only contractions that give nonzero contributions are

$$\overbrace{a_\alpha a_\beta^\dagger} = \delta_{\alpha\beta}, \tag{8.143}$$

the terms that contribute are reduced even more.

Wick's theorem provides us with an algebraic method for easy determination of the terms that contribute to the matrix element.

References

1. J.M. Lattimer, M. Prakash, Phys. Rep. **442**, 109 (2007)
2. J.M. Lattimer, Ann. Rev. Nucl. Part. Science **62**, 485 (2012)
3. K. Hebeler, J.M. Lattimer, C.J. Pethick, A. Schwenk, Astrophys. J. **773**, 11 (2013)
4. F. Weber, *Pulsars as Astrophysical Laboratories for Nuclear and Particle Physics* (Institute of Physics Publishing, London, 1999)
5. H. Heiselberg, M. Hjorth-Jensen, Phys. Rep. **328**, 237 (2000)
6. U. van Kolck, Phys. Rev. C **49**, 2932 (1994). DOI 10.1103/PhysRevC.49.2932. URL http://link.aps.org/doi/10.1103/PhysRevC.49.2932
7. R. Machleidt, D. Entem, Physics Reports **503**(1), 1 (2011). DOI 10.1016/j.physrep.2011.02.001. URL http://www.sciencedirect.com/science/article/pii/S0370157311000457
8. E. Epelbaum, H.W. Hammer, U.G. Meißner, Rev. Mod. Phys. **81**, 1773 (2009). DOI 10.1103/RevModPhys.81.1773. URL http://link.aps.org/doi/10.1103/RevModPhys.81.1773
9. H.W. Hammer, A. Nogga, A. Schwenk, Rev. Mod. Phys. **85**, 197 (2013)
10. S. Binder, P. Piecuch, A. Calci, J. Langhammer, P. Navrátil, R. Roth, ArXiv e-prints (2013)
11. H. Hergert, S. Binder, A. Calci, J. Langhammer, R. Roth, Phys. Rev. Lett. **110**, 242501 (2013). DOI 10.1103/PhysRevLett.110.242501. URL http://link.aps.org/doi/10.1103/PhysRevLett.110.242501
12. R. Roth, S. Binder, K. Vobig, A. Calci, J. Langhammer, P. Navrátil, Phys. Rev. Lett. **109**, 052501 (2012). DOI 10.1103/PhysRevLett.109.052501. URL http://link.aps.org/doi/10.1103/PhysRevLett.109.052501
13. G. Hagen, M. Hjorth-Jensen, G.R. Jansen, R. Machleidt, T. Papenbrock, Phys. Rev. Lett. **108**, 242501 (2012). DOI 10.1103/PhysRevLett.108.242501. URL http://link.aps.org/doi/10.1103/PhysRevLett.108.242501
14. G. Hagen, M. Hjorth-Jensen, G.R. Jansen, R. Machleidt, T. Papenbrock, Phys. Rev. Lett. **109**, 032502 (2012). DOI 10.1103/PhysRevLett.109.032502. URL http://link.aps.org/doi/10.1103/PhysRevLett.109.032502
15. A. Cipollone, C. Barbieri, P. Navrátil, Phys. Rev. Lett. **111**, 062501 (2013)
16. K. Hebeler, A. Schwenk, Phys. Rev. C **82**, 014314 (2010). DOI 10.1103/PhysRevC.82.014314. URL http://link.aps.org/doi/10.1103/PhysRevC.82.014314
17. T. Krüger, I. Tews, K. Hebeler, A. Schwenk, Phys. Rev. C **88**, 025802 (2013). DOI 10.1103/PhysRevC.88.025802. URL http://link.aps.org/doi/10.1103/PhysRevC.88.025802
18. A. Carbone, A. Polls, A. Rios, Phys. Rev. C **88**, 044302 (2013)
19. T. Inoue, S. Aoki, T. Doi, T. Hatsuda, Y. Ikeda, N. Ishii, K. Murano, H. Nemura, K. Sasaki, Phys. Rev. Lett. **111**, 112503 (2013)
20. B.D. Day, Rev. Mod. Phys. **39**, 719 (1967). DOI 10.1103/RevModPhys.39.719. URL http://link.aps.org/doi/10.1103/RevModPhys.39.719
21. K.A. Brueckner, C.A. Levinson, H.M. Mahmoud, Phys. Rev. **95**, 217 (1954)
22. K.A. Brueckner, Phys. Rev. **100**, 36 (1955)
23. M. Baldo, G.F. Burgio, Reports on Progress in Physics **75**, 026301 (2012)
24. M. Baldo, A. Polls, A. Rios, H.J. Schulze, I. Vidaña, Phys. Rev. C **86**, 064001 (2012). DOI 10.1103/PhysRevC.86.064001. URL http://link.aps.org/doi/10.1103/PhysRevC.86.064001
25. R.J. Bartlett, M. Musiał, Rev. Mod. Phys. **79**, 291 (2007)
26. I. Shavitt, R.J. Bartlett, *Many-body Methods in Chemistry and Physics* (Cambridge University Press, 2009)
27. S. Gandolfi, A.Y. Illarionov, K.E. Schmidt, F. Pederiva, S. Fantoni, Phys. Rev. C **79**, 054005 (2009). DOI 10.1103/PhysRevC.79.054005. URL http://link.aps.org/doi/10.1103/PhysRevC.79.054005
28. A. Lovato, O. Benhar, S. Fantoni, K.E. Schmidt, Phys. Rev. C **85**, 024003 (2012). DOI 10.1103/PhysRevC.85.024003. URL http://link.aps.org/doi/10.1103/PhysRevC.85.024003

29. W. Dickhoff, C. Barbieri, Progress in Particle and Nuclear Physics **52**(2), 377 (2004). DOI http://dx.doi.org/10.1016/j.ppnp.2004.02.038. URL http://www.sciencedirect.com/science/article/pii/S0146641004000535
30. J. Erler, C.J. Horowitz, W. Nazarewicz, M. Rafalski, P.G. Reinhard, Phys. Rev. C **87**, 044320 (2013)
31. A. Ekström, G. Baardsen, C. Forssén, G. Hagen, M. Hjorth-Jensen, G.R. Jansen, R. Machleidt, W. Nazarewicz, T. Papenbrock, J. Sarich, S.M. Wild, Phys. Rev. Lett. **110**, 192502 (2013). DOI 10.1103/PhysRevLett.110.192502. URL http://link.aps.org/doi/10.1103/PhysRevLett.110.192502
32. E. Epelbaum, A. Nogga, W. Glöckle, H. Kamada, U.G. Meißner, H. Witała, Phys. Rev. C **66**, 064001 (2002). DOI 10.1103/PhysRevC.66.064001. URL http://link.aps.org/doi/10.1103/PhysRevC.66.064001
33. P. Navrátil, Few-Body Systems **41**(3-4), 117 (2007). DOI 10.1007/s00601-007-0193-3. URL http://dx.doi.org/10.1007/s00601-007-0193-3
34. P. Navrátil, S. Quaglioni, I. Stetcu, B.R. Barrett, Journal of Physics G: Nuclear and Particle Physics **36**(8), 083101 (2009). URL http://stacks.iop.org/0954-3899/36/i=8/a=083101

Chapter 9

Variational and Diffusion Monte Carlo approaches to the nuclear few- and many-body problem

Francesco Pederiva, Alessandro Roggero, Kevin E. Schmidt

Abstract

9.1 Monte Carlo methods in quantum many-body physics

9.1.1 Expectations in Quantum Mechanics

In the previous chpaters the authors pointed out in several different ways the fact that the non-relativistic quantum many-body problem is equivalent to the solution of a very complicated differential equation, the many-body Schroedinger equation.

As it was illustrated, in the few-body case it is still possible to find exact solutions. At the very least, one can hope to be able to expand the solution on a basis set including $\mathcal{M}$ elements, and try to reach convergence as a function of $\mathcal{M}$. Unfortunately, this procedure becomes more and more expensive when the number of bodies A increases. There are many ingenuous ways to improve the convergence and the quality of the results. However, the price to pay is often the introduction of approximations. All these approaches have one characteristics in common: the end up with some close expression for the solution, i.e. they seek for an explicit (more or less approximated) wavefunction and for the corresponding eigenvalue.

However, we should remember that the wavefunction *per se* is not an observable. What we really need to compute in order to make predictions to be compared with the experiments are *expectations* of operators $\hat{O}$ describing the observables we are interested in. Therefore, given a many-body Hamiltonian $\hat{H}$, we might want to look, for instance, for the ground state solution:

$$\hat{H}|\Psi_0\rangle = E_0|\Psi_0\rangle. \tag{9.1}$$

We need at this point to provide a representation of the Hilbert space in term of some basis set. This set will be denoted as $\{|X\rangle\}$. Its elements could be for instance eigenstates of the position or of the momentum operators. In order to make the notation less cumbersome, we

Francesco Pederiva

Physics Department, University of Trento, and INFN-TIFPA, Trento, Italy , e-mail: `francesco.pederiva@unitn.it`

Kevin E. Schmidt

Department of Physics and Astronomy, Arizona State University, Tempe AZ (USA) e-mail: `kevin.schmidt@asu.edu`

Alessandro Roggero

Institute for Nuclear Theory, Washington University, Seattle WA (USA) , e-mail: `roggero@uw.edu`

will assume that the quantum numbers X characterizing the basis states are in the continuum. In the case of discrete quantum numbers, integrals have to be replaced by sums over all their possible values, without any loss of generality. As an example, X could include the positions or the momenta of A nucleons, and their spin and isospin values. All the physical information we need about the static problem is then included in integrals of the form:

$$\langle O \rangle \equiv \langle \Psi_0 | \hat{O} \Psi_0 \rangle = \frac{\int dX \langle \Psi_0 | X \rangle \langle X | \hat{O} | X \rangle \langle X | \Psi_0 \rangle}{\int dX | \langle X | \Psi_0 \rangle |^2}. \tag{9.2}$$

These integrals are apparently as hard to solve as the original problem, even if we had access to the explicit form of the wavefunction. Is there any gain in reformulating the problem this way?

We can first notice that expectations can in general be written in a slightly different form, independent of the nature of the operator $\hat{O}$:

$$\langle O \rangle = \frac{\int dX | \langle X | \Psi_0 \rangle |^2 \frac{\langle X | \hat{O} \Psi_0 \rangle}{\langle X | \Psi_0 \rangle}}{\int dX | \langle X | \Psi_0 \rangle |^2}. \tag{9.3}$$

For the moment we will just assume that the quotient appearing at numerator of the expectation is always well defined, and we will later discuss this aspect in more detail. The standard quantum mechanical interpretation of the wavefunction tells us that the quantity:

$$P[X] = \frac{| \langle X | \Psi_0 \rangle |^2}{\int dX | \langle X | \Psi_0 \rangle |^2}, \tag{9.4}$$

is the probability of finding the system in the state $|X\rangle$ labeled by the set of quantum numbers X. Thereby, the expectation integral has the general form:

$$\langle O \rangle = \int dX P[X] \frac{\langle X | \hat{O} \Psi_0 \rangle}{\langle X | \Psi_0 \rangle}, \tag{9.5}$$

i.e. the average of what we will call the *local* operator $O_{loc} \equiv \frac{\langle X | \hat{O} \Psi_0 \rangle}{\langle X | \Psi_0 \rangle}$ weighted with the probability of finding the system in a given state $|X\rangle$. Integrals like that in Eq. (9.5) have a direct physical interpretation. In a measurement process what we would observe is essentially the result of a *sampling process* of $P[X]$. The expectation of our operator is approximated by:

$$\langle O \rangle \simeq \frac{1}{M} \sum_{k=1}^{M} O(X_k), \tag{9.6}$$

where M is the number of measurements performed, and $O(X_k)$ is a shorthand notation to indicate the value assumed by the observable $\hat{O}$ in the observed state labeled by the quantum numbers X_k. The laws of statistics also give us a way of estimating a *statistical* error on $\langle O \rangle$, and we know that the error decreases by increasing the number of measurements. In the measurement process we have *no direct knowledge of the wavefunction*, we just *sample* its squared modulus!

This argument suggests that if we had a way of numerically sampling the squared modulus of the wavefunction, we could in principle compute expectations and make comparisons with experiments without needing an explicit expression of the wavefunction itself. Quan-

tum Monte Carlo methods aim exactly at solving the many-body Schroedinger equation by sampling its solutions, possibly without any need of an explicit analytical form.

The following of this chapter will be essentially divided in two parts. First we will discuss how to perform calculations based on an accurate, explicit ansatz for the wavefunction of an A-body system interacting via a purely central potential, exploiting the variational principle of quantum mechanics (Variational Monte Carlo methods). Then we will discuss how to sample the exact ground state of the system by projecting it out of an initial ansatz (Projection Monte Carlo methods). Finally, we will see how these methods need to be extended when we are interested in studying Hamiltonians that have an explicit dependence on the spin and isospin states of the particles, as it happens for modern interaction employed in nuclear physics.

9.2 Variational wavefunctions and VMC for central potentials

9.2.1 Coordinate space formulation

As previously discussed, we are in principle free to choose any representation of the Hilbert space of the system we like in order to compute expectations. There is, however, an option that appears quite natural, especially for particles interacting via a purely central potential, with no explicit dependence on the spin or isospin state. In this case the Hilbert space is conveniently represented in terms of eigenstates of the position operator. If $R = \mathbf{r}_1, \ldots \mathbf{r}_A$ are the coordinates of the A identical particles of mass m constituting the system, we have that:

$$|X\rangle \equiv |R\rangle = \delta(R - R'). \tag{9.7}$$

Notice that we are here considering a $3A$-dimensional Cartesian space, without decomposing it in the product of A 3-dimensional spaces. In this representation the wavefunction is simply given by:

$$\langle R|\Psi_0\rangle \equiv \Psi_0(R) = \Psi_0(\mathbf{r}_1, \ldots \mathbf{r}_A), \tag{9.8}$$

and the Hamiltonian reads:

$$\langle R|\hat{H}\rangle = -\frac{\hbar^2}{2m} \sum_{i=1}^{A} \nabla_i^2 + V(\mathbf{r}_1, \ldots \mathbf{r}_A), \tag{9.9}$$

where V is the interparticle potential. In this representation the states of the Hilbert space are sampled by sampling the particle positions from the squared modulus of the wavefunction $|\Psi_0(R)|^2$.

9.2.2 Variational principle and variational wavefunctions

As already seen in the previous chapters, one of the possible ways to approximate a solution of the many-body Schroedinger equation is to exploit the variational principle. Given a *trial state* $|\Psi_T\rangle$, the following inequality holds:

$$E_T = \frac{\langle \Psi_T|\hat{H}\Psi_T\rangle}{\langle \Psi_T|\Psi_T\rangle} \geq E_0, \tag{9.10}$$

where E_0 is the ground state eigenvalue of the Hamiltonian $\hat{H}$. The equality holds if and only if $|\Psi_T\rangle = |\Psi_0\rangle$. The variational principle holds for the ground state, but also for excited states,

provided that $|\Psi_T\rangle$ is orthogonal to all the eigenstates having eigenvalue lower than that of the state one wants to approximate.

In coordinate space the formulation of the variational principle can be directly transformed in a form equivalent to that of Eq. (9.5):

$$E_T = \frac{\int dR |\Psi_T(R)|^2 \frac{\hat{H}\Psi_T(R)}{\Psi_T(R)}}{\int dR |\Psi_T(R)|^2} \geq E_0, \tag{9.11}$$

where $\frac{\hat{H}\Psi_T(R)}{\Psi_T(R)}$ is called the *local energy*. Contrary to what happens in functional minimization approaches (such as the Hartree-Fock method), the variational principle is used to determine the best trial wavefunction within a class determined by some proper ansatz. The wavefunction will depend on a set of *variational parameters* $\{\alpha\}$. The solution of the variational problem will therefore be given by the solution of the Euler problem:

$$\frac{\delta E_T(\{\alpha\})}{\delta \{\alpha\}} = 0. \tag{9.12}$$

This means that we need to evaluate many times the integral of Eq.(9.11) for different values of the variational parameters, and find the minimum trial eigenvalue.

9.2.3 Monte Carlo evaluation of integrals

The integral giving us the trial eigenvalue is defined in a $3A$-dimensional space. Since particles interact, we expect that the solution cannot be expressed as a product of single particle functions, and therefore the integral cannot be factorized in a product of simpler integrals. In this sense, the problem is strictly analogous to that of a classical gas at finite temperature $\beta = 1/K_B T$. In that case, given a classical Hamiltonian $H(p,q) = \sum_{i=1}^{A} \frac{p_i^2}{2m} + V(q_1 \ldots q_A)$, the average energy of the system is given by:

$$E = \frac{3A}{2} K_B T + \frac{1}{Z} \int dq_1 \cdots dq_A V(q_1 \cdots q_A) e^{-\beta V(q_1 \cdots q_A)}, \tag{9.13}$$

where

$$Z \equiv \int dq_1 \cdots dq_A e^{-\beta V(q_1 \cdots q_A)} \tag{9.14}$$

is the *configurational partition function* of the system. Also in this case the integral to be evaluated is of the same form as Eq. (9.11). We can distinguish in the integrand the product of a *probability density*:

$$P(q_1 \ldots q_A) = \frac{e^{-\beta V(q_1 \cdots q_A)}}{Z}, \tag{9.15}$$

and a function to be integrated which is the potential energy V. For classical systems we have a quite intuitive of the way in which we could proceed. If could average a large set of measurements of the potential over many different configurations of the particle positions, we would obtain the estimate of the potential energy we need.

This fact can be easily frmalized by making use of the Central Limit Theorem. Given a probability density $P[X]$ defined in a suitable events space X, let us consider an arbitrary function $F(X)$, and let us define a stochastic variable:

$$S_N(F) = \frac{1}{N}\sum_{i=1}^{N} F(X_i),$$ (9.16)

where the events X_i are *statistically independent*, and are distributed according to $P[X]$. Obviously, the stochastic variable S_N will have its own probability density $P[S_N]$, which in general depends on the index N. The Central Limit Theorem states that for large N the probability density $P[S_N]$ will be a Gaussian, namely:

$$\lim_{N\to\infty} P[S_N] = \frac{1}{\sqrt{2\pi\sigma_N^2(F)}} e^{\frac{(S_N - \langle F\rangle)^2}{2\sigma_N^2(F)}},$$ (9.17)

where

$$\langle F\rangle = \int P[X]F(X)dX$$ (9.18)

is the average of the function F weighted with the probability density $P[X]$, and

$$\sigma_N^2(F) = \frac{1}{N-1}\left[\int P[X]F^2(X)dX - \langle F\rangle^2\right]$$ (9.19)

is the variance of the Gaussian. This well known result is at the basis of all measurement theory. Averages over a set of measurements of a system provide the correct expectation of the measured quantity with an error that can be in turn estimated, and that decreases with the square root of the number of measurements N.

This result is very important from the point of view of numerical evaluation of integrals. If we had a way to numerically sample an arbitrary probability density $P[X]$, we could easily estimate integrals like that in Eq. (9.11). The statistical error associated with the estimate would decrease as the square root of the sampled points *regardless of the dimensionality of the system*.

For a classical system configurations might be generated by solving Newton's equations, possibly adding a thermostat in order to be consistent with the canonical averaging. However, this is not certainly possible for a quantum system. The solution is to use an artificial dynamics, provided that it generates (at least in some limit) configurations that are distributed according to the probability density we want to use. In rder to simplify the description we will now work in an event space corresponding to the coordinates of the A particle in our system, but the treatment can be generalized to arbitrary spaces.

We start defining a *transition matrix* $T_k(R_{k+1} \leftarrow R_k)$ expressing the probability that in the k-th step of the dynamics the system moves from the configuration R to a configuration R'. If at the first step the system is in a configuration R_0, sampled from an arbitrary distribution $P_0[R_0]$, the probability density of finding the system in a configuration R_1 at the next step will be given by:

$$P_1[R_1] = \int dR_0 P_0[R_0] T_0(R_1 \leftarrow R_0).$$ (9.20)

We can define an integral operator $\hat{T}_0$ such that:

$$P_1[R_1] = \hat{T}_0 P[R_0].$$ (9.21)

With this notation, the probability density of the configuration at an arbitrary step k will become:

$$P_k[R_k] = \hat{T}_{k-1}P[R_{k-1}] = \hat{T}_{k-1}\cdots\hat{T}_1\hat{T}_0 P_0[R_0]$$ (9.22)

The sequence of stochastic variables R_k generated at each step of this procedure is called a *Markov Chain*. Let us assume that $\hat{T}_k$ does not depend on the index k. What we will generate

is then a *stationary* Markov Chain, for which the probability density generated at each step will only depend on the transition matrix and the probability density of the first element. In fact:

$$P_k[R_k] = \hat{T}P[R_{k-1}] = \hat{T}\cdots\hat{T}\hat{T}P_0[R_0] = \hat{T}^k P_0[R_0]. \tag{9.23}$$

Under these assumptions one might wonder if the sequence is convergent in functional sense, i.e. if a limiting probability density $P_\infty[R]$ exists. It is interesting to notice that if such function exists, it has to be an eigenvector of the integral operator $\hat{T}$. In fact, since we assume $\hat{T}$ to be independent of k we have:

$$\lim_{k\to\infty} \hat{T}P_k[R_k] = \lim_{k\to\infty} P_{k+1}[R_{k+1}]$$

$$\hat{T}P_\infty[R] = P_\infty[R].$$

It is also easy to realize that the eigenvalue is indeed 1. In fact, let us consider the general relation:

$$\hat{T}P_\infty[R] = \gamma P_\infty[R]. \tag{9.24}$$

The recursive application of $\hat{T}$ would give:

$$\hat{T}^k P_\infty[R] = \gamma^k P_\infty[R]. \tag{9.25}$$

If $\gamma \neq 1$ we would loose the normalization property of $P\infty[R]$. We will not discuss here in detail the mathematical conditions on $\hat{T}$ that guarantee the existence and uniqueness of such eigenvalue.

METTERE UNA BREVE DISCUSSIONE

These properties of stationary Markov chains can be exploited to sample a generic probability density $P[R]$. In fact, if we can determine the transition operator that has as eigenvector a *given* $P_\infty[R]$, a repeated application of such operator to an *arbitrary* initial distribution of points will eventually generate a chain in which each element is distributed according to $P_\infty[R]$. There is a simple recipe to construct such transition operator. We will assume that we have at hand a transition operator $\hat{\bar{T}}$ that we can sample (it could be as simple as a uniform probability within a given volume). We will split the searched transition operator in the product of $\hat{\bar{T}}$ and an unknown factor $\hat{A}$ that we will call "acceptance probability", and that is defined in such a way that:

$$\hat{\bar{T}}\hat{A} = \hat{T}. \tag{9.26}$$

At this point we should invoke the so-called detailed balance condition. If we reach equilibrium we have to expect that the dynamics described by the random walk will not change the density of sampled points anywhere in the events space. In equations this reads:

$$P(R)T(R' \leftarrow R) = P(R')T(R \leftarrow R') \tag{9.27}$$

The detailed balance condition translates into a condition on the acceptance probability. In fact:

$$\frac{A(R' \leftarrow R)}{A(R \leftarrow R')} = \frac{P(R')}{P(R)} \frac{\bar{T}(R \leftarrow R')}{\bar{T}(R' \leftarrow R)} \tag{9.28}$$

The quantities on the r.h.s. of Eq. (9.30) are all known. The configuration R' has to be sampled originating in R from the given transition probability $\bar{T}(R \leftarrow R')$. The probability density $P(r)$ is the one we actually want to asymptotically sample. Let us now consider a slightly modified version of Eq. ([**?**]):

$$\frac{A(R' \leftarrow R)}{A(R \leftarrow R')} = \min\left(\frac{P(R')}{P(R)} \frac{\bar{T}(R \leftarrow R')}{\bar{T}(R' \leftarrow R)}, 1\right). \tag{9.29}$$

We can interpret the ratio on the l.h.s. as a probability that we have to actually keep the forward transition $R' \leftarrow R$. rather than using the reverse transition $R \leftarrow R'$ in order to sample the correct transition $\hat{T}$ that will asymptotically converge to the distribution $P(R)$. This expression is often called *acceptance ratio*. In practice, it represents the probability according to which we have to *accept* the new configuration as the new member of the Markov chain, rather than keeping the original point as the next point in the chain.[1].

There is a case in which the Eq. (9.30) further simplifies. If the transition matrix is taken to be symmetric in the arguments R and R', the ratio becomes unity, and one is left with:

$$\frac{A(R' \leftarrow R)}{A(R \leftarrow R')} = \min\left(\frac{P(R')}{P(R)}, 1\right). \tag{9.30}$$

At this point we have all the ingredients to describe an algorithm that performs a Monte Carlo evaluation of an integral such that of Eq. (9.11). In the following we will describe the simplest version, i.e. the so called "Metropolis-Hastings algorithm".

1. Start from an arbitrary configuration of the A particles. If the potential has a repulsive core one has to pay attention to avoid overlapping pairs.
2. Sweep over the coordinates and generate new positions according to some transition probability. A simple choice is a uniform displacement within a cube of side Δ, i.e.:

$$\bar{T}(R' \leftarrow R) = \begin{cases} \frac{1}{\Delta} & \text{if } |R_i'^\alpha - R_i^\alpha| < \frac{\Delta}{2} \\ 0 & \text{otherwise} \end{cases} \tag{9.31}$$

   with $\alpha = x, y, z$, and $i = 1 \ldots A$. This choice has the advantage of being symmetric. If we imagine to store our configuration in an array $R[0...2][0...A-1]$ the implementation of this step would read:

   ```
   MC_Move()
   for i ∈ {0, A − 1} do
       for j ∈ {0, 2} do
           R_new[i][j] ← R[i][j] + (rand() − 0.5) ∗ Δ
       end for
   end for
   ```

   We will assume that the function rand() generates a random number uniformly distributed in $[0, 1)$.
3. At this point we need to evaluate the acceptance ratio. This is easily done with our choice of the transition matrix, since we only need to evaluate the probability densities in R and R':

$$\frac{A(R' \leftarrow R)}{A(R \leftarrow R')} = \min\left(\frac{|\Psi_T(R')|^2}{|\Psi_T(R)|^2}, 1\right). \tag{9.32}$$

4. Next we need to decide whether we keep the proposed configuration as the next element in the chain or if we want to resort to the original one. If we define $\text{acc} = \frac{A(R' \leftarrow R)}{A(R \leftarrow R')}$, then:

   ```
   Accept_reject()
   ξ = rand()
   if acc > ξ then
       R[i][j] ← R_new[i][j]
   end if
   ```

5. According to the Central Limit Theorem, we now need to cumulate the values of the rest of the integrand. In the case of our variational calculation we need to sum up the local

---

[1] The standard jargon refers to this as a "rejection" event. However one has not to be confused: this is the result of a *reversed* move, and generates a new element in the chain coincident with the starting point.

energies. Notice that this step has to be taken whatever is the result of the procedure described at the previous point. If we want to estimate the statistical error, we also need to cumulate he *square* of the local energy.

Acuest()
eloc $\leftarrow \frac{\hat{H}\Psi_T(R)}{\Psi_T(R)}$
ecum $\leftarrow$ ecum + eloc
ecum2 $\leftarrow$ ecum2 + eloc * eloc

6. Steps 2 to 5 need to be repeated N_{steps} times, where N_{steps} must be sufficiently large to provide a small enough statistical error. The final estimate of the energy is given by $\langle E \rangle \pm \Delta E$, where:

$$\langle E \rangle = \frac{1}{N_{steps}} * \text{ecum}$$

$$\Delta E = \sqrt{\frac{1}{N_{steps}-1}\left(\frac{1}{N_{steps}} * \text{ecum2} - \langle E \rangle^2\right)}$$

(9.33)

Notice that this algorithm could in principle be used to evaluate arbitrary integrals. In fact, it is always possible to multiply and divide the integrand by a probability density $P(X)$ that can be used to sample the values of X:

$$I = \int F(X)dX = \int P[X]\frac{F(X)}{P[X]}$$

(9.34)

[Aggiungere qualcosa su
- autocorrelazioni
- la scelta di Δ
- parallelizzazione]

9.1. Evaluate the following integral by means of the Metropolis algorithm

$$I = \int_0^1 e^x - 1\,dx$$

sampling points from

1. P(x) = 1 for $x \in [0,1]$
2. P(x) = x for $x \in [0,1]$

- Compare the average and the statistical error for the cases 1) and 2). Which is the best estimate?
- Try to figure out a way to sample a probability density proportional to x^n, and reevaluate the integral I. How is the convergence and the statistical error behaving by increasing n? Try to give an explanation of the result.

9.2. Try to sketch the general proof that for a generic integral I defined as in problem 9.1 the best statistical error is obtained when sampling from a probability density proportional to F(x).

9.3. Consider the one-dimensional Hamiltonian:

$$\hat{H} = \frac{1}{2}\frac{d^2}{dx^2} + \frac{1}{2}x^2$$

and consider the parametrized family of trial solutions $\psi(x,\alpha,\beta) = e^{-\alpha^2 x^2} - \beta$. Compute by means of the Metropolis algorithm the energy and the standard deviation of the energy as a function of α keeping $\beta = 0.01$. Is the minimum found at the same value than for $\beta = 0$? Why?

9.2.4 Wave function optimization

9.2.4.1 Reweighting methods

The optimization of the trial wave function might become quite cumbersome when the number of parameters exceeds a few units. In general the problem is equivalent to searching an absolute minimum in a multi-dimensional space, and does not admit a simple solution. If one is interested in a quick search for local minima, it is possible to compute the gradient of the energy in the parameter space, and use for instance some variant of the steepest descent method. Computation of gradients is based on the so-called "reweighting method". If we have a trial function depending on a set of parameters $\{\alpha\}$, and another depending on a set $\{\alpha + \delta\alpha\}$, it s not necessary to perform two independent calculations to compute the difference (which would also be affected by rather large statistical errors). In fact, the following identity holds):

$$\frac{\int dR |\Psi_T(R, \{\alpha + \delta\alpha\})|^2 O(R)}{\int dR |\Psi_T(R, \{\alpha + \delta\alpha\})|^2} = \frac{\int dR |\Psi_T(R, \{\alpha\})|^2 \frac{|\Psi_T(R, \{\alpha + \delta\alpha\})|^2}{|\Psi_T(R, \{\alpha\})|^2} O(R)}{\int dR |\Psi_T(R, \{\alpha\})|^2 \frac{|\Psi_T(R, \{\alpha + \delta\alpha\})|^2}{|\Psi_T(R, \{\alpha + \delta\alpha\})|^2}} \tag{9.35}$$

It is therefore possible to use the configurations sampled from a trial wavefunction with a given parametrization $\{\alpha\}$ to compute expectations over a wavefunction with a different parametrization $\{\alpha\delta\alpha\}$ by simply reweighting the values of the operator with the ration between the square moduli of the two wavefunctions:

$$\langle O_{\{\alpha + \delta\alpha\}} \rangle \equiv \frac{\langle \Psi_T(R_k, \{\alpha + \delta\alpha\}) | O(R_k) | \Psi_T(R_k, \{\alpha + \delta\alpha\}) \rangle}{\langle \Psi_T(R_k, \{\alpha + \delta\alpha\}) | \Psi_T(R_k, \{\alpha + \delta\alpha\}) \rangle} = \frac{\sum_k \frac{|\Psi_T(R_k, \{\alpha + \delta\alpha\}|^2}{|\Psi_T(R_k, \{\alpha\}|^2} O(R_k)}{\sum_k \frac{|\Psi_T(R_k, \{\alpha + \delta\alpha\}|^2}{|\Psi_T(R_k, \{\alpha\}|^2}} \tag{9.36}$$

where the R_k are sampled from $|\Psi_T(R, \{\alpha\})|^2$. Besides the obvious advantage of avoiding multiple calculations to compute the derivatives, the use of this reweighting technique allows for directly compute expectations of the gradients in the parameter space with very high accuracy. The access to gradients opens the way to the use of automated minimization algorithms such as the already mentioned steepest descent method or the Levemberg-Marquardt algorithm (cite Umrigar/Nightingale)

9.2.4.2 Power method

There is another class of algorithms that have been recently introduced, and based on the power method. We will here discuss in particular the algorithm due to Sandro Sorella. [2] This algorithm was originally discussed in terms of the Lanczos method, but for most of his variational calculations he only uses one multiplication by his propagator, so in that case his method is equivalent to the power method.

For Λ larger than the largest eigenvalue of the eigenvectors contained in $|\psi_n\rangle$, operating with $\Lambda - H$ will multiply the ground state by a larger number than any other state. Therefore iterating the equation

$$|\psi_{n+1}\rangle = (\Lambda - H)|\psi_n\rangle \tag{9.37}$$

will converge to the ground state. One way to implement this is to use a set of test functions (which, in principle, should be complete), $|\phi_m\rangle$. This gives the set of equations

[2] Sandro Sorella, *Generalized Lanczos algorithm for variational quantum Monte Carlo*, Phys. Rev. B **64**, 024512 (2001).

$$\langle \phi_m | \psi_{n+1} \rangle = \langle \phi_m | (\Lambda - H) | \psi_n \rangle. \tag{9.38}$$

In the original paper Sorella assumes $|\psi_n\rangle = |\Psi_T\rangle$, and next approximates $|\psi_{n+1}\rangle$ as a linear combination of the original state and the derivatives with respect to the parameters

$$|\psi_{n+1}\rangle \simeq \Delta \alpha_0 |\Psi_T\rangle + \sum_{n=1} \Delta \alpha_n \partial_{\alpha_n} |\psi_T\rangle \equiv \sum_{n=0} O^n |\psi_T\rangle \Delta \alpha_n \tag{9.39}$$

and he uses the same functions for $|\phi_m\rangle$, so that

$$|\phi_m\rangle = O^m |\Psi_T\rangle. \tag{9.40}$$

When evaluated in the position representation, the O^m for $m > 0$ correspond to multiplying by the derivative of the logarithm of the trial function. Substituting these expressions, and dividing by $\langle \Psi_T | \Psi_T \rangle$, Eq. 9.38 becomes

$$\frac{\langle \Psi_T | O^m (\Lambda - H) | \Psi_T \rangle}{\langle \Psi_T | \Psi_T \rangle} = \sum_{n=0} \frac{\langle \Psi_T | O^m O^n | \Psi_T \rangle}{\langle \Psi_T | \Psi_T \rangle} \Delta \alpha_n. \tag{9.41}$$

The expectation values can be calculated and the linear equations solved to get $\Delta \alpha_n$.

Alternatively, the $m = 0$ and $n = 0$ terms can be separated. Writing the trial function expectation of an operator O as $\langle O \rangle$, Eq. 9.41 becomes

$$\langle \Lambda - H \rangle = \Delta \alpha_0 + \sum_{n=1} \langle O^n \rangle \Delta \alpha_n \quad m = 0 \tag{9.42}$$

$$\langle O^m (\Lambda - H) \rangle = \langle O^m \rangle \Delta \alpha_0 + \sum_{n=1} \langle O^m O^n \rangle \Delta \alpha_n \quad m > 0. \tag{9.43}$$

Substituting Eq. 9.42 into Eq. 9.43 gives

$$\langle O^m (\Lambda - H) \rangle - \langle \Lambda - H \rangle \langle O^m \rangle = \sum_{n=1} [\langle O^m O^n \rangle - \langle O^m \rangle \langle O^n \rangle] \Delta \alpha_n. \tag{9.44}$$

Solving gives $\Delta \alpha_{n>0}$ and Eq. 9.42 then gives the value for $\Delta \alpha_0$.

In either case, the result gives an approximation to the next trial function as a linear combination of the original function and its derivatives. The new parameters are chosen to give this same linear combination as the first two terms in the Taylor series. Since dividing the approximate expression for $|\psi_{n+1}\rangle$ by $\Delta \alpha_0$ gives an expression that is the first two terms in the Taylor series, the new parameters are

$$\alpha_{n>0}^{(\text{new})} = \alpha_n^{(\text{old})} + \frac{\Delta \alpha_{n>0}}{\Delta \alpha_0} \tag{9.45}$$

9.2.5 Example

We will now describe a typical calculation for a central potential.

9.3 Projection Monte Carlo Methods in coordinate space

9.3.1 Propagation in imaginary time

9.3.2 General formulation

Variational calculations provide only an upper bound for the ground state eigenvalue of a given Hamiltonian. However, it is possible to use Monte carlo algorithms to actually solve the Schroedinger equation for an arbitrary number of interacting particles. This class of algorithms is bsed on the idea of imaginary time propagation

Let us consider a Hamiltonian $\hat{H}$. The imaginary time evolution of an arbitrary state is defined starting by the standard time-dependent Schroedinger equation:

$$-i\hbar\frac{\partial}{\partial t}|\Psi(t)\rangle = \hat{H}|\Psi(t)\rangle. \tag{9.46}$$

It is possible to operate a Wick rotation, and introduce an *imaginary time* $\tau = it$. The time dependent Schroedinger equation is transformed into an imaginary time dependent equation:

$$-\hbar\frac{\partial}{\partial \tau}|\Psi(\tau)\rangle = \hat{H}|\Psi(\tau)\rangle. \tag{9.47}$$

The formal solution can be written using the imaginary time propagator

$$|\Psi(\tau)\rangle = e^{-\frac{\tau}{\hbar}\hat{H}}|\Psi(0)\rangle \tag{9.48}$$

By setting $\hbar = 1$ we will define τ as an *inverse energy* that parametrizes the propagation of the quantum state. It is possible to expand the initial state $|\Psi(0)\rangle$ in eigenstates $|\phi_n\rangle$ of the Hamiltonian itself, such that $\hat{H}|\phi_n\rangle = E_n|\phi_n\rangle$. The imaginary time propagation of $|\Psi(0)\rangle = \sum_n c_n|\phi_n\rangle$ becomes:

$$|\Psi(\tau)\rangle = e^{-\tau\hat{H}}\sum_n c_n|\phi_n\rangle = \sum_n c_n e^{-\tau E_n}|\phi_n\rangle \tag{9.49}$$

Let us now consider the limit of the propagation for $\tau \to \infty$. The coefficients of the expansion $c_n e^{-\tau E_n}$ will either decrease (if $E_n > 0$) or increase (if $E_n < 0$) with the imaginary time, but in the limit the coefficient corresponding to the ground state of $\hat{H}$, i.e. $c_0 e^{-\tau E_0}$ will be dominant. This means that the imaginary time propagator has the interesting property of filtering out of an arbitrary state in the Hilbert space the ground state of a given Hamiltonian, provided that the state is not orthogonal to the ground state to begin with. We want to stress out a very important point. The ground state we are referring to is the *mathematical* ground state of the Hamiltonian $\hat{H}$. The *physical* ground state needs to take into account the symmetry of the particles, either bosons or fermions. It is very easy to convince oneself that such mathematical ground state is always a nodeless function (i.e. it is zero nowhere but possibly on the boundaries of the domain of existence of the wavefunction expressed in some representation). This is because the propagator is a positive definite function, at least for a Hamiltonian of the standard form $\hat{H} = \hat{T} + \hat{V}$, where $\hat{T}$ is the kinetic energy of a system of free particles and $\hat{V}$ is a local potential. In this case the eigenvector corresponding to the largest eigenvalue of the propagator is positive definite within the domain that defines the system. The largest eigenvalue of the propagator corresponds to the lowest eigenvalue of $\hat{H}$.

Notice that the imaginary time propagator is not unitary, and the normalization of the projected ground state is not guaranteed in general. By means of a small change in the propagator definition it is possible to guarantee the normalization of the projected ground state. In fact, let us define the propagator as:

$$|\Psi(\tau)\rangle = e^{-\tau(H-E_0)}|\Psi(0)\rangle. \tag{9.50}$$

It is easy to realize that in this case the amplitude of the component of the initial state along the ground state is preserved (while all other amplitudes decrease exponentially), and therefore the projected state is normalizable.

We will later discuss in details the implications of these properties for as concerns the application of imaginary time propagation to many-fermion systems.

9.3.3 Imaginary time propagator in coordinate representation

We will focus on a practical implementation of imaginary time propagation, and we will limit ourselves to a system of bosons (or boltzmannions) which do admit a ground state wavefunction that is positive definite. We will also consider Hamiltonians of the form mentioned in the previos subsection, in which the interaction is local. In this case the propagator is easily represented in coordinates. Formally we would have:

$$\langle R|\Psi(\tau)\rangle = \int dR' \langle R|e^{-\tau(H-E_0)}|R'\rangle\langle R'|\Psi(0)\rangle, \tag{9.51}$$

where we have inserted a completeness in terms of position eigenstates.The propagator

$$\langle R|e^{-\tau(\hat{H}-E_0)}|R'\rangle \tag{9.52}$$

seems to be still quite difficult to evaluate. However, let us break up the imaginary time interval τ in two equal intervals $\tau/2$. We can write

$$\langle R|e^{-\tau(\hat{H}-E_0)}|R'\rangle = \langle R|e^{-\frac{\tau}{2}(\hat{H}-E_0)}e^{-\frac{\tau}{2}(\hat{H}-E_0)}|R'\rangle, \tag{9.53}$$

since $\hat{H}$ obviously commutes with itself. Inserting a completeness we obtain:

$$\langle R|e^{-\tau(\hat{H}-E_0)}|R'\rangle = \int dR'' \langle R|e^{-\frac{\tau}{2}(\hat{H}-E_0)}|R''\rangle\langle R''|e^{-\frac{\tau}{2}(\hat{H}-E_0)}|R'\rangle, \tag{9.54}$$

This process can be iterated for an arbitrary large number of times M:

$$\langle R|e^{-\tau(\hat{H}-E_0)}|R'\rangle = \int \cdots \int dR'' \cdots dR^M \langle R|e^{-\frac{\tau}{2}(\hat{H}-E_0)}|R''\rangle \cdots \langle R^M|e^{-\frac{\tau}{2}(\hat{H}-E_0)}|R'\rangle. \tag{9.55}$$

Each of the factors in the integrand corresponds to a propagation for a *short* imaginary time $\Delta\tau = \tau/M$. In this case we can split the propagator using the Trotter-Suzuki formula:

$$e^{-\frac{\Delta\tau}{2}(\hat{H}-E_0)} \sim e^{-\frac{\Delta\tau}{2}(\hat{V}-E_0)}e^{-\Delta\tau\hat{T}}e^{-\frac{\Delta\tau}{2}(\hat{V}-E_0)} + o(\Delta\tau^2) \tag{9.56}$$

The representation in coordinates of each factor is known. The factors containing the potential, under the hypotheses made, are diagonal in the coordinates themselves, and simply become:

$$\langle R'|e^{-\frac{\Delta\tau}{2}(\hat{V}-E_0)}|R\rangle = e^{-\frac{\Delta\tau}{2}(V(R)-E_0)}, \tag{9.57}$$

while the kinetic term is the propagator of a set of A free particles obeying the equation:

$$-\frac{\partial}{\partial\tau}\Psi(R,t) = -\hbar 2m\nabla^2\Psi(R,t) \tag{9.58}$$

This is a classical *free diffusion* equation. If we interpret $\Psi(R,t)$ as a the density of the A particles, its evolution in time will be given by the well known diffusion law:

$$\Psi(R,t) = \frac{1}{(2\pi\frac{\hbar}{m}\Delta\tau)^{\frac{3A}{2}}} \int dR' e^{-\frac{(R-R')^2}{2\frac{\hbar}{m}\Delta\tau}} \Psi(R',0).$$
(9.59)

The short-time approximation for the propagator, correct at order $\Delta\tau$, will then become:

$$\langle R|e^{-\frac{\Delta\tau}{2}(\hat{H}-E_0)}|R'\rangle \sim \frac{1}{(2\pi\frac{\hbar}{m}\Delta\tau)^{\frac{3A}{2}}} e^{-\frac{\Delta\tau}{2}(V(R)-E_0)} e^{-\frac{(R-R')^2}{2\frac{\hbar}{m}\Delta\tau}} e^{-\frac{\Delta\tau}{2}(V(R)-E_0)}.$$
(9.60)

9.4. Prove that the propagator defined in the integrand of Eq.(9.59) is the Green's function of the differential equation (9.58).

At this point it is possible to proceed in different ways. By substituting Eq.(9.60) in Eq.(9.55), one obtains an integral in which the integrand is a function of M replicas of the coordinates of the particles in the system. The ground state expectation value of an operator that is a function of the coordinates can then be computed using on the left and on the right the imaginary time propagation started from an arbitrary state $\Psi(R,0)$. The resulting expression is:

$$\langle\phi_0|O(R)|\phi_0\rangle = \lim_{\tau\to\infty}\langle\Psi(R,\tau)|O(R)|\Psi(R,\tau)\rangle \sim \left(\frac{1}{(2\pi\frac{\hbar}{m}\Delta\tau)^{\frac{3A}{2}}}\right)^M \times$$

$$\times \int\int\cdots\int dR\,dR'\cdots dR^M \Psi(R,0)e^{-\frac{\Delta\tau}{2}(V(R)-E_0)}e^{-\frac{(R-R')^2}{2\frac{\hbar}{m}\Delta\tau}} e^{-\Delta\tau(V(R')-E_0)}\cdots O(R^{M/2})$$
(9.61)

$$\cdots e^{-\Delta\tau(V(R^{M-1})-E_0)}e^{-\frac{(R^{M-1}-R^M)^2}{2\frac{\hbar}{m}\Delta\tau}} e^{-\frac{\Delta\tau}{2}(V(R^M)-E_0)}\Psi(R^M,0)$$

This expression closely reminds a path-integral formulation of the problem. The integral can in principle be computed by means of a Metropolis-like algorithm, and gives the ground state expectation of an arbitrary observable, provided that the number of slices M used be large enough to guarantee a correct filtering of the ground state. This method is known as Path Integral Ground State Monte Carlo (PIGS-MC)[Cite Kevin etc]

However, there is a simpler way to implement the imaginary time propagation. Let us expand the initial state from which we want to project the ground state in eigenstates of the position:

$$|\Psi\rangle \simeq \sum_i \Psi(R_i)|R_i\rangle$$
(9.62)

We will call each of these points in coordinate space a *walker*, and we will refer to the whole ensemble of points as to the *population* of walkers. If we apply the short-time propagator to each walker, it is easy to understand its effect. We will call the application of the short-time propagator to the walker population an *imaginary time step* (or simply a *time step*). Each time step originates a new *generation* of walkers.

The Gaussian factor in the propagator tells us the probability that a walker positioned in R' is displaced in a new position R. Since the probability density is a Gaussian of variance $\sigma^2 = \frac{\hbar^2}{m}\Delta\tau$, the RMS displacement will be proportional to $\sqrt{\Delta\tau}$ by a constant, which plays the role of a *diffusion constant D*, equal to $\frac{\hbar^2}{m}$. For each coordinate of each particle we need to extract a random number η distributed as:

$$P[\eta] = \frac{1}{\sqrt{2\pi D \Delta \tau}} e^{-\frac{\eta^2}{2D\Delta \tau}} \qquad (9.63)$$

and sum it to to the original coordinate.

```
DMC_Move()
for i ∈ {0, A − 1} do
    for j ∈ {0, 2}  do
        R_new[i][j] ← R[i][j] + DΔτ[rgaus()]
    end for
end for
```

The function rgaus() generating normal distributed random numbers is now universally available as a library routine, but it can easily be implemented starting from a uniform distribution by using the Box-Muller formula. The part of the propagator depending on the potential has a slightly different interpretation. In the classical analogy we could say that the factor $W = e^{-\frac{\Delta\tau}{2}(V(R^M)-E_0)}$ represents the probability of a process to occur by which new points might be created in the time interval $\Delta\tau$ (if $W > 0$) or destroyed (if $W < 0$), or in other words, a process related to the presence of a source or a sink of walkers. W is interpreted as the average number of walkers that this process would generate over time at the position R. As we will later see, this creation/absorption (or *branching*) process is related to the fact that the normalization of the propagated state is not preserved. Since we cannot work with a non-integer number of walkers, we can use the following strategy

1. use the quantity W as a weight for the contribution to the estimates from the walker at a given position. Since in the short-time propagator we have two such factors, one from the initial position and on from te final position of the walker, we can use the product of the two as the total weight:

$$W = \exp\left\{-\Delta\tau\left[\frac{V(R)+V(R')}{2}-E_0\right]\right\} \qquad (9.64)$$

Estimates will be integrals of the form $\langle O \rangle = \int \phi_0(R)O(R)dR$, and they can be computed as:

$$\langle O \rangle = \frac{\sum_l^{N_{wk}} W_{kl} O(R_{kl})}{\sum_l^{N_{wk}} W_{kl}}, \qquad (9.65)$$

where N_{wk} is the number of walkers in a given generation. We will discuss later the specific form of the function O for interesting cases.

2. In order to generate a number of points that is correct on average, we can sample N_{mult}, the number of points to be generated for the next generation, in the following way:

$$N_{mult} = \text{int}(\text{int}(W)+\xi), \qquad (9.66)$$

where int() is the function truncating the argument to an integer, and ξ is a random number in $[0,1)$. N_{mult} could be ≥ 1, in which case the next generation will contain *Nmult* copies of the walker, or 0, in which case the walker is suppressed.

The projection of the ground state will be achieved when propagating for a sufficiently long imaginary time. This means that we need to evolve the population of walkers for a large number of time steps, and eventually we will sample a density of points with a distribution *proportional* to the ground state wavefunction. In the initial stage of the run, the energy and other estimators will have a value that is still strongly biased by the initial state. This means that the initial par of the propagation should be excluded from the averages. There is no automatic recipe to choose how much of the walk should be discarded. Usually it is

convenient to monitor some observable (typically energy) and try to see where its value stops having a systematic trend as a function of the imaginary time.

How is the constant E_0 fixed? In principle it should be equal to the ground state energy. This would mean that we need to know the solution of the problem... before solving it! In practice it is not strictly necessary to use the exact value of E_0, but it is sufficient to use a realistic variational estimate. The value of E_0 can also be used to reduce the fluctuations in the population of walkers due to the branching process, at the cost of introducing additional bias. For example, it is possible to modify the weight of a given configuration in the following way:

$$\tilde{W} = \frac{N_t}{N_g} \exp\left\{-\Delta\tau \left[\frac{V(R)+V(R')}{2} - E_0\right]\right\}$$
(9.67)

where N_t is a "target" number of walkers in the population and N_g is the number of walkers in the current generation. This modified weight reacts to the variations of the population, increasing or decreasing the weight depending on whether N_g is smaller or larger than N_t, respectively. This modification obviously introduces a bias in the results, since it modifies the propagator. However, this bias will be linearly decreasing with the time-step $\Delta\tau$. The weight can also be rewritten as:

$$\tilde{W} = \exp\left\{-\Delta\tau \left[\frac{V(R)+V(R')}{2} - \tilde{E}\right]\right\},$$
(9.68)

where

$$\tilde{E} = E_0 + \frac{1}{\Delta\tau} \log\left(\frac{N_t}{N_g}\right)$$
(9.69)

Therefore, at each generation the constant can be modified to keep the size of the population under control.

The weight can also be used to estimate the energy. In fact if we take the logarithm of both members of Eq. (9.68) we obtain:

$$\log\tilde{W} = -\Delta\tau \left[\frac{V(R)+V(R')}{2} - \tilde{E}\right]$$
(9.70)

from which we obtain:

$$E_0 = \log\left(\frac{N_g\tilde{W}}{N_t}\right) + \frac{V(R)+V(R')}{2}.$$
(9.71)

This is the so-called *growth energy* estimator, and it can be used in principle to evaluate the ground state eigenvalue.

A simpler way of evaluating the energy is to use a test function $\Psi_T(R)$. In this case the idea is to evaluate the following matrix element:

$$\langle E\rangle = \frac{\langle\phi_0|\hat{H}|\Psi_T\rangle}{\langle\phi_0|\Psi_T\rangle} = \frac{\int dR\,\phi_0(R)\hat{H}\Psi_T(R)}{\int dR\,\phi_0(R)\Psi_T(R)}$$
(9.72)

Both integrals at numerator and denominator are suitable to be evaluated in the Monte Carlo way. The probability density that we sample is $\phi_0(R)$, and the functions to be cumulated following the recipe in Eq. (**??** are
$hat{H}\Psi_T(R)$ and $\Psi_T(R)$. The latter is necessary whenever $\Psi_T(R)$ is not normalized. We will then have

$$\langle E\rangle = \frac{\langle\hat{H}\Psi_T\rangle}{\langle\Psi_T\rangle}.$$
(9.73)

However, due to the hermiticity of the hamiltonian, one has:

$$\langle E\rangle = \frac{\langle\phi_0|\hat{H}|\Psi_T\rangle}{\langle\phi_0|\Psi_T\rangle} = \frac{\langle\Psi_T|\hat{H}|\phi_0\rangle}{\langle\phi_0|\Psi_T\rangle} = E_0,$$
(9.74)

independent of the choice of $\Psi_T(R)$. This is the most practical way to evaluate the energy eigenvalue and its standard deviation. Other observables can be evaluated in a similar way. However the results will always depend on the choice of the test function. We will discuss this aspect later.

9.3.4 Application to the harmonic oscillator

9.3.5 Importance sampling

The simple diffusion algorithm we have illustrated above suffers of a substantial deficiency when particles interact with a potential having a repulsive or attractive core. Since the free particle diffusion propagator does not have any information about the potential, particles have no restrictions to come close to each other. This means that the weights will suffer of large fluctuations whenever a pair of particles find themselves at short distance. The consequent fluctuations in the population make the computation unmanageable.

The use of an importance function to guide the diffusion process [cite kalos, Anderson, Ceperley] was the key to make the Diffusion Monte Carlo algorithms usable. The idea is to give up on the request of sampling the ground state wavefunction, and rather try to sample a distribution that, asymptotically in imaginary time, is the product of the ground state wavefunction and of a known function that is the best possible approximation to the ground state obtained, for instance, by means of a variational calculation. We will call this function Ψ_G. Starting from Eq.(9.51) we can multiply both sides by Ψ_G and obtain:

$$\Psi_G(R)\Psi(R,\Delta\tau) = \int dR' G'(R',R,\Delta\tau)\Psi_G(R)\Psi(R',0), \tag{9.75}$$

where we have defined:

$$G'(R,R',\Delta\tau) = \frac{1}{(2\pi\frac{\hbar^2}{m}\Delta\tau)^{\frac{3A}{2}}} e^{-\Delta\tau(V(R')-E_0)} e^{-\frac{(R'-R)^2}{2\frac{\hbar^2}{m}\Delta\tau}}. \tag{9.76}$$

Since all the expressions we have written are correct at order $\Delta\tau$, for our purposes we can assume the equivalence of G' and G. We can multiply and divide the integrand in Eq.(9.75) by $\Psi_G(R')$ to obtain:

$$\Psi_G(R)\Psi(R,\Delta\tau) = \int dR' G'(R',R,\Delta\tau)\frac{\Psi_G(R)}{\Psi_G(R')}\Psi_G(R')\Psi(R',0),. \tag{9.77}$$

In Eq. (9.77) we can identify a new walker density to be propagated, namely:

$$f(R,\tau) = \Psi_G(R)\Psi(R,\tau), \tag{9.78}$$

and the corresponding propagator:

$$\tilde{G}(R,R',\Delta\tau) = G'(R,R',\tau)\frac{\Psi_G(R)}{\Psi_G(R')}. \tag{9.79}$$

The quotient of the wavefunctions can be included in the weight, and provides a correction that prevents the walkers to excessively multiply or die near the divergent points of the potential This point is better illustrated considering the short time limit it is possible to expand the ratio of the guiding functions. At first order in $\Delta\tau$ the result is:

$$\tilde{G}(R,R',\Delta\tau) \simeq G_0(R,R',\tau)\left[1 + \frac{\nabla\Psi_G(R')}{\Psi_G(R')}(R-R') + \cdots\right] \tag{9.80}$$

At the same order we can regard the terms in bracket as the expansion of an exponential and write:

$$\tilde{G}(R,R',\Delta\tau) \simeq G_0(R,R',\tau)e^{\frac{\nabla\Psi_G(R')}{\Psi_G(R')}(R-R')} \tag{9.81}$$

This can be combined with the Gaussian factor in G_0, and by completing the square (which introduces a term at order $\Delta\tau 2$), the propagator is modified as follows:

$$\tilde{G}(R,R',\Delta\tau) \simeq \frac{1}{(2\pi\frac{\hbar^2}{m}\Delta\tau)^{\frac{3A}{2}}}e^{-\frac{\Delta\tau}{2}(V(R')-E_0)}e^{-\frac{(R-R'-\frac{\hbar^2}{m}\Delta\tau\frac{\nabla\Psi_G(R')}{\Psi_G(R')})^2}{2\frac{\hbar^2}{m}\Delta\tau}}e^{-\frac{\Delta\tau}{2}(V(R)-E_0)}. \tag{9.82}$$

The same expansion can be performed to compute the *change in normalization* of the propagated density after a time step. The change in normalization is given by:

$$\mathcal{N} = \int dR\tilde{G}(R,R',\tau), \tag{9.83}$$

i.e. the total weight of the final points R that can be reached starting from R'. Once more we can expand the ratio of the guiding functions in the propagator, but this time up to second order:

$$\tilde{G}(R,R',\Delta\tau) \simeq G_0(R,R',\tau)\left[1 + \frac{\nabla\Psi_G(R')}{\Psi_G(R')}(R-R') + \frac{1}{2}\frac{\partial_{i\alpha}\partial_{j\beta}\Psi_G(R')(R-R')_{i\alpha}(R-R')_{j\beta}}{\Psi_G(R')} + \cdots\right] \tag{9.84}$$

Inserting the previous equation in Eq.(9.83) we can see that after integrating over R the terms containing odd powers of $(R-R')$ disappear by parity. We are therefore left with:

$$\mathcal{N} = e^{-\Delta\tau[V(R')-E_0]}\left[1 + \frac{1}{2}\frac{\nabla^2\Psi_G(R')}{\Psi_G(R')}\frac{\hbar^2}{m}\Delta\tau + \cdots\right] \tag{9.85}$$

We can now use the same trick used above to write the expression in square parenthesis as an exponential. The result is:

$$\mathcal{N} = \exp\left[-\Delta\tau\left(V(R') - \frac{\hbar^2}{2m}\frac{\nabla^2\Psi_G(R')}{\Psi_G(R')} - E_0 z\right)\right] \tag{9.86}$$

In the previous expression it is possible to immediately recognize the local energy. In fact, when using importance sampling, the normalization assumes the expression:

$$\mathcal{N} = \exp\left[-\Delta\tau\left(\frac{\hat{H}\Psi_G(R')}{\Psi_G(R')} - E_0\right)\right] \tag{9.87}$$

This is the new form of the weight factor that one needs to compute in order to determine the multiplicity of the walker at a given position. It is immediately clear that the fact that in the exponential we have the difference between the local energy, instead of the potential energy, and the reference eigenvalue E_0 essentially resolves the issue related to the fluctuations of the population related to a divergent behavior of the interaction. In fact, if we knew the exact solution the exponent would be identically zero, and the population would be absolutely stable. However, by means of an accurate variational calculation it is possible to obtain a very good approximation of the ground state wavefunction, thereby reducing the fluctuations in the population to a minimum.

The algorithm including impotance sampling is modified in the following way.

1. For each walker, and for each coordinate perform a "drift" move along the gradient of the guiding function. This displacement is deterministic.

    DMC_Drift()
    for $i \in \{0, A-1\}$ **do**
        for $j \in \{0, 2\}$ **do**
            $R_{drift}[i][j] \leftarrow R[i][j] + \frac{\nabla \Psi_G(R)}{\Psi_G(R)}|_{[i][j]} D \Delta \tau$
        end for
    end for

2. Cycle again over coordinates and diffuse the position from R_{drift} as in the non-importance sampled case.

3. Compute the new multiplicity of the walker and the weight to assign to estimators using

$$W = \exp\left[-\Delta \tau \left(\frac{\hat{H} \Psi_G(R')}{\Psi_G(R')} - E_0\right)\right] \qquad (9.88)$$

In this way the walkers will asymptotically sample the distribution:

$$f(R) = \Psi_G(R)\phi_0(R). \qquad (9.89)$$

This means that it is possible to evaluate integrals of the form:

$$\langle O \rangle = \frac{\int dR f(R) O(R)}{\int dR f(R)}. \qquad (9.90)$$

As in the previous case the evaluation of the exact energy eigenvalue can be easily obtained by using the local energy. In fact, the matrix element of the Hamiltonian between the guiding function[3] and the ground state wavefunction is:

$$\langle E \rangle = \frac{\langle \phi_0 | \hat{H} | \Psi_G \rangle}{\langle \phi_0 | \Psi_G \rangle} = \frac{\int dR f(R) \frac{\hat{H} \Psi_G(R)}{\Psi_G(R)}}{\int dR f(R)} \qquad (9.91)$$

Once more, because of the hermiticity of the Hamiltonian we will have that $\langle E \rangle = E_0$. All other estimators will be matrix elements of the operator between Ψ_G and ϕ_0.

9.3.6 The fermion sign problem

As we have mentioned

9.4 Quantum Monte Carlo for Nuclear Hamiltonians in coordinate space

9.4.1 Green's Function Monte Carlo

The GFMC method works well for calculating the low lying states of nuclei up to and including ^{12}C. Its major problem is that the computational costs scale exponentially with the number of particles, because of the full spin isospin summations. Full spatial integrations would also

---

[3] It is always possible to project the energy from a function Ψ_T other than Ψ_G, by introducing a further weighing factor $\frac{\Psi_T}{\Psi_G}$. However this is used very rarely in standard applications.

scale exponentially, and this problem is solved by Monte Carlo sampling the positions. The obvious solution to the exponential scaling of the spin-isospin sums is to perform them using Monte Carlo sampling as well.

Our goal is then to find a low variance method to sample the spin-isospin degrees of freedom. The usual historical route would be to begin with a variational Monte Carlo calculation with spin-isospin summations. For example, using Eq. **??**, and instead of summing over the spin degrees of freedom, we could sample them using a Metropolis et al. [**?**] method. For example, the energy expectation would be

$$
\begin{aligned}
E_V &= \frac{\sum_S \int dR \langle \Psi_T | H | RS \rangle \langle RS | \Psi_T \rangle}{\sum_S \int dR \langle \Psi_T | RS \rangle \langle RS | \Psi_T \rangle} \\
&= \sum_S \int dR P(R,S) E_L(R,S)
\end{aligned}
\tag{9.92}
$$

where

$$
\begin{aligned}
P(R,S) &= \frac{\langle \Psi_T | RS \rangle \langle RS | \Psi_T \rangle}{\sum_S \int dR \langle \Psi_T | RS \rangle \langle RS | \Psi_T \rangle} \\
E_L(R,S) &= \frac{\langle \Psi_T | H | RS \rangle}{\langle \Psi_T | RS \rangle} \,.
\end{aligned}
\tag{9.93}
$$

We could then sample the spin-isospin states. We could begin with any given up/down and proton/neutron spin state for each particle that gives a nonzero $\langle RS | \Psi_T \rangle$ value, and make Metropolis et al. moves by flipping spins and exchanging isospins. With a high quality trial function, the local energy $E_L(R,S)$ will have low variance, and the method would give an accurate variational energy upperbound.

The problem here is not in devising a Monte Carlo method or finding a way of sampling the spin-isospin variables. The problem, instead, is in the calculation of the trial function. The Calculation of the good trial functions described in section **??** scales exponentially with particle number even for a single spin-isospin state. In fact the difference in computational cost of calculating the value of these trial functions for one spin-isospin state and all off them is completely negligible. The VMC and GFMC methods described in section **??** can therefore lower the variance without increasing the computational complexity by summing over all of the spin-isospin states.

This tells us that in order to have an algorithm that has polynomial scaling with particle number, we require a basis that is complete or overcomplete, a trial state, and the evaluation of the wave function given by the overlap of our trial and basis states must be calculable in polynomial time.

To date, we have used the basis given by the outer product of nucleon position states, and the outer product of single nucleon spin-isospin spinor states. That is an element of this overcomplete basis is given by specifying the $3A$ cartesian coordinates for the A nucleons, and specifying four complex amplitudes for each nucleon to be in a $|p \uparrow, p \downarrow, n \uparrow, n \downarrow$ spin-isospin state. A basis state is then

$$
|R_n S_n \rangle = |r_1 s_1 \rangle \otimes |r_2 s_2 \rangle \cdots \otimes |r_n s_n \rangle
\tag{9.94}
$$

Our trial functions must be antisymmetric under interchange. The only such functions with polynomial scaling that we know how to write down are Slater determinants or Pfaffians (BCS pairing functions), for example,

$$
\begin{aligned}
\langle RS | \Phi_{\text{Slater}} \rangle &= \mathscr{A} \left[\langle \mathbf{r}_1 s_1 | \phi_1 \rangle \langle \mathbf{r}_2 s_2 | \phi_2 \rangle \ldots \langle \mathbf{r}_A s_A | \phi_n \rangle \right] \\
\langle RS | \Phi_{\text{BCS}} \rangle &= \mathscr{A} \left[\langle \mathbf{r}_1 s_1 \mathbf{r}_2 s_2 | \psi_{\text{cooper}} \rangle \langle \mathbf{r}_3 s_3 \mathbf{r}_4 s_4 | \psi_{\text{cooper}} \rangle \ldots \langle \mathbf{r}_{A-1} s_{A-1} \mathbf{r}_A s_A | \psi_{\text{cooper}} \rangle \right]
\end{aligned}
\tag{9.95}
$$

or linear combinations of them. Operating on these with the product of correlation operators, Eq. **??**, again gives a state with exponential scaling with nucleon number. For our AFDMC calculations, we multiply these wave functions by a state-independent, or central, Jastrow correlation. Calculations of the Slater determinants and Pfaffians scale like A^3 when using standard dense matrix methods, while the central Jastrow requires A^2 operations if its range is the same order as the system size.

These trial functions capture only the physics of the gross shell structure of the nuclear problem and the state independent part of the two-body interaction. Devising trial functions that are both computationally efficient to calculate and that capture the state-dependent two- and three-body correlations that we know are important would greatly improve both the statistical and systematic errors of quantum Monte Carlo methods for nuclear problems.

The trial wave functions above can be used for variational calculations. However, the results are poor since the functions miss the physics of the important tensor interactions. These functions can be used as importance functions for AFDMC calculations where they have been found adequate for this purpose in a variety of problems.

9.4.2 General Auxiliary Field Formalism

We begin by looking at the auxiliary field formalism without importance sampling. All such diffusion Monte Carlo methods can be formulated as

$$|\Psi(t+\Delta t)\rangle = \int dX P(X) T(X) |\Psi(t)\rangle \tag{9.96}$$

where X is a set of variables which will become our auxiliary fields, $P(X)$ is a probability density,

$$P(X) \geq 0$$
$$\int dX P(X) = 1 \,, \tag{9.97}$$

and $T(X)$ is an operator that operates in the Hilbert space of $|\Psi(t)\rangle$. We are free to choose the variables X, the probability density $P(X)$, and the operator $T(X)$ subject only to the constraint that the integral gives the desired propagator

$$e^{-(H-E_T)\Delta t} = \int dX P(X) T(X) \,, \tag{9.98}$$

at least in the limit that $\Delta t \to 0$.

In diffusion Monte Carlo methods, we represent the state $|\Psi(t)\rangle$ as a linear combination of basis states which obviously must span the Hilbert space. These can be a complete set. An example is the position eigenstates used for diffusion Monte Carlo for central potentials. They can also form an overcomplete set such as or the position and spin/isospin bases used in the nuclear GFMC method and the position and overcomplete outer product of single particle spinor basis used in AFDMC, or the overcomplete single particle bases used in auxiliarly field methods such as those developed by Zhang and coworkers. For either case, we can denote these basis states as possible "walkers." We will denote one of these walker states as $|RS\rangle$ since we will be applying the method to systems where the basis is given by the positions of the particles, R, and a spinor for each spin-isospin of the particles, S.

The state, $|\Psi(t)\rangle$, at time t is represented in diffusion Monte Carlo methods as a linear combination of walker states

$$|\Psi(t)\rangle = \sum_{i=1}^{N_W} w_i |R_i S_i\rangle \tag{9.99}$$

where w_i is a coefficient, often called the weight, and N_W is the number of walkers.

The key ingredient to implementing a diffusion Monte Carlo method is to choose the walker basis and the operator $T(X)$ such that when $T(X)$ operates on a walker basis state, it gives one and only one new walker basis state. That is we want

$$T(X)|RS\rangle = W(X,R,S)|R'S'\rangle \tag{9.100}$$

where $|R'S'\rangle$ is normalized in the same way as $|RS\rangle$, and $W(X,R,S)$ is the change in the normalization from the propagation.

Once we have arranged for Eq. 9.100 to be true, we can implement the diffusion Monte Carlo by starting with $|\Psi(0)\rangle$ written, as in Eq. 9.99, as any, not unreasonable, linear combination of walkers. For each walker, we sample X values from $P(X)$, and use Eq. 9.100 to propagate to a new walker $|R_i' S_i'\rangle$, with a new weight w_i' given by the proportionality constant of Eq. 9.100 multiplied by the original weight w_i. We branch on the magnitude of the weight, so usually, after branching, $w_i' = 1$, where we are ignoring the fermion sign or phase problem for now and assuming that all of the weights are greater than or equal to zero. We will deal with the fermion case below.

9.4.3 Operator expectations and importance sampling

9.4.3.1 Mixed averages

Diffusion Monte Carlo methods efficiently calculate ground-state mixed averages

$$\bar{O}_{\text{mixed}} = \frac{\langle \Psi_T | O | \Psi(t)\rangle}{\langle \Psi_T | \Psi(t)\rangle} \tag{9.101}$$

where $|\Psi_T\rangle$ is trial state. If O is the Hamiltonian, operating on $|\Psi(t)\rangle$ shows that the result is the ground-state energy for large t. For other operators, for which the ground state is not an eigenstate, either approximate extrapolation methods or forward walking or its equivalent must be used to extract the correct ground-state expection value.

Given a set of walkers as in Eq. 9.99, the mixed estimate can be calculated by

$$\bar{O}_{\text{mixed}} \simeq \frac{\sum_{i=1}^{N_w} w_i \langle \Psi_T | O | R_i S_i\rangle}{\sum_{i=1}^{N_w} w_i \langle \Psi_T | R_i S_i\rangle} \tag{9.102}$$

where the right hand side differs from the correct result because of statistical errors from the sampling which decreases as $N_W^{-1/2}$, and possible population size bias which decreases as N_W^{-1}. Statistical errors can be minimized by reducing the variance through importance sampling. Population bias also can be controlled with importance sampling, and, since it decays faster with population size, can be readily detected and removed by either taking larger numbers of walkers or extrapolation.

Efficient Monte Carlo methods need to have low variance so that the statistical error bars can be made small. For our walker propagation, this means that we should sample new walkers not only corresponding to the weight they will receive from our algorithm, but with this weight multiplied by their expected survival probability. The imaginary time Schrödinger equation is self adjoint, so the optimum importance function is the desired function [?]. Typically, a trial function that can be efficiently evaluated is determined variationally and used

as an approximation to the optimum trial function. Usually this trial wave function is used as the importance function. Sometimes a different importance function is used, so we will write this more general case.

9.4.3.2 Importance sampling

To add importance sampling, we arrange to sample our walkers from a new state which we call $|\Psi_I \Psi(t)\rangle$ such that

$$\langle RS|\Psi_I \Psi(t)\rangle = \langle \Psi_I|RS\rangle\langle RS|\Psi(t)\rangle \tag{9.103}$$

so that

$$|\Psi_I \Psi(t)\rangle = \sum_{i=1}^{N_w} w_i |R_i S_i\rangle \tag{9.104}$$

An alternative way of looking at this is that the sampling probability for the walkers at $R_i S_i$ has been modified so that

$$|\Psi(t)\rangle = \sum_{i=1}^{N_w} w_i \langle \Psi_I|R_i S_i\rangle^{-1}|R_i S_i\rangle. \tag{9.105}$$

Calculating a mixed average now becomes

$$\bar{O}_{\text{mixed}} = \frac{\sum_{i=1}^{N_w} w_i \frac{\langle \Psi_T|R_i S_i\rangle}{\langle \Psi_I|R_i S_i\rangle} \frac{\langle \Psi_T|O|R_i S_i\rangle}{\langle \Psi_T|R_i S_i\rangle}}{\sum_{i=1}^{N_w} w_i \frac{\langle \Psi_T|R_i S_i\rangle}{\langle \Psi_I|R_i S_i\rangle}}. \tag{9.106}$$

For the usual case where $|\Psi_I\rangle = |\Psi_T\rangle$, and $w_i = 1$, we have

$$\bar{O}_{\text{mixed}} = \frac{1}{N_w} \sum_{i=1}^{N_w} \frac{\langle \Psi_T|O|R_i S_i\rangle}{\langle \Psi_T|R_i S_i\rangle}. \tag{9.107}$$

We substitute Eqs. 9.103 and 9.104 into Eq. 9.96

$$|\Psi_I \Psi(t+\Delta t)\rangle = \sum_{i=1}^{N_w} w_i \int dX P(X) \frac{\langle \Psi_I|R_i' S_i'\rangle}{\langle \Psi_I|R_i S_i\rangle} T(X)|R_i S_i\rangle$$

$$= \sum_{i=1}^{N_w} w_i \int dX P(X) \frac{\langle \Psi_I|T(X)|R_i S_i\rangle}{\langle \Psi_I|R_i S_i\rangle} \frac{T(X)}{W(X,R_i,S_i)}|R_i S_i\rangle \tag{9.108}$$

where $|R_i' S_i'\rangle$ is defined as in Eq. 9.100. Notice that the operator $T(X)/W(X,R_i,S_i)$ operating on $|R_i S_i\rangle$ gives a normalized walker. The additional weight of this walker is given by $P(X)\frac{\langle \Psi_I|T(X)|R_i S_i\rangle}{\langle \Psi_I|R_i S_i\rangle}$. We want to minimize fluctuations in this weight factor, and to do this we normalize it and sample from the normalized distribution. The normalization will be the weight.

We write

$$\mathcal{N} = \int dX P(X) \frac{\langle \Psi_I|T(X)|R_i S_i\rangle}{\langle \Psi_I|R_i S_i\rangle}$$

$$= \frac{\langle \Psi_I|e^{-(H-E_T)\Delta t}|R_i S_i\rangle}{\langle \Psi_I|R_i S_i\rangle}$$

$$= e^{-(E_L(R_i,S_i)-E_T)\Delta t} + O(\Delta t^2) \tag{9.109}$$

where the local energy $E_L(R_i,S_i)$ is defined by

$$E_L(R_i,S_i) = \frac{\langle \Psi_I|H|R_i S_i\rangle}{\langle \Psi_I|R_i S_i\rangle} \tag{9.110}$$

and we now sample X variables from the normalized distribution

$$\tilde{P}(X) = \mathcal{N}^{-1} P(X) \frac{\langle \Psi_I | T(X) | R_i S_i \rangle}{\langle \Psi_I | R_i S_i \rangle} \, .$$
(9.111)

The importance sampled diffusion Monte Carlo in the auxiliary field formalism becomes

$$|\Psi_I \Psi(t+\Delta t)\rangle = \sum_{i=1}^{N_w} w_i \int dX \tilde{P}(X) e^{-(E_L(R_i,S_i)-E_T)\Delta t} \frac{T(X)}{W(X,R_i,S_i)} |R_i S_i\rangle \, .$$
(9.112)

We propagate a walker by sampling an X value from $\tilde{P}(X)$, we include the local energy expression in the weight, and construct the new normalized walker position and spin state as $W^{-1}(X,R_i,S_i)T(X)|R_i S_i\rangle$. In each of the equations above, the ratio of the wave function terms gives the walker weight. In Eq. 9.112 these terms have been combined to give a weight that depends on the local energy expectation value. All of the expectation values and weights contain ratios of trial wave functions so that any normalization factor multiplying the $|RS\rangle$ cancels and any convenient normalization can be used. We can therefore drop the W factors and normalize our walker kets at the end of a step. Typically just the walker positions are stored and the walker spinors are normalized to have magnitude 1.

9.4.3.3 Importance sampling with a Hubbard-Stratonovich transformation

We often have Hamiltonians where the Hubbard-Stratonovich transformation

$$e^{\frac{O^2}{2}} = \frac{1}{\sqrt{2\pi}} \int_{-\infty}^{\infty} dx e^{-\frac{x^2}{2}} e^{xO}$$
(9.113)

can be used to write a propagatator in the form of Eq. 9.100. Examples are writing the kinetic energy as an integral over translations, or writing terms like $\sigma_i \cdot \sigma_j = (\sigma_i + \sigma_j)^2 - 6$ as an integral over spin rotations.

Since we primarily use the Hubbard-Stratonovich transformation to define our auxiliary fields, it is useful to work out how importance sampling can be included within the short-time approximation for this particular case. We begin with a Hamiltonian that is quadratic in a set of N_O operators (which for our nuclear problems will be momentum and spin-isospin operators) O_n,

$$H = \frac{1}{2} \sum_{n=1}^{N_O} \lambda_n O_n^2$$
(9.114)

so that the imaginary time propagator is

$$e^{-H\Delta t} = \int dx \frac{1}{(2\pi)^{N_O/2}} e^{-\frac{1}{2}\sum_{n=1}^{N_O} x_n^2} e^{-i\sum_{n=1}^{N_O} x_n \sqrt{\lambda_n \Delta t} O_n}$$
$$+ O(\Delta t^2)$$
(9.115)

where the Δt^2 terms comes from the possible noncommutivity of the O_n.

As before, we choose our walker basis and the operators O_n such that operating on a walker, $|RS\rangle$, with a term sampled from the integrand, gives a result proportional to another walker

$$e^{-i\sum_{n=1}^{N_O} x_n \sqrt{\lambda \Delta t} O_n} |RS\rangle = W(\{x_n\},R,S)|R'S'\rangle$$
(9.116)

where $\{x_n\}$ represents the set of sampled x_n values.

We now sample $\tilde{P}(X)$ which is

$$\tilde{P}(X) = \mathcal{N}^{-1} e^{-\frac{1}{2}\sum_{n=1}^{N_O} x_n^2} \frac{\langle \Psi_T | e^{-i\sum_{n=1}^{N_O} x_n \sqrt{\lambda_n \Delta t} O_n} | RS \rangle}{\langle \Psi_T | RS \rangle}$$

$$= \mathcal{N}^{-1} e^{-\frac{1}{2}\sum_{n=1}^{N_O} x_n^2} \left(1 - i \sum_{n=1}^{N_O} x_n \sqrt{\lambda_n \Delta t} \frac{\langle \Psi_T | O_n | RS \rangle}{\langle \Psi_T | RS \rangle} - \frac{1}{2} \sum_{n=1,m=1}^{N_O} x_n x_m \sqrt{\lambda_m \lambda_n} \Delta t \frac{\langle \Psi_T | O_n O_m | RS \rangle}{\langle \Psi_T | RS \rangle} + ... \right)$$

$$(9.117)$$

Notice that if we were to expand $T(X)/W(X,R_i,S_i)$ it would have the form $1 + O(x_n \Delta t^{1/2}) + O(x_n x_m \Delta t) + ...$. Therefore if we drop terms of order Δt^2, the $O(\Delta t)$ term of $P(X)$ contributes only when it multiplies the 1 term from $T(X)/W(X,R_i,S_i)$. We can therefore integrate it over X without changing the result to this order in Δt. This term cancels the normalization, so that

$$\tilde{P}(X) = e^{-\frac{1}{2}\sum_{n=1}^{N_O} x_n^2} \left(1 - i \sum_{n=1}^{N_O} x_n \sqrt{\lambda_n \Delta t} \frac{\langle \Psi_T | O_n | RS \rangle}{\langle \Psi_T | RS \rangle} + O(\Delta t^{3/2}) \right)$$

$$= e^{-\frac{1}{2}\sum_{n=1}^{N_O} x_n^2} e^{-i\sum_{n=1}^{N_O} x_n \sqrt{\lambda_n \Delta t} \frac{\langle \Psi_T | O_n | RS \rangle}{\langle \Psi_T | RS \rangle} + \sum_{n=1}^{N_O} \lambda_n [\frac{\langle \Psi_T | O_n | RS \rangle}{\langle \Psi_T | RS \rangle}]^2} + O(\Delta t^{3/2})$$

$$= \exp \left\{ -\frac{1}{2} \sum_{n=1}^{N_O} \left[x_n + i\sqrt{\lambda_n \Delta t} \frac{\langle \Psi_T | O_n | RS \rangle}{\langle \Psi_T | RS \rangle} \right]^2 \right\}$$

$$(9.118)$$

where in the last line, we have written the linear term in x in the exponent, and included a canceling term so that only the linear term survives integration to order Δt.

We sample our expression by sampling x_n from the shifted gaussian (Again, we assume here that $i\sqrt{\lambda_n \Delta t}\langle O_n \rangle$ is real. We will discuss what to do for the complex case below.)

$$x_n = \chi_n - i\sqrt{\lambda_n \Delta t}\langle O_n \rangle \tag{9.119}$$

where χ_n is sampled from a gaussian with unit variance. The new unnormalized ket is

$$|R'S'\rangle = e^{-i\sum_{n=1}^{N_O} x_n \sqrt{\lambda \Delta t} O_n} |RS\rangle \langle \Psi_T | RS \rangle \tag{9.120}$$

and its weight is given by the local energy expression

$$W(R',S') = e^{-[\langle H \rangle - E_T]\Delta t} \tag{9.121}$$

9.4.4 Application to standard diffusion Monte Carlo

9.4.4.1 Diffusion Monte Carlo without importance sampling

It is helpful to apply the formalism above to derive the well known central potential diffusion Monte Carlo algorithm [**?**]. The Hamiltonian is

$$H = \sum_{j=1}^{A} \sum_{\alpha=1}^{3} \frac{p_{j\alpha}^2}{2m} + V(R) \tag{9.122}$$

where $p_{j\alpha}$ and R operate on Hilbert space, and $p_{j\alpha}$ is the α component of the momentum operator for the jth particle. Making the short-time approximation, the propagator can be written as

$$e^{-(H-E_T)\Delta t} = e^{\sum_{j=1}^{A} \sum_{\alpha=1}^{3} \frac{p_{j\alpha}^2}{2m}\Delta t} e^{-[V(R)-E_T]\Delta t} + O(\Delta t^2). \tag{9.123}$$

Since the Hamiltonian does not operate on the spin, we can drop the spin variable from the our walker expressions and take just a position basis $|R\rangle$. Operating with the potential term

$$e^{-[V(R)-E_T]\Delta t}|R_j\rangle = e^{-[V(R_j)-E_T]\Delta t}|R_j\rangle \tag{9.124}$$

clearly satisfies Eq. 9.100. The kinetic energy part of the propagator does not satisfy Eq. 9.100. However, by using the Hubbard-Stratonovich transformation, we can write the kinetic energy in terms of the translation operators $e^{-\frac{i}{\hbar}P_{j\beta}a}$. We introduce the auxiliary field or Hubbard-Stratonovich variables, $x_{j\alpha}$, and write

$$e^{-\sum_{j=1}^A \sum_{\alpha=1}^3 \frac{p_{j\alpha}^2}{2m}\Delta t} =$$
$$\prod_{j\alpha} \frac{1}{(2\pi)^{3/2}} \int dx_{j\alpha} e^{-\frac{x_{j\alpha}^2}{2}} e^{-\frac{i}{\hbar}\mathbf{P}_{j\alpha}x_{j\alpha}\sqrt{\frac{\hbar^2\Delta t}{m}}} \tag{9.125}$$

With this definition, X is the set $\{x_{j\alpha}\}$, for the A particles,

$$P(X) = \prod_{j\alpha} \frac{1}{\sqrt{2\pi}} e^{-\frac{x_{j\alpha}^2}{2}}, \tag{9.126}$$

and

$$T(X)|R\rangle = e^{-[V(R)-E_T]\Delta t}|R+\Delta R\rangle \tag{9.127}$$

where $R' = R + \Delta R$ is given by translating each particle's position in R

$$r'_{j\alpha} = r_{j\alpha} + x_{j\alpha}\frac{\hbar^2\Delta t}{m}. \tag{9.128}$$

This is identical to the standard diffusion Monte Carlo algorithm without importance sampling. We move each particle with a gaussian distribution of variance $\frac{\hbar^2\Delta t}{m}$, and include a weight of $e^{-[V(R)-E_T]\Delta t}$. We would then include branching on the weight to complete the algorithm.

While the Hubbard-Stratonovich transformation is the most common, there are many other possibilities. For example, the propagator for the relativistic kinetic energy $\sqrt{p^2c^2+m^2c^4}-mc^2$ can be sampled by using

$$e^{-\left[\sqrt{p^2c^2+m^2c^4}-mc^2\right]\Delta t} = \int d^3x f(x) e^{-\frac{i}{\hbar}\mathbf{p}\cdot\mathbf{x}} \tag{9.129}$$

with

$$f(x) = \int \frac{d^3p}{(2\pi)^3} e^{\frac{i}{\hbar}\mathbf{p}\cdot\mathbf{x}} e^{-\left[\sqrt{p^2c^2+m^2c^4}-mc^2\right]\Delta t}$$
$$= e^{mc^2\Delta t} K_2\left(\frac{mc}{\hbar}\sqrt{x^2+c^2\Delta t^2}\right) \tag{9.130}$$

where K_2 is the modified Bessel function of order 2 [**?**].

9.4.4.2 Importance sampled Diffusion Monte Carlo in the auxiliary field formulism

We break up the Hamiltonian as a kinetic and potential part. The potential part gives the usual $e^{-V(R)\Delta t}$ weight, and we need to work only with the importance sampled kinetic energy part. The kinetic energy operator is already written as a sum of squares,

$$KE = \sum_{j\alpha} \frac{p_{j\alpha}^2}{2m} \tag{9.131}$$

where j is the particle label and α is the x, y, or z coordinate. We can identify $\lambda_{j\alpha} = m^{-1}$, and $O_{j\alpha} = p_{j\alpha}$. Substituting this into our previous formalism, we have

$$
\begin{aligned}
i\sqrt{\lambda_{j\alpha}\Delta t}\langle O_{j\alpha}\rangle &= i\sqrt{\frac{\Delta t}{m}} \frac{\langle \Psi_T | p_{j\alpha} | RS \rangle}{\langle \Psi_T | RS \rangle} \\
&= -\sqrt{\frac{\hbar^2 \Delta t}{m}} \frac{\partial_{j\alpha}\langle \Psi_T | RS \rangle}{\langle \Psi_T | RS \rangle} .
\end{aligned}
\tag{9.132}
$$

The sampled value of $x_{j\alpha}$ will be

$$x_{j\alpha} = \chi_{j\alpha} + \sqrt{\frac{\hbar^2 \Delta t}{m}} \frac{\partial_{j\alpha}\langle \Psi_T | RS \rangle}{\langle \Psi_T | RS \rangle} \tag{9.133}$$

where the $\chi_{j\alpha}$ are sampled from a gaussian with unit variance. The new walker will be

$$|R'S'\rangle = e^{-\frac{i}{\hbar}\sum_{j\alpha} x_{j\alpha}\sqrt{\frac{\hbar^2 \Delta t}{m}} p_{j\alpha}} |RS\rangle . \tag{9.134}$$

Since $e^{-\frac{i}{\hbar} p_{j\alpha} a}$ is the translation operator that translates the ket's $j\alpha$ position coordinate by a. We have

$$
\begin{aligned}
S' &= S \\
R'_{j\alpha} &= R_{j\alpha} + x_{j\alpha}\sqrt{\frac{\hbar^2 \Delta t}{m}} \\
&= R_{j\alpha} + \chi_{j\alpha}\sqrt{\frac{\hbar^2 \Delta t}{m}} + \frac{\hbar^2 \Delta t}{m}\frac{\partial_{j\alpha}\langle \Psi_T | RS \rangle}{\langle \Psi_T | RS \rangle}
\end{aligned}
\tag{9.135}
$$

which is the standard diffusion Monte Carlo propagation. The weight factor is the local energy.

9.4.5 Fixed-phase importance-sampled Diffusion Monte Carlo

The fixed-phase approximation [?] was developed to extend the fixed-node approximation to electrons in a magnetic field where the ground-state wave function is complex. The approximation enforces the trial function's phase as the phase for the calculated ground state. Diffusion Monte Carlo is used to sample the magnitude of the ground state.

If the walker phase has been chosen so that $\langle \Psi_T | R \rangle$ is real, the fixed-phase approximation requires that after propagation $\langle \Psi_T | R' \rangle$ would also be real since an imaginary part would correspond to the calculated ground-state having a different phase than the trial function. Therefore in the implementation of the fixed-phase approximation we discard the imaginary part of the weight of a propagated walker. For an arbitrary initial phase, we discard the imaginary part of the ratio $\frac{\langle \Psi_T | R' \rangle}{\langle \Psi_T | R \rangle}$ which means that the we replace the importance sampled factor in Eq. **??** with its real part

$$\frac{\langle \Psi_T | e^{-i\sum_{n=1}^{N_O} x_n \sqrt{\lambda_n \Delta t} O_n} | RS \rangle}{\langle \Psi_T | RS \rangle} \rightarrow$$

$$\text{Re}\left[\frac{\langle \Psi_T | e^{-i\sum_{n=1}^{N_O} x_n \sqrt{\lambda_n \Delta t} O_n} | RS \rangle}{\langle \Psi_T | RS \rangle} \right]. \tag{9.136}$$

The fixed-phase algorithm for propagating a walker is then

1. Propagate to the new position (the spin does not change with a central potential)

$$S' = S$$

$$R'_{j\alpha} = R_{j\alpha} + \chi_{j\alpha}\sqrt{\frac{\hbar^2 \Delta t}{m}} + \frac{\hbar^2 \Delta t}{m}\text{Re}\left[\frac{\partial_{j\alpha}\langle \Psi_T | RS \rangle}{\langle \Psi_T | RS \rangle}\right] \tag{9.137}$$

2. Include a weight factor for the walker of

$$W = e^{-(\text{Re}\langle H \rangle - E_T)\Delta t} \tag{9.138}$$

This is identical to the fixed-phase algorithm of Ortiz et al.

We will see that similar approximations can be used for our spin-isospin dependent problems.

9.4.6 Application to quadratic forms

Quadratic forms in operators that change from one walker to another can be diagonalized to produce the sum of squares needed for Eq. 9.114. That is for

$$H = \frac{1}{2}\sum_{ij} O_i A_{ij} O_j \tag{9.139}$$

with A_{nm} real and symmetric, we can calculate the normalized real eigenvectors and eigenvalues of the matrix A,

$$\sum_j A_{ij} \psi_j^{(n)} = \lambda_n |\psi_i\rangle$$

$$\sum_j \psi_j^{(n)} \psi_j^{(m)} = \delta_{nm}. \tag{9.140}$$

The matrix is then

$$A_{ij} = \sum_n \psi_i^{(n)} \lambda_n \psi_j^{(n)} \tag{9.141}$$

and substituting back we have

$$H = \frac{1}{2}\sum_n \lambda_n \mathscr{O}_n^2$$

$$\mathscr{O}_n = \sum_j \psi_j^{(n)} O_j, \tag{9.142}$$

which is now in the form of Eq. 9.114.

9.4.7 Auxiliary Field Breakups

There are many possible ways to break up the nuclear Hamiltonian using the auxiliary field formalism. As a concrete example let's look at the spinor propagator when we have a spin-exchange potential between A neutrons

$$V = \sum_{i<j} v^\sigma(r_{ij}) \sigma_i \cdot \sigma_j \tag{9.143}$$

Taking the operators to be the x, y, and z components of the Pauli operators for each particle, we have a quadratic form in these $3A$ operators. Since walker gives the positions of the neutrons, we know the value of $v^\sigma(r_{ij})$ for all pairs. We can then write

$$V = \frac{1}{2} \sum_{ij}^A B_{ij} \sigma_{ix} \sigma_{jx} + \frac{1}{2} \sum_{ij}^A B_{ij} \sigma_{iy} \sigma_{jy} + \frac{1}{2} \sum_{ij}^A B_{ij} \sigma_{iz} \sigma_{jz} \tag{9.144}$$

where $B_{ii} = 0$, and $B_{ij} = v^\sigma(r_{ij})$ for $i \neq j$. Finding the eigenenvectors $\psi_i^{(n)}$ and eigenvalues λ_n of the B matrix, we can write

$$V = \frac{1}{2} \sum_n \lambda_n (\mathcal{O}_{nx})^2 + \frac{1}{2} \sum_n \lambda_n (\mathcal{O}_{ny})^2 + \frac{1}{2} \sum_n \lambda_n (\mathcal{O}_{nz})^2$$

$$\mathcal{O}_{nx} = \sum_{i=1}^A \psi_i^{(n)} \sigma_{ix}$$

$$\mathcal{O}_{ny} = \sum_{i=1}^A \psi_i^{(n)} \sigma_{iy}$$

$$\mathcal{O}_{nz} = \sum_{i=1}^A \psi_i^{(n)} \sigma_{iz} . \tag{9.145}$$

Using the Hubbard-Stratonovich transformation would give us $3A$ auxiliary fields.

We can modify this transformation. For example, the diagonal elements of the B matrix are zero. Adding a nonzero diagonal term B_{jj}, would give us additional terms proportonal to $\sigma_{jx}^2 = \sigma_{jy}^2 = \sigma_{jz}^2 = 1$, that is, these would be additional purely central terms. Subtracting a corresponding central contribution would then give an identical interaction, but different eigenvectors and therefore different spin rotation operators.

Another alternative would be to look at each term in the sum separately as a quadratic form of two operators. The resulting 2×2 matrices have two eigenvalues and eigenvectors so that

$$v^\sigma(r_{ij}) \sigma_{ix} \sigma_{jx} = \frac{1}{4} v^\sigma(r_{ij}) [\sigma_{ix} + \sigma_{jx}]^2 - \frac{1}{4} v^\sigma(r_{ij}) [\sigma_{ix} - \sigma_{jx}]^2 \tag{9.146}$$

and each of the $3A(A-1)/2$ terms would require 2 auxiliary fields or $3A(A-1)$ total. We can reduce the number of auxiliary fields by including diagonal terms to our 2×2 matrix equal to the off diagonal terms. These make the eigenvector $(1,-1)/\sqrt{2}$ have a zero eigenvalue, which then does not contribute

$$v^\sigma(r_{ij}) \sigma_{ix} \sigma_{jx} = \frac{1}{2} v^\sigma(r_{ij}) [\sigma_{ix} + \sigma_{jx}]^2 - v^\sigma(r_{ij}) \tag{9.147}$$

where the second term on the right hand side is a central potential counter term that would be added to the physical central potential, and $3A(A-1)/2$ auxiliary fields would be required. This form could also be derived by expanding the square $[\sigma_{ix} + \sigma_{jx}]^2$.

Each of these breakups gives the same net propagator after integration of the auxiliary fields. If a good importance function is used, and the sampling can be carried out, we would

expect the local energy for a complete step to have low variance, and therefore the propagation to have low variance. The trade off then would be the complexity of constructing the operator combination versus the number of auxiliary fields needed in the propagation. In our work to date, we have used the full diagonalization to minimize the number of auxiliary field integrations. The cost of the diagonalization is order A^3 which is the same order as the cost for calculating a Slater determinant for the trial functions we need. However, it is easy to imagine having more complicated Hamiltonians where the cost of full diagonalization would be prohibitive (for example adding Δ degrees of freedom to the nuclei) and a simpler breakup using more auxiliary fields would be more efficient.

The best break up will be the one which optimizes the accuracy and variance of the results for a given amount of computational resources.

9.4.8 AFDMC with the v'_6 potential for nuclear matter

The Argonne v'_6 potential includes central, spin and isospin exchange, and tensor interactions. Writing out the components, the Hamiltonian is

$$
H = \sum_{i\alpha} \frac{p_{i\alpha}^2}{2m} + \sum_{i<j} v^c(r_{ij}) + \sum_{i<j,\alpha\beta} \left\{ v^\sigma(r_{ij})\delta_{\alpha\beta} + v^t(r_{ij}) \left[3\hat{\alpha}\cdot\hat{r}_{ij}\hat{\beta}\cdot\hat{r}_{ij} - \delta_{\alpha\beta} \right] \right\} \sigma_{i\alpha}\sigma_{j\beta}
$$
$$
+ \sum_{i<j,\alpha\beta\gamma} \left\{ v^{\sigma\tau}(r_{ij})\delta_{\alpha\beta} + v^{t\tau}(r_{ij}) \left[3\hat{\alpha}\cdot\hat{r}_{ij}\hat{\beta}\cdot\hat{r}_{ij} - \delta_{\alpha\beta} \right] \right\} [\sigma_{i\alpha}\tau_{i\gamma}][\sigma_{j\beta}\tau_{j\gamma}] + \sum_{i<j,\gamma} v^\tau(r_{ij})\tau_{i\gamma}\tau_{j\gamma} \quad (9.148)
$$

where α and β refer to the x, y, and z components and $\hat{\alpha}$ $\hat{\beta}$ are the corresponding unit vectors. We work in a position basis. The potential is quadratic in the 15A spin-isospin operators $\sigma_{i\alpha}$, $\tau_{i\gamma}$, $\sigma_{i\alpha}\tau_{i\gamma}$. Since each spin-isospin operator can rotate the corresponding spin-isospinor the natural basis is the overcomplete basis of the outer product of these spin-isospinors – one for each particle. A walker consists of an overall weight factor, and x, y, and z coordinates and four complex numbers for the components of $|p\uparrow\rangle$, $|p\downarrow\rangle$, $|n\uparrow\rangle$, $|n\downarrow\rangle$ for each of the A particles.

9.4.8.1 The v'_6 Hamiltonian as a sum of operator squares

We now follow section 9.4.6 and define matrices

$$
C_{i\alpha,j\beta}^\sigma = v^\sigma(r_{ij})\delta_{\alpha\beta} + v^t(r_{ij}) \left[3\hat{\alpha}\cdot\hat{r}_{ij}\hat{\beta}\cdot\hat{r}_{ij} - \delta_{\alpha\beta} \right]
$$
$$
C_{i\alpha,j\beta}^{\sigma\tau} = v^{\sigma\tau}(r_{ij})\delta_{\alpha\beta} + v^{t\tau}(r_{ij}) \left[3\hat{\alpha}\cdot\hat{r}_{ij}\hat{\beta}\cdot\hat{r}_{ij} - \delta_{\alpha\beta} \right]
$$
$$
C_{i,j}^\tau = v^\tau(r_{ij}) \quad (9.149)
$$

which have zero matrix elements when $i = j$. Their eigenvalues and normalized eigenvectors are defined as

$$
\sum_{j\beta} C_{i\alpha,j\beta}^\sigma \psi_{j\beta}^{\sigma\,(n)} = \lambda_n^\sigma \psi_{i\alpha}^{\sigma\,(n)}
$$
$$
\sum_{j\beta} C_{i\alpha,j\beta}^{\sigma\tau} \psi_{j\beta}^{\sigma\,(n)} = \lambda_n^{\sigma\tau} \psi_{i\alpha}^{\sigma\tau\,(n)}
$$
$$
\sum_j C_{i,j}^\tau \psi_j^{\tau\,(n)} = \lambda_n^\tau \psi_i^{\tau\,(n)} \quad (9.150)
$$

with operator combinations

$$O_n^\sigma = \sum_{i\alpha} \psi_{i\alpha}^{\sigma\ (n)} \sigma_{i\alpha}$$

$$O_{n\beta}^{\sigma\tau} = \sum_{i\alpha} \psi_{i\alpha}^{\sigma\tau\ (n)} \sigma_{i\alpha} \tau_{i\beta}$$

$$O_{n\alpha}^\tau = \sum_i \psi_i^{\tau\ (n)} \tau_{i\alpha} \tag{9.151}$$

The Hamiltonian becomes

$$H = \sum_{i=1}^{A} \sum_{\alpha=1}^{3} \frac{p_{i\alpha}^2}{2m} + \sum_{i<j} v^c(r_{ij}) + \frac{1}{2} \sum_{n=1}^{3A} \lambda_n^\sigma (O_n^\sigma)^2$$

$$+ \frac{1}{2} \sum_{n=1}^{A} \sum_{\alpha=1}^{3} \lambda_n^\tau (O_{n\alpha}^\tau)^2 + \frac{1}{2} \sum_{n=1}^{3A} \sum_{\alpha=1}^{3} \lambda_n^{\sigma\tau} (O_{n\alpha}^{\sigma\tau})^2$$

$$\tag{9.152}$$

This is, of course, identical to the original Hamiltonian given in Eq. 9.148, but now it is in a form that makes the propagator easy to sample using auxiliary fields.

9.4.8.2 Complex auxiliary fields

In realistic nuclear physics problems, the fermion sign problem necessarily becomes a phase problem since conservation of angular momentum requires that flipping a spin changes the orbital angular momentum, which induces an angular phase to the wave function. Various fixed-phase approximations can be used. The Hubbard-Stratonovich transformation integrates the auxiliary field over all real values with a gaussian weight. With importance sampling, the gaussian for x_n is shifted by $i\sqrt{\lambda_n \Delta t}\langle O_n \rangle$ as shown in the last line of Eq. **??**. As Zhang and Krakauer [**?**] showed for electronic structure problems, it is equally valid to integrate the auxiliary field over any shifted contour, and by shifting the contour so that x_n becomes complex and takes on the values $x_n = z + i\sqrt{\lambda_n \Delta t}\langle O_n \rangle$, $-\infty < z < \infty$. Integrating over these values does not change the result. However, now this factor is real. We implement the fixed phase approximation by taking the real part of $\langle H \rangle$.

Note that this method cannot be used for the momentum operator. This is because the operator $e^{-\frac{i}{\hbar} p_{j\alpha} a}$ is not bounded if a has an imaginary part. We therefore implement the kinetic energy terms exactly as in the central potential fixed-phase approximation.

There are of course other possible approximations that can be used. The auxiliary fields can be kept real. We find that the approximation is more accurate with Zhang-Krakauer prescription for auxiliary fields for the spin operators.

9.4.8.3 The v_6' algorithm

We can now give the complete algorithm used for the v_6' potential.

1. We begin with a set of walkers $|R_i S_i\rangle$ which we sample from our trial function magnitude squared, $|\langle RS|\Psi_T\rangle|^2$, with Metropolis Monte Carlo. The walkers consist of the $3A$ coordinates of the A particles, and A 4-component normalized spinors.
2. For each walker in turn we calculate the C^σ, C^τ and $C^{\sigma\tau}$ matrices, their eigenvalues, and their eigenvectors.
3. From the trial function and spinor values we evaluate $\langle \sigma_{j\alpha} \rangle$, $\langle \sigma_{j\alpha} \tau_{j\beta} \rangle$, $\langle \tau_{j\alpha} \rangle$, $\langle p_{j\alpha} \rangle$, and $\langle H \rangle$.
4. We sample the complex values for the spin-isospin auxiliary fields

$$x_n = \chi_n + i\sqrt{\lambda_n \Delta t}\langle O_n\rangle \tag{9.153}$$

and transform our walker spinors using

$$|RS'\rangle = e^{-i\sum_{n=1}^{N_O} x_n \sqrt{\lambda \Delta t} O_n}|RS\rangle \tag{9.154}$$

and normalize the spinors

5. We sample the new positions from

$$r'_{j\alpha} = r_{j\alpha} + \chi_{j\alpha}\sqrt{\frac{\hbar^2 \Delta t}{m}} + \frac{\hbar^2 \Delta t}{m}\mathrm{Re}\frac{\partial_{j\alpha}\langle \Psi_T|RS\rangle}{\langle \Psi_T|RS\rangle} \tag{9.155}$$

6. The weight of the new walker is given by $W = e^{-[\mathrm{Re}\langle H\rangle - E_T]\Delta t}$

7. We branch on the walker weight, taking the number of new walkers to be the integer part of W plus a uniform random value on $(0,1)$. If the weight W is negative, we discard the walker.

9.4.9 Isospin-independent spin-orbit interaction

Without isospin exchange, the spin orbit term for particles j and k is

$$\frac{1}{4\hbar}v_{LS}(r_{jk})[(\mathbf{r}_j - \mathbf{r}_k)\times(\mathbf{p}_j - \mathbf{p}_k)]\cdot(\boldsymbol{\sigma}_j + \boldsymbol{\sigma}_k) \tag{9.156}$$

We can write the kinetic energy plus spin-orbit interaction Hamiltonian as

$$\sum_{j\alpha}\frac{p_{j\alpha}^2}{2m} + \frac{1}{4\hbar}\sum_{j<k}v_{LS}(r_{jk})[(\mathbf{r}_j - \mathbf{r}_k)\times(\mathbf{p}_j - \mathbf{p}_k)]\cdot(\boldsymbol{\sigma}_j + \boldsymbol{\sigma}_k)$$

$$= \sum_{j\alpha}\frac{(p_{j\alpha} + \frac{m}{4\hbar}\sum_{k\neq j}v_{LS}(r_{jk})[(\boldsymbol{\sigma}_j + \boldsymbol{\sigma}_k)\times(\mathbf{r}_j - \mathbf{r}_k)]_\alpha)^2}{2m} + V_{\text{Counter}}$$

$$V_{\text{Counter}} = -\frac{1}{2m}\sum_{j\alpha}\left[\frac{m}{4\hbar}\sum_{k\neq j}v_{LS}(r_{jk})[(\boldsymbol{\sigma}_j + \boldsymbol{\sigma}_k)\times(\mathbf{r}_j - \mathbf{r}_k)]_\alpha\right]^2 \tag{9.157}$$

where the counter terms subtract off the unwanted interaction from completing the square. The counter terms do not depend on $\mathbf{p}_j$, so they can be included with the rest of the local potential, and will contribute to the drift and the local energy for that part. However, we will see that the local energy part is canceled below (that is the final weight will be just the correct total local energy which does not include the counter terms).

Using the Hubbard-Stratonovich break up with importance sampling, we have $\lambda_{j\alpha} = m^{-1}$, and

$$i\sqrt{\lambda_{j\alpha}\Delta t}\langle O_{j\alpha}\rangle = -\sqrt{\frac{\hbar^2 \Delta t}{m}}\frac{\partial_{j\alpha}\langle \Psi_T|RS\rangle}{\langle \Psi_T|RS\rangle} + i\sqrt{\frac{m\Delta t}{16\hbar^2}}\sum_{k\neq j}[(\langle \boldsymbol{\sigma}_j\rangle + \langle \boldsymbol{\sigma}_k\rangle)\times \mathbf{r}_{jk}]_\alpha v_{LS}(r_{jk}). \tag{9.158}$$

The sampled value of $x_{j\alpha}$ will be

$$x_{j\alpha} = \chi_{j\alpha} + \sqrt{\frac{\hbar^2 \Delta t}{m}} \frac{\partial_{j\alpha}\langle \Psi_T | RS \rangle}{\langle \Psi_T | RS \rangle} - i\sqrt{\frac{m\Delta t}{16\hbar^2}} \sum_{k \neq j} [(\langle \sigma_j \rangle + \langle \sigma_k \rangle) \times \mathbf{r}_{jk}]_\alpha v_{LS}(r_{jk}). \qquad (9.159)$$

where our fixed-phase like approximation will modify this to keep the translation real, so that

$$x_{j\alpha} = \chi_{j\alpha} + \mathrm{Re}\left\{ \sqrt{\frac{\hbar^2 \Delta t}{m}} \frac{\partial_{j\alpha}\langle \Psi_T | RS \rangle}{\langle \Psi_T | RS \rangle} - i\sqrt{\frac{m\Delta t}{16\hbar^2}} \sum_{k \neq j} [(\langle \sigma_j \rangle + \langle \sigma_k \rangle) \times \mathbf{r}_{jk}]_\alpha v_{LS}(r_{jk}) \right\}. \qquad (9.160)$$

The walker propagator is

$$|R'S'\rangle = e^{-\frac{i}{\hbar}\sum_{j\alpha} x_{j\alpha}\sqrt{\frac{\hbar^2\Delta t}{m}}p_{j\alpha}} e^{i\sum_{j\alpha}x_{j\alpha}\sqrt{\frac{m\Delta t}{16\hbar^2}}\sum_{k\neq j}[(\sigma_j+\sigma_k)\times\mathbf{r}_{jk}]_\alpha v_{LS}(r_{jk})}|RS\rangle \qquad (9.161)$$

The local energy term for the spin orbit will contain the kinetic energy, the spin orbit, and the negative of the counter terms. Therefore, the counter term contribution cancels in the weight, and the final weight is the local energy.

9.5 General projection algorithms in Fock space and non-local interactions

In recent years, a number of projection algorithms working in a discrete Fock space (configuration space) rather than in coordinate space have been proposed [?, ?, ?, ?]. While more similar to more standard many–body techniques (*like perturbation theory or coupled cluster [cite previous chapters]**), the advantage here is that by using Monte Carlo sampling one is able to deal with much larger number of basis sets that build up the total Hilbert space. Also, working on a finite many-body space allows practical calculations with non-local interactions, like those developed within the Chiral Effective Field Theory approach to nuclear forces, in a far more controllable way than not with the continuous coordinate-space formulation exposed so far.

Finally, another great advantage of performing the Monte Carlo on a discrete Hilbert space is the possibility to devise an efficient strategy to reduce the impact of the sign-problem by using cancellation techniques [?, ?]. Unfortunately we won't have space here to cover these aspects.

9.5.1 Fock space formulation of Diffusion Monte Carlo

To set the stage let us take a finite set $\mathscr{S}$ of single-particle (sp) states of size $\mathscr{N}_s$ and consider a general second–quantized fermionic Hamiltonian including two and possibly many–body interactions

$$H = \sum_{\alpha \in \mathscr{S}} \varepsilon_\alpha a_\alpha^\dagger a_\alpha + \sum_{\alpha\beta\gamma\delta \in \mathscr{S}} V_{\alpha\beta\gamma\delta} a_\alpha^\dagger a_\beta^\dagger a_\delta a_\gamma + \dots . \qquad (9.162)$$

In this expression Greek letter indices indicates sp states (ie. α is a collective label for all sp quantum numbers), the operator $a_\alpha^\dagger$ (a_α) creates (destroys) a particle in the sp state α and the $V_{\alpha\beta\gamma\delta}$ are general (anti–symmetrized) two-body interaction matrix elements:

$$V_{\alpha\beta\gamma\delta} = \langle \alpha\beta | \hat{V} | \gamma\delta \rangle - \langle \alpha\beta | \hat{V} | \gamma\delta \rangle. \qquad (9.163)$$

. For an N-fermion system the resulting Fock space would be spanned by the full set of N-particle Slater determinants that can be generated using the sp orbitals $\alpha \in \mathscr{S}$. We will denote these Slater–determinants in the occupation number basis by $|\mathbf{n}\rangle$, where $\mathbf{n} \equiv \{n_\alpha\}$ and $n_\alpha = 0, 1$ are occupation number of the single–particle orbital α satisfying $\sum_\alpha n_\alpha = N$. Using these, any state vector in our many–body Hilbert space can then be expressed as

$$|\Psi\rangle = \sum_{\mathbf{n}} \langle \mathbf{n}|\Psi\rangle |\mathbf{n}\rangle \equiv \sum_{\mathbf{n}} \Psi(\mathbf{n})|\mathbf{n}\rangle \tag{9.164}$$

where the sum is over all possible basis vectors that one can obtain from the $\mathscr{N}_{\mathscr{S}}$ single-particle orbitals.

It is important to notice at this point that no assumption is made on the locality of the interaction, which translates into restrictions on the structure of the tensor $V_{\alpha\beta\gamma\delta}$. This implies that possible non-local interactions can be cleanly incorporated in the formalism.

As was already introduced in the previous sections, the core idea behind any Diffusion Monte Carlo algorithm is to extract ground-state informations on the system by evolving in imaginary-time an initial guess for the lowest eigenstate of the hamiltonian H:

$$\Psi_{\tau+\Delta\tau}(\mathbf{m}) = \sum_{\mathbf{n}} \langle \mathbf{m}|P|\mathbf{n}\rangle \Psi_\tau(\mathbf{n}). \tag{9.165}$$

with a suitable projecton operator P (cf. Eq. (9.96) and discussion above). In order to illustrate how the evolution in (9.165) can be implemented in a stochastic way, it will be usefull first to express the matrix elements of P as follows

$$\langle \mathbf{m}|P|\mathbf{n}\rangle = p(\mathbf{m}, \mathbf{n})g(\mathbf{n}) \tag{9.166}$$

with

$$g(\mathbf{n}) = \sum_{\mathbf{m}} \langle \mathbf{m}|P|\mathbf{n}\rangle \tag{9.167}$$

and

$$p(\mathbf{m}, \mathbf{n}) = \frac{\langle \mathbf{m}|P|\mathbf{n}\rangle}{\sum_{\mathbf{m}} \langle \mathbf{m}|P|\mathbf{n}\rangle} \tag{9.168}$$

. At this point, provided the matrix elements $\langle \mathbf{m}|P|\mathbf{n}\rangle \geq 0$ we can interpret $p(\mathbf{m}, \mathbf{n})$ for fixed $\mathbf{n}$ as (normalized) probability distribution for the states $\mathbf{m}$ and $g(\mathbf{n})$ as a weight factor. This is analogous to what happened in conventional coordinate–space formulations (cf. Sec. **??**) where the propagator is splitted into an off–diagonal part times a weight factor.

Imagine now that at a given imaginary–time τ the wave–function Ψ_τ is non–negative in configuration space (ie. $\Psi_\tau(\mathbf{n}) \geq 0 \forall \mathbf{n}$), then we can represent it as an ensemble of configurations. Due to the non–negativity of the matrix elements of P, we also have that the evolution described in (9.165) preserves the signs, ie. $\Psi_{\tau+\Delta\tau}(\mathbf{m}) \geq 0 \forall \mathbf{m}$. This suggests the following procedure for the stochastic imaginary–time evolution:

1. walker starts at configuration $\mathbf{n}$ with weight $w(\mathbf{n})$
2. a new configuration $\mathbf{m}$ is chosen from the probability distribution $p(\mathbf{m}, \mathbf{n})$
3. the walker's weight gets rescaled as $w(\mathbf{n}) \to w(\mathbf{m}) = w(\mathbf{n})g(\mathbf{n})$
4. reapeat from 1.

In order to improve efficiency one can include a *branching* step where the new configuration in $\mathbf{m}$ is replicated according to its weight as explained in Sec. **??**.

In practice we have to choose some form for the evolution operator that appears in (9.165), a common choice in discrete spaces is the following

$$\begin{aligned}\langle \mathbf{m}|P|\mathbf{n}\rangle &= \langle \mathbf{m}|1 - \Delta\tau(H - E_T)|\mathbf{n}\rangle \\ &= \delta_{\mathbf{m},\mathbf{n}} - \Delta\tau \langle \mathbf{m}|H - E_T|\mathbf{n}\rangle\end{aligned} \tag{9.169}$$

where E_T is an energy shift used in the simulation to preserve the norm of the solution (the trial energy introduced in Sec. **??**. Convergence to the ground–state by repeated application of the projector P to the initial state $|\Psi_0\rangle$

$$|\Psi_{gs}\rangle = \lim_{M\to\infty} P^M |\Psi_0\rangle \tag{9.170}$$

is guaranteed provided that the eigenvalues of P lie between -1 and 1 in order to ensure the diagonal part remains positive definite. This requirement translates into a condition on the imaginary–time step $\Delta\tau$ which has to satisfy

$$\Delta\tau < 2/(E_{max} - E_{min}) \tag{9.171}$$

where E_{max} and E_{min} are respectively the maximum and minimum eigenvalue of H in our finite basis. This upper bound becomes tighter and tighter as we increase the number of particle N and/or the number of sp–states $\mathcal{N}_s$. As a consequence the number M of iterations needed for convergence to the ground state increases dramatically. A way to deal with this problem is to employ a different algorithm proposed in [**?**] (see also [**?**, **?**]) that allows us to sample directly from the exponential propagator

$$\langle \mathbf{m}|P|\mathbf{n}\rangle = \langle \mathbf{m}|e^{-\Delta\tau(H-E_T)}|\mathbf{n}\rangle \tag{9.172}$$

without any limitation on the choice of the imaginary time step $\Delta\tau$. We leave the discussion of its details in Sec. **??**.

So far we assumed that the matrix elements on the projector that defines $p(\mathbf{m},\mathbf{n})$ in Eq. (9.168) are actually positive definite. Under general circumstances, this is however not the case, thus preventing the interpretation of $p(\mathbf{m},\mathbf{n})$ as a probability distribution. In order to circumvent the problem we can use the same idea behind the fixed node (phase) approximation introduced in Sec. **??**: use importance sampling.

Necessary condition for the applicability of the algorithm discussed so far is that the matrix elements of P in configuration space are positive, in general however P will have negative–matrix elements which will cause problems, this is once again a manifestation of the sign–problem.

[*******************] In principle, one can still produce a stochastic evolution absorbing the signs into the renormalization factor and sampling off-diagonal moves using $|\langle\mathbf{m}|P|\mathbf{n}\rangle|$, but this is accompanied by an exponential decay of the signal to noise ratio as a function of the total projection time $\tau = M\Delta\tau$. Recently it was shown that by employing an annihilation step in the evolution this problem can be substantially alleviated [**?**, **?**, **?**]. At the end however these algorithms have still an exponential scaling with system–size, though with a reduced exponent. [*******************]

9.5.2 Importance sampling and fixed-node approximation

AS we just mentioned, we can deal with the sign–problem in a way which is similar to standard coordinate–space QMC: we will use an initial ansatz Φ_T for the ground–state wave–function and use that to constrain the random walk in a region of the many–body Hilbert space where $\langle\mathbf{m}|P|\mathbf{n}\rangle \geq 0$ is satisfied. In order to this scheme to be practical one needs a systematic way for reducing the bias coming from this approximation, e.g. we want the bias to go to zero as the ansatz Φ_T goes towards the ground–state Ψ_{gs}. That's exactly what is done in coordinate-space fixed–node QMC simulations presented in the previous sections.

In this derivation we will follow the work in [**?**, **?**] and generalize it to the case of complex–hermitian hamiltonians usually found in nuclear theory. First a comment is necessary due to the fact that the trial–wave function will now have both a real and imaginary part and in principle we should evolve both according to their evolution equation ****reference discussion above****, here instead we choose to work in the so–called *fixed–phase* approximation where the imaginary part of the solution is constrained to be the same of the trial wave–function, ie. $\Re[\Psi^*(\mathbf{n})\Phi_T(\mathbf{n})] = 0$ for every distribution $\Psi(\mathbf{n})$ sampled in the random walk.

We start by defining for any configurations $\mathbf{n}$ and $\mathbf{m}$ for which $|\Phi_T(\mathbf{n})| \neq 0$ the following quantity:

$$
\begin{aligned}
\mathfrak{s}_{\mathbf{mn}} &= \text{sign } \Re\left[\Phi_T^*(\mathbf{m})H_{\mathbf{mn}}\Phi_T^*(\mathbf{n})^{-1}\right] \\
&= \text{sign } \frac{\Re\left[\Phi_T^*(\mathbf{m})H_{\mathbf{mn}}\Phi_T(\mathbf{n})\right]}{|\Phi_T(\mathbf{n})|^2} = \mathfrak{s}_{\mathbf{nm}}
\end{aligned}
\tag{9.173}
$$

where $\Re$ stands for the real part and * is complex–conjugation. Now define a one–parameter family of Hamiltonians $\mathscr{H}_\gamma$ defined over configurations $\mathbf{n}$ (again such that $|\Phi_T(\mathbf{n})| \neq 0$) with off–diagonal matrix elements given by

$$
\langle \mathbf{m}|\mathscr{H}_\gamma|\mathbf{n}\rangle = \begin{cases} -\gamma\langle \mathbf{m}|H|\mathbf{n}\rangle & \mathfrak{s}(\mathbf{m},\mathbf{n}) > 0 \\ \langle \mathbf{m}|H|\mathbf{n}\rangle & \text{otherwise} \end{cases} ,
\tag{9.174}
$$

while the diagonal terms are

$$
\begin{aligned}
\langle \mathbf{n}|\mathscr{H}_\gamma|\mathbf{n}\rangle &= \langle \mathbf{n}|H|\mathbf{n}\rangle + (1+\gamma)\sum_{\substack{\mathbf{m}\neq\mathbf{n} \\ \mathfrak{s}(\mathbf{m},\mathbf{n})>0}} \mathfrak{s}(\mathbf{m},\mathbf{n}) \\
&= \langle \mathbf{n}|H|\mathbf{n}\rangle + \sum_{\mathbf{m}} h_{\mathbf{mn}}
\end{aligned}
\tag{9.175}
$$

.

In the limit where $\gamma \to -1$ we clearly recover the original Hamiltonian $\mathscr{H}_{\gamma=-1} \equiv H$. We proceed now to define a corresponding family of propagators $\mathscr{P}_\gamma$ for configurations $\mathbf{n}$ with $|\Phi_T(\mathbf{n})| \neq 0$ by

$$
\langle \mathbf{m}|\mathscr{P}_\gamma|\mathbf{n}\rangle = \delta_{\mathbf{m},\mathbf{n}} - \Delta\tau\frac{\Re\left[\Phi_T^*(\mathbf{m})\langle \mathbf{m}|\mathscr{H}_\gamma - E_T|\mathbf{n}\rangle\Phi_T(\mathbf{n})\right]}{|\Phi_T(\mathbf{n})|^2} .
\tag{9.176}
$$

It is clear now that for any $\gamma \geq 0$ we have $\langle \mathbf{m}|\mathscr{P}|\mathbf{n}\rangle \geq 0$ and so the propagator $\mathscr{P}$ is, by construction, free from the sign–problem and performing the corresponding random–walk allows us to filter the state $\Phi_T(\mathbf{n})\phi_\gamma^0(\mathbf{n})$, where now $\phi_\gamma^0(\mathbf{n})$ is the ground–state of the hamiltonian $\mathscr{H}_\gamma$. The ground–state energy E_γ obtained following this procedure is a strict upper bound for the true ground–state energy E_{gs} of the true hamiltonian H and, moreover, this upper bound is tighter than the variational upper–bound provided by $\langle \Phi_T|H|\Phi_T\rangle$. ****Include eqn. for p and g with IS. Also,should we include the proof here?****

9.5.2.1 Upper bound proof in the complex hermitian case

As shown ****in the appendix/above**** any linear extrapolation of E_γ from any two values $\gamma \geq 0$ to $\gamma = -1$ (which would correspond to the original hamiltonian) also provides an upper–bound on E_{gs} that is tighter than the individual E_γ's. A good compromise between the tightness of the upper–bound and the statistical noise in the extrapolation is to choose two values of γ: 0 and 1, thus giving the following energy estimator:

$$
E_{CIMC} = 2E_{\gamma=0} - E_{\gamma=1}
\tag{9.177}
$$

To ensure the success of the proposed method a good choice for the importance function $|\Phi_T\rangle$ is crucial, we need a wave–function flexible enough to account for the relevant correlations in the system and that at the same time can be evaluated sufficiently quickly on a computer. In many strongly–interacting systems coupled–cluster theory provide an ansatz that fulfills the first criterion.

9.5.3 Trial wave–functions from Coupled Cluster

As have been pointed out before, a crucial role is played by the importance function Φ_G used to impose the constraint. This is especially true if we want to estimate expectation values of operators other than the energy [**MIXED ESTIMATOR ref**]. Within a Fock space formulation, an excellent choice for Φ_G is given by the wave function generated in a Coupled Cluster (CC) calculation. Starting from a reference state, which usually is the Hartree-Fock solution of the problem, CC theory allows to include dynamical correlations into a new state

$$|Psi_{CC}\rangle = e^{\hat{T}}|\Phi_{HF}\rangle. \tag{9.178}$$

In the above equation, correlations are introduced trough the excitation operator $\hat{T}$ which in CC theory is hierarchically divided as $\hat{T} = \hat{T}_1 + \hat{T}_2 + \hat{T}_3 + \cdots$ counting the number of creation/annihilation operators that compose them. The firt two terms are:

$$\hat{T}_1 = \sum_{ia} t_i^a a_a^\dagger a_i \quad \hat{T}_2 = \frac{1}{4}\sum_{ijab} t_{ij}^{ab} a_a^\dagger a_b^\dagger a_i a_j \quad \cdots \tag{9.179}$$

A fundamental prerequisite for a viable importance function, other than being accurate for the problem at hand, is the possibility to evaluate efficiently its overlap with an arbitrary element of the Hilbert space we are exploring during the random walk. To set the notation, we will express a generic Slater-Determinant state describing an M-particle–M-hole state as

$$|\mathbf{m}\rangle = a_{p_1}^\dagger \ldots, a_{p_M}^\dagger a_{h_1} \ldots, a_{h_M}|\Phi_{HF}\rangle \equiv |\Phi_{h_1,\ldots,h_M}^{p_1,\ldots,p_M}\rangle. \tag{9.180}$$

In order to simplify the discussion we will focus here on the case of a homogeneous system that can be described dropping the one-particle–one-hole excitation operator $\hat{T}_1$ in the expansion (which do not contribute due to translational inveriance)[4]. In this situation the lowest order of CC theory is the Coupled Cluster Doubles (CCD) approximation.

The required amplitude can then be expressed as a superposition of $M-2$ particle/hole states that can be generated from $\mathbf{m}$. Eventually (the proof is tedious but straightforward) one obtains:

$$\langle\mathbf{m}|\Phi_{CCD}\rangle = \sum_{\gamma=2}^{M}\sum_{\mu<\nu}^{M}(-1)^{\gamma+\mu+\nu}t_{h_1,h_\gamma}^{p_\mu p_\nu}\Phi_{CCD}^{M-2}\binom{p_1,p_2,\ldots,p_{\mu-1},p_{\mu+1},\ldots,p_{\nu-1},p_{\nu+1},\ldots,p_M}{h_2\ldots,h_{\gamma-1},h_{\gamma+1},\ldots,h_M} \tag{9.181}$$

assuming $p_1 < p_2 < \cdots < p_M$ and $h_1 < h_2 < \cdots < h_M$. The normalization is fixed in such a way that $\langle\Phi_{HF}|\Phi_{CCD}\rangle = 1$.

Within CC theory the coefficients t_{ij}^{ab} appearing in the previous equations are to be obtained as the self–consistent solutions of the following non–linear equation:

$$\langle\Phi_{ij}^{ab}|\hat{H}\left(1+\hat{T}_2+\frac{1}{2}\hat{T}_2^2\right)|\Phi_{HF}\rangle = \left(\frac{1}{4}\sum_{ijab}\langle ij||ab\rangle t_{ij}^{ab}\right)t_{ij}^{ab} \tag{9.182}$$

---

[4] Extension to singlets (p-h states) and triplets (3p-3h states) is simple

where $\langle ij||ab\rangle \equiv V_{ijab} - V_{ijba}$ are the anti–symmetrized two–body matrix elements of the inter-action (cf. Eq. (**??**)).

Solving Eq. (9.182) is in general a very expensive computational problem and within the fixed–node approach all that matters are the signs in Eq. (**??**). It could then be possible to find cheaper approximate ways to determine the doubles coefficients t_{ij}^{ab} while still preserving a good quality in the fixed–node approximation. A quite precise and very cheap approximation that have been used successfully is to obtain the coefficients within second order Moeller–Plesset perturbation theory:

$$t_{ij}^{ab} = \frac{\langle ij||ab\rangle}{\eta_i + \eta_j - \eta_a - \eta_b} \quad \text{with} \quad \eta_i = \varepsilon_i + \sum_k \langle ik||ik\rangle. \tag{9.183}$$

This is equivalent to truncating the self–consistent solution of (9.182) after the first iteration.

9.5.3.1 Efficient recursive evaluation of CCD wave-function

9.5.4 Propagator sampling with no time-step error

As we pointed out before, in simulations employing the linear propagator (**??**) raising the dimension of the basis set has a detrimental effect on the efficiency of the algorithm since in order to satisfy the bound Eq. (9.171) we are forced to employ an exceedingly small time step. Moreover, in practice values of τ much smaller than the maximum value are usually employed due to the difficulty in obtaining reliable estimates of E_{max} in realistic situations.

To further complicate the scenario, when lattice fixed–node methods are employed (ie. diagonal–dumping) this maximum value is reduced even further because the diagonal matrix elements of P gets pushed towards the negative region by the addition of the sign–violating contributions. If this method is used to control the sign–problem additional care has to be devoted in the choice of the time–step, greatly deteriorating the efficiency of the overall scheme.

In discrete space however we can cope with the problem by using an algorithm firstly introduced by Trivedi and Ceperley [**?**], which shares similarities with the Domains Green's Function Monte Carlo by Kalos, Levesque, and Verlet [**?**]. The idea is to use directly (meaning sample from) the exponential propagator

$$P^e(\tau, \mathbf{m}, \mathbf{n}) = \langle \mathbf{m}|e^{-\tau(H-E_T)}|\mathbf{n}\rangle, \tag{9.184}$$

that clearly has no problem with negative diagonal elements. These schemes usually come with the name of *continuous–time* evolution.

For simplicity let us forget the sign–problem for the time being and imagine we are working with the fixed–node importance–sampled greens function (9.176) with $\gamma = 0$ (and the corresponding Hamiltonian $\tilde{H}$) in order to avoid such problems, i.e. we will assume that $\tilde{H}_{\mathbf{m},\mathbf{n}} \leq 0 \forall \mathbf{m} \neq \mathbf{n}$. Furthermore, we will neglect the energy shift E_T since its addition is straight-forward.

Recall that the Green's function can be written as a product of a stochastic matrix $\tilde{p}_{\mathbf{m},\mathbf{n}}$ and a weight factor $\tilde{b}_{\mathbf{n}}$ (see Sect.):

$$\tilde{G}_{\mathbf{m},\mathbf{n}}(\Delta\tau) = \delta_{\mathbf{m},\mathbf{n}} - \Delta\tau\tilde{H}_{\mathbf{m},\mathbf{n}} = \tilde{p}_{\mathbf{m},\mathbf{n}}\tilde{g}_{\mathbf{n}} \tag{9.185}$$

where the two factors are given by:

$$\tilde{p}_{\mathbf{m},\mathbf{n}} = \frac{\tilde{G}_{\mathbf{m},\mathbf{n}}(\Delta\tau)}{\tilde{b}_{\mathbf{n}}},$$

$$\tilde{g}_{\mathbf{n}} = \sum_{\mathbf{m}} \tilde{G}_{\mathbf{m},\mathbf{n}}(\Delta\tau) \tag{9.186}$$

$$= 1 - \Delta\tau E_L(\mathbf{n})$$

and in the last equation we have used the expression for the local energy

$$E_L(\mathbf{n}) = \frac{\langle\Phi_T|H|\mathbf{n}\rangle}{\Phi_T|\mathbf{n}\rangle} = \sum_{\mathbf{m}} \frac{\langle\Phi_T|\mathbf{m}\rangle\langle\mathbf{m}|H|\mathbf{n}\rangle}{\Phi_T|\mathbf{n}\rangle} \equiv \sum_{\mathbf{m}} \tilde{H}_{\mathbf{m},\mathbf{n}}. \tag{9.187}$$

The continuous–time limit is recovered by applying M times $\tilde{G}(\Delta\tau)$ and letting $\Delta\tau \to 0$ while preserving constant the product $\tau = M\Delta\tau$:

$$\tilde{G}_{\mathbf{m},\mathbf{n}}(\tau) = \lim_{M\to\infty} \left(1 - \frac{\tau}{M}\tilde{H}_{\mathbf{m},\mathbf{n}}\right)^M$$

$$= \lim_{\Delta\tau\to 0} \left(1 - \Delta\tau\tilde{H}_{\mathbf{m},\mathbf{n}}\right)^{\frac{\tau}{\Delta\tau}} \tag{9.188}$$

$$= \langle\mathbf{m}|e^{-\tau\tilde{H}}|\mathbf{n}\rangle = P^e(\tau,\mathbf{m},\mathbf{n}).$$

Now note that if we let $\Delta\tau \to 0$ then the probability to make a diagonal move in a single step among the M will accordingly go to ≈ 1, in fact:

$$P_{diag} = \frac{\tilde{G}_{\mathbf{n},\mathbf{n}}(\Delta\tau)}{\tilde{b}_{\mathbf{n}}}$$

$$= \frac{1 - \Delta\tau\tilde{H}_{\mathbf{n},\mathbf{n}}}{1 - \Delta\tau E_L(\mathbf{n})} \tag{9.189}$$

$$\xrightarrow{\Delta\tau\to 0} 1$$

since the local–energy E_L does not depend on the time step but just on the current configuration $\mathbf{n}$. Accordingly, the probability of making K consecutive diagonal moves will be:

$$P_{diag}^K = \left(\frac{\tilde{G}_{\mathbf{n},\mathbf{n}}(\Delta\tau)}{\tilde{g}_{\mathbf{n}}}\right)^K = \left(\frac{1 - \Delta\tau\tilde{H}_{\mathbf{n},\mathbf{n}}}{1 - \Delta\tau E_L(\mathbf{n})}\right)^K \tag{9.190}$$

$$\xrightarrow{K\to\infty} e^{\tau(E_L(\mathbf{n})-\tilde{H}_{\mathbf{n},\mathbf{n}})} \equiv e^{-\tau\tilde{H}_{\mathbf{n}}^{off}} = f_{\mathbf{n}}(\tau)$$

where we have implicitly defined the off–diagonal sum

$$\tilde{H}_{\mathbf{n}}^{off} = \sum_{\mathbf{m}\neq\mathbf{n}} \tilde{H}_{\mathbf{m},\mathbf{n}} < 0.$$

Therefore the elapsed time between consecutive off–diagonal moves is distributed as an exponential distribution $f_{\mathbf{n}}(\tau)$ with average time given by

$$\int_0^\infty \tau f_{\mathbf{n}}(\tau) = -\frac{1}{\tilde{H}_{\mathbf{n}}^{off}} = \left|\frac{1}{\tilde{H}_{\mathbf{n}}^{off}}\right|. \tag{9.191}$$

We can then sample the time when the off-diagonal move happens by using a transformation technique: suppose we have a way to sample values ξ from a uniform distribution $g(\xi) = $ const, due to conservation of probability the samples τ drawn from the wanted $f_{\mathbf{n}}(\tau)$ will satisfy:

$$|f(\tau)d\tau| = |g(\xi)d\xi| \quad\longrightarrow\quad \left|\frac{d\xi(\tau)}{d\tau}\right| = f_{\mathbf{n}}(\tau) \tag{9.192}$$

where τ are the samples drawn from the wanted PDF $f_{\mathbf{n}}$. By solving now equation (9.192) for $\xi(\tau)$ and performing the inversion to $\tau = \tau(\xi)$ we obtain the following relation

$$\tau_\xi = \frac{log(\xi)}{\tilde{H}_{\mathbf{n}}^{off}}. \tag{9.193}$$

that allows to sample exactly from $f_{\mathbf{n}}$ using only samples from a uniform distribution $\xi \in (0,1)$.

Walkers undergoing such random walk accumulate weight during the K diagonal–moves as well as from performing the off–diagonal step. The weight coming from the diagonal moves is given by

$$w_{\mathbf{n}} = \tilde{g}_{\mathbf{n}}^K = (1 - \Delta\tau E_L(\mathbf{n}))^K \xrightarrow{\Delta\tau \to 0} e^{-\tau E_L(\mathbf{n})}. \tag{9.194}$$

For the off–diagonal moves instead we can either sample $\mathbf{m}$ from the normalized probability $P_1(\mathbf{m},\mathbf{n}) = \tilde{H}_{\mathbf{m},\mathbf{n}}/\tilde{H}_{\mathbf{n}}^{off}$ using for instance a heat–bath algorithm, and in this case the off–diagonal weight would be $w_{\mathbf{m},\mathbf{n}} = 1$, or we can sample off–diagonal moves using a uniform probability $P_2(\mathbf{m},\mathbf{n}) = 1/N_{conn}$, where N_{conn} is the number of connected state to the starting point $\mathbf{n}$, and then reweight the walker with $w_{\mathbf{m},\mathbf{n}} = P_1(\mathbf{m},\mathbf{n})/P_2(\mathbf{m},\mathbf{n})$. In our current implementation we have used the first of these options.

Furthermore, in order for the measurements along the path to be unbiased we want to define equidistant "time–slices" along the random walk, in order to this we simply choose a target time–step τ_t at the beginning then for each move we first sample a value of τ_ξ from (9.193), if $\tau_\xi > \tau_t$ we set $\tau = \tau_t$ and use correspondingly a diagonal move if instead $\tau_\xi < \tau_t$ we have to sample an off–diagonal move. The process is preformed until the sum of all the sampled τ_ξ reaches the target time τ_t.

The final algorithm is then as follows:

for walker $w = 1, N_w$ **do**
    Accept_reject()
    $\xi = \text{rand}()$
    if acc $> \xi$ **then**
        $R_[i][j] \leftarrow R_{new}[i][j]$
    end if
end for

1. starting from state x, sample a time–step τ_ξ from (9.193)
2. if $\tau_\xi > \tau_t$, apply the diagonal weight $w_{\mathbf{n}} = e^{-\tau_t E_L(\mathbf{n})}$ and exit (go to next walker)
3. apply diagonal weight $w_{\mathbf{n}} = e^{-\tau_\xi E_L(\mathbf{n})}$
4. choose a new state $\mathbf{m} \neq \mathbf{n}$ according to $P_1(\mathbf{m},\mathbf{n}) = \tilde{H}_{\mathbf{m},\mathbf{n}}/\tilde{H}_{\mathbf{n}}^{off}$
5. move walker to state $\mathbf{m}$, the time remaining becomes $\tau_t - \tau_\xi \to \tau_t$, replace $\mathbf{n}$ with $\mathbf{m}$ and repeat from 1

The basic idea is to use the limiting case discussed in Eq. (**??**). The idea is to first consider the probability of making K consecutive diagonal moves ($\mathbf{n} \to \mathbf{n}$) :

$$P_{diag}^K(\mathbf{n}) = p(\mathbf{n},\mathbf{n})^K, \tag{9.195}$$

which in the limit $\Delta\tau \to 0$ goes to

$$P_{diag}^K(\mathbf{n}) \to e^{-K\Delta\tau \sum_{\mathbf{m} \neq \mathbf{n}} \langle \mathbf{m}|H - E_T|\mathbf{n}\rangle} \tag{9.196}$$

We see then that the time elapsed between consecutive off-diagonal moves, $K\Delta\tau$, is distributed according to a truncated exponential distribution (the distribution is truncated because $K \leq M$). [**maybe include algorithm for this**] A prectical way to obtain this is set a target time-step $\delta\tau$ and sample a time $\delta\tau_{od}$ for the off–diagonal move. If $\delta\tau < \delta\tau_{od}$ no off–

digonal move happened for the entire time span of $\delta\tau$ and the state gets re-weighted by $e^{-\delta\tau\sum_{\mathbf{m}\neq\mathbf{n}}\langle\mathbf{m}|H-E_T|\mathbf{n}\rangle}$. If instead, we have $\delta\tau > \delta\tau_{od}$ an off–diagonal move is performed selecting a new state $|\mathbf{n}'\rangle$ from the probability

$$\frac{\langle\mathbf{n}'|H-E_T|\mathbf{n}\rangle}{\sum_{\mathbf{m}\neq\mathbf{n}}\langle\mathbf{m}|H-E_T|\mathbf{n}\rangle} \tag{9.197}$$

This process is then repeated by setting $\delta\tau \leftarrow \delta\tau - \delta\tau_{od}$ and $\mathbf{n} \leftarrow \mathbf{n}'$ until $\delta\tau < \delta\tau_{od}$. This procedure defined above exactly samples:

$$\langle\mathbf{m}|\mathscr{P}|\mathbf{n}\rangle = \langle\mathbf{m}|e^{-\Delta\tau(H-E_T)}|\mathbf{n}\rangle \tag{9.198}$$

without any time-step error. The computational bottelneck of this approach is the off-diagonal sum in Eq. (9.196) and this has historically limited a wide-spread application of the algorithm, however recently [**cite brand new Cyrus paper and Clark & Koludrubez**] efficient approximations are being explored with some success. When used together with the fixed–node approximation this off–diagonal sums are need anyway and we usually employ this directly

Chapter 10
In-medium SRG approaches to infinite nuclear matter

Scott K. Bogner, Heiko Hergert, Justin Leitz, Titus Morris, Sam Novario, Nathan Parzuchowski, and Fei Yuan

Abstract We present a comprehensive review of the In-Medium Similarity Renormalization Group (IM-SRG), a novel *ab inito* method for nuclei. The IM-SRG employs a continuous unitary transformation of the many-body Hamiltonian to decouple the ground state from all excitations, thereby solving the many-body problem. Starting from a pedagogical introduction of the underlying concepts, the IM-SRG flow equations are developed for systems with and without explicit spherical symmetry. We study different IM-SRG generators that achieve the desired decoupling, and how they affect the details of the IM-SRG flow. Based on calculations of closed-shell nuclei, we assess possible truncations for closing the system of flow equations in practical applications, as well as choices of the reference state.

Scott Bogner

Department of Physics and Astronomy and National Superconducting Cyclotron Laboratory, Michigan State University, East Lansing, Michigan USA, e-mail: `bogner@nscl.msu.edu`,

Heiko Hergert

Department of Physics and Astronomy and National Superconducting Cyclotron Laboratory, Michigan State University, East Lansing, Michigan USA, e-mail: `hergert@nscl.msu.edu`,

Justin G. Lietz

Department of Physics and Astronomy and National Superconducting Cyclotron Laboratory, Michigan State University, East Lansing, Michigan, USA, e-mail: `lietz@nscl.msu.edu`,

Titus Morris

Department of Physics and Astronomy and National Superconducting Cyclotron Laboratory, Michigan State University, East Lansing, Michigan USA, e-mail: `morrist@nscl.msu.edu`,

Samuel Novario

Department of Physics and Astronomy and National Superconducting Cyclotron Laboratory, Michigan State University, East Lansing, Michigan, USA, e-mail: `novarios@nscl.msu.edu`,

Nathan Parzuchowski

Department of Physics and Astronomy and National Superconducting Cyclotron Laboratory, Michigan State University, East Lansing, Michigan USA, e-mail: `parzuchowski@frib.msu.edu`,

Fei Yuan

Department of Physics and Astronomy and National Superconducting Cyclotron Laboratory, Michigan State University, East Lansing, Michigan USA, e-mail: `yuan@nscl.msu.edu`

10.1 Introduction

10.2 IM-SRG Flow Equations

10.2.1 Preliminaries

The Similarity Renormalization Group (SRG) was first formulated by Wegner [**?**] and Glazek and Wilson [**?**] to study condensed matter systems and light-front quantum field theories, respectively. From a mathematical point of view, the philosophy behind the SRG is to render the Hamiltonian $H(s)$ diagonal via a continuous unitary transformation

$$H(s) = U(s)H(0)U^{\dagger}(s) \,, \tag{10.1}$$

where $H(s = 0)$ is the starting Hamiltonian and s denotes the so-called flow parameter, for reasons that will become apparent shortly. In practice, the demand for strict diagonality is usually relaxed to requiring band- or block-diagonality of the Hamiltonian matrix in a chosen basis, e.g., in relative momentum or harmonic oscillator (HO) spaces. These specific cases are realized in nuclear physics applications, where the SRG is used to decouple momentum or energy scales, and thereby render the nuclear Hamiltonian more suitable for *ab initio* many-body calculations [**?**, **?**, **?**, **?**].

With the IM-SRG, we want to use this strategy to solve the many-body problem directly. Taking the derivative of Eq. (10.1) with respect to the flow parameter s, we obtain the operator flow equation

$$\frac{d}{ds}H(s) = [\eta(s), H(s)] \,, \tag{10.2}$$

where the generator $\eta(s)$ is related to the unitary transformation $U(s)$ by

$$\eta(s) = \frac{dU(s)}{ds}U^{\dagger}(s) = -\eta^{\dagger}(s) \,. \tag{10.3}$$

By rearranging this relation, we obtain a differential equation for $U(s)$ whose formal solution is given by the *path-* or *S-ordered* exponential

$$U(s) = \mathscr{S} \exp \int_{0}^{s} ds' \eta(s') \,. \tag{10.4}$$

We leave $\eta(s)$ unspecified for now and defer the discussion of suitable choices to Sec. 10.3.

Naively, one could try to solve the flow equation (10.2) by choosing a suitable basis of the many-body Hilbert space and turning Eq. (10.2) into a matrix differential equation, but such an approach would ultimately amount to a diagonalization of the many-body Hamiltonian. To make matters worse, implementing the flow means we would deal with the Hamiltonian's full spectrum rather than just some extremal eigenvalues that can be extracted efficiently in state-of-the-art, large-scale Lanczos approaches like the NCSM [**?**, **?**].

For the IM-SRG, we follow a different route, and formulate the flow equation as well as the decoupling conditions underlying the definition of $\eta(s)$ in the language of second quantization. This approach has been very successful in producing powerful and numerically efficient many-body schemes, chief among them the CC method (see, e.g., [**?**, **?**, **?**, **?**]).

10.2.2 Normal Ordering and Wick's Theorem

Let us consider the usual fermionic creation and annihilation operators, $a_i^\dagger$ and a_i, with

$$\{a_i^\dagger, a_j^\dagger\} = \{a_i, a_j\} = 0, \quad \{a_i^\dagger, a_j\} = \delta_{ij}. \tag{10.5}$$

The indices are collective labels for the quantum numbers of the single-particle states. Using these operators, we can construct a representation of any A-body operator, and a complete basis for the A-body Hilbert space is obtained by acting with products of $a_i^\dagger$ on the particle vacuum,

$$|\Phi\{i_1 \ldots i_A\}\rangle = \prod_{k=1}^{A} a_{i_k}^\dagger |0\rangle. \tag{10.6}$$

The states $|\Phi\{i_1 \ldots i_A\}\rangle$ are simple A-particle Slater determinants.

When we consider an actual A-body nucleus, it is inefficient to work with the basis states (10.6) because of the existence of characteristic energy and momentum scales. The low-lying excitation spectrum is dominated by excitations of particles in the vicinity of the Fermi level, and the coupling between states, particularly between the ground state and excitations, is suppressed if their energies differ by much more than the characteristic energy $\hbar^2 \lambda^2 / 2m$ associated with the nuclear interaction's resolution scale λ. Typical values for λ are on the order of $3 - 4 \, \text{fm}^{-1}$ for interactions from chiral EFT [?], or lower after softening with the free-space SRG [?]. For such interactions, we can find a single Slater determinant $|\Phi\rangle$ that is a fair approximation to the nucleus' ground state, and use $|\Phi\rangle$ rather than the particle vacuum $|0\rangle$ as a reference state to construct a complete many-body basis.

To account for the fact that $|\Phi\rangle$ is an A-particle state, we introduce normal-ordered operators by defining

$$a_i^\dagger a_j \equiv \, :a_i^\dagger a_j: + \overbracket{a_i^\dagger a_j}, \tag{10.7}$$

where the contraction is the expectation value of the operator in the reference state $|\Phi\rangle$:

$$\overbracket{a_i^\dagger a_j} \equiv \langle \Phi | a_i^\dagger a_j | \Phi \rangle \equiv \rho_{ji}. \tag{10.8}$$

By definition, the contractions are identical to the elements of the one-body density matrix of $|\Phi\rangle$ [?]. A normal-ordered A-body operator is now defined recursively by evaluating all contractions between creation and annihilation operators:

$$\begin{aligned}
&a_{i_1}^\dagger \ldots a_{i_A}^\dagger a_{j_A} \ldots a_{j_1} \\
&\equiv \, :a_{i_1}^\dagger \ldots a_{i_A}^\dagger a_{j_A} \ldots a_{j_1}: \\
&\quad + \overbracket{a_{i_1}^\dagger a_{j_1}} :a_{i_2}^\dagger \ldots a_{i_A}^\dagger a_{j_A} \ldots a_{j_2}: - \overbracket{a_{i_1}^\dagger a_{j_2}} :a_{i_2}^\dagger \ldots a_{i_A}^\dagger a_{j_A} \ldots a_{j_3} a_{j_1}: + \text{singles} \\
&\quad + \left(\overbracket{a_{i_1}^\dagger a_{j_1}} \overbracket{a_{i_2}^\dagger a_{j_2}} - \overbracket{a_{i_1}^\dagger a_{j_2}} \overbracket{a_{i_2}^\dagger a_{j_1}} \right) :a_{i_3}^\dagger \ldots a_{i_A}^\dagger a_{j_A} \ldots a_{j_3}: + \text{doubles} \\
&\quad + \ldots + \text{full contractions}, \tag{10.9}
\end{aligned}$$

where we have used quantum chemistry parlance (singles, doubles, etc.) for the number of contractions in a term. Note that the shown double contraction corresponds to the factorization formula for the two-body density matrix of a Slater determinant,

$$\rho_{j_1 j_2 i_1 i_2} \equiv \langle \Phi | a_{i_1}^\dagger a_{i_2}^\dagger a_{j_2} a_{j_1} | \Phi \rangle = \rho_{i_1 j_1} \rho_{i_2 j_2} - \rho_{i_1 j_2} \rho_{i_2 j_1}. \tag{10.10}$$

From Eq. (10.7), it is evident that $\langle \Phi | :a_i^\dagger a_j: | \Phi \rangle$ must vanish, and this is readily generalized for the expectation values of general normal-ordered operators in the reference state $|\Phi\rangle$,

$$\langle \Phi | :a_{i_1}^\dagger \ldots a_{i_1} : |\Phi\rangle = 0\,, \tag{10.11}$$

which facilitates calculations of operator matrix elements in a space spanned by all possible excitations of $|\Phi\rangle$. Even more useful is Wick's theorem (see e.g. [?]), which is a direct consequence of Eq. (10.9) and allows us to expand products of normal-ordered operators:

$$
\begin{aligned}
&:a_{i_1}^\dagger \ldots a_{i_N}^\dagger a_{j_N} \ldots a_{j_1} ::a_{k_1}^\dagger \ldots a_{k_M}^\dagger a_{l_M} \ldots a_{l_1} : \\
&= (-1)^{M\cdot N} :a_{i_1}^\dagger \ldots a_{i_N}^\dagger a_{k_1}^\dagger \ldots a_{k_M}^\dagger a_{j_N} \ldots a_{j_1} a_{l_M} \ldots a_{l_1} : \\
&\quad + (-1)^{M\cdot N} \overline{a_{i_1}^\dagger a_{l_1}} :a_{i_2}^\dagger \ldots a_{k_M}^\dagger a_{j_N} \ldots a_{l_2} : \\
&\quad + (-1)^{(M-1)(N-1)} \overline{a_{j_N} a_{k_1}^\dagger} :a_{i_1}^\dagger \ldots a_{k_M}^\dagger a_{j_N} \ldots a_{j_2} : \\
&\quad + \text{singles} + \text{doubles} + \ldots .
\end{aligned}
\tag{10.12}
$$

Here, the phases appear because we anti-commute the $a_k^\dagger$ operators past the a_j, and we encounter a new type of contraction,

$$\overline{a_i a_j^\dagger} \equiv \langle \Phi | a_i a_j^\dagger |\Phi\rangle = \delta_{ij} - \rho_{ij}\,, \tag{10.13}$$

as expected from the basic fermionic anti-commutator algebra. The important feature of Eq. (10.12) is that only contractions between one index from each of the two strings appear in the expansion, because contractions between indices within a single normal-ordered string vanish by construction. This leads to a substantial reduction of terms in practical calculations. Another immediate consequence of Wick's theorem is that a product of normal-ordered M and N-body operators has the general form

$$A^M B^N = \sum_{k=|M-N|}^{M+N} C^{(k)}\,. \tag{10.14}$$

10.2.3 Normal-Ordered Hamiltonian

Let us now consider an intrinsic nuclear A-body Hamiltonian containing both NN and 3N interactions,

$$H = \left(1 - \frac{1}{A}\right)T + T^{(2)} + V^{(2)} + V^{(3)}\,, \tag{10.15}$$

where the one- and two-body kinetic energy terms are

$$T \equiv \sum \frac{p_i^2}{2m}\,, \tag{10.16}$$

$$T^{(2)} \equiv -\frac{1}{Am}\sum_{i<j} p_i \cdot p_j \tag{10.17}$$

(see Sec. ?? and Ref. [?]). Choosing a single Slater determinant $|\Phi\rangle$ as the reference state, we can rewrite the Hamiltonian *exactly* in terms of normal-ordered operators,

$$H = E + \sum_{ij} f_{ij} :a_i^\dagger a_j: + \frac{1}{4}\sum_{ijkl} \Gamma_{ijkl} :a_i^\dagger a_j^\dagger a_l a_k: + \frac{1}{36}\sum_{ijklmn} W_{ijklmn} :a_i^\dagger a_j^\dagger a_k^\dagger a_n a_m a_l:\,, \tag{10.18}$$

where the labels for the individual contributions have been chosen for historical reasons. For convenience, we will work in the eigenbasis of the one-body density matrix in the following,

so that

$$\rho_{ab} = n_a \delta_{ab}, \quad n_a \in \{0, 1\}. \tag{10.19}$$

The individual normal-ordered contributions in Eq. (10.18) are then given by

$$E = \left(1 - \frac{1}{A}\right) \sum_a \langle a | T | a \rangle n_a + \frac{1}{2} \sum_{ab} \langle ab | T^{(2)} + V^{(2)} | ab \rangle n_a n_b$$
$$+ \frac{1}{6} \sum_{abc} \langle abc | V^{(3)} | abc \rangle n_a n_b n_c, \tag{10.20}$$

$$f_{12} = \left(1 - \frac{1}{A}\right) \langle 1 | T | 2 \rangle + \sum_a \langle 1a | T^{(2)} + V^{(2)} | 2a \rangle n_a$$
$$+ \frac{1}{2} \sum_{ab} \langle 1ab | V^{(3)} | 2ab \rangle n_a n_b, \tag{10.21}$$

$$\Gamma_{1234} = \langle 12 | T^{(2)} + V^{(2)} | 34 \rangle + \sum_a \langle 12a | V^{(3)} | 34a \rangle n_a, \tag{10.22}$$

$$W_{123456} = \langle 123 | V^{(3)} | 456 \rangle. \tag{10.23}$$

Due to the occupation numbers in Eqs. (10.20)–(10.22), the sums run over occupied (hole) states only. Note that the zero-, one-, and two-body parts of the Hamiltonian all contain in-medium contributions from the free-space 3N interaction.

10.2.4 *M-Scheme Flow Equations*

After discussing normal ordering and Wick's theorem in the previous sections, we are now ready to turn back to the operator flow equation, Eq. (10.2).

When carried out exactly, the IM-SRG is a continuous unitary transformation in A-body space, and consequently, $\eta(s)$ and $H(s)$ are A-body operators even if they initially have a lower rank at $s = 0$. From the discussion of the previous sections, we see that every evaluation of the commutator on the right-hand side of Eq. (10.2) increases the particle rank of $H(s)$, e.g.,

$$[:a_a^\dagger a_b^\dagger a_d a_c:, :a_i^\dagger a_j^\dagger a_l a_k:] = \delta_{ci} :a_a^\dagger a_b^\dagger a_j^\dagger a_l a_k a_d: + \dots. \tag{10.24}$$

All of these induced contributions will in turn contribute to the parts of $H(s)$ with lower particle rank in subsequent integration steps. Because an explicit treatment of all contributions up to the A-body level is clearly not feasible, we have to introduce a truncation to close the system of IM-SRG flow equations. We follow a simple approach, and truncate $\eta(s)$ and $H(s)$ at a given particle rank $n \leq A$, which is motivated by the cluster decomposition principle for short-range interactions (see, e.g., [?]). For $n = 2$, this yields the so-called IM-SRG(2) truncation, our primary truncation scheme in past works [?, ?, ?], which will serve as the basis of the discussion in the remainder of this work. On occasion, we will also consider the next truncation in the hierarchy, denoted IM-SRG(3). The corresponding flow equations are given in Appendix **??**, but they have not been used in numerical calculations because of the computational demands associated with handling three-body operators.

Let us assume, then, that for each flow parameter s

$$H(s) \approx E(s) + f(s) + \Gamma(s), \tag{10.25}$$

$$\eta(s) \approx \eta^{(1)}(s) + \eta^{(2)}(s). \tag{10.26}$$

We introduce the permutation symbol P_{ij} to interchange the attached indices in any expression, i.e.,

$$P_{ij}g(\ldots,i,\ldots,j) \equiv g(\ldots,j,\ldots,i), \tag{10.27}$$

and use the fundamental commutators from Appendix **??** to obtain

$$\frac{dE}{ds} = \sum_{ab}(n_a - n_b)\eta_{ab}f_{ba} + \frac{1}{2}\sum_{abcd}\eta_{abcd}\Gamma_{cdab}n_a n_b \bar{n}_c \bar{n}_d, \tag{10.28}$$

$$\frac{df_{12}}{ds} = \sum_{a}(1+P_{12})\eta_{1a}f_{a2} + \sum_{ab}(n_a-n_b)(\eta_{ab}\Gamma_{b1a2}-f_{ab}\eta_{b1a2})$$
$$+ \frac{1}{2}\sum_{abc}(n_a n_b \bar{n}_c + \bar{n}_a \bar{n}_b n_c)(1+P_{12})\eta_{c1ab}\Gamma_{abc2}, \tag{10.29}$$

$$\frac{d\Gamma_{1234}}{ds} = \sum_{a}\{(1-P_{12})(\eta_{1a}\Gamma_{a234}-f_{1a}\eta_{a234}) - (1-P_{34})(\eta_{a3}\Gamma_{12a4}-f_{a3}\eta_{12a4})\}$$
$$+ \frac{1}{2}\sum_{ab}(1-n_a-n_b)(\eta_{12ab}\Gamma_{ab34}-\Gamma_{12ab}\eta_{ab34})$$
$$- \sum_{ab}(n_a-n_b)(1-P_{12})(1-P_{34})\eta_{b2a4}\Gamma_{a1b3}, \tag{10.30}$$

where $\bar{n}_i = 1 - n_i$, and the s-dependence has been suppressed for brevity. To obtain ground-state energies, we integrate Eqs. (10.28)–(10.30) from $s = 0$ to $s \to \infty$, starting from the initial components of the normal-ordered Hamiltonian (Eqs. (10.20)–(10.22)).

As we will discuss in more detail in Sec. **??**, Eqs. (10.28)–(10.30) can easily be translated into Goldstone or Hugenholtz diagrams for the flowing Hamiltonian $H(s)$. This provides us with an intuitive understanding of the mechanism through which the IM-SRG is non-perturbatively re-summing the many-body expansion. The second and third rows of Eq. (10.30), in particular, re-sum pp/hh-ladder and ph-ring diagrams, respectively. Due to the use of $H(s)$, ladder-ring interference diagrams are generated in the limit $s \to \infty$, and therefore the IM-SRG(2) goes beyond the more traditional Brueckner G-matrix or Random-Phase Approximation-type summations [**?**,**?**,**?**]. Furthermore, the commutator structure of Eq. (10.2) ensures that the IM-SRG is size-extensive, and only connected diagrams are generated and re-summed by the IM-SRG flow [**?**,**?**]. This property is preserved even if the commutators are truncated at a given operator rank, as in the IM-SRG(2) case presented here.

From Eqs. (10.28)–(10.30), it is clear that the computational effort for solving the IM-SRG(2) flow equations is dominated by the two-body flow equation, which scales polynomially like $\mathcal{O}(N^6)$ with the single-particle basis size N. This puts the IM-SRG(2) in the same category as other numerically efficient non-perturbative methods[1] like Coupled Cluster with Singles and Doubles (CCSD) [**?**,**?**], the Self-Consistent Green's Function Approach (SCGF) [**?**,**?**,**?**], or canonical transformation theory [**?**,**?**].

---

[1] The mentioned methods can make use of the distinction between particle and hole states in the single-particle basis to further reduce the effort. For instance, the amplitude equations of CCSD can be solved at $\mathcal{O}(N_h^2 N_p^4)$ cost, where typically the number of hole states N_h is much smaller than the number of particle states $N_p \sim N$. Note that the construction of the CCSD effective Hamiltonian from the amplitudes requires $\mathcal{O}(N^6)$ effort. In the IM-SRG(2), we are working directly with the analogous effective Hamiltonian.

10.2.5 J-Scheme Flow Equations

When the nuclear Hamiltonian is normal-ordered with respect to a general reference state, its manifest symmetries may become hidden and implicitly reliant on cancellations which are spoiled by the introduction of finite bases or other truncations. For systems with explicit spherical symmetry, e.g., for closed-shell nuclei, we can use a spherically symmetric $|\Phi\rangle$, and preserve the manifest rotational symmetry of H on a term-by-term basis. In this case, the flow equations become block-diagonal in angular momentum, and independent of the angular momentum projection quantum numbers, which leads to a significant reduction in numerical effort.

In the following, the single-particle indices collectively represent the radial, angular momentum, and isospin quantum numbers $i = (k_i l_i j_i \tau_i)$. Then the matrix elements of single-particle operators are diagonal in all but the radial quantum numbers, e.g.,

$$f_{12} = f_{k_1 k_2}^{l_1 j_1 \tau_1} \delta_{l_1 l_2} \delta_{j_1 j_2} \delta_{\tau_1 \tau_2}. \tag{10.31}$$

Likewise, two-body matrix elements are diagonal in total two-body angular momentum J and independent of M. In this case, the IM-SRG(2) flow equations reduce to

$$\frac{dE}{ds} = \sum_{ab} \hat{j}_a^2 \eta_{ab} f_{ba} (n_a - n_b) + \frac{1}{2} \sum_{abcdJ} \hat{J}^2 \eta_{abcd}^J \Gamma_{cdab}^J n_a n_b \bar{n}_c \bar{n}_d, \tag{10.32}$$

$$\frac{df_{12}}{ds} = \sum_a (1 + P_{12}) \eta_{1a} f_{a2} + \frac{1}{\hat{j}_1^2} \sum_{abJ} \hat{J}^2 (n_a - n_b) \left(\eta_{ab} \Gamma_{b1a2}^J - f_{ab} \eta_{b1a2}^J \right)$$

$$\qquad + \frac{1}{2\hat{j}_1^2} \frac{1}{2} \sum_{abcJ} \hat{J}^2 \left(n_a n_b \bar{n}_c + \bar{n}_a \bar{n}_b n_c \right) (1 + P_{12}) \eta_{c1ab}^J \Gamma_{abc2}^J, \tag{10.33}$$

$$\frac{d\Gamma_{1234}^J}{ds} = \sum_a \left(\left(1 - (-1)^{J - j_1 - j_2} P_{12} \right) \left(\eta_{1a} \Gamma_{a234}^J - f_{1a} \eta_{a234}^J \right) \right.$$

$$\qquad \left. - \left(1 - (-1)^{J - j_3 - j_4} P_{34} \right) \left(\eta_{a3} \Gamma_{12a4}^J - f_{a3} \eta_{12a4}^J \right) \right)$$

$$\qquad + \frac{1}{2} \sum_{ab} \left(\eta_{12ab}^J \Gamma_{ab34}^J - \Gamma_{12ab}^J \eta_{ab34}^J \right) (1 - n_a - n_b)$$

$$\qquad + \sum_{abJ'} (n_a - n_b) \left(1 - (-1)^{J - j_1 - j_2} P_{12} \right)$$

$$\qquad \times \hat{J}'^2 \begin{Bmatrix} j_1 & j_2 & J \\ j_3 & j_4 & J' \end{Bmatrix} \left(\overline{\eta}_{1\bar{4}a\bar{b}}^{J'} \overline{\Gamma}_{a\bar{b}3\bar{2}}^{J'} - \overline{\Gamma}_{1\bar{4}a\bar{b}}^{J'} \overline{\eta}_{a\bar{b}3\bar{2}}^{J'} \right), \tag{10.34}$$

where $\hat{j} \equiv \sqrt{2j+1}$, indices with a bar indicate time-reversed states, and the $\overline{\eta}$ and $\overline{\Gamma}$ matrix elements in the last line of Eq. (10.34) are obtained by a generalized Pandya transform (see, e.g., [?]),

$$\overline{\mathcal{O}}_{1\bar{2}3\bar{4}}^J = -\sum_{J'} \hat{J}'^2 \begin{Bmatrix} j_1 & j_2 & J \\ j_3 & j_4 & J' \end{Bmatrix} O_{1432}^{J'}. \tag{10.35}$$

Alternatively, the particle-hole terms in the last line of Eq. (10.34) can also be expressed in terms of the cross-coupled matrix elements introduced in Ref. [?]. If the same angular-momentum coupling order is used, the two types of matrix elements are related by a trivial phase factor (-1).

10.2.6 General Observables

In principle, the evaluation of observables other than the Hamiltonian is a straightforward task: We need to normal-order the operator $\mathscr{O}(s)$ with respect to the same reference state as the Hamiltonian, and then plug it into the flow equation

$$\frac{d}{ds}\mathscr{O}(s) = [\eta(s), \mathscr{O}(s)], \tag{10.36}$$

with $\eta(s)$ the same as in the Hamiltonian flow equation. For consistency with the overall IM-SRG(2) scheme, $\mathscr{O}(s)$ is truncated at the two-body level. We then obtain an additional set of flow equations for the normal-ordered zero-, one- and two-body parts of $\mathscr{O}(s)$ which need to be solved alongside Eqs. (10.28)–(10.30). We will follow this route in later sections of this work to investigate radii (Sec. **??**) and the center-of-mass separation in the IM-SRG(2) ground-state wave function (Sec. **??**). Due to the size of the system of flow equations, and the associated storage needs of numerical differential equation solvers, this procedure becomes unfeasible if we are interested in more than one or two additional operators.

Unfortunately, we cannot resort to the same strategy as in the free-space SRG case [**?**, **?**], where the unitary transformation can be reconstructed from the eigenvectors of the initial and final Hamiltonians in the two-nucleon, three-nucleon,... system. To do so, we would have to solve the eigenvalue problem of the Hamiltonian in the A-body system through exact diagonalization, and we could not even resort to large-scale NCSM machinery because it does not provide the full eigenbasis, but only the lowest eigenvalues and eigenvectors via Lanczos methods. The cost for exact diagonalization increases factorially with the single-particle basis, and it is precisely this high computational effort that motivated the development of mildly scaling methods like CC or the IM-SRG. A more efficient alternative for the evaluation of observables exists in the form of the so-called Magnus expansion [**?**, **?**], which we briefly discuss in Sec. **??**.

10.3 Choice of Generator

10.3.1 Decoupling

After setting up the general IM-SRG flow equation framework in Sec. 10.2, we have to specify the generator η. To this end, we first need to identify the off-diagonal parts of the Hamiltonian that the IM-SRG transformation is supposed to suppress for $s \to \infty$. The freedom to partition the Hamiltonian into suitably defined diagonal and off-diagonal pieces gives the IM-SRG flexibility to target different states, and is key to extending the method to open-shell nuclei, see Secs. **??** and **??**. To illustrate the general idea of a targeted decoupling, let us assume our goal is to extract the ground-state energy of a closed-shell nucleus, i.e., the lowest eigenvalue of the nuclear many-body Hamiltonian. In the left panel of Fig. 10.1, we show a schematic representation of the initial Hamiltonian $H(0)$, in a basis consisting of A-particle-A-hole (ApAh) excitations of the reference state $|\Phi\rangle$. For the following illustration of the IM-SRG's basic concept, we assume that $H(0)$ has been truncated to two-body operators, that is, it can at most couple npnh to $(n \pm 2)$p$(n \pm 2)$h states. The extension to three-body operators is straightforward.

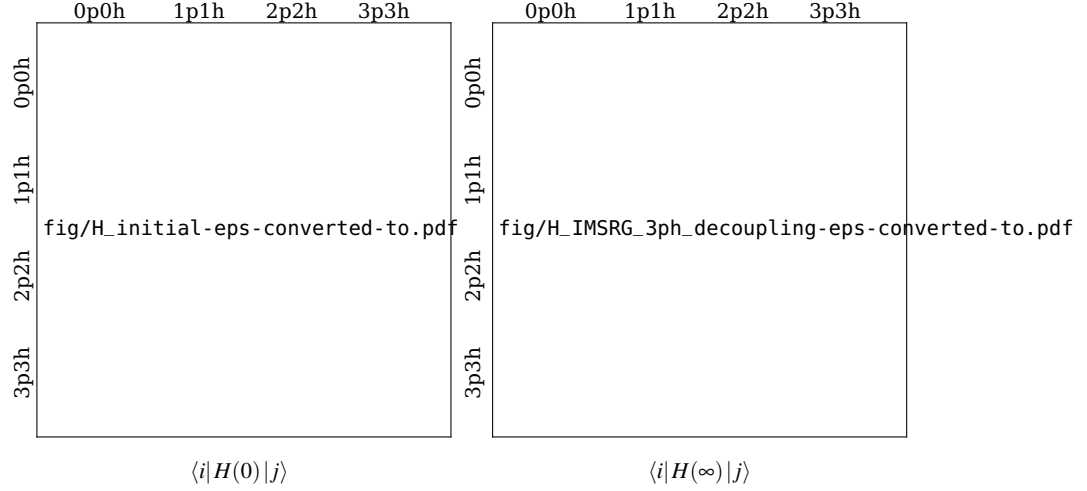The 0p0h reference state is coupled to 1p1h and 2p2h excitations by the matrix elements

Fig. 10.1 Schematic representation of the initial and final Hamiltonians, $H(0)$ and $H(\infty)$, in the many-body Hilbert space spanned by particle-hole excitations of the reference state.

$$\langle\Phi|H(0):a_p^\dagger a_h:|\Phi\rangle = f_{ph}\,, \tag{10.37}$$

$$\langle\Phi|H(0):a_p^\dagger a_{p'}^\dagger a_{h'} a_h:|\Phi\rangle = \Gamma_{pp'hh'}\,, \tag{10.38}$$

and their Hermitian conjugates. Thus, we define the off-diagonal part of the Hamiltonian as

$$H^{od}(s) = \sum_{ph} f_{ph}:a_p^\dagger a_h: +\frac{1}{4}\sum_{pp'hh'}\Gamma_{pp'hh'}:a_p^\dagger a_{p'}^\dagger a_{h'} a_h: + \text{H.c.}\,. \tag{10.39}$$

During the flow, matrix elements between the reference state and higher excitations acquire non-zero values,

$$\langle\Phi|H(s):a_{p_1}^\dagger\ldots a_{p_A}^\dagger a_{h_A}\ldots a_{h_1}:|\Phi\rangle \neq 0\,, \tag{10.40}$$

because $H(s > 0)$ has induced $3-,\ldots,A-$body contributions (cf. Eq. (10.24)), just as in a free-space SRG evolution [**?**, **?**, **?**]. By truncating operators to two-body rank in the IM-SRG(2) (or any rank $n \leq A$ in a higher truncation), we force these (and other) matrix elements to vanish, at the cost of violating unitarity. We will have to check that this violation remains sufficiently small in practical calculations.

If we eliminate the matrix elements (10.37), (10.38) as $s \to \infty$, the final IM-SRG(2) Hamiltonian $H(\infty)$ has the shape shown in the right panel of Fig. 10.1: the one-dimensional 0p0h space spanned by the reference state is completely decoupled from other states, and therefore an eigenspace of $H(\infty)$, with the eigenvalue given by the corresponding matrix element. In essence, this means that the IM-SRG provides a mapping between the reference state $|\Phi\rangle$ and an exact eigenstate $|\Psi\rangle$ of the nucleus.

At this point, a few remarks are in order. In a finite system, i.e., in the absence of phase transitions, it is always possible to obtain a mapping between the reference state $|\Phi\rangle$ and an exact bound eigenstate $|\Psi\rangle$ of H by performing a diagonalization, provided there are no symmetry or other restrictions on the ApAh basis built from $|\Phi\rangle$. Thus, the IM-SRG is guaranteed to yield an exact energy and wave function for the A-body system if the IM-SRG flow equations are not truncated. Induced couplings between the 0p0h reference state and excited 3p3h,...,ApAh states (Eq. (10.40)) are included in $H^{od}(s)$, and consequently suppressed for $s \to \infty$. By truncating the flow equations, we only obtain an approximation to an exact eigenvalue and eigenstate, of course. Similarly, we note that eigenvalue spectrum of $H(s)$

is variational only if the IM-SRG equations are solved without truncation, since the unitary equivalence with H is otherwise only approximate.

In general, we cannot guarantee that the IM-SRG will necessarily extract the lowest eigenstate of H. As in other methods which make use of a reference state, we expect to be able to reach the lowest eigenvalue if the reference state itself is a fair approximation to the ground state, e.g., a Hartree-Fock Slater determinant. We will revisit this issue in Sec. **??**.

As indicated in Fig. 10.1, we have also eliminated the outermost side diagonals of $H(\infty)$ by suppressing the coupling between the reference state and 2p2h excitations. This implies that any subsequent calculation which uses $H(\infty)$ as input, e.g., a diagonalization to obtain the full excitation spectrum, can be expected to converge much more rapidly (see Sec. **??**).

Finally, we want to address why we have decided to target only a single eigenvalue and eigenstate of the Hamiltonian by means of IM-SRG decoupling. We might wish to extend the definition of $H^{od}(s)$ to encompass matrix elements that mix 1p1h excitations or couple the 1p1h and 2p2h blocks of the Hamiltonian, in order to diagonalize $H(s)$ completely in the 0p0h and 1p1h blocks (cf. Fig. **??**). In practice, this results in uncontrolled behavior of the generator and (approximate) ground and excited-state energies during the flow, because we have truncated strong induced three- and higher-body operators that feed back into the flow of the zero-, one-, and two-body operators that we do track in the IM-SRG(2) scheme. To avoid these complications in our ground-state calculations, we restrict ourselves to decoupling the 0p0h block, similar to the CC method (see, e.g., [**?**]). We refer to this as the *minimal decoupling* scheme.

10.3.2 White Generators

Starting from the off-diagonal Hamiltonian, Eq. (10.39), we can define several classes of generators which will suppress the matrix elements of H^{od} as we integrate the IM-SRG flow equations for $s \to \infty$. Our standard choice is motivated by the work of White on canonical transformation theory in quantum chemistry [**?**, **?**]:

$$\eta^{\text{IA/B}}(s) \equiv \sum_{ph} \frac{f_{ph}(s)}{\Delta_{ph}^{\text{A/B}}(s)} :a_p^\dagger a_h: + \sum_{pp'hh'} \frac{\Gamma_{pp'hh'}(s)}{\Delta_{pp'hh'}^{\text{A/B}}(s)} :a_p^\dagger a_{p'}^\dagger a_{h'} a_h: - \text{H.c.}. \tag{10.41}$$

The generalization to three-body or higher rank is obvious. Note that the energy denominators must cause a sign change under transposition in Eq. (10.41) to ensure the anti-Hermiticity of $\eta(s)$, because f and Γ are Hermitian.

The superscripts in (10.41) distinguish two different choices for the energy denominators which we will be studying in the following. They correspond to the Epstein-Nesbet and Møller-Plesset partitionings used in MBPT (see, e.g., [**?**]). A straightforward application of White's construction described in Ref. [**?**] leads to the Epstein-Nesbet case, with energy denominators which are defined in terms of the diagonal matrix elements of the Hamiltonian in our chosen npnh-representation (Fig. 10.1):

$$\Delta_{ph}^{\text{A}} \equiv \langle ph|H|ph \rangle - \langle \Phi|H|\Phi \rangle = f_p - f_h + \Gamma_{phph} = -\Delta_{hp}^{\text{A}}, \tag{10.42}$$

$$\Delta_{pp'hh'}^{\text{A}} \equiv \langle pp'hh'|H|pp'hh' \rangle - \langle \Phi|H|\Phi \rangle = f_p + f_{p'} - f_h - f_{h'} - A_{pp'hh'} \equiv -\Delta_{hh'pp'}^{\text{A}}, \tag{10.43}$$

where $f_p = f_{pp}, f_h = f_{hh}$, and

$$A_{pp'hh'} \equiv \Gamma_{pp'pp'} + \Gamma_{hh'hh'} - \Gamma_{phph} - \Gamma_{p'h'p'h'} - \Gamma_{ph'ph'} - \Gamma_{p'hp'h}. \tag{10.44}$$

In the Møller-Plesset case, on the other hand,

$$\Delta^{\mathrm{B}}_{ph} \equiv f_p - f_h \equiv -\Delta^{\mathrm{B}}_{hp}\,, \tag{10.45}$$

$$\Delta^{\mathrm{B}}_{pp'hh'} \equiv f_p + f_{p'} - f_h - f_{h'} \equiv -\Delta^{\mathrm{B}}_{hh'pp'}\,. \tag{10.46}$$

By expanding the Epstein-Nesbet denominators in Eq. (10.41) in terms of geometric series, we see that η^{A} corresponds to a generator with Møller-Plesset denominators where certain MBPT diagrams have been summed to all orders.

If we want to work with the *J*-scheme flow equations (10.32)–(10.34), it is not unambiguously clear how to treat the two-body matrix elements in the Epstein-Nesbet denominators (10.42), (10.43) in the angular momentum coupling process. As a pragmatic solution to this issue, we use the monopole matrix elements

$$\Gamma^{(0)}_{abcd} \equiv \frac{\sum_J (2J+1)\Gamma^J_{abcd}}{\sum_J (2J+1)} \tag{10.47}$$

in Eqs. (10.42)–(10.44).

The big advantage of White-type generators in practical calculations lies in the fact that they suppress *all* off-diagonal matrix elements with a decay scale identical (or close to) 1 (see Sec. 10.3.5). Thus, the flow is *not* a proper RG flow that suppresses matrix elements between states with large energy differences first. This is inconsequential if we are only interested in $H(\infty)$, because all unitary transformations which suppress H^{od} must must be equivalent up to differences caused by truncating the IM-SRG flow equations.

The use of $\eta^{\mathrm{A/B}}$ has additional benefits in numerical applications: First, the effort for their construction scales as $\mathcal{O}(N_h^2 N_p^2)$, where $N_h \ll N$ and $N_p \sim N$ are the number of hole and particle states in a single-particle basis of dimension N. Second, because the generator's matrix elements are given by ratios of energies, f and Γ only contribute linearly to the magnitude of the right-hand side of the IM-SRG flow equations (10.28)–(10.30). The flow equations are significantly less stiff than those for the canonical Wegner generator (Sec. 10.3.4), where third powers of f and Γ appear (see below). This greatly reduces the number of integration steps which are required to solve the IM-SRG flow equations. However, the White generators also have an obvious drawback: It is clear from Eq. (10.41) that we might encounter problems with small energy denominators [**?**, **?**]. Fortunately, this is not the case if we deal with closed-shell nuclei, as in the present work.

We conclude our discussion by remarking that the White-type generators $\eta^{\mathrm{A/B}}$ provide a manifest link between the IM-SRG and MBPT, which will be explored further in Section **??**.

10.3.3 Imaginary-Time Generators

A second class of generators which are used in our calculations are inspired by imaginary-time evolution techniques that are frequently used in Quantum Monte Carlo methods, for instance (see, e.g., [**?**] and references therein). Using the off-diagonal Hamiltonian, Eq. (10.39), we define

$$\eta^{\mathrm{IIA/B}}(s) \equiv \sum_{ph} \mathrm{sgn}\left(\Delta^{\mathrm{A/B}}_{ph}(s)\right) f_{ph}(s)\; :a^\dagger_p a_h:$$

$$+ \sum_{pp'hh'} \mathrm{sgn}\left(\Delta^{\mathrm{A/B}}_{pp'hh'}(s)\right) \Gamma_{pp'hh'}(s)\; :a^\dagger_p a^\dagger_{p'} a_{h'} a_h: - \mathrm{H.c.}\,, \tag{10.48}$$

where $\Delta^{\mathrm{A/B}}$ are the Epstein-Nesbet and Møller-Plesset energy denominators defined in Eqs. (10.42)–(10.46). As we will see in Sec. 10.3.5, the sign functions are necessary to ensure that off-diagonal matrix elements are suppressed instead of enhanced during the flow.

The decay scale for these matrix elements is approximately given by the linear energy difference between the reference state and 1p1h or 2p2h excitations, respectively, which can be expressed via $\Delta^{A/B}$. Note that this implies that $\eta^{IIA/B}$ generates a proper RG flow.

For the imaginary-time generator, the IM-SRG(2) flow equations are quadratic in the Hamiltonian. While this leads to a mild increase in the stiffness compared to the use of White generators, the flow is not susceptible to small or vanishing energy denominators. Combined with the low $\mathscr{O}(N_h^2 N_p^2)$ effort for its construction, the imaginary-time generator is a robust numerical fallback option in cases where singular White generators stall the IM-SRG flow.

10.3.4 Wegner Generators

In his initial work on flow equations and the SRG [?], Wegner proposed the canonical generator

$$\eta^{III}(s) = [H^d(s), H^{od}(s)]. \tag{10.49}$$

Using the definition of the off-diagonal Hamiltonian, Eq. (10.39), and the commutators from Appendix **??**, it is straightforward to derive the individual one-body, two-body, etc. matrix elements of $\eta(s)$. Keeping up to two-body operators, just as in the IM-SRG(2) flow equations, we obtain

$$\eta_{12} = \sum_a (1 - P_{12}) f_{1a}^d f_{a2}^{od} + \sum_{ab} (n_a - n_b)(f_{ab}^d \Gamma_{b1a2}^{od} - f_{ab}^{od} \Gamma_{b1a2}^d)$$
$$+ \frac{1}{2} \sum_{abc} (n_a n_b \bar{n}_c + \bar{n}_a \bar{n}_b n_c)(1 - P_{12}) \Gamma_{c1ab}^d \Gamma_{abc2}^{od}, \tag{10.50}$$

$$\eta_{1234} = \sum_a \left\{ (1 - P_{12})(f_{1a}^d \Gamma_{a234}^{od} - f_{1a}^{od} \Gamma_{a234}^d) - (1 - P_{34})(f_{a3}^d \Gamma_{12a4}^{od} - f_{a3}^{od} \Gamma_{12a4}^d) \right\}$$
$$+ \frac{1}{2} \sum_{ab} (1 - n_a - n_b)(\Gamma_{12ab}^d \Gamma_{ab34}^{od} - \Gamma_{12ab}^{od} \Gamma_{ab34}^d)$$
$$- \sum_{ab} (n_a - n_b)(1 - P_{12})(1 - P_{34})\Gamma_{b2a4}^d \Gamma_{a1b3}^{od}. \tag{10.51}$$

Structurally, Eqs. (10.50) and (10.51) are identical to the flow equations except for signs stemming from the overall anti-Hermiticity of the generator. The J-scheme expressions for $\eta^{III}(s)$ are easily obtained from Eqs. (10.33) and (10.34).

Clearly, a fixed point of the Wegner flow is reached when $\eta(s)$ vanishes. At finite s, this can occur when $H^d(s)$ and $H^{od}(s)$ commute due to a degeneracy in the spectrum of $H(s)$, e.g., because of symmetries. A fixed point at $s \to \infty$ exists if $H^{od}(s)$ vanishes as required. When we work with a truncated, finite-dimensional Hilbert space, it is easy to show that [?, ?]

$$\frac{d}{ds} \text{tr} \left(H^{od}(s) \right)^2 = -2\text{tr} \left(\eta^\dagger(s) \eta(s) \right) \leq 0 \tag{10.52}$$

due to $\eta^\dagger(s)\eta(s)$ being positive semi-definite, so $H^{od}(s)$ is increasingly suppressed and $H(s)$ is indeed diagonalized.

An interesting consequence of Eq. (10.52) is that the flow generated by the generator (10.49) follows a steepest-descent trajectory in the manifold of unitarily transformed Hamiltonians. The flow itself has proper RG character, i.e., it eliminates off-diagonal matrix elements between states with large energy differences first, as we will demonstrate in Sec. 10.3.5. While the proper RG behavior, the steepest-descent property Eq. (10.52), and absence of small energy denominators as in the White generators are useful formal features, Wegner

generators are much less efficient in numerical applications than our other choices. The cost for constructing η^{III} is of the order $\mathcal{O}(N^6)$, with little to be gained by distinguishing particle and hole states, and therefore similar to the cost for evaluating the IM-SRG(2) flow equations themselves. In addition, the flow equations become very stiff because the RHS terms are cubic in the Hamiltonian, and the appropriate stiff ODE solvers have higher storage and computing time demands than those for non-stiff or weakly stiff cases resulting from the use of White or imaginary-time generators.

10.3.5 Decay Scales

Further insight into the IM-SRG flows that result from our different generator choices can be gained from a schematic analysis of the flow equations, analogous to prior work for the free-space SRG [**?**, **?**]. Let us again assume that the Hamiltonian is split into a diagonal and an off-diagonal part,

$$H(s) = H^d(s) + H^{od}(s), \tag{10.53}$$

where $H^{od}(s)$ is supposed to be suppressed as $s \to \infty$. Further, we work in the eigenbasis of $H^d(0)$, which is assumed to be invariant under s, so that at each step of the flow

$$H^d(s)\,|n\rangle = E_n(s)\,|n\rangle \,. \tag{10.54}$$

In this basis representation, Eq. (10.2) becomes

$$\frac{d}{ds}\langle i|H|j\rangle = \sum_k \left(\langle i|\,\eta\,|k\rangle\langle k|H|j\rangle - \langle i|H|k\rangle\langle k|\,\eta\,|j\rangle \right)$$
$$= -(E_i - E_j)\langle i|\,\eta\,|j\rangle + \sum_k \left(\langle i|\,\eta\,|k\rangle\langle k|H^{od}|j\rangle - \langle i|H^{od}|k\rangle\langle k|\,\eta\,|j\rangle \right), \tag{10.55}$$

and $\langle i|H^{od}|i\rangle = 0$.

Consider now a generator of White type, which can be written as

$$\langle i|\,\eta^I\,|j\rangle = \frac{\langle i|H^{od}|j\rangle}{E_i - E_j}, \tag{10.56}$$

so that the flow equation reads

$$\frac{d}{ds}\langle i|H|j\rangle = -\langle i|H^{od}|j\rangle + \sum_k \frac{E_i + E_j - 2E_k}{(E_i - E_k)(E_j - E_k)}\langle i|H^{od}|k\rangle\langle k|H^{od}|j\rangle. \tag{10.57}$$

Let us assume that the transformation generated by η truly suppresses H^{od}, and consider the asymptotic behavior for large flow parameters $s > s_0 \gg 0$. If $||H^{od}(s_0)|| \ll 1$ in some suitable norm, the second term in the flow equation can be neglected compared to the first one. In this case, Eq. (10.57) implies

$$\left.\frac{dE_i}{ds}\right|_{s=s_0} = 2\sum_k \frac{\langle i|H^{od}|k\rangle\langle k|H^{od}|i\rangle}{E_i - E_k} \approx 0\,, \tag{10.58}$$

and the energies stay (approximately) constant:

$$E_i(s) \approx E_i(s_0), \quad s > s_0\,. \tag{10.59}$$

Consequently, Eq. (10.57) can be integrated, and we have

$$\langle i| H^{od}(s)|j\rangle \approx \langle i| H^{od}(s_0)|j\rangle\, e^{-(s-s_0)}, \quad s > s_0, \tag{10.60}$$

as already mentioned in Sec. 10.3.2. If the initial $H_{od}(0)$ is perturbative, we will observe this behavior from the very onset of the flow (see the discussion in Sec. **??**).

For the imaginary-time generator, we have

$$\langle i| \eta^{\mathrm{II}}|j\rangle = \mathrm{sgn}\,(E_i - E_j)\,\langle i| H^{od}|j\rangle, \tag{10.61}$$

and the flow equation

$$\frac{d}{ds}\langle i| H|j\rangle = -\left| E_i - E_j\right| \langle i| H^{od}|j\rangle$$
$$+ \sum_k \left(\mathrm{sgn}(E_i - E_k) + \mathrm{sgn}(E_j - E_k)\right) \langle i| H^{od}|k\rangle \langle k| H^{od}|j\rangle. \tag{10.62}$$

Note that the sign function in the definition of η^{II} ensures that only the absolute value of the energy difference between the states $|i\rangle$ and $|k\rangle$ appears in the first term. Integration of Eq. (10.62) yields

$$\langle i| H^{od}(s)|j\rangle \approx \langle i| H^{od}(s_0)|j\rangle\, e^{-|E_i - E_j|(s-s_0)}, \quad s > s_0, \tag{10.63}$$

and off-diagonal matrix elements are suppressed, with a decay scale set by $|E_i - E_j|$.

Finally, we perform the same kind of analysis for the Wegner generator

$$\langle i| \eta^{\mathrm{III}}|j\rangle = \langle i| [H^d, H^{od}]|j\rangle = (E_i - E_j)\langle i| H^{od}|j\rangle. \tag{10.64}$$

The flow equation reads

$$\frac{d}{ds}\langle i| H|j\rangle = -(E_i - E_j)^2\,\langle i| H^{od}|j\rangle + \sum_k (E_i + E_j - 2E_k)\,\langle i| H^{od}|k\rangle \langle k| H^{od}|j\rangle, \tag{10.65}$$

and we obtain

$$\langle i| H^{od}(s)|j\rangle \approx \langle i| H^{od}(s_0)|j\rangle\, e^{-(E_i - E_j)^2(s-s_0)}, \quad s > s_0. \tag{10.66}$$

Thus, we see that the imaginary-time and Wegner generators yield proper RG transformations, in the sense that matrix elements between states with large energy differences $\Delta E_{ij} = |E_i - E_j|$ decay at smaller flow parameters s than states with small ΔE_{ij}. The White generator, on the other hand, acts on all matrix elements simultaneously. If we are only interested in the limit $s \to \infty$, this should not make a difference. In Sec.**??**, we will explore to which extent this is indeed the case, and quantify differences which are caused by the terms we have omitted in our schematic analysis, and the necessary truncations in the IM-SRG flow equations.

10.4 In-medium SRG studies of infinite matter

Chapter 11
Green's function approaches

Carlo Barbieri and Adriana Carbone

Abstract We discuss Green's function methods with a focus on infinite nuclear matter

11.1 Concluding remarks

Carlo Barbieri
Department of Physics, University of Surrey, Surrey, UK, e-mail: c.barbieri@surrey.ac.uk,

Adriana Carbone
Germany, e-mail: carbone@lnf.infn.it

Chapter 12
Concluding remarks and perspectives

Morten Hjorth-Jensen, Maria Paola Lombardo, and Ubirajara van Kolck

Abstract Here Morten the Roman-Viking (who has never admitted his Norse roots) goes finally berserk in a classical Norse way and and Bira, clad in his befitting apologetic suit, presents himself as the true messiah of EFT and shouts stand up all ye infidels and hail the master. Halleluja and amen. Maria Paola is left speechless and runs for shelter somewhere in lovely Frascati (we envy her).

12.1 Concluding remarks

12.2 Perspectives

Morten Hjorth-Jensen

Department of Physics and Astronomy and National Superconducting Cyclotron Laboratory, Michigan State University, East Lansing, Michigan, USA and Department of Physics, University of Oslo, Oslo, Norway, e-mail: hjensen@msu.edu,

Maria Paola Lombardo

INFN, Laboratori Nazionali di Frascati, Frascati, Italy, e-mail: mariapaola.lombardo@lnf.infn.it,

Ubirajara van Kolck

Department of Physics, University of Arizona, Tucson, Arizona, USA and Institut de Physique NuclÃl'aire, Orsay, France, e-mail: vankolck@ipno.in2p3.fr